S

SALINITY

C. K. Jain
National Institute of Hydrology, Centre for Flood Management Studies, Dispur, Guwahati, Assam, India

Synonyms

Brininess; Salinity; Salt; Saltiness

Definition

Concentration of dissolved salts found in a sample of water. It is measured as the total amount of dissolved salts in parts per 1,000. Seawater has an average salinity of about 35 parts/1,000.

Nearly all water contains dissolved chemicals, even rainwater. These dissolved chemicals are called salts. The salinity of normal ocean water is about 35 parts per 1,000, total dissolved solids. This is written as 35‰ or 35 ppth. A salinity of 35‰ is the same as 3.5%. The symbol resembles a percentage sign (%), but percent means per 100. But the symbol with two zeros on the bottom of the fraction (‰) means per 1,000.

Salinity varies slightly from place to place around the world, and also varies somewhat with the seasons (affected by temperature and precipitation). The salinity of seawater ranges from about 30‰ to 40‰. Warm temperatures and high evaporation rates (particularly in shallow seas) raise the salinity. Warmer waters will tend to have higher salinity than cooler waters.

Water of salinity between freshwater and seawater is called brackish. Brackish water can be found in estuaries. Water with salinity greater than normal seawater is called hypersaline. For example, the Great Salt Lake, Utah, and the Dead Sea are hypersaline. Hypersaline lakes tend to occur in arid areas. They are land-locked basins with no outlet for the waters to flow from the lake. The salts are concentrated as a result of evaporation. Evaporation is so extreme in some lakes (ephemeral lakes or playa lakes) that they dry up completely every few years, leaving a saltpan.

Freshwater input (rivers, precipitation, or melting ice) lowers the salinity. In polar areas where glaciers and ice caps are melting, the seawater has lower salinity.

SALTATION

C. K. Jain
National Institute of Hydrology, Centre for Flood Management Studies, Dispur, Guwahati, Assam, India

Saltation is a specific type of particle transport by fluids such as wind, or the denser fluid water. It occurs when loose material is removed from a bed and carried by the fluid, before being transported back to the surface. Examples include pebble transport by rivers, sand drift over desert surfaces, soil blowing over fields, or even now drift over smooth surfaces such as those in the Arctic or Canadian Prairies.

At low-fluid velocities, loose material rolls downstream, staying in contact with the surface. This is called *creep*. Here the forces exerted by the fluid on the particle are only enough to roll the particle around the point of contact with the surface. At higher speeds, the lift and moment exerted by the fluid on the particle is enough to pull it away from the surface and into the flow. Initially the particle moves quite rapidly compared to the flow and so has high lift, moving it away from the surface. As the particle moves into the faster flow away from the bed, the velocity difference between particle and flow decreases and so lift decreases. When the particle weight is greater than the lift force, the particle sinks back toward the

Vijay P. Singh, Pratap Singh & Umesh K. Haritashya (eds.), *Encyclopedia of Snow, Ice and Glaciers*, DOI 10.1007/978-90-481-2642-2,

surface. During its descent, the particle keeps some of the speed it picked up in the faster moving flow, and so returns to the surface at higher speed than the fluid near the surface. This gives the particle a parabolic trajectory through the fluid, which is the defining characteristic of saltation. Depending on the surface, more loose material could be dislodged by the impacting particle, the particle might disintegrate on impact, or the particle could continue bouncing downstream. In rivers, this process repeats continually, gradually eroding away the riverbed, but also transporting in fresh material from upstream.

SCANDINAVIAN GLACIERS

Juha P. Lunkka
Institute of Geosciences, University of Oulu,
Oulu, Finland

Definition

Scandinavia: Geographical area in northern Europe consisting Norway, Sweden, and northwestern part of Finnish Lapland.

Introduction

Scandinavia is located in northern Europe between latitudes 55–71° North (Figure 1). The mountains that run through mainland Scandinavia from south to north are not very high but in many places they are very steep. The highest peaks reach well over 2,000 m above the present sea level. Their northern location and moisture from the North Atlantic Ocean to the west of Scandinavia has caused the formation of many glaciers in the coastal areas as well as further inland several times, particularly during the past 2.6 million years. At present, the glaciers in Scandinavia are relatively small and cover mostly mountainous areas, occurring in a wide latitudinal range from ca. 60° N to 70°N. Although glaciated areas in Scandinavia consist of only 0.2% of the ice coverage in Arctic regions (Dowdeswell and Hagen, 2004), they have provided valuable records on the behavior of glaciers and proxy data for recent climate events in northwestern Europe.

History of the Scandinavian glaciers

The Fennoscandian Shield, including Scandinavia, has hosted glaciers many times throughout Earth's history, although its latitudinal position and topography has changed constantly in time as a result of plate tectonism. The geological record from Scandinavia, extending back to the Precambrian, includes metasedimentary rocks of glacial origin, for example, in Finnish North Karelia, on the Kola Peninsula, and on the Varanger Peninsula, Norway. This evidence indicates that glaciers covered Fennoscandia several times during the Early Proterozoic around 2.4–2.2 billion years ago and in the Neoproterozoic Era ca. 700–600 million years ago (cf. Siedlecka and Roberts, 1992; Melezhik, 2006). However, there is no geological evidence to indicate that any major glaciers existed in the Fennoscandian shield between the Palaeozoic and Mesozoic Era (540–65 million years ago).

Results from the central Arctic Ocean and Norwegian-Greenland Sea suggest that continental glaciers were present around the Arctic Basin during the Late Eocene as early as 35 million years ago (Moran and ACEX Members, 2006; Eldrett et al., 2007), but the distribution and extent of these ice masses are not known in detail. Ice-Rafted Detritus (IRD) in the deep-sea sediments west of Norway indicate that glaciers must have existed in Scandinavia already about 11 million years ago (Mangerud et al., 1996).

Glaciers in the Scandinavian mountains are thought to have been the nucleus of the Scandinavian Ice Sheet (SIS) that spread over the southern and eastern continental areas adjacent to Scandinavian mountains and was confluent with the Barents and British Ice Sheets several times during the Quaternary period (cf. Mangerud, 2004) (Figure 2). It has been estimated that during the past 2.6 million years, the Scandinavian mountains were covered by glacial ice ca. 90% of the time (cf. Holmlund, 2005). Geological evidence indicates the presence of an ice sheet over Scandinavia for most part of the Elsterian (ca. 500,000–450,000 years ago), Saalian (ca. 390,000–130,000 years ago), and Weichselian (115,000–11,500 years ago) glaciations (cf. Donner, 1995; Mangerud, 2004; Svendsen et al., 2004). During the last glacial maximum (LGM) ca. 20,000–18,000 years ago the Scandinavian Ice Sheet was at its largest for at least the past 130,000 years extending from the North Sea and the Norwegian shelf areas to the Russian Plain (Figure 2). At the LGM, the modelled thickness of the ice sheet over Scandinavia was ca. 2.5 km (Siegert and Dowdeswell, 2004) and during the Younger Dryas cold climate event (ca. 12,500–11,500 years ago) SIS still covered most of Fennoscandia (Figure 1). It is thought that glaciers started to melt relatively fast at the beginning of the Holocene and may have disappeared completely at least once during the period from 8,000–4,000 years ago (Nesje et al., 2008). After their disappearance most of the Scandinavian glaciers attained their largest extent during the Little Ace Age most likely about 1,750 A.D. (cf. Whalley, 2004).

Present glaciers in Scandinavia

At present the total number of glaciers in Scandinavia is ca. 1,900, of which slightly over 1,600 in Norway and ca. 300 in Sweden (Østrem and Haakensen, 1993; Schytt, 1993). The average sizes of the glaciers in Norway and Sweden are 2.6 km^2 and 1 km^2, respectively (cf. Holmlund, 2005). Morphologically the largest glaciers are categorized as ice caps and ice fields or plateau glaciers while the medium-size glaciers are valley glaciers and cirque glaciers. The largest glacier in Scandinavia, and also in mainland Europe, is Jostedalsbreen (487 km^2), which is located in Norway. Other sizeable

Scandinavian Glaciers, Figure 1 Location map of the glaciers in Scandinavia (*squares*) with names of the glaciers mentioned in text. The Younger Dryas ice limit (ca. 12,500–11,500 years ago) is also indicated.

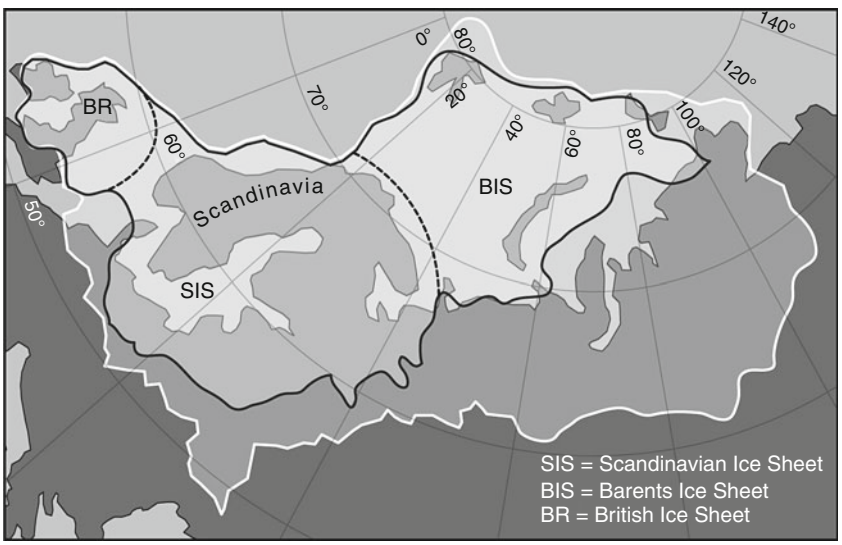

Scandinavian Glaciers, Figure 2 The reconstruction of the Eurasian ice sheet at the Saalian glaciation ca. 160,000–140,000 years ago (*white line*) and at the last glacial maximum ca. 20,000–18,000 years ago (*black line*).

glaciers in Norway are Svartisen West (221 km^2), Folgefonna South (168 km^2), and Svartisen East (148 km^2) (Figure 2). The total glacier volume of Norway is estimated to be 164 km^3 (Nesje et al., 2008). Glaciers in Sweden are relatively small compared to those in Norway. The largest glaciers in Sweden are Stourrajekna and Ålmaijekna both less than 12 km^2 (Schytt, 1993).

Glaciers in mainland Scandinavia cover an area of approximately 2,900 km^2 (cf. Whalley, 2004). In this area, glaciers occur mainly in mountainous areas, that is, in the Scandinavian Mountain range (Figure 2). Climate in the western part of the mountain range is locally maritime, becoming more continental on the eastern side of the mountains. In the maritime climatic areas, the glaciers on the mountains are normally fed by orographic precipitation while in the climatically more continental eastern part of the mountain range precipitation is lower and the glaciers here are fed by wind-driven snow accumulation (cf. Holmlund, 2005).

The largest glaciers are built up in the maritime climate of the Norwegian west coast between 60–62° N and 66–70° N latitudes within 180 km of the coast (Østrem and Haakensen, 1993; Grove, 2004). Annual accumulation in the glaciated areas close to the western coast of Norway is ca. 3–4 m (snow water equivalent), while the annual accumulation in the more easterly located glaciers in Sweden and Norway is less than 1 m (snow water equivalent) (cf. Holmlund, 2005). The glaciers in

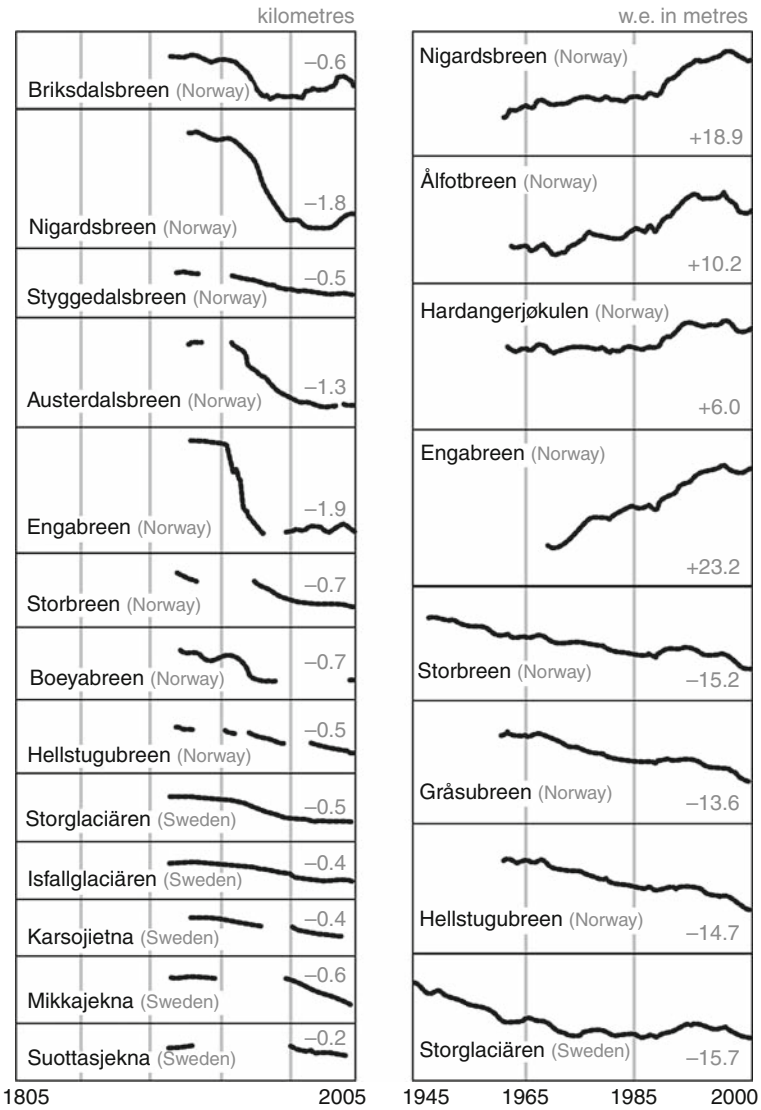

Scandinavian Glaciers, Figure 3 The diagram on the *left* shows glacier frontal changes and the total frontal change in kilometers of different Scandinavian glaciers (*left* panel) up to the year 2005. The diagram on the *right* panel shows the mass balance variations and the total mass balance change in water equivalent of different glaciers up to the year 2005 in Scandinavia.

Scandinavia are mainly warm-based but a few glaciers are polythermal and some glaciers on high mountain plateaux are cold-based (cf. Whalley, 2004 and references therein).

Glacier frontal position and mass balance

Systematic monitoring of the Scandinavian glaciers already began at the turn of the twentieth century with observations on the ice-marginal positions (the glacier change in length) in many glaciated areas. At present data on changes of ice-marginal position from around the world are reported in every fifth year by the World Glacier Monitoring Service (http://www.geo.uzh.ch/wgms/) in their report entitled *Fluctuations of Glaciers*. The ice-frontal position record of most outlet glaciers in Scandinavia indicates a clear overall receding trend of the glacial margins from the mid-1930s to the present (Figure 3). The ice-frontal position for the past ca. 70 years generally indicates a total retreat between 0.3 km and 2.4 km in most of the glaciers observed (Zemp and van Woerden, 2008). During the twentieth century the retreat of the ice margins has not been continuous. While most of the inland glaciers have retreated during the whole observation period starting at the turn of twentieth century, many maritime glacier margins have experienced several advance periods. Maritime glaciers have advanced particularly around 1910 and 1930, late 1970s and 1990s (cf. Andersen et al., 2005; Zemp and van Woerden, 2008). A relatively fast retreating trend has been observed in most glaciers in Scandinavia since 2001 (Andersen et al., 2005).

Mass balance measurements are highly important when studying and describing glacier behavior and their response to variations in climate. The first mass balance measurements of the Scandinavian glaciers were begun late in the 1940s (Schytt, 1959; Liestøl, 1967). The summer, winter, and net-mass balance record of Storglaciären in the Kebnekaise area, Sweden extends back to 1945 and that of Storbreen in Jotunheimen, Norway back to 1949. These two mass balance records are the longest records in the world. Nowadays mass balance data from a number of glaciers from around the world are reported every second year by World Glacier Monitoring Service (http://www.geo.uzh.ch/wgms/) in their *Glaciers Mass Balance Bulletin*.

The mass balance record from the Scandinavian glaciers indicates slight variation over time within individual glaciers depending on local climate conditions, such as the amount of precipitation, but the general trend over the past decades is relatively clear (Figure 3). In general, the maritime glaciers have had a positive mass balance trend from the beginning of the early 1960s. Mass balance became even more positive between the late 1980s and 2000. It has also been shown that there is a clear correlation between the North Atlantic Oscillation (NAO) index and the mass balance records of the maritime glaciers in southern Norway (Nesje et al., 2000; Reichert et al., 2001). In contrast, the mass balances of the more continental glaciers, such as Storglaciären and Storbreen, have had a negative trend over decades. However, all glaciers in Scandinavia have lost mass since 2001 (Anderssen et al., 2005).

Conclusion

Research on past and present Scandinavian glaciers has a long history. Datasets on past and present glaciers, compiled over a century, are one of the most extensive in the world. Despite this fact, the behavior of the past glaciers and ice sheets, their environmental impact, and the relationship between climate and glaciers are still not fully understood. It seems to be vital to seek more high resolution proxy data from terrestrial and marine archives and integrate that with ice sheet modelling in order to understand the causes and mechanisms of the past environmental and climate changes.

Extensive mass balance and other glaciological data on Scandinavian glaciers, together with climatic records, have formed a firm foundation for a detailed study of diverse range of glaciers throughout the region. In addition, reliable field data is essential to test models of glacier behavior. Research on mass balance variations of the Scandinavian glaciers and climate has already shown important results on glaciers' behavior under different climate conditions. Mass balance changes are strongly dependent on climate and therefore it is highly important to understand the mechanisms and response times behind glaciers' mass balance variations in different climate and glacial settings in order to predict glacial behavior in the future climate change.

Bibliography

Andreassen, L. M., Elvehøy, H., Kjøllmoen, B., Engeset, R. V., and Haakensen, N., 2005. Glacier mass balance and length variations in Norway. *Annals of Glaciology*, **42**, 317–325.

Donner, J., 1995. *The Quaternary History of Scandinavia*. Cambridge: Cambridge University Press.

Dowdeswell, J. A., and Hagen, J. O., 2004. Arctic ice masses. Chapter 15. In Bamber, J. L., and Payne, A. J. (eds.), *Mass Balance of the Cryosphere*. Cambridge: Cambridge University Press, pp. 527–557.

Eldrett, J. S., Harding, I. C., Wilson, P. A., Butler, E., and Roberts, A. P., 2007. Continental ice in Greenland during the Eocene and Oligocene. *Nature*, **446**, 176–179.

Grove, J. M., 2004. *Little Ice Ages: Ancient and Modern*. London/New York: Routledge, Vol. I–II.

Holmlund, P., 2005. Glaciers. In Seppälä, M. (ed.), *The Physical Geography of Fennoscandia*. Oxford: Oxford University Press, pp. 175–184.

Liestøl, O., 1967. Storbreen glacier in Jotunheimen, Norway. *Norsk Polarinstitut Skrifter*, **141**, 1–63.

Mangerud, J., 2004. Ice sheet limits in Norway and on the Norwegian continental shelf. In Ehlers, J., and Gibbard, P. L. (eds.), *Quaternary Glaciations – Extent and Chronology, Part I: Europe*. Amsterdam: Elsevier, pp. 271–294.

Mangerud, J., Jansen, E., and Landvik, J. Y., 1996. Late Cenozoic history of the Scandinavian and Barents sea ice sheets. *Global and Planetary Change*, **12**, 11–26.

Melezhik, V. A., 2006. Multiple causes of Earth's earliest global glaciation. *Terra Nova*, **18**, 130–137.

Moran, K., and ACEX Members, 2006. The Cenozoic palaeoenvironments of the Arctic ocean. *Nature*, **441**, 601–605.
Nesje, A., Lie, Ø., and Dahl, S. V., 2000. Is the North Atlantic oscillation reflected in Scandinavian glacier mass balance records? *Journal of Quaternary Science*, **15**, 587–601.
Nesje, A., Bakke, J., Dahl, S. O., Lie, Ø., and Matthews, J. A., 2008. Norwegian mountain glaciers in the past, present and future. *Global and Planetary Change*, **60**, 10–17.
Østrem, G., and Haakensen, N., 1993. Glaciers in Europe – glaciers in Sweden. In Williams, R. S., Jr., and Ferringo, J. G. (eds.), *Satellite Image Atlas of Glaciers of the World*. Washington: U.S. Geological Survey professional paper, 1386-E-3, pp. 63–109.
Reichert, B. K., Bengtsson, L., and Oerlemans, J., 2001. Mid latitude forcing mechanisms for glacier mass balance investigated using general circulation models. *Journal of Climate*, **14**, 3767–3784.
Schytt, V., 1959. The glaciers of the Kebnekaise-Massif. *Geografiska Annaler*, **41**, 213–227.
Schytt, V., 1993. Glaciers in Europe – glaciers in Sweden. In Williams, R. S., Jr., and Ferringo, J. G. (eds.), *Satellite Image Atlas of Glaciers of the World*. Washington: U.S. Geological Survey professional paper, 1386-E-3, pp. 111–125.
Siedlecka, A., Roberts, D., 1992. *The Bedrock Geology of Varanger Peninsula, Finnmark, North Norway: An Excursion Guide*. Trondheim, Norway: Norges Geologiske Undersøkelse Special Publication 5.
Siegert, M. J., and Dowdeswell, J. A., 2004. Numerical reconstructions of the Eurasian Ice Sheet and climate during the Late Weichselian. *Quaternary Science Reviews*, **23**, 1273–1283.
Svendsen, J. I., Alexanderson, H., Astakhov, V. I., Demidov, I., Dowdeswell, J. A., Funder, S., Gataullin, V., Henriksen, M., Hjort, C., Houmark-Nielsen, M., Hubberten, H. W., Ingólfsson, Ó., Jakobsson, M., Kjær, K. H., Larsen, E., Lokrantz, H., Lunkka, J. P., Lyså, A., Mangerud, M., Matiouchkov, A., Murray, A., Möller, P., Niessen, F., Nikolskaya, O., Polyak, L., Saarnisto, M., Siegert, C., Siegert, M. J., Spielhagen, R., and Stein, R., 2004. Late quaternary ice sheet history of northern Eurasia. *Quaternary Science Reviews*, **23**, 1229–1271.
Whalley, W. B., 2004. Glacier research in mainland Scandinavia. In Cecil, L. D., Green, J. R., and Thompson, L. G. (eds.), *Earth Paleoenvironments: Records Preserved in Mid- and Low-Latitude Glaciers*. Secaucus: Kluwer, pp. 121–143.
Zemp, M., and van Woerden, J., 2008. *Global Glacier Changes: Facts and Figures*. Zürich: World Glacier Monitoring Service. URL: http://www.grip.unep.ch/glaciers/.

SEA ICE

Matti Leppäranta
Department of Physics, University of Helsinki, Helsinki, Finland

Definition

Any form of ice found at sea that has originated from the freezing of seawater (WMO, 1970). Icebergs and ice islands, also found in the polar oceans, are *ice of land origin*.

Introduction

Sea ice occurs in about 10% of the surface of the world ocean. Perennial ice is found in high polar latitudes in the Central Arctic Ocean, in the East Greenland Current, and in the western Weddell Sea. The seasonal sea ice zone extends on average to 60° latitudes, not so low in the Northeast Atlantic Ocean but more south in subarctic shallow semi-enclosed seas. Sea ice renewal time is short due to ice melting and advection; perennial ice is mostly less than 10 years old. Solid sea ice lids are statically unstable and break into fields of ice floes, undergoing transport, as well as opening and ridging that altogether create the exciting sea ice landscape as it appears to a human eye (Figure 1).

The history of sea ice science initiated in the l800s with the polar expeditions constructing the geographical picture of the sea ice world (Weeks, 1998b). Microscale structural sea ice models were prepared in the 1950s, and sea ice thermodynamics problem and the closure of sea ice dynamics problem were completed. The modern era commenced in the 1970s based on new technological innovations. Satellite remote sensing revealed the character of time-space variations of sea ice conditions, computing technology made realistic sea ice models possible, and automatic monitoring systems were introduced. The present research focuses on scaling issues, ice thickness observation methods, and the climate problem, with applications to shipping, oil, and gas exploration and ecology of freezing seas.

Sea ice structure and properties

Sea ice physics covers a wide range of scales. *Microscale* includes individual grains and impurities extending from sub-millimeter size to 0.1 m. *Local scale*, 0.1–10 m, considers sea ice as a polycrystalline continuum, and *ice floe scale* extends from 10 m to 10 km, including ice floes and types such as pressure ridges. When the scale exceeds the floe size, the sea ice medium is called *drift ice*.

Microscale – crystal structure and impurities. The freezing point of seawater is $T_f = -1.8°C$. In calm weather, a thin primary ice layer forms first but in windy conditions frazil crystals are generated forming a solid sheet when their buoyancy overcomes the turbulence. Ice crystal platelets overlain together form macrocrystals. Due to constitutional supercooling in the molecular diffusion of salt and heat, cellular ice–water interface forms and encloses liquid brine pockets between the crystal platelets and the crystal boundaries become jagged (Weeks, 1998a). The salinity of new ice is 25–50% of the water salinity. The brine salinity always corresponds to the freezing point of the ambient temperature, that is, brine volume changes with temperature, and salts crystallize in their eutectic temperatures (Figure 2). In summer, the brine pockets expand into drainage network and much brine flows out. Brine pockets serve as biological habitats, for algae with primarily light-limited growth. The most active layer is the bottom layer or so-called skeleton layer.

Local scale – forms of sea ice. Sea ice formation is based on three main mechanisms resulting in *congelation ice*, *frazil ice*, and *superimposed ice* (Weeks, 1998a). Congelation ice crystals are columnar and grow down from the

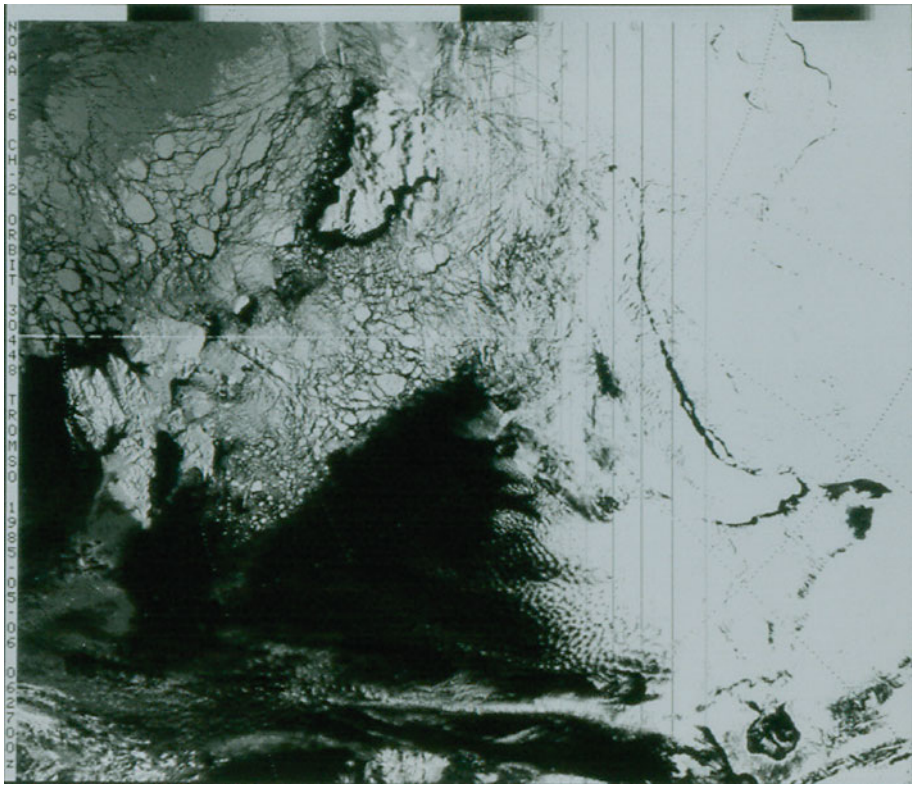
a


b

Sea Ice, Figure 1 Sea ice cover over the Barents Sea and part of the Central Arctic Ocean shown in a NOAA image and a field photograph.

ice–water interface; it is dominant type in the Arctic Ocean. Frazil ice forms in open water areas, with small crystal size; in Antarctica, this is the dominant type. In shallow waters, frazil may attach into the sea bottom to form anchor ice, which may rise up with bottom material. In superimposed ice formed of slush, the crystals are small. Sea ice contains gas bubbles, which have a major influence on scattering of electromagnetic waves, and sediment particles originating from the water body, sea bottom, or atmospheric fallout. Optical properties of sea ice

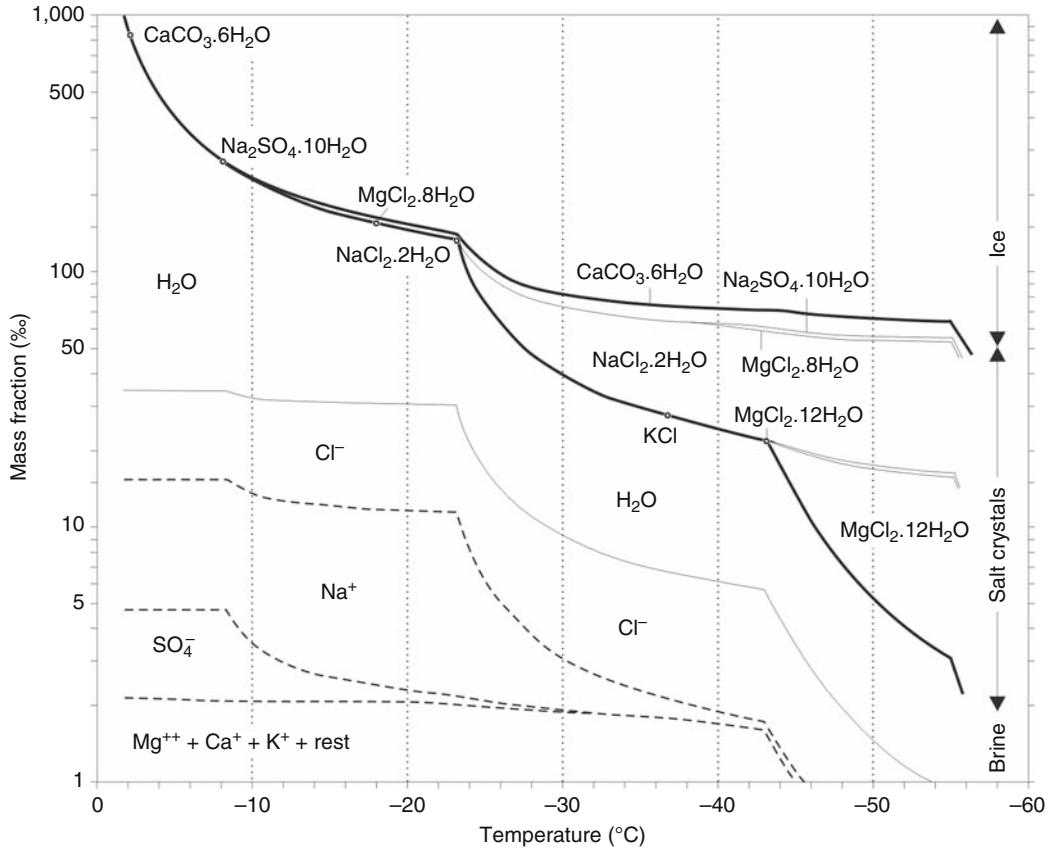

Sea Ice, Figure 2 Sea ice phase diagram with the proportions of ice, brine, and solid salts as a function of temperature. The chemical symbols show the eutectic points of the main salts. Redrawn from Assur (1958).

are influenced by the salt and gas content. Sea ice is less transparent than seawater, the attenuation coefficient being around 1 m^{-1} for normal sea ice.

Drift ice – fields of ice floes. A sea ice landscape consists of ice floes with ridges and other morphological features, as well as *leads* and *polynyas*. The central drift ice pack is free of influence from the boundaries, and the length scale is the size of the basin. (Land) fast ice extends from the shore to about 10–20 m depths. Further out is the shear zone (width 10–200 km), where the mobility of the ice is restricted by the boundary and strong deformation takes place. Marginal ice zone (100 km) lies along the boundary to open sea, characterized as the zone, which "feels the presence of the open ocean." Drift ice is a peculiar geophysical medium (Leppäranta, 2005). It is granular – ice floes are the basic elements – compressible, and highly nonlinear. For continuum models, the size of material particles D must be satisfied, $d << D << \Lambda$, where d is the floe size and Λ is the gradient length scale. The ranges are in nature $d \sim 10^1$–10^4 m, $D \sim 10^3$–10^5 m, and $\Lambda \sim 10^4$–10^6 m. An ice state is defined for the material description, usually taken as the ice thickness distribution (Thorndike et al., 1975), defined by the spatial density function $\pi = \pi(h)$ in a grid cell.

Sea ice growth and decay

In ice growth, latent heat is released and conducted through the ice to the atmosphere. The thicker the ice, the slower is the conduction and growth – mostly less than 5 cm/day for very thin ice and less than 1 cm/day for ice thicker than 1 m. Sea ice has no definite melting point, but always there is melting involved when sea ice warms to dilute the brine and vice versa. The melt rate is of the order of 1 cm/day, mainly due to the net radiation and oceanic heat flux. Where the summer melt is less than the winter growth, multi-year ice develops. First-year ice grows up to 2 m and multi-year ice to 3–4 m.

A simple, analytic approach for the ice growth problem is Zubov's model. The basic assumptions are to ignore solar radiation, oceanic heat flux, and snow. The thickness of ice is

$$h = \sqrt{aS + d^2} - d \tag{1}$$

where $a = 2\kappa/\rho L \approx 11$ cm $(°C \cdot day)^{-1}$, κ is thermal conductivity of ice, ρ is ice density, L is latent heat of freezing, $S = \int_o^t (T_f - T_a)dt'$, usually referred as the "sum of freezing-degree-days," T_a is air temperature ($T_a \leq T_f$), and $d \approx 10$ cm is the insulation efficiency of the atmospheric

surface layer. In the melting season, there is no conduction but the ice melts at the boundaries by the surface fluxes and inside by the solar radiation. Melting of ice goes into ice thickness and porosity ν:

$$\frac{\mathrm{d}\nu h}{\mathrm{d}t} = -\frac{Q}{\rho L} < 0 \tag{2}$$

where Q is the total heat flux into the ice. Snow protects the ice cover due to its high albedo and small optical depth. The equilibrium thickness of multiyear ice is obtained when the summer melt Δh equals the winter growth:

$$h_e = \frac{h_1^2}{2\Delta h} - \frac{\Delta h}{2} \tag{3}$$

where h_1 is the thickness of first-year ice; h_1 = 2 m, and Δh = ½ m gives h_e = 3.75 m. More detail level thermodynamics are examined by numerical modeling (Maykut and Untersteiner, 1971). The results show that the thickness of first-year ice is sensitive to snowfall and oceanic heat flux and the thickness of multi-year ice additionally to albedo.

Drift ice dynamics

Ice kinematics. Drift ice speed is 1–100 cm/s. In the Arctic Ocean, the Transpolar Drift Stream takes ice across the Eurasian side through the Fram Strait into the Greenland Sea, while in the American side ice rotates clockwise in the Beaufort Sea Gyre. Average velocities are 1–5 cm/s, higher toward the Fram Strait. In Antarctica, the governing features are westward flow zone close to the continent and eastward drift zone farther out, driven by the easterly and westerly winds. Meridional displacements interchange ice floes between the two annuli, in particular up along the Antarctic Peninsula in the Weddell Sea. Frequency spectra of ice velocity reach highest levels at the synoptic time scales, and secondary peaks appear at tidal and inertial periods. The ice–wind–ocean current correlation is usually good, but remarkable noncoherent changes appear due to the internal friction of the ice.

Conservation of ice. Ice conditions are modified by thermal and mechanical processes, dictated by the ice conservation law. Mechanical deformation occurs as opening and closing of leads, rafting, and ridging. The general form is (Thorndike et al., 1975)

$$\frac{\partial \pi}{\partial t} + u \cdot \nabla \pi = \psi - \pi \nabla \cdot u + \frac{\partial \phi(h)\pi}{\partial h} \tag{4}$$

where ψ is the mechanical ice thickness redistributor and ϕ is the growth rate of ice.

Drift ice rheology. The main mechanisms behind internal ice stress σ is friction between ice blocks in mechanical deformation (secondary, come floe collisions, floe breakage, and potential energy production). Stress level is negligible for compactness less than 0.7, but compact ice has significant yield strength. The rheological law is formally $\sigma = \sigma(\pi, \varepsilon, \dot{\varepsilon})$, where ε is strain and $\dot{\varepsilon}$ is strain-rate (Figure 3). At compactness more than 0.8 floe collisions

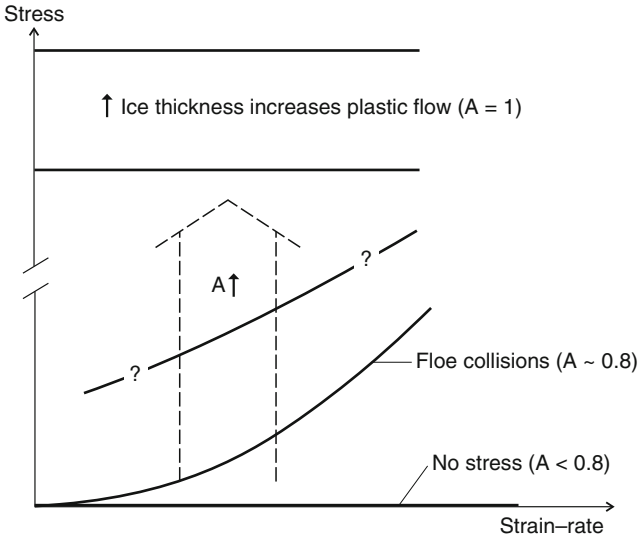

Sea Ice, Figure 3 Schematic presentation of the sea ice rheology as a function of ice compactness *A* and thickness *h*. The cut in the ordinate axis tells of a jump of several orders of magnitude (Leppäranta, 2005).

and shear friction between ice floes increase the stress and plastic flow results, yield strength increasing with ice thickness. Normally, compressive strength is taken twice the shear strength, and for changes in compactness the e-folding strength scale is taken as 5%.

Equation of motion. Integration through the thickness of ice gives the two-dimensional system as (e.g., Leppäranta, 2005)

$$\rho H\left(\frac{\partial u}{\partial t} + u \cdot \nabla u + f k \times u\right) = \nabla \cdot \sigma + \tau_a + \tau_w - \rho H g \beta \tag{5}$$

where ρ is ice density, f is the Coriolis parameter, g is acceleration due to gravity, and β is the sea surface slope. The air and water stresses are turbulent drag laws with drag coefficients and Ekman angles as their parameters. The sea ice dynamics solution is divided to three cases/categories. *Stationary ice cover* results when the forcing is below the yield level. In *free drift*, internal friction is absent and the solution is obtained as vector addition:

$$u = u_a + U_w \tag{6}$$

where U_w is the geostrophic surface current and u_a is the wind-driven ice drift, 2–3% of the wind speed and 20–40° to the right (left) of the wind direction in the northern (southern) hemisphere (Figure 4).

For *ice drift in the presence of internal friction*, numerical continuum models are employed (Hibler, 1979; Hibler and Bryan, 1987). A full model consists of four elements: ice state, rheology, equation of motion, and ice conservation law. The first and second elements constitute

the heart of the model. The primary geophysical parameters are the air and water drag coefficients and compressive strength of ice. The mean annual velocity comes out well from the simulation together with the mean thickness field, validated against submarine data (Figure 5). Models predict that there is always a small amount of open water or thin ice present in the Central Arctic, and further that the annual cycle of the mean thickness has about the same amplitude as in thermodynamic models but the level drops down by about one meter. The maximum ice thicknesses are 5–8 m due to mechanical deformation off the northern coast of Greenland.

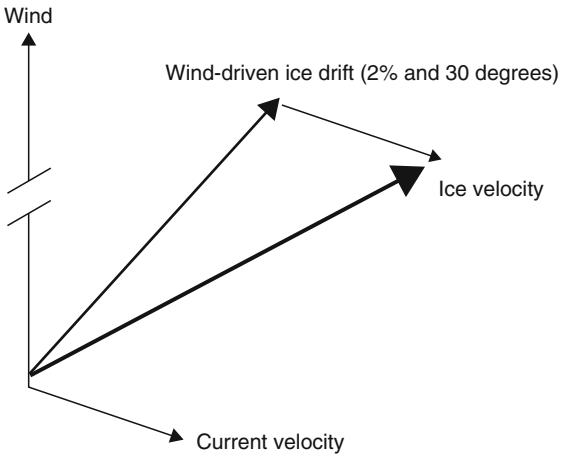

Sea Ice, Figure 4 The free drift solution as the vector sum of wind-driven ice drift and geostrophic ocean current.

Short-term modeling (1 h to 10 days) applications are in shipping and marine technology, while in long-term modeling (1 month to 100 years) the main objective is the climate problem. Sea ice drift transports latent heat and fresh water, modifies the ice boundary and air-sea interaction, and by freezing and melting the ice has a major influence on the hydrographic structure of the ocean. Differential ice drift opens and closes leads bringing major changes to the air-sea heat fluxes, and ridging accumulates ice blocks adding large amounts to the total volume of ice.

Sea ice literature is rather limited. Extensive lecture notes from summer schools are given in Untersteiner (1986) and Leppäranta (1998). Wadhams (2000) presented an excellent general book of the sea ice geophysics, Leppäranta (2005) focused on the drift of sea ice, and McPhee (2008) on the ice–ocean interaction.

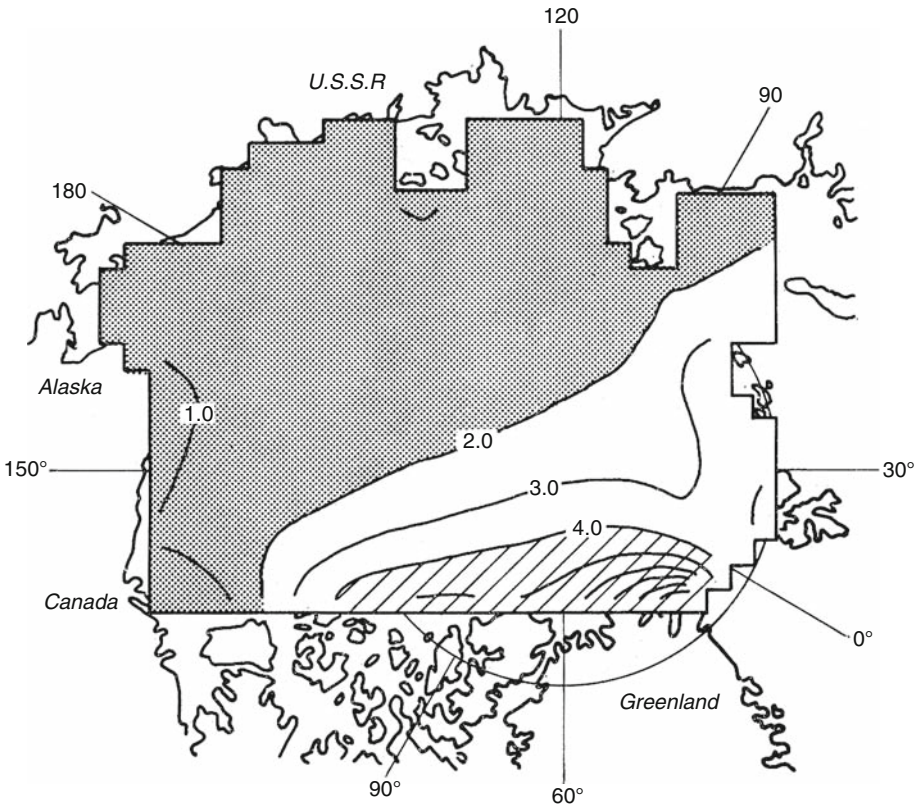

Sea Ice, Figure 5 Ice thickness field in April in the Arctic Ocean as produced by the Hibler (1979) model.

Bibliography

Assur, A., 1958. Composition of sea ice and its tensile strength. In Thurston, W. (ed.), *Arctic Sea Ice*. U.S. National Academy of Science/National Research Council: Publ. No 598, pp. 106–138.
Hibler, W. D., III, 1979. A dynamic-thermodynamic sea ice model. *Journal of Physical Oceanography*, **9**, 815–846.
Hibler, W. D., III, and Bryan, K., 1987. A diagnostic ice–ocean model. *Journal of Physical Oceanography*, **17**, 987–1015.
Leppäranta, M. (ed.), 1998. *Physics of Ice-Covered Seas*. Helsinki: Helsinki University Press, Vol. II, pp. 715–773.
Leppäranta, M., 2005. *The drift of sea ice*. Germany: Springer-Praxis.
Maykut, G. A., and Untersteiner, N., 1971. Some results from a time-dependent, thermodynamic model of sea ice. *Journal of Geophysical Research*, **76**, 1550–1575.
McPhee, M. G., 2008. *Air–Ice–Ocean Interaction: Turbulent Ocean Boundary Layer Exchange Processes*. New York: Springer. 215 p.
Thorndike, A. S., Rothrock, D. A., Maykut, G. A., and Colony, R., 1975. The thickness distribution of sea ice. *Journal of Geophysical Research*, **80**, 4501–4513.
Untersteiner, N. (ed.), 1986. *Geophysics of Sea Ice*. New York: Plenum.
Wadhams, P., 2000. *Ice in the Ocean*. Amsterdam, The Netherlands: Gordon and Breach Science.
Weeks, W. F., 1998a. Growth conditions and structure and properties of sea ice. In Leppäranta, M. (ed.), *Physics of Ice-Covered Seas, Vol. 1*. Helsinki: Helsinki University Press, pp. 25–104.
Weeks, W. F., 1998b. The history of sea ice research. In Leppäranta, M. (ed.), *Physics of Ice-Covered Seas, Vol. 1*. Helsinki: Helsinki University Press, pp. 1–24.
WMO, 1970. *WMO sea-ice nomenclature*. Terminology, codes and illustrated glossary. Edition 1970. Geneva, Secretariat of the World Meteorological Organization, 1970, 147 p. (WMO/OMM/BMO, No. 259, TP. 145.)

Cross-references

Albedo
Arctic Hydroclimatology
Atmosphere–Snow/Ice Interactions
Biogeochemistry of Sea Ice
Estuary Ice Cover
Fast Ice
Finger Rafting
Marginal Ice Zones
Pancake Ice
Thinning of Arctic Sea Ice

SEA-LEVEL

Anny Cazenave
Laboratoire d'Etudes en Géophysique et Océanographie Spatiales (LEGOS), LEGOS-CNES, Observatoire Midi-Pyrénées, Toulouse, France

Definition

Sea level is the height of the sea surface with respect to a given reference. Sea level variations are called "absolute" or "relative" depending in which reference frame (inertial or terrestrial) they are expressed. Absolute sea level variations generally represent change in the volume of water in ocean basins (either due to water density change or water mass change) while relative sea level variations designate sea surface height changes with respect to the ground (accounting thus for both "absolute" sea level variations plus ground motions).

Spatiotemporal scales of sea level variations

Sea level may vary globally or regionally depending on the causes. Global (uniform) variations are sometimes called eustatic. However this term should be avoided because it is sometimes misused and attributed to water mass change of the oceans only (by opposition to water density change). Superimposed to any global mean sea level change, regional variations may also occur (see below). Temporal sea level variations spread over a very broad spectrum. The largest global-scale sea level changes (10–100 m amplitude) occur on geological time scales (10–100 Myr) and depend primarily on tectonics processes (e.g., large-scale change in the shape of ocean basins associated with seafloor spreading and mid-ocean ridges expansion). Formation of long-live ice sheets (e.g., formation of the Antactica ice sheet about 30 Myr ago) is also able to produce >50 m global sea level variations. On shorter time scales (tens to hundred thousand years), quasiperiodic growth and decay of polar ice caps driven by changes of the Earth's obliquity and orbit around the sun represent another cause of global-scale sea level change, with amplitude on the order of 100 m. Century- to millenium-scale sea level fluctuations are mainly driven by climate change in response to natural forcing factors (e.g., solar radiation, volcanic eruptions) and internal variability of the climate system (related, for example, atmosphere-ocean perturbations such as El Nino-Southern Oscillation –ENSO, North Atlantic Oscillation –NAO, Pacific Decadal Oscillation-PDO, etc.).

Recent past and present-day sea level variations

For the last century and past few decades, sea level variations depend on global climate changes induced by natural climate variability and eventually anthropogenic forcing. The two main factors causing sea level change (globally and regionally) are thermal expansion of sea waters and fresh water mass exchange between land and oceans. For example, as the ocean warms in response to global warming, sea waters expand, and thus sea level rises. When mountain glaciers melt in response to increasing air temperature, sea level rises because of fresh water mass input to the oceans. Similarly, ice mass loss from the ice sheets causes sea level rise. Modification of the land hydrological cycle due to climate variability and direct anthropogenic forcing may lead to increased or decreased runoff, hence ultimately to sea level change.

Observations of recent past and present-day sea level variations

Twentieth century

Our knowledge of past century sea level change comes from tide gauge measurements located along continental coastlines and islands. The largest tide gauge database of monthly and annual mean sea level records is the Permanent Service for Mean Sea Level (PSMSL, www.pol.ac.uk/psmsl/) which contains data for the twentieth century from ~2,000 sites maintained by about 200 nations. The records are somewhat inhomogeneous in terms of data length and quality. For long-term sea level studies, only ~10% of this data set is useable because of data gaps and limited tide gauge distribution in the past. Tide gauges measure sea level relatively to the ground, hence monitor also ground motions. In active tectonic and volcanic regions, or in areas subject to strong ground subsidence due to natural causes (e.g., sediment loading in river deltas) or human activities (ground water pumping and oil/gas extraction), tide gauge data are directly affected by the corresponding ground motions. Post glacial rebound, the elastic response of the Earth crust to last deglaciation (also called Glacial Isostatic Adjustment), is another process that gives rise to vertical land movement.

After the ~120 m sea level rise associated with the last deglaciation that started about 15,000 years ago, geological and archeological observations indicate that the mean sea level remained almost stable during the last 2–3 millennia (Lambeck et al., 2010). But tide gauges available since the late nineteenth century have reported significant sea level rise during the twentieth century, especially since 1950, with a mean rate of ~1.7 mm/year over the past 50 years (Church et al., 2004).

Satellite altimetry era

Since the early 1990s, satellite altimetry has become the main tool for precisely and continuously measuring sea level with quasi global coverage and a few days revisit time. Compared to tide gauges which provide sea level relative to the ground, satellite altimetry measures "absolute" sea level variations. The concept of the satellite altimetry measurement is simple: the onboard radar altimeter transmits microwave radiation toward the sea surface which partly reflects back to the satellite. Measurement of the round-trip travel time of the signal provides the height of the satellite above the instantaneous sea surface (called "range"). The quantity of interest in oceanography is the sea surface height above a reference fixed surface (typically a conventional reference ellipsoid). It is obtained by the difference between the altitude of the satellite above the reference (deduced from precise orbitography) and the range measurement. The estimated sea surface height needs be corrected for various factors due to atmospheric delay and biases between the mean electromagnetic scattering surface and sea at the air–sea interface. Other corrections due to geophysical effects, such as solid Earth, pole, and ocean tides, are also applied. High-precision altimetry started with the launch of the Topex/Poseidon satellite in 1992. Its successors, Jason-1 and Jason-2, were launched in 2001 and 2008, respectively. The precision of an individual sea surface height measurement based on these missions has reached the 1–2 cm level, allowing a precision on the global mean rate of rise of ~0.4 mm/year (Ablain et al., 2009). The temporal evolution of the global mean sea level from satellite altimetry since early 1993 (Figure 1) shows an almost linear increase (except for two temporary anomalies associated with the 1997–1998 El Nino and the 2008 La Nina). Over this 18-year-long period, global mean sea level has been rising at a rate of ~3.3 $\pm$ 0.4 mm/year (Ablain et al., 2009; Nerem et al., 2010), a value significantly higher than the mean rate recorded by tide gauges over the past decades.

Sea level budget for the recent years/decades

Ocean warming

Analyses of in situ ocean temperature data collected over the past 50 years by ships and recently by profiling floats indicate that ocean heat content, and hence ocean thermal expansion, has significantly increased since 1950. Ocean warming explains about 25% of the observed sea level rise of the last few decades (Bindoff et al., 2007). This number is likely a lower bound, due to the lack of hydrographic data in remote regions of the southern hemisphere and in the deep ocean (below 1,000 m) (Dominguez et al., 2008). A steep increase is observed in thermal expansion over the decade 1993–2003 (Bindoff et al., 2007). Since about 2003, thermal expansion rate has reduced (Cazenave and Llovel, 2010) but this likely reflects short-term natural variability rather than a new long-term trend. On an average, over the satellite altimetry era (1993–2009), the contribution of ocean warming to sea rise accounts for ~30% (Cazenave and Llovel, 2010).

Glaciers melting

Being very sensitive to global warming, mountain glaciers and small ice caps have retreated worldwide during the recent decades, with significant acceleration during the 1990s. From mass balance studies of a large number of glaciers, estimates have been made of the contribution of glacier's ice melt to sea level (Lemke et al., 2007; Cogley, 2009). For the period 1993–2009, glaciers and ice caps have accounted for ~30% of sea level rise (Cazenave and Llovel, 2010).

Ice sheets

If totally melted, Greenland and West Antarctica would raise sea level by about 7 and 5 m, respectively. Thus, even a small amount of ice mass loss from the ice sheets would produce substantial sea level rise, with adverse societal and economical impacts on vulnerable low-lying coastal regions. Since the early 1990s, different remote sensing observations based on airborne laser and satellite

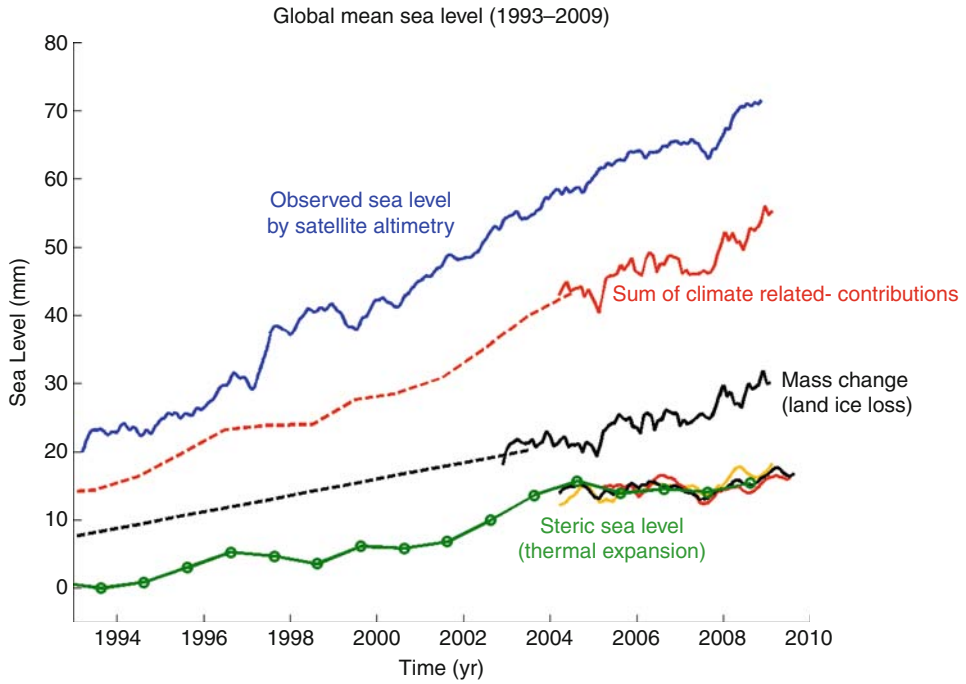

Sea-Level, Figure 1 Evolution of the global mean sea level observed by satellite altimetry (*upper blue curve*), thermal expansion (*botton green curve*), land ice contribution (*middle black curve*), and total climate contributions (*middle red curve*).

altimetry, as well as Synthetic Aperture Radar Interferometry (InSAR) technique and space gravimetry (GRACE space mission), have provided important observations of the mass balance of the ice sheets. These indicate accelerated ice mass loss in coastal regions of Greenland and West Antarctica (Allison et al., 2009; Velicogna, 2009; Steffen et al., 2010). For 1993–2003, <15% of the rate of global sea level rise was due to the mass loss of the ice sheets of Greenland and Antarctica (Lemke et al., 2007), but this contribution has clearly increased after 2003 (Velicogna, 2009) (Figure 2). On an average, over 1993–2009, the two ice sheets have contributed by 30% to sea level rise, with almost equal amount from Greenland and West Antarctica (Cazenave and Llovel, 2010).

Land water storage

Change in land water storage, due to natural climate variability and human activities (i.e., anthropogenic changes in the amount of water stored in soils, reservoirs and aquifers as a result from dam building, underground water mining, irrigation, urbanization, deforestation, etc.), is another potential contribution to sea level change. Model-based estimates of land water storage change caused by natural climate variability suggest no long-term contribution to sea level for the past few decades, although interannual/decadal fluctuations may have been significant. Since 2002, space gravimetry observations from the GRACE space mission now allow determination of the total (i.e., due to climate variability and human activities) land water contribution to sea level. The land water signal is dominated by interannual variability with only a modest contribution (<10%) to the trend (Cazenave and Llovel, 2010).

Sea level budget over the years 1993–2009

Although none of the climate factors discussed above change linearly with time, on an average over the 1993–2009 time span, ocean warming, glaciers melting, and ice sheet mass loss have each contributed by ~30% to global mean sea level rise (Cazenave and Llovel, 2010). Figure 1 compares the thermal expansion and total land ice loss contributions with observed sea level rise.

Regional variability in sea level trends

Satellite altimetry has revealed that sea level is not rising uniformly. In some regions (e.g., western Pacific), the rates of sea level rise are faster by a factor up to three times the global mean rate. In other regions rates are slower than the global mean (e.g., eastern Pacific). The regional variability in sea level trends is mainly due to large-scale changes in the density structure of the oceans and its interaction with the ocean circulation (Wunsch et al., 2007). The largest regional changes in sea level trends result from ocean temperature change (i.e., from non uniform thermal expansion), but in some regions, change in water salinity is also important (Wunsch et al., 2007). Observations of

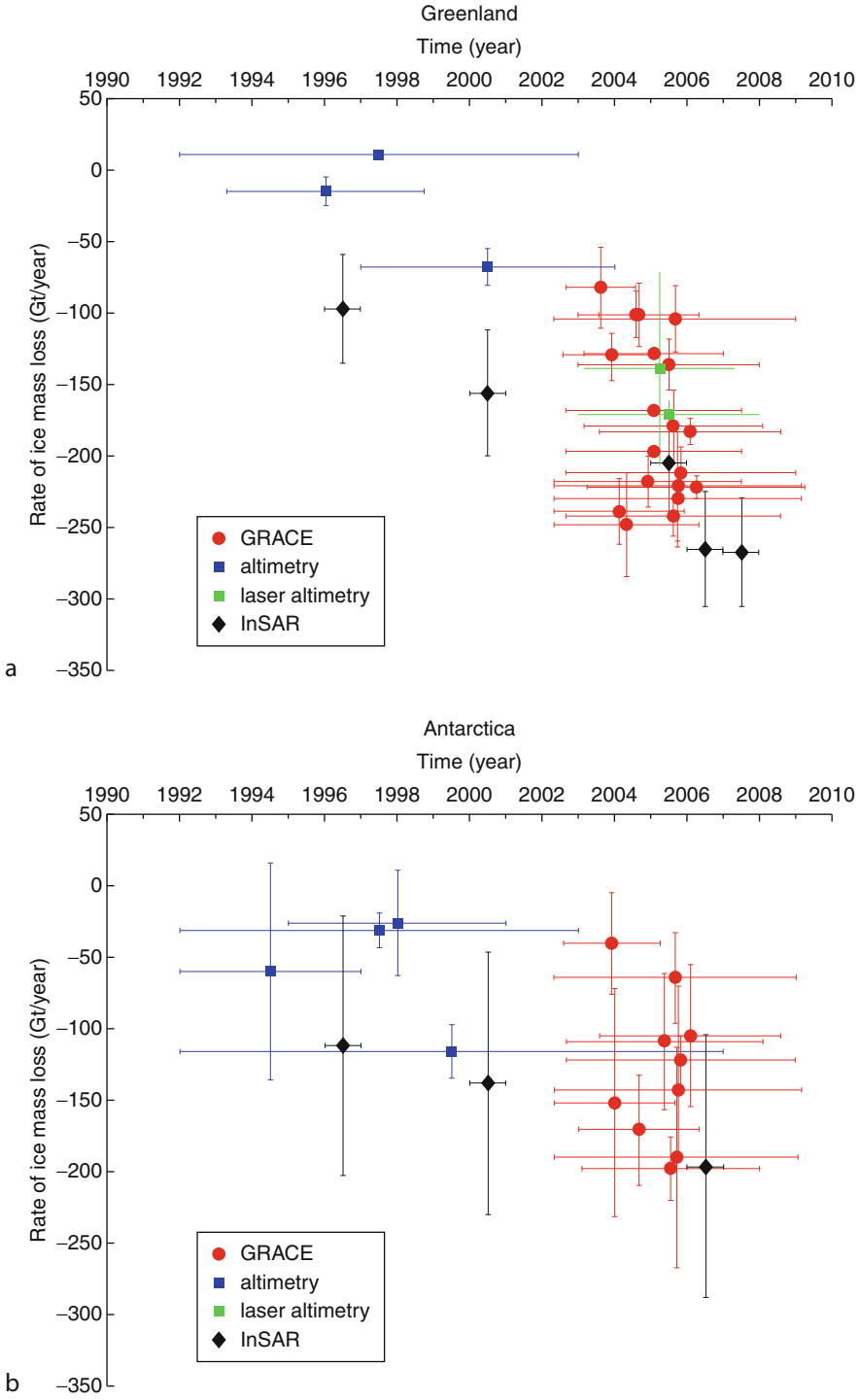

Sea-Level, Figure 2 Mass balance of the ice sheets estimated by remote sensing techniques; compilation of published results (see Cazenave and Llovel, 2010); *horizontal bars* correspond to the time span of data analysis and *vertical bars* represent uncertainty. (**a**) Greenland ice sheet; (**b**) Antarctica ice sheet.

ocean temperature over the past few decades show that trend patterns in thermal expansion are not stationary but fluctuate both in space and time in response to natural perturbations of the climate system such as ENSO (El Nino-Southern Oscillation), NAO (North Atlantic Oscillation), and PDO (Pacific Decadal Oscillation) (Bindoff et al., 2007). As a result, sea level trend patterns observed by satellite altimetry over the last 18 years may be different from those of the last 50 years.

Future sea level rise

IPCC AR4 projections based on coupled climate models indicate that sea level should be higher than today's value by ~38 cm by 2100 (within a range of ±15 cm due to model results dispersion and uncertainty on future greenhouse gases emissions) (Meehl et al., 2007). However this value is possibly a lower bound because AR4 projections only accounted for future ocean warming and glaciers melting. A large proportion of Greenland and West Antarctica ice mass loss results from coastal glacier flow into the ocean through complex dynamical instabilities (Allison et al., 2009; Steffen et al., 2010). Such processes have begun to be understood only recently and were not taken into account in the AR4 sea level projections.

Present-day sea level rise is not uniform; this is also expected for the future. The regional sea level map for 2090–2100 provided by IPCC AR4 (average of an ensemble of models) shows higher than average sea level rise in the Arctic Ocean and along a narrow band in the south Atlantic and south Indian ocean. However, as noticed in IPCC AR4 (Meehl et al., 2007), geographical patterns of sea level change from different models are not generally similar, reflecting current model deficiency in modeling regional changes, in particular those associated with decadal/multidecadal natural variability. This is a research area where improvements are crucially needed, in particular for assessing future coastal impacts of sea level rise. It is worth noticing that IPCC AR4 regional projections are different from present-day observed patterns of sea level rise, a result of spatiotemporal change in spatial trend patterns.

Impacts of sea level rise

Sea level rise is a major concern for populations living in low-lying coastal regions (about 25% of human beings) because it will give rise to inundation, wetland loss, shoreline erosion, saltwater intrusion in surface water bodies and aquifers, and will rise water tables (Nicholls, 2010). Moreover, in many coastal regions of the world, the effects of rising sea level act in combination with other natural and/or anthropogenic factors, such as decreased rate of fluvial sediment deposition in deltaic areas, ground subsidence due to tectonic activity or ground water pumping, and hydrocarbon extraction.

Besides factors that modify shoreline morphology (e.g., sediment deposition in river deltas, change in coastal waves and curren), what does matter in coastal regions is relative sea level rise, i.e., the combination of sea level rise and vertical ground motions. In many coastal regions of the world, these two factors are currently of the same order of magnitude and most often of opposite sign (sea level rises and ground subsides). Accelerated ground subsidence is reported in many regions, either because of local groundwater withdrawal or hydrocarbon extraction. Whatever the causes, ground subsidence directly interacts with and amplifies climate-related sea level rise (long-term trend plus regional variability). However, if sea level continues to rise at current rates and more likely accelerates, the climate factors (sea level rise) will become dominant. But as mentioned above, IPCC AR4 sea level projections could be underestimated. In addition climate models do not yet provide reliable regional variability projections (that superimposes to the global mean rise) for the next few decades. Hence, it is very difficult to quantify future sea level rise in specific regions where various factors interfer in a complex way.

Summary

Measuring sea level rise and understanding its causes has considerably improved in the recent years, essentially because new in situ and remote sensing observations have become available. Sea level is presently rising at a sustained rate and will continue in the future decades because of expected increased global warming. However, the exact amount of sea level rise by 2100 is presently an open question. The main source of uncertainty is the future behavior of the Greenland and Antarctica ice sheets in a changing climate. Ice mass loss in these regions has accelerated in the recent years but we do not know yet how fast and how much the ice sheets will continue to lose mass, hence how they will affect sea level in the future. Improved understanding and modeling of the complex dynamical response of the ice sheets to global warming is one of the priorities of current climate research.

Bibliography

Ablain, M., Cazenave, A., Valladeau, G., and Guinehut, S., 2009. A new assessment of the error budget of global mean sea level rate estimated by satellite altimetry over 1993–2008. *Ocean Science*, **5**, 193–201.

Allison, I., Alley, R. B., Fricker, H. A., Thomas, R. H., and Warner, R. C., 2009. Ice sheet mass balance and sea level. *Antarctic Science*, **21**, 413–426.

Bindoff, N., Willebrand, J., Artale, V., Cazenave, A., Gregory, J., Gulev, S., Hanawa, K., Le Quéré, C., Levitus, S., Nojiri, Y., Shum, C. K., Talley, L., and Unnikrishnan, A., 2007. Observations: oceanic climate and sea level. In Solomon, S., Qin, D., Manning, M., Chen, Z., Marquis, M., Averyt, K. B., Tignor, M., and Miller, H. L. (eds.), *Climate change 2007: The physical Science Basis: Contribution of Working Group I to the Fourth Assessment Report of the Intergovernmental Panel on Climate Change*. Cambridge/New York: Cambridge University Press.

Cazenave, A., and Llovel, W., 2010. Contemporary sea level rise. *Annual Review of Marine Science*, **2**, 145–173.

Church, J. A., White, N. J., Coleman, R., Lambeck, K., and Mitrovica, J. X., 2004. Estimates of the regional distribution of

sea-level rise over the 1950–2000 period. *Journal of Climate*, **17**(13), 2609–2625.
Cogley, J. C., 2009. Geodetic and direct mass balance measurements: comparison and joint analysis. *Annals of Glaciology*, **50**, 96–100.
Dominguez, C., Church, J., White, N., Glekler, P. J., Wijffels, S. E., Barker, P. M., and Dunn, J. R., 2008. Improved estimates of upper ocean warming and multidecadal sea level rise. *Nature*, **453**, 1090–1093, doi:10.1038/nature07080.
Lambeck, K., Woodroffe, C. D., Antonioli, F., Anzidei, M., Gehrels, W. R., Laborel, J., and Wright, A. J., 2010. Paleoenvoronmental records, geophysical modelling and reconstruction of sea level trends and variability on centennial and longer time scales. In Church, J. A., et al. (eds.), *Understanding Sea Level Rise and Variability*. Oxford: Wiley-Blackwell.
Lemke, P., et al., 2007. Observations: changes in snow, ice and frozen ground. In Solomon, S., Qin, D., Manning, M., Chen, Z., Marquis, M., Averyt, K. B., Tignor, M., and Miller, H. L. (eds.), *Climate Change 2007: The Physical Science Basis. Contribution of Working Group I to the Fourth Assessment Report of the Intergovernmental Panel on Climate Change*. Cambridge/New York: Cambridge University Press.
Meehl, G. A., et al., 2007. Global climate projections. In Solomon, S., Qin, D., Manning, M., Chen, Z., Marquis, M., Averyt, K. B., Tignor, M., and Miller, H. L. (eds.), *Climate Change 2007: The Physical Science Basis. Contribution of Working Group I to the Fourth Assessment report of the Intergovernmental Panel on Climate Change*. Cambridge/New York: Cambridge University Press.
Nerem, R. S., Chambers, D. P., Choe, C., and Mitchum, G. T., 2010. Estimating mean sea level change from the Topex and Jason altimeter missions. *Marine Geodesy*, **33**, 435–446.
Nicholls, R. J., 2010. Impacts of and responses to sea level rise. In Church, J. A., et al. (eds.), *Understanding Sea Level Rise and Variability*. Oxford: Wiley-Blackwell.
Steffen, K., Thomas, R. H., Rignot, E., Cogley, J. G., Dyugerov, M. B., Raper, S. C. B., Huybrechts, P., and Hanna, E., 2010. Cryospheric contributions to sea level rise and variability. In Church, J. A., et al. (eds.), *Understanding Sea Level Rise and Variability*. Oxford: Wiley-Blackwell.
Velicogna, I., 2009. Increasing rates of ice mass loss from the Greenland and Antarctica ice sheets revealed by GRACE. *Geophysical Research Letters*, **36**, L19503.
Wunsch, C., Ponte, R. M., and Heimbach, P., 2007. Decadal trends in sea level patterns: 1993–2004. *Journal of Climate*, **20**(24), 5889–5911, doi:10.1175/2007JCLI1840.1.

Cross-references

Calving Glaciers
Catastrophic Rock Slope Failures and Mountain Glaciers
Climate Change and Glaciers
Deglaciation
Glacioeustasy
Glacioisostasy
Glaciology
Global Warming and its Effect on Snow/Ice/Glaciers
Greenland Ice Sheet
Hydrologic Cycle and Snow
Ice Age
Ice Sheet Mass Balance
Impacts of Snow and Glaciers on Runoff
Last Glacial Maximum Glaciation (LGM/LGP) in High Asia (Tibet and Surrounding Mountains)
Quaternary Glaciation
Surface Energy Balance

SEASONAL FROST

Chelamallu Hariprasad
Centre for Studies in Resource Engineering, IITB Powai, Mumbai, Maharashtra, India

The occurrence of ground temperatures below 0°C for only part of the year is known as seasonal frost. This may occur in the regions where temperature prevails at subzero temperature for a period of time.

SEASONAL SNOW COVER

Amit Kumar
Department of Geology, Centre of Advanced Study in Geology, Punjab University, Chandigarh, India

During winter, when climate conditions do not allow melt of the deposited snow, a snow cover is formed by the deposition of successive snowfall events. Although highly stratified with many layers, the seasonal snow cover is often treated as a homogeneous medium. Each layer has its own physical properties due to the initial snow condition at the time of deposition on the previous surface layer and subsequent metamorphosis, which is mainly determined by the varying field conditions and load and arrangement of ice particles in the layer. Thus, a snow cover has a stratified structure because snowfall is deposited in a series of layers. Individual layers corresponding to different snowfall event may be thick or thin. Thick layers are the result of steady snowfall in calm weather, whereas thin layers occur due to ice crusts formed due to melting, freezing, and wind conditions on the surface of deposited snow cover depends on the topography and the presence of vegetation. A seasonal snow cover is deposited and melted within 1-year cycle, and is normally developed from a series of winter storm. In addition to being an important component of water considered it is also a major component of regional and global hydrology balance. Permanent snowfields, which turn into glacier gradually, are developed at high places where total accumulated snow is not melted away in the summer season.

The changes in snow cover depend upon the prevailing weather conditions such as temperature, precipitation radiation, and wind. In warm conditions, the snow may melt away or stay for a short period. Snow cover that stays only for a few days and then depleted due to climate conditions is known as temporary snow cover.

Snow cover constitutes the largest component of the cryosphere and plays a significant role in the global climate and climate response to global changes. The extent and variability of seasonal snow cover are important parameters in climate and hydrologic systems due to effects on energy and moisture budgets. Seasonal snow can cover more than 50% (50 million km^2) of the Northern

Hemisphere land surface during the winter, making it the largest single component of the cryosphere.

Bibliography

Benn, D. I., Evans, D. J. A., 1998. *Glaciers and glaciation*. Arnold: London.

Singh, P., Singh, V. P., 2001. Snow and glacier hydrology. *Water Science and Technology Library*, Kluwer Academic: Dordrecht.

SEDIMENT BUDGETS

Helen E. Reid, Gary J. Brierley
School of Environment, The University of Auckland, Auckland, New Zealand

Definition

A sediment budget is an account of sediment movement within a defined spatial unit (e.g., hillslope, river reach, or catchment) over a given time frame. It is measured as:

$$O - I \pm \Delta S = 0$$

where O = sediment output, I = sediment input, and ΔS refers to the change in sediment storage over a given time frame. If sediment inputs exceed outputs then net deposition (storage) has occurred within the system. If outputs exceed inputs, then net erosion has occurred.

Introduction

Sediment budgets are an integral part of geomorphic enquiry (Slaymaker, 2003). They can be applied to any situation where sediment is being transported, whether over land, within water bodies, or within the atmosphere (Thomas and Goudie, 2000). In terrestrial terms, sediment budgets can be performed over a wide range of spatial scales for differing compartments of a landscape. In general, however, they are applied at the (sub)catchment scale (Reid and Dunne, 1996), reflecting the primacy of the catchment as the fundamental geomorphic unit (Chorley, 1969). As drainage basins operate as closed systems, they are the ideal unit/spatial scale at which sediment budgets can be performed (e.g., Reid and Dunne, 1996). However, sediment budgets may be a useful tool at smaller scales, such as reach-scale analyses of sediment transfer along a river or plot-scale analyses of soil erosion on farms.

River systems act as conveyer belts that move sediments from source zones (hillslopes of headwater areas, where net erosion occurs) through transfer zones in mid-catchment where erosion and deposition are approximately in balance, to accumulation zones (i.e., oceans or inland basins; Schumm, 1977). Analysis of sediment budgets entails identification of sediment sources and erosion rates (whether primary erosion or reworking of sediment stores), measurement of sediment accumulation within landscape compartments (i.e., deposition and restorage of materials), and determination of sediment output at the outlet of the spatial unit that is being studied. Changes to relationships between sediment sources, storage elements, and pathways of sediment movement may bring about dramatic changes to landscape form and sediment flux.

Sediment yield refers to the quantity of sediment that reaches the outlet of a drainage basin (Thomas and Goudie, 2000). The primary difference between analysis of sediment yield and derivation of sediment budgets is consideration of the processes that fashion sediment storage, and the efficiency with which sediment stores are reworked. The sediment delivery ratio defines the "proportion of sediment leaving an area, relative to the amount of sediment eroded in that area" (Brown et al., 2009: 37). Residence times for sediment reworking vary markedly for differing sediment storage units, whether on hillslopes or along the valley floor (both channel and floodplain compartments). In a sense, the nature and pattern of sediment stores reflects spatial variability in accommodation space within a landscape (i.e., places where sediments may be stored, however effectively) and the nature of geomorphic processes that rework these sediments (i.e., the magnitude–frequency relationships of reworking processes, and the sequence of events that determine whether sediments in stores are eroded, or additional materials are added to that store). Meaningful differentiation can be made between short-term *stores* that are prone to reworking (e.g., mobile sediments that make up mid-channel bars in river systems) and long-term *sinks* that are spatially isolated from reworking processes (e.g., cohesive sediments that make up floodplain and/or terrace features; Fryirs and Brierley, 2001). Residence time for sediment storage within a unit reflects the effectiveness of erosion, transport, and deposition processes that fashion the behavior of that landscape compartment which, in turn, is affected by the position of that feature within the landscape, the surrounding topography, climatic conditions, and vegetation cover (Brown, 1987). Residence times usually increase downstream within a catchment, as slopes decrease and accommodation space increases (Fryirs et al., 2007a).

The nature and rate of sediment movement through a landscape reflects the connectivity of the system (Harvey, 2002; Fryirs et al., 2007b). In highly coupled systems, sediment from hillslopes is delivered directly to the channel. High gradient, headwater channels are highly coupled with their hillslopes, directly inputting materials into channels. High slopes generate high steam power; so competence-limited channels are able to flush all but the largest material. As a result, sediment stores are limited in these highly connected parts of landscapes. Once slope flattens in downstream reaches, accommodation space and sediment stores increase. Floodplain pockets disconnect hillslope-derived sediments from within-channel features such as mid-channel bars and benches. Terraces have even longer residence times than the contemporary floodplain, further acting to decouple the system. In general terms, the residence time of sediment stores tends to

increase with distance downstream. Indeed, as sediments are buried and the thickness of the basin fill increases, subsidence increasingly traps and compresses sediments, facilitating their incorporation into the rock record.

Buffers, barriers, and blankets impede sediment conveyance within a catchment (Fryirs et al., 2007a, b). Buffers restrict sediment transfer from hillslopes to the channel network, as sediments are stored within features such as intact valley fills, piedmont zones, alluvial fans, floodplain pockets, and terraces. Barriers inhibit downstream movement of sediment along channels, as features such as dams and bedrock steps induce base level controls along longitudinal profiles. Blankets smother landforms, protecting underlying sediments from reworking. The more connected the system, the more efficient the rate of sediment transfer.

Sediment movement is not uniform over time. Rather, pulses in sediment reflect stochastic inputs and transfer mechanisms, such as landslides, rainfall events, earthquakes, and fires (Benda and Dunne, 1997). The amount of sediment moved by a single event is linked to the magnitude and duration of the event, whereas the amount of sediment that is moved over a period of time reflects the frequency of events of different sizes. Each landscape compartment is subjected to a suite of processes that have their own magnitude–frequency domain (or spectra). The sediment budget reflects the synchronicity of these relationships across differing compartments of the landscape (i.e., sediments sourced from one unit may be flushed to the outlet, or become trapped elsewhere within the system). This is most readily exemplified by the transfer of sediments from hillslopes to a channel system. If sediment generation from hillslopes is too high, and the channel is unable to remove all sediments, aggradation occurs on the valley floor. Alternatively, if sediment supply from hillslopes is too low, the channel will incise into its bed. In both instances, the channel adjusts to mediate conditions operating on hillslopes. The relationship between hillslope and river processes determines the rate of sediment flux (and storage) in differing parts of river systems.

Using sediment budgets to place landscape responses to human disturbance in light of natural variability

Long-term changes in sediment flux must be understood before the imprint of human disturbance upon a system can be determined (Brierley and Fryirs, 2005; Houben et al., 2009). Sediment storage and movement reflect the interaction of geologic, climatic, and anthropogenic memory, highlighting how the imprint of the past upon sediment stores is key to predicting future sediment fluxes (Brierley, 2010). For example, Pleistocene glacial stores continue to influence contemporary sediment fluxes in some systems (Church and Slaymaker, 1989). In their modelling of sediment flux at the global scale, Syvitski and Milliman (2007) found that geological controls explained 65%, climate 14%, and anthropogenic factors 16% of the viability in sediment loads. Therefore, natural geologic characteristics including basin area, lithology (i.e., erodibility), relief (i.e., erosivity, as determined by potential energy), and ice erosion are major determinants on the amount of sediment a landscape generates.

As sediment movement is largely stochastic, large events may cause fundamental shifts in the functioning of the system, prospectively bringing about a change in system state as threshold conditions are exceeded (Schumm, 1977; Reid and Dunne, 1996; Brierley and Fryirs, 2005). For example, landslides may block a channel system from reworking sediments. Sediment budgets can be used to understand landscape responses to natural, commonly high magnitude events such as volcanic eruptions (Tagata et al., 2005), landslides (Peart et al., 2005), bush fires (Wallbrink et al., 2005), and system responses to climatic fluctuations (Aalto et al., 2003).

Human activities have had a profound impact upon sediment movement in landscapes, and sediment budgets are commonly used to analyze the nature and extent of system responses to human disturbance (Houben et al., 2009). Every system is unique, its functioning driven by landscape history and more contemporary patterns of anthropogenic activity (Brierley, 2010). Wilkinson and McElroy (2007) assert that reworking of sediment stores generated in response to forest clearance is testimony to the primacy of human disturbance as the greatest influence upon contemporary sediment budgets across the Earth's surface. Examples of the use of sediment budgets to analyze the impact of contemporary land uses include agricultural impacts (Trimble 1983, 2009), mining (Knighton, 1991), logging (Roberts and Church, 1986), dams (Bogen and Bonsnes, 2005), roads (Megahan et al., 1986; Ramos-Scharron and MacDonald, 2007), and urbanization (Nelson and Booth, 2002). Tracking of contaminants and heavy metal pollutants, and analyses of carbon, nitrogen, and phosphorus cycles can be a component of sediment budget analyses (e.g., Houghton et al., 1999; Prosser et al., 2001; Slaymaker et al., 2003). Vorosmarty et al. (2003) highlight the primary role of dams in storing sediments of river systems. Understanding how human activities have altered sediment flows between compartments of a system allows for targeted management, identifying and mitigating the areas that are having the most detrimental affect on the system.

What techniques are used to derive sediment budgets?

Any sediment budget must give careful consideration to the spatial scale at which it is to be applied. Typically, a trade-off must be made between scale and precision and the level of accuracy that is sought (Brown et al., 2009). Local scale studies tend to be more fieldwork intensive, involving in-depth investigation into the relationships among specific components that make up the system (e.g., Bartley et al., 2007; Trimble, 1983). In contrast, sediment budgets undertaken at national

(Hicks et al., 1996) or global (Syvitski and Milliman, 2007) scales tend to consider sediment yields (outputs) rather than identification of sources and stores.

Given the stochastic nature of the forcing elements that determine sediment movement and storage, timescale of analysis is a critical consideration in the derivation of sediment budgets. Long-term perspectives may incorporate changes in climatic periods, land use, and sea level whereas short-term, more contemporary analyses can be used to analyze system responses to a given event (or sequence of events), such as impacts of floods, fire, or land-use alterations. Seasonal changes may be an important driver of sediment flux (e.g., tropical wet-dry seasonality, or impacts of snowmelt). Sediment flux at any given time is greatly influenced by the amount of sediment that is available to be moved at that time, especially the availability of readily accessible stores. Conditions experienced at the time of measurement have major implications when extrapolating data over longer time periods.

Techniques used to derive and analyze sediment budgets range from simple qualitative conceptualizations used to examine process interactions to in-depth quantitative analyses that derive volumetric information about the rates at which sediment is entering and leaving landscape components (Reid and Dunne, 2003). Most budgets use a mixture of desk, field, and analytical techniques.

Conceptual models of sources, sinks, and the pathways of transfer are used to identify the primary processes and units that influence sediment flux within a system (Reid and Dunne, 1996; Bartley et al., 2007). Various analytical techniques are used to assess processes of erosion, transport, and deposition that affect different units. Aerial photographs and maps aid identification of erosion rates for differing surfaces such as erosion scarps or gully complexes (Reid and Dunne, 1996). Historical images can be used to interpret the types and magnitude of channel and hillslope change (e.g., differences in active versus vegetated bar surface areas over time (Ham and Church, 2000)). The availability of map, photograph, and archival sources makes it much easier to interpret human impacts upon natural systems in the New World than elsewhere (Brown et al., 2009).

Most small-scale sediment budgets have a fieldwork component applying repeat surveys such as cross section analysis, erosion pins, flumes, ground-penetrating radar, bed load transport, floodplain coring, or trenches to assess the level of floodplain deposition (Bartley et al., 2006, 2007; Brown et al., 2009; Trimble, 1983; Walling et al., 1998; Reid and Dunne, 1996). Sediment-rating curves can be derived from analyses of turbidity (suspended sediment loads) and bed load sampling at gauging stations. Fieldwork provides important contextual information with which to ground modelling applications. However, use of field techniques in isolation can be problematic, as getting accurate data is very expensive and time consuming, and issues always arise regarding reliability and representativeness (Brown et al., 2009). Ideally, modelling techniques are supported and verified using field-based evidence (e.g., Bartley et al., 2007). However, more ground can be covered with higher accuracy when computer-based techniques are used (Brown et al., 2009).

Advances in computer-based technology, remote sensing imagery, and Geographic Information Science (GIS) have aided the development of more detailed and complex sediment budgets, increasing what can be achieved in terms of speed, accuracy, and scale (Brooks et al., 2008; Brown et al., 2009). GIS allows large datasets to be overlayed with greater spatial accuracy (e.g., Ramos-Scharron and MacDonald, 2007). Repeat surveys using advanced remote sensing technologies such as light detection and ranging (LiDAR) can be applied to generate precise digital elevation models from which fine resolution sediment budgets can be derived (Brown et al., 2009).

Paleo-records can be used to interpret how sediment fluxes have changed over time, isolating responses to different forcing mechanisms such as different cycles in climate or extreme events. The further back that analysis is based, the more likely it is that changes in climate and morphology have driven the system, altering cause–response relationships (Houben et al., 2009). Applications of dating techniques to derive sediment age and source are an integral part of sediment budget analyses. While dating can be expensive and have a degree of error, it allows more accurate interpretation of the timescales and rates over which landscape evolution has occurred. Finally, sediment fingerprinting using environmental and fallout radionuclides and chemical sediment characteristics can be used to trace the sources and pathways of sediment movement and accumulation (Walling, 2003; Walling and Horowitz, 2005; Wallbrink et al., 2005).

Summary

Sediment budgets are an integral part of geomorphic investigations into sediment movement through landscapes. Recent conceptual and technological advances in sediment budgeting aid interpretations of landform development and responses to anthropogenic disturbance. Hence, sediment budgets are a key conceptual framework in the analysis of landscape systems, allowing researchers and managers to gain critical insights into how landscapes look and operate, aiding spatial prioritization of management applications.

Bibliography

Aalto, R., Maurice-Bourgoin, L., Dunne, T., Montgomery, D. R., Nittrouer, C. A., and Guyot, J. L., 2003. Episodic sediment accumulation on Amazonian flood plains influenced by El Niño/Southern Oscillation. *Nature*, **425**, 493–497.

Bartley, R., Roth, C., Ludwig, J., McJannet, D., Liedloff, A., Corfield, J., Hawdon, A., and Abbott, B., 2006. Runoff and erosion from Australia's tropical semi-arid rangelands: influence of ground cover for differing space and time scales. *Hydrological Processes*, **20**, 3317–3333.

Bartley, R., Hawdon, A., Post, D. A., and Roth, C. H., 2007. A sediment budget for a grazed semi-arid catchment in the Burdekin basin, Australia. *Geomorphology*, **87**, 5–28.

Benda, L., and Dunne, T., 1997. Stochastic forcing of sediment supply to channel networks from landsliding and debris flow. *Water Resources Research*, **33**(12), 2849–2863.

Bogen, J., and Bonsnes, T. E., 2005. The impact of hydropower development on the sediment budget of the river Beiarelva, Norway. In Horowitz, A. J., and Walling, D. E. (eds.), *Sediment Budgets 2*. Willingford, UK: IAHS Pub 292, pp. 214–222.

Brierley, G. J., 2010. Landscape memory: the imprint of the past on contemporary landscape forms and processes. *Area*, **42**(1), 76–85.

Brierley, G. J., and Fryirs, K. A., 2005. *Geomorphology and River Management: Applications of the River Styles Framework*. Oxford: Blackwell.

Brooks, A. P., Spencer, J., Shellberg, J. G., Knight, J., and Lymburner, L., 2008. Using remote sensing to quantify sediment budget components in a large tropical river-Mitchell River, Gulf of Carpentaria. In Schmidt, J., Cochrane, T., Philips, C., Elliott, S., Davies, T., and Basher, L. (eds.), *Sediment Dynamics in Changing Environments*. Willingford: IAHS Pub 325, pp. 225–236.

Brown, A. G., 1987. *Long-Term Sediment Storage in the Severn and Wye Catchments*. In Gregory, K. J., Lewin, J., and Thornes, J. B. (eds.), Palaeohydrology in Practice. John Wiley and Sons Ltd. Great Britain, pp. 307–332.

Brown, A. G., Carey, C., Erkens, G., Fuchs, M., Hoffmann, T., Macaire, J. J., Moldenhauer, K. M., and Walling, D. E., 2009. From sedimentary records to sediment budgets: multiple approaches to catchment sediment flux. *Geomorphology*, **108**, 35–47.

Chorley, R. J., 1969. The drainage basin as the fundamental unit. In Chorley, R. J. (ed.), *Water, Earth and Man: A synthesis of Hydrology*. Methuen, London: Geomorphology and Socioeconomic geography, pp. 77–99.

Church, M., and Slaymaker, O., 1989. Disequilibrium of Holocene sediment yield in glaciated British Columbia. *Nature*, **337**(6206), 452–453.

Fryirs, K., and Brierley, G. J., 2001. Variability in sediment delivery and storage along river courses in Bega catchment, NSW, Australia: implications for geomorphic river recovery. *Geomorphology*, **38**, 237–265.

Fryirs, K. A., Brierley, G. J., Preston, N. J., and Kasai, M., 2007a. Buffers, barriers and blankets: the (dis)connectivity of catchment-scale sediment cascades. *Catena*, **70**, 49–67.

Fryirs, K. A., Brierley, G. J., Preston, N. J., and Spencer, J., 2007b. Catchment-scale (dis)connectivity in sediment flux in the upper Hunter catchment, New South Wales, Australia. *Geomorphology*, **84**, 297–316.

Ham, D. G., and Church, M., 2000. Bed-material transport estimated from channel morphodynamics: Chilliwack river, British Columbia. *Earth Surface Processes and Landforms*, **25**, 1123–1142.

Harvey, A. M., 2002. Effective timescales of coupling within fluvial systems. *Geomorphology*, **44**, 175–201.

Hicks, M. D., Hill, J., and Shankar, U., 1996. Variation of suspended sediment yields around New Zealand: the relative importance of rainfall and geology. In Walling, D. E., and Webb, B. W. (eds.), *Erosion and Sediment Yield: Global and Regional Perspectives*. Willingford: IAHS Pub 236, pp. 149–156.

Houben, P., Wunderlich, J., and Schrott, L., 2009. Climate and long-term human impact on sediment fluxes in watershed systems. *Geomorphology*, **108**, 1–7.

Houghton, R. A., Hacker, J. L., and Lawrence, K. T., 1999. The U.S. carbon budget: contributions from land-use change. *Science*, **285**, 574–578.

Knighton, A. D., 1991. Channel bed adjustment along mine affected rivers of northeast Tasmania. *Geomorphology*, **4**(3/4), 205–219.

Megahan, W. F., Seyedbagheri, K. A., Mosko, T. L., and Ketcheson, G. L., 1986. Construction phase sediment budget for forest roads on granitic slopes in Idaho. In Hadley, R. (ed.), *Drainage Basin Sediment Delivery*. Willingford: IAHS Pub 159, pp. 31–39.

Nelson, E. J., and Booth, D. B., 2002. Sediment sources in an urbanizing, mixed land use watershed. *Journal of Hydrology*, **264** (1–4), 51–68.

Peart, M. R., King, J. P., and Ruse, M. E., 2005. Sediment production by landslides in Hong Kong: two case studies. In Walling, D. E., and Horowitz, A. (eds.), *Sediment Budgets 1*. Willingford: IAHS Pub 291, pp. 29–36.

Prosser, I. P., Rutherfurd, I. D., Olley, J. M., Young, W. J., Wallbrink, P. J., and Moran, C. J., 2001. Large-scale patterns of erosion and sediment transport in river networks with examples from Australia. *Marine and Freshwater Research*, **52**, 81–99.

Ramos-Scharron, C. E., and MacDonald, L. H., 2007. Development and application of a GIS-based sediment budget model. *Journal of Environmental Management*, **87**(2), 157–172.

Reid, L. M., and Dunne, T., 1996. *Rapid Evaluation of Sediment Budgets*. Germany: Catena.

Reid, L. M., and Dunne, T., 2003. Sediment budgets as an organising framework. In Kondolf, G. M., and Piegay, H. (eds.), *Tools in Fluvial Geomorphology*. Chichester: Wiley, pp. 463–500.

Roberts, R. G., and Church, M., 1986. The sediment budget in severely disturbed watersheds, Queen Charlotte Ranges, British Columbia. *Canadian Journal of Forest Research*, **16**, 1092–1106.

Schumm, S. A., 1977. *The Fluvial System*. New York: Wiley.

Slaymaker, O., 2003. The sediment budget as conceptual framework and management tool. *Hydrobiologia*, **494**, 71–82.

Slaymaker, O., Souch, C., Menounos, B., and Filippelli, G., 2003. Advances in Holocene mountain geomorphology inspired by sediment budget methodology. *Geomorphology*, **55**, 305–316.

Syvitski, J. P. M., and Milliman, J. D., 2007. Geology, geography and humans battle for dominance over the delivery of fluvial sediment to the coastal ocean. *Journal of Geology*, **115**, 1–19.

Tagata, S., Yamakoshi, T., Doi, Y., Sasahara, K., Nishimoto, H., and Nagura, H., 2005. Post-eruption sediment budget of a small catchment on the Miyakejima volcano, Japan. In Walling, D. E., and Horowitz, A. J. (eds.), *Sediment Budgets 1*. Willingford: IAHS Pub 291, pp. 37–45.

Thomas, D. S. G., and Goudie, A., 2000. *The Dictionary of Physical Geography*. Malden: Blackwell.

Trimble, S. W., 1983. A sediment budget for Coon Creek basin in the driftless area, Wisconsin, 1853–1977. *American Journal of Science*, **283**, 454–474.

Trimble, S. W., 2009. Fluvial processes, morphology and sediment budgets in the Coon Creek basin, WI, USA, 1975–1993. *Geomorphology*, **108**, 8–23.

Vorosmarty, C. J., Meybeck, M., Fekete, B., Sharma, K., Green, P., and Syvitski, J. P. M., 2003. Anthropogenic sediment retention: major global impact from registered river impoundments. *Global and Planetary Change*, **39**(1–2), 169–190.

Wallbrink, P., Blake, W., Doerr, S., Shakesby, R., Humphreys, G., and English, P., 2005. Using tracer based sediment budgets to assess redistribution of soil and organic material after severe bush fires. In Horowitz, A., and Walling, D. E. (eds.), *Sediment Budgets 2*. Willingford: IAHS Pub 292, pp. 223–230.

Walling, D. E., 2003. Using environmental radionuclides as tracers in sediment budget investigations. In Bogen, J., Fergus, T., and Walling, D. E. (eds.), *Erosion and Sediment Transport Measurements in Rivers: Technological and Methodological Advances*. Willingford: IAHS Pub 283, pp. 57–78.

Walling, D. E., and Horowitz, A. J., 2005. Preface. In Walling, D. E., and Horowitz, A. (eds.), *Sediment Budgets 1*. Willingford: IAHS Pub 291, pp. v–viii.

Walling, D. E., Owens, P. N., and Leeks, G. J. L., 1998. The role of channel and floodplain storage in the suspended sediment budget of the river Ouse, Yorkshire, UK. *Geomorphology*, **22**, 225–242.
Wilkinson, B. H., and McElroy, B. J., 2007. The impact of humans on continental erosion and sedimentation. *Geological Society of America Bulletin*, **119**(1–2), 140–156.

Cross-references

Glacial Erosion
Sediment Entrainment, Transport, and Deposition
Sediment Transfer Modeling
Sediment Yield

SEDIMENT CORE AND GLACIAL ENVIRONMENT RECONSTRUCTION

Jostein Bakke[1], Øyvind Paasche[2,3]
[1]Department of Geography/Bjerknes Centre for Climate Research, University of Bergen, Bergen, Norway
[2]Bjerknes Centre for Climate Research, University of Bergen, Bergen, Norway
[3]Department of Research Management, University of Bergen, Bergen, Norway

Synonyms

Glacier reconstructions

Definition

Sediment core and glacial environment reconstructions describe the methods used to reconstruct past glacier activity based on sediments deposited in distal glacier-fed lakes (Figure 1). By quantifying physical properties of glacial and extra-glacial sediments deposited in catchments, and in downstream lakes and fjords, it is possible to isolate and identify past glacier activity – size and production rate – that subsequently can be used to reconstruct changing environmental shifts and trends. Moreover, detailed glacier reconstructions can also be used to assess denudation rates, chemical and physical weathering, as well specific glaciological changes.

Introduction

Alpine glaciers are often located in remote and high-altitude regions of the world, areas that only rarely are covered by instrumental records. Understanding the behavior of glaciers and linking their activity to climate changes can therefore be challenging, but when successful glacier reconstructions can shed light on past and present climate variability on both shorter and longer time scales.

Few, if any, other proxies have responded in a more unambiguous way to global warming than glaciers, which now are receding in a hitherto unrecognized pattern.

Robust glacier reconstructions can thus be an important source of knowledge for a better understanding of not only natural climate variability, but also change induced by anthropogenic emissions of greenhouse gases. Producing glacier records is not straightforward and is frequently based on a blend of different methods, which occasionally is difficult to reconcile. This can, for instance, be due to the method applied for estimating the equilibrium-line-altitude (ELA) or even the preferred physical parameter that is interpreted to reflect glacier activity.

One major drawback with glacier reconstructions based solely on moraine chronologies – by far the most common – is that due to selective preservation of moraine

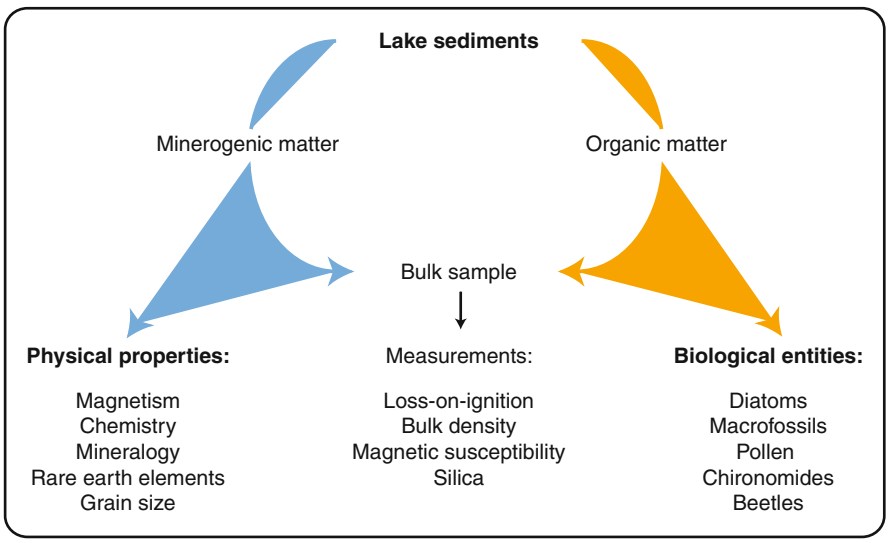

Sediment Core and Glacial Environment Reconstruction, Figure 1 Shows a simplified representation of different organic and minerogenic components making up the bulk sediments typically found in records retrieved from distal glacier-fed lakes. It is commonly the physical properties of the sediments that are used for glacier reconstructions.

ridges such records do not exclude the possibility of multiple Holocene glacier advances. This problem is true regardless of whether cosmogenic isotopes or lichenometry have been used to date the moraines, or also radiocarbon dating of mega fossils buried in till or underneath the moraines themselves.

To overcome this problem, Karlén (1976) initially suggested that glacial erosion and the associated production of rock-flour deposited in downstream lakes could provide a continuous record of glacial fluctuations, hence overcoming the problem of temporal incomplete reconstructions. Reading the glacial signal, as preserved in downstream lake sediments, now includes the application of various methods such as measuring the amount of minerogenic versus biologic matter (typically inferred from Loss-on-Ignition (LOI)), grain-size analysis (GSA), magnetic properties (MP), geochemical elements (GE), Rare-Earth Elements (REE), Bulk Sediment Density (BSD), but also other techniques (e.g., Bakke et al., 2009; Guyard et al., 2007; Leeman and Niessen, 1994; Leonard and Reasoner, 1999; Lie et al., 2004; Paasche et al., 2007).

Paleorecords of natural climate variability based on glacier reconstructions are arguably more reliable if separate events, like those that happened to produce individual moraines, can be compared relative to each other. Being able to do so requires knowledge not only about the conditions during the deposition of a single moraine, but also the conditions both prior and after the advance. It is not until such knowledge is made available through continuous glacier reconstructions that changing climate conditions adequately can be evaluated in terms of glacier response. Being able to do so is the main advantage with using sediment cores as basis for glacial environment reconstruction. Here we offer a brief review on prospects and problems associated with the employment of such an approach and also how continuous glacier reconstructions can be used as proxies for past climates.

Methods review

Changes in average sediment evacuation from alpine glaciers are mainly governed by glacier size and the mass turnover gradient, determining the deformation rate at any given time. The amount of solid precipitation (mainly winter accumulation) versus loss due to melting during the ablation-season (mainly summer temperature) determines the mass turnover gradient in either positive or negative direction. In this simplified world, a prevailing positive net balance will lead to higher sedimentation rates and vice versa, which in turn can be recorded in downstream lakes. To retrieve these glacial sediments it is necessary to collect sediment cores from the lake bottom. A range of coring equipment is now available, with different operating mechanisms and different levels of success in core recovery (see Table 1). A number of problems (often overlooked) are encountered during coring operations or during subsequent transport: (1) sediment disturbance/deformation due to coring, (2) cores not capturing all sedimentary units, (3) not enough cores retrieved, and (4) potential onsite pollution of the sediments in the cores.

To optimize the coring effort it is preferable to carry out seismic or similar investigations. New technology has made it possible to do advanced imaging of the soft sediments in glacial lakes using, for instance, Ground Penetrating Radar (GPR) or light-weighted Pinger or Kirp systems (see Moorman, 2001). With these tools it is possible to measure the actual sediment distribution within a basin, which can ensure that the selected coring sites indeed are representative for the overall sediment distribution.

Extra-glacial and also paraglacial sediment sources represent a source of error in glacier lakes because they may influence the way the bulk sediment samples are interpreted. Many are well-known and typically include debris flows, talus cones, dirty snow avalanches, subaquatic slumping, melt-out of permafrost, and so forth.

Sediment Core and Glacial Environment Reconstruction, Table 1 An overview of available coring devices, how they are operated, what maximum water coring depth they are suited for and what the maximum length of the retrieved core is expected to. The last column contains reference to some papers describing these devices

Coring device	Operation	Operating water depth	Core length (m)	References
Piston corers driven by rods (also modified with hammer or percussion)[a]	Hand operated and motorized	<100 m	40 m	(e.g., Livingstone, 1955; Nesje, 1992)
Cable-operated piston corers[a]	Motor, hydraulics	<500 m	40 m	(e.g., Kelts et al., 1986)
Box cores and dredges[a]	Hand operated	<10 m	10–20 cm	(e.g., Murdoch and Azcue, 1995)
Open-barrel and gravity corers[a]	Hand operated	<40–50 m	>1 m	(e.g., Renberg, 1991)
Chamber-type samplers[a]	Hand operated	<15 m	<15 m	(e.g., Russian peat corers, Hiller corers)
Vibracorers[a]	Motorized	<50 m	<15 m	(e.g., Thompson et al., 1991)
Freeze samplers	Hand operated	<50 m	<1 m	(e.g., Lotter et al., 1997)
Modified gravity corers[a]	Motorized for deep water	<500 m	2–4 m	(e.g., Cushing et al., 1997)
Pneumatic corers[a]	Motorized	<30 m	6 m	(e.g., Mackereth, 1969)

[a]Tube diameter varies between 30 and 200 mm

The shortcomings of many lake sediment studies are precisely that they do not distinguish different processes affecting lake sedimentation from each other (Bakke et al., 2005; Snowball and Sandgren, 1996). More recent studies build on multi-proxy approaches (Figure 2), taking advantage of the sediment's different physical qualities, which in due turn allows for the possibility of discriminating glacial flour produced at the sole of the glacier from extra-glacial and paraglacial sediments (Paasche et al., 2007; Rosqvist et al., 2004).

The landscape relief around lakes is also important as gentle slopes reduce the risk of snow avalanches and rock falls, which otherwise might impact the overall sediment budget of the lake (Dahl et al., 2003). Using lacustrine sediments retrieved from downstream glacier-fed lakes to reconstruct past glacier activity requires careful validation of the records in question since several sources of error are present. The bulk sediment composition, as seen from the lake-sedimentary archive, consists of extra-glacial components that need to be identified and isolated, as this would otherwise corrupt the glacier reconstruction. Being able to unmix bulk sediments is the most important research frontier in work dealing with glacial reconstructions based on continuous sedimentary records.

Methods that potentially can be used to distinguish different sedimentary components include rock magnetic properties (magnetic grain size, magnetic mineralogy, signal strength), XRF core scanning, and changes in physical grain-size composition (Bakke et al., 2005, 2010; Guyard et al., 2007; Paasche et al., 2007).

Sedimentary fingerprinting by means of magnetic properties usually requires a suit of measurements, which in sum might allow for a more accurate glacial reconstruction (Paasche et al., 2007; Rosenbaum and Reynolds, 2004). Variations in magnetic mineralogy are, for instance, widely used in environmental magnetism to ascertain contributions from different sediment sources, utilizing variations in provenance when erosion of different lithologies occurs. Not only will magnetic properties yield insight to provenance, it is also possible to identify chemical processes associated with transport and subsequent deposition. Magnetic measurements required to perform such a task typically involve bulk magnetic susceptibility (scrutinizing between paramagnetic susceptibility, diamagnetic susceptibility, and ferromagnetic susceptibility), saturation isothermal magnetization (sIRM), anhysteretic remanent magnetization (ARM), coercivity specters (IRM-H curves), first-order-reversal-curves (FORCS), and hysteresis loops.

XRF count rate of titanium in distal glacier-fed lakes have been employed with some success to detect glacier activity, as observed from lake sediments (Bakke et al., 2009, 2010). Other stable geochemical elements that also can be used – they are present in many lithologies – are Silicon, Potassium, and Rubidium (Guyard et al., 2007). Rubidium can, for instance, be used to monitor the amount of detrital clays (i.e., glacier flour), indicative of glacier erosion (Guyard et al., 2007). The relative new XRF scanning technology provides tools for further unmixing of the lake sediments derived from non-glacial processes.

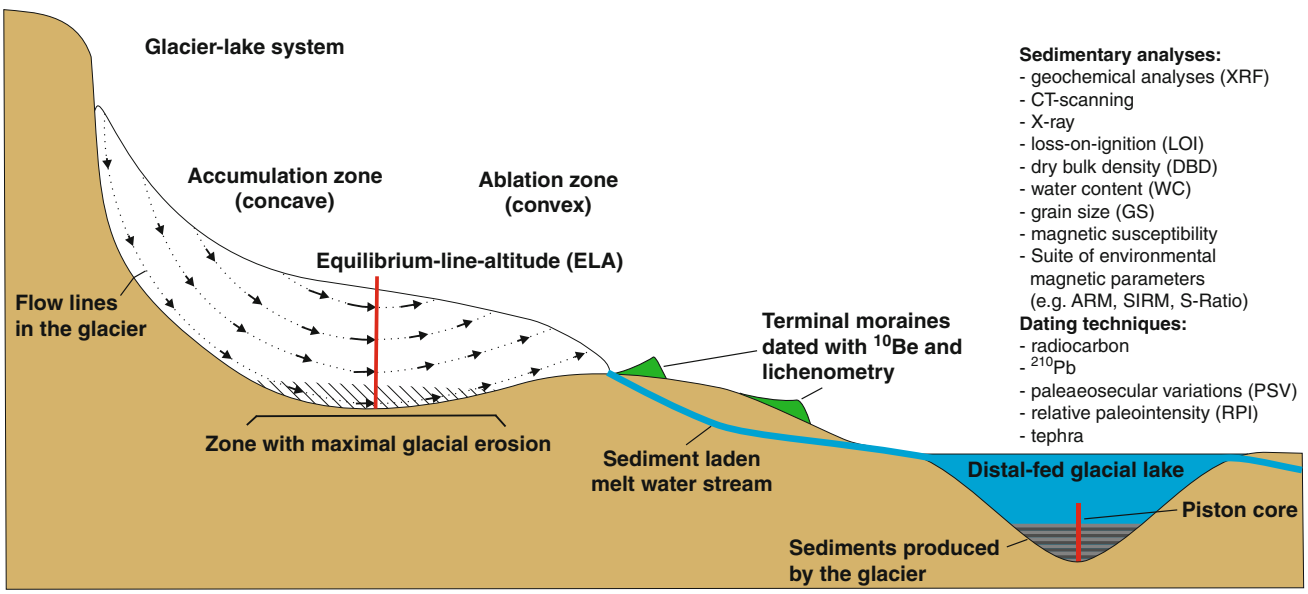

Sediment Core and Glacial Environment Reconstruction, Figure 2 Shows a conceptual illustration of an alpine glacier in relation to a distal glacial-fed lake that receives sediment-laden meltwater directly from the glacier through the glaciofluvial system. Possible sedimentary analyses that can be performed are listed together with the possible dating techniques that will make it possible to integrate the sedimentary records with, e.g., independently dated terminal moraines. Parts of this methodology have previously been used; however, few studies use all the available methods to validate the sedimentary records in question.

By employing different ratios such as Titanium/Iron and Titanium/Magnesium, which are metals assumed to be redox-sensitive and redox-insensitive, respectively, inferences about slope wash or paraglacial processes can be inferred.

X-rays and CT scanners can also be used to identify any sedimentological signatures that may indicate disturbance in the sedimentary records (e.g., erosional contact, drop stones, bioturbation, etc.).

A complementary approach is to use grain sizes that may reflect transport capacity of meltwater entering a lake. Given that this assumption is valid it may be possible to link variability in the distribution of grain sizes directly to variations in glacier runoff and hence indirectly to size (Bakke et al., 2009, 2010). The critical assumption here is that larger glaciers, on average, release more meltwater than smaller glaciers and that such changes do not also change the potential sediment contribution from other extra-glacial sources. On shorter time scales (annual) large deviations are likely, but on longer timescales (decadal to centennial) this assumption might be valid.

Paleoclimatic reconstructions based on sediment cores

Temperate glaciers respond both to temperature and solid winter precipitation. The importance of these two climatic parameters varies from glacier to glacier, but for maritime glaciers winter precipitation tends to be more important in explaining changes in the overall mass balance budget, whereas for continental glaciers temperature tends to be more important.

The potential of disentangling the climate forcing that plays such a crucial role in most glaciers 'health-state' is precisely the reason for them being sought after as proxies for past and present climate change. By reconstructing maritime glaciers along a certain transect it is, for instance, possible to assess changes of past atmospheric circulation anomalies (cf. Bakke et al., 2008) because such patterns govern the distribution of precipitation.

Over the last 30 years numerous glacial reconstructions based on sediments from distal glacier-fed lakes worldwide are published. They all provide important information about glacier and climate variations from regions often without any other paleoclimatic archives available. It is however critical that each glacier record is seen in the context of both local and regional climate before the results are upscaled.

Many reconstructions during the 1980s and 1990s were based on the pioneer work from Northern Sweden where Karlén (1976) used the organic content of lacustrine sediments (measured by loss-on-ignition, LOI) to quantify glacial erosion and its associated rock-flour production. From North America/Canada and Scandinavia several studies are based on this approach covering the time span from the deglaciation towards present day (e.g., Leonard and Reasoner, 1999). It is especially the Neo-glacial time period that is suited for the methods based on sediments from distal glacier-fed lakes because it is crucial to standardize the sedimentary archives when the boundary conditions are similar to present day. Also in the Alps several glacier reconstructions are based on sediments from distal glacier-fed lakes, such as from Lake Silvaplana (Leeman and Niessen, 1994) and Lake Bramant (Guyard et al., 2007). However, due to few lakes and high sedimentation rates the most important source for information about glacier variability in the Alps still comes from radiocarbon dating of mega fossils as well as historical sources.

State-of-the-art glacier reconstructions from distal glacier-fed lakes should aim for a quantitative-based reconstruction of the ELA. When sediment records are validated (i.e., intra-core comparison, stacking records, and/or establishing a masterstratigraphy), the next critical step involves connecting the continuous sediment record to corresponding shifts in ELA of the glacier in question. The ELAs (present and past) of dated glacier advances can be reconstructed with established methods such as, for instance, area-altitude balance ratio (AABR) (Osmaston, 2005).

In certain studies dry bulk density (DBD) or SIRM have been used for such a quantification (Bakke et al., 2010; Bakke et al., 2005). First step in this approach is, nevertheless, to integrate an independently dated moraine chronology with an independently dated sedimentary record. As evident from Figure 3, it is possible to establish a statistical relationship between the ELAs calculated from dated moraines and the corresponding sedimentary values obtained from sediment core analysis.

The second step is to use (if available) ^{210}Pb-dated sections in the sedimentary records to correlate sedimentary values to historical documented glacier-front positions recalculated to ELA. Taken together, this allows for a construction of a continuous record of ELA variations, which is based on two independently dated archives (Figure 3). The ELA reconstruction at hand must then be, if necessary, adjusted for potential land uplift before values are used for whatever reason. In Figure 3 the strong statistical relationship between ELA and winter precipitation suggests one area where such an ELA reconstruction can be valuable.

Holocene paleoclimatic trends and future prospects

Alpine glaciers located in the mid- to high latitudes in Northern Hemisphere is small or absent glaciers from 9,000 to 8,000 years BP until ca. 6,000 years BP, which possibly is the most characteristic trend for glacier records during the entire Holocene. After ca. 6,000 years BP the big picture gets more complicated and numerous advances are recorded several places, including South America, North America, Canada, the Alps, and Scandinavia (see Wanner et al., 2008). The major trend in the Holocene glacier variations in the NH seems to be connected to the gradually decreasing summer insolation due to orbital forcing.

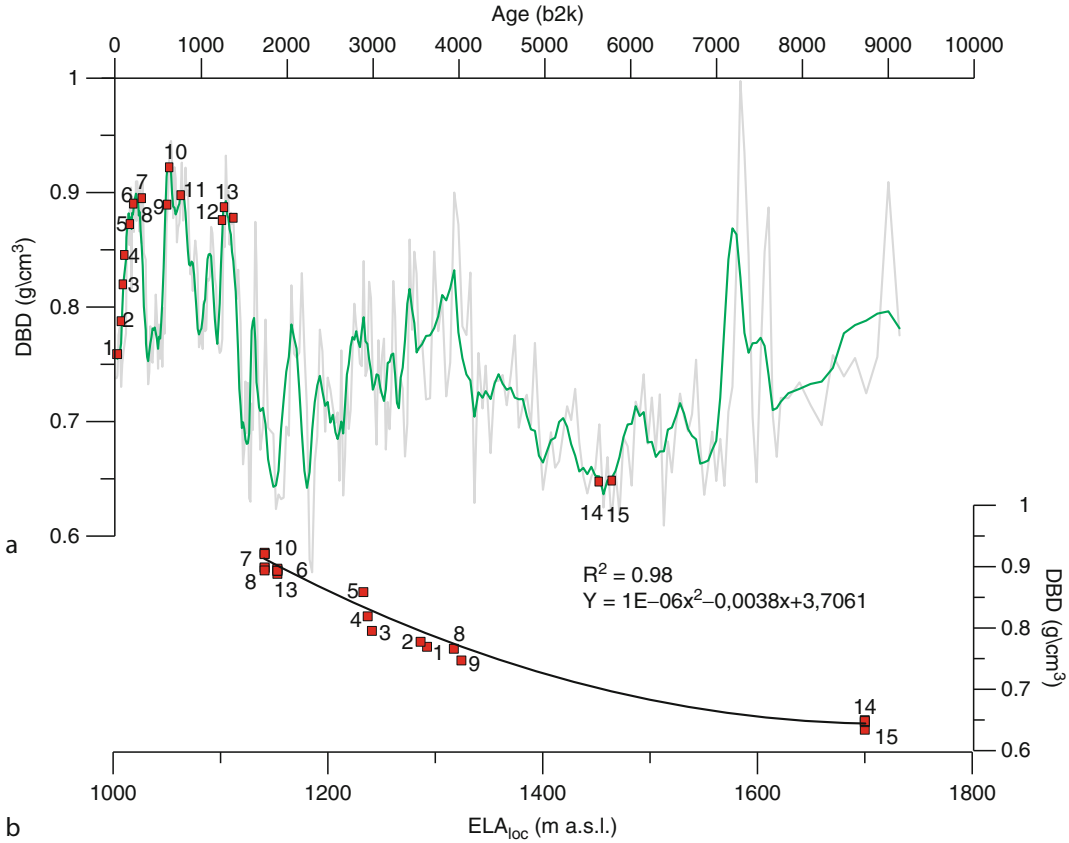

Sediment Core and Glacial Environment Reconstruction, Figure 3 (**a**) Diagram illustrating how it is possible to transform a sedimentary proxy into a continuously record of past ELA fluctuation. *Red dots* indicate periods when the ELA is known, either based on historical data, lichenometric data, and/or interpretation of lake sediments. (**b**) Shows the statistical relationship between periods with known ELA (meter above sea level) and dry bulk density (DBD) values. The regression model is used to model a continuous ELA_{loc} for Holocene. (Modified after Bakke et al., 2010).

Besides the 3,000-year period during the early Holocene when glaciers are small or even absent, another common feature for NH-glaciers is that many of them reach Holocene maximum advances during the Little Ice Age (LIA), occurring sometime between AD 1450 and AD 1910.

A challenge for future studies that seek to extract paleoclimatic information from continuous glacier sediment archives is to more actively use Earth System Models, and also modern meteorological observations. Such an approach can allow for positive identification of regions and areas where glaciers are (or are likely to be) most sensitive to changing climate conditions, and also to explore the critical number of glacier reconstructions required in order to adequately represent a particular region or weather system such as the North Atlantic Oscillation (NAO).

Another possibility for future studies is to aim for improving coring techniques by for instance combining the use of short and long cores in order to retrieve pristine sediment stratigraphies from lakes and fjords. Only when in possession of undisturbed top sediments, overlapping with the longer cores, can crucial calibration against modern processes and environment be carried out.

Overlapping time series with glacier mass-balance measurements are important for verifying and quantifying past ELAs. Using modern mass-balance data in combination with simple flow models can shed light on glacier behavior in both long and short perspectives, specifically when it comes to understanding sediment release from glaciers during advance and subsequent retreats.

Modern multi-proxy approaches, partly outlined here, have opened up new avenues for quantifying glacier process in alpine environments and linking them to changing environmental conditions. Furthermore, improving the accuracy of continuous glacier reconstructions hinges on our ability to better decipher lake sediments, i.e., connect the different sedimentary components to their factual source, and also to identify what processes that might have affected them during production, transport, and deposition. Unless we are able to improve the understanding of the glacier-lake system much of the paleoclimatic inferences will be hampered by noise. Distal glacier-fed lakes are, for instance, frequently perturbed by floods, which

can be difficult to recognize in lake-sedimentary cores, but by employing new methods such as XRF and CT scanning it is now possible to generate reconstructions for avalanche and flooding activity from the same lakes that earlier were only used for glacier reconstructions. This represents an optimization of the sediment core–based glacier reconstructions, but it also implies more accurate paleoclimatic reconstructions.

Bibliography

Bakke, J., Lie, Ø., Nesje, A., Dahl, S. O., and Paasche, Ø., 2005. Utilizing physical sediment variability in glacier-fed lakes for continous glacier reconstructions during the Holocene, northern Folgefonna, western Norway. *Holocene*, **15**(2), 161–176.

Bakke, J., Lie, Ø., Dahl, S. O., Nesje, A., and Bjune, A. E. 2008. Strength and spatial patterns of the Holocene wintertime westerlies in the NE Atlantic region. *Global and Planetary Change*, **60**(1–2), 28–41. doi:10.1016/j.gloplacha.2006.07.030.

Bakke, J., et al., 2009. Rapid oceanic and atmospheric changes during the Younger Dryas cold period. *Nature Geoscience*, **2**(3), 202–205.

Bakke, J., et al., 2010. A complete record of Holocene glacier variability at Austre Okstindbreen, northern Norway: an integrated approach. *Quaternary Science Reviews*, **29**, 1246–1262.

Cushing, S. J., Desjardins, S. J., and Fillion, J. M., 1997. Parachute-assisted gravity sediment corer (Algonquin Corer). *Journal of Paleolimnology*, **18**, 380–384.

Dahl, S. O., Bakke, J., Lie, O., and Nesje, A., 2003. Reconstruction of former glacier equilibrium-line altitudes based on proglacial sites: an evaluation of approaches and selection of sites. *Quaternary Science Reviews*, **22**(2–4), 275–287.

Guyard, H., et al., 2007. High-altitude varve records of abrupt environmental changes and mining activity over the last 4000 years in the Western French Alps (Lake Bramant, Grandes Rousses Massif). *Quaternary Science Reviews*, **26**, 2644–2660.

Karlén, W., 1976. Lacustrine sediments and tree-line variations as indikators of climatic fluctuations in Lappland, northern Sweden. *Geografiska Annaler*, **58A**, 1–34.

Kelts, Z., Briegel, K. G., and Husu, K., 1986. The limnology-ETH coring system. *Schweizerische Zeitschrift für Hydrologie*, **48**, 104–115.

Leeman, A., and Niessen, F., 1994. Holocene glacial activity and climatic variations in the Swiss Alps: reconstructing a continuous record from proglacial lake sediments. *Holocene*, **4**, 259–268.

Leonard, E. M., and Reasoner, M. A., 1999. A continuous Holocene glacial record inferred from proglacial lake sediments in Banff National Park, Alberta, Canada. *Quaternary Research*, **51**, 1–13.

Lie, O., Dahl, S. O., Nesje, A., Matthews, J. A., and Sandvold, S., 2004. Holocene fluctuations of a polythermal glacier in high-alpine eastern Jotunheimen, central-southern Norway. *Quaternary Science Reviews*, **23**(18–19), 1925–1945.

Livingstone, D. A., 1955. A lightweight piston sampler for lake depostis. *Ecology*, **36**, 137–139.

Lotter, A., Renberg, I., Hannsson, H., Stöckli, R., and Strum, M., 1997. A remote controlled freeze corer for sampling unconsolidated surface sediments. *Aquatic Sciences*, **59**, 295–303.

Mackereth, F. J. H., 1969. A short core sampler for sub-aqueous deposits. *Limnology and Oceanography*, **3**, 181–191.

Moorman, B. J., 2001. Ground-penetrating radar applications in paleolimnology. In Last, W. M., and Smol, J. P. (eds.), *Tracking Environmental Change Using Lake Sediments*. Dordrecht: Kluwer. Basin Analysis, Coring, and Chronological Techniques, Vol. 1, pp. 23–47.

Murdoch, A., and Azcue, J. M., 1995. *Manual of Aquatic Sediment Sampling*. Boca Raton: Lewis, p. 219.

Nesje, A., 1992. A piston corer for lacustrine and marine-sediments. *Arctic and Alpine Research*, **24**(3), 257–259.

Osmaston, H., 2005. Estimates of glacier equilibrium line altitudes by the Area × Altitude, the Area × Altitude Balance Ratio and the Area × Altitude Balance Index methods and their validation. *Quaternary International*, **138**, 22–31.

Paasche, O., Dahl, S. O., Bakke, J., Lovlie, R., and Nesje, A., 2007. Cirque glacier activity in arctic Norway during the last deglaciation. *Quaternary Research*, **68**(3), 387–399.

Renberg, I., 1991. The HON-Kajak sediment corer. *Journal of Paleolimnology*, **6**, 167–170.

Rosenbaum, J. G., and Reynolds, R. L., 2004. Record of Late Pleistocene glaciation and deglaciation in the southern Cascade Range: II. Flux of glacial flour in a sediment core from Upper Klamath Lake, Oregon. *Journal of Paleolimnology*, **31**, 235–252.

Rosqvist, G., Jonsson, C., Yam, R., Karlen, W., and Shemesh, A., 2004. Diatom oxygen isotopes in pro-glacial lake sediments from northern Sweden: a 5000 year record of atmospheric circulation. *Quaternary Science Reviews*, **23**(7–8), 851–859.

Snowball, I. F., and Sandgren, P., 1996. Lake sediment studies of Holocene glacial activity in the Kårsa valley, northern Sweden: contrasts in interpretation. *Holocene*, **6**, 367–372.

Thompson, T. A., Miller, C. S., Doss, P. K., Thompson, L. D. P., and Baedke, S. J., 1991. Land-based vibracoring and vibracore analysis: tips, tricks, and traps. Indiana Geological Survey Occasional Paper, vol. 58, 13 p.

Wanner, H., et al., 2008. Mid- to Late Holocene climate change: an overview. *Quaternary Science Reviews*, **27**(19–20), 1791–1828.

Cross-references

Atmospheric Circulation and Glaciochemical Records
Cirque Glaciers
Climate Change and Glaciers
Glacial Erosion
Glacier Mass Balance
Glacier Motion/Ice Velocity
Proglacial Lakes
Retreat/Advance of Glaciers
Scandinavian Glaciers
Suspended Sediment Concentration
Temperate Glaciers

SEDIMENT ENTRAINMENT, TRANSPORT, AND DEPOSITION

Michael J. Hambrey, Neil F. Glasser
Centre for Glaciology, Institute of Geography & Earth Sciences, Aberystwyth University, Aberystwyth, Ceredigion, Wales, UK

Definition

Sediment entrainment, transfer and deposition explains how debris is incorporated into the base or onto the surface of a glacier, then modified and deformed during glacier flow, and finally deposited beneath or in front of the glacier, including its subsequent reworking.

Introduction

Importance of glacial sediments

Glacial sediments provide a vital legacy for interpreting past climates of the Quaternary and earlier geological periods. Their importance can be gauged from the facts that 30% of the Earth's land surface was under ice during the last ice age, and that even today 10% of the land is still covered by glaciers and ice sheets. During the Quaternary Period, in addition to those that survive in Antarctica and Greenland, vast ice sheets grew over North America, Scandinavia and the British Isles, northern Russia, Tibet, and Patagonia. Smaller icefields grew over the Alps, New Zealand, and central Asian ranges, together with smaller ice masses in many other of the Earth's mountain ranges. Glacier ice has left a complex but often patchy record of deposition on land, but offshore has contributed substantially to the buildup of high-latitude continental shelves.

Glacial transport and deposition is intimately associated with a wide range of other processes, including ice deformational and glaciotectonic, fluvial, mass flowage, aeolian, lacustrine, and marine. The resulting sedimentary facies associations are highly variable, and even with detailed investigation can be interpreted in widely different ways. It is only within the last 4 decades that studies of glacial processes in modern settings have made it possible to develop plausible models of past glacial depositional environments.

Understanding the nature of Quaternary glacial sediments and their associated landforms is crucial in the glaciated areas of North America, Europe, and elsewhere. This is because sand and gravel extraction, notably from glaciofluvial sequences, is essential for construction purposes, as well as informed management of water resources and waste disposal. Some pre-Quaternary glacigenic facies are also economically important in some regions, such as in the Permo-Carboniferous and Neoproterozoic basins of the Middle East and South America, where they constrain the presence of petroleum resources.

Glacial sediments also have an important aesthetic appeal. In mountain regions, they add to the character of impressive glacial erosional landscapes, while in lowland regions they provide a rolling topography of lakes and hills, all of which underpin the tourism business.

The wider implications of focusing on glacial sediments and their associated landforms center on reconstructing past ice sheets. This topic, referred to as paleoglaciology, is of increasing importance as we seek to understand past response of ice masses to climate. Using this concept provides us with constraints on predictions of climate change.

This article is an updated version of that published in the *Encyclopedia of Sediments and Sedimentary Rocks* (Hambrey and Glasser, 2003).

Historical background

It is widely recognized today that the Earth experienced a series of ice ages. However, when the concept was first promoted in the early nineteenth century, it met with fierce opposition. At that time, most of the unconsolidated deposits (so-called drift) that were familiar to geologists were attributed to the biblical Noah's flood. Indeed, the flood concept was used to explain the presence of large boulders displaced from their source bedrock ("erratics") that were deposited from icebergs (Hambrey, 1994, Chap. 1 for review). The Swiss natural historian, Agassiz, became the chief protagonist of the "Ice Age Theory," and when he delivered his ideas in 1837, they had a Europe-wide impact. In the following decades, through Agassiz's influence, geologists in the UK and North America gradually accepted the theory as being also applicable to their regions. In the second half of the nineteenth century, "ancient" glacial deposits (*tillites*) were recognized in many parts of the world. However, even in the second half of the twentieth century, the glacial origin of supposed tillites was challenged, notably those of Neoproterozoic age. It has taken systematic sedimentological investigations, coupled with an appreciation of modern glacial processes, to settle these debates.

Glaciological aspects of debris entrainment and transport

To evaluate the processes whereby sediment is entrained and deposited, we need to understand a number of key glaciological phenomena; several of these are dealt with more thoroughly in this volume (see Section "Cross-references").

Mass balance

The state of health of a glacier and its capacity to carry debris is a reflection of its mass balance, and the supply of debris from surrounding headwalls and from the base. A positive mass balance allows rapid burial of supraglacial debris and transport through an englacial pathway, while a negative mass balance sees the exposure and emergence of greater quantities of debris at the surface. The basal conditions also vary, with a positive mass balance causing the glacier to flow more rapidly and erode the bed more intensely, and a negative mass balance allowing stagnation and rapid deposition of the sediment load (Figure 1).

Glacier dynamics

In order to interpret the origin of glacial sediments and landforms, it is necessary to understand the mechanisms of ice deformation and glacier flow. Glaciers flow by one or more of three main mechanisms: internal deformation, basal sliding, and movement over a soft, deformable bed (Paterson, 1994). In simple terms, *internal deformation* results in the slowest flow occurring at the margins and at the base of a glacier, but large-scale reorganization of preexisting structures, with or without debris, through folding and foliation development is also common. *Basal sliding* is important where rain or meltwater is able to lubricate the bed, and varies according to the season and

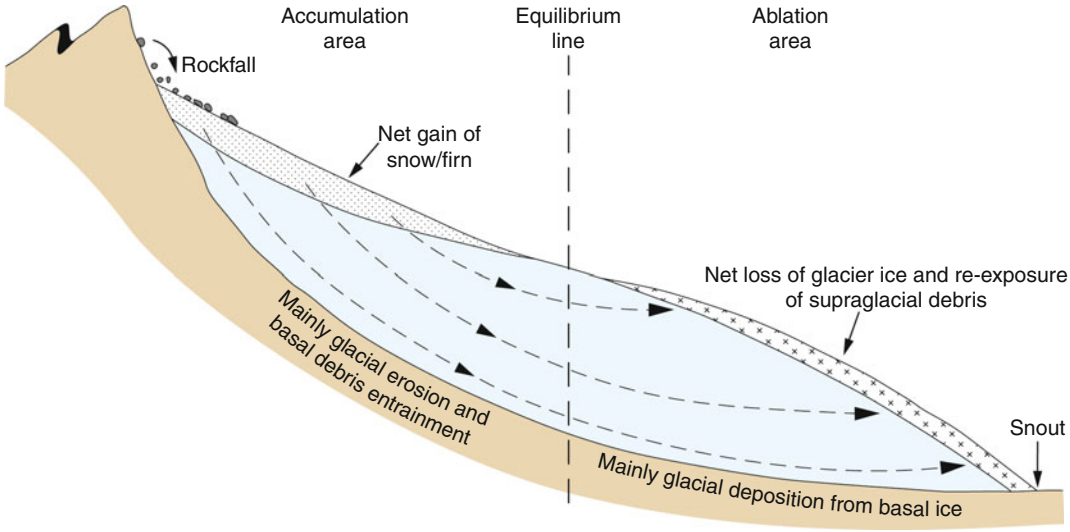

Sediment Entrainment, Transport, and Deposition, Figure 1 Longitudinal profile through a valley or cirque glacier, illustrating the relationship between mass balance, particle paths (*arrows*), and debris entrainment processes.

time of day or night. Frictional and geothermal heating may add to the availability of meltwater. All these factors control erosion and regelation at the glacier bed. Many glaciers flow over a *deformable bed* of unconsolidated sediment which, when saturated, can behave as a slurry that enhances the flow of the glacier. Deformable beds exist beneath modern fast-flowing ice streams in Antarctica and Greenland, as well as many ice caps and outlet glaciers. Much of the movement of the Quaternary ice sheets in North America has also been linked to deformation of the bed. The relative importance of these mechanisms is highly variable. In moist temperate regions as much as 80% of glacier flow is from sliding. Cold polar glaciers, which are frozen to their beds, flow almost entirely by internal deformation. Polythermal glaciers (with both cold and warm ice) have a combination of sliding and frozen bed conditions. Debris entrainment commonly occurs where there is a transition between the two modes of flow. Where a deformable bed exists, the bulk of movement may be within the sediment layer beneath the ice, while the sediment itself is transported in conveyor belt–like fashion. In *surge-type glaciers*, flow is unstable, with long periods (often decades) of quiescence punctuated by short bursts (several months to a few years) of high velocity (*surges*). During the most active phase of a surge, the velocity may reach several orders of magnitude above normal, and the glacier may advance rapidly, and redistribute large volumes of sediment.

Glacier structure

Glacier structures are principally the product of internal deformation, and are intimately associated with the transport of debris (Paterson, 1994; Hambrey and Lawson, 2000). Glacier ice is similar to any other type of geological material in that it comprises strata that progressively deform to produce a wide range of structures. Primary structures in glacier ice include stratification derived from snow and superimposed ice, and unconformities. Regelation layering, resulting from pressure melting and refreezing at the base of a glacier, the latter also sometimes being referred to as stratified ice, although not strictly in the geological sense. Secondary structures are the result of deformation, and include both brittle features (crevasses, crevasse traces, faults, and thrusts) and ductile features (foliation, folds, boudinage). All these structures are associated with debris, whether by direct accumulation as rockfall (as in stratification), or by concentration in foliation as in shear zones between two merging flow units. Typically, a glacier reveals a sequential development of structures as in deformed rocks, so that by the time the glacier snout is reached, ice may record several "phases" of deformation. Similarly, the cumulative strain which glacier ice has undergone commonly changes the original geometry of the structure and associated sediment out of all recognition.

Thermal regime

The temperature distribution or *thermal regime* of a glacier is fundamental to glacier flow, meltwater production and routing, and to styles of glacial erosion and deposition. *Temperate* or *warm* glaciers, in which the ice is at the pressure-melting point throughout, tend to slide rapidly on their beds and are highly erosive. These glaciers are typical of alpine regions. *Cold* glaciers are the end member at the opposite temperature extreme, the ice being below the pressure melting point throughout; they occur in high polar regions or at very high altitudes only. These glaciers have long been thought incapable of eroding their

bed, although evidence from Antarctica indicates that this is not strictly true. An intermediate type of glacier, found especially in the high Arctic, is referred to as *polythermal*. In such glaciers, it is typical for the snout, margins and surface layer of the glacier to be below the pressure-melting point, whereas thicker, higher-level ice is warm based.

Glacier hydrology

Glacial erosion and sediment transport would be much less effective were it not for the presence of meltwater within, beneath, and beyond the glacier. Water, derived from melting snow and ice, flows in supraglacial rills, channels, and canyons cut into the glacier surface. If structural weaknesses exist, the meltstreams commonly plunge into the interior or bed of the glacier via moulins, before emerging at the snout. Drainage routes, and therefore sediment transport paths, differ according to the thermal regime of the glacier. In cold and polythermal glaciers, meltwater tends to be forced toward the glacier margins, as subzero ice prevents surface water penetrating far below the glacier surface. In contrast, water flows in discrete channels at the bed in temperate glaciers, often emerging from the glacier at a single portal. Glaciers act as natural storage reservoirs, retaining water and sediment in winter and releasing them in summer. Thus discharge is markedly seasonal and diurnal. On a typical braided outwash plain, beyond the glacier, marked fluctuations in discharge result in rapid, continuous channel shifts, and deposition of both suspended and bed-load sediment. Meltwater and sediment also accumulates in ice-constrained lakes, including ice-dammed, proglacial, supraglacial, and subglacial types. Many of these are ephemeral, and those dammed by ice, which are most commonly associated with polythermal glaciers, are particularly prone to catastrophic failure, resulting in outburst floods called *jökulhlaups*. Moraine-dammed lakes, which typically grow behind Little Ice Age moraines are also prone to catastrophic failure, notably in the Andes and the Himalaya. Glacial meltwater is not only a powerful erosive agent, but is also responsible for among the most important sedimentary facies in glacierized regions.

Morphological controls on sediment transport

As documented elsewhere in this volume, glaciers range in size from ice masses only a few hundred meters across to the huge ice sheets that cover Antarctica and Greenland, and there are thus many different morphological types (Hambrey, 1994; Bennett and Glasser, 2009; Benn and Evans, 2010). Ice sheets and ice caps carry most of their sediment load in the bed, where regelation processes have entrained the debris. Conversely, they carry little supraglacial debris, other than dust, or where compressive flow causes upward movement of basal debris in the terminal region. Valley and cirque glaciers carry much more supraglacial debris as a result of rockfall, induced by freeze-thaw processes, especially in high-relief temperate zones. Dealing with the past record, one of the key roles of the glacial sedimentologist is to reconstruct the morphological characteristics of former ice masses, in order to constrain the interpretation of past climates and sea-level response.

Glacial erosion

The processes whereby a glacier or ice sheet picks up and transports rock fragments and sediment, and transfers this material to another location are referred to as glacial erosion. In summary, glacial erosion occurs by means of four main processes: *glacial abrasion*, *glacial plucking* (or *quarrying*), *glacial meltwater erosion*, and *subglacial sediment deformation*, and gives rise to a wide range of spectacular landforms (Figure 2). Since glacial erosion is the starting point for debris entrainment and transport by glaciers and ice sheets, an understanding of this topic is essential if we are to understand the sedimentary products of ice masses.

Glacial abrasion is the process by which particles entrained in the basal layer of a glacier are dragged across the subglacial surface. The scratching and polishing associated with glacial abrasion tends to create smoothed rock surfaces, commonly with striations or grooves.

Glacial quarrying (or *plucking*) is the process whereby a glacier removes and entrains large fragments of its bed. The processes of rock fracture are controlled by the density, spacing, and depth of preexisting joints in bedrock, together with the stresses applied by the glacier. Fracturing of bedrock is also aided by the presence of meltwater beneath the glacier, where bedrock is loosened by subglacial water-pressure fluctuations. Material ranging from quarried blocks to fine material is then entrained in basal ice by freezing-on (*regelation*), when surrounded by flowing ice, or when incorporated along thrusts. Entrainment is most pronounced in polythermal glaciers, especially where there is a transition from sliding-bed to frozen-bed conditions, and a complex layer several meters thick may develop (Figure 3a). In contrast, the abundance of meltwater precludes substantial entrainment of debris in temperate glaciers, and the basal debris layer may be less than a meter thick (Figure 3b). Although not noted for being erosional agents, cold glaciers can entrain blocks of frozen subglacial sediment and bedrock as a result of shear at the ice/substrate contact (Figure 3c).

Glacial meltwater erosion involves both mechanical and chemical processes. Mechanical erosion occurs primarily through fluvial abrasion by the transport of suspended sediment and bedload within meltwater at the base of the glacier. Locally, fluvial *cavitation* (the sudden collapse of bubbles within turbulent meltwater under high pressure) may also be important. In subglacial channels, chemical erosion involves the removal of rock and rock debris in solution, especially in areas of carbonate bedrock. Rates of chemical erosion beneath ice masses are high because of high flushing rates, the availability of large amounts of chemically reactive rock flour, and the enhanced solubility of CO_2 at low temperatures.

Sediment Entrainment, Transport, and Deposition, Figure 2 Glacially sculpted peaks of Piz Morteratsch and Piz Bernina, Graubünden, Switzerland, with the glacier Vadret da Tschierva in the center. The huge lateral moraines on either side of the valley and the hummocky moraine in the foreground date from the Little Ice Age.

Subglacial sediment deformation is a relatively new concept, and is believed to be a major component of glacier flow beneath ice streams and valley glaciers (Boulton, 1996). The process involves net removal of wet sediment in conveyor belt–like fashion and can contribute to the progradation of sediment aprons or wedges where there is a sharp break in slope, for example, at the edge of a continental shelf or in a lake.

Debris entrainment and transport

Debris is entrained within a glacier both at the bed as basal glacial debris and at the surface as supraglacial debris. In addition, there is transfer of debris from low to high level and vice versa by means of a range of processes related to deformation of the ice (Figure 4). The following discussion considers both low- and high-level transport and stages in between, but in effect entrainment is a continuum of processes at different levels within the glacier. Transport paths and textural character of glacial sediments are related to the dynamic and thermal characteristics of the glacier. Broadly speaking, polythermal glaciers tend to carry a high basal debris load (Figure 3a), and the surface rarely has a substantial cover of debris. In contrast, temperate glaciers, especially those in high-relief regions, normally carry relatively little basal debris (Figure 3b), but the surface commonly has an extensive cover of supraglacial debris. The resulting sedimentary products can thus be used to infer the thermal and topographic regimes of a former glacier regime.

Low-level debris entrainment and transport

Debris is entrained at the bed by a combination of pressure melting and refreezing (regelation). Freezing to the base of the glacier occurs when the 0°C isotherm migrates into the substrate, sometimes even allowing sediment or bedrock to be entrained en masse. The thickness of the basal ice layer can be increased by folding and thrusting, or concentration around obstacles. These complex processes create a basal debris layer that comprises a wide range of ice types (or facies), involving frozen meteoric water, glacier ice, different concentrations of debris, and even solid sediment (Knight, 1997; Hubbard et al., 2009), as is well known from studies of both temperate and polythermal glacier margins (Figure 5). Basally derived debris is subject to abrasion, fracturing, and crushing at the ice/bedrock interface. The resulting entrained sediment is dominated by clasts up to boulder-size, with subangular and subrounded shapes, faceted surfaces, and striations (if the lithologies are fine grained) (Figure 6). In addition, much clay- or silt-grade sediment is produced by abrasion. Together, on deposition, the resulting sediment is poorly sorted with a wide range of clast shapes and sizes.

A second mechanism of debris entrainment at the glacier bed, discovered in recent years at a temperate glacier in Alaska, is associated with glaciohydraulic supercooling. This involves sediment-laden supercooled water refreezing to the glacier sole on the upslope side of an overdeepening in the glacier bed. The process preferentially selects finer-grained sediment, and can lead to the buildup of a several-meters-thick basal ice layer.

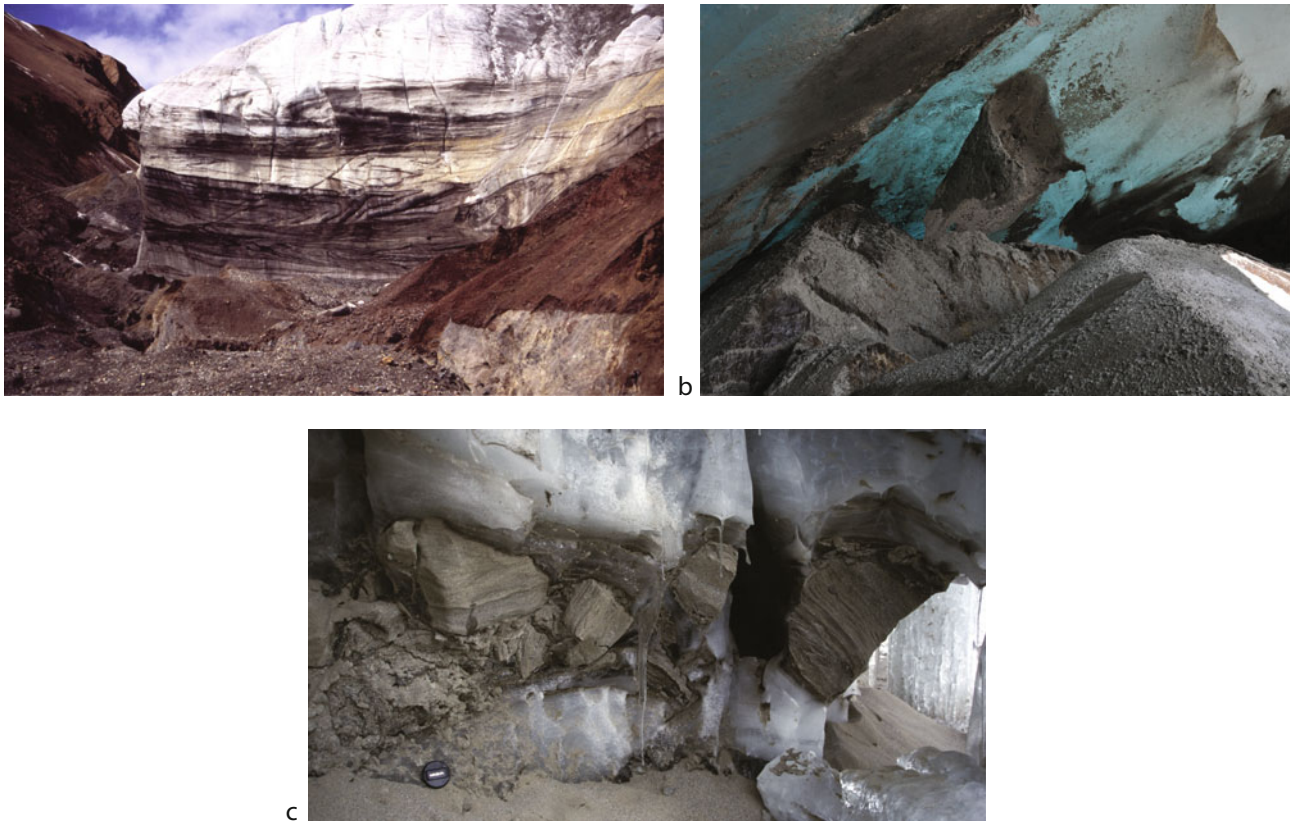

Sediment Entrainment, Transport, and Deposition, Figure 3 Debris entrainment compared in the base of thermally contrasting glaciers. (**a**) Several-meters-thick basal debris layer, repeated by folding in polythermal Trapridge Glacier, Yukon; the cliff is c. 10 m in height. (**b**) Minimal basal debris in a cave at the snout of temperate Rhonegletscher, Switzerland; a thin film of granitic sand mantles the bedrock, while a 1-m-wide folded layer of debris hangs from the roof. (**c**) Solid frozen blocks of glaciofluvial sand incorporated, boudinaged, and rotated in the base of cold Wright Lower Glacier, Dry Valleys, Antarctica.

High-level debris entrainment and transport

In high-relief areas, freeze-thaw processes on exposed bedrock in the accumulation area of a glacier result in rockfall onto the snowpack below, where it is buried as the layer of stratified snow, firn, and ice buildups. Similarly, along the flanks of the glacier in the ablation zone, rockfall allows debris to drape large areas of the glacier surface, sometimes covering it completely to a depth of several meters (Figure 7). Debris falling high in the accumulation area tends to take an englacial path and emerge near the snout, following the flow lines through the glacier, whereas debris falling close to the equilibrium line will follow a shallow englacial path and emerge a short distance down glacier (Figure 1). However, superimposed on this simple pattern are the complexities of folding, as discussed below. Supraglacial debris is generally dominated by gravel (pebble to boulder-sized) material, with few fines, and clast shapes are typically angular and very angular (Figure 7).

Debris on the surface of a glacier is commonly concentrated into flow-parallel ridges of debris, referred to as medial moraines, of which there are two types: *flow-unit interaction moraines* (also confusingly referred to as ice-stream interaction moraines) and *ablation-dominant moraines*. An understanding of structural glaciology is necessary to infer which is the correct mechanism involved. Flow-unit interaction moraines are formed by the confluence of two lateral moraines at the junction of two glacier flow units (Figure 8). The medial moraine consists of a debris-covered ridge that represents the surface expression of a vertical debris septum that may extend down to the bed of the glacier. The internal structure of the septum may be complex, consisting, for example, of anastomosing shears and isoclinal folding. Texturally, these moraines are highly variable; some consist of angular supraglacial debris, but others are mixed with sediment reworked at the ice/bed interface and so comprises more rounded material. *Ablation-dominant moraines* form

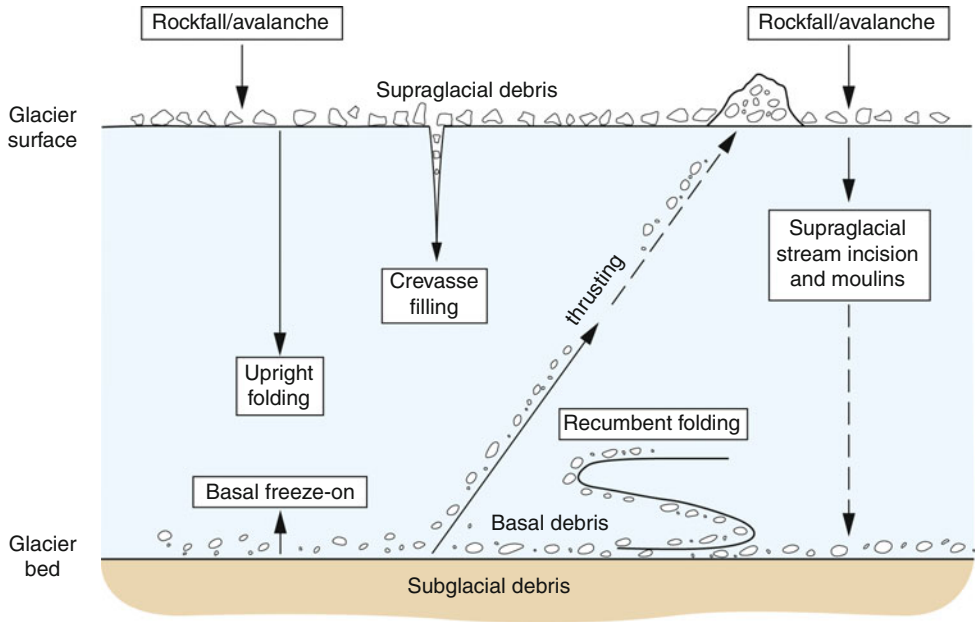

Sediment Entrainment, Transport, and Deposition, Figure 4 Schematic longitudinal cross section through a glacier, summarizing the various processes whereby debris is entrained and transported.

Sediment Entrainment, Transport, and Deposition, Figure 5 Deformed basal ice layer in a cave at the snout of Glacier de Tsanfleuron, Valais, Switzerland. The glaciologist (Bryn Hubbard) is standing on striated limestone bedrock, and there is a folded multilayered basal ice sequence to his right.

where ridges of englacial debris emerge from the ice surface in the ablation zone and extend to the snout. This type of moraine may form in two ways:

1. From a point source between two flow units in the accumulation area where the debris is initially buried and then takes an englacial path through the glacier. Structurally, these are similar to flow-unit interaction moraines.
2. Incorporation of angular rockfall material within the stratified sequence of snow and firn (Figure 9).

This debris takes an englacial path through the glacier, and becomes folded, especially in zones of lateral compression, such as where multiple accumulation basins feed into a narrow tongue. Fold styles range from the broad open "similar" type to isoclinal folds (with parallel limbs). In the ablation area, the debris emerges at the surface on the flow-parallel hinges and upper limbs of the folds, producing medial moraines that merge toward the snout. The resulting lines of debris are deposited on the proglacial area in the form of regular trains of angular debris, as the glacier recedes. This process has been inferred from several small valley glaciers in Svalbard and the Alps (Hambrey et al., 1999).

Sediment Entrainment, Transport, and Deposition, Figure 6 Striated and faceted clast of limestone on the proglacial basal till surface of Austre Lovenbreen, Svalbard.

The above mechanisms result in typical flow-parallel medial moraines than can be tracked long distances downglacier. However, perturbations in flow resulting from surging can distort the moraines into folds and loops (Figure 10). These contortions allow surge-type glaciers to be identified even when there is no historical record of a surge having taken place. Another situation where folded moraines develop is where narrow tongues spread out into piedmont lobes. In this case, the folds generate axes normal to the maximum compression that is parallel to the ice margin.

Debris transfer between low and high levels

An understanding of glacier structure is once again vital to appreciate how debris is redistributed within the glacier, especially where basal debris is uplifted to a higher-level position. In this context, glacier ice behaves no differently from any other geological material deforming where the Earth's crust is subject to lateral stresses. Debris in glaciers is transferred from the bed to an englacial and even a supraglacial position by three main glaciotectonic processes: thrusting, basal crevasse-filling, and incorporation within longitudinal foliation. Of these, the role of thrusting versus crevasse-filling has been much debated, and certainty of the mechanism cannot always be achieved.

Thrusts, typically inclined upglacier at angles ranging from a few to c. 40°, develop under longitudinal

Sediment Entrainment, Transport, and Deposition, Figure 7 Thick layer of largely angular avalanche-derived supraglacial debris draping the surface of Khumbu Glacier, Mt. Everest region, Nepal.

Sediment Entrainment, Transport, and Deposition, Figure 8 Medial moraines of the flow-unit interaction type on Kaskawulsh Glacier, Yukon.

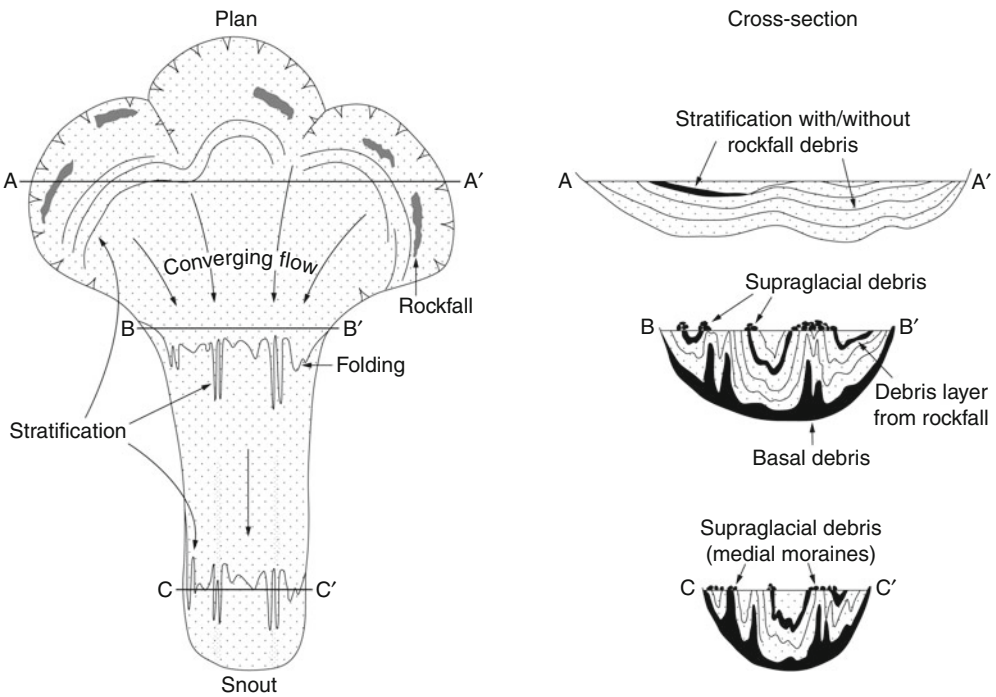

Sediment Entrainment, Transport, and Deposition, Figure 9 Conceptual models of debris entrainment and the development of ablation-dominant moraines, illustrating both high-level folding of supraglacial debris and low-level folding of basal debris. (After Hambrey et al., 1999; published with permission of the International Glaciological Society.)

Sediment Entrainment, Transport, and Deposition, Figure 10 Complex folding and looped moraines are characteristic features of surge-type glaciers, this example being Lowell Glacier in the Icefield Ranges, Yukon.

compression in three main situations: (1) where there is a downstream transition from a sliding to a frozen bed, as in polythermal glacier; (2) where ice flows against a reverse bedrock or sediment slope; and (3) in surging glaciers as the strongly compressive surge front moves down glacier. Thrusts carrying abundant debris are a feature of many polythermal and cold glaciers, but they also occur to a limited extent in temperate glaciers. Specifically, debris-rich basal ice (including regelation ice) and rafts of subglacial sediments are uplifted into an englacial position, sometimes emerging at the ice surface (Figure 11). This material is more varied than rockfall debris, and reflects the substrate lithologies: typically poorly sorted sediment (diamicton) with striated clasts (inferred to be basal till), sandy gravel (glaciofluvial sediment, and even laminated or stratified mud and sand (glaciolacustrine or glaciomarine sediment). The thrusts may extend upward to the ice surface and be associated with recumbent folding with lower limbs being sheared off at the thrust surface. Other so-called blind thrusts may terminate within the ice mass. As thrusts melt out at the glacier surface, groups of roughly aligned, commonly arcuate ridges and hummocks of basally derived sediment are formed.

Flowage of subglacial sediment into basal crevasses, followed by rotation during glacier flow, has also been inferred to explain the emergence of debris on inclined planes at the glacier surface. There are few direct sightings of basal crevasses, but such fractures are thought to occur especially when a glacier surges over a soft deformable bed of till. Once they attain a moderate angle, they resemble thrusts, and discrimination between the two processes relies on whether the feature is associated with basal ice, in which case the thrusting mechanism is most likely. The sedimentary product of incorporation of debris into basal crevasses is a suite of meter-scale landforms referred to as crevasse-fill ridges.

A third mechanism involves incorporation of debris of both supraglacial and basal character within longitudinal foliation. This process is particularly evident at the glacier margins and at flow-unit boundaries where the folding is commonly isoclinal. The folding has an axial planar relationship with the foliation. At depth, it is inferred (but not so far observed) that the lateral compressive regime that produces high-level folding, also induces folding is soft subglacial and basal sediments of the same geometry (Figure 9). As these features melt out, low (meter-scale) longitudinal ridges form that are similar to, but genetically different from, flutes; these are referred to as "foliation-parallel ridges."

Debris transfer between high and intermediate levels

In addition to burial and folding of supraglacial debris, described above, debris can enter an englacial position via crevasses. Crevasses generally do not penetrate to the bed, and in temperate glaciers are theoretically no more than 30 meters deep unless water filled. Structures commonly influence the pattern of supraglacial and englacial drainage. For example, a moulin that captures a supraglacial stream may form along a crevasse trace, which acts as a plane of weakness in the ice. Supraglacial sediment washed into the stream may tumble into the moulin and enter an englacial position or even reach the bed.

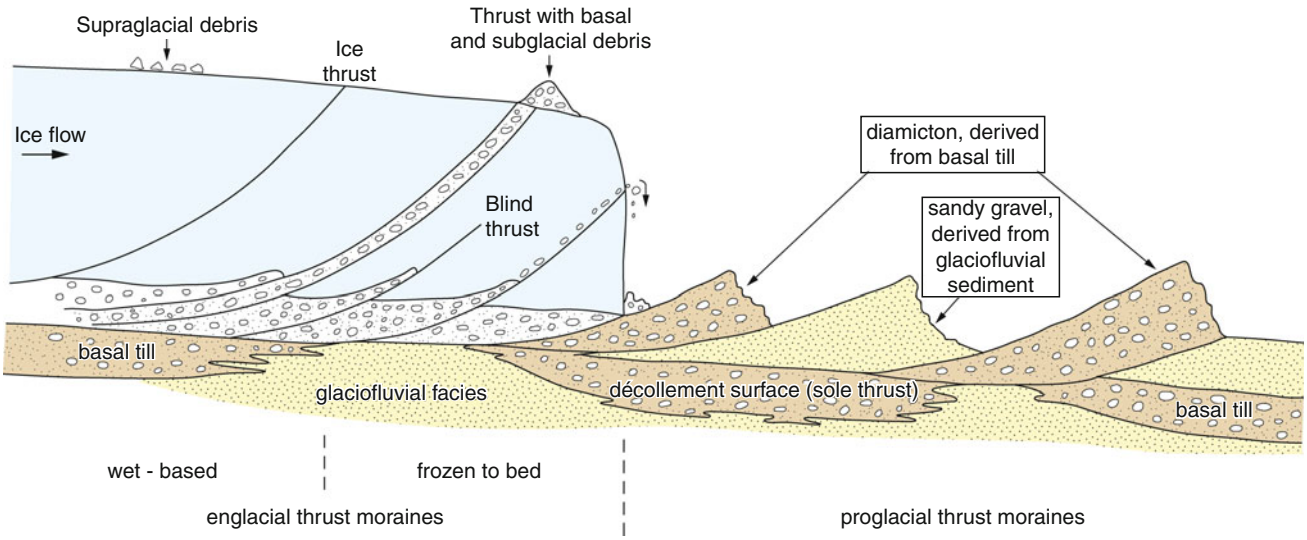

Sediment Entrainment, Transport, and Deposition, Figure 11 Simplified model of thrusting as exemplified by an advancing polythermal glacier, with thrusts propagating beyond the ice margin into frozen ground of the forefield.

Glacial depositional processes and facies

Glacial sedimentation involves the direct release of debris that has been transported on or within glacier ice. Debris is modified during transport primarily by basal processes (e.g., abrasion, crushing, and quarrying during intra-clast collision, subglacial sediment deformation), and by water in subglacial, englacial, and supraglacial stream channels. Debris that follows a passive transport path (supraglacially or englacially) tends to retain its primary characteristics.

Sediment may be deposited directly beneath the glacier or at its margins, or it can be transported significant distances from the glacier itself by other agents such as rivers or by iceberg calving. During release from the ice, numerous glacier-related processes, including reworking in marginal streams and lakes, debris flows, and aeolian activity, may modify sediment. Many glacigenic sediments may be related to specific glacial environments. For example, the temperate terrestrial glacier system is commonly regarded as being dominated by a mixture of basal (actively transported) and supraglacial (passively transported) sediment, with a strong element of glaciofluvial modification upon release (Figure 12a). Glaciers terminating in fjords produce a suite of sediments that is also dependent on thermal regime. Temperate and polythermal glaciers, such as those in Alaska and Greenland, respectively (Figure 12b), not only provide basal and supraglacial debris inputs, but also sediments released from subglacial streams emanating at or below water level close to the ice margin, sediment released from suspension over the whole depositional basin, and iceberg-rafted debris. The resulting sediment associations reflect thermal regime, which primarily controls the balance between direct glacial deposition and fluvial inputs. For the coldest glaciers, terminating as ice shelves on the continental shelf, as in Antarctica today, direct glacial deposition is restricted to the grounding line, while the volume of meltwater sediments is limited. Rather, biogenic sedimentation in the form of diatom ooze may become dominant (Figure 12c). Indeed, rather than releasing sediments, some ice shelves accrete saline ice at their base, trapping sediment, which is released only when the tabular icebergs, calved from the ice shelf, disintegrate.

Glaciotectonism

Glaciotectonic deformation is now recognized as a widespread phenomenon (Maltman et al., 2000). Commonly visible at the scale of entire moraine complexes (Figure 13), it is also widely recognized at the microscopic level and recent years have seen substantial advances in understanding the role played by deformation in the character of glacial sediments. Not only is deformation associated with internal processes, such as folding and thrusting, as noted above, but it is also transmitted subglacially and proglacially. Glaciotectonic deformation operates in any topographic setting, both during advancing and recessional phases, and involves all types of material, including frozen, saturated, and dry unconsolidated sediments, as well as bedrock. Deformation may detach blocks of rock and sediment, occasionally hundreds of meters across, incorporating them into the ice by thrusting or pushing them in front of the glacier. Faults and brecciated zones are common in such materials. Sediments may also be deformed in ductile fashion, especially if wet and fine grained. Beneath ice sheets, deformation may affect sediment and bedrock to depths of several hundred meters.

Reworking of glacigenic sediments

Glacigenic sediments are typically subject to syn-depositional and postdepositional modification by fluvial, mass-movement, and aeolian processes. In terrestrial settings, fluvial modification by proglacial streams is

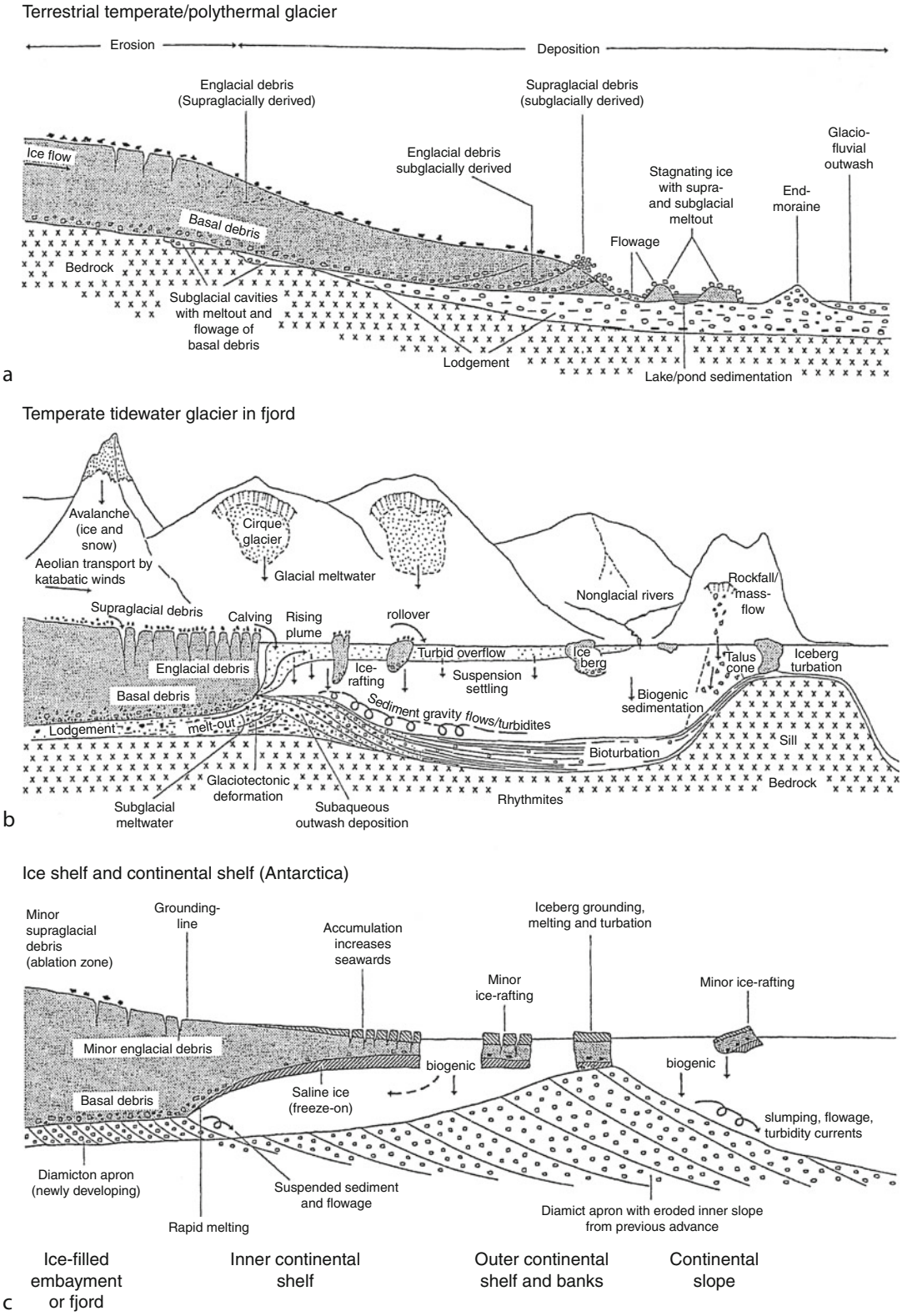

Sediment Entrainment, Transport, and Deposition, Figure 12 Depositional processes and products in a selection of glacial environments: (**a**) terrestrial, (**b**) fjord with temperate tidewater glacier, and (**c**) ice shelf on the Antarctic continental margin. (After Hambrey, 1999; published by permission of Terra Antartica, Museo Nazionale dell'Antartide, Siena.)

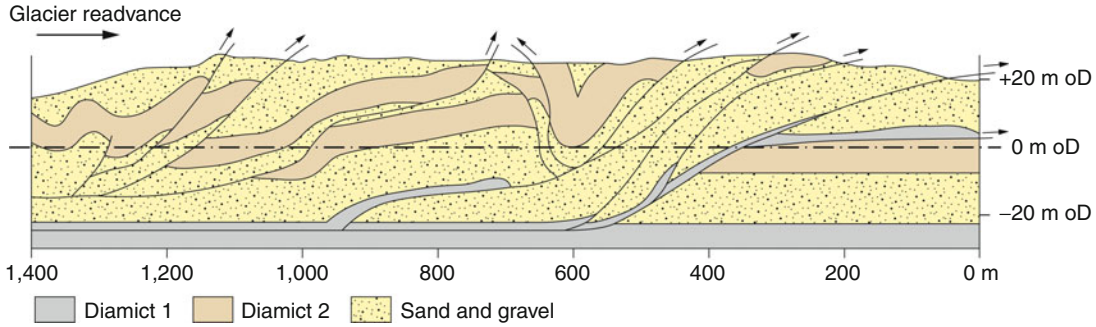

Sediment Entrainment, Transport, and Deposition, Figure 13 Glaciotectonic deformation exemplified by the push moraine complex at Dinas Dinlle, North Wales. The section is exposed in a coastal cliff and the subsurface geometry was revealed by a seismic survey. (Modified from Harris et al., 1997.)

particularly important in temperate climates, and many temperate glaciers terminate at the head of large *outwash* or *sandur* plains composed almost entirely of reworked glacial sediments. Resedimentation by mass-movement processes is common in ice-cored terrain where water, released by the melting of buried glacier ice or permafrost, mixes with sediment to create *glacigenic sediment flows*. Modification by wind, especially in cold arid environments such as Antarctica, involves the redistribution of sand and silt, creating *deflation surfaces* and *ventifacts*. The extent to which each of these processes operates is controlled to a great extent by the local topographic, meteorological, and climatological conditions. Resedimentation by subaqueous gravity flows is also important in glaciomarine and glaciolacustrine environments, where large volumes of sediment may accumulate on relatively steep ice-contact slopes that become unstable during recession.

Terminology of terrestrial glacigenic sediments

The terminology used to describe glacigenic sediment has always been in a state of flux, and the evolution of terms may be linked to progressive improvement of understanding glacial processes. For an objective study of glacigenic sediments, a nongenetic classification of poorly sorted sediments is required. The use of process-focused terms such as "till" should only follow from careful description of a wide range of attributes, including texture, clast-shape and surface characteristics, bed-geometry, and boundary relationships.

The terms *diamicton* (unlithified), *diamictite* (lithified), and *diamict* (both) are now well established for "a nonsorted or poorly sorted terrigenous sediment that contains a wide range of particle sizes" (Flint et al., 1960). However, this definition hides a vast range of textures, and the literature abounds with conflicting ideas about what constitutes a "diamicton." A textural classification, based on the relative proportions of sand and gravel, has subsequently been developed (Hambrey and Glasser, 2003) (Table 1).

The genetic terminology is perhaps even more confused. First, we need to define some widely used general terms:

Glacigenic sediment: "of glacial origin"; the term is used in the broad sense to embrace sediments that have been influenced by glacier ice.

Glacial debris: material being transported by a glacier and thus in contact with glacier ice.

Glacial drift: a general term embracing all rock material in transport by glacier ice, all deposits released by glaciers, and all deposits predominantly of glacial origin deposited in the sea by icebergs, or from glacial meltwater.

Till: sediment deposited directly by glacier ice that has not been subsequently disaggregated by flow or gravity. There are several subcategories of till, which are explained below.

Subglacial sedimentary processes

It is evident from the general nature of the above terms that texturally glacigenic sediments are exceedingly variable, and therefore a lack of consensus as to their appearance is apparent in the literature. Nevertheless, there are several processes which have been identified by which debris in transport is deposited: lodgement, meltout, flow, subglacial deformation, and sublimation. All these processes give rise to subcategories of till, and all are widespread except sublimation till, which is confined to the cold arid environment of Antarctica. This classification of till has traditionally been widely used and adopted by the International Quaternary Association (Dreimanis, 1989; Hambrey, 1994), but these distinctions have been challenged over the past decade following the development of microstructural (micromorphological) analysis of till in thin section. Indeed, most "tills" form by a combination of processes, especially in the subglacial environment, and they are thought by some to be the product of deformation rather than depositional processes; hence the new term *tectomict* (Bennett and Glasser, 2009 give an up-to-date synthesis of this issue).

Sediment Entrainment, Transport, and Deposition, Table 1 Textural classification of poorly sorted sediments (From Hambrey, 1994; modified from Moncrieff 1989). In order to derive sediment name, percent of gravel is first estimated (horizontal axis) and then the proportion or percent of sand in the matrix (vertical axis)

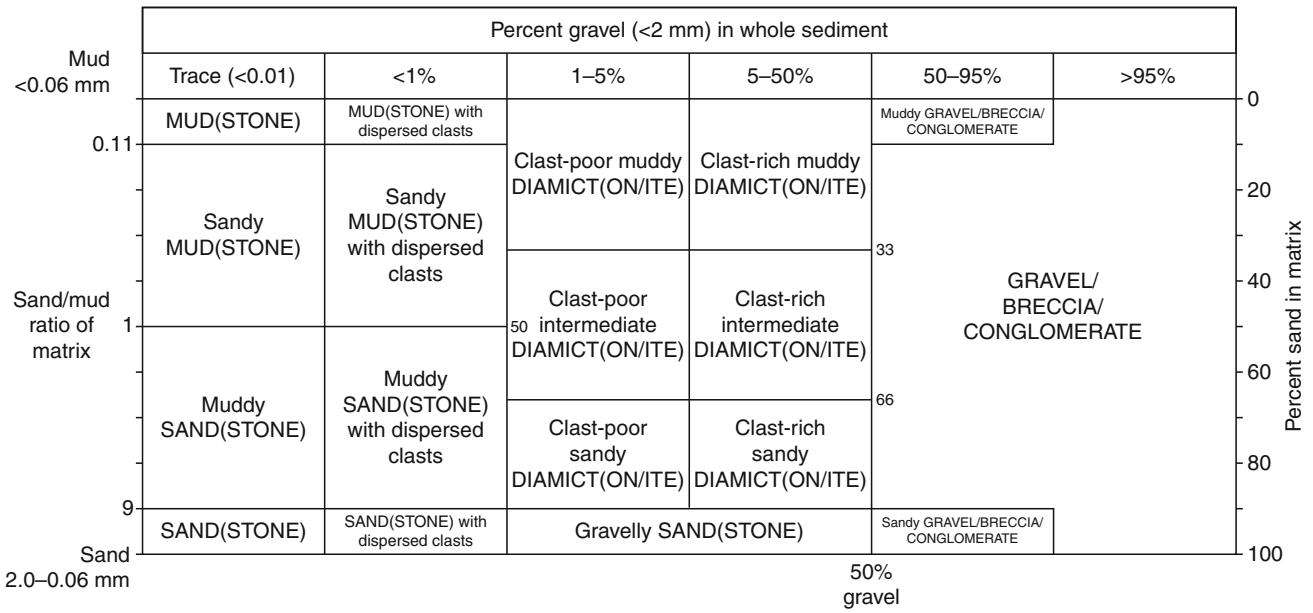

Supraglacial sedimentary processes

Debris on the glacier surface includes material that has fallen on the surface via rockfalls and passively transported as well as basally derived debris that originates where flow units combine, or where glaciotectonic processes have lifted basal sediments from the bed. This debris accumulates as a result of melting under the influence of solar radiation. A thin cover of debris will enhance melting, but as the debris accumulates, it retards melting, so debris-covered areas tend to be elevated compared with surrounding ice surfaces. Debris is concentrated into mounds and ridges, and as slopes increase in angle by the differential melting, it is prone to constant movement by sliding and slumping. Sediment thus accumulates in hollows which, when sufficiently thick, retards ablation so gradually becoming a new high point – a process known as topographic inversion.

Glaciomarine (or glacimarine) sedimentation

Glaciomarine sediments are much less studied than terrestrial glacigenic sediments, but nevertheless considerable strides in understanding have been made in recent years. Sediments are released into the ocean via several processes, giving rise to a distinctive suite of attributes that are subtly different from their terrestrial counterparts.

Ice-proximal glaciomarine sediment comprises debris that is released either from floating basal glacier ice or by continuous rain-out from icebergs, without subsequent winnowing by currents and waves.

Ice-distal glaciomarine sediment is debris that is released from icebergs, but in this case subject to winnowing and admixing with other marine sediment, including biogenic components. Texturally, this facies is sandy mud or muddy sand with dispersed clasts, and in modern environments is often rich in diatoms.

Iceberg turbate is sediment deposited on the sea floor that is subsequently reworked by grounded icebergs. The end product is commonly a massive diamicton with a heavily grooved upper surface.

Cyclopels (silt/mud couplets) and *cyclopsams* (graded sand/mud couplets) are rhythmically laminated sediments derived from turbid overflow plumes originating from subglacial discharge, especially in fjords, typically producing two couplets a day according to the tidal cycle.

Subaqueous sediment flows are the product of remobilization of all of the above sediment types. They range from massive uniform diamicton, resulting from down-slope creep or mobile flow, as on land, to well-graded beds of mud, sand and gravel where disaggregated in a turbidity flow.

Glaciolacustrine (or glacilacustrine) sedimentation

Glaciolacustrine sediments are similar to those in glaciomarine environments. In addition, lakes commonly have rhythmically laminated sand and mud called *varves*. They are similar to cyclopsams and cyclopels, but each couplet forms over 1 year.

Facies analysis of glacigenic sediments

The facies approach

For objective treatment of glacial sediments, and following other branches of sedimentology, the facies approach must be used. The first step is to describe the *lithofacies* (types of sediment) found in a vertical section or core, using a wide range of criteria (texture, sedimentary structures, bed geometry and boundary relations, clast characteristics), and avoiding genetic terms such as "till." Some authors use a formal lithofacies code (Eyles et al., 1983) which has been widely adopted, but this is thought by others (e.g., Hambrey, 1994; Miller, 1996) to be too inflexible and not totally objective as it includes interpretative elements.

The next step is to group the lithofacies into *facies associations* that contain a set of attributes that will allow the depositional setting to be determined, such as glacioterrestrial or glaciomarine. On a regional scale, given sufficient three-dimensional exposure on land, or extensive seismic and borehole stratigraphy offshore, derivation of the *facies architecture* is a desirable aim, allowing one to address larger issues, such as basin evolution, ice sheet–scale fluctuations and sea-level changes. Representative facies associations from terrestrial, lacustrine, and glaciomarine settings are illustrated in Figure 14.

Glacial sediment/landform associations

The concept of *glacial sediment/landform associations* (the "*landsystem*" approach) rests on the assumption that, at the large scale, it is possible to identify areas of land with common attributes, distinct from the surrounding areas, that can be related to the processes involved in their development (Benn and Evans, 2010; Evans, 2003). The landsystem approach was pioneered for glaciated terrain in an attempt to identify tracts of land created by similar till-forming processes and therefore of similar geotechnical properties. The *glacial landsystem* concept was then applied to former ice-sheet beds. Originally, three distinct landsystems were defined: (1) the *subglacial landsystem*, in which the dominant glacial sediment/landform associations are formed at the glacier bed; (2) the *supraglacial landsystem*, in which the dominant glacial sediment/landform associations are largely composed of a drape of supraglacial debris; and (3) the *glaciated valley landsystem*, in which the dominant glacial sediment/landform association is that formed by mountain glaciation.

As the concept has developed, other landsystems have been added to this simple list (Evans, 2003). These include landsystems formed in proglacial and glaciomarine environments, as well as those found in settings where surge-type glaciers are common. It is also possible to define landsystems according to glacier thermal regime. Thus we can identify landsystems related to warm-based ("temperate"), polythermal, and cold-based ("polar") glacier margins. A criticism of the landsystems approach is that it takes little account of spatial patterns of ice-sheet erosion and deposition, and how these vary during ice-sheet growth and decay.

Glacial depositional landforms

Glaciers and ice sheets produce a huge variety of depositional landforms that are commonly grouped according to their origin into ice-marginal and subglacial types (Hambrey, 1994; Menzies, 1995, 1996; Bennett and Glasser, 2009; Benn and Evans, 2010). Distinguishing between the different types of moraine is important for reconstructing the size, morphology, and dynamics of former ice masses.

Ice-marginal landforms. Ice-marginal landforms can be produced by advancing, stationary, or receding ice margins, as well as during seasonal fluctuations of the glacier terminus. These landforms include *glaciotectonic moraines, push moraines, dump moraines*, and *thrust-block moraines* (Figure 11).

Ablation moraines (sometimes referred to as *ice-cored moraines*) form wherever ice-melt is retarded beneath a cover of supraglacial debris (Figure 12). If the cover of insulating debris is irregular, irregular ridges and mounds of debris, referred to as *hummocky moraines* or *moraine-mound complexes*, will develop.

Subglacial landforms (sometimes referred to as *subglacial bedforms*) are produced beneath actively flowing ice. They provide information about former subglacial conditions, including ice-flow directions, thermal regime, and paleohydrology. The most common of these is a family of ice-molded landforms, all of which are parallel to ice flow. This includes *flutes, megaflutes, mega-scale glacial lineations*, and *drumlins.*

Ribbed moraines (also known as *Rogen moraines*) are large, regularly and closely spaced moraine ridges consisting of glacigenic sediment.

Geometric ridge networks and *crevasse-fill ridges* are subglacial landforms that are not generally ice-molded. They form by the squeezing of subglacial material into basal crevasses or former subglacial tunnels, commonly during surges, or beneath glaciers as a result of the intersection of foliation-parallel ridges and englacial thrusts.

Eskers are glaciofluvial landforms created by the flow of meltwater in subglacial, englacial, or supraglacial channels. *Concertina eskers* are deformed eskers, created by compression beneath overriding ice.

Outwash fans and *outwash plains* (or *sandar*, plural; *sandur*, singular) are formed as glacial meltwater emerges from the glacier and sediment is deposited at or beyond the ice margin. Outwash fans form at stationary ice margins where meltwater is concentrated at a particular point for a length of time. Outwash plains are much larger features, formed where individual fans coalesce away from the glacier to create a braided-river facies association. Characteristics of the glaciofluvial environment are braided river channels with rapidly migrating bars, terraces, frequent channel avulsions, and the formation of *kettle holes* where sediment is deposited over buried ice.

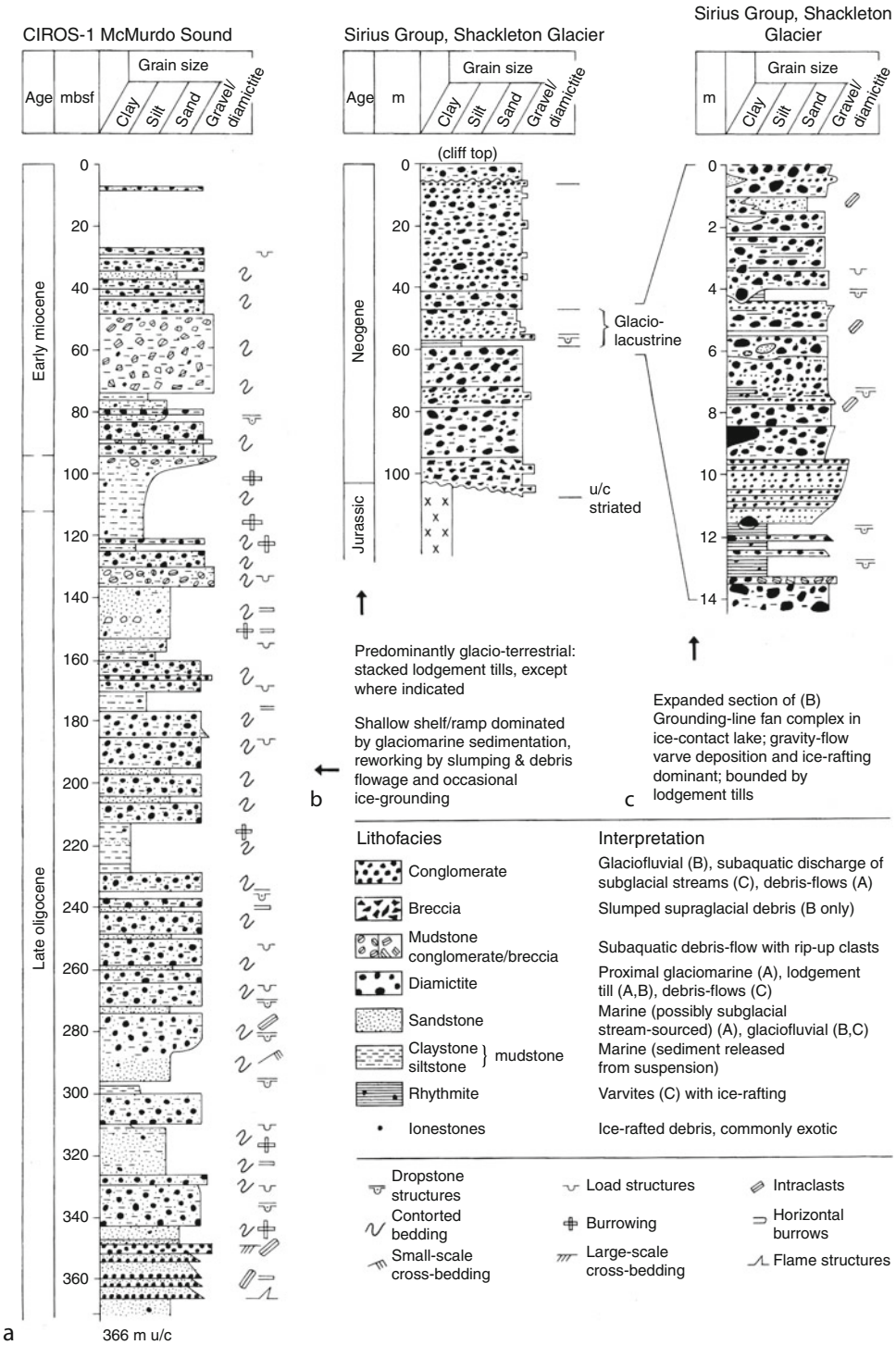

Sediment Entrainment, Transport, and Deposition, Figure 14 Characteristic glacigenic facies associations from marine and terrestrial settings in Antarctica. (**a**) Late Oligocene – Early Miocene proximal continental shelf facies association, upper part of CIROS-1 drill-core, McMurdo Sound, illustrating deposition in a subsiding rift-basin, with occasional ice-grounding events (after Barrett, 1989). (**b**) A terrestrial glacigenic facies association dominated by repeated lodgement till deposition, represented by stacked diamictites, but with a lacustrine phase of sedimentation in midsection: Sirius Group (Neogene), Shackleton Glacier, Transantarctic Mountains. (**c**) Enlargement of the glaciolacustrine facies association in B illustrating ice-proximal deposition dominated by slumping and debris flowage of rain-out diamictite and varve-sedimentation. (From Middleton, 2003 published with permission of Kluwer Publishers, Dordrecht.)

Kame terraces are formed when sediment is deposited by meltwater flowing laterally along an ice margin. *Kames* are more fragmentary features, formed in a similar manner, but often in ice-walled tunnels and against steep valley sides. *Kame-and-kettle topography* is the term used to describe the landform-sediment assemblage often found on glacier forefields where there was formerly a high proportion of buried ice.

Bathymetric forms resulting from glacial processes

Erosional forms

Various erosional phenomena, mainly associated with grounded ice or subglacial meltwater are found in marine settings. The larger-scale forms are filled by sediment and may be recognizable in seismic profiles (e.g., Anderson, 1999). *Submarine troughs* are found on continental shelves, and are genetically equivalent to fjords and other glacial troughs, but are generally much broader. Formed by ice streams, the largest occur in Antarctica where they attain dimensions of over 400 km in length, 200 km in width, and 1,100 m in depth. Where two ice streams merge, an *ice-stream boundary ridge* is formed. Steep-sided channels a few kilometers wide, carved out by subglacial meltwater and subsequently filled by sediment are known as *tunnel valleys*. These are well known from the NW European continental shelf around Britain, the Scotian Shelf off Canada, and in Antarctica. Icebergs can also cause considerable erosion as they become grounded on the sea floor. Large tabular bergs can scour the bed of the sea for several tens of kilometers, leaving impressions up to 100 m wide and several meters deep. *Slope valleys* are groups of gullies forming a dendritic pattern that develop just beyond the ice margin, on the continental slope, as a result of erosion by sediment gravity flows that emanate from sediment accumulation at the ice margin. On continental shelf areas, where the ice repeatedly becomes grounded, and then releases a large amount of rain-out sediment, alternations of diamicton and *boulder pavements* may be observed. The pavements build up by accretion of boulders around an obstacle, by subglacial erosion, or they represent a lag deposit from winnowing by bottom currents.

Depositional forms

The morphology and sediment composition of subaquatic features, particularly in fjords and on continental shelves are less well known than their terrestrial counterparts, but major strides have been made in identifying such features in the last 3 decades. As on land, depositional assemblages reflect the interaction of a wide range of processes and they comprise a diverse range of sediments.

Ice-contact features form when a glacier terminus remains almost stationary in water, particularly in fjords (Powell and Cooper, 2002). *Morainal banks* form by a combination of meltout from basal ice, dumping of englacial and supraglacial debris, push and squeeze processes, combined with glaciofluvial discharge. The end product is an assemblage of poorly sorted deposits with some evidence of glaciotectonically disturbed stratification (Figure 15). *Grounding-line fans* extend from a subglacial tunnel that discharges meltwater and sediment into the sea, and are typically composed of sand and gravel. A series of such fans may develop if glacier recession is interrupted. Developing out of grounding-line fans are *ice-contact deltas* that form when the terminus remains stable long enough for sediment to build up to the surface of the fjord. Where a glacier becomes disconnected from the water body, alluvial sediments may prograde to form *fluviodeltaic complexes*, which comprise sand and gravel. In addition to these large-scale forms (measured in hundreds of meters), there are small-scale features (measured in meters or less), found particularly on beaches, such as iceberg tool-marks, ridges, depressions from melting of buried ice, bounce-marks, chattermarks, and roll-marks. Icebergs can also churn up submarine sediment, particularly on shoals, producing *iceberg turbates*.

Depositional forms on continental shelves are best known from a combination of deep drilling and seismic profiling. Some, as in Alaska, are simply larger-scale analogues of fjordal features, such as delta-fan complexes, but others form under floating tongues that are typical of the colder ice of the polar regions. These include subglacial deltas, till tongues, diamicton aprons, and the immense (up to 400 km wide) trough-mouth fans, all of which are commonly associated with ice streams. Other features are similar to those on land, including shelf moraines, flutes, mega-scale glacial lineations, and transverse ridges.

Glacial sediments in the geological record

Identification of glaciation in the geological record

The recognition of glacigenic sediments and landforms in the rock record is of fundamental importance to the emerging field of paleoglaciology, which embraces paleoclimatological and paleoenvironmental reconstructions. Even where exposure is good, evidence for glaciation may be equivocal as, for example, in alpine regions where mass-movement and fluvial processes may overprint direct evidence for glacial deposition, or in those areas where tectonic deformation has overprinted depositional features. However, detailed analysis may yield sufficient criteria that, taken together, could form the basis of a glacial interpretation.

Preservation potential of glacigenic successions

Tectonic setting is the principal control on whether a glacial succession is preserved. Eyles (1993) provided a detailed review of the wide range of tectonic settings suitable for preservation. Intracratonic basins, rifts, forearc and backarc basins, and subsiding continental shelves are particularly suitable receptacles for accumulation and preservation of glacial sediments, especially if those sites are first buried and later uplifted and exposed. Except for deposits of Quaternary age, land areas are less likely to preserve glacial sediment, as continued erosion tends to

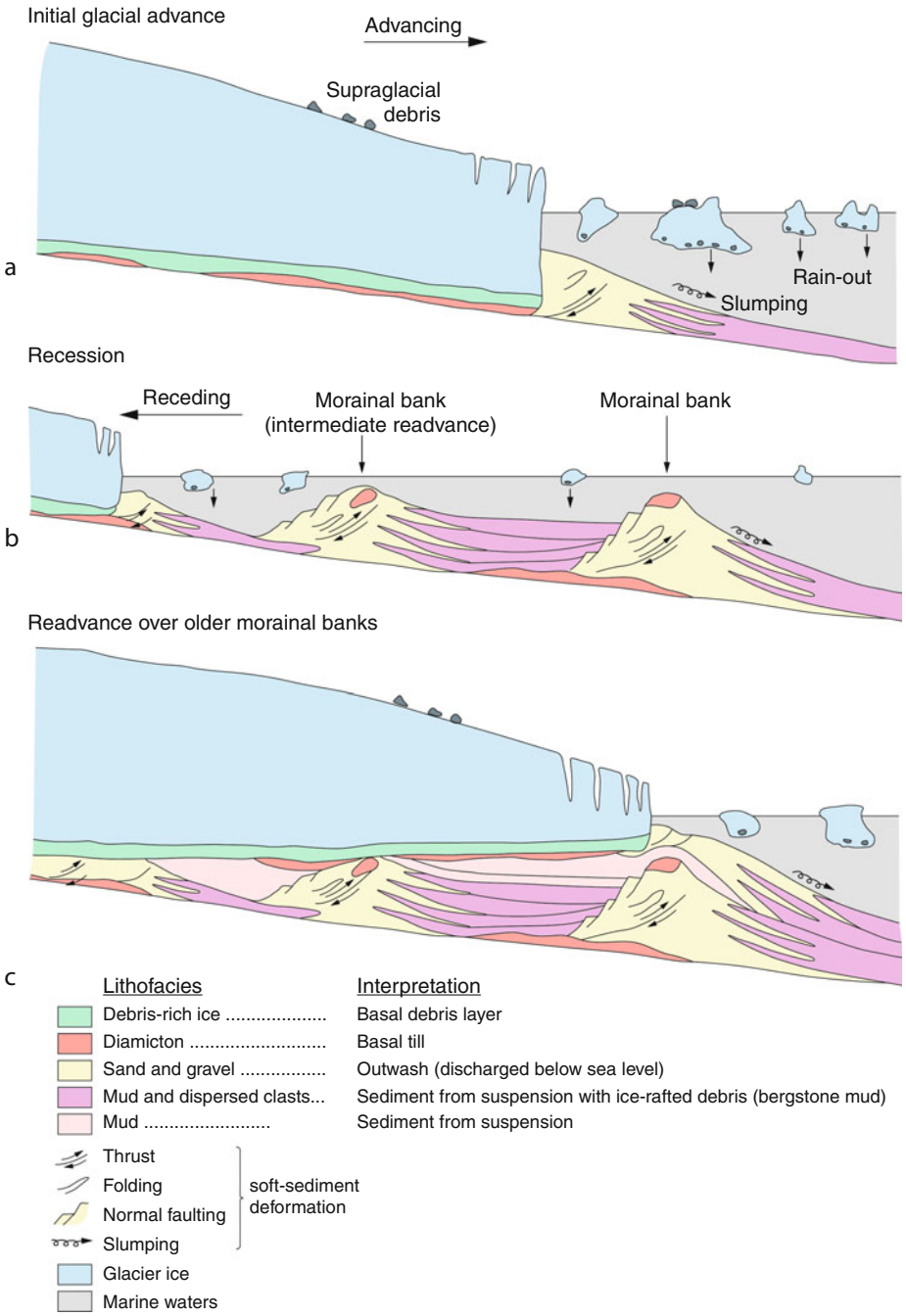

Sediment Entrainment, Transport, and Deposition, Figure 15 Conceptual model for the development of the morainal bank facies association, as exemplified by the succession recovered by the Cape Roberts Drilling Project, western McMurdo Sound, Antarctica. (Simplified from Powell and Cooper, 2002.)

remove traces of glaciation. There are, however, notable exceptions in the geological record.

Earth's glacial record

Far more is known about the Quaternary glaciations than all previous glaciations put together, even though some of those earlier events were equally dramatic in terms of scale. Since the International Geological Correlation Programme compiled an inventory of all known pre-Quaternary glacigenic sequences (Hambrey and Harland, 1981), several syntheses have been undertaken (e.g., Eyles, 1993; Deynoux et al., 1994; Crowell, 1999). For the Quaternary Period there is a vast literature from which to choose.

The oldest known glacigenic sediments are of late Archaean age (2,600–3,100 Ma) from South Africa. Extensive Paleoproterozoic (2,500–2,000 Ma) tillites are known from South Africa, Australia, and Finland. The most prolonged and globally extensive glacial era took place in Neoproterozoic time (1,000–550 Ma). Evidence for glaciation occurs on all continents, leading to the "snowball earth" hypothesis that envisages the Earth being totally ice covered, although this concept has proved highly controversial (Allen and Etienne, 2008). Sporadic Early Paleozoic glacial events are best represented by the late Ordovician to early Silurian deposits and erosional features of the supercontinent of Gondwana, notably in Africa. The most prolonged and extensive phase of glaciation during the Phanerozoic Eon spanned about 90 Ma of the Carboniferous and Permian Periods, affecting all Gondwana continents. Finally, after a phase of global warmth, with little evidence of ice on Earth, the Cenozoic glaciations began in Antarctica at the Eocene/Oligocene transition (c. 34 Ma). Northern Hemisphere glaciation followed, with minor ice-rafting events recorded in the North Atlantic from late Miocene time, until full-scale glaciations began in late Pliocene time (2.4 Ma) and continued through the Quaternary to the present day.

Summary

Sediment entrainment, transport, and deposition are important in understanding the legacy of former glaciers and ice sheets. The entrainment and transport processes depend primarily on glacier mass balance, dynamics, structure, thermal regime, hydrology, and morphology. Sediment entrainment takes place at the bed and the surface of a glacier, and there are transfers between both zones. Structural evolution plays a key role in defining the distribution of sediment through a glacier. Structural processes are also evident in the depositional environment, especially in terms of glaciotectonic deformation of sediments and landforms, for example, through folding and thrusting. Systematic analysis of the sedimentary record following deposition, through the facies approach, allows inferences to be made about the environments of deposition and paleoclimates, and approach which is valid not only for understanding the Quaternary record, but also that of ancient glaciations.

Bibliography

Allen, P. A., and Etienne, J. L., 2008. Sedimentary challenge to snowball Earth. *Nature Geoscience*, **1**, 817–825.

Anderson, J. B., 1999. *Antarctic Marine Geology*. Cambridge: Cambridge University Press, 297 p.

Barrett, P. J. (ed.), 1989. *Antarctic Cenozoic History from the CIROS-1 Drillhole, McMurdo Sound*. Wellington: DSIR Publishing. DSIR Bulletin 245.

Benn, D. I., and Evans, D. J. A., 2010. *Glaciers and Glaciation*, 2nd edn. London: Arnold.

Bennett, M. R., and Glasser, N. F., 2009. *Glacial Geology: Ice Sheets and Landforms*. Chichester: Wiley.

Boulton, G. S., 1996. Theory of glacial erosion, transport and deposition as a consequence of subglacial sediment deformation. *Journal of Glaciology*, **42**, 43–62.

Crowell, J. C., 1999. Pre-Mesozoic ice ages: Their bearing on understanding the climate system. Geological Society of American Memoir 192, pp. 1–106.

Deynoux, M., Miller, J. M. G., Domack, E. W., Eyles, N., Fairchild, I. J., and Young, G. M., 1994. *Earth's Glacial Record*. Cambridge: Cambridge University Press.

Dreimanis, A., 1989. Tills, their genetic terminology and classification. In Goldthwait, R. P., and Matsch, C. L. (eds.), *Genetic Classification of Glacienic Deposits*. Rotterdam: Balkema, pp. 17–84.

Evans, D. J. A. (ed.), 2003. *Glacial Landsystems*. London: Arnold.

Eyles, N., 1993. Earth's glacial record and its tectonic setting. *Earth Science Reviews*, **35**, 1–248.

Eyles, N., Eyles, C. H., and Miall, A. D., 1983. Lithofacies types and vertical profile models; an alternative approach to the description and environmental interpretation of glacial diamict and diamictite sequences. *Sedimentology*, **30**, 393–410.

Flint, R. F., Sanders, J. E., and Rodgers, J., 1960. Diamictite: a substitute term for symmictite. *Geological Society of America Bulletin*, **71**, 1809–1810.

Hambrey, M. J., 1994. *Glacial Environments.* Vancouver: University of British Columbia Press, and London: UCL Press.

Hambrey, M. J., 1999. The record of Earth's glacial history during the last 3000 Ma. In Barrett, P. J., and Orombelli, G. (eds.), *Geological Records of Global and Planetary Changes*. Terra Antartica Reports 3, Siena, Italy, pp. 73–107.

Hambrey, M. J., and Glasser, N. F., 2003. Glacial sediments: processes, environments and facies. In Middleton, G. V. (ed.), *Encyclopedia of Sediments and Sedimentary Rocks*. Dordrecht: Kluwer, pp. 316–331.

Hambrey, M. J., and Harland, W. B., 1981. *Earth's Pre-Pleistocene Glacial Record*. Cambridge: Cambridge University Press.

Hambrey, M. J., and Lawson, W. J., 2000. Structural styles and deformation fields in glaciers: a review. In Maltman, A. J., Hubbard, B., and Hambrey, M. J. (eds.), *Deformation of Glacial Materials*. London: Geological Society of London. Special Publication, 176, pp. 59–83.

Hambrey, M. J., Bennett, M. R., Dowdeswell, J. A., Glasser, N. F., and Huddart, D., 1999. Debris entrainment and transfer in polythermal valley glaciers. *Journal of Glaciology*, **45**, 69–86.

Harris, C., Brabham, P. J., Williams, G. D., and Eaton, G., 1997. The nature and significance of glaciotectonic structures at Dinas Dinlle, northwest Walesm UK. *Quaternary Science Reviews*, **18**, 109–127.

Hubbard, B., Cook, S., and Coulson, H., 2009. Basal ice facies: a review and unifying approach. *Quaternary Science Reviews*, **28**, 1956–1969.

Knight, P. G., 1997. The basal ice layer of glaciers and ice sheets. *Quaternary Science Reviews*, **16**, 975–993.

Maltman, A. J., Hubbard, B., and Hambrey, M. J. (eds.), 2000. *Deformation of Glacial Materials*. London: Geological Society of London. Special publication, 176.

Menzies, J. (ed.), 1995. *Modern Glacial Environments: Processes, Dynamics and Sediments*. Oxford: Butterworth-Heinemann.

Menzies, J. (ed.), 1996. *Past Glacial Environments: Sediments, Forms and Techniques*. Oxford: Butterworth-Heinemann.

Middleton, G. V. (ed.), 2003. *Encyclopedia of Sediments and Sedimentary Rocks*. Dordrecht: Kluwer.

Miller, J. M. G., 1996. Glacial sediments. In Reading, H. G. (ed.), *Sedimentary Environments: Processes, Facies and Stratigraphy,* 3rd edn. Oxford: Blackwell Science, Chap. 11, pp. 454–484.

O'Cofaigh, C., and Dowdeswell, J. A. (eds.), 2002. *Glacier-Influenced Sedimentation on High-Latitude Continental Margins*. London: Geological Society. Special publication, 203.

Paterson, W. S. B., 1994. *Physics of Glaciers*. Oxford: Pergamon.
Powell, R. D., and Cooper, J. M., 2002. A glacial sequence stratigraphic model for temperate, glaciated continental shelves. In O'Cofaigh, C., and Dowdeswell, J. A. (eds.), *Glacier-Influence Sedimentation on High-Latitude Continental Margins*. London: Geological Society, Special publication 203, pp. 215–244.

Cross-references

Cold-Based Glaciers
Debris
Debris-Covered Glaciers
Englacial Processes
Formation and Deformation of Basal Ice
Glacier Hydrology
Glacier Motion/Ice Velocity
Glacier Surging
Meltwater Channels
Moraine
Polythermal Glaciers
Retreat/Advance of Glaciers
Sediment Core and Glacial Environment Reconstruction
Structural Glaciology
Temperate Glaciers
Till
Transformations of Snow at the Earth's Surface and its Climatic and Environmental Consequences

SEDIMENT FLUX SOURCE-TO-SINK

Achim A. Beylich
Quaternary Geology and Climate Group, Geological Survey of Norway (NGU), Trondheim, Norway
Department of Geography, Norwegian University of Science and Technology (NTNU), Trondheim, Norway

Synonyms

Sediment transfer source-to-sink; Sediment transport source-to-sink

Definition

Erosion (mobilization), transport (transfer), and deposition (accumulation, storage) of sediment within a defined area (landscape unit).

Introduction

Geomorphologic processes, responsible for transferring sediments and affecting landform change, are highly dependent on climate, and it is anticipated that climate change will have a major impact on the behavior of Earth surface systems. Research on sedimentary fluxes from source to sink in a variety of different climatic environments is very well documented in the literature. Studies on source-to-sink fluxes generally refer to the development of sediment budgets. A sediment budget is an accounting of the sources and disposition of sediment as it travels from its point of origin to its eventual exit from a defined landscape unit like a drainage basin (e.g., Reid and Dunne, 1996). Accordingly, the development of a sediment budget necessitates the identification of processes of erosion, transport, and deposition within a defined area, and their rates and controls (Reid and Dunne, 1996; Slaymaker, 2000; Beylich and Warburton, 2007). The fundamental concept underpinning source-to-sink sediment flux and sediment budget studies is the basic sediment mass balance equation:

$$I = O + -\Delta S$$

where inputs (I) equal outputs (O) plus changes in net storage of sediment (ΔS). Source-to-sink study allows quantification of the transport and storage of sediment in a system. A thorough understanding of the current sediment production and flux regime within a system is fundamental to predict likely effects of changes to the system, whether climatic induced or human influenced. Source-to-sink sediment flux and sediment budget research therefore enables the prediction of changes to erosion and sedimentation rates, knowledge of where sediment will be deposited, how long it will be stored, and how much sediment will be remobilized (Gurnell and Clark, 1987; Reid and Dunne, 1996; Beylich and Warburton, 2007).

Sediment sources

Sediments are eroded and mobilized in source areas. Sediment sources are diverse and subject to variation in response to climate change. Global warming leads to the loss of glacial ice, which in turn increases slope instability caused by glacial de-buttressing, and flooding from glacial and moraine-dammed lakes (Evans and Clague, 1994; Ballantyne, 2002). All these processes redistribute sediments and operate at different rates as a result of change to the system. Glaciers and ice sheets exert strong controls on the supply of sediments. For example, Knight et al. (2002) identify the basal ice layer of a section of the Greenland ice sheet as the dominant source of sediment production. There is, however, only limited knowledge of debris fluxes from ice sheets and glaciers, and its variability. The main mechanisms of sediment production in source areas can be described in terms of contemporary environmental conditions. However, in order to fully understand sediment supply, a longer-term perspective is needed. Over the Quaternary, glacier fluctuations have had profound influences in depositing extensive mantles of sediments. More-widely, periglacial activity has altered the landscape under non-glacial cold climate conditions. The obvious imprint of this legacy is often reflected in contemporary sediment transfer rates where preexisting deposits are eroded by present-day processes (Ballantyne, 2002; Warburton, 2007).

Sediment transfers

Sediment transfers move eroded sediments from their source area to an area of temporal storage or long-term deposition in sinks. Rates of sediment transfer are not only conditioned by competence of geomorphic processes but

also by the availability of sediment for transport. Accordingly, in assessing sediment transfer, we need to quantify the forces that drive transport processes but equally account for the factors that control sediment supply (Warburton, 2007). Glacial fluxes are arguably the most significant processes for contemporary sediment flux (Harbor and Warburton, 1992). Small-scale process studies very often focus on sedimentary fluxes from areas of weathering and erosion to areas of storage within defined landscape units like drainage basins, whereas large-scale sediment systems couple headwaters to oceanic sinks. For example, Gordeev (2006), applying models developed by Morehead et al. (2003), estimates the increase in sediment load in Arctic rivers in response to a rise in surface temperature of the drainage basins. Based on this model, increases in river discharge lead to an increase in the sediment flux of the six largest Arctic rivers, predicted to range from 30% to 122% by the year 2100.

Sediment stores/sinks

The identification of storage elements and sinks is critical to the effective study and understanding of source-to-sink sedimentary fluxes (Reid and Dunne, 1996). The setting of a particular drainage basin defines the boundary conditions for storage within that landscape unit. In a defined landscape unit like a drainage basin, the slope and valley infill elements constitute the key storage units and storage volumes are important for addressing time-dependent sediment budget dynamics. Dating of storage in sedimentary source-to-sink flux studies is applied to determine or estimate the age and chronology of the storage components within the system. An understanding of the nature of primary stores, secondary stores, and the potential storage capacities of different types of drainage basins is important along with knowledge of sediment residence times. Of growing importance is the development of innovative field methods, such as geophysical techniques for estimating sediment storage volumes (Schrott et al., 2003; Sass, 2005; Hansen et al., 2009). Within large-scale sediment systems, oceanic sinks are most important and provide the opportunity to estimate rates of sediment production and delivery at long-term temporal as well as continental spatial scales (Rise et al., 2005; Dowdeswell et al., 2006).

Summary

Studies on sedimentary fluxes from source to sink are an accounting of the sources and deposition of sediment as it travels from its point of origin to its eventual exit from a defined area. The connected development of a sediment budget necessitates the identification of processes of erosion, transport, and deposition within this defined area, and their rates and controls. Within the scope of climate change research, knowledge on the contemporary sediment production and flux regime within a system enables the prediction of possible future changes to erosion and sedimentation rates. In addition, improved knowledge of where sediment will be deposited, how long it will be stored and how much sediment will be remobilized can be achieved. The main mechanisms of sediment production in source areas can be described in terms of contemporary environmental conditions. However, in order to fully understand sediment supply also a long-term perspective is required. Sediment transfers move eroded sediments from their source area to an area of temporal storage or long-term deposition in sinks, with glacial fluxes being arguably the most significant processes for sediment flux. An understanding of the nature of primary stores, secondary stores, and the potential storage capacities of different types of drainage basins is important along with knowledge of residence times. Within large-scale sediment systems oceanic sinks are most important and provide the opportunity to estimate rates of sediment production and delivery at large temporal and spatial (continental) scales.

Bibliography

Ballantyne, C. K., 2002. Paraglacial geomorphology. *Quaternary Science Reviews*, **21**, 1935–2017.

Beylich, A. A., and Warburton, J. (eds.), 2007. Analysis of source-to-sink-fluxes and sediment budgets in changing high-latitude and high-altitude cold environments: SEDIFLUX Manual. *NGU Report* 2007.053.

Dowdeswell, J. A., Ottesen, D., and Rise, L., 2006. Flow switching and large-scale deposition by ice streams draining former ice sheets. *Geology*, **34**, 313–316.

Evans, S. G., and Clague, J. J., 1994. Recent climate change and catastrophic geomorphic processes in mountain environments. *Geomorphology*, **10**, 107–128.

Gordeev, V. V., 2006. Fluvial sediment flux to the Arctic Ocean. *Geomorphology*, **80**, 94–104.

Gurnell, A. M., and Clark, M. J. (eds.), 1987. *Glacio-Fluvial Sediment Transfer: An Alpine Perspective*. Chichester: Wiley.

Hansen, L., Beylich, A. A., Burki, V., Eilertsen, R., Fredin, O., Larsen, E., Lysså, A., Nesje, A., Stalsberg, K., and Tønnesen, J.-F., 2009. Stratigraphic architecture and infill history of a deglaciated bedrock-valley based on georadar, seismic profiling and drilling. *Sedimentology*, **56**, 1751–1773.

Harbor, J., and Warburton, J., 1992. Glaciation and denudation rates. *Nature*, **356**, 751.

Knight, P. G., Waller, R. I., Patterson, C. J., Jones, A. P., and Robinson, Z. P., 2002. Discharge of debris from ice at the margin of the Greenland ice sheet. *Journal of Glaciology*, **48**, 192–198.

Morehead, M. D., Syvitski, J. P., Hutton, E. W., and Peckham, S. D., 2003. Modeling the temporal variability in the flux of sediment from ungauged river basins. *Global and Planetary Change*, **39**, 95–110.

Reid, L. M., and Dunne, T., 1996. *Rapid evaluation of sediment budgets*. Cremlingen: Catena.

Rise, L., Ottesen, D., Berg, K., and Lundin, E., 2005. Large-scale development of the mid-Norwegian margin during the last 3 million years. *Marine and Petroleum Geology*, **22**, 33–44.

Sass, O., 2005. Spatial patterns of rockfall intensity in the northern Alps. *Zeitschrift für Geomorphologie N.F. Suppl.-Bd*, **138**, 51–65.

Schrott, L., Hufschmidt, G., Hankammer, M., Hoffmann, T., and Dikau, R., 2003. Spatial distribution of sediment storage types and quantification of valley fill deposits in an alpine basin, Reintal, Bavarian Alps, Germany. *Geomorphology*, **55**, 45–63.

Slaymaker, O., 2000. Research developments in the hydrological sciences in Canada (1995–1998): Surface water – quantity, quality and ecology. *Hydrological Processes*, **14**, 1539–1550.
Warburton, J., 2007. Sediment budgets and rates of sediment transfer across cold environments in Europe: a commentary. *Geografiska Annaler*, **89A**(1), 95–100.

Cross-references

Climate Change and Glaciers
Glacial Erosion
Sediment Budgets
Sediment Yield

SEDIMENT GRAVITY FLOW

George Postma
Faculty of Geosciences, EUROTANK Laboratories, TA Utrecht, The Netherlands

Synonyms

Density currents; Gravity currents; Mass flows; Sediment flows

Definition

Sediment gravity flows are mixtures of water and sediment particles where the gravity acting on the sediment particles moves the fluid, in contrast to rivers, where the fluid moves the particles.

Introduction

Sediment gravity flows are catastrophic subaerial and subaqueous events that occur at various frequencies. An event can originate from sliding of unstable sediment mass on a slope, in which case the trigger is often by storm, tidal wave, seismic shock, or heavy rainfall. It can also originate from flood wave in a river that debouches onto the delta slope, where it, if denser than the basin water, first plunges down as hyperpycnal flow and continues as sediment gravity flow.

Sediment gravity flows have the ability to transport large masses of coarse-grained sediment into places, where otherwise only fines are deposited from suspension. Their deposits have been found in oceanic basins at 5 km depth at more than 2,000 km away from the continental slope, but also occur almost everywhere on land and in shallow seas and lakes and occur also in present-day glacial environments.

Since the rheology of sediment gravity flows varies and has great impact on the type of deposits, first an overview is given of this variation, which is followed by an impression of how rheology and flow characteristics (density, velocity) is reflected in the deposits. Finally, their occurrence in the glacial environments is highlighted.

Rheology of sediment gravity flows

The rheology of sediment gravity flows falls into two main classes of flow behavior that are fundamentally different and which difference is often reflected in the final deposit. The first class is characterized by fluidal behavior similar to Newtonian fluid, where shear stress is linearly related to strain according to

$$\sigma_s = \mu \,.\, \varepsilon_s \quad \left[\mathrm{N/m^2}\right] \tag{1}$$

where σ_s is the shear stress, μ is the apparent viscosity, and ε_s is rate of shear strain. In a fluid the shear strain is measured by the velocity gradient, hence dU/dz, where U is velocity at height z in the flow. Characteristic for waning, fluidal flow is that deposition occurs from the bed upward. Such depositional behavior is in sharp contrast with the second class of sediment gravity flow with plastic-viscous flow behavior. Such flows exhibit strength, while above the yield point viscous deformation occurs. Their rheology is described by the Coulomb-viscous model (Johnson, 1970, Figure 1):

$$\sigma_s = k + \mu_b.\varepsilon_s \quad \left[\mathrm{N/m^2}\right] \tag{2}$$

where k is the yield strength, μ_b is the Bingham viscosity, and ε_s rate of shear strain. The expression tells us that above the yield strength k the flow behaves viscous and has a linear viscosity called the Bingham or plastic viscosity. The apparent viscosity may be shear stress related and deformation above the yield strength is in such case non-Newtonian. Flow of plastic-viscous sediment mass is characterized by a nondeforming rigid plug which is riding on a viscously deforming basal layer, a behavior that

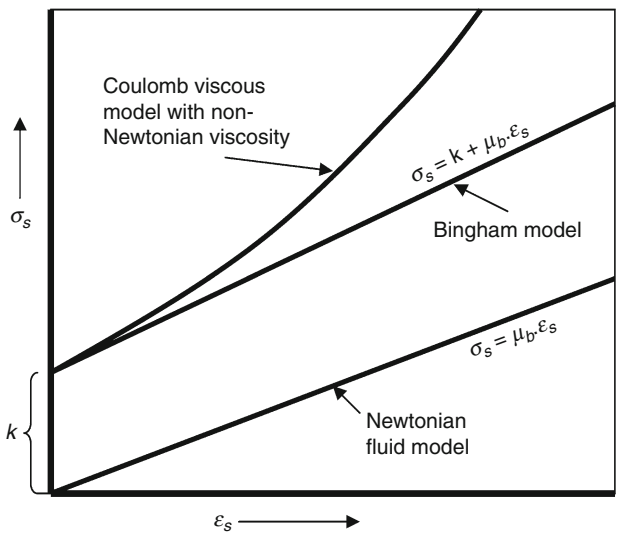

Sediment Gravity Flow, Figure 1 Diagram showing the Bingham rheological model: If strength $k = 0$, the flow experiences only Newtonian viscous deformation. In case of nonlinear viscous deformation, the viscosity is stress depended and non-Newtonian.

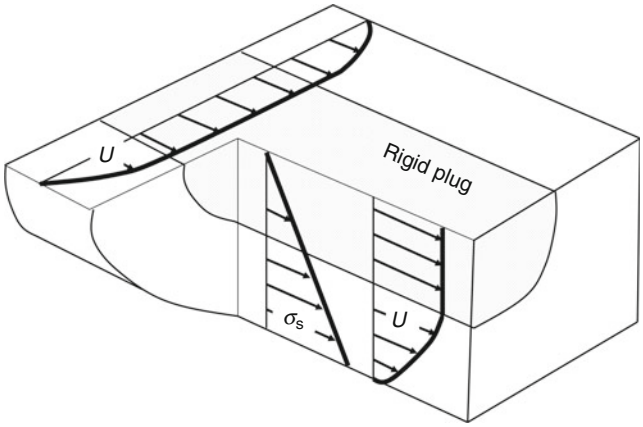

Sediment Gravity Flow, Figure 2 Plastic-viscous flow characterized by the formation of a rigid plug if the shear stress σ_s is equal or less than the shear strength k (see Eq. 2). The velocity gradient in the plug is zero.

is exemplified by the flow of concrete cement (Figure 2). The plug exists for $\sigma_s \leq k$.

The strength k within a debris flow mass is a function of the effective normal stress (σ') through the relationship

$$k = c' + \sigma \tan \Phi \quad [\mathrm{N/m^2}] \tag{3}$$

where c' is the effective cohesion and Φ' is the effective angle of internal friction (Rodine and Johnson, 1976). Extreme poor sorting reduces the internal friction; whereas the normal stress is reduced by

$$\sigma' = \sigma - p \quad [\mathrm{N/m^2}] \tag{4}$$

where σ is the total normal stress (the total weight of the debris and p is the pore pressure, which if positive (excess pressure) reduces the normal stress. Hence the excess pore pressure may locally (in most cases it is maximal at the base of the flow) significantly reduce the strength (up to 100%). The ability of the flow to trap pore pressure depends on the particle-size distribution (Rodine and Johnson, 1976). Very poorly sorted fabrics can maintain high excess pore pressure, because the narrow passageways (pore necks) hinder the fluid to escape upward. The presence of minimum amount of silt and clay (as little as 5%) appears to be important trapping the pore fluid and hinders draining of the flow, which greatly enhances its mobility.

Flow transformations

If a flow accelerates or decelerates, its behavior may change due to dilution or to deposition. Four types of flow transformations are feasible (Fisher, 1983): Body transformation, when the flow changes between laminar and turbulent; Gravity transformation, when initial turbulent, particle charged flows become gravitationally segregated into a 2-phase flow with a high-concentrated lower and a low-concentrated upper suspension layer; Surface transformation, when fluid becomes mixed or lost at flow boundaries resulting in dilution; Fluidization transformation, which develops by upward-moving fluids from the substrate or at the head of the flow also diluting the sediment gravity flow.

All types of transformations may play a role during the lifetime of a sediment gravity flow. Upon failure of a sediment mass on a slope, fluidization can make entire sediment slice on a slope unstable and initiate movement of the slice due to failure of, what can be, a thin weak layer where pore pressure could build up sufficiently to reduce its strength (e.g., Brunsden and Prior, 1984). At low rates of shear clast concentrations over 35–58 vol% still form a supporting framework of clasts in contact with each other (Rodine and Johnson, 1976) in which strength derives from both frictional resistance and cohesion. Hence, the slice can start to move as a rigid body riding on a thin shear zone behaving essentially as a plastic body, i.e., if its movement stops its original internal structure is still intact. If the slice accelerates it dilates by water intake from below (fluidization transformation), and from above (surface transformation). This may enhance body transformation, causing the sediment mass to move in either plastic-viscous or fluidal fashion depending on the remaining strength.

Experiments show that sustained, quasi-steady fluidal flows can have concentrations of up to 35 vol% (see Baas et al., 2004). In such highly concentrated fluidal flows, grains are held in suspension mainly by grain-to-grain collisions that cause an upward directed dispersive pressure (Bagnold, 1954). At concentrations less than 9 vol%, grains can be fully supported by turbulence of the fluid (Bagnold, 1954; Sohn, 1997). Flume experiments on high-concentration sandy to gravelly turbulent suspensions by Postma et al. (1988; Figure 3) show how behind the fully turbulent head of the flow the coarsest particles separated out into a highly concentrated basal layer by gravity transformation. The experiments reveal the presence of so-called traction carpets that are overridden by a low-concentrated turbulent suspension (2-phase suspension flows, see Postma et al., 2009).

Deposits of sediment gravity flows

Middleton and Hampton (1973) were the first to summarize a range of sediment gravity flow deposits based on sediment support mechanisms during flow. Later, Lowe (1982), Nemec and Steel (1984), Postma (1986), Nemec (1990), Mutti (1992), Kneller and Branney (1995), Sohn (1997), Russell and Arnott (2003), Postma et al. (2009), and many others addressed in detail the variety of deposits that stems from plastic-viscous and fluidal flow behavior of sediment mixtures. Although some controversies about whether to relate some structureless poorly sorted, coarse-grained deposits to plastic-viscous or to fluidal flow behavior still exist to date (and the just cited papers give a fair insight into these controversies), a fair overview of flow rheology and related deposits can be given, without

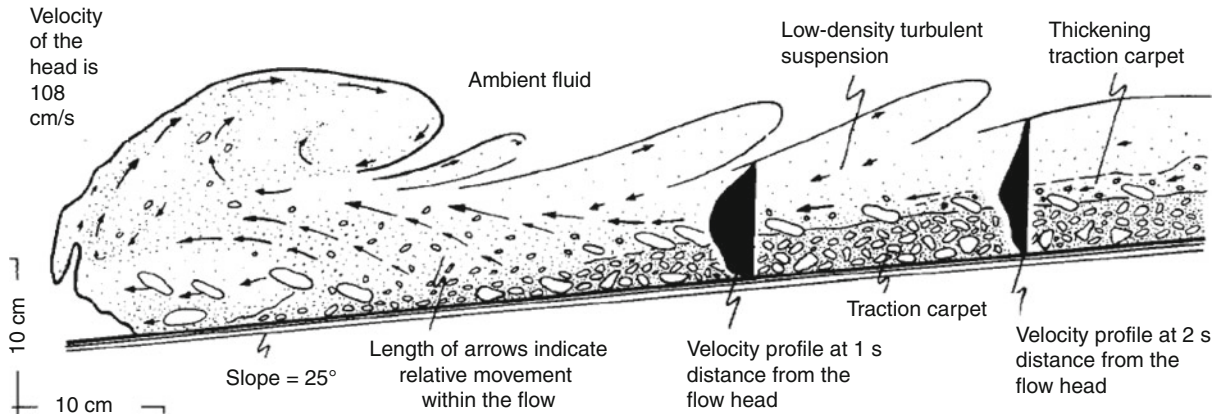

Sediment Gravity Flow, Figure 3 An initial high-concentration turbulent flow transforms by gravity transformation as observed through time (head of flow passes observer at 0 s). The passing head of the current is a fully turbulent 1-phase suspension flow and just before 1 s has passed, a density interface has developed separating the high-concentration traction carpet from the low concentration overriding suspension flow (2-phase flow). The drawing is traced from photographs with a high-speed film camera (70 frames per second (Slightly modified from Postma et al., 1988).

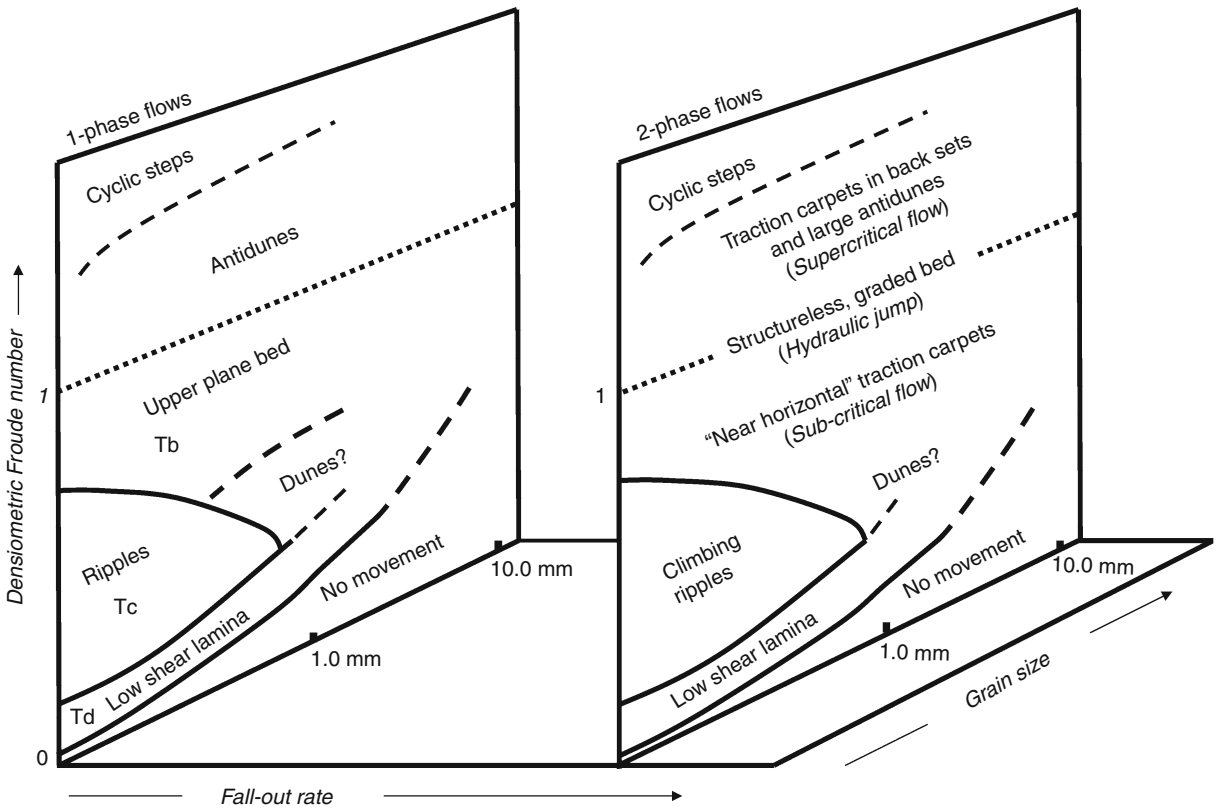

Sediment Gravity Flow, Figure 4 Three-dimensional bed-form stability diagram for 1- and 2-phase suspension flows. To illustrate the position of the hydraulic jump, the stability fields of the various bed forms are given relative to critical flow conditions ($Fr' = 1$). Hence, the boundaries of the stability feeds are only approximate (From Postma et al., 2009).

discussing extensively the right or wrong of certain interpretations.

Deposits of plastic-viscous sediment gravity flow

The deposit of a plastic-viscous flow is called debris flow deposit, or debrite. The basal layer of such deposit is often finer grained than its body and could have a "ropy" appearance representing the original shear zone underlying the rigid plug: The latter is often structureless and nongraded, with large clasts floating in a matrix (similar to *diamicton*). The strength of the debris flow is measured by its largest clast size (Hampton, 1975), and a good correlation between max particle size and bed thickness has been demonstrated in studies of Nemec and Steel (1984).

Deposits of fluidal sediment gravity flow

To fully understand the deposits of fluidal sediment gravity flows it is imperative to realize that deposition can take place under both supercritical, critical, and subcritical flow conditions as defined by the densimetric Froude number. The densiometric Froude number is determined by

$$\mathrm{Fr}' = \frac{U}{\sqrt{g' h}} \quad [-] \tag{5}$$

where U is the flow velocity, h is the flow thickness, and g' is the reduced gravity

$$g' = g\,\frac{\rho_{\mathrm{mix}} - \rho}{\rho} \quad \left[\mathrm{m/s^2}\right] \tag{6}$$

and where ρ_{mix} is the density of the flow, ρ is the density of the ambient water, and g is the gravity constant. For $\mathrm{Fr}' < 1$, the turbidity current is called subcritical, for $\mathrm{Fr}' > 1$ the flow is supercritical, and when $\mathrm{Fr}' \approx 1$ it is critical. When a supercritical flow switches to a subcritical flow it passes the hydraulic jump. Most fluidal sediment gravity flows are already supercritical on slopes of 0.001.

The various bed forms that may develop from a fluidal sediment gravity flow are depicted in the diagram of Figure 4, which illustrates that bed forms are different for 1-phase and 2-phase suspension flows. In 1-phase flows, suspension concentration is below 9 vol% criterion. In such flows fallout rate is low and bed-load transport is dominant, a flow behavior very similar to unidirectional water flow. In 2-phase suspension flows the fallout rate is sufficiently high to form traction carpets (gravity transformation). Various styles of traction-carpet deposits have been recognized as a function of the varying rheology of the layer during its deposition, as was discussed by Sohn (1997). Field and flume evidence indicate that traction

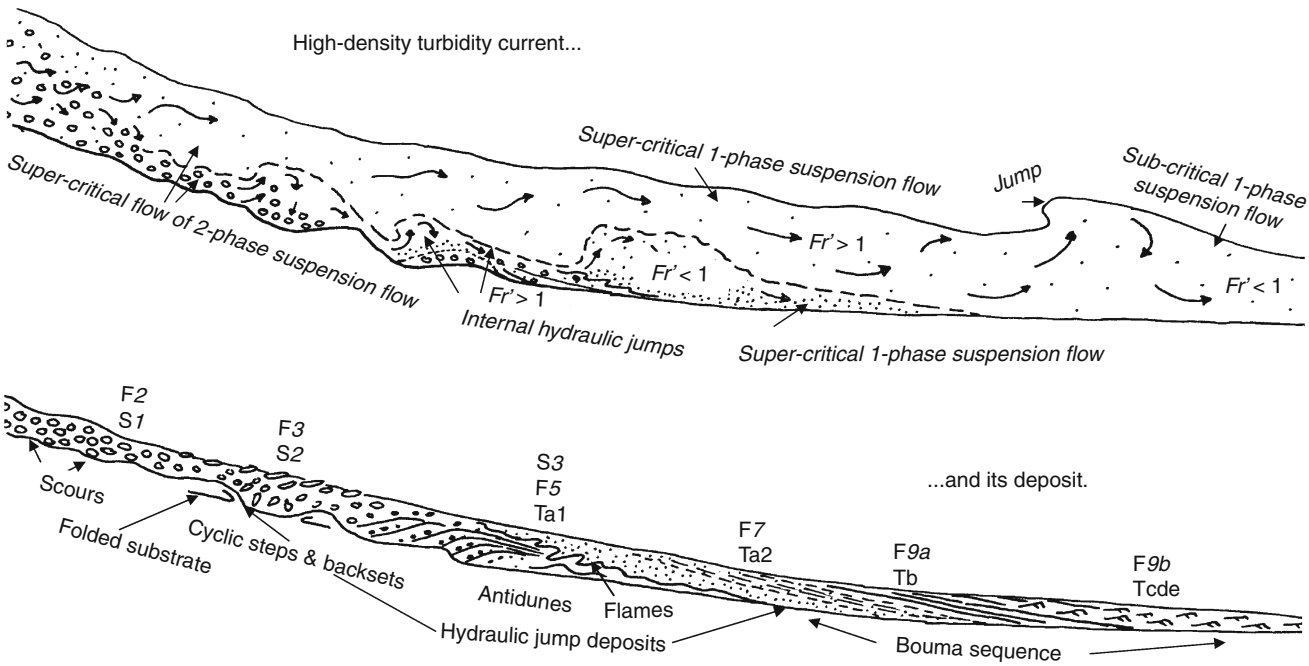

Sediment Gravity Flow, Figure 5 Flow transformation from supercritical to subcritical, with an internal hydraulic jump that leads to the development of Bouma Ta_1 (structureless coarse-tail graded gravelly sand) with flame structures at the base of the unit. In the supercritical region traction carpets deposit in back sets and large wavelength antidunes, whose deposits can be truncated by Bouma Ta_1. In the subcritical region, down slope of the internal jump, weakly stratified Bouma Ta_2 may develop truncated by Bouma Tbcd units of the subcritical flow regime.

carpets can form under both super and subcritical flows, as long as the required fallout rate is achieved.

The evolution of a decelerating high-concentration sediment gravity flow is depicted in Figure 5, together with the resultant deposits, a sketch inspired by Mutti (1992). The F numbers refer to detailed descriptions and illustrations of deposits by Mutti (1992), the S numbers refer to deposits described by Lowe (1982) and the T numbers refer to deposits described by Bouma (1962). The number addition for Ta1 and Ta2 gives the difference between structureless and weakly stratified deposits in the Bouma Ta unit (Postma et al., 2009).

Traction carpets formed under supercritical condition are deposited as large backsets, long-wave (>30 m) antidunes, and large sand and gravel waves (cyclic steps). Backsets and long-wave antidunes have been described from Gilbert-type deltas (see review by Nemec, 1990) and from ice-marginal lakes in deposits formed by subaqueous water jets occurring at the outlet of subaqueous tunnel valleys (e.g., Russell and Arnott, 2003). Traction carpets formed under subcritical conditions are straight and tabular often deposited in association with plane bed lamination (Bouma Tb) and climbing ripple sets (Bouma Tc, see Postma et al., 1983). The deposit of a waning, low concentration turbidity current is described in detail by the Bouma Ta–e sequence with coarse-tail graded basal unit (Ta) followed by plane bed lamination (Tb), small-scale ripple sets (Tc), and silt lamina formed by low shear and suspension fall out (Tde).

Sediment gravity deposits in the various glacigenic environments

Sediment gravity flows and their deposits occur in many present-day glacial environments, and have, for instance, been encountered in fjords in association with deltas (e.g., Bornhold and Prior, 1990), in glacial lakes (e.g., Postma et al., 1983; Gilbert and Crookshanks, 2008), and in many subaerial and subaqueous ice-contact environments. In the latter case, deposits are not necessarily from sediment gravity flows *sensu stricto*, because the high-concentration suspension is for great part driven by the subaqueous jet efflux originating from subglacial melt water drainage systems (tunnel valleys). Yet, their deposits show many close similarities with those of sediment gravity flows (Postma et al., 1983; Russell and Arnott, 2003; Hornung et al., 2007). At the terminus of glaciers, subaerial sediment gravity flows originate where sediment overlies the ice. The ablation of ice disaggregates the overlying sediment and mixes it with the melt water resulting in watery debris slurries. A beautiful example of debris flow deposits has been studied on James Ross Island (Antarctica). The debris flow deposits attain thicknesses of up to 150 m and extend over 4 km laterally. The high volume of glacigenic sediment delivery implicit in the James Ross Island successions indicates that a series of dynamic ice fronts crossed the region during the late Miocene and Pliocene epochs (Nelson et al., 2009). The highly fossiliferous glacigenic debris flows are well dated and signify episodes of ice expansion during relatively warm periods (interglacials).

Summary

The deposits of sediment gravity flows are common in both subaerial and subaqueous glacial environments. They are strongly related to the rheology of the suspension carrying flow and flow characteristics such as speed, densiometric Froude number, and particle concentration and size. The deposits of fluidal sediment gravity flow class are varied and have been organized here in a bedform stability diagram and a longitudinal cross-section.

Bibliography

Baas, J. H., Van Kesteren, W., and Postma, G., 2004. Deposits of depletive, quasi-steady high-density turbidity currents: a flume analogue of bed geometry, structure and texture. *Sedimentology*, **51**, 1053–1089.

Bagnold, R. A., 1954. Experiments on a gravity free dispersion of large solid spheres in a Newtonian fluid under shear. *Proceedings of the Royal Society of London. Series A*, **225**, 49–63.

Bornhold, B. D., and Prior, D. B., 1990. Morphology and sedimentary processes on the subaqueous Noeick River delta, British Columbia, Canada. In Colella, A., Prior, D. B. (eds.), *Coarse Grained Deltas*. International Association of Sedimentologists Special Publication 10. UK: Blackwell, pp. 160–184.

Bouma, A. H., 1962. *Sedimentology of Some Flysch Deposits: A Graphic Approach to Facies Interpretation*. Amsterdam: Elsevier, p. 168.

Brunsden, D., and Prior, D. B. (eds.), 1984. *Slope Instability*. New York: Wiley, p. 620.

Gilbert, R., and Crookshanks, S., 2008. Sediment waves in a modern high-energy glacilacustrine environment. *Sedimentology*, **56**, 645–659.

Fisher, R. V., 1983. Flow transformations in sediment gravity flows. *Geology*, **11**, 273–274.

Hampton, M. A., 1975. Competence of fine grained debris flows. *Journal of Sedimentary Petrology*, **49**, 753–793.

Hornung, J. J., Asprion, U., and Winsemannn, J., 2007. Jet-efflux deposits of a subaqueous ice-contact fan, glacial Lake Rinteln, north western Germany. *Sedimentary Geology*, **193**, 197–192.

Johnson, A. M., 1970. *Physical Processes in Geology*. San Francisco: Freeman, Cooper and Co, p. 577.

Kneller, B. C., and Branney, M. J., 1995. Sustained high-density turbidity currents and the deposition of thick massive sands:. *Sedimentology*, **42**, 607–616.

Lowe, D. R., 1982. Sedimentary gravity flows: II depositional models with special reference to the deposits of high density turbidity currents. *Journal of Sedimentary Petrology*, **52**, 279–297.

Middleton, G. V., and Hampton, M. A., 1973. Subaqueous sediment transport and deposition by sediment gravity flows. In Middleton, G. V., and Bouma, A. H. (eds.), *Turbidites and Deep Water Sedimentation*. Anaheim: Society of Economic Paleontologists Mineralogists, Short course 1, pp. 1–38.

Mutti, E., 1992. *Turbidite Sandstones*. Agip Special Publication, Istituto de geologia, Universita di Parma, p. 275.

Nemec, W., and Steel, R. J., 1984. Alluvial and coastal conglomerates: their significant features and some comments on gravelly mass-flow deposits. In Kosters, E. H., and Steel, R. J. (eds.), *Sedimentology of Gravels and Conglomerates*. Canada: Canadian Society of Petroleum Geologists, Galcary, pp. 1–32.

Nemec, W., 1990. Aspects of sediment movement on steep delta slopes. In Colella, A., and Prior, D. B. (eds.), *Coarse Grained*

Deltas. International Association of Sedimentologists Special Publication 10. UK: Blackwell, pp. 29–74.
Nelson, A. E., Smellie, J. L., Hambrey, M. J., Williams, M., Vautravers, M., Salzmann, U., McArthur, J. M., and Regelous, M., 2009. Neogene glacigenic debris flows on James Ross Island, northern Antarctic Peninsula, and their implications for regional climate history. *Quaternary Science Reviews*, **28**, 3138–3160.
Postma, G., Roep, Th. B., and Ruegg, G. J. H., 1983. Sandy gravelly mass flow deposits in an ice-marginal lake (Saalian, Leuvenumsche Beek Valley, Veluwe, The Netherlands), with emphasis on plug-flow deposits. *Sedimentary Geology*, **34**, 59–82.
Postma, G., 1986. Classification for sediment gravity-flow deposits based on flow conditions during sedimentation. *Geology*, **14**, 291–294.
Postma, G., Nemec, W., and Kleinspehn, K. L., 1988. Large floating clasts in turbidites – a mechanism for their emplacement. *Sedimentary Geology*, **58**(1), 47–61.
Postma, G., Cartigny, M., and Kleverlaan, K., 2009. Structureless, coarse-tail graded Bouma Ta formed by internal hydraulic jump of the turbidity current? *Sedimentary Geology*, doi:10.1016/j.sedgeo.2009.05.018.
Rodine, J. D., and Johnson, A. M., 1976. The ability of debris, heavily freighted with coarse material, to flow on gentle slopes. *Sedimentology*, **23**, 213–234.
Russell, H. A. J., and Arnott, R. W. C., 2003. Hydraulic-jump and hyperconcentrated-flow deposits of a glacigenic subaqueous fan: Oakridges moraine, southern Ontario, Canada. *Journal of Sedimentary Research*, **73**(6), 887–905.
Sohn, Y. K., 1997. On traction-carpet sedimentation:. *Journal of Sedimentary Research*, **67**, 502–509.

Cross-references

Glacier Lake Outburst Floods
Gravitational Mass Movement Deposits
Gravity Flow (Mass Flow)

SEDIMENT ROUTING

Subhajit Sinha
DBS College, Dehradun, Uttarakhand, India

Sediment is transported from areas of uplift and erosion into adjacent sedimentary basins. The relationship between transport processes and storage sites of the sediments is sediment routing. From its generation to its reaching the depozones, the position a sediment particle occupies, depends on its location at the time of deposition. Large sediment routing systems are among the largest geological features on earth, commonly spanning ocean–continent boundaries and occasionally crossing plate boundaries.

Basin models conventionally involve modeling of the filling of sedimentary basins is dependent on incorporating surface processes of weathering, sediment release and dispersal, and long-term burial in the basin. This integrated process system from source to sink is the sediment routing system. Tectonics and sediment routing systems are closely coupled. Dispersal of a mixed sediment supply into a basin with a certain spatial pattern of tectonic subsidence also controls the regional slope and downstream granulometric fining of the depositional system, the positioning of discontinuities such as the gravel front, and gross depositional facies. This offers the possibility that certain basin types may be occupied by particular styles of sediment routing system.

SEDIMENT TRANSFER MODELING

Richard Hodgkins
Department of Geography, Loughborough University, Leicestershire, UK

Synonyms

Sediment transport modeling

Definition

Simulation of rates of suspended-sediment transport in glacial meltwaters, by statistical or physical methods.

Introduction

Models of suspended-sediment transfer in glacially fed rivers have been developed in order to forecast sediment yields for engineering purposes (e.g., Bezinge et al., 1989; Bogen, 1989), to predict erosion rates for geomorphological purposes (e.g., Swift et al., 2002, 2005), to investigate fluvial processes (e.g., Church and Gilbert, 1975; Gurnell and Fenn, 1984), and to identify and interpret seasonal changes in suspended-sediment transfer from glacierized catchments (e.g., Gurnell et al., 1992, 1994; Hodgkins, 1996). Although sophisticated, computational fluid dynamics approaches are well established in hydraulic engineering, the modeling of sediment transfer in glacial environments is typically restricted by the perennial difficulties of acquiring continuous, high-quality hydrometric and sediment transport data at fine spatial and temporal resolutions, in unstable proglacial and inaccessible subglacial environments. Parameterizations of complex models require detailed data such as precise fluvial network topology, bed characteristics and velocity profiles that are usually impractical to obtain in proglacial locations, and even less so in subglacial ones.

Rating-curve approaches

Because of the difficulties of parameterizing physical models, statistical approaches to sediment transfer modeling are much more widespread. By far the most common model is a rating curve derived from linear regression of Suspended-Sediment Concentration (SSC), or sometimes (spuriously, from a statistical point of view) Suspended-Sediment Load (SSL), on discharge (e.g., Repp, 1988). Swift et al. (2005) used residuals from linear regressions of daily SSL on discharge to highlight important changes in the seasonal efficiency of sediment transfer, which were investigated further at a sub-seasonal scale using SSC as

the dependent variable. The popularity of the rating curve stems from its simplicity of construction and interpretation, with SSC deterministically predicted from discharge. However, the discharge-SSC relationship is far from simple in reality, and the performance of rating curves is frequently poor. For instance, Parks and Madison (1984) derived rating curves for glacierized basins in Alaska that had standard errors ranging from −50% to +100%, while Fenn (1989) found that rating curves developed for one season's data from the Glacier de Tsidjiore Nouve (Switzerland) predicted suspended loads from 34% to 278% of measured values when applied beyond that season. Such limitations arise because the bivariate discharge-SSC relationship is unstable over a range of temporal scales. Fenn et al. (1985) summarized the effects that limit the performance of sediment rating curves as follows:

1. Variations in sediment supply at the seasonal scale, such as from early-season flushing (Liestøl, 1967; Collins, 1989), late-season exhaustion (Østrem, 1975; Gurnell et al., 1992), or changing sediment sources (Gurnell et al., 1994; Hodgkins, 1996).
2. Variations in sediment supply at the diurnal scale, between the rising and falling limbs of the hydrograph, leading to diurnal hysteresis (Bogen, 1980; Hodgkins, 1996). This is a particular problem for forecasting SSC from discharge alone, since there are distinct, rising- and falling-limb values of SSC for any one value of discharge.
3. Transient SSC pulses, which are independent of discharge (Gurnell, 1982; Gurnell and Warburton, 1990).
4. Variable entrainment and deposition of sediment in the proglacial region (Maizels, 1979; Warburton, 1990; Hodgkins et al., 2003).
5. Variations in sediment supply associated with rainfall-induced events (Church, 1972; Richards, 1984).

Time-series (stochastic) approaches

The limitations of the rating curve are usually reflected in the presence of autocorrelation in the residual series. *Quasi-autocorrelation* results from shortcomings in the formulation of the model: nonlinearity, omission of relevant independent variables, the presence of response lags/leads, and hysteresis at different time scales (Fenn et al., 1985). *True-autocorrelation*, however, indicates that the SSC series is generated not through a linear dependence on discharge, but by a stochastic process in which the present value of SSC is not independent of previous values of SSC, but a probabilistic function of them and of present and previous random disturbances (Richards, 1979).

Gurnell and Fenn (1984) took advantage of true-autocorrelation, estimating a Box-Jenkins transfer function (Box and Jenkins, 1976) between discharge and SSC series from Glacier de Tsidjiore Nouve. AutoRegressive Integrated Moving-Average (ARIMA) stochastic time-series models of discharge and SSC series were developed for an estimation period, and the transfer function used to bring them into phase and apply a scaling factor. Predictions from the transfer-function model were far superior to those from rating curves, such that Gurnell and Fenn (1984) recommended a similar approach be used whenever possible. Fenn (1989) found that a transfer-function model gave predictions of SSL from 96% to 105% of measured values at Glacier de Tsidjiore Nouve, even when applied beyond the season in which it was developed. Nevertheless, despite the advantages of the transfer-function approach, it has not been widely adopted, because: (1) it requires an unbroken series of uniformly spaced observations for estimation, (2) it is sometimes difficult to place physical interpretations on the ARIMA parameters (Swift et al., 2005).

Simpler implementations of time-series approaches are available, however. Linear regression models for successive subperiods of an SSC time series acquired at Scott Turnerbreen (Svalbard), using discharge as the independent variable, accounted for between none (when not significant) and about 52% of the variance in SSC (Hodgkins, 1996). However, *autoregression* models, incorporating both discharge, Q, and an ARIMA (1,0,0) component ($SSC_t = aQ_t + bSSC_{t-1} + \varepsilon_t + c$, where a and b are regression coefficients, c the regression intercept, and ε is a random disturbance), indicate that the latter dominates the regression relationship, and is relatively constant with a value close to unity, throughout the melt season (Hodgkins, 1999). Likewise, Gurnell et al. (1994) found that a first-order autoregressive ARIMA model was largely sufficient to describe an SSC time series obtained at Austre Brøggerbreen (Svalbard), although a second-order autoregressive, or sometimes also a diurnal moving-average, model was required for series obtained at Haut Glacier d'Arolla (Switzerland): this is a temperate glacier with a seasonally evolving, multi-reservoired, subglacial drainage network (Gurnell et al., 1992) of greater complexity than the largely sub-serial networks of the essentially non-temperate Svalbard examples. Inferring the structure of the glacial drainage system was an early motivation of sediment transfer modeling, and remains important. For example, Swift et al. (2005) noted increasing sediment availability through a strong relationship between daily SSL and discharge amplitude at Haut Glacier d'Arolla, and inferred that increasing subglacial water pressure variation as a consequence of increasingly peaked diurnal run-off cycles was likely to have increased access to basal sediment, by encouraging extra-channel flow excursions and/or enhancing basal sediment deformation.

Subdivision of time series

Other attempts to improve rating-curve performance have involved subdividing the discharge and SSC series into shorter intervals of more uniform response, for which a linear relationship may be more valid. Collins (1979) estimated rating curves for individual rising and falling limbs of the diurnal hydrograph at Gornergletscher

(Switzerland). Hammer and Smith (1983) derived early- and late-season rating curves for Hilda Glacier (Canada). Richards (1984) obtained separate rating curves for periods of meltwater runoff and storm runoff at Storbreen (Norway). Gurnell et al. (1992) divided discharge and SSC series from Haut Glacier d'Arolla into five subperiods on the basis of variations in diurnal maximum and minimum discharge, prior to estimating regression and ARIMA models. Statistical hydrograph classification has also been used as a tool to trace the seasonal evolution of subglacial drainage configuration, which has in turn been used to define periods of consistent run-off sediment transfer response for further statistical analysis, e.g., Orwin and Smart (2004) and Swift et al. (2005) used principal components and hierarchical clustering analyses to classify hydrographs on the basis of shape and magnitude at Small River Glacier (Canada) and Haut Glacier d'Arolla, respectively. Orwin and Smart (2004) also applied these analyses to diurnal suspended-sediment cycles, and compared the resulting classes with discharge and meteorological data to analyze sediment transfer patterns. This approach showed that relatively low SSC and clear diurnal cycling were the norm, but that about 70% of the total seasonal sediment load occurred in "irregular," relatively high-SSC events associated with rainfall and enhanced snowmelt: the proglacial area was the source for up to 80% of the sediment yield of the glacier basin. Proglacial storage effects are particularly relevant to the modeling of sediment transfer in glacierized catchments, and careful field experimental design is required to distinguish the glacial sediment transfer signal from the proglacially modulated one, though it is not always possible to achieve this in intractable glacial locations.

Multivariate approaches

A further approach has been to develop multivariate rating curves incorporating additional explanatory variables, which may represent components of variability at different temporal scales. Richards (1984) introduced the *rate of change of discharge per hour*, positive during rising and negative during falling stages, to represent diurnal hysteresis. It was found that this variable was the main control on SSC variation during periods of meltwater runoff. Willis et al. (1996) found that the variables *discharge*, *rate of change of discharge,* and *days since discharge was equalled or exceeded* were all significant in a multivariate rating curve from Midtdalsbreen (Norway), although the improvement over a rating curve using discharge alone was slight, and the residuals were autocorrelated. Likewise, Swift et al. (2005) found that the variables *days since discharge was equalled or exceeded*, *rate of change of discharge* and *rainfall* were significant in multivariate regression models at Haut Glacier d'Arolla; again, autocorrelation, though reduced compared with bivariate models, was not removed. However, autocorrelation was absent from models that included the variable SSC_{t-1}, indicating true-autocorrelation arising either from a dependence of the current value of SSC on recent values of SSC (denoting sediment availability), from the settling velocity of fine particles being lower than that required for their entrainment (Hodson and Ferguson, 1999), or from some combination of these factors. In all models, SSC_{t-1} became the most significant explanatory variable at the expense of Q. Note that lagging an independent variable in a regression is not the same process as building an ARIMA (1,0,0) model: the former still uses the least-squares approach to estimate its parameters, while the latter takes a maximum-likelihood approach (Akaike, 1974). However, both methods can reduce autocorrelation. Hodgkins (1999) earlier noted that the dependence of SSC on the magnitude of discharge in time series from Scott Turnerbreen was weak and highly variable, whereas the dependence of current SSC on recent values of SSC, revealed through an ARIMA(1,0,0) term, was strong (an order of magnitude greater than Q) and relatively constant. The dominant control on SSC was therefore short-term sediment availability: a corollary of this is that forecasting becomes problematic in the absence of recent SSC data. The challenge is therefore presented of identifying and modeling processes that control sediment *availability.*

Physical approaches

Physical models of sediment transfer are far less developed than statistical ones. A notable contribution is that of Clarke (1996), who developed a lumped-element model of the subglacial hydraulic system. He related the sediment flux from the bed into suspension (erosion), $F_S^{\uparrow}$, to the porosity of the bed, n, the sediment density, ρ_S, and the bed shear stress, τ_0:

$$F_S^{\uparrow} = \rho_S(1-n)k_E(\tau_0 - \tau^*)^N \quad \tau_0 > \tau^*$$

where k_E is a constant relating to the character of the flow and the bed surface, τ^* is a threshold boundary shear stress for erosion and N is an experimentally derived constant. Clarke (1996) assumed an unlimited sediment supply, but this is not a necessary assumption of the model. τ^* depends on grain size, and can be approximately zero for silt particles. Assuming that Stokes' Law governs the processes of sedimentation, the sediment flux from suspension into the bed (deposition), $F_S^{\downarrow}$, can be written

$$F_S^{\downarrow} = c_S v_S = c_S \frac{(\rho_S - \rho)gD_P^2}{18\mu}$$

where c_S is SSC (essentially supplied from upstream), v_S is the settling velocity of grains of diameter D_P, and density ρ_S from a fluid of density ρ and viscosity μ. Mass conservation requires the flux of sediment per unit time from a drainage element of volume V and bed surface A to be equal to the flux in, plus erosion, minus deposition. Therefore a sediment balance can be written:

$$\frac{dc_S}{dt} = \frac{1}{V}\left[-c_S\frac{dV}{dt} + c_S^{in}Q^{in} - C_S^{out}Q^{out} = A\left[\rho_S(1-n)k_E(\tau_0-\tau^*)^N - \frac{c_S(\rho_S-\rho)gD_P^2}{18\mu}\right]\right]$$

Clarke (1996) notes astutely that the main limitations on subglacial hydraulic modeling are not in the mathematical treatment, but in our poor knowledge of drainage configurations and of sediment sources and sinks.

Jones and Arnold (1999) applied Clarke's (1996) equations to a subglacial water routing model (Arnold et al., 1998) and obtained reasonable results for the period when conduits were well established in the mid-to-late melt season, though not before. An observed reduction in peak diurnal SSCs toward very end of melt season was not seen in modeled data, which suggested it was not caused by any reduction in water discharge or velocity. Instead, it was suggested that sediment exhaustion was occurring, as at that point of the melt season the conduits had been established for some 30 days, with little headward expansion, and therefore without potential access to fresh sediment sources (though note Swift et al.'s (2005) interpretations, above). The diurnal range of SSC was more sensitive than the mean SSC to changing parameter values, and diurnal SSC maxima and minima tended to increase/decrease together. This suggested that, to improve model performance, it would probably be necessary to include additional physical processes, such as sediment exhaustion, hiding of grains, and the exposure of fine particles if and when larger particles become entrained. This is to reiterate the point that sediment availability is probably the key control of sediment transfer, and that while variations in availability can be identified by statistical analysis of SSC/SSL time series, there are currently no effective means to model it.

Summary

Sediment transfer rates in glacial meltwaters have so far mainly been modeled by statistical means, and the rating-curve approach has been the most important of these. However, while it can be improved by subdividing time series and incorporating independent variables other than runoff, the rating curve is essentially simplistic and fails to account for the true-autocorrelation that is pervasive in sediment transfer series. Stochastic methods, such as ARIMA, can model autocorrelation explicitly, but are more complex to estimate, more demanding of data, and more difficult to interpret. Autocorrelation at short lags shows that sediment availability is probably the key control of sediment transfer rates. An expanding range of statistical approaches, including the classification of hydrographs and sedigraphs by principal components and clustering analyses, have shed valuable light on temporal patterns of sediment availability, but a really effective means to model the availability of sediment in a predictive manner remains elusive. Physical models of sediment transfer are underdeveloped by comparison with statistical approaches, but they may become more widely adopted as our ability to parameterize complex hydrological processes improves.

Bibliography

Akaike, H., 1974. A new look at the statistical model identification. *IEEE Transaction on Automatic Control*, **AC-19**, 716–723.

Arnold, N., Richards, K., Willis, I., and Sharp, M., 1998. Initial results from a distributed, physically-based model of glacier hydrology. *Hydrological Processes*, **12**(2), 191–219.

Bezinge, A., Clark, M. J., Gurnell, A. M., and Warburton, J., 1989. The management of sediment transported by glacial melt-water streams and its significance for the estimation of sediment yield. *Annals of Glaciology*, **13**, 1–5.

Bogen, J., 1980. The hysteresis effect of sediment transport systems. *Norsk Geografisk Tidsskrift*, **34**, 45–54.

Bogen, J., 1989. Glacial sediment production and development of hydro-electric power in glacierized areas. *Annals of Glaciology*, **13**, 6–11.

Box, G. E. P., and Jenkins, G. M., 1976. *Time Series Analysis, Forecasting and Control*, rev. edn. San Francisco: Holden-Day.

Church, M. A., 1972. Baffin Island Sandurs: a study of Arctic fluvial processes. *Bulletin of the Geological Survey of Canada*, **216**, 208 pp.

Church, M. A., and Gilbert, R., 1975. Proglacial fluvial and lacustrine environments. In Jopling, A. V., and MacDonald, B. C. (eds.), *Glaciofluvial and Glaciolacustrine Sedimentation*. Tulsa, Oklahoma, USA: Society of Economic Palaeontologists and Mineralogists Special Publication, 23, pp. 22–100.

Clarke, G. K. C., 1996. Lumped-element model for subglacial transport of solute and suspended sediment. *Annals of Glaciology*, **22**, 152–159.

Collins, D. N., 1979. Sediment concentration in meltwaters as an indicator of erosion processes beneath an Alpine glacier. *Journal of Glaciology*, **23**(89), 247–257.

Collins, D. N., 1989. Seasonal development of subglacial drainage and suspended sediment delivery to melt waters beneath an Alpine glacier. *Annals of Glaciology*, **13**, 45–50.

Fenn, C. R., 1989. Quantifying the errors involved in transferring suspended sediment rating equations across ablation seasons. *Annals of Glaciology*, **13**, 64–68.

Fenn, C. R., Gurnell, A. M., and Beecroft, I. R., 1985. An evaluation of the use of suspended sediment rating curves for the prediction of suspended sediment concentration in a proglacial stream. *Geografiska Annaler*, **67A**(1–2), 71–82.

Gurnell, A. M., 1982. The dynamics of suspended sediment concentration in an Alpine pro-glacial stream network. In *Hydrological Aspects of Alpine and High Mountain Areas* (*Proceedings of the Symposium*), Exeter, July 1982. International Association of Hydrological Sciences Publication Number, 138, pp. 319–330.

Gurnell, A. M., and Fenn, C. R., 1984. Box-Jenkins transfer function models applied to suspended sediment concentration-discharge relationships in a proglacial stream. *Arctic and Alpine Research*, **16**, 93–106.

Gurnell, A. M., and Warburton, J., 1990. The significance of suspended sediment pulses for estimating suspended sediment load and identifying suspended sediment sources in alpine glacier basins. In *Hydrology in Mountainous Regions. I. Hydrological Measurements; the Water Cycle* (*Symposium*), Lausanne, 1990. International Association of Hydrological Sciences Publication Number, 193, pp. 463–470.

Gurnell, A. M., Clark, M. J., and Hill, C. T., 1992. Analysis and interpretation of patterns within and between

hydroclimatological time series in an Alpine glacier basin. *Earth Surface Processes and Landforms*, **17**, 821–839.
Gurnell, A. M., Hodson, A., Clark, M. J., Bogen, J., Hagen, J. O., and Tranter, M., 1994. Water and sediment discharge from glacier basins: an arctic and alpine comparison. In Variability in Stream Erosion and Sediment Transport (*Symposium*), Canberra, 1994. International Association of Hydrological Sciences Publication Number, 224, pp. 325–334.
Hammer, K. M., and Smith, N. D., 1983. Sediment production and transport in a proglacial stream: Hilda Glacier, Alberta, Canada. *Boreas*, **12**, 91–106.
Hodgkins, R., 1996. Seasonal trends in suspended-sediment transport at an Arctic glacier, and their implications for drainage system structure. *Annals of Glaciology*, **22**, 147–151.
Hodgkins, R., 1999. Controls on suspended-sediment transfer at a High-Arctic glacier, determined from statistical modelling. *Earth Surface Processes and Landforms*, **24**, 1–21.
Hodgkins, R., Cooper, R., Wadham, J., and Tranter, M., 2003. Suspended sediment fluxes in a High-Arctic glacierised catchment: implications for fluvial sediment storage. *Sedimentary Geology*, **165**, 105–117.
Hodson, A. J., and Ferguson, R. I., 1999. Fluvial suspended sediment transport from cold and warm-based glaciers in Svalbard. *Earth Surface Processes and Landforms*, **24**(11), 957–974.
Jones, H., and Arnold, N., 1999. Modelling the entrainment and transport of suspended sediment in subglacial hydrological systems. *Glacial Geology and Geomorphology*, http://boris.qub.ac.uk/ggg/papers/full/1999/rp091999/rp09.html.
Liestøl, O., 1967. *Storbreen glacier in Jotunheimen*. Norway: Norsk Polarinstitutt Skrifter, p. 141.
Maizels, J. K., 1979. Proglacial aggradation and changes in braided channel patterns during a period of glacier advance: an Alpine example. *Geografiska Annaler*, **61A**(1–2), 87–101.
Orwin, J. F., and Smart, C. C., 2004. Short-term spatial and temporal patterns of suspended sediment transfer in proglacial channels, Small River Glacier, Canada. *Hydrological Processes*, **18**, 1521–1542.
Østrem, G., 1975. Sediment transport in glacial meltwater streams. In Jopling, A. V., and MacDonald, B. C., (eds.), *Glaciofluvial and Glaciolacustrine Sedimentation*. Tulsa, Oklahoma, USA: Society of Economic Palaeontologists and Mineralogists Special Publication, 23, pp. 101–122.
Parks, B., and Madison, R. J., 1984. *Estimation of selected flow and water quality characteristics of Alaskan streams*. U.S. Geological Survey Water Resources Investigations Report 84-4247.
Repp, K., 1988. The hydrology of Bayelva, Spitsbergen. *Nordic Hydrology*, **19**, 259–268.
Richards, K. S., 1979. *Stochastic processes in one-dimensional series; an introduction*. Norwich: Geo-abstracts. Concepts and Techniques in Modern Geography, Vol. 23.
Richards, K. S., 1984. Some observations on suspended sediment dynamics in Storbregrova, Jotunheim. *Earth Surface Processes and Landforms*, **9**, 101–112.
Swift, D. A., Nienow, P. W., Spedding, N., and Hoey, T. B., 2002. Geomorphic implications of subglacial drainage configuration: rates of basal sediment evacuation controlled by seasonal drainage system evolution. *Sedimentary Geology*, **149**, 5–19.
Swift, D. A., Nienow, P. W., and Hoey, T. B., 2005. Basal sediment evacuation by subglacial meltwater: suspended sediment transport from Haut Glacier d'Arolla, Switzerland. *Earth Surface Processes and Landforms*, **30**(7), 867–883.
Warburton, J., 1990. An alpine proglacial sediment budget. *Geografiska Annaler*, **72A**(3–4), 261–272.
Willis, I. C., Richards, K. S., and Sharp, M. J., 1996. Links between proglacial stream suspended sediment dynamics, glacier hydrology and glacier motion at Midtdalsbreen, Norway. *Hydrological Processes*, **10**, 629–648.

Cross-references

Glacier Hydrology
Hydrographs
Hysteresis
Meltwater Erosion
Rating Curve
Sediment Budgets
Sediment Yield
Suspended Sediment Dynamics

SEDIMENT YIELD

Kelly MacGregor
Geology Department, Macalester College, Saint Paul, MN, USA

Synonyms

Annual sediment yield; Integrated sediment flux

Definition

Sediment yield: Total quantity of sediment, expressed in units of mass (or volume) per unit time. In the case of glacial or fluvial environments, sediment yield is typically the volume of sediment transported from a drainage basin over a given time period.
Annual sediment yield: Total quantity of sediment fluxed from a basin during an entire year, expressed in units of mass or volume per annum.

Introduction

Sediment yield is broadly understood in earth surface processes to mean the total volume or mass of sediment evacuated, transported, or deposited from a drainage basin. As the term yield implies, the amount of sediment removed is estimated or measured over a known period of time. Yield is then reported as mass per year (typically tons/year) or volume per year. Sediment yield refers to the inorganic fraction of sediment, ignoring organic material frequently in transport in fluvial systems.

Source of sediment in glacierized basins

Measurements of sediment yield are typically difficult to make, in part because of the large distribution in grain size produced by glacial processes. Accurate measurements of sediment yield consider the coarse-grained fraction (from headwall processes and subglacial quarrying) and the finer-grained material (produced during subglacial abrasion). Fine-grained sediments (silts and clays) are often carried to proglacial lakes and fjords in streams, while coarser material is transported more slowly and over shorter distances. The production of sediment is either subglacial (subglacial abrasion and quarrying) and therefore impossible to observe directly, or sourced from the valley walls but incorporated into glacier ice in the accumulation zone or from rockfall into the bergschrund or

crevasses. Some rockfall from the valley walls either falls or emerges in the ablation zone; this material is eventually moved to the proglacial zone and deposited in the form of moraines. While there may be a contribution of subglacial or proglacial fluvial bedrock erosion contributing to sediment yield, this is typically assumed to be many orders of magnitude less than the glacial contribution of sediment.

Measurement of sediment yield in glacierized basins

The variety of methods for quantifying sediment yield fall into three general categories: measurement of active suspended sediment and bedload flux in proglacial streams and ice proximal marine settings; mapping terrestrial deposits and landforms; and bathymetric, ground-penetrating radar, and/or coring studies of subaqueous sedimentary deposits.

A key study of sediment yield using measurements of sediment flux from an active glacier is Humphrey and Raymond (1994). Using measurements of suspended sediment at Variegated Glacier in Alaska, the authors constrained sediment yield from the glacier over a wide range of measured ice velocities. The techniques used to measure sediment flux in proglacial streams are well documented (e.g., Ostrem, 1975; Gurnell, 1987; Bogen, 1989). Measurement of the bedload fraction is difficult to constrain; examples of studies that have successfully quantified bedload contributions to sediment yield include Pearce et al. (2003) and Riihimaki et al. (2005). In addition to measuring sediment concentration and flux in proglacial streams, some studies of active glaciers utilize sediment traps to assess yield. Direct measurements of settling sediment in lakes have been used (e.g., Hunter, 1994); uncertainties can be high over daily to seasonal timescales.

Terrestrial measurements of moraine volume and debris cover have been used to estimate basin-wide sediment yield (e.g., Reheis, 1976; Heimsath and McGlynn, 2008). Calculations of sediment yield are made using mapping and estimates of moraine density. An important uncertainty with this technique is constraining the timescales over which the deposits were formed. The use of cosmogenic radionuclides (CRN) to determine sediment yield in non-glacierized basins has been used with good success (e.g., Blanckenburg, 2005; Kirchner et al., 2002), and is beginning to be used in alpine settings to constrain the timescales over which sediment accumulates on moraines (e.g., Heimsath and McGlynn, 2008). An important challenge for utilizing CRN in glacierized basins is the shielding of subglacial sediment and rock with ice and snow, as well as the extremely steep angles of valley walls, both of which complicate the estimated exposure and inheritance of basin surfaces (discussed in Bierman and Nichols, 2004).

Measurements of total sediment volume deposited in well-defined traps such as proglacial lakes, fjords, and debris fans in subaqueous ocean environments have been used with some good success (in addition to the summary provided in Hallet et al. (1996), Koppes and Hallet (2002) provide a new methodology for determining the time series of sediment yield from a retreating tidewater glacier). Ground-penetrating radar and bathymetric measurements have been used to image and constrain sediment volume and density in these areas. Lake coring has also been used to constrain sediment yields from glacierized basins; sediment accumulation rates from cores are converted to volume by averaging across the surface area of the lake (Foster et al., 1990) or an averaging technique using multiple cores (e.g., O'Hara et al., 1993; Evans and Church, 2000). Loso et al. (2004) quantified sediment yield by measuring the accumulation of fine and coarse-grained sediment in an ice-dammed lake that had drained. This work highlighted the uncertainties associated with measuring only suspended sediment yield as a proxy for total sediment flux.

Sediment yield is frequently converted to basin-averaged (or glacier-averaged) erosion rate. The effective erosion rate is simply the sediment yield divided by the basin area or glacier footprint. A key assumption in these calculations is that subglacial storage of sediment is either zero (i.e., the bed beneath the glacier is bare bedrock) or storage of sediment is steady (input of sediment into the glacier is equal to sediment output). It is difficult to assess the validity of this assumption in subglacial settings.

Sediment yields from glacierized basins

An excellent summary of sediment yield from glacierized basins can be found in Hallet et al. (1996). Typically, sediment yield is converted to basin-averaged erosion rate and reported in mm a^{-1}. Hallet et al. (1996) reported rates of erosion in glacierized basins exceed those in fluvial settings by an order of magnitude or more, with sediment yields increasing with greater ice cover. Sediment yields converted to erosion rates vary from 0.01 mm a^{-1} for polar glaciers, to 10–100 mm a^{-1} beneath fast-moving temperate glaciers (Hallet et al., 1996). Koppes and Hallet (2002) document variability in sediment yield and, therefore, erosion rate in Alaskan tidewater glaciers. Their work suggests the extremely high modern rates of erosion (greater than 30 mm a^{-1} in this region) are about five times greater than long-term erosion rates because of rapid ice motion and calving resulting from warming since the Little Ice Age.

Summary

Sediment yield from glacierized basins is a key measurement for constraining rates of glacial erosion. Models of exhumation and range-scale evolution are sensitive to the timing and distribution of rock removal, and quantifying sediment yield is an important aspect of constraining these models and their predictions. While measurements of sediment yield are difficult to make, they offer insight into basin-wide erosional dynamics in arctic and alpine systems.

Bibliography

Bierman, P. R., and Nichols, K. K., 2004. Rock to sediment, slope to sea with ^{10}Be; rates of landscape change. *Annual Review of Earth and Planetary Sciences*, **32**, 215–255.
Bogen, J., 2008. The impact of climate change on glacial sediment delivery to rivers; sediment dynamics in changing environments. *IAHS-AISH Publication*, **325**, 432–439.
Evans, M., and Church, M., 2000. A method for error analysis of sediment yields derived from estimates of lacustrine sediment accumulation. *Earth Surface Processes and Landforms*, **25**(11), 1257–1267.
Foster, I. D. L., Dearing, J. A., Grew, R., and Orend, K., 1990. The sedimentary database; an appraisal of lake and reservoir sediment based studies of sediment yield; erosion, transport and deposition processes. *IAHS-AISH Publication*, **189**, 19–43.
Gurnell, A. M., 1987. Fluvial sediment yield from alpine, glacierized catchments. In Gurnell, A. M., and Clark, M. J. (eds.), *Glacio-Fluvial Sediment Transfer; an Alpine Perspective*. Chichester, UK (GBR): Wiley.
Hallet, B., Hunter, L., and Bogen, J., 1996. Rates of erosion and sediment evacuation by glaciers; a review of field data and their implications. *Global and Planetary Change*, **12**(1–4), 213–235.
Heimsath, A. M., and McGlynn, R., 2008. Quantifying periglacial erosion in the Nepal High Himalaya. *Geomorphology*, **97** (1–2), 5–23.
Humphrey, N. F., and Raymond, C. F., 1994. Hydrology, erosion and sediment production in a surging glacier; Variegated Glacier, Alaska, 1982–83. *Journal of Glaciology*, **40**(136), 539–552.
Hunter, L. E., 1994. *Grounding-Line Systems of Modern Temperate Glaciers and Their Effects on Glacier Stability*. PhD thesis, De Kalb, IL, Northern Illinois University, 467 p.
Koppes, M. N., and Hallet, B., 2002. Influence of rapid glacial retreat on the rate of erosion by tidewater glaciers. *Geology (Boulder)*, **30**(1), 47–50.
O'Hara, S. L., Street-Perrott, F. A., and Burt, T. P., 1993. Accelerated soil erosion around a Mexican highland lake caused by pre-Hispanic agriculture. *Nature*, **362**, 48–51.
Ostrem, G., 1975. Sediment transport in glacial meltwater streams. In Jopling, A. V., and McDonals, B. C. (eds.), *Glaciofluvial and Glaciolacustrine Sedimentation, Vol 23*. Tulsa, OK: Society of Economic Paleontologists and Mineralogists (special publication), pp. 101–122.
Pearce, J. T., Pazzaglia, F. J., Evenson, E. B., Lawson, D. E., Alley, R. B., Germanoski, D., and Denner, J. D., 2003. Bedload component of glacially discharged sediment; insights from the Matanuska Glacier, Alaska. *Geology (Boulder)*, **31**(1), 7–10.
Reheis, M. J., 1975. Source, transportation and deposition of debris on Arapaho glacier, Front Range, Colorado, USA. *Journal of Glaciology*, **14**, 407–420.
Riihimaki, C. A., MacGregor, K. R., Anderson, R. S., Anderson, S. P., and Loso, M. G., 2005. Sediment evacuation and glacial erosion rates at a small alpine glacier. *Journal of Geophysical Research*, **110**(F3), 17.

Cross-references

Basal Sediment Evacuation by Subglacial Drainage System
Discharge/Streamflow
Glacial Erosion
Glacier Motion/Ice Velocity
Glaciofluvial
Sediment Budgets
Sediment Core and Glacial Environment Reconstruction
Sediment Entrainment, Transport, and Deposition
Subglacial Processes
Suspended Sediment Dynamics

SEM ANALYSIS OF GLACIAL SEDIMENTS

William C. Mahaney
Quaternary Surveys, Thornhill, ON, Canada

Definition

Microtextures studied by SEM are found on quartz and other mineral grains from different sedimentary environments, and these along with grains from bedrock release, are transported by glaciers which inflict the most extensive array of fracture and abrasion microfeatures. Anywhere from 10% to 20% of grains in glaciers may escape contact with other grains, and hence sojourn in the ice without suffering physical damage. The other 80–90% of glacial grains will exit the system with fractured and abraded surfaces some of which are diagnostic of the glacial environment. These grains record damage that, to a large extent, depends on the thickness of the ice and the distance of transport with temperatures close to pressure-melting (p-melting). While the distance of transport is nearly impossible to compute with total accuracy, it would seem that long-distance transport close to p-melting will yield a triangular faceted quartz grain totally reformed from its original shape and size, and with the greatest damage inflicted on it. No other geological agent is capable of this transformation and none have the damaging effect that glaciers can inflict on quartz and other minerals entrained in the ice.

SEM analysis of glacial sediments

Sand grain surface microtexture analysis, using the Scanning Electron Microscope (SEM), was initiated by Dave Krinsley and John Doornkamp (1973), who introduced the subject to sedimentology. The original atlas became a repository of sand grain imagery and provided the first attempt to collate microtextures on sands, specifically quartz sands, linking them to specific geologic agents and/or sedimentary environments. After five decades of research on sand grain morphometry/fractography, it is now known that only a few microtextures are unique to specific environments, or geologic processes. Many microtextures, previously believed to be unique signatures of a particular environment, are now known on sands emplaced by different geologic/geomorphic processes. Thus, microtextures ranging across many environments perfectly illustrate the *Principle of Equifinality*, that is, in open systems a given end state can be reached by many potential means (Mahaney, 2002). Beyond this, investigators need the power of a representative population of grains to definitively identify the conditions under which grains are sourced, transported, and emplaced. The initiation of SEM analysis of sediments was pioneered by Biederman (1962), Porter (1962), and Krinsley and Takahashi (1962), and has since undergone several modifications as equipment has evolved into the digital age. During the inception of SEM

investigations in the early 1960s, research emphasis focused on sedimentological and mineralogical applications. However, increasingly over the years, the method has been applied to other fields where SEM-EDS (Energy Dispersive Spectrometry) methods can be employed to build a database of microtextures, microstructures, and chemical spectra that help to answer questions related to weathering in paleoenvironments as well as generate new ones. For example, standard databases on precipitates and coatings, information lacking in the Krinsley and Doornkamp (1973) volume, are now frequently used to help solve questions related to weathering of glacial grains (Mahaney, 2002), the coating chemistry offering new insight into wetting depths and paleoleaching in paleosols (Mahaney, 1990a), all of which may provide valuable information on preweathering prior to glacial transport (Mahaney et al., 1991) and relative dating of sediments (Mahaney et al., 2009).

The 1973 volume on glacial grain surface microtextures, although long out of date, remains a basic reference for researchers interested in the application of the technique since that time. Additional work by Whalley (1978) and Marshall (1987) has added numerous case studies in the microtexture field since that time. The new SEM atlas by Mahaney (2002) contains additional case studies intended to complement and expand upon these earlier reference works; however, the intent here is to bring the reader up to date on current techniques used and the range of microtextures now recognized on sands from glacial environments. From the evidence discussed by Mahaney (2002), it is possible, for example, to separate till from glaciolacustrine and glaciofluvial grains within the glacial sedimentary environment. Similarly, while it has proved difficult to separate tills genetically (Mahaney et al., 2001), it is possible to generate information related to glacial thickness and differences between warm and cold-based ice (Mahaney et al., 1988), as well as the relative amount of water transport within the glacier system.

In general terms, the pathway of grains from initial bedrock release (Figure 1a; quarrying process) leads to the production of *fracture faces* (Mahaney, 2002), the one common, but by no means the only, microtexture resulting from mechanical weathering. The fracture face is undeniably the common microtexture found on grains entering alpine glacial systems (Mahaney et al., 1991) and one that is soon overridden by a complex of new signatures comprised of subparallel linear fractures, conchoidal fractures, arc-shaped steps, uplifted plates, deep grooves, and microstriations, the latter being the one unique glacial microtexture, just as striations can be taken as evidence of glacial movement. Hence, glacial signatures can only be assessed from individual samples of till if the ice responsible attained a minimum thickness (~50–100 m) and applied a minimum force (Mahaney et al., 1988). Indeed, SEM microtexture imagery of α-quartz grains grown in an ice column and subjected to uniaxial stress under controlled conditions has indicated the importance of greatly increased glacial crushing that occurs along a transition from cold-based to warm-based ice with a minimum thickness in excess of ~100 m. At temperatures close to p-melting, and with cryostatic pressures equal to 1- and 2-km thick ice sheets, stick–slip motions appear to induce an array of microtextures on quartz sand grains that closely resemble microtextures observed on grains in tills deposited by the thickest Pleistocene glaciers of Canada, Europe, and the Antarctic. Aside from striated surfaces, it is not the presence of individual microfeatures that identifies the mechanism of glaciation, but the range of microtextures associated with varying degrees of glacial crushing. With decreasing ice thickness the range of microfeatures diminishes until, with thin cirque ice, little damage appears on grains transported from source to end moraines (Mahaney et al., 1988).

Grains subjected to aeolian processes (Figure 1b) produce bulbous edges, rounding and frosting on larger grains due to abrasion, along with occasional upturned plates and the presence of numerous craters of variable geometry (abrasion fatigue). Aeolian grains may be subject to multiple turbulent collisions during transport and later subjected to glacial transport which adds a whole new array of microtextures. The very fact that aeolian and glacial grains were differentiated in an analysis of Saharan ergs (Mahaney and Andres, 1996), without any previous knowledge of sedimentary processes on the part of the SEM operator, should convince skeptics that there is, indeed, an advantage in using SEM imagery in sedimentological analyses of various kinds. Aeolian microtextures are generally limited to superficial "skin" disruption and damage to individual grains which distinguishes them from deeper, more linear oriented "Wallner lines" produced by glaciation (Mahaney, 1991, 2002). Grains subjected to aeolian transport may retain their windblown signatures after transport in glacial systems but most often deeply embedded glacial crushing microfeatures may completely obliterate the aeolian source markings.

The fluvial environment, like the aeolian one, produces an array of superficial fractures and abrasion microfeatures often superficially disrupting the surfaces of grains, all of which are fine-tuned in the glacial environment. However, for the most part, fluvial transport tends to produce severe rounding and abrasion correlated with the discharge and turbulence of river or tsunami wave flow, the latter with optimal geomorphological parameters often results in resurfacing of quartz with a high count of v-shaped percussion scars (Mahaney et al., 2010b). Overprinting of fluvial grains brings forceful grain collisions that produce v-shaped percussion scars (Figure 1c), the one microtexture exclusive to the fluvial and geothermal environments. Interpretive difficulties arise because similar microfeatures are also produced by meltwater transport within glaciers, as for instance, in moulin systems or in fast moving, turbulent subglacial and englacial meltwater channels. If such grains are fluvially overprinted upon leaving the glacial system, the origin of the grain may be difficult or impossible to decipher. Of course, in nonglacial areas, streams leave an indelible record of water transport on quartz and other mineral

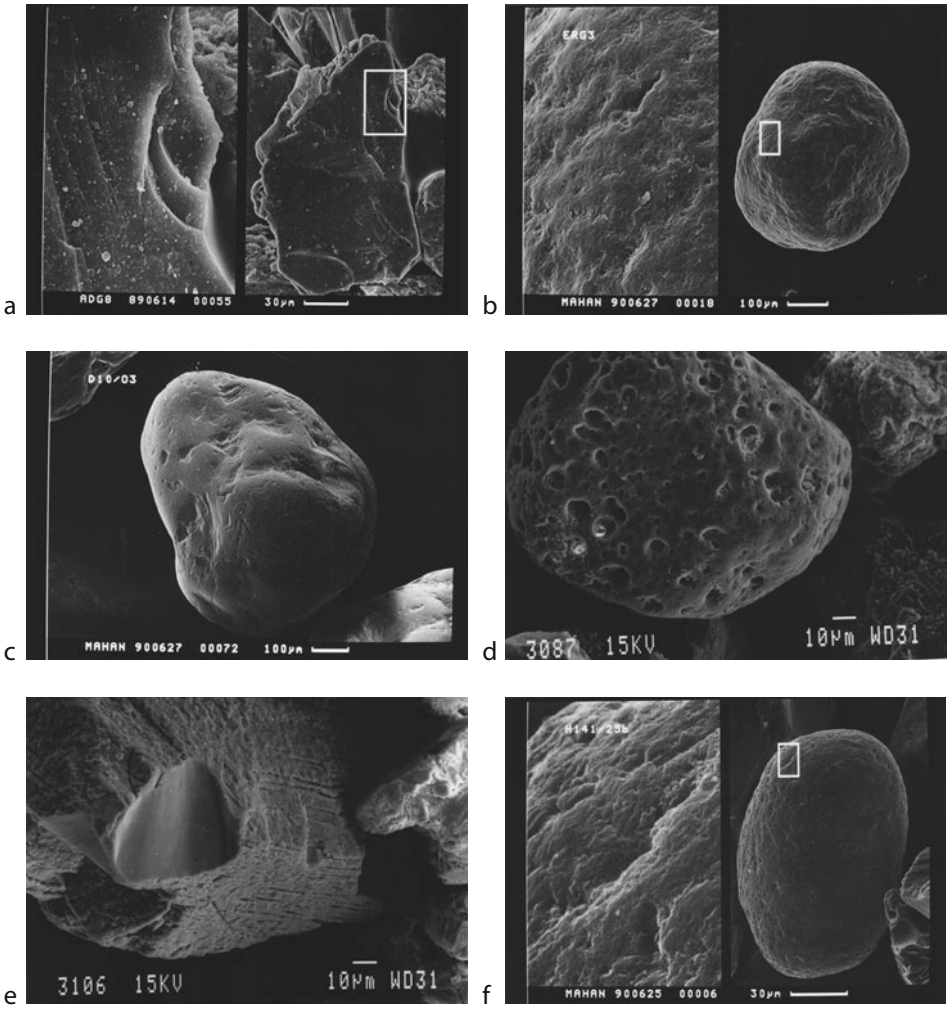

SEM Analysis of Glacial Sediments, Figure 1 (**a**) Mass wasted quartz grain, Adishy Glacier Area, Caucasus Mountains, Russia. The fracture face on the grain is typical of bedrock release accompanied by deep conchoidal fractures. The reverse side appears to be partly etched and covered with coating. Close up of the fractues is ×5. (**b**). Round quartz from Saharan ergs shows slight bulbous microfeatures (*right and top left facets*) and minor abrasion fatigue, a type of disrupted lattice formed from dry grinding. The disrupted lattice consists of broken surface structures of mm or micron size made up of small cracks, dislocations. The elongate depressions shown in the enlargement (×10) produce microrelief not seen with hand lens and probably result from saltation. (**c**), Aeolian grain with bulbous edges overprinted with v-shaped percussion cracks from transport in the Nile River; (**d**), Subround shock melted quartz with interconnecting melt cavities from Clear Creek, Colorado (K/T ejecta); (**e**), Shock lamellae on partially melted quartz, partially melted and annealed (From Mahaney, 2002, courtesy Oxford University Press). (**f**), Round quartz from lacustrine sand in the Thorncliffe Formation, Middle Wisconsinan age, Little Rouge Creek, Ontario, Canada. A plethora of v-shaped percussion scars attest to continual movement in Upper Flow Regime water masses (lacustrine or fluvial) prior to the ingress of Last Glacial Maximum ice in Southern Ontario.

fragments. Mass wasting, a neglected geologic agent in microtextural studies (Bull et al., 1987), initially leaves a record of bedrock release on grains just as in the glacial environment; however, fast or slow movement in gravitationally induced systems leads to the generation of new microtextures that involve grain packing and slickensides, microfeatures that are quickly erased in later glacial transport. The most distinctive microtexture in mass wasted sediments is the fracture face, a relatively clean break on the grain surface, often surrounded by varying degrees of chemical dissolution, microfeatures that survive transport in alpine glaciers, but are usually obliterated with long-distance transport in continental ice sheets. Thus, SEM investigations offer the chance to reconstruct source microtextures, followed by glacial, aeolian, and fluvial transport.

Some researchers (Oberbeck et al., 1993) consider that bolide (asteroid) impacts provide a plausible explanation for the occurrence of some tillites (ancient glacial deposits), characterized mainly by fragmented and

fractured quartz particles (Figures 1d and e). The tillites in question, however, are lacking in shock-melted quartz and planar deformation features (pdfs) which are the main product of extreme high-energy impacts ([15–25 km/s] [Boggs et al., 2001; Kennett et al., 2009; Firestone et al., 2007; Mahaney et al., 2010b]). Additional investigations of tillites are needed to determine if shock-melted quartz can be located in sufficient quantity to support the impact theory.

Glacial grains (Figures 2a–c and 3a–b) probably carry the greatest range of deeply embedded microtextures when compared with grains affected by other geologic agents. This includes the full range of fractures (Figures 2a–c and 3a–b), grooves, and abrasion microfeatures listed in Mahaney (2002), as well as solution-precipitation microfeatures and other coatings that may predate or postdate a glacial episode. Moreover, some grains (perhaps as many as 1 in 5) make the "glacial trip" unscathed by their sojourn in the ice and carry only microtextures related to previous environments. These fragments may carry a record of release from bedrock with unremarkable fracture faces, without the usual grain-to-grain contact in glacial systems that produce triangular faceted, sharp-edged grains with moderate to high relief, the latter usually well abraded with a multitude of fractures, grooves, and well-worn abrasion microfeatures.

As recorded in most studies, quartz is the ubiquitous and well-studied recorder of glaciation in many environmental settings (Krinsley and Doornkamp, 1973; Helland and Diffendal, 1993), major mineral suites, including all the plagioclase and orthoclase minerals, as well as many heavy minerals and gold, may also be analyzed to determine the degree of damage inflicted during glacial transport (Mahaney, 2002). This discussion, however, concentrates on quartz as the prime environmental recorder.

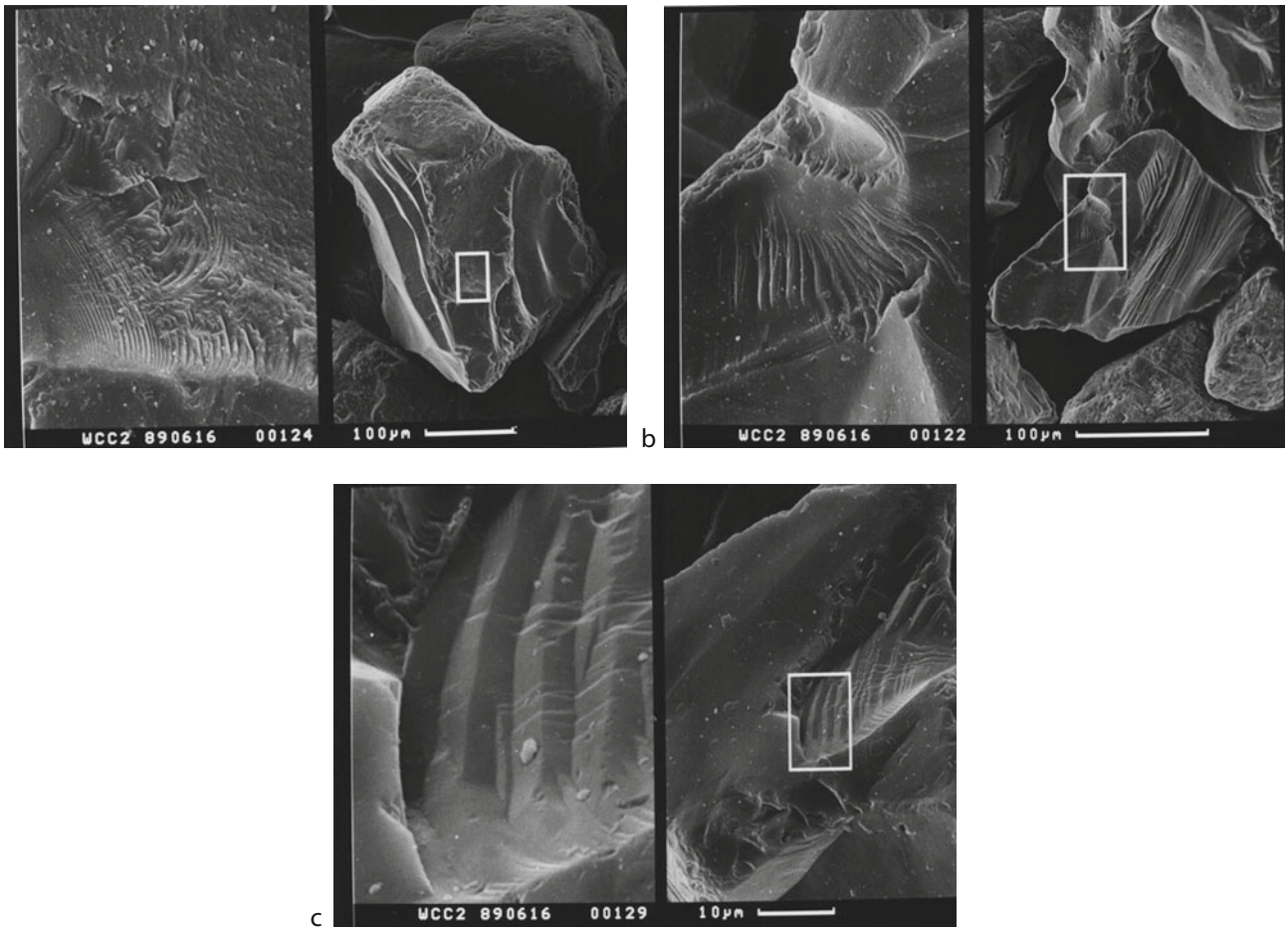

SEM Analysis of Glacial Sediments, Figure 2 (**a**), Deep troughs in subangular quartz from basal till, Wildcat Creek, Indiana. Linear troughs to left, curved troughs to right. Pseudo-chattermarks terminate on an upper ridge. See Folk (1975) for similar microfeatures on garnet. Upper grain is subrounded quartz and carries numerous v-shaped percussion scars from transport in meltwater. Crossed fractures, like crossed striae, depict typical high frequency younger fractures overprinting low frequency, higher wavelength microfeatures to the right in the enlargement (×10). (**b**), Quartz, heavily abraded and fractured; (**c**), Quartz with deep striations.

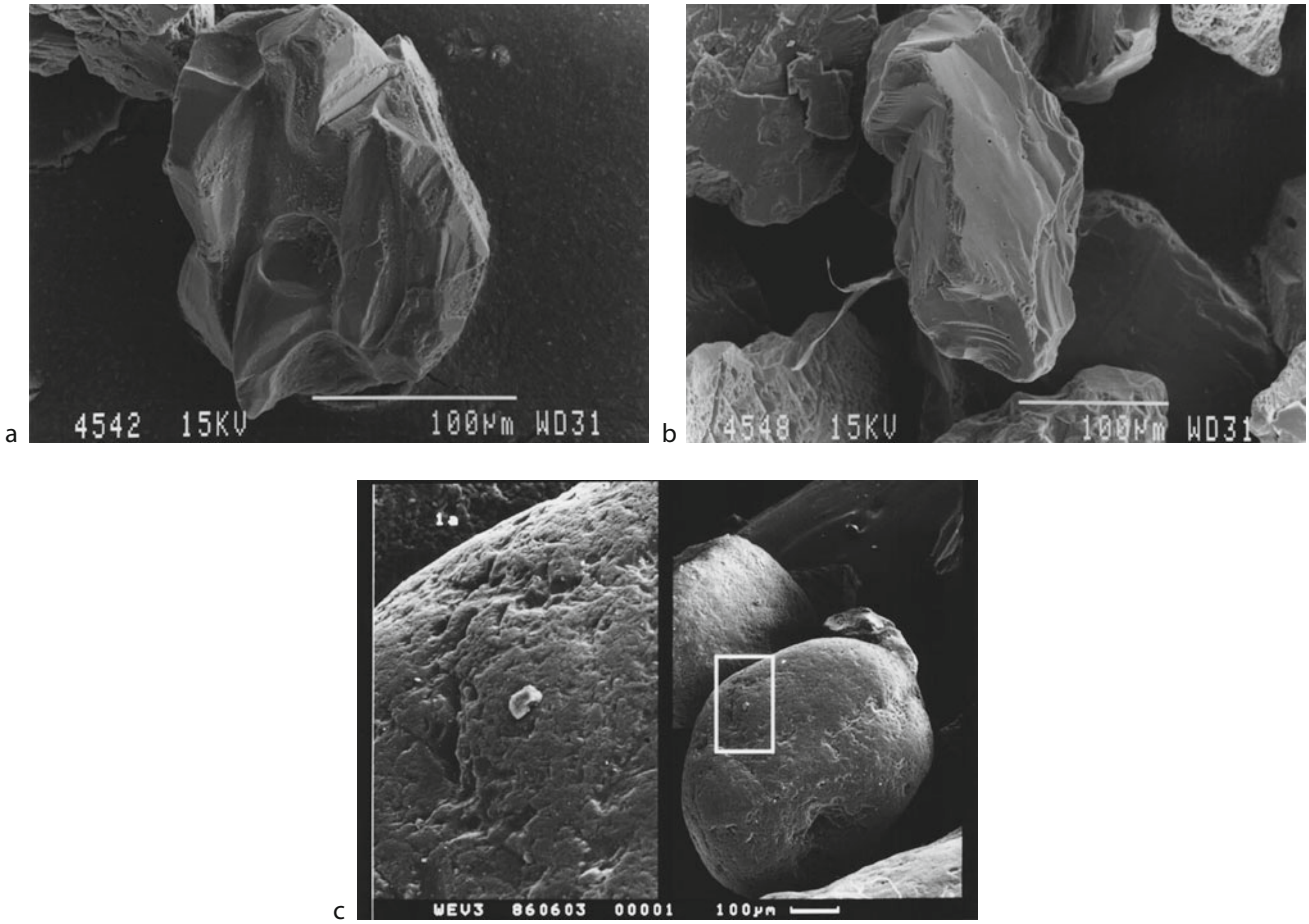

SEM Analysis of Glacial Sediments, Figure 3 (**a**) Angular quartz with partial abraded edges in Weichselian Till from sample TAR 3/3, Estonia. The sample shows deep grooves, multiple striations, deep cavities, well-abraded facets, and minor preweathering as indicated by minor etching; (**b**) from the same section, angular quartz with wavy, smoothed top and multiple grooves, striations and conchoidal fractures along the *c*-axis; (**c**) Two subround quartz grains with numerous v-shaped percussion cracks in the lowermost till, WEV3 Section, Wellsch Valley, Saskatchewan, Canada. The number of round grains with fluvial transport signatures depends on whether the till has a warm- or cold-based history. These grains have a warm-based history that becomes depleted up-section.

The relative hardness of quartz (7.0 on Mohs hardness scale) and its widespread occurrence in nearly every environment make it an ideal candidate for microtextural study. Grains are often unblemished, existing as colorless, hexagonal crystals, although sometimes colored by impurities. With an absence of cleavage, especially in the coarse fractions (2,000–50 µm), it is composed exclusively of silica-oxygen tetrahedra with oxygen atoms joined with silicon into a strong geometrical network (Frondel, 1962). Unlike weaker minerals, quartz is capable of transiting the glacier system many times and it is possible to examine complex quartz grains that have undergone many trips in the ice. Because quartz is subject to slow dissolution and precipitation, it is also an ideal mineral to record subaerial and diagenetic weathering events; moreover, it is possible to observe preweathered microfeatures overprinted with the fresh scars of glacial transport, followed by more recent weathering events. Hence, a single grain may carry evidence of several transport/weathering episodes (Mahaney, 2002).

Load

The load transported by ice ranges from clay to boulder and block sized material. It also includes a minor amount of aeolian-delivered grains as well as mass wasted material derived from nunataks and high-cirque walls. The supraglacial load may be light to heavy, depending on the nature of the source rocks and the climatic setting (tropical mountains to Arctic or Antarctic environments), and consist of material delivered by airfall influx and gravity to the glacier surface. There must be grain-to-grain contact even at pressures close to 1–2 atm to achieve sufficient stress in the basal ice to comminute mineral

material. The englacial environment, however, is relatively free of clastic load, although subsurface channels may move large volumes of meltwater that may occasionally carry clastic load. In these turbulent sluiceways grains may suffer heavy abrasion, giving overprints partially masking previously inherited weathering (e.g., preweathering) and other fractures and/or abrasion inflicted during the initial stage of ice transport.

The basal ice, containing the bulk of the clastic load in a glacier, together with variable amounts of water, provides the environment with the highest probability of grain-to-grain contact. Increasing water content tends to create hydrostatic pressures close to one bar and nearly equal in all directions. With decreasing water content, shear stress rises somewhat but falls far below the pressures that result from stick–slip processes (up to ~200 bars) where sudden slippage generates vibrations, the sudden convergence of kinetic energy to elastic energy. The vibrations produced by glacier movement are manifest in the array of fractures seen in great numbers on glacial grains. No other geologic agent can generate the strong vibrations, cones of energy that produce deeply embedded microfeatures in clasts nicely demonstrated by the multitude of fracture microfeatures often observed on glacial grains.

Of the many pathways by which clasts may enter, move through, and exit a glacier, grains of any description may: (a) sink into the ice from the glacial surface, (b) be carried by surface and subsurface meltwater streams to exit the terminal areas, (c) be forced to the surface by thrusting, and/or (d) be entrained from contact with underlying bedrock and/or till. This raises the question as to where to sample till, and whether it is best to concentrate on subglacial deposits where glacial grinding is apt to be at a maximum, or alternatively sample end or lateral moraines, which might likely contain a mix of material deposited directly in contact with ice or from meltwater.

Unlike aeolian and fluvial grains, glacial grains are generally held in bondage by the ice, or by other grains in rigid suspension, so that the ultimate amount of grinding occurs with movement down glacier. Aeolian and fluvial grains, as previously discussed, are capable of considerable turbulent random movement, and while they are capable of high-energy collisions, they are not subjected to the sustained and concentrated high-energy fields inflicted on glacial grains. While aeolian grains may produce scars somewhat reflecting microfeatures resulting from glaciation, the damage is far less deeply imbedded in the former grain surfaces.

As suggested by Barcilon and MacAyeal (1993) and Mahaney (1995, 2002) stick–slip motions at the base of glaciers tend to fracture and abrade particles in ice. Particle surface microtextures are governed partly by bedrock release (mechanical weathering), preweathering, resultant transport by different geologic agents and diagenesis/pedogenesis in a depositional environment. Within the ice body, quartz grains form inhomogeneous elastic inclusions with different strengths depending on preweathered states and these respond to variable stresses by forming fracture and abrasion microfeatures. If the particles are already weakened by chemical preweathering, and if they have fracture faces (Mahaney, 1995) derived from frost riving (Mahaney et al., 1991), they may easily comminute into smaller particles. This is particularly the case if they come into contact with one another in the basal ice layer where stick–slip processes produce high basal shear stresses and high strain rates (Barcilon and MacAyeal, 1993). Basal till, with meltwater lubrication, glides over bedrock and occasionally surges, subjecting particles carried as load to high fracture and abrasive stress, engendering low velocity impacts which impart microtextures onto quartz sand surfaces. While there are similar shallow, conchoidal and linear fractures on quartz from aeolian (Mahaney and Andres, 1996) and fluvial environments, the angular shape, deep entrenchment of conchoidal and linear fractures, and frequent directionality of troughs and grooves (striations) are unique to grains emplaced by glacial transport. As shown by Sweet and Soreghan (2010), Soreghan et al. (2008) and Strand et al. (2003) glacial microtextures may remain in the rock record for tens of millions of years.

Microtexture recognition

Almost all the microfeatures listed and discussed in Mahaney (2002) can be found on glacial grains. All dissolution and weathering microfeatures resulting from subaerial weathering and or diagenesis are presumably inherited from interstadial or interglacial climates having survived the damages inflicted on a large proportion of grains moving through glaciers.

Taking the array of microtextures as possible candidates for microfeatures likely observed on glacial grains, the researcher is faced with the question of how many grains to analyze and at what resolution. All microtextures should be logged by their frequency of occurrence, and it is necessary to analyze several samples and several fractions of each sample in order to arrive at a meaningful interpretation. A quick overview of each sample can be obtained by analysis of the fine and very fine sand fraction taking into account that angularity is often extreme in the finer fractions. This should be followed by analysis of at least 20 grains in the medium sand fraction (500–250 μm) and 20 grains in the coarse to very coarse fractions (2,000–500 μm). These grains should be collected as randomly as possible and studied under the light microscope prior to using the SEM.

The degree of relief is one of the first assessments to make when analyzing a sample suite. Because of heavy fracturing and abrasion, high relief often dominates on glacial grains. This needs to be assessed and given a percent frequency of occurrence. Next, among the population of grains studied, the degree of angularity, edge rounding, and all fracture and abrasion microfeatures need to be identified and frequency of occurrence tabulated. Last, all weathering, precipitation, and dissolution

features should be assessed in a similar fashion. Glacial grains should be compared and contrasted with grains resulting from the action of other geological agents, perhaps in the same section or between sections.

Continental glaciation

Wisconsinan and pre-Wisconsinan tills provide a wealth of information on glacial processes and preweathering that occurred prior to glacial entrainment (Mahaney, 1990a). One of the most striking microfeatures on grains from thick and extensive valley glaciers and continental glaciers are curved grooves, striations similar to those forms on bedrock or on pebble, and cobble clasts residing in tills (Figure 3a, b). Linear grooves may be glacial but they may also result from fault movement although with tectonic origins there is usually lattice distortion, very high abrasion, and uplifted surfaces that allow differentiation from glacial processes. Curvilinear grooves are unidirectional features that are as much an indisputable proof of the glacial environment as striations on rock. Whether these grains are frozen into the ice and dragged along the surface or affected by ice drag on particles, which eventually break off from bedrock; they are clearly the product of ice contact similar to macrofeatures that have been invoked to prove glaciation for nearly two centuries since the advent of the Glacial Theory proposed by Louis Agassiz.

Another microfeature typically observed on glacial grains is the v-shaped percussion crack (Figure 3c) that indicates the effect of water transport, presumably in this case, meltwater flow. Also with attrition along the edge of the grain some rounding appears to have been in progress when these grains were incorporated into till. Edge rounded grains, nearly equant, often carry surface scars of meltwater transport in somewhat greater abundance than is usual in fluvial systems. Often they are associated with grains showing directional grooves, steplike features, cirque-like amphitheater, overprinted with superficial radiating fractures less deeply inscribed and uplifted surface plates that have been lifted out leaving the amphitheater-like feature, the radiating fractures of which indicate plate removal may have come from a high-stress collision.

Antarctic tills

Grains in polar environments show heavily damaged surfaces representative of tills emplaced by continental ice. Often refashioned into triangular-shaped particles (Figure 4a–b), they exhibit deep fractures, upturned plate along the bottom of the grain, somewhat curved directional trough from top to mid region and steplike features on top right; much of the grain is extensively abraded. Considered to be the product of high stress fields, such microfeatures might be expected in thick continental ice with low water content where high local stick–slip motion might produce pressure capable of starting to dislocate the lattice. Polar grains display grains with high degrees of abrasion and directional troughs. While adhering particles are rather scarce on most of the sands shown here, they are more prevalent on the abraded grains.

The most intense crushing comes from the thickest ice as indicated by observations made by Mahaney et al. (1988) following a thorough examination of samples from Mount Kenya and southern Canada. Quartz sand grains in thick ice, such as the Antarctic Ice Sheet, are presumably subjected to transport over long distances with maximum stress generated by stick–slip mechanisms at the base of the ice.

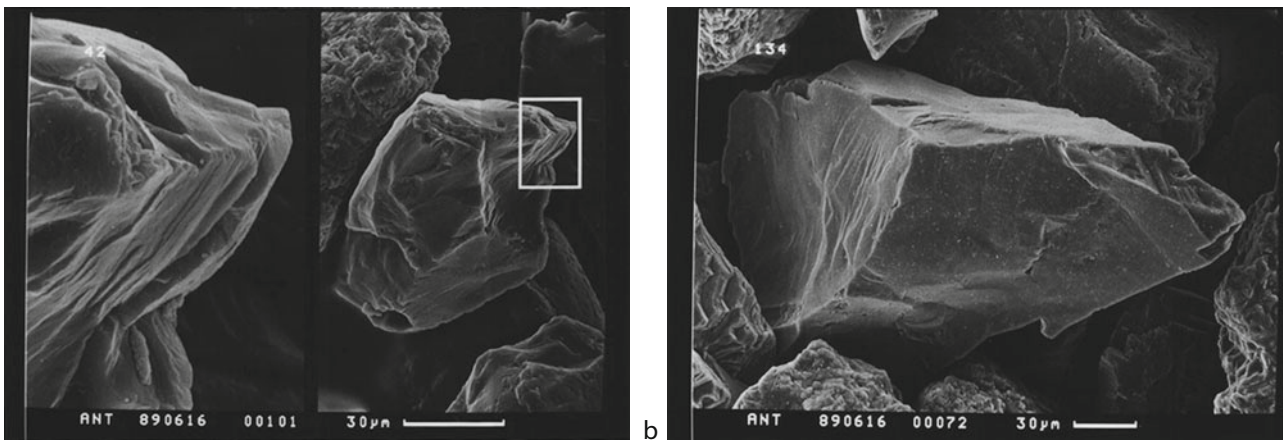

SEM Analysis of Glacial Sediments, Figure 4 (**a**) Angular quartz from till 42 (Mahaney et al., 1996) exhibiting multiple fractures, deposited by the Inland Ice Sheet, Antarctica. Edge of fractured quartz lower right; preweathered plagioclase in upper left; (**b**) Angular quartz with multiple fractures and minor preweathered etching in upper left surrounded by preweathered calcite and plagioclase.

Alpine glaciation

Quartz and other mineral grains, recovered from various tropical and middle latitude alpine areas (Figure 5a, b), show ranges of fracture microfeatures, striations, and abrasion that appear to be related to ice thickness and distance of transport (see Mahaney, 2002). Quartz and other minerals surviving transport in alpine ice carry a range of fractured and abraded preweathered grains showing varying degrees of *minor* subparallel linear fractures, conchoidal fractures, and abrasion that suggest low shear stress, low stress field conditions for stick–slip occurrences, and, of course, minimum transport distance. As previously discussed, many alpine subglacial tills are well lubricated with water giving them very low shear stress and high pore water pressure making it difficult to fracture grains carried as basal load. This condition must also affect stick–slip processes (Barcilon and MacAyeal, 1993; Mahaney, 1995) creating a situation where, even if stick–slip were to occur, the resulting shear stress would not overcome the shear resistance of the grain.

Reworking of grains from other environments through the glacial system is evidenced from several suites of samples from African massifs, the Andes, Tibet, Rocky Mountains, and the European Alps. The greatest ratio of preweathered to fresh grains is often observed in alpine areas for both Neoglacial and late Pleistocene tills studied to date. For example, the imagery indicates glacially crushed grains may carry extensive dissolution features, overprinted with a glacial signature followed by younger weathering and re-entrainment in an active glacier.

Experimental fractography

The theory of brittle and ductile fracture, the central canon of microtexture theory, requires the fracturing of quartz and other minerals to result from increasing stress until strain produces slow to catastrophic crack propagation. The resulting fractures may open along preexisting flaws in minerals (Griffith cracks) and/or generate new flaws extending across mineral surfaces, either as shallow or deeply embedded cracks. These fractures are predetermined by the stress–strain energy field, much as vibrational energy is released through the grain (Mahaney, 1995). In a glacier, large sand grains of very coarse to coarse (2,000–500 μm) grade size require less stress to fracture than smaller ones (500–50 μm), but much depends on the applied stress field, strength of the minerals undergoing strain, and particularly their weathered state. In general smaller grains require, on average, higher stress fields to induce failure leading to crack propagation. Put another way, the probability of fracture by breaking the weakest mineral increases with increasing size of fragments. Particularly susceptible are mineral intergrowths, as for example, quartz and biotite, with the latter mineral prone to rupture. Analysis of different grade sizes of glacial sands (Mahaney, 2002) within the same till sample reveals that coarse fractions exhibit about the same range of glacial microtextures as fine ones.

Analysis of different fragment grade sizes of sands in glacial sediment has shown that repeated fracturing results in increased fragmentation. Increased fragmentation, and hence smaller size material, requires increased stress to achieve continual fracturing as particle size diminishes from sand to silt. Small silt-size fragments (<50 μm) continually fragmented/comminuted and/or liberated from larger grains by grinding at the base of the ice lie at the end of their size reduction run (Dreimanis and Vagners, 1971), and are apt to be preserved intact in till after their sojourn in the ice. These smaller grains may carry the final range of microtextures from glacial crushing, the end product of a long series of grinding and fragmentation from very coarse sand to silt. Other small fragments of

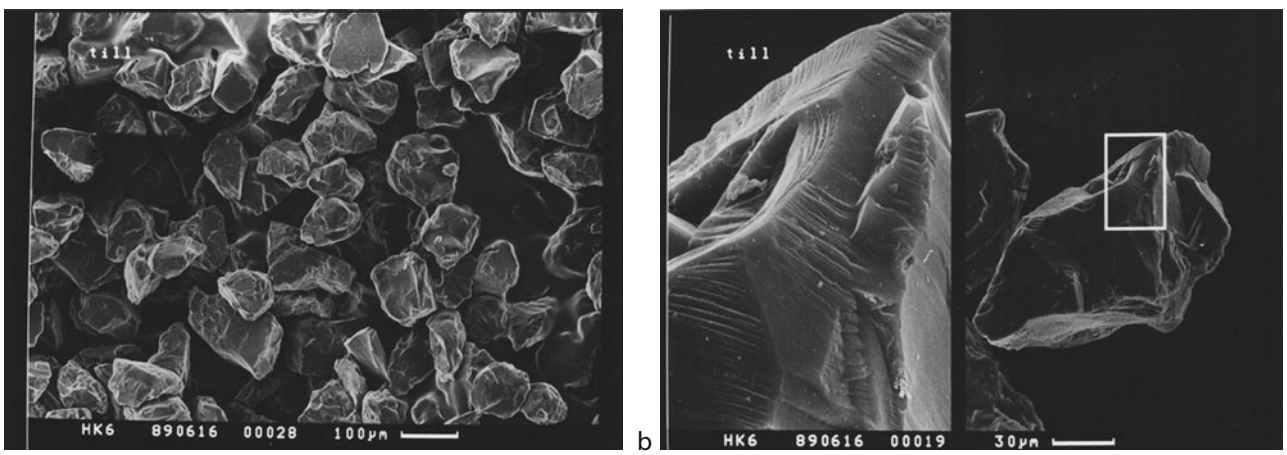

SEM Analysis of Glacial Sediments, Figure 5 (**a**) General frame showing angular and subangular grains, a mix of plagioclase, orthoclase, minor biotite, and quartz in till from section HK6, Zillertal Alps, Austria; (**b**) Angular quartz with multiple fractures and deep grooves.

the same size, subjected to low pressure mechanical action by either mass wasting, aeolian, and/or fluvial agencies long before they are added as load to a glacier, are likely to be little modified by the mechanical forces of an active glacier although they may be overprinted with a glacial signature. This is why fine sand–silt fractions are important to study with the objective of cataloging the range of microtextures at close to the final stage of comminution. Therefore, depending on grain-to-grain contact within the ice some of the grains in the fine and medium silt fractions may have a microtexture record entirely unrelated to travel in the ice; that is, some grains make the glacial trip in isolation, without contact with other grains.

Fractography, that is the identification and interpretation of fractures on particle surfaces (Krinsley and Donahue, 1968; Krinsley and Doornkamp, 1973; Margolis and Krinsley, 1974; Mahaney et al., 1988; Mahaney, 1990a, b, 1995; Marshall, 1987), has been pursued with the objective of analyzing individual fracture markings, and their frequency of occurrence, as a means to gain insight into glacial grain history. All attempts to target certain microtextures as "glacial" have made it necessary to pose several important questions: (1) Do characteristic mechanical damage microfeatures reside on grains subjected to glacial transport? (2) If glacial microfeatures exist, are they related to glacial dynamics? (3) If unique glacial microtextures exist, is it possible to deduce distance of transport and ice thickness from the fractography?

Many different minerals have been used to study crack propagation in glacial grains but quartz is the usual material selected as test material for stress–strain relationship tests because it is abundant in glacial deposits and its hardness ensures it to be an excellent long-lived recorder of damage inflicted on it. As a test, amorphous silica glass spheres have been utilized: (1) as an analog of quartz that could be subjected to low stress in a confined space, (2) using a spherical shaped object makes it possible to compare with crushed mineral grains, and (3) to determine the shape and number of fractured particles.

Since several previous fractographic studies were performed on till particles in the 50–500 μm range (Krinsley and Donahue, 1968), and on larger particles of 16–26.5 mm diameter (Iverson, 1990), it seemed logical to carry out laboratory experiments using quartz of a similar size. In the first three tests, particles were selected from fragments of a large single piece of optically translucent α-quartz (from Brazil), crushed by low velocity impact. After separating the particles into three size categories of 50–500 μm sizes, they were subjected to compression in a cylindrical volume of ice at 2,000 psi capacity (see Mahaney, 2002). Compression was achieved in a piston cylinder that contained a cooling agent maintained at a constant low-test temperature.

Mineral fragments were sprinkled widely on ice, which was grown by layer to insure particle segregation. Each layer was periodically subjected to a low vacuum of ~1 Torr to eliminate as much air as possible. The first three tests were run on quartz fragments. In Test 1 the ice temperature was below −10°C, thus similar to a cold glacier. Tests 2 and 3 were carried out using quartz (2) and silica glass (3) and with the temperature raised to p-melting simulating warm glacier conditions. The objective of the experiment was to determine the amount of fracturing that occurred in the charge before and after compression in ice.

Test 1 (Figure 6a) used the *fine* sand fraction (125–250 μm), selected as load with a maximum pressure of 2,000 psi or 17.5 Mpa on the ice cylinder, as before equating to an ice thickness of 1.98 km, applied for 30 min. Recovered grains showed several new fragments with sizes finer than the starting size. Original fragments with protrusions were subjected to considerable edge rounding and several flaky particles were likely due to physically induced spalling probably from lattice disruption.

In Test 2 (Figure 6b), the grain size and cylinder pressure were approximately the same as in Test 1. In this experiment, grains were subjected to similar pressure as in Test 2 for 40 min while temperature was brought up to p-melting. The imagery of the resultant charge shows considerable change in particle size and distribution. Here, several small fragments and fine fragments cling to larger ones, which survived compression. P-melting conditions in the test cylinder led to formation of meltwater; ice bridges melted, allowing particles to join. Particles at the base of the brass cylinder were subjected to high hydraulic pressure causing some quartz to become embedded in the brass base. In this third test, quartz grains were fractured into numerous particles brought into mutual contact under high load. These particles exhibited unmistakable arc-shaped steps with numerous and deeply imbedded conchoidal and subparallel linear fractures, with a sizable population of fine adhering particles.

Test 3 (Figures 6c and d), the concluding test in this series, was designed to study the effect of compression on a population of well-isolated, untouched, and perfectly spherical silica glass spheres. These were situated to represent inhomogeneous inclusions exactly as would occur with fresh quartz released from bedrock. Because of their sphericity, they represented a set of particles with equal geometric stress concentrating factors, easily amenable to theoretical analysis but different from what would occur in nature. Pressure was applied at 17.5 Mpa as in the previous tests, and after a short time, the temperature was raised to p-melting. Mechanical damage on this load was severe with four spheres totally shattered into small fragments of fine sand and silt size, others greatly reduced in diameter, and still others escaping with only a few craters produced. Apparently the nine spheres suffering the greater damage released fine particles simulating glacial grinding, the latter process originally postulated by Smalley (1966).

These experiments show that coarse silt inclusions in ice apparently unaffected escape compression. Sizes ranging from fine to medium sand are affected by compression depending on temperature. Clearly, the p-melting temperature is critical to produce the greatest degree of fragmentation as shown in Tests 2 and 3. Large particles of equal

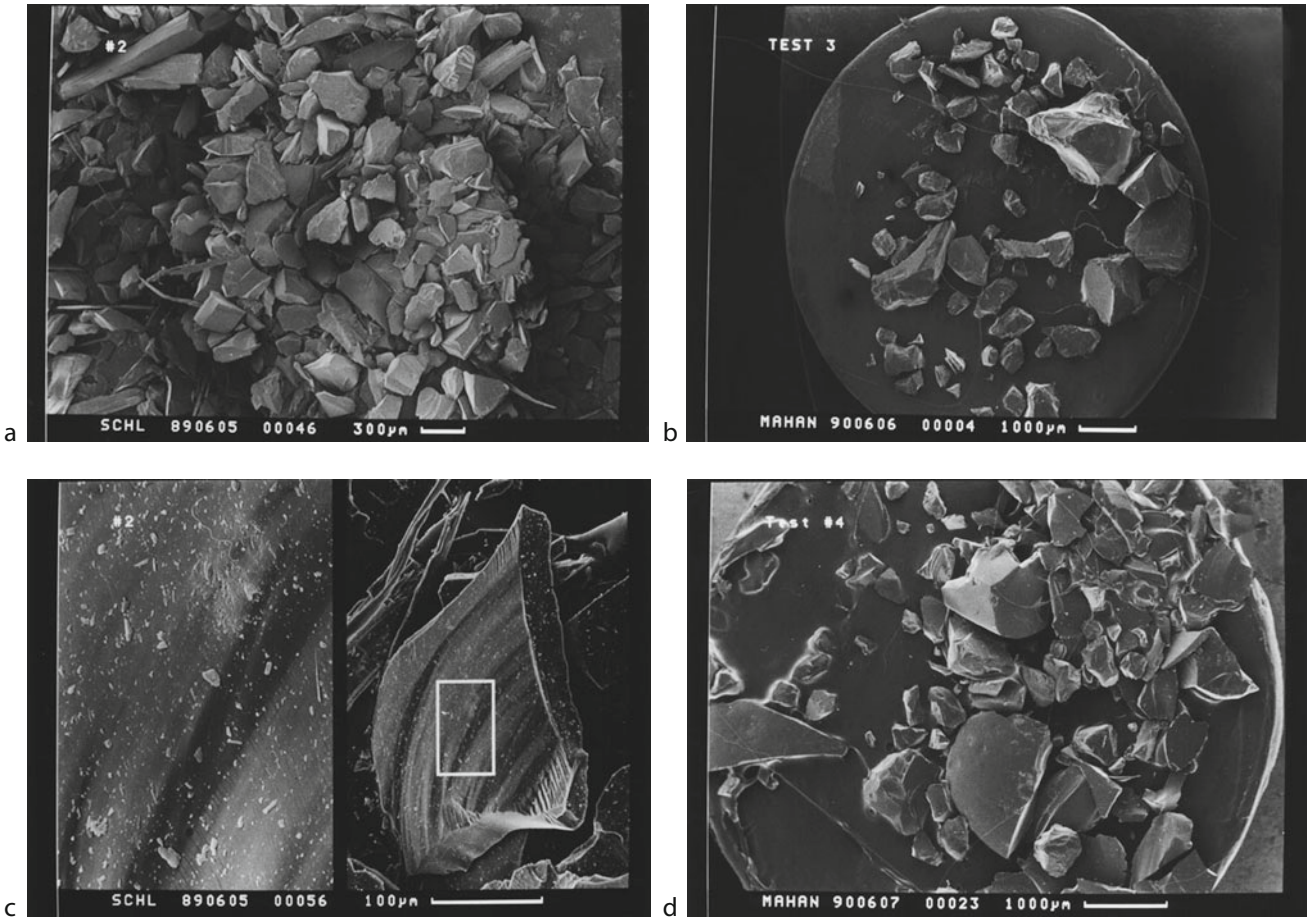

SEM Analysis of Glacial Sediments, Figure 6 (**a**) Recovered charge of fragmented sands originally sieved to medium and fine sand size (125–250 μm diameter). Approximately 25–30 grains of the sample were fragmented into smaller sizes; (**b**) Representative quartz fragments from Test 2 of approximately 125 μm diameter, with deeply imbedded conchoidal and subparallel linear fractures and sharp edges with numerous adhering particles; (**c**) Fragments of silica spheres, originally of 250–1,000 μm size recovered (Test 3) after compression in ice at simulated thickness of 1.98 km; (**d**) Recovered fragmented charge from Test 4. Original size of the silica spheres was 3.5 cm. Simulated ice thickness was 1.98 km. Experimental laboratory work compressing alpha quartz and silica spheres at simulated glacial crushing pressures was done in the laboratory of Prof. H. Schloessin, University of Western Ontario, London.

sphericity are subject to considerable comminution when temperature is raised to the p-melting point. The experimental data show that ice of varying thickness is capable of glacial crushing as originally postulated by Krinsley and Doornkamp (1973), but much depends on grain to grain contact, glacial overprinting on preweathered grains, and cold versus warm ice.

Conclusions

The triangular faceted "glacial grain," depicted in Krinsley and Doornkamp (1973), as a triangular faceted, refashioned quartz, with a multitude of fracture and abrasion features is one of the *common* particles found in the sand fraction of tills. As shown here it is by no means the only well-fractured and abraded particle in till, although depending on the ice thickness and distance of transport it could amount to 40% or 50% of grains observed. There are other grains including equant grains with minor damage, flake-shaped grains often with an abundance of abrasion and little fracture, partly streamlined abraded particles with variable damage, and preweathered grains. The preweathered grains often reach 30% of the total population of grains in till observed under the SEM, which means that perhaps as many as 1 in 3 of the grains analyzed might carry important information about preglacial weathering. Indeed, in some instances, the degree of preweathering might yield important information about paleoleaching and the strength of interglacial climates (see Mahaney, 1990a). Indeed, on Mount Kenya, plagioclase and quartz from the last interglacial carried coatings of fibrous and nodular gibbsite in considerable

quantity as determined by XRD and SEM/EDS, the product of aggressive leaching and removal of Si leading to meta-halloysite degradation (Mahaney, 1995).

Microtextures considered of unequivocal glacial origin include directional curved and straight grooves or troughs. Groove is a useful term for lightly imbedded striations, with troughs reserved for deeply embedded features, to the order of 5 μm or more. These are as much the exclusive product of the glacial environment as macrostriations that have been used for nearly two centuries as chief indicators of glaciation. In the microworld it may be that minerals harder than quartz (topaz, zircon, etc.), while of low mass in most tills, could, when in contact with quartz, leave directional troughs and grooves. Perhaps this leads to the production of pencil-shaped zircons commonly found in some tills (Mahaney and Milner, 1998).

Deeply inscribed fractures are common on glacial grains, but not exclusive to the glacial environment. Over a large population of grains, however, conchoidal and subparallel linear fractures would be expected to dominate as one of the most frequently occurring forms. Only thick valley glaciers and glaciers of continental proportions would be expected to produce deeply imbedded features of this type. Sharp edges, where grains have been worn away by abrasion, are also a hallmark of the glacial environment. They are not unequivocally glacial, but taken as a proportion of the whole in a large population of samples they can be expected to have a frequent occurrence.

Relief on glacial grains is often considered high but with extreme abrasion, common with thick ice, grain surfaces may be worn to produce minimum relief. Grains deposited by cirque ice and outlet glaciers often exhibit moderate to high relief, which may in fact mislead investigators into thinking considerable grain modification and reformation has been achieved.

Chattermarks (Folk, 1975; Peternecht and Tietz, 2010), often touted as the common glacial microtexture, are in reality extremely rare, despite infrequent observations that seem to attract attention. Trails of chattermarks forming rune-like grooves, while infrequently common on glacial grains, are now known to be the product of mechanically induced fractures that become visible after chemical etching, a process originally envisioned by Bull (1981). Experimental work carried out by Peternecht and Tietz (2010) confirms that collision of minerals leads to disruption of the internal crystal lattice, the fracture sites dissolving faster than the surrounding mineral fabric. Once the mechanically induced fractures are subjected to chemical weathering, the fracture sites become visible. Chattermarks are therefore considered to be part of a two-stage process; first, mechanical collision during transport followed by chemical weathering at a later stage.

Steplike features resulting from well placed and deeply embedded fractures are unequivocally glacial in origin (Mahaney, 2002). These mechanically induced microfeatures may result from larger grains blasting fragments off smaller grains as a result of their increased mass/energy relationships. Much depends on random events within the ice mass and the probability of grain-to-grain contact, impact angle, force (cone of energy), bulk mass, and hardness of the material.

The fact that so many preweathered grains make the glacial trip without damage means that not all glacial grains come into contact with one another. While preweathered grains provide important information on interglacial climates, their coatings can range from carbonate and silica to iron and manganese; even clay coats have been documented (Mahaney et al., 1996) from the Antarctic. As with other geologic agents, to prove a glacial origin requires a large number of samples from different size fractions (very coarse–coarse; medium; and fine–very fine sand), all documented with replicates.

Bibliography

Barcilon, V., and MacAyeal, D. R., 1993. Steady flow of a viscous ice stream across a no slip/free transition at the bed. *Journal of Glaciology*, **39**, 167–185.

Biederman, E., 1962. Destruction of shoreline environments in New Jersey. *Journal of Sedimentary Petrology*, **32**, 181–200.

Boggs, S., Krinsley, D. H., Goles, G. G., Seyedolali, A., and Dypvik, H., 2001. Identification of shocked quartz by scanning cathodoluminescence imaging. *Meteoritics and Planetary Science*, **36**, 783–791.

Bull, P. A., 1981. Environmental reconstruction by scanning electron microscopy. *Progress in Physical Geography*, **5**, 368–397.

Bull, P. A., Goudie, A. S., Price-Williams, D., and Watson, A., 1987. Colluvium: a Scanning Electron Microscopy analysis of a neglected sediment type. In Marshall, J. R. (ed.), *Clastic Particles*. New York: Van Nostrand Reinhold, pp.16–35.

Dreimanis, A., and Vagners, U. J., 1971. Bimodal distribution of rock and mineral fragments in basal tills. In Goldthwaite, R. P. (ed.), *Till-A Symposium*. Columbus: Ohio State University Press, pp. 237–250.

Firestone, R. B., West, A., Kennett, J. P., Becker, L., Bunch, T. E., Revay, Z. S., Schultz, P. H., Belgya, T., Kennett, D. J., Erlandson, J. M., Dickenson, O. J., Goodyear, A. C., Harris, R. S., Howard, G. A., Kloosterman, J. B., Lechler, P., Mayewski, P. A., Montgomery, J., Poreda, R., Darrah, T., Que Hee, S. S., Smith, A. R., Stich, A., Topping, W., Wittke, J. H., and Wolbach, W. S., 2007. Evidence for an extraterrestrial impact 12, 900 years ago that contributed to the megafaunal extinctions and the Younger Dryas cooling. *Proceedings of the National Academy of Sciences*, **104**, 16016–16021.

Folk, R. L., 1975. Glacial deposits identified by chattermark tracks in detrital grains. *Geology*, **3**, 475–479.

Frondel, C., 1962. *The System of Mineralogy, Vol. II, Silica Minerals*. New York: Wiley, 334 p.

Helland, P. E., and Diffendal, R. F., Jr., 1993. Probable glacial climatic conditions in source areas during deposition of parts of the Ash Hollow Formation, Ogallala Group (Late Tertiary), of western Nebraska. *American Journal of Science*, **293**, 744–757.

Iverson, N. R., 1990. Laboratory simulations of glacial abrasion: comparison with theory. *Journal of Glaciology*, **36**, 304–314.

Kennett, D. J., Kennett, J. P., West, A., Mercer, C., Que Hee, S. S., Bement, L., Bunch, T. E., Sellers, M., and Wolbach, W. S., 2009. Nanodiamonds in the Younger Dryas boundary sediment. *Science*, **323**(5910), 94.

Krinsley, D., and Donahue, J., 1968. Environmental interpretation of sand grain surface textures by electron microscopy. *Geological Society of America Bulletin*, **79**, 743–748.

Krinsley, D., and Doornkamp, J. C., 1973. *Atlas of Sand Grain Surface Textures*. Cambridge: University Press, p. 91.
Krinsley, D., and Takahashi, T., 1962. The surface textures of sand grains: an application of electron microscopy. *Science*, **135**, 923–925.
Mahaney, W. C., 1990a. *Ice on the Equator*, Ellison Bay, WI: William Caxton Ltd, 386 p.
Mahaney, W. C., 1990b. Macrofabrics and quartz microstructures confirm glacial origin of Sunnybrook drift in the Lake Ontario Basin. *Geology*, **18**, 145–148.
Mahaney, W. C., 1991. Two distinct particle types in the Lanzhou Loess. *Naturwissenschaften*, **78**, 167.
Mahaney, W. C., 1995. Pleistocene and Holocene glacier thicknesses, transport histories and dynamics inferred from SEM microtextures on quartz particles. *Boreas*, **24**, 293–304.
Mahaney, W. C., 2002. *Atlas of Sand Grain Surface Textures and Applications*. Oxford, UK: Oxford University Press. 237 p.
Mahaney, W. C., and Andres, W., 1996. Scanning electron microscopy of quartz sand from the north-central Saharan desert of Algeria. *Zeitschrift für Geomorphologie N.F, Suppl-BD.*, **103**, 179–192.
Mahaney, W. C., and Milner, M., 1998. Zircon microstriators in the sand of auriferous Andean tills: fine tools and noble metals. *Boreas*, **27**, 140–152.
Mahaney, W. C., Vortisch, W. A., and Julig, P., 1988. Relative differences between glacially crushed quartz transported by Mountain and continental ice-some examples from North America and East Africa. *American Journal of Science*, **288**, 810–826.
Mahaney, W. C., Vaikmae, R., and Vares, K., 1991. Scanning Electron Microscopy of quartz grains in surpraglacial debris, Adishy Glacier, Caucasus Mountains, USSR. *Boreas*, **20**, 395–404.
Mahaney, W. C., Claridge, G., and Campbell, I., 1996. Microtextures of quartz grains in tills from Antarctica. *Paleo-3*, **121**, 89–103.
Mahaney, W. C., Stewart, A., and Kalm, V., 2001. Quantification of SEM microtextures useful in sedimentary environmental discrimination. *Boreas*, **30**, 165–171.
Mahaney, W. C., Kalm, V., Kapran, B., Milner, M. W., and Hancock, R. G. V., 2009. Soil chronosequence, Humboldt Glacier, northwestern Venezuelan Andes. *Geomorphology*, **10**, 99–110.
Mahaney, W. C., Dohm, J., Costa, P., and Krinsley, D. H., 2010a. Tsunamis on Mars: Earth analogues of projected Martian sediment. *Journal of Planetary and Space Science* (in press).
Mahaney, W. C., Kapran, B., Milner, M. W., Kalm, V., Krinsely, D., Beukens, R., Boccia, S., and Hancock, R. G. V., 2010b. Evidence from the northwestern Venezuelan Andes for extraterrestrial impact. *Geomorphology* (in press).
Margolis, S., and Krinsley, D., 1974. Processes of formation and environmental occurrence of microfeatures on detrital quartz grains. *American Journal of Science*, **274**, 449–464.
Marshall, J. R., 1987. *Clastic Particles*. New York: Van Nostrand Reinhold Co. 346 p.
Oberbeck, V. R., Marshall, J. R., and Aggarwal, H., 1993. Impacts, tillites and the breakup of Gondwanaland. *Journal of Geology*, **101**, 1–19.
Peterknecht, K. M., and Tietz, G. F., 2010. Chattermark trails: surface features on detrital quartz grains indicative of a tropical climate. *Journal of Sedimentary Research* (In press).
Porter, J., 1962. Electron microscopy of sand surface textures. *Journal of Sedimentary Petrolgy*, **32**, 124–135.
Smalley, I. J., 1966. The properties of glacial loess and the formation of loess deposits. *Journal of Sedimentary Petrology*, **36**, 669–676.
Soreghan, G. S., Soreghan, M. J., Poulsen, C. J., Young, R. A., Eble, C. F., Sweet, D. E., and Davogustto, O. C., 2008. Anomalous cold in the Pangaean tropics. *Geology*, **36**, 659–662.
Strand, K., Passchier, S., Nasi, J., 2003. Implications of quartz grain microtextures for onset of Eocene/Oligocene glaciation in Prydz Bay, ODP Site 1166, Antarctica. *Palaeo*-3, **198**, 101–111.
Sweet, D. E., and Soreghan, G. S., 2010. Application of quartz sand microtextural analysis to infer cold-climate weathering for the equatorial Fountain Formation (Pennsylvanian-Permian, Colorado, USA). *Journal of Sedimentary Research*, **80**, 666–677.
Whalley, W. B. (ed.), 1978. *Scanning Electron Microscopy in the Study of Sediments*. Norwich: GeoAbstracts.

Cross-references

Alps
Andean Glaciers
Antarctica
Cirque Glaciers
Dynamics of Glaciers
Geocryology
Glacial Grooves
Glacial Striations
Glacier
Glacier System
Ice Age
Little Ice Age
Moraine
Quaternary Glaciation

SEPTA OF ENGLACIAL DEBRIS

Subhajit Sinha
DBS College, Dehradun, Uttarakhand, India

Debris input to glaciers occurs most commonly at ice margins and is thus concentrated along the base of cirques and in medial debris septa that ultimately become medial moraines. Proximal debris addition from rockfalls and increasing debris concentration from below by ice sublimation results in supraglacial debris mantles in the distal direction with great spatial variability in thickness and grain size. As ablation proceeds, debris accumulations represented by englacial septa emerge and form longitudinal or transverse debris ridges separated by areas of cleaner or bare ice.

SERAC

Markus Konz
ETH Zürich Institut für Umweltingenieurwissenschaften, Hydrologie und Wasserwirtschaft, Zürich, Switzerland

The word “serac” originated from the Swiss French sérac, which is a type of a crumbly white cheese. Seracs are needle-like towers, individual blocks, or columns of ice on the surface of a glacier. Their height varies between few meters to tens of meters. They can be found within icefalls or on the lower edge of hanging glaciers (e.g., Post

and Lachapelle, 2000). Seracs are commonly formed by intersecting crevasses where the glacier is periodically broken as it passes over a steep slope. They can cause disastrous hazards and are dangerous to mountaineers due to rapid toppling often with little advance warning time.

Bibliography

Post, A., and Lachapelle, E. R., 2000. Glacier ice. University of Washington Press, Seattle.

SIBERIA

Kazuyoshi Suzuki
Research Institute for Global Change, Japan Agency for Marine-Earth Science and Technology, Yokohama, Japan

Definition

Siberia: a region of northern Asia of Russia, stretching from the Ural Mountains to the Pacific Ocean.
Continental air mass: vast body of air that forms over the interior of a continent, excluding mountainous areas.
Anticyclone: weather phenomenon in which there is a descending movement of the air and a high pressure area over the part of the planet's surface affected by it.
Continental arctic air: air that are extremely cold and dry due to their continental source region between 60° and 90° north latitude.
Tundra: a biome in which tree growth is hindered by low temperatures and short growing seasons.
Taiga: a biome characterized by coniferous forests.

Introduction

Siberia has the largest area of permafrost in the world. Furthermore, the freshwater in the large Arctic rivers of Eurasia that flow from Siberia to the Arctic Ocean plays an important role in the control of the global thermohaline circulation by modifying salinity and sea-ice formation in the Arctic Ocean. In addition, snow and ice greatly affect the lives of the people inhabiting Siberia. This article discusses the characteristics of snow and ice in Siberia.

Geography and climate

Siberia occupies the Asian part of Russia and consists of three major subregions shown in Figure 1a. In the west, abutting the Ural Mountains, is the huge West Siberian Plain, drained by the Ob and Yenisey rivers. It varies little in relief and includes wide tracts of swampland. East of the Yenisey River is central Siberia, a vast area that consists mainly of plains and the central Siberian Plateau. Farther east, the basin of the Lena River separates central Siberia from the complex series of mountain ranges, upland massifs, and intervening basins that make up East Siberia.

According to *Climates of the U.S.S.R.* by Borisov (1965), there are four major climate zones in Siberia. The climate zones of West and East Siberia are each subdivided into two climate zones according to the dominant vegetation, tundra or taiga. Here, West Siberia as used here includes the central Siberian Plateau. West Siberia is characterized by many days dominated by continental arctic air and East Siberia by prevailing continental temperate climate and continental arctic air masses, which converge to form mainly extensive anticyclones, especially in winter. The taiga corresponds with regions of subarctic and cold continental climate with long, severe winters (up to 6 months with mean temperatures below freezing) and short summers as characteristic, as has a wide range of temperatures between the lows of winter and highs of summer. On the other hand, tundra corresponds with the regions of polar climate with extremely short growing season (6–10 weeks) and long, cold, dark winters. Tundra occupies the region between tree line and polar ice cap. Tundra–taiga boundary is corresponding to the arctic front (Bryson, 1966).

Figure 1b denotes the four major climate regions. The West Siberian tundra region is characterized by contrast in the intensity of solar radiation during the year and by a long, severe winter with frequent passage of low-pressure systems accompanied by violent gales and heavy snowstorms. In contrast, a high-pressure system typically develops over the East Siberian tundra region in winter, leading to stable winter weather and a negligible snow cover. Because of its great continentality, the region is characterized by contrasting conditions between summer and winter. The West Siberian taiga region is characterized by the active movement of air masses from the Atlantic and Arctic oceans with the continental air mass and anticyclones formed in Siberia. The East Siberian taiga region is characterized by marked continentality such as the prevalence of clear-cut anticyclonic weather conditions, very frosty and cold cloudless winter weather and hot summers with high solar radiation, and the sudden onset of seasons.

Frozen ground

Permafrost is the dominant component of the Siberian soil; about 80% of area in the subsurface in Siberia is composed of permafrost. Kondratjeva et al. (1993) showed that permafrost in Siberia mostly developed in the Late Pleistocene during the Sartanian glaciation (Late Wisconsinan/Weichselian, 18,000–27,000 years ago). The average air temperature at that time was 8–10°C lower than at present, and under these very cold conditions, permafrost spreads over Siberia, eventually extending its southern boundary to 48–49° N during the Sartanian glaciation. Subsequently, in the Holocene, the spatial extent of the permafrost was greatly reduced in West Siberia, where the southern permafrost border has been displaced northward to 60° N. Although in East Siberia the permafrost has retained almost the same spatial coverage as during the last glacial period, it has likely become reduced in thickness. Duchkov (2006) showed that permafrost reaches its greatest thickness (more than 1 km) in Yakutia, central Siberia, where it forms the lowest temperature block of

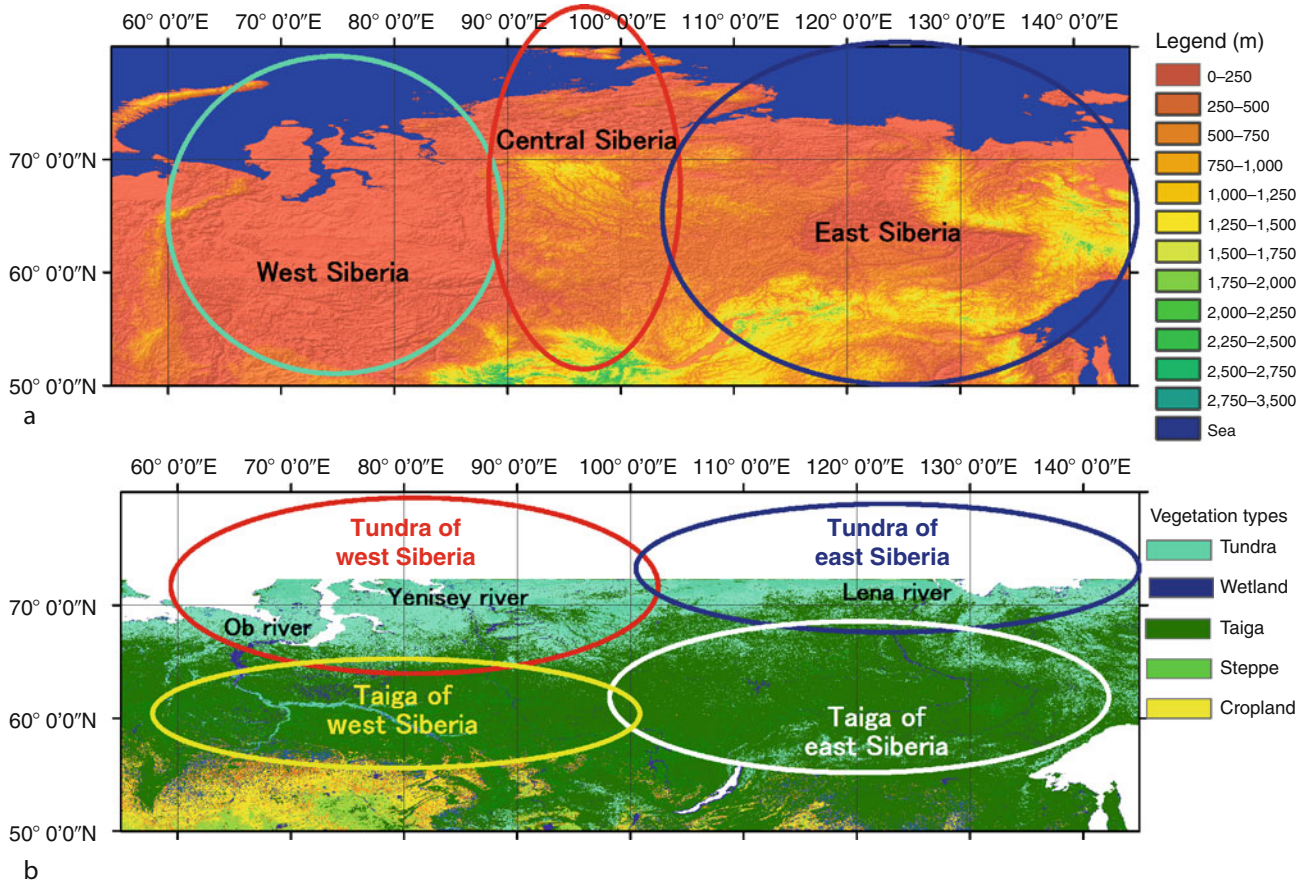

Siberia, Figure 1 Map of Siberia. (**a**) Topography map for geography indicated West, central, and East Siberia and (**b**) vegetation map for climate for tundra and taiga of West and East Siberia.

lithosphere in northern Eurasia. Terrestrial heat flow acts as one of the heat sources for permafrost to determine the lower limit of the permafrost depth. Terrestrial heat flow in the area of Yakutia does not exceed 30 mW m^{-2}, in contrast to other Siberian regions, where terrestrial heat flow is 50–70 mW m^{-2} and the permafrost is no more than 400–600-m thick.

The top layer of soil above the permafrost layer thaws seasonally and is called the active layer. The active layer affected direct runoff and peak flow in a small permafrost watershed, as shown by Yamazaki et al. (2006). Water within the active layer has a role of memory in previous years, because water within the active layer has a residence time of more than a half year and it affects snowmelt runoff due to the change of the capability of infiltration into frozen ground (Suzuki et al., 2006a) and transpiration due to recovering shortage of water for transpiration from the thawing ground water during the summer (Sugimoto et al., 2003). Rest of the parts of Siberia without permafrost are covered by seasonal frost, where the ground freezes in winter and thaws in summer. Zimov et al. (2006) showed that the permafrost stores a large amount of carbon, and if it were to thaw, a great deal of carbon would be released. One of the pathways for terrestrial carbon cycle in permafrost region is carbon transport in the rivers. Suzuki et al. (2006b) showed that a large quantity of dissolved organic matter is transported from the upper catchments of the Lena river to the Arctic Ocean.

Snow

During winter, snow covers all of Siberia. The snowpack structure in Siberia is characterized by a thick layer of depth hoar at the bottom, which forms as a result of the large temperature gradient between the relatively warm soil and cold air. Kitaev et al. (2005) analyzed the distribution of snow over Russia from 1936 to 2000. In East Siberia, the mean snow depth, snow cover days from 1936 to 2000, and snow water equivalent from 1966 to 1996 were 34 cm, 220 days, and 90 mm, respectively, and in West Siberia, they were 34 cm, 192 days, and 133 mm, respectively. In both West and East Siberia, snow depth and snow cover days generally increased from 1936 to 2000.

The presence of snow cover influences the depth of the active layer and of seasonal frost in Siberia. In addition,

snowmelt runoff contributes greatly to the discharge of Siberian Rivers, rather than rain. Tree growth as indicated by tree ring width is related to winter precipitation as snow, because recent tree growth is not only related to air temperature but also to the timing of snow disappearance (Vaganov et al., 1999). A few snow researches have been carried out in the southern mountain region of East Siberia, where Suzuki et al. (2006c) showed that sublimation accounts for nearly 10% of snow ablation beneath larch forest. Furthermore, Suzuki et al. (2006c) found that snow albedo is related to snow density. In the tundra region of East Siberia, Hirashima et al. (2004) developed a land surface model that incorporated blowing snow and estimated that about 40% of winter precipitation sublimated during blowing snow events. Tundra regions of Siberia are characterized by a shallow snowpack and a heterogeneous snow cover because of the small topographic relief, because strong wind induced blowing snow events occasionally, but taiga regions tend to have a uniform snow cover since forest canopy reduced wind speed and large snow-folding capacity.

Glaciers and river and lake ice

Ice in Siberia occurs in glaciers and as river and lake ice. The large volume of ice constitutes an important water resource and influences the inhabitants of Siberia. According to Kotlyakov et al. (1996) and UNEP (United Nations Environment Programme) (2007), from 1950 to 1970, Siberia's glaciers were widely dispersed on mountain ranges, from the Ural Mountains to Kamchatka, covering a total area of about 3,600 km^2 (USSR Glacier Inventory). Since 1970, Siberian glaciers have generally retreated, mainly from lower elevations and southern latitudes, and the amount of retreat has a wide variety in the places.

River and lake ice are of more importance to the people living in Siberia than glaciers because they are an important freshwater resource. The timing of the break-up or freeze-up of lake ice depends primarily on air temperature. Walter et al. (2006) reported that during thaws, a lake in northern East Siberia emits a large amount of methane.

The break-up of river ice in spring occasionally causes large floods in Siberia, especially in permafrost-dominated regions. By incorporating river ice into a river run-off model, Ma et al. (2005) showed that river ice volume greatly affects estimations of snowmelt run-off in the Lena River. Vuglinsky (2002) noted that the knowledge of river ice is important for understanding run-off processes, and the duration of river ice each year also greatly affects the use of large rivers for transporting cargo from or to the sea. Smith (2000) showed that the river ice in central and East Siberia is melt onset 1–3 weeks earlier since 1930s but found no trend in West Siberian river.

Thick icing is commonly observed in the permafrost regions of the northern hemisphere, including Siberia. Icing is often seen on the river in Siberia. In southern East Siberia, aufeis (icing) can be 5–10-m thick. Icing contributes about 10% of annual river discharge (Sokolov and Vuglinsky, 1997). Icing may be an important indicator of groundwater movement in permafrost regions of Siberia.

Summary

Because of the extremely cold winter climate of Siberia, the region is characterized by a thick and extensive winter snow cover and many frozen water bodies in winter. However, people in Siberia are more aware of global warming and its effects on snow and ice in Siberia are posing a threat to infrastructures due to thawing snow and ice. Warming air temperature by itself can cause the shorter periods or less volume of snow and ice in Siberia, but it cannot explain all of the observed changes such as the small changes of timing of river ice freeze-up or permafrost thawing. Vegetation characteristics also influence how warmer air temperatures affect snow and ice in Siberia. Most of Siberia is covered by taiga forest. In East Siberia, the taiga forests consist mainly of larch, which is a deciduous conifer, whereas West Siberia is characterized by wetlands and evergreen coniferous forest. Suzuki et al. (2007) showed that a moss layer protects the soil from heating by the atmosphere and helps to maintain a constant ground temperature and moisture content. Thus, the vegetation type affects snow and ice in Siberia and complicates our understanding of snow and ice cover changes in Siberia. In the future, this subject should be studied by a multidisciplinary approach.

Bibliography

Borisov, A. A., 1965. *Climates of the U.S.S.R.* Chicago: Aldine.

Bryson, R. A., 1966. Airmasses, streamlines and the boreal forest. *Geographical Bulletin (Canada)*, **8**, 228–269.

Duchkov, A. D., 2006. Characteristics of permafrost in Siberia. In Lombardi, S., Altunina, L. K., and Beaubien, S. E. (eds.), *Advances in the Geological Storage of Carbon Dioxide*. New York: Springer, pp. 81–91.

Hirashima, H., Ohata, T., Kodama, Y., Yabuki, H., Sato, N., and Georgiadi, A., 2004. Nonuniform distribution of tundra snow cover in eastern Siberia. *Journal of Hydrometeorology*, **5**, 373–389.

Kitaev, L., Forland, E., Razuvaev, V., Tveito, O. E., and Krueger, O., 2005. Distribution of snow cover over Northern Eurasia. *Nordic Hydrology*, **36**, 311–319.

Kondratjeva, K. A., Khrutzky, S. F., and Romanovsky, N. N., 1993. Changes in the extent of permafrost during the late quaternary period in the territory of the former Soviet Union. *Permafrost and Periglacial Processes*, **4**, 113–119.

Kotlyakov, V. M., et al., 1996. *Glaciation in North and Central Eurasia at present time*. Moscow: Nauka.

Ma, X. Y., Yasunari, T., Ohata, T., and Fukushima, Y., 2005. The influence of river ice on spring runoff in the Lena river, Siberia. *Annals of Glaciology*, **40**, 123–127.

Smith, L. C., 2000. Trends in Russian Arctic river-ice formation and breakup, 1917 to 1994. *Physical Geography*, **21**, 46–56.

Sokolov, B. L., and Vuglinsky, V. S., 1997. *Energy and water exchange in mountain Taiga in the south of east Siberia*. St. Petersburg: State Hydrological Institute, pp. 1–90.

Sugimoto, A., Naito, D., Yanagisawa, N., Ichiyanagi, K., Kurita, N., Kubota, J., Kotake, T., Ohata, T., Maximov, T. C., and Fedorov, A. N., 2003. Characteristics of soil moisture in permafrost

observed in East Siberian taiga with stable isotopes of water. *Hydrological Processes*, **17**, 1073–1092.
Suzuki, K., Konohira, E., Yamazaki, Y., Kubota, J., Ohata, T., and Vuglinsky, V., 2006a. Transport of organic carbon from the Mogot Experimental Watershed in the southern mountainous taiga of eastern Siberia. *Nordic Hydrology*, **37**, 303–312.
Suzuki, K., Kubota, J., Ohata, T., and Vuglinsky, V., 2006b. Influence of snow ablation and frozen ground on spring runoff generation in the Mogot Experimental Watershed, southern mountainous taiga of eastern Siberia. *Nordic Hydrology*, **37**, 21–29.
Suzuki, K., Kubota, J., Zhang, Y. S., Kadota, T., Ohata, T., and Vuglinsky, V., 2006c. Snow ablation in an open field and larch forest of the southern mountainous region of eastern Siberia. *Hydrological Sciences Journal*, **51**, 465–480.
Suzuki, K., Kubota, J., Yabuki, H., Ohata, T., and Vuglinsky, V., 2007. Moss beneath a leafless larch canopy: influence on water and energy balances in the southern mountainous taiga of eastern Siberia. *Hydrological Processes*, **21**, 1982–1991.
UNEP, 2007. *Global Outlook for Ice & Snow*. Birkeland: Birkeland Trykkeri A/S.
Vaganov, E. A., Hughes, M. K., Kirdyanov, A. V., Schweingruber, F. H., and Silkin, P. P., 1999. Influence of snowfall and melt timing on tree growth in subarctic Eurasia. *Nature*, **400**, 149–151.
Vuglinsky, V. S., 2002. Peculiarities of ice events in Russian Arctic rivers. *Hydrological Processes*, **16**, 905–913.
Walter, K. M., Zimov, S. A., Chanton, J. P., Verbyla, D., and Chapin, F. S., 2006. Methane bubbling from Siberian thaw lakes as a positive feedback to climate warming. *Nature*, **443**, 71–75.
Yamazaki, Y., Kubota, J., Ohata, T., Vuglinsky, V., and Mizuyama, T., 2006. Seasonal changes in runoff characteristics on a permafrost watershed in the southern mountainous region of eastern Siberia. *Hydrological Processes*, **20**, 453–467.
Zimov, S. A., Schuur, E. A. G., and Chapin, F. S., 2006. Permafrost and the global carbon budget. *Science*, **312**, 1612–1613.

Cross-references

Icing
Inverted Cup Depth Hoar Crystals
Lake Ice
Permafrost
River Ice Hydrology
Snow Hydrology

SLUSH AND SLEET OF SNOW

A. K. Singh
DIAT (Deemed University), Girinagar, Pune, Maharashtra, India

Snow that partially melts upon reaching the ground, to the point that it accumulates in puddles of partially frozen water, is slush, whereas sleet is snow falling mixed with rain, that is, rain containing snow. Slush is slurry, mixture of liquid and solid forms of water. A slushy layer of snow also results when rain or meltwater percolates downward from the snow surface but cannot penetrate an icy layer or the ground surface beneath. Because of its low binding strength, slush that forms in hilly terrain, can sometimes pose a hazard by releasing wet snow avalanches. These avalanches can occur even on very gentle slopes where, though they are unable to gather much speed, the large mass of slush can make avalanches destructive. In the natural environment, slush forms as ice and snowmelts. This often mixes with dirt and other materials, resulting in a gray or muddy brown color. Solid ice or snow often blocks the drainage of liquid water from slushy areas and slush goes through multiple freeze/thaw cycles before disappearing completely.

In dry snow crystal growth rate is limited by the rate at which water vapor diffuses across the pores from smaller particles to larger ones. However, in slush, the pores between the ice crystals are occupied by liquid water rather than air and hence the crystal growth rate is driven by thermal diffusion between particles through the water filled pores.

As raindrops pass through layers of air at varying temperatures, while passing through a layer with temperature below the freezing point, they turn into sleet, that is, precipitation of small, partially melted grains of ice. Snowflakes that have melted by passing through a warm layer will turn into sleet if they happen to pass through a freezing layer. Sleet often falls together with snow and rain. It occurs only during the winter, while hail, a different form of icy precipitation, may fall at any time of the year. Sleet is less prevalent than freezing rain and is more difficult to forecast as it develops under specialized atmospheric conditions.

SNOW

A. K. Singh
DIAT (Deemed University), Girinagar, Pune, Maharashtra, India

Snow is a form of precipitation, measured using snow gauge, in the form of ice crystals, usually flakes of star-like crystals that can be in a variety of shapes and sizes. Snow stakes and simple scales can be used to determine the depth of the snow pack. Snow is less dense than liquid water by a factor of $\approx$10 (fresh and dry snow). By the time flakes reach the ground they undergo transformations resulting from growth, disintegration, or agglomeration. Highly branched or dendrite crystals occupy more space between the arms of ice that form the snowflake and this snow will therefore have a lower density, referred to as dry snow and is highly reflective (0.9 and higher albedo). Conditions that create columnar or plate-like crystals will have much less air space within the crystal and will therefore be denser. When all the snow does not melt in the summer it evolves into firn, where individual granules become more spherical in nature, evolving into glacier ice.

Snow is a thermodynamically active material, exhibiting strange behavior near the melting temperature and constantly undergoing metamorphism. Structurally, snow is a granular material characterized by a continuous ice network, formed through cohesion between ice grains, to form

a porous structure. Snow behavior, properties, and processes often fall far outside of those normally encountered in granular materials. Unique properties of snow include its high compressibility.

Once the snow is on the ground, it will settle under its own weight. Recrystallization under stress caused by the weight of the overlying snow becomes predominant, and grains change in size and shape in order to minimize the stress on them with large or favorably oriented grains growing at the expense of others. Increases in density above this initial compression occur primarily due to melting and refreezing, caused by temperatures above freezing or by direct solar radiation. By late spring, snow densities typically reach a value half of water density. This densification of the snow proceeds more slowly after reaching this density and many of the processes become less and less effective.

In many parts of the world, snow is the primary source of water during summer and autumn. Water equivalent is of great interest to water managers wishing to predict spring runoff and the water supply of cities downstream. Sudden melting of snow can cause flooding. Snow is also a source of recreational activity and at the same time turns into a deadly avalanche. Climate is also influenced by snow cover due to its reflection character as compared to other surface materials, and also the absorption of solar radiations.

SNOW BED/SNOW BED VEGETATION

Nadine Konz
Institute of Environmental Geosciences, University of Basel, Basel, Switzerland

Snow beds are defined through the duration of snow cover and snow height leading to an individual geomorphology and a specific microclimatology (Huelber et al., 2006). These conditions lead to an ecological niche for different plants; the snow bed vegetation.

The term snow bed is currently adopted to designate plant communities whose occurrence is determined by the geomorphological situations favoring a long duration of the snow cover (Tomaselli, 1991). One of the most extreme sets of conditions under which plants may grow is those of snow beds. Generally, the snow does not cover the ground to the same depth everywhere: small depressions are filled with snow; ridges are blown free from snow. Places with more snow than a medium depth form the snow beds. Duration of snow cover, character of bedrock, and quantity of available moisture are the three dominating factors that influence the mountain vegetation. The snow cover is generally the one of greatest physiognomic importance (Faegri, 1957). The plant communities of the snow bed belong to the class of *Salicetea herbacea*. These plants are snow covered between seventh and tenth month a year. Snow bed vegetation can be divided into vegetation on siliceous bedrock and limestone. Some examples of snow bed vegetation on siliceous bedrock are *Salicaceae* (e.g., *Salix herbacea*), *Poaceae* (e.g., *Poa alpina*), *Polytrichaceae* (e.g., *Polytrichum sexangulare*), and *Peltigeraceae* (e.g., *Solorina crocea*). Some examples of snow bed vegetation on limestone are *Poaceae* (e.g., *Sesleria albicans*), *Plantaginaceae*, (e.g., *Veronica alpina*), and *Ranunculaceae* (e.g., *Ranunculus alpestris*) (Merz, 2000).

Bibliography

Faegri, K., 1957. Snow-bed vegetation. *Ecology*, **38**, 668–669.
Huelber, K., Gottfried, M., Pauli, H., Reiter, K., Winkler, M., and Grabherr, G., 2006. Phenological responses of snowbed species to snow removal dates in the central alps: implications for climate warming. *Arctic Antarctic and Alpine Research*, **38**, 99–103.
Merz, P., 2000. *Pflanzengesellschaften mitteleuropas und der alpen – erkennen, bestimmen*. Landsberg/Lech: Bewerten.
Tomaselli, M., 1991. The snow-bed vegetation in the Northern Apennines. *Vegetatio*, **94**, 177–189.

SNOW COURSE

A. K. Singh
DIAT (Deemed University), Girinagar, Pune, Maharashtra, India

Snow course consists of a series of manually marked sampling points or locations where depth and snow water equivalent measurements are made by trained observers. It is an established line, usually from several hundred feet to as much as *a mile long*, traversing representative terrain in a mountainous region of appreciable snow accumulation. Snow course length and the frequency of sampling points are defined depending on site specific conditions such as slope, aspect, land cover, and uniformity of snow cover. Snow course data are, however, subject to a systematic bias because the measurements, obtained by inserting a tube through the snowpack to the soil to cut and hold a snow core, tend to underestimate snow water equivalent due to sampling difficulties associated with ground ice and depth hoar. The size of the sampling cutter can also influence accuracy. Besides, other aspects regarding snow course data that must also be taken into account are consistency of equipment, procedures, and measurement locations over time, and the degree to which a real snow cover condition can be represented by a series of point measurements.

Snowmelt is a major source of water supply to areas in temperate zones near mountains that catch and hold winter snow, especially those with a prolonged dry summer. In such places, water equivalent is of great interest to water managers wishing to predict spring runoff and the water supply of cities downstream.

Bibliography

Dressler, K. A., Fassnacht, S. R., and Bales, R. C., 2006. A comparison of snow telemetry and snow course measurements in the Colorado River Basin. *Journal of Hydrometeorology*, **7**(4), 705–712.

SNOW COVER AND SNOWMELT IN FOREST REGIONS

Tobias Jonas[1], Richard Essery[2]
[1]Snow Hydrology Research Group, WSL Institute for Snow and Avalanche Research SLF, Davos, Switzerland
[2]School of GeoSciences, University of Edinburgh, Edinburgh, UK

Definition

Snow cover. Snow that accumulates on the ground due to snow precipitation and snow redistribution processes. Typically used for seasonal snow, excluding firn and ice.
Snowmelt. Snow ablation process and/or meltwater originating from the snow cover.

Introduction

The evolution and ablation of the seasonal snow cover in a forest is very different compared to the snow in open terrain. Snow precipitation is partly intercepted by the canopy, from where the snow may subsequently evaporate directly, melt and drip down, or fall off. The canopy also absorbs shortwave radiation and changes the longwave radiation budget. The presence of trees decelerates wind fields near the snow cover surface and thus constrains the turbulent exchange of heat and moisture. Finally, litter fall from trees (e.g., conifer needles or lichens) can have a significant impact on the snow surface albedo, increasing the absorption of shortwave radiation. Due to these differences, the maximum snow water equivalent and the subsequent amount of melt water can easily differ by some 10% from the respective amounts at neighboring open sites, while melt-out dates may be shifted by several weeks. As boreal and subalpine forests cover large areas of the northern hemisphere land surface, snow-forest processes have an important influence on weather and hydrology, even at hemispheric scales. See also the entry on *Snow and Vegetation Interaction*, which covers related topics from an alternative perspective.

Measuring relevant data

A forest canopy typically features a complex and heterogeneous structure. The canopy density may display spatial variability on different scales, e.g., shortwave radiation and snowfall rates below the canopy can significantly differ on the meter scale. The same applies to the distribution of stems and other parts of the vegetation which emit longwave radiation. Given the spatial complexity of important snow cover energy budget forcing terms, it is not surprising that snow cover thickness inside forests often shows great levels of spatial variation. It is hence difficult to measure "representative" data. In this respect, single point measurements below the canopy are typically useless, and snow depth, snow water equivalent (SWE), or snow accumulation rates are normally measured on transects, grids, snow courses, etc. that represent the area of interest (and the spatial scales to be resolved).

Several setups have been used to measure radiation inside forests. Most commonly, arrays of fix sensors have been used to capture the spatial variability of radiation below the canopy (e.g., Link et al., 2004; Pomeroy et al., 2008). Alternatively, radiation sensors have been moved manually or automatically along ground transects, cables, or rails (Sturm et al., 2005; Stähli et al., 2009). Also, infrared thermography has been used to map the emission of longwave radiation (Pomeroy et al., 2009).

Quantitative measurement of snow interception is challenging. While qualitative interception levels can be gathered from periodic observations (e.g., by webcams), the mass of snow intercepted per unit area is a difficult parameter to obtain. Techniques that have been applied include (a) weighing trees or tree-like structures mounted on or suspended from scales (Hedstrom and Pomeroy, 1998; Storck et al., 2002), (b) optically tracking the vertical position of branches, which bend down under the weight of intercepted snow (Brundl et al., 1999), (c) measuring canopy snow using radar absorption (Gustafsson et al., 2010), or (d) absorbing gamma radiation (Calder, 1990).

As important boundary conditions for snow-forest processes, information about the canopy structure/density is required, usually specified through parameters such as sky-view fraction (SVF; the projected fraction of the sky hemisphere visible from a point below the canopy) and leaf area index (LAI; the total projected leaf area per unit area of ground). Manual or optical methods of measuring canopy parameters (e.g., destructive sampling or hemispherical photography) can be time consuming and subject to large uncertainties (Chen et al., 1997). Airborne laser scanning (LiDAR) offers the possibility of canopy structure mapping at landscape scales (Riaño et al., 2004).

Snow distribution in forests

On the meter scale, forest snow cover is typically heterogeneous. Snow depth patterns often mirror canopy gaps, the distribution of shorter vegetation on the ground and thermal radiation effects in the vicinity of stems. As a useful first-order predictor for such small-scale patterns, the sky-view fraction has been found to correlate well with the maximum SWE below forest canopies of varying density (e.g., Pomeroy et al., 2002; Lundberg et al., 2004; Lopez-Moreno and Latron, 2008). Since denser canopies intercept more snow, locations with higher sky-view fractions generally accumulate more snow on the ground than locations with lower sky-view fractions (within the same stand). Some studies even report forest openings to accumulate more snow than nearby unforested sites (Lopez-Moreno and Latron, 2008).

However, snow distribution patterns within forests are certainly not just driven by interception. In addition to snow accumulation phenomena, spatially variable snow ablation processes also contribute to complex distribution dynamics of snow in forests. Energy budget

considerations are therefore covered in a separate section below in more detail.

Understanding snow distribution dynamics in forests is important, since snow accumulated on the ground directly drives runoff from snowmelt. But also, the fate of snow that is intercepted in the canopy is important to consider for the water balance. A significant part of intercepted snow may be evaporated (e.g., 20–30% in a study by Montesi et al., 2003) and hence does not contribute to runoff. Further information is given in the entry on Interception of Snow.

Energy budget of snow in forests

Insight into the specific and interacting effects of physical forest snow processes can be gained by assessing the energy budget of a forest snow cover (Figure 1).

Terms that counterbalance the rate of change in snowpack heat storage are:

- SWR: Net shortwave radiation
- LWR: Net longwave radiation
- THF: Turbulent heat fluxes (sensible and latent)
- PHF: Heat advected by precipitation
- GHF: Heat exchange with the ground (including advection by meltwater)
- PCH: Energy of snowpack phase changes

At a global scale, forests in regions with seasonal snow have characteristics that are so diverse with respect to canopy structure and ambient conditions that there is no general rule for the relative importance of the terms in the energy balance (but see King et al., 2008). In the following, some of the terms are discussed in more detail.

Shortwave radiation (SWR): Transmission of short wave radiation through a forest canopy is a truly three-dimensional phenomenon. Naturally, canopy structure and density are the main predictors for the transmissivity τ_{SWR}, which is the ratio between the radiation below and above the canopy. The simplest way to describe this relationship adopts Beer's law,

$$\tau_{SWR} = \exp(-\kappa \cdot LAI)$$

where, κ is an empirical extinction parameter related to the orientation and clumping of canopy elements. Such descriptions can be enhanced by additionally accounting, e.g., for (a) solar angle, which affects the path length of direct radiation through the canopy or (b) snow interception, which enhances diffuse radiation below the canopy (Stähli et al., 2009). Moreover, multiple reflection effects can entail increased τ_{SWR} during cloudy weather when diffuse radiation dominates the SWR budget below the canopy; these effects can be accounted for using a two-stream radiative transfer approximation (Niu and Yang, 2004). The net SWR on the other hand is also determined by snow albedo, which is the ratio between reflected and incoming radiation at the snow surface. Albedo generally decreases as a snow surface ages because increasing contaminants in the snow increase absorption of visible radiation and increasing snow grain sizes increase near-infrared absorption. Snow albedos may be lower in forests than in the open due to both decreases in the proportion of visible radiation and increases in litter accumulation under forest canopies (Melloh et al., 2002), although net SWR may still be higher in the open due to the higher incoming shortwave radiation.

Longwave radiation (LWR): A forest snowpack receives longwave radiation from the canopy and from the atmosphere through canopy gaps. Since canopy surface temperatures are often very different from atmospheric temperatures, the sky-view fraction (SVF) is an important parameter for the net LWR budget of the snow cover in semi-closed forests. The simplest way to describe the net LWR is:

$$LWR_{net} = SVF \cdot LWR_{from\ atmosphere} + (1 - SVF) \times LWR_{from\ canopy} - LWR_{from\ snow\ cover}$$

or using the Stefan–Boltzmann law

$$LWR_{net} = SVF \cdot LWR_{from\ atmosphere} + (1 - SVF) \cdot \sigma T_c^4 - \sigma T_s^4$$

where, T_c and T_s denote the temperatures of canopy and snow surface, σ is the Stefan–Boltzmann constant, and the emissivities of canopy and snow surface are approximated to be 1 (both around 0.97). In practice, T_c is often simplified to equal the air temperatures measured below the canopy, while incoming LWR above canopy can be estimated from air temperature, humidity, and cloud cover using bulk formulae (e.g., Flerchinger et al., 2009). These parameterizations have been evaluated against measurements by Essery et al. (2008) and Pomeroy et al. (2009).

Turbulent heat flux (THF): Latent and sensible heat fluxes can constitute important contributions to the energy balance of a forest snow cover (e.g., Li et al., 2008), which

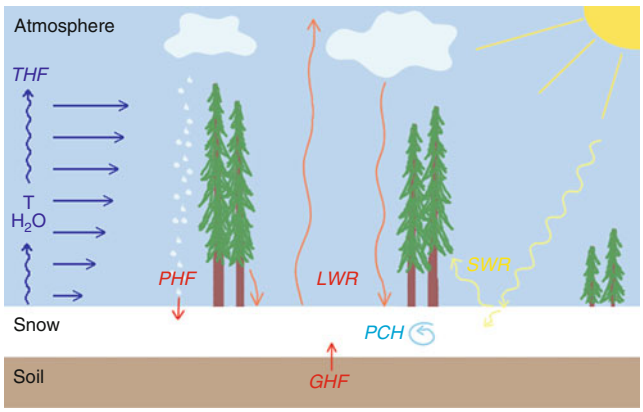

Snow Cover and Snowmelt in Forest Regions,
Figure 1 Schematic of the energy budget of snow in forests.

may appear surprising given that wind speeds are typically low inside forests. Estimating turbulent heat fluxes for a forest snow cover is comparatively difficult and imprecise, since it involves a combination of parameterizing wind speeds, temperature, and humidity gradients. However, snow models that incorporate interactions with vegetation/forest do so with differing levels of complexity (Essery et al., 2009). Only a few attempts have been made so far to measure latent and sensible heat fluxes inside forests over snow using eddy covariance (EC) systems (Molotch et al., 2006; Marks et al., 2008), since applying EC systems in such environments is associated with significant uncertainties. More research is certainly needed to improve the understanding and prediction of turbulent heat exchange inside snow-covered forests.

Snowpack modeling for forest regions

Because of the importance of forest snow processes, many snow models have been developed or modified recently to include vegetation canopies. Thirty-three such models, listed by Rutter et al. (2009), participated in the second Snow Model Intercomparison Project (SnowMIP2) by performing simulations driven by meteorological observations for paired open and forested plots at five sites. The models generally perform complete mass and energy balance calculations for forest canopies and snowpacks, but they were primarily evaluated by comparison with measurements of SWE on the ground. Although the evaluation is complicated by uncertainties in meteorological and snowpack observations, the intercomparison revealed a wide range in the ability of models to simulate snow in open and forested situations. On the larger scales used in climate modeling, Roesch (2006) suggested that the models participating in the IPCC Fourth Assessment Report showed difficulties in determining the extent of snow albedo masking by forests.

Summary

Forest snow is subject to very different ambient conditions compared to snow in open terrain. Accumulation patterns are predominantly altered by interception of snow in the canopy, while melting dynamics are driven by complex processes such as the transfer of shortwave and longwave radiation through the canopy and the turbulent transport of heat and water. Today, many snow models try to reproduce interactions between snow and vegetation, emerging from the need to involve forest snow processes in distributed land-surface models.

Bibliography

Brundl, M., Bartelt, P., Schneebeli, M., and Fluhler, H., 1999. Measuring branch defection of spruce branches caused by intercepted snow load. *Hydrological Processes*, **13**, 2357–2369.

Calder, I. R., 1990. *Evaporation in the uplands*. Chichester, UK: Wiley.

Chen, J. M., Rich, P. M., Gower, S. T., Norman, J. M., and Plummer, S., 1997. Leaf area index of boreal forests: theory, techniques, and measurements. *Journal of Geophysical Research-Atmospheres*, **102**, 29429–29443.

Essery, R., Pomeroy, J., Ellis, C., and Link, T., 2008. Modelling longwave radiation to snow beneath forest canopies using hemispherical photography or linear regression. *Hydrological Processes*, **22**, 2788–2800.

Essery, R., Rutter, N., Pomeroy, J., Baxter, R., Stähli, M., Gustafsson, D., Barr, A., Bartlett, P., and Elder, K., 2009. SnowMIP2 – An evaluation of forest snow process simulations. *Bulletin of the American Meteorological Society*, **90**, 1120–1135.

Flerchinger, G. N., Xaio, W., Marks, D., Sauer, T. J., and Yu, Q., 2009. Comparison of algorithms for incoming atmospheric long-wave radiation. *Water Resources Research*, **45**, 13.

Gustafsson, D., Magnusson, J., and Granlund, N., 2010. Impulse radar measurements of snow interception – laboratory tests and field application to a forest stand in northern Sweden. *Cold Regions Science and Technology*, in prep.

Hedstrom, N. R., and Pomeroy, J. W., 1998. Measurements and modelling of snow interception in the boreal forest. *Hydrological Processes*, **12**, 1611–1625.

King, J. C., Pomeroy, J., Gray, D. M., Fierz, C., Föhn, P. M. B., Harding, R. J., Jordan, P., Martin, E., and Plüss, C., 2008. Snow-atmosphere energy and mass balance. In Armstrong, R. A., and Brun, E. (eds.), *Snow and Climate Physical Processes, Surface Energy Exchange and Modeling*. Cambridge: Cambridge University Press, pp. 70–124.

Li, W. P., Luo, Y., Xia, K., and Liu, X., 2008. Simulation of snow processes beneath a boreal Scots pine canopy. *Advances in Atmospheric Sciences*, **25**, 348–360.

Link, T. E., Marks, D., and Hardy, J. P., 2004. A deterministic method to characterize canopy radiative transfer properties. *Hydrological Processes*, **18**, 3583–3594.

Lopez-Moreno, J. I., and Latron, J., 2008. Influence of canopy density on snow distribution in a temperate mountain range. *Hydrological Processes*, **22**, 117–126.

Lundberg, A., Nakai, Y., Thunehed, H., and Halldin, S., 2004. Snow accumulation in forests from ground and remote-sensing data. *Hydrological Processes*, **18**, 1941–1955.

Marks, D., Reba, M., Pomeroy, J., Link, T., Winstral, A., Flerchinger, G., and Elder, K., 2008. Comparing simulated and measured sensible and latent heat fluxes over snow under a pine canopy to improve an energy balance snowmelt model. *Journal of Hydrometeorology*, **9**, 1506–1522.

Melloh, R. A., Hardy, J. P., Bailey, R. N., and Hall, T. J., 2002. An efficient snow albedo model for the open and sub-canopy. *Hydrological Processes*, **16**, 3571–3584.

Molotch, N. P., Blanken, P. D., Williams, M. W., Turnipseed, A. A., Monson, R. K., and Margulis, S. A., 2006. Estimating sublimation of intercepted and sub-canopy snow using eddy covariance systems. *Hydrological Processes*, **21**, 1567–1575.

Montesi, J., Elder, K., Schmidt, R. A., and Davis, R. E., 2003. Sublimation of intercepted snow within a subalpine forest canopy at two elevations. *Journal of Hydrometeorology*, **5**, 763–773.

Niu, G. Y., and Yang, Z. L., 2004. Effects of vegetation canopy processes on snow surface energy and mass balances. *Journal of Geophysical Research-Atmospheres*, **109**, 15.

Pomeroy, J. W., Gray, D. M., Hedstrom, N. R., and Janowicz, J. R., 2002. Prediction of seasonal snow accumulation in cold climate forests. *Hydrological Processes*, **16**, 3543–3558.

Pomeroy, J., Rowlands, A., Hardy, J., Link, T., Marks, D., Essery, R., Sicart, J. E., and Ellis, C., 2008. Spatial variability of shortwave irradiance for snowmelt in forests. *Journal of Hydrometeorology*, **9**, 1482–1490.

Pomeroy, J., Marks, D., Link, T., Ellis, C., Hardy, J., Rowlands, A., and Granger, R., 2009. The impact of coniferous forest

temperature on incoming longwave radiation to melting snow. *Hydrological Processes*, **23**, 2513–2525.
Riaño, D., Valladares, F., Condes, S., and Chuvieco, E., 2004. Estimation of leaf area index and covered ground from airborne laser scanner (Lidar) in two contrasting forests. *Agricultural and Forest Meteorology*, **124**, 269–275.
Roesch, A., 2006. Evaluation of surface albedo and snow cover in AR4 coupled climate models. *Journal of Geophysical Research-Atmospheres*, **111**, 18.
Rutter, N., Essery, R., Pomeroy, J., Altimir, N., Andreadis, K., Baker, I., Barr, A., Bartlett, P., Boone, A., Deng, H. P., Douville, H., Dutra, E., Elder, K., Ellis, C., Feng, X., Gelfan, A., Goodbody, A., Gusev, Y., Gustafsson, D., Hellstrom, R., Hirabayashi, Y., Hirota, T., Jonas, T., Koren, V., Kuragina, A., Lettenmaier, D., Li, W. P., Luce, C., Martin, E., Nasonova, O., Pumpanen, J., Pyles, R. D., Samuelsson, P., Sandells, M., Schadler, G., Shmakin, A., Smirnova, T. G., Stähli, M., Stockli, R., Strasser, U., Su, H., Suzuki, K., Takata, K., Tanaka, K., Thompson, E., Vesala, T., Viterbo, P., Wiltshire, A., Xia, K., Xue, Y. K., and Yamazaki, T., 2009. Evaluation of forest snow processes models (SnowMIP2). *Journal of Geophysical Research-Atmospheres*, **114**, 18.
Stähli, M., Jonas, T., and Gustafsson, D., 2009. The role of snow interception in winter-time radiation processes of a coniferous sub-alpine forest. *Hydrological Processes*, **23**, 2498–2512.
Storck, P., Lettenmaier, D. P., and Bolton, S. M., 2002. Measurement of snow interception and canopy effects on snow accumulation and melt in a mountainous maritime climate, Oregon. *United States. Water Resources Research*, **38**, 16.
Sturm, M., Douglas, T., Racine, C., and Liston, G. E., 2005. Changing snow and shrub conditions affect albedo with global implications. *Journal of Geophysical Research-Biogeosciences*, **110**, 13.

Cross-references

Depletion of Snow Cover
Glacier Mass Balance
Hydrologic Cycle and Snow
Radiative Transfer Modeling
Snow and Vegetation Interaction
Sublimation from Snow and Ice
Surface Energy Balance

SNOW COVER CHANGES IN THE ALPS

Christoph Marty
WSL Institute for Snow and Avalanche Research SLF, Davos, Switzerland

Definition

HS: Snow Depth
RCM: Regional Climate Model
Snow day: A day with a snow depth larger than a given threshold
Winter snow cover duration: Continuous snow depth of at least 1 cm

Introduction

Snow influences life and society in many ways. The amount and duration of snow in the Alps has a high socioeconomic significance in terms of both tourism and hydropower. Many Alpine towns and villages heavily depend on snow, because their economy is dominated up to 90% by winter tourism (Abegg et al., 2007). The vast majority of customers of such ski areas live in the pre-Alpine regions of Switzerland, Austria, Germany, Italy, and France. A longer sequence of almost snowless winters in these heavily populated regions, as was observed between the late 1980s and mid-1990s, caused a discussion about the uniqueness of such a situation and the possible connection to climate change.

Observed changes

The importance of snow for hydrology and tourism in the Alps has led to quite a few studies, which investigated the past variability and trends of the Alpine snow cover. Some of the Alpine countries have a relatively dense network of manual measurement stations available, where daily snow depth and snowfall have been measured with the help of a permanently mounted snow stake, respectively a new snowboard for 50 years or more. This comprehensive dataset and the above-mentioned socioeconomic importance of snow make the Alps a preferred region to investigate changes in snow cover. Remote sensing data of Alpine snow cover have not been used for climatological purposes due to the lack of longer time series and due to the limited data quality, which is caused by the steep topography of the Alps.

In the Swiss Alps, a significant decrease of HS for elevations below 1,300 m asl was observed in the late twentieth century with measurements from more than 100 stations, whereas no significant differences could be detected for high-altitude stations above 2,000 m asl (Scherrer et al., 2004). It was shown that the long-term snow trends in the Swiss Alps are similar for snow depth, the duration of the continuous snow cover and the number of snowfall days (Laternser and Schneebeli, 2003). Earlier investigations concluded that the length of snow season and snow amount have substantially decreased since the mid-1980s, but there have been periods in the records (e.g., 1930s) where snow depth was as low as during the late 1980s (Beniston, 1997). However, a newer study with more data available points out the uniqueness of the series of snow-poor winters over the period of 20 years from 1988 to 2007 (Marty, 2008), in comparison with at least the last 130 years. In particular, it could be shown that the decline is rather caused by an abrupt change than by a continuous decrease. The number of snow days ($HS > 5$ cm) below 800 m asl, for example, dropped by about 50% in the last 20 years compared to the long-term mean before the change.

In the Austrian Alps, an investigation on different snow parameters at 98 long-term stations revealed a more diverse picture (Jurkovic, 2008). The two 20-year periods between 1980 and 2000 and between 1896 and 1916 were compared and tested for changes. Statistical tests detected decreasing trends at the majority of the stations, but

the decline was only significant at the southern Austrian stations. There, a clear decreasing trend was found for the winter snow cover duration and the snow days with HS > 1 cm. A separate analysis of 14 stations with 100 years of data revealed similar results with mostly significantly decreasing snow day trends in southern Austria and no significant trends in the remaining part of the country.

In the Italian Alps, a general decrease in snowfall in the last 20 years of the analyzed time series between 1920 and 2004 could be found using data from 40 stations (Valt et al., 2005).

In the German Alps, a 20–30% reduction of the snow cover duration was found for low-lying areas between 1952 and 1996 (Günther et al., 2006). A smaller reduction was generally observed in higher areas.

In the French Alps, data from only one long-term station at 1,320 m asl was analyzed. There, a clear decreasing trend in the mean snow depth and in the number of days with snow on the ground was detected (Martin and Etchevers, 2005).

Only one study found an increase of snow depth at high altitude based on one station at 2,500 m asl (Beniston et al., 2003), whose data seem to be questionable due to the measurements on a mountain summit and several displacements of the snow stake.

Future changes

Climate models successfully reproduce large-scale parameters such as temperature today. However, investigations on the evolution of the future snowpack under changing climate conditions all battle with the fact that the current climate models have difficulties in representing fine-scaled spatial and temporal variability of snow. Some studies therefore use physical models driven by artificially generated data of future weather to predict the snow depth and duration at local level. Other studies estimate future snow conditions based on a sensitivity analysis of the current variability.

Such a simple approach was chosen by Hantel and Hirtl-Wielke (2007). They assessed the snow-temperature sensitivity in the European Alps based on data of the last 40 years from 268 stations and came to conclusion that the number of snow days (HS > 5 cm) will decrease by 33% per 1°C warming. This corresponds to a reduction of snow cover duration of about 1 month at the height of maximum sensitivity (about 700 m) but falls rapidly above and below that level. The future snow reliability of 666 Alpine ski resorts in six countries was investigated by Abegg et al. (2007). The authors calculated the impact of a 1°C, 2°C, and 4°C temperature increase based on the assumption that the altitudinal limit of natural snow reliability will rise by 150 m per 1°C warming. They concluded that the number of naturally snow-reliable areas would drop by 25% with 1°C, by 40% with 2°C, and by 70% with a 4°C warming.

In the Swiss Alps, the sensitivity of the snow cover to future climate was analyzed for 20 Swiss ski resorts with a more sophisticated approach and came to similar results (Uhlmann et al., 2008). The authors used the HIRHAM RCM model results of the IPCC A2 scenario and an energy balance model to compute future snow reliability. They pointed out that snow will become scarce on the lower ski runs in all resorts and that days with more than the critical 30 cm snow depth will drastically decrease at more than half of the stations. Future changes in two alpine river basins (above 800 m asl) in the Swiss Alps have been investigated with the help of the distributed catchment model WaSiM-ETH (Jasper et al., 2004). A 2.5°C warming and small changes in precipitation were elaborated from 23 regional climate models calculated for the end of the twenty-first century. The authors found a decrease of 70% in the annual mean snow-water equivalent. The duration of continuous snow cover was shortened by about 2 months, while the snow line was raised by about 450 m. A similar study assessed two other alpine river basins (above 1,600 m asl) in the Swiss Alps using the model system Alpine3D and the IPCC A2 and B2 scenarios from 12 RCMs (Bavay et al., 2009). According to these results, the snow volume and the maximum snow-water equivalent at the end of the twenty-first century will be reduced by about 40%. The complete melt of the snow cover will occur about 40 days earlier and the snow line will be shifted by about 900 m, which would be the end of most of the glaciers in these basins.

The future Austrian snow conditions have been analyzed using a simple temperature- and precipitation-dependent snow model by Breiling and Charamza (1999). An assumed 2°C warming and no change in precipitation showed a 50% reduction of snow cover at the mean altitude of residential population in the 85 Austrian districts. The authors also mention that the 2,000 m mark does not seem to be problematic concerning the amount of snow.

For the French Alps, a similar study was undertaken assuming a temperature increase of 1.8°C (Martin and Etchevers, 2005). They used the more elaborated model chain Safran-Crocus, which is usually used for operational avalanche warning and found a 50% reduction of snow depth below 1,500 m asl and 30% snow-covered area in midwinter.

Conclusions

The seasonal snow cover in the Alps is primarily influenced by a high year-to-year variability due to natural large-scale weather patterns. Despite this fact, a general decrease of the snow depth and snow cover duration could be detected since the end of the 1980s for low-lying stations throughout the European Alps. The decline could be linked to anomalous warm winter temperatures in the last 20 years (Scherrer et al., 2004; Marty, 2008), which seem to be unique for at least the last 500 years (Luterbacher et al., 2007).

Regarding future snow cover the two different approaches, the one based on physical models and the other on the current snow-temperature sensitivity, both came to similar results, which, for a 2°C warming, point to a drastic decrease of snow depth and snow-water equivalent of about 40–60% below 1,800 m, a reduction of the snow cover duration of 4–6 weeks and a rise of the snow line by about 300–500 m. According to the RCM projections, the warming in the Alps will be accompanied by a small increase in winter precipitation. Some authors therefore concluded that higher altitudes, where the temperatures are still cold enough for snowfall might experience an increase in snow depth with climate warming. However, the outcomes of two newer studies revealed that the projected increase in winter precipitation over the Alps will not even in the higher resorts compensate for the projected increase in temperature (Uhlmann et al., 2008; Bavay et al., 2009).

Because of the sensitivity of the Alpine snow cover to temperature, the depth, length, and duration of the snow cover is highly influenced by climate change. As warming progresses in future, regions where snowfall is the current norm will increasingly experience rain and the snow on the ground will melt faster. These perspectives leave no doubt that the projected changes will have a large impact on the economic, social, hydrological, and biological systems in the Alpine region.

Bibliography

Abegg, B., Agrawala, S., Crick, F., and de Montfalcon, A., 2007. *Climate change impacts and adaptation in winter tourism. Climate Change in the European Alps*. Paris:OECD: S. Agrawala, pp. 25–60.

Bavay, M., Lehning, M., Jonas, T., and Löwe, H., 2009. Simulations of future snow cover and discharge in Alpine headwater catchments. *Hydrological Processes*, **23**(1), 95–108, doi:10.1002/hyp. 7195.

Beniston, M., 1997. Variatons of snow depth and duration in the Swiss Alps over the last 50 years: Links to changes in large-scale climatic forcings. *Climatic Change*, **36**, 281–300.

Beniston, M., Keller, F., Koffi, B., and Goyette, S., 2003. Estimates of snow accumulation and volume in the Swiss Alps under changing climatic conditions. *Theoretical and Applied Climatology*, **76**(3), 125–140, doi:10.1007/s00704–003–0016–5.

Breiling, M., and Charamza, P., 1999. The impact of global warming on winter tourism and skiing: a regionalised model for Austrian snow conditions. *Regional Environmental Change*, **1**(1), 4–14, doi:10.1007/s101130050003.

Günther, T., Rachner, M., and Matthäus, H., 2006. Langzeitverhalten der Schneedecke in Baden-Württemberg und Bayern. KLIWA-Projekt A 1.1.4: "Flächendeckende Analyse des Langzeitverhaltens verschiedener Schneedeckenparameter in Baden-Württemberg und Bayern. *KLIWA Berichte*. A. KLIWA: 76.

Hantel, M., and Hirtl-Wielke, L.-M., 2007. Sensitivity of Alpine snow cover to European temperature. *International Journal of Climatology*, **27**(10), 1265–1275, doi:10.1002/joc.1472.

Jasper, K., Calanca, D., Gyalistras, D., and Fuhrer, J., 2004. Differential impacts of climate change on the hydrology of two alpine river basins. *Climate Research*, **26**(2), 113–129, doi:10.3354/cr026113.

Jurkovic, A., 2008. Gesamtschneehöhe – Vergleichende Zeitreihenanalyse. *Meteorology*. Vienna: University of Vienna. Magistra der Naturwissenschaften (Mag.rer.nat.).

Laternser, M., and Schneebeli, M., 2003. Long-term snow climate trends of the Swiss Alps (1931–99). *International Journal of Climatology*, **23**(7), 733–750, doi:10.1002/joc.912.

Luterbacher, J. r., Liniger, M. A., Menzel, A., Estrella, N., Della-Marta, P. M., Pfister, C., Rutishauser, T., and Xoplaki, E., 2007. Exceptional European warmth of autumn 2006 and winter 2007: Historical context, the underlying dynamics, and its phenological impacts. *Geophysical Research Letters*, **34**, 10.1029/2007GL029951.

Martin, E., and Etchevers, P., 2005. Impact of climatic changes on snow cover and snow hydrology in the French Alps. In Huber, U. M., Bugmann, H. K. M., and Reasoner, M. A. (eds.), *Global Change and Mountain Regions: An Overview of Current Knowledge*. New York: Springer, pp. 235–242.

Marty, C., 2008. Regime shift of snow days in Switzerland. *Geophys. Res. Lett.* 35. 10.1029/2008GL033998.

Scherrer, S. C., Appenzeller, C., and Laternser, M., 2004. Trends in Swiss Alpine snow days: the role of local- and large-scale climate variability. *Geophysical Research Letters*, **31**, 10.1029/2004GL020255.

Uhlmann, B., Goyette, S., and Beniston, M., 2008. Sensitivity analysis of snow patterns in Swiss ski resorts to shifts in temperature, precipitation and humidity under conditions of climate change. *International Journal of Climatology*, doi:10.1002/joc.1786.

Valt, M., Cagnati, A., Crepaz, A., and Marigo, G., 2005. *Snow precipitation in the last years on Italian Alps*. Zadar, Croatia: International Conference on Alpine Meteorology ICAM.

Cross-references

Alps
Depletion of Snow Cover
Global Outlook of Snowcover, Sea Ice, and Glaciers
Global Warming and its Effect on Snow/Ice/Glaciers

SNOW CRYSTAL STRUCTURE

Kenneth G. Libbrecht
Department of Physics, Caltech, Pasadena, CA, USA

Synonyms

Ice crystal structure; Snow crystal morphology

Definition

Snow Crystal Structure refers to the various morphologies of snow crystals that form from condensing water vapor in the atmosphere.

Introduction

Snow crystals, also called snowflakes, are single crystals of ice that grow from water vapor. They form in copious numbers in the atmosphere and are well known for their elaborate, symmetrical patterns. Figure 1 shows several examples of natural snow crystals.

The origin of the varied structures of snow crystals has been the source of considerable curiosity and scientific study for centuries (for a detailed historical account,

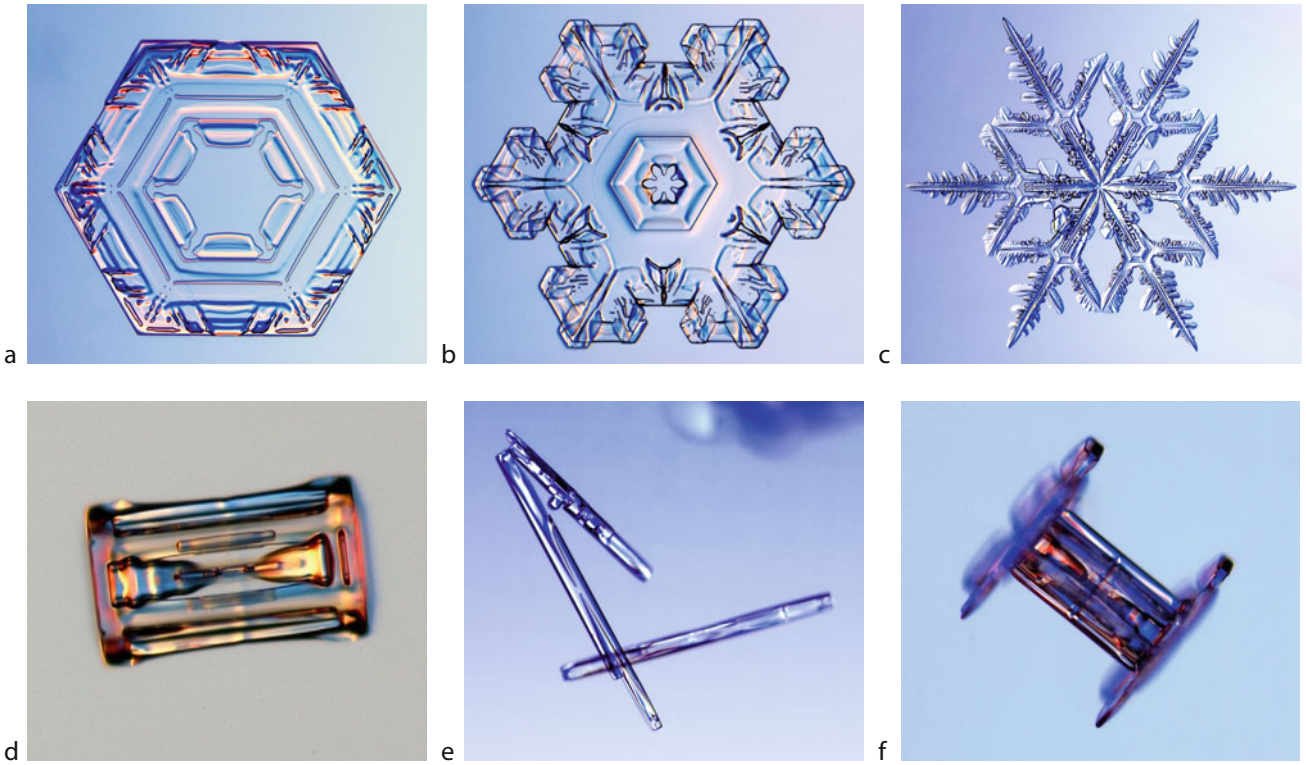

Snow Crystal Structure, Figure 1 Examples of several different morphological types of snow crystals found in natural snowfalls in temperate climates. (**a**) A relatively simple platelike crystal, 1.4 mm from tip to tip, with surface markings. Plates with smooth, featureless facets are less common in nature, except at low temperatures ($T < -20°C$) and low humidities. (**b**) A more elaborate platelike crystal, 2.1 mm from tip to tip, with an unusually high degree of complex symmetry. (**c**) A multibranched stellar dendrite crystal, 3.0 mm from tip to tip. These typically form at higher humidities when the temperature is near $T = -15°C$. (**d**) A simple hexagonal columnar crystal, 0.45 mm in length. Some internal hollowing resulted when the initially hollow ends of the column grew over. (**e**) Needlelike crystals, the largest being 1.1 mm in length. Note one needle grew as a slender hollow column before the ends branched. These crystals only grow near $T = -5°C$. (**f**) A capped column crystal, 0.6 mm in length. This crystal began growing as a stout hollow column, and then platelike stellar crystals grew on the two ends of the column. Photos by the author (Libbrecht, 2003).

see Kobayashi and Kuroda (1987) and Nakaya (1954)). With the development of photography in the late nineteenth century, Wilson Bentley (1931) catalogued several thousand snow crystal images in 1931 that he had acquired over many decades. Bentley's images popularized the snow crystal as a winter icon and were largely responsible for the widespread notion that no two snowflakes are alike.

Faceting

When water molecules condense from the vapor phase onto a growing ice surface, the rate of incorporation into the solid lattice is governed by complex molecular dynamics known as *attachment kinetics* (Libbrecht, 2005). Molecules attach especially slowly to molecularly flat surfaces, which have fewer dangling molecular bonds. As a crystal grows, the faster-growing surfaces fill in more readily, so with time one is left with only the slower growing surfaces, which become the crystal facets.

Faceting is the dominant mechanism determining snow crystal structure when the growth is slow or the crystals are small. The resulting structure is that of a hexagonal prism, with two *basal surfaces* and six *prism surfaces*. The process of faceting is how the geometry of the ice crystal lattice is transferred to the structure of a macroscopic snow crystal.

Branching

Snow crystal growth behavior is typically dominated by attachment kinetics in combination with effects of water molecule diffusion through the air. If we begin with a platelike hexagonal prism crystal, then particle diffusion will bring molecules to the six tips of the hexagon at a slightly faster rate than to the neighboring flat surfaces. With a greater supply of material, the tips grow out, which increases the water supply even more. This positive feedback effect is called the *Mullins–Sekerka instability* (see Saito, 1996; Langer, 1980), and it is a ubiquitous feature of diffusion-limited growth. Much of the complex structure seen in snow crystals ultimately derives from this instability.

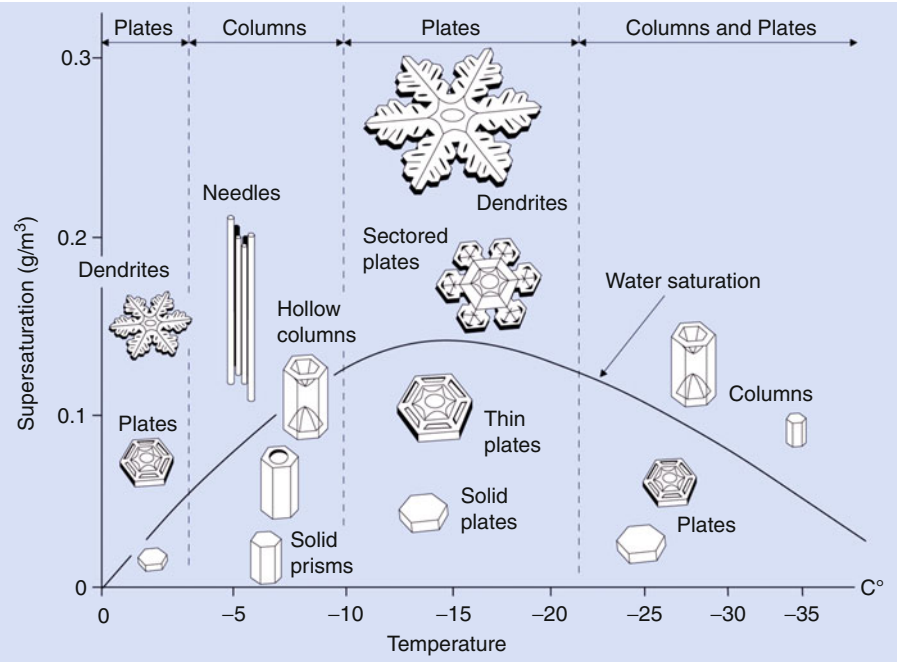

Snow Crystal Structure, Figure 2 The snow crystal morphology diagram, showing different types of snow crystals that grow in air at atmospheric pressure, as a function of temperature and water vapor supersaturation relative to ice. The water saturation line gives the supersaturation of supercooled water, as might be found within a dense cloud. The morphology switches between platelike and columnar forms as a function of temperature, while higher supersaturations produce more complex structures.

Snow crystal morphology diagram

The observed variety of snow crystal forms prompted the first laboratory investigations of snow crystal growth in 1930s. Nakaya (1954) observed the different growth morphologies as a function of ambient temperature and water vapor supersaturation, and he combined these observations into what is now called a *snow crystal morphology diagram*, shown in Figure 2. This diagram refers to snow crystals growing in air at a pressure near 1 bar, so applies to natural snow crystals.

The increase in structural complexity with increasing supersaturation is explained by the mechanics of diffusion-limited growth and the branching instability, but the changing morphology with temperature remains something of a scientific mystery.

Complexity and symmetry

The sensitivity of snow crystal growth to temperature and supersaturation allows a straightforward explanation for the combination of complexity and symmetry seen in many specimens like those shown in Figure 1. When a snow crystal is first nucleated inside a cloud, faceting dictates that the growth initially takes the form of a simple hexagonal prism. Diffusion limits the growth as the crystal becomes larger, and eventually this causes branches to form. Because ice growth is so sensitive to the local environment, it frequently happens that an abrupt change of some kind will cause all six corners of a simple platelike crystal to sprout arms at the same time.

As the growing crystal travels through the cloud, it experiences different temperatures and humidities along the way, and thus the growth behavior changes as a function of time. All six arms, however, experience the same changing conditions as they grow. The result is a rather complex growth pattern for each arm of the crystal, with all six arms developing roughly the same pattern. Under ideal conditions – for which the growth must be unperturbed by collisions with other ice or water particles – a snow crystal can grow into an elaborate, sixfold symmetrical shape, like those shown in Figure 1. Turbulent motions in the atmosphere cause each crystal path to be different, so each grows into a slightly different complex structure.

There are a number of naming conventions for snow crystals as they are falling (e.g., Kobayashi and Kuroda, 1987) and after metamorphosis of the crystals has taken place on the ground (IACS, 2009).

Bibliography

Bentley, W. A., and Humphreys, W. J., 1931. *Snow Crystals*. New York: McGraw-Hill.

IACS Working Group, 2009. International classification for seasonal snow on the ground, IHP-VII technical documents in hydrology N° 83.

Kobayashi, T., and Kuroda, T., 1987. Snow crystals. In Sunagawa, I. (ed.), *Morphology of Crystals–Part B*. Tokyo: Terra Scientific, pp. 645–743.

Langer, J. S., 1980. Instabilities and pattern formation in crystal growth. *Reviews of Modern Physics*, **52**, 1–28.
Libbrecht, K. G., 2003. *The Snowflake: Winter's Secret Beauty*. Stillwater: Voyageur.
Libbrecht, K. G., 2005. The physic of snow crystals. *Reports on Progress in Physics*, **68**, 855–895.
Nakaya, U., 1954. *Snow Crystals: Natural and Artificial*. Cambridge: Harvard University Press.
Saito, Y., 1996. *Statistical Physics of Crystal Growth*. Singapore: World Scientific.

SNOW DEFORMATION

Jerome B. Johnson
Institute of Northern Engineering, University of Alaska Fairbanks, Fairbanks, AK, USA

Synonyms

Snow creep; Snow strain

Definition

Snow deformation. A change in the shape and/or size of snow due to an applied stress.

Introduction

Snow deformation complexity arises because it is composed of ice that exists on the ground near its melting temperature as an intricate three-dimensional porous material formed from new and sintered snow grains that metamorphose over relatively short timescales (Flin et al., 2004; Schneebeli and Sokratov, 2004). Ice exhibits elastic, viscous, viscoelastic, viscoplastic, and brittle deformation that is a function of temperature and loading/deformation rates, and can lead to cohesive failure (Petrenko and Whitworth, 1999). Metamorphism changes the microstructure of snow through the sublimation and diffusion of water molecules from high surface energy surfaces to surfaces with less surface energy or through melting/freezing processes (Bartelt and Buser, 2004; Fierz et al., 2009). Sintering is the process of forming bonds between snow grains by "freezing" the disordered layers on snow grain surfaces that come into contact, or diffusing water molecules to points of contact between snow grains. The size of bonds increase through molecular diffusion of water at rates that increase dramatically as the snow temperature approaches the melting temperature of ice (Blackford, 2007) and with increasing pressure in the bond (Szabo and Schneebeli, 2007). Changes in snow microstructure, and the size of bonds between snow grains, change the mechanical properties of snow that control the deformation response of snow to stress.

Snow microstructure

The microstructure of deposited snow is highly variable because snowflakes take many different forms (Nakaya, 1954). New snow is highly porous with fragile and intricate structures similar to foam materials. Snow self-weight densification and metamorphosis can produce microstructures that consist of random variations of grain and bond sizes or stiff, brittle, vertically oriented large grains connected by small bonds (Figure 1) (Armstrong, 1980; Trabant and Benson, 1972). Melting and refreezing of snow produces clusters of extremely large grains, polycrystals, and bonds (Fierz et al., 2009). As the density of snow increases, its microstructure becomes more uniform with decreasing porosity and heterogeneity.

Continuum-scale uniaxial compression, uniaxial tension, and shear

At the continuum scale, snow subjected to stress or deformation in compression, tension, or shear has fundamentally different deformation paths. Under the influence of uniaxial compressive stresses or deformations, low-density snow ($<$300–400 kg/m^3) will initially deform with little resistance (stress or load). The resistance to deformation increases gradually with density until about 450 kg/m^3 whereupon a dramatic increase in resistance occurs with density. The specific path of deformation and overall resistance to compression depends on snow initial density and microstructure, temperature, and the rate of loading/deformation. At relatively high initial densities, greater than about 500 kg/m^3, resistance to compression is a strong function of density and deformation paths coalesce (Figure 2).

Uniaxial tension at constant temperature causes snow to elongate with increasing resistance to deformation that eventually ends in failure. The form of deformation is a strong function of deformation rate. At high rates of deformation ($>10^{-4}$/s), the resistance to deformation increases rapidly until the snow undergoes a brittle failure (Figure 3a). As the rate of deformation decreases (10^{-5}/s), the resistance to deformation initially increases with strain to a relatively constant value and then decreases with strain as microcracks form. Eventually, microcracks will coalesce to form larger cracks that may gradually expand with deformation or cause the snow to rupture (Figure 3b and c). Higher density snow resists deformation more than lower density snow and will deform to a greater extent than low-density snow. At low deformation rates ($<10^{-6}$/s), the resistance to deformation gradually increases with strain (Figure 3d), eventually forming slow opening cracks (Narita, 1980).

Shear deformation occurs when a plane within snow displaces relative to adjacent parallel planes under the influence of shear stresses or displacements. For low-density snow at low loading/deformation rates, resistance to shear increases with shear displacement, often with an associated decrease in snow volume. The magnitude of resistance to shear, at a given shear displacement increases as stresses acting perpendicular to shear planes increase. As the loading/deformation rate increases, for constant temperature, resistance to shear will increase to a maximum, and then decrease to relatively constant values,

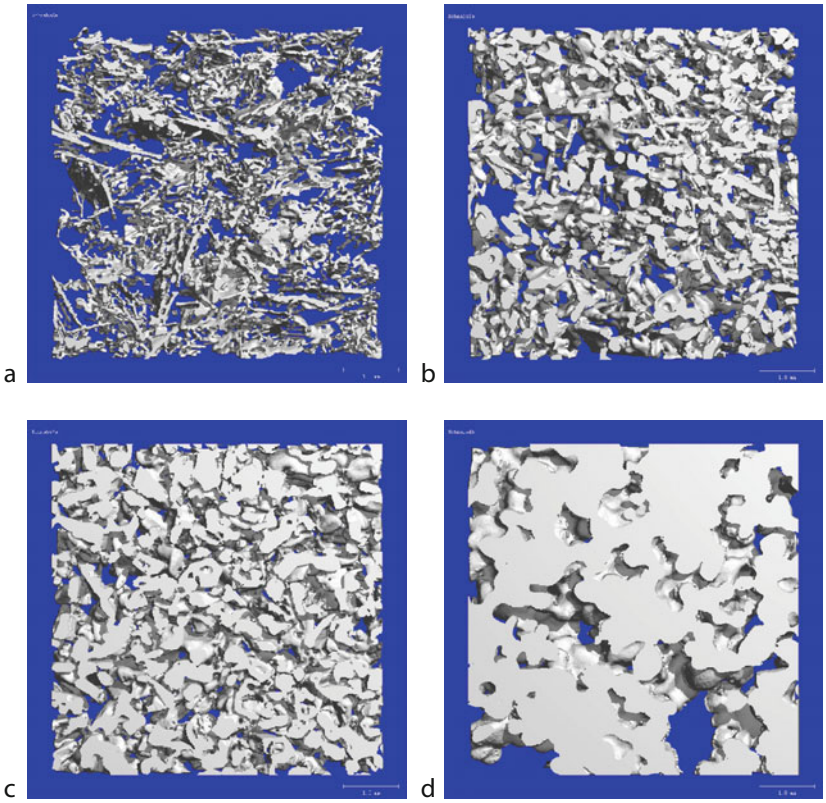

Snow Deformation, Figure 1 Snow microstructure at different stages of metamorphism and sintering. New snow with density $\rho = 110$ kg/m^3 (**a**), equilibrium temperature metamorphosed snow, $\rho = 240$ kg/m^3 (**b**), depth hoar, $\rho = 380$ kg/m^3 (**c**), and high-density snow, $\rho = 610$ kg/m^3 (**d**) (Images: M. Schneebeli, WSL Institute for Snow and Avalanche Research SLF).

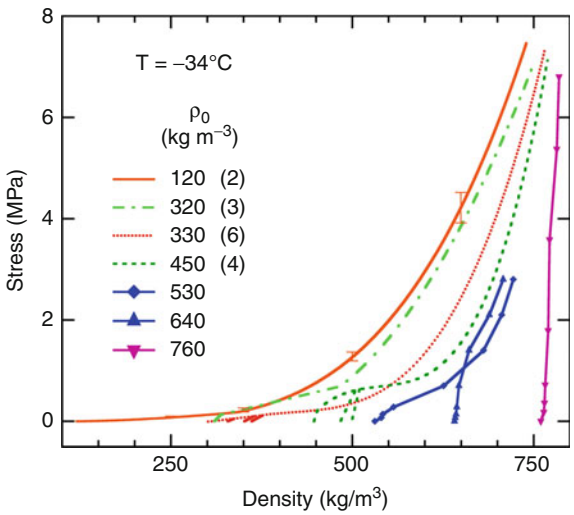

Snow Deformation, Figure 2 Uniaxial compression deformation of snow (Data from Abele and Gow, 1975, 1976). Numbers in parentheses indicate the number of tests.

as shear layers within the snow fail. As temperature increases, resistance to shear decreases. The magnitude of peak shear stresses at failure are functions of the magnitude of the stress perpendicular to the shear planes, temperature, rate of loading/deformation, and density (Figure 4) (McClung, 1977; Montmollin, 1982).

Microstructural and grain-scale processes that control snow deformation

Snow microstructure varies significantly over the range of possible densities from new snow to ice. New snow has no, or very small, bonds connecting grains together (Figure 1a). Metamorphosed snow grains are larger than in new snow (Figure 1b and c). Well-metamorphosed, high-density snow exhibits little microstructural variety, and differences between bond and grain sizes are relatively small (Figure 1d).

The intricate microstructure and small size of bonds compared to grain sizes in low-density snow influences deformation in two important ways. First, loads that cause deformation are not uniformly supported by the microstructural geometry and some geometric pathways support more load than others (Kry, 1975). This means that deformation occurs more rapidly in some parts of the bulk of

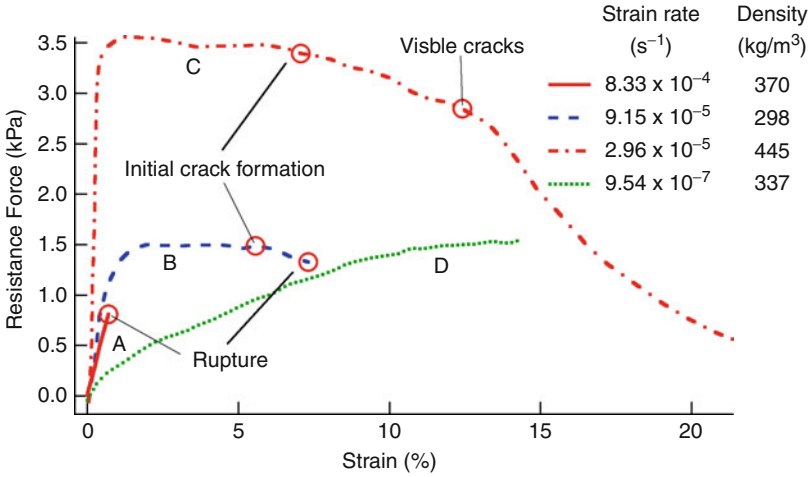

Snow Deformation, Figure 3 Resisting force as a function of uniaxial tension strain (Data from Narita, 1980).

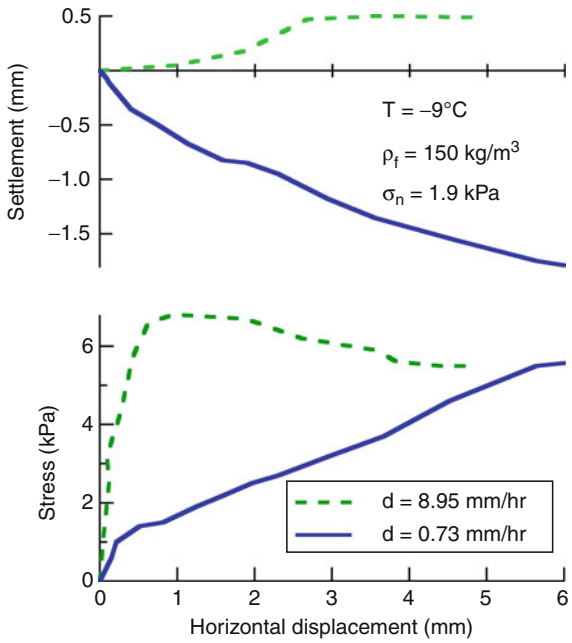

Snow Deformation, Figure 4 Shear stress as a function of horizontal (shear) displacement. Negative settlement indicates densification and positive settlement indicates dilation (Data from McClung, 1977).

snow than in others and that as deformation proceeds more of the microstructure geometry may become involved. Alternatively, as some parts of the microstructure fail, other parts of the microstructure will experience increased loading and deformation. Snow microstructure is more uniform in high-density snow so that stress and deformation will also be more uniform. Secondly, stresses applied to bulk snow concentrate at the bonds with the result that most of the deformation occurs in the bonds, not the grains. As bond sizes approach the size of grains, the distinction between grains and bonds disappears and snow deforms as porous ice.

Grain-scale deformation processes act similarly for deformation in compression, tension, and shear. Differences in the expression of the grain-scale processes at continuum scales are due to the differences in the way the loads are applied. At the grain scale, bonds can be subjected to tension, compression, linear or torsional (twisting) shear, bending, or a combination of those (Johnson and Hopkins, 2005). Tension causes bonds to elongate and thin, and eventually to rupture, while compression causes bonds to thicken. Shear allows grains to move past each other, or rotate in place, via creep deformation while remaining bonded, or sliding if the bond ruptures. Bending is a response to combined tension and compression loads that can eventually lead to rupture. Combined conditions of loading or deformation, such as shear and compression, can cause grains to rotate (Faraday, 1859). Sintering affects grain-scale deformation by changing bond thickness and snow microstructure, especially near the melting temperature where sintering rates are high.

Uniaxial compression

During uniaxial compression, assuming that the rate of loading/deformation and temperature are held constant, the bonds between snow grains can thicken or thin, depending on their orientation to stress. At densities below about 300–400 kg/m^3, grains rearrange through viscous creep in the bonds or fracture of the bonds that permit grains to be displaced with respect to each other. This is a shear deformation process at the grain scale even though the continuum-scale deformation is compression (Shapiro et al., 1997). The process of grain rearrangement is generally accommodated within the pore space of the snow such that confinement of the snow has little effect on deformation (Scapozza and Bartelt, 2003). Sintering continues to operate during deformation, producing changes in the

bonds that can be more important in controlling deformation magnitude and rate than the applied stress, at low loading rates or at high temperatures. As grains rearrange, the microstructure tightens and the density of the snow increases resulting in more grain contacts and new sintered bonds that can produce a wide range of values in the mechanical properties of snow. Often, an *apparent* relationship between density and deformation can be established because both the deformation response of snow to stress and the density depend on the snow microstructure and the form of the bonding/grain contacts. Thus, it is the microstructure and bonding, and not the density, which are important for determining snow deformation response to applied stresses.

At initial densities of between 500 and 700 kg/m^3, snow microstructure makes a transition from complex forms to a form that resembles distributed interconnected pores in an ice matrix. The resistance to uniaxial compression of snow increases significantly as the pore space is no longer able to accommodate snow grain rearrangement. The size of bonds between grains grow to become a significant percentage of the grain size causing stress concentrations to decrease to negligible levels that are related to the ratio of the pore space to the overall volume of ice. At these higher densities, deformation becomes a strong function of density.

Uniaxial tension

Uniaxial tension deformation in relatively low-density snow occurs as viscous creep in bonds, or elastic deformation and rupture of bonds, to allow grains to rearrange in an alignment parallel to the axis of tension. Grains that are initially randomly distributed will undergo shear within their bonds and grain rearrangement to achieve alignment with the tensile stress field. As grains become aligned with the tension axis, bonds will elongate and thin. Bonds will begin to rupture in tension producing progressive failure of the snow at low rates of loading or catastrophic failure of the snow at high loading rates (Narita, 1980). As bonds rupture, stress is transferred to the remaining bonds. As snow density increases, the influence of microstructure decreases, and deformation becomes more ice-like.

Shear

During shear, grains attempt to move past each other along shear planes and may be able to do so without change in volume when grains do not interfere with each other and there are no loads perpendicular to the planes of shearing. When loads act perpendicular to planes of shear, grains will move past each other and fill available pore space, reducing snow volume. If grains interfere with each other during deformation, the grains must fail or the snow volume increase (dilate) to allow grains to rearrange into an easy glide configuration. Increasing the perpendicular loading on a shear plane makes it more difficult for interfering grains to move around each other, thus requiring larger shear stresses to dilate the snow or cause grain failure. For higher-density snow, or at higher loading/deformation rates, interference of grains with each other will cause the deformation resistance to increase to a maximum. At this point, deformation resistance decreases to a relatively constant value determined by the sliding resistance between grains and/or the rates of bond or grain rupture, sintering, and re-sintering (Figure 4).

Conclusions

Snow deformation at the continuum scale is complex because of the cumulative influences of snow microstructures that change under the influence of sintering and multiple grain-scale deformation processes. Sintering and grain-scale deformation are both temperature and loading/deformation rate dependent. Continuum-scale reflections of grain-scale mechanisms in uniaxial compression include decreasing volume with an associated increasing deformation resistance. Uniaxial tension produces an initial increase in deformation resistance as grains align themselves with the axis of tension. Once grains are aligned, bonds will fail as deformation continues, causing the resistance to deformation to decrease and cracks to form in the snow. Resistance to shear deformation increases until grains fail or rearrange themselves to move past neighboring grains. If grains can move into available pore space without interfering with each other, then snow density will increase along with resistance to shear. If grain movement is restricted then resistance will increase to a maximum followed by a decline to a relatively constant value as grains fail or arrange themselves in an easy glide orientation. The importance of microstructure and grain-scale processes decreases with increasing snow density such that, at densities greater than about 500 kg/m^3, deformation mechanisms transition to those associated with porous ice.

Bibliography

Abele, G., and Gow, A., 1975. *Compressibility characteristics of undisturbed snow.* Research Report, USA Cold Regions Research and Engineering Laboratory.

Abele, G., and Gow, A. J., 1976. *Compressibility characteristics of compacted snow.* CRREL Report, USA Cold Regions Research and Engineering Laboratory.

Armstrong, R. L., 1980. An analysis of compressive strain in adjacent temperature-gradient and equi-temperature layers in a natural snow cover. *Journal of Glaciology*, **26**(94), 283–289.

Bartelt, P., and Buser, O., 2004. The principle of minimum entropy production and snow structure. *Journal of Glaciology*, **50**(170), 342–352.

Blackford, J. R., 2007. Sintering and microstructrure of ice: a review. *Journal of Physics. D. Applied Physics*, **40**, R355–R385.

Faraday, M., 1859. On regelation, and on the conservation of force. *Philosophical Magazine*, **17**, 162–169.

Fierz, C. et al., 2009. *The International Classification for Seasonal Snow on the Ground.* IHP-VII Technical documents in hydrology N°83, IACS contribution N°1, UNESCO-IHP, Paris, 80 pp. http://unesdoc.unesco.org/images/0018/001864/186462e.pdf

Flin, F., et al., 2004. Three-dimensional gemoetric measurements of snow microstructural evolution under isothermal conditions. *Annals of Glaciology*, **38**, 39–44.
Johnson, J. B., and Hopkins, M. A., 2005. Identifying microstructural deformation mechanisms in snow using discrete element modeling. *Journal of Glaciology*, **51**, 432–442.
Kry, P. R., 1975. The relationship between the visco-elastic and structural properties of fine-grained snow. *Journal of Glaciology*, **14**(72), 479–500.
McClung, D. M., 1977. Direct simple shear stress tests on snow and their relation to slab avalanche formation. *Journal of Glaciology*, **19**(81), 101–109.
Montmollin, V. d, 1982. Shear tests on snow explained by fast metamorphism. *Journal of Glaciology*, **28**(98), 187–198.
Nakaya, U., 1954. *Snow crystals: natural and artificial*. Cambridge: Harvard University Press.
Narita, H., 1980. Mechanical behavior and structure of snow under uniaxial tensile stress. *Journal of Glaciology*, **26**(94), 275–282.
Petrenko, V. F., and Whitworth, R. W., 1999. *Physics of ice*. New York: Oxford University Press, p. 373.
Scapozza, C., and Bartelt, P., 2003. Triaxial tests on snow at low strain-rate. Part II. Constitutive behavior. *Journal of Glaciology*, **49**(164), 91–101.
Schneebeli, M., and Sokratov, S. A., 2004. Tomography of temperature gradient metamorphism of snow and associated changes in heat condutivity. *Hydrological Processes*, **18**, 3655–3665.
Shapiro, L. H., et al., 1997. *Snow mechanics: review of the state of knowledge and applications.* CRREL Report, Research and Engineering Laboratory, US Army Cold Regions, 35 pp.
Szabo, D., and Schneebeli, M., 2007. Subsecond sintering of ice. *Applied Physics Letters*, **90**, 3.
Trabant, D., and Benson, C., 1972. Field experiments on the development of depth hoar. *Geological Society of America Memoirs*, **135**, 309–322.

Cross-references

Creep
Firn
Seasonal Snow Cover
Snow Density
Snow Grains

SNOW DENSITY

Steven Fassnacht
Snow Hydrology, Watershed Science Program,
Colorado State University, Fort Collins, CO, USA

Definition

Snow density is the ratio of snow water equivalent (SWE) to snow depth. When SWE is given in mm of water and snow depth in m, the units of density are kg m^{-3}.

The density of snow can vary by more than an order of magnitude. The density of freshly fallen snow has been observed to range from 20 kg m^{-3} to 250 kg m^{-3} (e.g., Reek et al., 1992; Fassnacht and Soulis, 2002) and is a function of formation conditions in the clouds and the atmospheric conditions through which the snow crystals fall. Upon reaching the ground, snow crystals begin to metamorphose. Prior to melt, the snow can attain a density of 300 kg m^{-3} (e.g., Fassnacht and Soulis, 2002) to 500 kg m^{-3}, depending on the length of time on the ground, meteorological conditions, and the depth of overlying snow.

Bibliography

Fassnacht, S. R., and Soulis, E. D., 2002. Implications during transitional periods of improvements to the snow processes in the Land Surface Scheme – Hydrological Model WATCLASS. *Atmosphere-Ocean*, **40**(4), 389–403.
Reek, T., Doty, S. R., and Owen, T. W., 1992. A deterministic approach to the validation of historical daily temperature and precipitation data from the cooperative network. *Bulletin of the American Meteorological Society*, **73**, 753–762.

SNOW DEPTH

Gavin Gong
Department of Earth and Environmental Engineering,
Henry Krumb School of Mines, Columbia University,
New York, NY, USA

Definition

The amount of snow on the Earth's surface at a specific point in space and time, measured as the actual vertical distance from the ground surface to the snowpack surface.

Introduction

Snow depth is arguably the most basic and fundamental descriptive feature of snow that resides on the Earth's surface. It is an intuitive measure of the magnitude of a solid precipitation event, for example, "last night's storm dumped 10 in. of snow on the ground". However the familiarity of snow depth belies its spatiotemporal variability, its physiological importance to the cryosphere, hydrosphere, lithosphere, and atmosphere, and also its societal importance as a water resource, especially in a changing climate (Doesken and Judson, 1997).

Snow depth refers to the actual thickness of a snowpack that overlays the surface, and has some important distinctions from other common snow cover descriptors. The binary presence/absence or the spatial extent of snow cover is the most extensively documented feature since it is the easiest to observe. Although snow extent and snow depth are inherently related, their fluctuations do not necessarily coincide in magnitude, timing, or even phase. This distinction is innate at local scales, where snow depth can vary between two different locations within a snow-covered domain, and can vary at a given location throughout the course of its snow season. At broader regional or continental scales, this distinction is often overlooked; for example, a year with a more extensive October snow cover over North America may be incorrectly assumed to have an anomalously deep snowpack throughout the snow-covered region.

Snow water equivalent refers to the depth of water that would result from a melted snowpack. Although this parameter also represents the amount of snow on the ground, it is not interchangeable with snow depth. The difference lies in the highly variable density of snow (typically 50–400 kg m^{-3}) in contrast to the relatively fixed density of liquid water (~1,000 kg m^{-3}). The density of freshly fallen snow depends on the meteorological conditions producing the snowfall event, and the density of a snowpack varies with depth and from seasonal down to hourly timescales even in the absence of melting. Thus, especially during the winter season, snow depth can vary considerably relative to snow water equivalent.

Observed spatial and temporal patterns of variability

Snow depth is represented as a continuous, nonnegative variable defined over an *x, y, t* coordinate system, where *x* and *y* define a location on the land surface (including glaciers and sea ice), and *t* is an instantaneous point in time. Local spatial variability can arise from factors such as heterogeneous precipitation rates, hillslope orientation, vegetation interception, and wind interaction with surface features. On regional scales (e.g., a watershed), the local variations are often averaged out to consider a homogenous snow depth for hydrologic and water resource applications. An important regional phenomenon is lake-effect snow, where atmospheric warming over lakes induces lifting, condensation, and snowfall over downstream land areas, resulting in regions with high snow depth. At the mesoscale, snow depth generally increases with latitude, but orography and proximity to oceans are key geographic determinants. Snow depths tend to be greater over mountain ranges where consistently lower temperatures facilitate solid precipitation and sustain surface snowpacks. The high heat capacity of water has a warming effect on coastal regions, so that Northern Hemisphere snow depth actually decreases with latitude near the Arctic coasts due to reduced snowfall. Hence, maximum snow depths tend to occur in the high-elevation interior of the North American and Eurasian continents (Foster and Davy, 1988).

Temporal variability can occur over multiple timescales. Snow depth can decrease on hourly-daily timescales via ablation processes such as melting, sublimation, and metamorphic transition from crystalline to granular structure which increases snowpack density. Ablation also occurs on weekly-monthly timescales, but is less apparent since periodic snowfall events increase snow depths. The interaction of snowfall and ablation generally lead to a broad delineation of the snow season, into an accumulation period with increasing snow depth, followed by a melt period with decreasing snow depths. On interannual to decadal timescales, snow depth exhibits structured periodicities as well as unstructured random variability, especially at large spatial scales. For example, twentieth century snow depth measurements gridded over North America indicate a decreasing trend from about 1970 to 2000, especially in late winter and early spring, preceded by an increasing trend from about 1900 to 1970 (Ge and Gong, 2008; Dyer and Mote, 2006). Early twenty-first century records do not clearly continue the late twentieth century decreasing trend; hence, the existence of any long-term anthropogenic trend in the snow depth record is ambiguous.

Measurement methods

Snow depth can be easily measured with a ruled stick or snow board inserted through the snowpack, typically to 1 in. or 1 cm precision. The drawbacks of this method are the limitation to point measurements, and the manual effort required and associated inconsistencies (Doesken and Judson, 1997). Nevertheless, it is commonly used for a wide range of scientific and nonscientific activities due to its simplicity and low cost. Snow depth station measurement networks exist throughout North America and Eurasia, and some stations have records dating back for over a century. Recent efforts have been made to interpolate the station measurements into gridded snow depth time series, particularly over North America (Brown, 2000; Dyer and Mote, 2006), which offer a new opportunity to fully characterize the large-scale spatiotemporal variability of snow depth. However, the gridded values can be constrained by irregular station distribution, which can lead to local biases, relatively coarse gridcell resolution that can dampen the true spatial variability, and insufficient accounting of elevation differences. Therefore, individual gridcell values far removed from station observations should be used with caution.

An alternative method for measuring snow depth utilizes remote sensing of electromagnetic waves. At local scales, an ultrasonic sensor is typically mounted on a permanent stand, and measures the time required for an ultrasonic (~50 kHz) pulse to travel through the air down to and back up from the surface. A shorter travel time is indicative of a shorter travel distance due to deeper snow. A temperature probe is also required since the speed of sound is sensitive to air temperature. At the mesoscale, passive microwave sensors mounted onto orbiting satellites are used to measure the degree of scattering caused by snow grains, which can be related to snow depth or snow water equivalent over broad regions (Cavalieri et al., 2004). The principal advantage of satellite remote sensing over station measurements is consistent spatial coverage, but the precision of satellite-based snow depth estimates is still evolving.

Data assimilation has also been used to infer snow depth values at locations far removed from station measurements. Deterministic snowpack models are used to simulate gridcell snow depth based on more readily available meteorological inputs, and model outputs are constrained to match station measurements where

available. Assimilation techniques for snow depth are still developing, but one available product provides daily snow depth for 1 km gridcells over the continental United States dating back to 2003 (NOHRSC, 2004).

Physical processes and modeling

The physical processes that govern snow depth are driven by energy fluxes as well as moisture fluxes (Dingman, 2002). Snow depth, of course, increases directly in response to snowfall events, but this increase can be short-lived if temperatures do not consistently remain below ~0°C. If the snowpack experiences a sustained net energy loss, snowpack temperatures will decrease, ablation will be minimal, and successive snowfall events will accumulate leading to sustained snow depth increases. If the snowpack experiences a net energy gain, snowpack temperatures will increase toward a maximum of ~0°C. During this warming phase, snow depth changes in the absence of snowfall events are minimal since ablation results from sublimation but not evaporation or melting. Even upon reaching ~0°C, snow depth changes are modest at first since initial melting is retained by surface retention onto snow particles within the snowpack; during this ripening period, ablation results from sublimation and evaporation. Only after surface retention has reached capacity does a melt period commence, in which melted snow infiltrates into the underlying soil, and snow depth decreases conspicuously.

Although the energy fluxes are the primary drivers of snow depth, other physical processes can also have an important influence. Wind-driven transport (i.e., blowing snow) during and between snowfall events can spatially redistribute snow depths, affecting sublimation rates and increasing avalanche risks due to locally high accumulations (Pomeroy et al., 2008). Dust deposition onto a snowpack affects snow depths by decreasing the albedo and hence increasing snowmelt rates at the snow surface. Metamorphic processes within a snowpack, such as gravitational settling, refreezing of snowmelt and water vapor transport, result in the densification of a snowpack over time, which can decrease snow depths even in the absence of snowmelt losses.

Mathematical models have been developed to simulate the evolution of a snowpack and its associated physical processes, by solving the governing equations of mass and energy balance for a one-dimensional system comprised of multiple snow and underlying soil layers. Radiative, turbulent, and diffusive energy exchanges are computed between each layer, from specified optical and thermal properties for snow and the underlying soil, and meteorological inputs at the snow–air interface. These fluxes determine the temperature and density of each layer, which in turn control the snowpack accumulation and ablation processes, and the resulting snowpack depth. Examples of such models include SNTHERM, CROCUS, and SNOWPACK, and they are used for a variety of applications from water supply planning to avalanche warning (Rasmus et al., 2007).

Snow depth is also a prominent land surface feature simulated in large-scale climate models, as part of a land surface parameterization scheme. Because of the gridcell structure of most climate models that is very coarse relative to the physical snow accumulation and ablation processes, these snow parameterizations are necessarily simplified. Typically, only a single snow layer is modeled, primary processes such as albedo are computed simply from vegetation type, snow depth, and snow temperature, and other important metamorphic processes such as refreezing are ignored. Recent improvements have increased vertical resolution, improved vertical physics, and incorporated sub-grid-scale heterogeneity to represent snow depth variability within a gridcell. Overall, climate models capture the broad features of the observed land surface snow regime, although ablation processes at low snow depths are a significant source of both scatter between individual models and overall modeling weakness (Slater et al., 2001).

Socioeconomic importance

Land surface snow depth is of tremendous social and economic importance, affecting many sectors such as water supply, agriculture, fishery, forestry, manufacturing, and tourism (Doesken and Judson, 1997; Frederick and Gleick, 1999). The potential influence of insufficient winter snowpack on water supply and drought risk during the subsequent spring and summer seasons is a major concern in the densely populated mid-latitude regions of the world. The lack of water stored in the form of snow also limits agricultural irrigation, creates shortages of water for industrial users, and damages wildlife habitats. Less snow accumulation in winter or early snow melt in spring are also a major reason for more frequent and prolonged forest fires that put ecosystems and humans in peril. Another impact of snow depth is its influence on the tourism sector, in particular skiing and other winter activities that serve as a major contributor to regional economies in many places around the world. Snow depth variations even on a weekly basis can have a direct financial impact on the local ski and snow sports industry and related businesses, while seasonal to interannual variations can affect employment patterns and construction decisions.

Conversely, excessive snow depths can jeopardize livelihoods and disrupt local economies. The consequences of severe snow storms are usually devastating, resulting in power outages, agricultural damage, and property loss (Doesken and Judson, 1997). Deep snowpacks pose an obvious avalanche risk in mountainous areas, and can also be a primary reason for floods when combined with excessive rainfall during the snow melting season, which may require massive evacuations and damage buildings, bridges, dams, and other infrastructure. Rapid melt of deep snowpacks can also trigger landslides and debris flows which could impair downstream water quality, cause

serious soil erosion, and limit agricultural productivity (Frederick and Gleick, 1999).

The SNOTEL system operated by the United States Natural Resources Conservation Service (http://www.wcc.nrcs.usda.gov/snow/about.html) illustrates the socio-economic value of snow depth. This service regularly collects, transmits, and processes snowpack and related climatic data at roughly 2,000 manual and/or automated sites in the western United States and Alaska, as well as streamflow forecasts for about 740 locations. This information is critical to regional water managers and decision makers in these regions, where, winter snowpack represent the largest component of water storage (Mote et al., 2005). It is used to inform crop optimization plans for irrigation-dependent agricultural land, drought management plans for water supply reservoirs, and flood diversion plans for municipalities. It is also used by local businesses to inform staffing, equipment, and other operational decisions.

Climatic relationships

Land surface snow depth is being increasingly recognized for exhibiting physically based relationships with the overlying climate system, distinct from the more widely studied snow extent relationships (Ge et al., 2009). Although the presence of a snow cover is known to suppress local air temperature, deeper snow has been shown to enhance the temperature suppression. Climate modeling studies suggest that snow depth may have a greater impact on the Indian monsoon than snow extent, via alterations to the hydrological cycle and surface energy budget. Extending to larger scales, snow depth anomalies over Siberia have also been found to influence the dominant mode of extratropical North Hemisphere climate variability.

Conversely, large-scale climate teleconnection patterns have been shown to influence snow depth, particularly over North America. Many of these studies are motivated largely by socioeconomic issues such as water supply in the western United States, and therefore use snow water equivalent rather than snow depth as the snow cover metric. These studies have identified various regional-scale statistical relationships with a disparate set of climatic drivers, for example, the Pacific–North American Pattern (PNA), El-Nino Southern Oscillation (ENSO), Pacific Decadal Oscillation (PDO), and the North Atlantic Oscillation (NAO). More recently, a gridded snow depth dataset covering all of North America has been used to identify more coherent continental-scale relationships with climate phenomena that originate in the extratropical North Pacific. Overall, snow depth is emerging from the shadow of the more readily measured snow extent as having meaningful climatic causes and consequences.

Bibliography

Brown, R. D., 2000. Northern hemisphere snow cover variability and change, 1915–1997. *Journal of Climate*, **13**, 2339–2355.

Cavalieri, D., Markus, T., and Comiso, J., 2004. *AMSR-E/Aqua Daily L3 12.5 km Brightness Temperature, Sea Ice Conentration, and Snow Depth Polar Grids V002*. Boulder, CO: National Snow and Ice Data Center. Digital media.

Dingman, S. L., 2002. *Physical Hydrology*. Upper Saddle River, NJ: Prentice-Hall.

Doesken, N. J., and Judson, A., 1997. *The Snow Booklet – A Guide to the Science, Climatology, and Measurement of Snow in the United States*. Fort Collins, CO: Colorado State University.

Dyer, L. J., and Mote, T. L., 2006. Spatial variability and trends in snow depth over North America. *Geophysical Research Letters*, **33**, L16503, doi:10.1029/2006GL027258.

Foster, D. J., and Davy, R. D., 1988. *Global Snow Depth Climatology, USAFETAC/TN-88/006*. Illinois: USAF Environmental Technical Applications Center, Scott Air Force Base.

Frederick, K. D., and Gleick, P. H., 1999. *Water and Global Climate Change: Potential Impacts on U.S. Water Resources*. Washington, DC: Pew Center on Global Climate Change.

Ge, Y., and Gong, G., 2008. Observed Inconsistencies Between Snow Extent and Snow Depth Variability at Regional/Continental Scales. *Journal of Climate*, **21**, 1066–1082.

Ge, Y., Gong, G., and Frei, A., 2009. Physical Mechanisms Linking the Winter Pacific – North American Teleconnection Pattern to Spring North American Snow Depth. *Journal of Climate,* in press.

Mote, P. W., Hamlet, A. F., Clark, M. P., and Lettenmaier, D. P., 2005. Declining Mountain Snowpack in Western North America. *Bulletin of the American Meteorological Society*, **86**, 39–49.

National Operational Hydrologic Remote Sensing Center (NOHRSC), 2004. *Snow Data Assimilation System (SNODAS) Data Products at NSIDC*. Boulder, CO: National Snow and Ice Data Center. Digital Media.

Pomeroy, J. W., Gray, D. M. and Marsh, P., 2008. Studies on Snow Redistribution by Wind and Forest, Snow-Covered Area Depletion, and Frozen Soil Infiltration in Northern and Western Canada. *Cold Region Atmospheric and Hydrologic Studies. The Mackenzie GEWEX Experience. Volume 2: Hydrologic Processes*. doi:10.1007/978-3-540-75136-6_5. 81–96.

Rasmus, S., Gronholm, T., Lehning, M., Rasmus, K., and Kulmala, M., 2007. Validation of the SNOWPACK model in five different snow zones in Finland. *Boreal Environment Research*, **12**, 467–488.

Slater, A. G., et al., 2001. The representation of snow in land surface schemes: results from PILPS 2(d). *Journal of Hydrometeorology*, **2**, 7–25.

Cross-references

Frequency Analysis of Snow Storms
Global Outlook of Snowcover, Sea Ice, and Glaciers
Snow Density
Snow Water Equivalent
Surface Energy Balance

SNOW DRIFT

Richard Bintanja
Royal Netherlands Meteorological Institute (KNMI),
De Bilt, The Netherlands

The process of transporting snow particles due to strong winds is called snowdrift.

In regions with permanent snow cover such as Antarctica, and in regions with seasonal snow cover, blizzards, snowstorms, and snowdrift are common phenomena. Loose surface snow particles are usually present whenever temperatures are below 0°C. When surface winds exceed about 7 m s^{-1}, these particles are picked up by the wind and become airborne. At moderate winds, individual snow particles bounce along the surface – a process called saltation – thereby ejecting more particles at each bounce. This is also referred to as drifting snow, and takes place in the lowest 0.1 m or so of the atmosphere. When wind speeds increase further, the particles become fully detached from the surface. This state of snowdrift is usually referred to as suspension, or blowing snow, and can reach heights of tens to even hundreds of meters. During snowdrifting conditions, individual particles collide, break, and generally become more round while airborne. Starting as snowflakes, they quickly turn into much smaller, rounded particles, which can be more densely stacked when they are deposited again. This process is usually referred to as wind packing.

Persisting winds may transport snow particles tens to hundreds of kilometers before settling down again. The erosion, horizontal transport, and subsequent deposition of snow lead to a significant redistribution of the surface snow, often resulting in surface features like snow dunes. Over the vaste flat snowplains of Antarctica, snow dunes thus formed can reach heights of about 1 m. However, when orography or buildings induce irregular wind patterns, snowdrift can potentially lead to accumulation of tens of meters of snow. Another adverse and potential dangerous effect of snowdrift is the reduced visibility caused by the airborne snow particles; during strong blizzards, the visibility may be reduced to almost zero.

Snowdrift not only involves the transport of snow from one location to the other, it also causes the snowdrifting particles to sublime. Traveling downwind, turbulent updrafts within the snowstorm will keep the particles afloat. Hence, the airborne particles are continuously ventilated, inducing a turbulent moisture flux, or sublimation, which steadily eats away mass from the particle. Snowdrift sublimation is a fairly efficient process, since the airborne particles are ventilated on all sides (in contrast to particles at the surface). This constitutes a two-step mechanism by which the snow surface loses mass: first snow particles are being swept up by the winds, after which they are slowly sublimated away while traveling downstream. Calculations have shown that snowdrift sublimation is generally a significant term in removing mass from the snow surface; averaged over Antarctica, about 15% of all precipitated snow is thus sublimed to water vapor again.

Bibliography

Bintanja, R., 1998. The contribution of snowdrift sublimation to the surface mass balance of Antarctica. *Annals of Glaciology*, **27**, 251–259.

Bintanja, R., 2001. Modification of the wind speed profile caused by snowdrift: results from observations. *Quart J R Meteorol Soc*, **127**, 2417–2434.

SNOW GAUGE

A. K. Singh
DIAT (Deemed University), Girinagar, Pune, Maharashtra, India

A snow gauge is an instrument used by meteorologists and hydrologists to measure the amount of snow precipitation over a set period of time. Snow stakes and simple rulers can be used to determine the depth of the snowpack, though they will not evaluate either its density or liquid equivalent. Snow gauges measure snowfall water equivalent directly. The snow gauge consists of two parts, a copper catchment container and a funnel-shaped gauge. The snow collection container is generally shielded to reduce wind turbulence around the orifice, as shown in Figure 1, and is mounted on a pipe outdoors and is approximately 1.5 m high, far enough above the snow surface to minimize the accumulation of blowing snow in the gauge, while the container is 51.5 cm in length. When snow has fallen the container is removed and replaced with a spare.

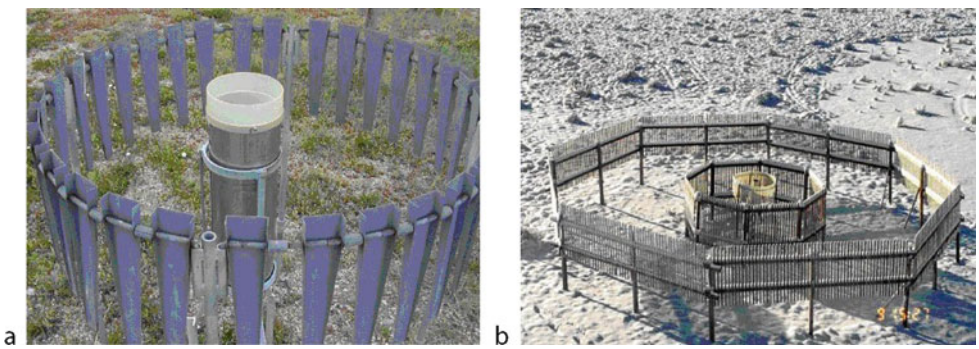

Snow Gauge, Figure 1 Snow gauge. Single alter shield (**a**); double fenced intercomparison reference shield (**b**). (Taken from ams.confex.com/ams/pdfpapers/119076.pdf.)

Snow Gauge, Figure 2 Tipping bucket rain gauges, that is, electric rain/snow gauges (www.omega.com).

The snow is then melted and poured into a measuring glass. While the depth of snow is normally measured in centimeters, the measurement of melted snow (water equivalent) is in millimeters. An estimate of the snow depth can be made by multiplying the water equivalent by ten.

The snow gauge suffers from the problem as that of the rain gauge when conditions are windy as the amount of snow may be under or over reported. Another problem may occur when there is both snowfall and rainfall leading to inaccurate measurement. In all of these cases the observer judgment is of critical importance to ascertain the accuracy of measurement.

Remote reading gauges used by weather stations that work similar to rain gauges have a large catch area that collects a critical weight of snow after which it tips and empties the snow catch. This activates a switch and sends a signal (Figure 2). If the catch container has a heater in it the snow weight is measured accurately. There is a possibility to tip the switch based on volume instead of weight leading to appropriate fill sensing.

Bibliography

Landolt, S. D., and Rasmussen, R. M., National Center for Atmospheric Research, Boulder, CO (taken from ams.confex.com/ams/pdfpapers/119076.pdf).

SNOW GRAINS

Thomas H. Painter
Jet Propulsion Laboratory/Caltech, Pasadena, CA, USA

Definition and introduction

Changes in snow grains and their bonds contribute to changes in snow's albedo, microwave scattering, thermal conductivity, mechanical properties, and gas adsorption. The concept of the snow grain would seem to be easily defined and yet the complexity of the snow matrix and forms resulting from initial conditions and metamorphism renders an exact definition impossible (Mätzler, 1997). This lack of a simple definition results largely because the degree of sintering between the (always) monocrystalline particles varies enormously and concave or highly asymmetric forms are not uncommon. The concept of the snow grain to a remote sensor is substantially different from that to an avalanche forecaster, and their respective defined sizes for the same snow can vary by two orders of magnitude. Here, the concept of snow grains is described through the characterization of shape and size. (Note: sintering is described in the entry on snow bonding.)

We tend to conceptualize snow as a collection of grains because snow precipitates discretely to the Earth's surface and scrapes discretely from a snow pit face (Figure 1). However, the concept of the snow grain is most sound when the degree of metamorphism is modest, and the principal axes of the crystals are similar. The advent of micro-tomography has shown that snow has a much more complex structure than previously thought, and traditional grain-bond models are of little scientific use. Still, grain size and shape is the only possible morphometric measure that can be observed in the field.

Grain shape

In the new International Classification for Seasonal Snow on the Ground (Fierz et al., 2009), the snow grain is defined by its shape and its size. The shape is based mainly on morphological criteria, but also to some degree by its assumed state of metamorphism as described below. This definition relies methodologically on the traditional way of estimating grain size by scraping snow particles from the wall of a snow profile and studying these particles on a gridded black board using a magnifying hand lens or loupe.

The ICSSG (International Classification of Seasonal Snow on the Ground) suggests classification of snow grains according to the following classes: precipitation particles, machine-made snow, decomposing and fragmented precipitation particles, rounded grains, faceted grains, depth hoar, surface hoar, melt forms, and ice formations. As such, the first seven classes are specific to dry snow whereas the last two are specific to a period of

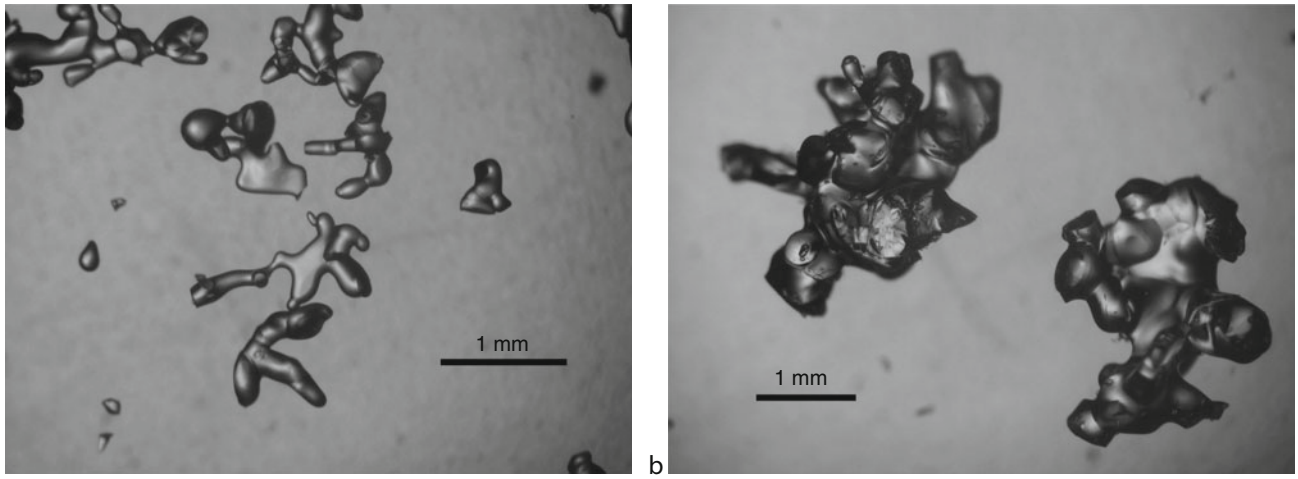

Snow Grains, Figure 1 (**a**) Decomposing precipitation particles from near-surface layer, Mammoth Lakes, California, February, 2001 (Photo: T. H. Painter, from Painter and Dozier (2004), Figure 6). (**b**) Rounded polycrystals from near-surface layer, Mammoth Lakes, California, March, 2001 (Photo: T. H. Painter, from Painter and Dozier (2004), Figure 6).

wet snow. The classes are further divided into subclasses for which the description of the physical process is relied upon to assist in assignment of subclass. These classes and subclasses are used in most applications with little confusion but it is understood that the observations involve human interpretation and as such are inexact.

When modeling radiative transfer and thermal conductivity, these classes are often approximated with analytical forms that resemble atmospheric forms (Macke and Mishchenko, 1996; Mishchenko et al., 1999; Painter and Dozier, 2004) but more detailed treatments are emerging (Kokhanovsky and Zege, 2004). Techniques for automatically retrieving grain shape from X-ray microtomography and digital imagery with the metrics of dendricity (to distinguish "new" from "old" snow) and sphericity (to distinguish faceted from rounded grains) have been demonstrated with modest success (Flin et al., 2005; Bartlett et al., 2008).

Grain size

The complexity of grain shapes and bonds in snow renders the description of grain size difficult. In the ICSSG, the size is defined by the range of the longest extent of a collection of grains. The maximum dimension of a fresh stellar snowflake can be as large as 10 mm whereas the minimum dimension can be as small as 0.05 mm, having an aspect ratio of 200. By contrast, a rounded polycrystal particle that has experienced persistent melt-freeze cycles can be quasi-spherical with a radius of 1 mm (Figure 1b). Without quantitative description of the grain shapes, comparison of single grain sizes for these two particles would be meaningless for any application.

Grain size therefore is often described as the equivalent grain size within the context of application or process. For example, grain size with respect to visible and near-infrared radiative transfer (reflectance, transmission) is described by an optically equivalent grain size, given by the radius of the ice sphere that can represent the optical properties of the observed nonspherical snow. Likewise, equivalent grain size is described for microwave radiative transfer and current efforts are investigating how these equivalent grain sizes are related across the electromagnetic spectrum.

While the concept of "equivalent grain size" is useful from a practical, computational standpoint, a more physically explicit and comparable description of snow grain "size" comes from the specific surface area (SSA). SSA is defined as surface area per unit ice volume ($mm^2/mm^3 = mm^{-1}$) or surface area per unit mass (m^2/kg). The SSA is an essential microstructural parameter for the characterization of sintered materials such as snow, determining radiative properties, adsorption and release of trace gases, and permeability. The radius of the equivalent sphere for a specific surface area is 3/SSA (units of m).

The most fundamental modern method to measure snow SSA is through the determination of adsorption isotherm of gases such as nitrogen or methane (Adamson and Dormant, 1966; Legagneux et al., 2002; Kerbrat et al., 2008). Micro-X-ray tomography and stereology of vertical sections are equally precise (Kerbrat et al., 2008), and have the advantage that they can resolve spatial heterogeneities and very thin layers. Near-infrared photography (Matzl and Schneebeli, 2006) and contact spectroscopy (Painter et al., 2007) likewise give precise results but for the entire snow column at vertical resolutions of <1 mm to ~ 2 cm and far more rapidly than possible with the previous techniques (Figure 2). By resolving heterogeneities and thin layers with these

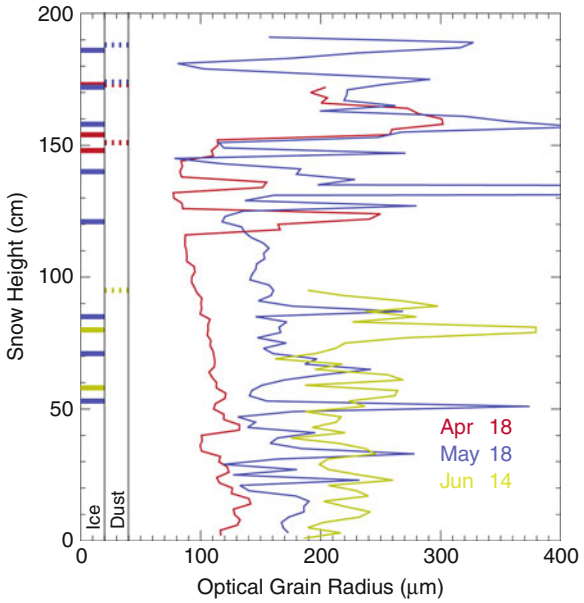

Snow Grains, Figure 2 Optical equivalent grain radius from contact spectroscopy in the San Juan Mountains, Colorado (From Painter et al. (2007), Figure 4).

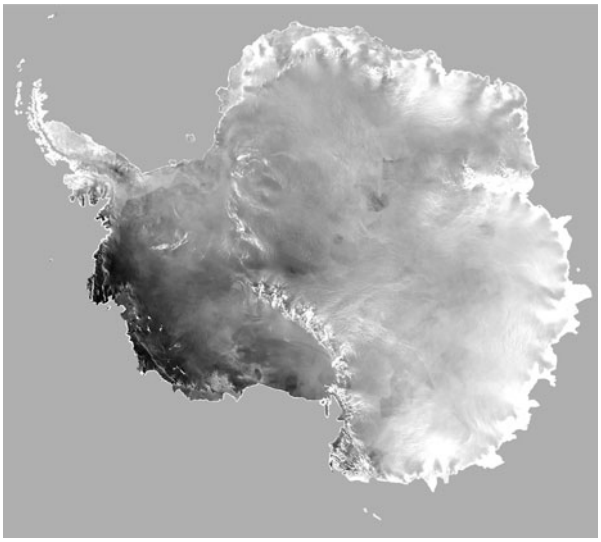

Snow Grains, Figure 3 Optical grain size map of Antarctica from the Mosaic of Antarctica from the NASA Moderate Resolution Imaging Spectroradiometer (MODIS) (Haran et al., 2005; Scambos et al., 2007). The OGS range was 40 μm (*dark*) to 1,100 μm (*light*) in radius (Image courtesy of the National Snow and Ice Data Center [NSIDC]).

techniques, we can better understand the influence on optical and microwave radiative transfer and mechanical properties of the snow column (Painter et al., 2007). These techniques do not presently treat grain shapes but in the future, directional retrievals will facilitate simultaneous retrievals of metrics of grain shape and grain size (Painter et al., 2003).

Remote sensing of snow grains

The spectral reflectance of snow is sensitive to changes in the optical grain size and grain shapes. Because of this sensitivity, multispectral and hyperspectral optical remote sensing from airborne and spaceborne platforms has the capacity to invert the measured reflectance for near-surface, optical grain size (Figure 3). The spatial distribution of optical grain size (which can be inverted for SSA) can be mapped using absolute reflectance at discrete bands in the near infrared (Fily et al., 1997), the integral of ice absorption features from imaging spectrometer data (Nolin and Dozier, 2000), and the general shape of the reflectance spectrum (Scambos et al., 2007; Painter et al., 2009).

Summary

Our understanding of the snow grain has come to more quantitative terms since the seventeenth-century observations by Descartes, Grew, Hooke, and Kepler. Even since the previous International Snow Classification of Seasonal Snow on the Ground in 1990, technological and modeling advances have contributed the X-ray tomograph, portable optical spectroscopy, and performance computing. These most recent technologies have allowed us to explore the three-dimensional structure of snow, specific surface area, and the influences of changes in the concepts of grains on energy and mass transfer. At the time of writing, laboratory, field, and remote sensing experiments are exploring the consistency between wavelength specific equivalent grain sizes and our ability to accurately infer SSA, new reflectance technologies, and relationship between passive and active microwave retrievals of snow water equivalent and our best understanding of the grain.

Bibliography

Adamson, A. W., and Dormant, L. M., 1966. Adsorption of nitrogen on ice at 78 Degrees K. *Journal of the American Chemical Society*, **88**, 2055–2057.

Bartlett, S. J., Rüedi, J.-D., Craig, A., and Fierz, C., 2008. Assessment of techniques for analyzing snow crystals in two dimensions. *Annals of Glaciology*, **48**, 103–112.

Fierz, C., Armstrong, R. L., Durand, Y., Etchevers, P., Greene, E., McClung, D. M., Mishimura, K., Satyawali, P. K., and Sodratov, S. A., 2009. *The International Classification for Seasonal Snow on the Ground*. Paris: UNESCO-IHP.

Fily, M., Bourdelles, B., Dedieu, J. P., and Sergent, C., 1997. Comparison of in situ and Landsat Thematic Mapper derived snow grain characteristics in the Alps. *Remote Sensing of Environment*, **59**(3), 452–460.

Flin, F., Brzoska, J. B., Coeurjolly, D., Pieritz, R. A., Lesaffre, B., Coleou, C., Lamboley, P., Teytaud, O., Vignoles, G. L., and Delesse, J. F., 2005. Adaptive estimation of normals and surface area for discrete 3-D objects: Application to snow binary data from X-ray tomography. *IEEE Transactions on Image Processing*, **14**(5), 585–596.

Haran, T., Bohlander, J., Scambos, T., Painter, T. H., and Fahnestock, M., 2005. *MODIS Mosaic of Antarctica (MOA) Image Map*. Boulder, CO: National Snow and Ice Data Center.
Kerbrat, M., Pinzer, B., Huthwelker, T., Gaggeler, H. W., Ammann, M., and Schneebeli, M., 2008. Measuring the specific surface area of snow with X-ray tomography and gas adsorption: comparison and implications for surface smoothness. *Atmospheric Chemistry and Physics*, **8**(5), 1261–1275.
Kokhanovsky, A. A., and Zege, E. P., 2004. Scattering optics of snow. *Applied Optics*, **43**(7), 1589–1602, doi:10.1364/AO.43.001589.
Legagneux, L., Cabanes, A., and Dominé, F., 2002. Measurement of the specific surface area of 176 snow samples using methane adsorption at 77 K. *Journal of Geophysical Research*, **107**, 4335–4349.
Macke, A., and Mishchenko, M., 1996. Applicability of regular particle shapes in light scattering calculations for atmospheric ice particles. *Applied Optics*, **35**(21), 4291–4296.
Matzl, M., and Schneebeli, M., 2006. Measuring specific surface area of snow by near infrared photography. *Journal of Glaciology*, **52**(179), 558–564.
Mätzler, C., 1997. Autocorrelation functions of granular media with free arrangement of spheres, spherical shells or ellipsoids. *Journal of Applied Physics*, **81**(3), 1509–1517.
Mishchenko, M., Dlugach, J. M., Yanovitskij, E. G., and Zakharova, N. T., 1999. Bidirectional reflectance of flat, optically thick particulate layers: an efficient radiative transfer solution and applications to snow and soil surfaces. *Journal of Quantitative Spectroscopy and Radiative Transfer*, **63**, 409–432.
Nolin, A. W., and Dozier, J., 2000. A hyperspectral method for remotely sensing the grain size of snow. *Remote Sensing of Environment*, **74**(2), 207–216.
Painter, T. H., Paden, B., and Dozier, J., 2003. Automated spectro-goniometer: a spherical-robot for the measurement of the directional reflectance of snow. *Reviews of Scientific Instruments*, **74**(12), 5179–5188.
Painter, T. H., and Dozier, J., 2004, Measurements of the hemispherical-directional reflectance of snow at fine spectral and angular resolution, *Journal of Geophysical Research-Atmospheres*, 109(D18): D1811510.1029/2003JD004458.
Painter, T. H., Molotch, N. P., Cassidy, M. P., Flanner, M. G., and Steffen, K., 2007. Contact spectroscopy for the determination of stratigraphy of snow grain size. *Journal of Glaciology*, **53**(180), 121–127.
Painter, T. H., Rittger, K., McKenzie, C., Slaughter, P., Davis, R. E., and Dozier, J., 2009. Retrieval of subpixel snow covered area, grain size, and albedo from MODIS. *Remote Sensing of Environment*, **113**, 868–879, doi:10.1016/j.rse.2009.01.001.
Scambos, T., Haran, T., Fahnestock, M., Painter, T. H., and Bohlander, J., 2007. MODIS-based Mosaic of Antarctica (MOA) data sets: Continent-wide surface morphology and snow grain size. *Remote Sensing of Environment*, **111**(2–3), 242–257, doi:10.1016/j.rse.2006.12.020.

Cross-references

Albedo
Atmosphere-Snow/Ice Interactions
Dry Snow
Firn
Layering of Snow
Melting Processes
Radiative Transfer Modeling
Snow Crystal Structure
Snow Hydrology
Stratigraphy of Snowpacks

SNOW HYDROLOGY

Sarah Boon, Katie Burles
Department of Geography, University of Lethbridge, Lethbridge, AB, Canada

Definition

Snow hydrology is the study of snow contributions to the hydrologic cycle, particularly snowmelt, meltwater movement within the snowpack, and meltwater contributions to surface runoff.

Snow hydrology processes

The snow accumulation period is characterized by accumulating snow water equivalent (SWE), as observed in many parts of the northern hemisphere and high-elevation locations in the southern hemisphere. During the accumulation period, net energy inputs to the snowpack are negligible: average air temperatures decrease while SWE increases.

The snowmelt period is initiated when air temperatures begin to rise, net energy becomes positive, and SWE begins to decrease. The melt period can be separated into three phases:

1. *Warming*: snowpack temperature increases until the snowpack is isothermal at 0°C.
2. *Ripening*: melt occurs but meltwater remains within the snowpack. At the end of this phase, the snowpack is "ripe": all available pore spaces are saturated with meltwater, and no additional water can be stored (see *Snow Ripening*).
3. *Output*: continuing energy inputs create additional melt. Since the snowpack is saturated, additional melt leaves the pack and contributes to surface hydrology (soil moisture, surface runoff).

The average snowpack may not necessarily follow this exact sequence; in many cases, meltwater is produced at the snow surface prior to the pack becoming isothermal. This meltwater then percolates down through the pack and freezes, releasing latent heat which can act to warm the pack. Alternatively, the snow surface may become isothermal then refreeze until air temperatures increase and melting continues. Snowmelt can be empirically assessed using remote sensing approaches that quantify the areal extent of snowpack and the phase of melt (warming, ripening, output); however, it is difficult to quantify the volume and timing of snowmelt using these approaches (Rango, 1980; Déry et al., 2005; Derksen and MacKay, 2006; Wolken et al., 2009).

Factors influencing snowmelt

The rate and timing of snowmelt is determined mainly by the amount of available energy (Pomeroy and Goodison, 1997), which varies with topography (elevation, aspect), climate and meteorological conditions (maritime,

continental; rain-on-snow events, chinooks), and vegetation cover (open, sub-canopy, shrub, glacier surface). South-facing slopes have higher melt rates than north-facing slopes given increased radiation inputs, while lower elevations melt earlier than high elevations due to higher air temperatures. In maritime climates, rain-on-snow events enhance snowmelt, while in continental climates with frequent föhn (chinook) events, winter melt can occur. Vegetation cover plays a significant role in altering the energy reaching the snow surface, thus melt processes are often divided into open versus forested environments. In open environments (prairie, clear-cut, glacier surface), melt is driven by a combination of both radiative and turbulent fluxes. In forested environments, however, turbulent fluxes are significantly reduced, and radiative fluxes are much more complex. Shrub environments, however, lie between open and forested environments, with reduced longwave radiation inputs relative to a forest, but only slightly reduced turbulent fluxes, and very similar shortwave radiation inputs to open environments.

Snowmelt production: temperature index methods

Snowmelt has historically been calculated using temperature index (degree-day) approaches, which approximate snowmelt as a function of average air temperature (Anderson, 1973):

$$\text{SWE} = M(T_a - T_m) \text{ when } T_a \geq T_m \quad (1)$$

$$\text{SWE} = 0 \text{ when } T_a < T_m \quad (2)$$

where SWE is the snow water equivalent; M is the melt coefficient (also termed melt factor or degree-day factor); and T_a and T_m are the temperature of the atmosphere and snowpack, respectively. This approach assumes that, during melt, $T_m \approx 0°C$, that energy inputs to the pack from longwave and turbulent sources are linear functions of air temperature, and that solar radiation is well correlated with air temperature (Braithwaite, 1984). The melt coefficient can be difficult to determine and is dependent on latitude, elevation, aspect, forest cover, and day of year, all of which must be empirically measured or assumed for various watersheds (Gray and Prowse, 1993). The strength of these models lies in their minimal input data requirements, as air temperature is the most readily available meteorological variable, and their minimal computational requirements. However, these models are highly calibrated (Walter et al., 2005) and are limited to larger spatial scales and longer time periods (i.e., exceeding hourly and daily intervals) (Gray and Prowse, 1993). They are most commonly applied in large-scale watershed models with limited input data; for example, the HBV (Bergström, 1995), SRM (Martinec and Rango, 1986), UBC (Quick and Pipes, 1977), and SWAT (Fontaine et al., 2002) models. Despite their simplistic representation of the snowmelt process, temperature index–based model outputs have been validated in many environments (Beven, 2001).

To improve the physical basis of degree-day models, researchers have defined modified degree-day methods that incorporate additional variables such as snow surface albedo (e.g., Hock, 1999; Pellicciotti et al., 2008). While these models require additional input data and are more computationally intensive than the standard temperature index method, they remain more accessible than energy balance approaches, which can require significant amounts of data and data processing time.

Snowmelt production: energy balance methods

Energy balance models are more complex than temperature index approaches, as they are based on the fundamental physical principles of conservation of energy and mass. Designed for short-term forecasts (e.g., hourly and daily intervals) and highly data intensive (Gray and Prowse, 1993), energy balance models are the most thorough and accurate methods for calculating snowmelt. Figure 1 shows a basic schematic of the vertical energy fluxes during snowmelt in a forested environment. Here we describe the snow surface energy balance in a forested environment, as it is most complex given the ability of the forest canopy (e.g., density, height to live crown, crown depth and diameter, tree condition) to absorb and reflect incoming shortwave radiation, emit longwave radiation, and alter snow surface albedo (Link and Marks, 1999). Forest canopy also increases surface roughness, thereby decreasing wind speeds (Gray and Prowse, 1993).

The energy balance during snowmelt is calculated as:

$$Q_m = Q^* + Q_h + Q_e + Q_g + Q_r - Q_\Theta \quad (3)$$

where: Q_m = energy available for melt; Q^* = net radiation Q_h = convective transport of sensible heat between the air and snowpack; Q_e = latent heat released through condensation of water vapor onto the snowpack or lost through evaporation; Q_g = conduction of heat to the snowpack from the ground; Q_r = advection of heat to the snowpack through rain; Q_θ = rate of change of internal energy per unit surface area per unit time (all in MJ m^{-2} day^{-1}).

Net radiation (Q^*) is the sum of net shortwave (K^*) and net longwave (L^*) radiation fluxes and is the dominant energy flux contributing to snowmelt in forested environments (Link and Marks, 1999; Woo and Giesbrecht, 2000; Koivusalo and Kokkonen, 2002; Spittlehouse and Winkler, 2002). K^* is the total amount of incoming shortwave radiation (K↓) minus outgoing shortwave radiation (K↑). K↓ is representative of the total amount of solar radiation that has reached the ground or snow surface. This includes the portion that is not reflected by clouds or absorbed and scattered by the atmosphere (direct beam [S]), and the portion that is scattered by the atmosphere or above-surface objects such as trees (diffuse solar radiation [D]). K↑ is a function of the surface albedo (α), or reflectivity, which is calculated as the ratio of incoming solar radiation reflected by a surface to the total amount incident on that surface. Albedo declines as snow ages and melts (Table 1), and is also affected by organic debris

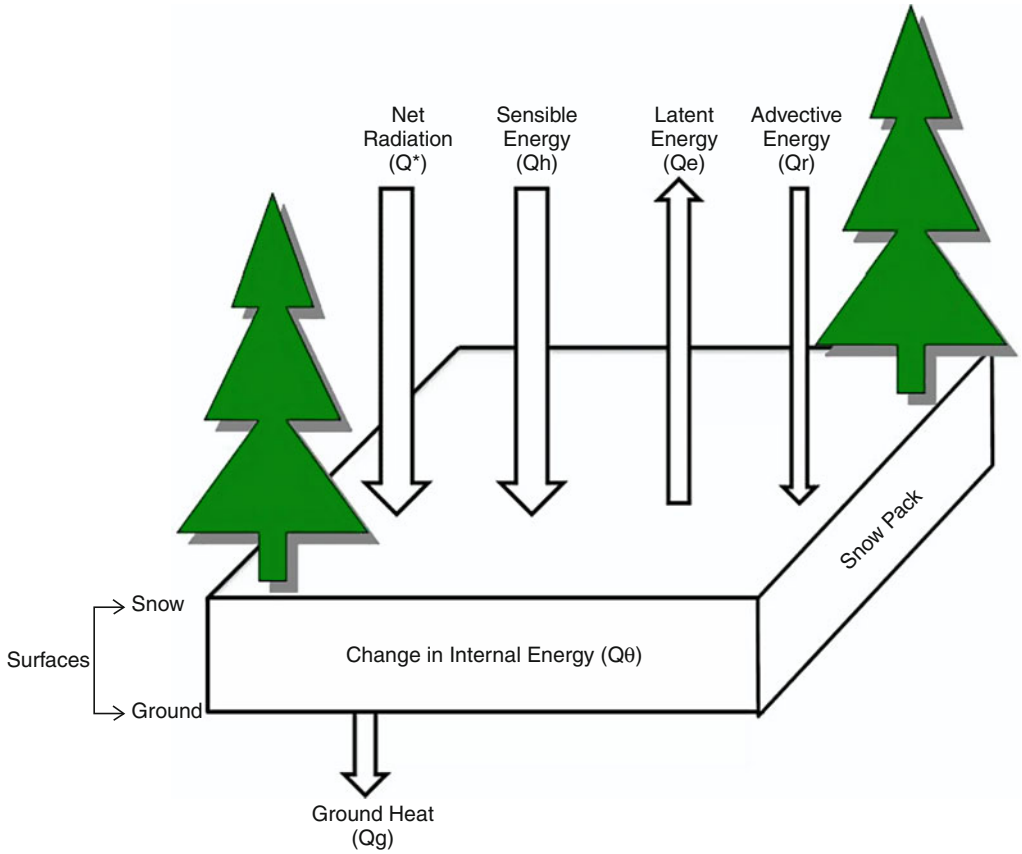

Snow Hydrology, Figure 1 Schematic of vertical energy fluxes in a forested environment (Modified from Gray and Prowse, 1993).

Snow Hydrology, Table 1 Albedo of various surfaces (From Gray and Prowse, 1993)

Surface	Typical range in albedo
New snow	0.80–0.90
Old snow	0.60–0.80
Melting snow-porous-fine grained	0.40–0.60
Forests-conifers, snow	0.25–0.35
Forests-green	0.10–0.20
Water	0.05–0.15
Snow ice	0.30–0.55
Black ice: intact → candled → granulated	0.10→0.40→0.55

accumulating on the snow surface (Link and Marks, 1999; Melloh et al., 2001; Winkler et al., 2010). Albedo can also be significantly affected later in the melt season, when the snowpack becomes patchy and the underlying ground surface is exposed (Liston, 1995). K↓ is not limited to the snow surface, but can penetrate up to 10 cm into the snowpack (Brock et al., 2000) , and reach the ground surface in shallow packs (DeWalle and Rango, 2008) with subsequent implications for the energy balance.

K^* in forested stands can be calculated as:

$$K^* = K \downarrow \tau_c(1 - \alpha) \quad (4)$$

where canopy transmissivity (τ_c) is the amount of K↓ transmitted through the forest canopy (Boon, 2009) and is largely dependent on tree type, stand characteristics, stand age, and stand productivity (Geiger et al., 2003). In coniferous forests, up to 90% of incident shortwave radiation may be absorbed by the canopy (Gray and Prowse, 1993).

L^* is the sum of all longwave radiation emitted by the atmosphere (L↓) minus the amount emitted by the Earth's surface (L↑). In the absence of clouds, L↓ is a function of atmospheric temperature and emissivity (ε), the latter of which is dependent on the vertical distribution of atmospheric temperature, water vapor, and carbon dioxide (Oke, 1988). Periods of low cloud cover increase L↓ from the atmosphere (Gray and Prowse, 1993). L↓ is important for snowmelt in dense forests, where a significant proportion of incident shortwave radiation is absorbed by the canopy and reemitted to the snow surface. As snow can more effectively absorb longwave versus shortwave radiation, this causes higher snowmelt rates near tree trunks (Reifsnyder and Lull, 1965) and results in high

spatial variability in melt rates (Bohren and Thorud, 1973). As with L↓, L↑ is dependent on the temperature and ε of the ground surface (Table 2). In forested environments, L^* at the snow surface is the sum of L↓ from the atmosphere, canopy, and tree stems; and L↑ from the snow surface:

$$L^* = \tau_L L\downarrow + (1-\tau_L)\varepsilon_c \sigma {T_c}^4 + (H_t/H)\varepsilon_t \sigma {T_t}^4 - \varepsilon_{ss}\sigma {T_{ss}}^4 \quad (5)$$

L↓ from the atmosphere and canopy is dependent on the sky view factor (τ_L) which is the proportion of hemisphere visible beneath the forest canopy. L↓ from the canopy is a function of the Stefan–Boltzmann law ($\varepsilon\sigma T^4$); where σ is the Stefan-Boltzmann constant = 5.67×10^{-8} W m^{-2} K^{-4} and the fraction of the hemisphere covered by canopy. L↓ from the tree stems is a function of the ratio of the hypothetical hemisphere surface area affected by longwave radiation from the tree trunk (H_t) and the hypothetical hemispherical area emitting longwave radiation to a point on the snow surface located at a distance from the tree trunk (H), multiplied by the energy emitted by the tree stems (Woo and Giesbrecht, 2000). Finally, L↑ from the snow surface is determined by the temperature and emissivity of the snow surface (Table 2).

The turbulent heat fluxes – sensible (Q_h) and latent (Q_e) heat – represent the exchange of energy between the snow surface and overlying air due to temperature and vapor pressure gradients, respectively (Andreas, 2002). These transfers occur not only at the snow surface, but also within the top few centimeters of the snowpack as wind is "pumped" into the pore spaces of the pack itself (Colbeck, 1997). Under dense forest canopies, where wind speeds are generally low, turbulent heat transfers are small (Woo and Giesbrecht, 2000). However, Q_h and Q_e can dominate the snowpack energy balance under strong warm winds, resulting in high short-term melt rates (Moore, 1983; Hayashi et al., 2005).

These fluxes are calculated as:

$$Q_h = \rho C_a D_k (T_a - T_s s) \quad (6)$$

$$Q_e = \rho \lambda_v D_e \left(\frac{0.622}{P}\right)(e_a - e_{ss}) \quad (7)$$

Snow Hydrology, Table 2 Emissivity of various surfaces (From Oke, 1988)

Surface	Typical emissivity range
Snow old → fresh	0.82–0.99
Forests deciduous bare → leaved	0.97–0.98
Forest coniferous	0.97–0.99
Water	0.92–0.97
Ice	0.92–0.97

where: ρ = density of air (kg m^{-3}); C_a = heat capacity of air (J kg^{-1} K^{-1}); D_h = bulk transfer coefficient for sensible heat (m s^{-1}); T_a, T_{ss} = temperature of the atmosphere and snow surface (°C), respectively; P = atmospheric pressure (kPa); λ_v = latent heat of vaporization (2.48×10^6 J kg^{-1}); D_e = bulk transfer coefficient for latent heat (m s^{-1}); and e_a, e_{ss} = atmospheric and snow surface vapor pressure (kPa), respectively.

The bulk transfer coefficients for latent and sensible heat vary with atmospheric condition. Under neutral atmospheric conditions, $D_h = D_e$ (Price, 1977):

$$D_h = D_e = \frac{k^2 u_a}{\left[\ln\left(\frac{z_a}{z_o}\right)\right]^2} \quad (8)$$

where k is Von Karman's constant (0.40), u_a is the wind speed (m s^{-1}), z_a is the height of the wind measurement (m), and z_o is the roughness length of the snow surface (m). Values of z_o range from 0.0002 to 0.02 m, with the greatest roughness lengths over older snow (Moore, 1983). When atmospheric conditions become highly stratified, the bulk aerodynamic method (Richardson number) is used:

$$R_i = \frac{g(T_a - T_{ss})z_a}{{u_a}^2 T_k} \quad (9)$$

where g is the gravitational acceleration (m s^{-2}) and T_k is the mean temperature of the air layer. Conditions are stable when $R_i > 0$, and unstable when $R_i < 0$. Air temperatures during snowmelt are usually >0°C, resulting in log-linear profiles for wind, temperature, and vapor pressure above the snow surface and stable atmospheric conditions, with $D_m = D_h = D_e$ (Price, 1977; Moore, 1983), calculated as:

$$D_m = D_m/(1 + 10R_i) \quad (10)$$

where D_m is the bulk exchange coefficient for momentum.

Ground heat (Q_g) flux occurs at the base of the snowpack and is estimated using soil temperature and moisture data (Gray and Prowse, 1993). Soil temperature generally increases with depth as a result of energy stored during the summer months and geothermal heat, thus establishing a temperature gradient that results in heat conduction upward to the ground surface and the base of the snowpack:

$$Q_g = k_G\left(\frac{T}{z}\right) \quad (11)$$

where k_G is the thermal conductivity of the soil, which varies spatiotemporally as a function of soil texture, soil density, and moisture content (Oke, 1988); T is the soil temperature (°C); and z is the depth of measurement below the ground surface (m). In comparison with Q^*, Q_h and Q_e, Q_g is relatively small on a daily time step (0–6 W m^{-2}); thus it is either assumed to be negligible, or to be a constant value in the energy balance equation

(USACE, 1956; Melloh, 1999). While the effects of Q_g on snowmelt can be ignored over short time periods (Gray and Prowse, 1993), the cumulative ground heat flux should be considered over entire winter seasons (Pomeroy and Goodison, 1997).

Advective energy (Q_r) is supplied to the snowpack by rainfall during the snowmelt period; the magnitude of the energy contribution depends on the regional climate and the frequency and magnitude of rain-on-snow events (e.g., Storck et al., 2002). Q_r is measured as the ratio between rainfall energy content while airborne (prior to contact with the snow surface) and energy content on reaching thermal equilibrium within the pack (Gray and Prowse, 1993). Two main scenarios are considered: (1) rainfall on an isothermal pack where the rain does not freeze; or (2) rainfall on a frozen pack (<0°C) at which point the rainfall freezes, releasing the heat of fusion (Male and Gray, 1981). These processes are calculated as:

$$Q_r = \rho_w C_w P(T_r - T_{ss}) \tag{12}$$

$$Q_r = \rho_w C_w P(T_r - T_{ss}) + \rho_w \lambda_F P \tag{13}$$

where ρ_w = density of liquid water (~1,000 kg m^{-3}); C_w = specific heat of liquid water (~0.0042 MJ kg^{-1}°C^{-1}); P = rainfall rate (L s^{-1}); T_r = temperature of rain (°C); T_{ss} = temperature of the volume of snow (°C); and λ_F = latent heat of fusion (~0.334 MJ kg^{-1}).

Finally, Q_θ is the rate of change of internal energy in the snowpack (Gray and Prowse, 1993). Within deep snowpacks, Q_θ can be relatively small in comparison to other energy fluxes, and is often considered negligible as snowpack temperature during ablation is ~0°C. However, midday snowmelt followed by overnight freezing can result in large changes in internal energy in both shallow snowpacks and the upper layers of deep packs. Q_θ is calculated as:

$$Q_\theta = (\rho_i C_i + \rho_w C_w + \rho_v C_v)\Delta T_i Z_i \tag{14}$$

where: ρ_i = density of snow and ice (~922 kg m^{-3}); C_i = specific heat of snow and ice (~0.0021 MJ kg^{-1}°C^{-1}); ρ_v = density of water vapor (kg m^{-3}); C_v = specific heat of water vapor (MJ kg^{-1}°C^{-1}); ΔT_i = the change in snow temperature (°C); and Z_i = snow depth (m).

Internal changes in snowpack temperature can also be measured using thermistor strings, or modelled using one-dimensional snow temperature and energy balance models such as SNTHERM (Jordan, 1991; Melloh, 1999).

Once the total energy available for melt (Q_m) is calculated, the total amount of meltwater or snow water equivalent (SWE) (in m) can be calculated as (Pomeroy and Goodison, 1997):

$$\mathrm{SWE} = Q_m/(\rho_w \lambda_F B_i) \tag{15}$$

where the thermal quality of snow (B_i) is the fraction of ice in a unit mass of snow (approximately 0.95–0.97) (Male and Gray, 1981).

Water movement through the snowpack

Once melt is initiated, meltwater can flow through the snowpack as both Darcian flow through an unsaturated porous medium (Colbeck, 1976) and as flow "fingers" that concentrate in particular regions of the pack (Colbeck, 1979; Albert et al., 1999). Water movement is a function of the temperature, structure, and water content of the snowpack (USACE, 1956; Waldner et al., 2004); for example, the presence of ice lenses or weaker snowpack layers can cause preferential flow paths within the pack. Observed time lags between melt onset and runoff production are a function of cold content, the liquid-water-holding capacity of the pack, and meltwater transmission through the snowpack as a function of permeability and gravity (Fountain, 1996; DeWalle and Rango, 2008) (see Cross-references).

Runoff generation from the snowpack

Meltwater outflow is generated from the snowpack once it can no longer hold meltwater within its internal pore spaces. This meltwater is then routed to surface runoff via overland flow, subsurface stormflow, and groundwater flow, the timing of which is critical for basin-scale runoff. Thus, snow hydrology is strongly linked with soil moisture and runoff generation, groundwater recharge, spring freshet, and climate change (see Cross-references).

New directions in snow hydrology

Current snow hydrology research is examining key topics around the relative importance of topography and vegetation cover in driving the snowmelt energy balance. Research suggests that south-facing slopes are more sensitive to changes in forest canopy cover than north-facing slopes, given the role of the canopy in attenuating incoming shortwave radiation and driving fluxes of incident radiation at the snow surface. Research is also detailing the role of forest litter and atmospheric dust on snow surface albedo, the snowmelt energy balance, and subsequent melt and runoff. Shifting weather patterns have increased long-range dust transport from arid/semi-arid regions to mountain snowpacks (Painter et al., 2007), while increasing rates of forest disturbance have enhanced forest litter production and incorporation into the snowpack (Winkler et al., 2010). While both dust and forest litter have significant impacts on snow surface albedo, they behave differently in terms of their effect on spectral albedo – thus new research is examining the spectral reflectance properties of both contaminant types in an effort to quantify their impact on snowmelt and runoff. Additional research is examining the relationship between snow hydrology and soil moisture (Seyfried et al., 2009; Williams et al., 2009), which is critical for determining patterns of runoff generation at the watershed scale (James and Roulet, 2009). Finally, research continues to assess the effects of shifts in air temperature and precipitation amount and type

as a result of climate change, and associated forest cover change, on snow hydrology (Bales et al., 2006; Lundquist et al., 2008; Jost et al., 2009). See Cross-references.

Bibliography

Albert, M., Koh, G., and Perron, F., 1999. Radar investigations of melt pathways in a natural snowpack. *Hydrological Processes*, **13**(18), 2991–3000.

Anderson, E. A., 1973. *National Weather Service River Forecast System – Snow Accumulation and Ablation Model*. NWS Hydro-17. Silver Spring: US Dept. Commerce, NOAA, National Weather Service.

Andreas, E. L., 2002. Parameterizing scalar transfer over snow and ice: A review. *Journal of Hydrometeorology*, **3**(4), 417–432.

Bales, R. C., Molotch, N. P., Painter, T. H., Dettinger, M. D., Rice, R., and Dozier, J., 2006. Mountain hydrology of the western United States. *Water Resources Research*, **42**(8), 13. W08432.

Bergström, S., 1995. The HBV model. In Singh, V. P. (ed.), *Computer Models of Watershed Hydrology*. Colorado: Water Resources Publications, pp. 443–476.

Beven, K. J., 2001. *Rainfall-Runoff Modelling – The Primer*. London: Wiley.

Bohren, C. F., and Thorud, D. B., 1973. Two theoretical models of radiation heat transfer between forest trees and snowpacks. *Agricultural Meteorology*, **11**, 3–16.

Boon, S., 2009. Snow ablation energy balance in a dead forest stand. *Hydrological Processes*, **23**(18), 2600–2610.

Braithwaite, R. J., 1984. Calculation of degree-days for glacier-climate research. *Zeitschrift für Gletscherkunde und Glazialgeologie*, **20**, 1–8.

Brock, B. W., Willis, I. C., and Sharp, M. J., 2000. Measurement and parameterization of albedo variations at Haut glacier d'Arolla, Switzerland. *Journal of Glaciology*, **46**(155), 675–688.

Colbeck, C., 1976. Analysis of water flow in dry snow. *Water Resources Research*, **12**(3), 523–527.

Colbeck, C., 1979. Water flow through heterogeneous snow. *Cold Regions Science and Technology*, **1**(1), 37–45.

Colbeck, C., 1997. Model of wind pumping for layered snow. *Journal of Glaciology*, **43**(143), 60–65.

De Walle, D. R., and Rango, A., 2008. *Principles of Snow Hydrology*. New York: Cambridge University Press, p. 410.

Derksen, C., and MacKay, M., 2006. The Canadian northern boreal snow water equivalent band. *Atmosphere-Ocean*, **44**(3), 305–320.

Déry, S. J., Salomonson, V. V., Stieglitz, M., Hall, D. K., and Appel, I., 2005. An approach to using snow areal depletion curves inferred from MODIS and its application to land surface modelling in Alaska. *Hydrological Processes*, **19**, 2755–2774.

Fontaine, T. A., Cruickshank, T. S., Arnold, J. G., and Hotchkiss, R. H., 2002. Development of a snowfall-snowmelt routine for mountainous terrain for the soil water assessment tool (SWAT). *Journal of Hydrology*, **262**, 209–223.

Fountain, A. G., 1996. The effect of snow and firn hydrology on the physical and chemical characteristics of glacial runoff. *Hydrological Processes*, **10**, 509–521.

Geiger, R., Aron, R. H., and Todhunter, P., 2003. *The climate near the Ground*. Langham: Rowman & Littlefield, p. 584.

Gray, D. M., and Prowse, T. D., 1993. Snow and floating ice. In Maidment, D. (ed.), *Handbook of Hydrology*. New York: McGraw-Hill, pp. 7.1–7.58.

Hayashi, M., Hirota, T., Iwata, Y., and Takayabu, I., 2005. Snowmelt energy balance and its relation to foehn events in Tokachi, Japan. *Journal of the Meteorological Society of Japan*, **93**, 783–798.

Hock, R., 1999. A distributed temperature-index ice- and snowmelt model including potential direct solar radiation. *Journal of Glaciology*, **45**(149), 101–111.

James, A. L., and Roulet, N. T., 2009. Antecedent moisture conditions and catchment morphology as controls on spatial patterns of runoff generation in small forest catchments. *Journal of Hydrology*, **377**, 351–366.

Jordan, R., 1991. A one-dimensional temperature model for a snow cover: technical documentation for SNTHERM89. Hanover, NH: US Army Corps of Engineers, Cold Regions Research and Engineering Lab, Special Report 91-16.

Jost, G., Moore, R. D., Weiler, M., Gluns, D. R., and Alila, Y., 2009. Use of distributed snow measurements to test and improve a snowmelt model for predicting the effect of forest clearcutting. *Journal of Hydrology*, **376**(1–2), 94–106.

Koivusalo, H., and Kokkonen, T., 2002. Snow processes in a forest clearing and in a coniferous forest. *Journal of Hydrology*, **262**, 145–164.

Link, T. E., and Marks, D., 1999. Point simulation of seasonal snowcover dynamics beneath boreal forest canopies. *Journal of Geophysical Research*, **104**(D22), 27841–27857.

Liston, G. E., 1995. Local advection of momentum, heat and moisture during the melt of patchy snow covers. *Journal of Applied Meteorology*, **34**, 1705–1715.

Lundquist, J. D., Neiman, P. J., Martner, B., White, A. B., Gottas, D. J., and Ralph, F. M., 2008. Rain versus snow in the Sierra Nevada, California: Comparing radar and surface observations of melting level. *Journal of Hydrometeorology*, **9**, 194–211.

Male, D. H., and Gray, D. M., 1981. Snowcover ablation and runoff. In Gray, D. M. (ed.), *Handbook of Snow*. New Jersey: The Blackburn Press, pp. 360–430.

Martinec, J., and Rango, A., 1986. Parameter values for snowmelt runoff modeling. *Journal of Hydrology*, **84**, 197–219.

Melloh, R. A., 1999. A synopsis and comparison of selected snowmelt algorithms. Cold Regions Research and Engineering Lab Report 99-8.

Melloh, R. A., Hardy, J. P., Davis, R. E., and Robinson, P. B., 2001. Spectral albedo/reflectance of littered forest snow during the melt season. *Hydrological Processes*, **15**(18), 3409–3422.

Moore, R. D., 1983. A comparison of the snowmelt energy budget in two alpine basins. *Archives of Meteorology, Geophysics and Bioclimatology Series A*, **33**, 1–10.

Oke, T., 1988. *Boundary Layer Climates*. New York: Routledge, p. 464.

Painter, T. H., Barrett, A. P., Landry, C. C., Neff, J. C., Cassidy, M. P., Lawrence, C. R., McBride, K. E., and Farmer, G. L., 2007. Impact of disturbed desert soils on duration of mountain snow cover. *Geophysical Research Letters*, **34**(12), 6. L12502.

Pellicciotti, F., Helbing, J., Rivera, A., Favier, V., Corripio, J., Araos, J., Sicart, J. E., and Carenzo, M., 2008. A study of the energy balance and melt regime on Juncal Norte glacier, semi-arid Andes of central Chile, using melt models of different complexity. *Hydrological Processes*, **22**(19), 3980–3997.

Pomeroy, J. W., and Goodison, B. E., 1997. Winter and Snow. In Bailey, W. G., Oke, T. R., and Rouse, W. R. (eds.), *The Surface Climates of Canada*. Montreal: McGill-Queen's University Press, pp. 68–100.

Price, A. G., 1977. *Snowmelt runoff processes in a subarctic area*. Climatology Research Series No. 10. Montreal: McGill University.

Quick, M. C., and Pipes, A., 1977. UBC watershed model. *Hydrological Sciences Bulletin*, **22**(1), 153–161.

Rango, A., 1980. Remote sensing of snow covered area for runoff modelling. *International Association of Hydrological Sciences*, **129**, 291–297.
Reifsnyder, W. E., and Lull, H. W., 1965. *Radiant energy in relation to the forest*. USDA Agricultural Technical Bulletin No. 1344, 111 pp. (Reprinted by AMS Press, 1979).
Seyfried, M. S., Grant, L. E., Marks, D., Winstral, A., and McNamara, J., 2009. Simulated soil water storage effects on streamflow generation in a mountainous snowmelt environment, Idaho, USA. *Hydrological Processes*, **23**, 858–873.
Spittlehouse, D. L., and Winkler, R. D., 2002. Modelling snowmelt in a forest and clearcut. In *Proceedings 25th Conference on Agricultural and Forest Meteorology*, 20–24 May 2002, Norfolk Virginia. American Meteorological Society, Boston, MA, pp. 121–122.
Storck, P., Lettenmaier, D. P., and Bolton, S., 2002. Measurement of snow interception and canopy effects on snow accumulation and melt in mountainous maritime climate, Oregon, USA. *Water Resources Research*, **38**(11), 1223–1238.
United States Army Corps of Engineers, 1956. *Snow hydrology: summary report of the snow investigations*. US Army Corps of Engineers, North Pacific Division, Portland, OR.
Waldner, P. A., Schneebeli, M., Schultze-Zimmerman, U., and Fluhler, H., 2004. Effect of snow structure on water flow and solute transport. *Hydrological Processes*, **18**(7), 1271–1290.
Walter, M. T., Brooks, E. S., McCool, D. K., King, L. G., Molnau, M., and Boll, J., 2005. Process-based snowmelt modeling: does it require more input data than temperature-index modeling? *Journal of Hydrology*, **300**(1–4), 65–75.
Williams, C. J., McNamara, J. P., and Chandler, D. G., 2009. Controls on the temporal and spatial variability of soil moisture in a mountainous landscape: the signature of snow and complex terrain. *Hydrology and Earth System Sciences*, **13**, 1325–1336.
Winkler, R., Boon, S., Zimonick, B., and Baleshta, K., 2010. Assessing the effects of post pine beetle forest litter on snow albedo. *Hydrological Processes*, **24**, 803–812.
Wolken, G., Sharp, M., and Wang, L., 2009. Snow and ice facies variability and ice layer formation on Canadian Arctic ice caps, 1999–2005. *Journal of Geophysical Research, Earth Surface*, **114**, 14, doi:10.1029/2008JF001173. F03011.
Woo, M., and Giesbrecht, M. A., 2000. Simulation of snowmelt in a subarctic spruce woodland: 1. Tree model. *Water Resources Research*, **36**, 2275–2285.

Cross-references

Albedo
Atmosphere–Snow/Ice Interactions
Degree-Days
Depletion of Snow Cover
Global Warming and its Effect on Snow/Ice/Glaciers
Hydrologic Cycle and Snow
Impacts of Snow and Glaciers on Runoff
Latent Heat of Condensation
Latent Heat of Fusion/Freezing
Latent Heat of Sublimation
Latent Heat of Vaporization/Condensation
Melt Runoff Modeling
Melting Processes
Rain-Induced Snowmelt
Runoff Generation
Snow and Vegetation Interaction
Snow Cover and Snowmelt in Forest Regions
Snow Metamorphism
Snow Ripening
Snow Water Equivalent
Specific Melt Rate

SNOW LAYER

A. K. Singh
DIAT (Deemed University), Girinagar, Pune, Maharashtra, India

Snow cover forms layer by layer (Figure 1), from one storm to another through interaction with atmosphere along with densification, accumulating in high-altitude geographic regions. In order to follow the evolution of a given snow layer, it is necessary to construct a time profile, based on a series of pits excavated through the snow cover at periodic intervals where density, crystal size and type, temperature, and other properties of the individual layers can be analyzed.

Assessing the formation and stability of snow layer is important in the study and prediction of avalanches. Many of the mechanical and thermal properties of snow that are significant to avalanche formation are related to a large extent on snow density. Temperature, crystal type, superimposed load, and temperature gradient all play a role in determining snow density. There is a strength variation in the snowpack due to its multilayered character. The mechanical properties of snow layers determine if it is stable enough to prevent an avalanche. Such stability information requires analysis of snow on avalanche slopes on a regular basis. The snow layers in which depth hoar formation (TG metamorphism) takes place show a distinctly different densification pattern. The density increases very slowly (reflecting the common observation that depth hoar layers undergo little settlement), and

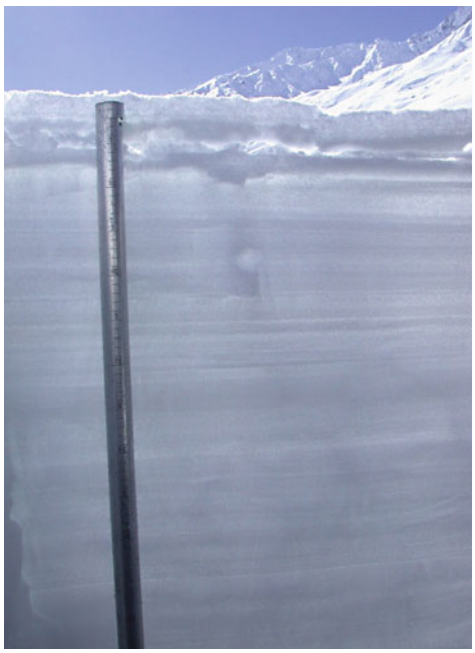

Snow Layer, Figure 1 Snow layers in snow cover.

requires over 100 days to reach a value of 300 kg/m^3. The density values are also of importance in evaluation of forecasting snowmelt runoff as snow covers are important water resources that feed streams and rivers. Snowpacks are also studied in relation to climatic change and global warming.

SNOW LOAD

A. K. Singh
DIAT (Deemed University), Girinagar, Pune, Maharashtra, India

Snow load is the force acting on a structure. Load causes stress, deformation, and displacement in structures. Assessment of its effects is carried out by the methods of structural analysis. Excess load or overloading may cause structural failure. In addition to the load magnitude, its frequency of occurrence, distribution, and nature (static or dynamic) are important factors in design.

The load resulting from the accumulation of snow on a roof in a severe winter must be taken into account in designing buildings in snow-bound hilly regions. The unit weight factor is used in the design of a flat or pitched roof for the probable amount of snow lying upon it. Roof failures in snow-bound regions are often associated with early spring rains, and, therefore, it is advisable to add to the snow load, the load of rainwater also, that might be retained in the snow.

SNOW METAMORPHISM

A. K. Singh
DIAT (Deemed University), Girinagar, Pune, Maharashtra, India

Since snow, in nature, exists close to its melting point, it transforms with time depending on the physical parameters of the snow environment. This process is called metamorphism. Under metamorphism we study change in crystal structure with change in temperature and pressure conditions. Fresh snow crystal is a branched structure (Figure 1a and b), which immediately after touching the ground starts decaying (Figure 1c and d). Researchers have described three types of thermal metamorphism, namely, Equi-temperature (ET) or equilibrium forms,

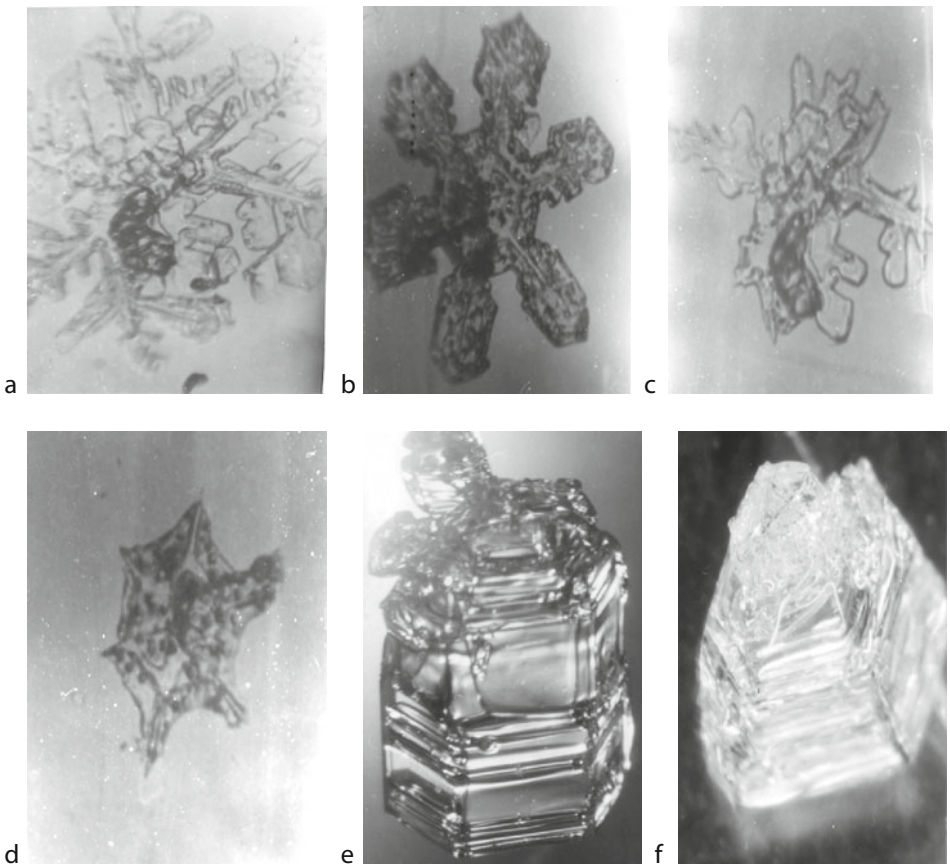

Snow Metamorphism, Figure 1 Snow grains, (**a, b**) new snow (**c, d**) rounding of snow (**e, f**) depth hoar (TG) snow.

Temperature-gradient (TG) metamorphism or kinetic growth forms (Figure 1e and f), and Melt-freeze (MF) metamorphism. Depending upon the temperature and temperature gradient inside snow cover, felt-like crystal may either convert to round or ET or TG grains. In almost all the situations there is fast destruction of branches of fresh snow crystal to felt-like structure. TG metamorphism is the source of weak layer formation in the snow cover and is of importance in avalanche studies and is an active research field in snow and ice community. Metamorphic modification of structure, texture, and density of snow is accompanied by changes in the mechanical properties of snow.

For ET growth, curvature effects are dominant in changing the crystal morphology, and vapor pressure over convex region is higher than that over concave region. Due to this, vapor transfer takes place from convex to concave surface thereby rounding off fresh snow crystal or felt-like crystal. During ET metamorphism the density changes from approximately 80 to 250 kg m^{-3}. Equilibrium form dominates snow pack at low temperature gradients and temperatures above −6°C.The process of equilibrium form goes through various stages, that is, rounding, growth of neck or bond, and further rounding and becoming almost equi-dimensional. This process has great significance in avalanche formation. The rounding of the snow grains and the neck formation tend to increase snow strength in tension, compression, as well as in shear.

For TG growth, if air temperature is very low or snow pack is very shallow, there exists a strong temperature gradient. Vapor migrates from higher temperature to lower temperature regions upwardly. On countering an obstruction or grain the vapor is directly deposited over the grain surface, thereby forming faceted or inverted cup-like crystal structures (Figure 1e and f) that are instrumental to avalanche formation. These depth hoar grains, being angular in character, generally do not bond well and exhibit extremely poor strength in shear. The depth hoar layers have high compressive viscosity and therefore snow density remains constant during formation.

The melt-freeze (MF) process occurs due to cyclic variation in snow surface temperature, resulting in formation of large poly-granular grains after repeated cycles of melting and refreezing and is known as MF metamorphism. In spring, the entire snowpack becomes isothermal near 0°C, however, the temperature varies considerably between day and night, resulting in melting and refreezing.

SNOW MICROSTRUCTURE

Christine Pielmeier
WSL Institute for Snow and Avalanche Research SLF, Warning and Prevention, Davos Dorf, Switzerland

Synonyms

Snow texture

Definition

The most recent definition of snow microstructure is given in the International Classification of Seasonal Snow on the Ground (Fierz et al., 2009, p. 3): "Snow on the ground is a highly porous, sintered material made up of a continuous ice structure and a continuously connected pore space, forming together the snow microstructure." Hence, snow microstructure is the size, shape, and number of structural elements and their arrangement in a sample of snow. A previous definition by Arons and Colbeck (1995) distinguished between snow microstructure and snow texture. They defined snow texture in terms of microstructure and mesostructure. Snow texture combines on the microscale the size and shape of individual ice particles with the three-dimensional arrangement and interconnectedness of the grains and pore spaces in a mesoscale specimen of snow.

Genesis

The microstructure of snow in the atmosphere (new snow) is initially determined by the meteorological (crystal type, snow fall intensity, temperature, wind, radiation) disposition during the snow fall period. After the snow reaches the ground it forms the snowpack. Properties of the ground or of the existing snowpack influence the deposition process. Postdepository metamorphism as well as mechanical and meteorological impacts produce large and persistent changes in the snow microstructure as long as the snowpack exists on the ground. Snow microstructure disappears either by melting of the snowpack or by the transformation of firn to glacial ice.

Relevance of snow microstructure

The snow microstructure is complex, since size, shape, and number of structural elements and their arrangement vary widely spatially and also temporarily in natural snowpacks. Thermodynamic, electromagnetic, and mechanical processes in snow depend highly on the microstructure of snow. Hence, the current state of the snow microstructure itself has a feedback effect on all processes within the snowpack and consequently on the future microstructure.

Measurement and simulation

Traditionally, snow microstructure is approximated by measuring the properties of isolated grains, knowing that it is an incomplete model of the three-dimensional ice-air-matrix (Fierz et al., 2009). Porous materials such as snow can be described by their porosity, specific surface area, and curvature. Recent progress has been made to simulate the thermal, mechanical, and electromagnetic properties of snow (Schneebeli, 2004; Flin and Brzoska, 2008; Kaempfer and Plapp, 2009; Satyawali et al., 2009), and to correlate to specific surface area and porosity (Johnson and Schneebeli, 1999; Matzl and Schneebeli, 2006; Dadic et al., 2008; Toure et al., 2008).

Conclusion

Recent studies show the importance of considering the snow microstructure in order to explain the snow

properties correctly. To improve our knowledge of thermodynamic, electromagnetic, and mechanical processes in snow, the snow microstructure has to be quantified and considered in the analysis and in simulations.

Bibliography

Arons, E. M., and Colbeck, S. C., 1995. Geometry of heat and mass transfer in dry snow: a review of theory and experiment. *Reviews of Geophysics*, **33**(4), 463–493.

Dadic, R., Schneebeli, M., Lehning, M., Hutterli, M. A., and Ohmura, A., 2008. Impact of microstructure of snow on its temperature: a model validation with measurements from summit, Greenland. *Journal of Geophysical Research*, **113**, 11, doi:10.1029/2007JD0009562. D14303.

Fierz, C., Armstrong, R. L., Durand, Y., Etchevers, P., Greene, E., McClung, D. M., Nishimura, K., Satyawali, P. K., and Sokratov, S. A., 2009. *The International Classification for Seasonal Snow on the Ground*. IHP-VII Technical Documents in Hydrology N°83, IACS Contribution N°1, UNESCO-IHP, Paris.

Flin, F., and Brzoska, J.-B., 2008. The temperature-gradient metamorphism of snow: vapour diffusion model and application to tomographic images. *Annals of Glaciology*, **49**, 17–21.

Johnson, J. B., and Schneebeli, M., 1999. Characterizing the micro structural and micro mechanical properties of snow. *Cold Regions Science and Technology*, **30**, 91–100.

Kaempfer, T. U., and Plapp, M., 2009. Phase-field modeling of dry snow metamorphism. *Physical Review E*, **79**(3), 17. 031502.

Matzl, M., and Schneebeli, M., 2006. Measuring specific surface area of snow by near-infrared photography. *Journal of Glaciology*, **52**(179), 558–564.

Satyawali, P. K., Schneebeli, M., Pielmeier, C., Stucki, T., and Singh, A. K., 2009. Preliminary characterization of alpine snow using SnowMicroPen. *Cold Regions Science and Technology*, **55**, 311–320.

Schneebeli, M., 2004. Numerical simulation of elastic stress in the microstructure of snow. *Annals of Glaciology*, **38**, 339–342.

Toure, A. M., Goïta, K., Royer, A., Mätzler, C., and Schneebeli, M., 2008. Near-infrared digital photography to estimate snow correlation length for microwave emission modeling. *Applied Optics*, **47**(36), 6723–6733.

Cross-references

Seasonal Snow Cover
Snow
Snow Crystal Structure
Snow Deformation
Snow Density
Snow Grains
Snow Layer
Snow Metamorphism
Stratigraphy of Snowpacks

SNOW PELLET

A. K. Singh
DIAT (Deemed University), Girinagar, Pune, Maharashtra, India

Snow pellets are symbolized by white ice particles that fall as precipitation, grow by supercooled water, and break apart easily when landing on surface. Falling snow may partially melt and refreeze into a rain drop before it reaches the ground, as shown in Figure 1. These snow pellets are also referred to as sleet. Snow pellets can also occur when snowflakes melt about half way then refreeze as they fall. Soft hail also grows in a way similar to the growth of snow pellets. Snow pellets have whiter appearance than sleet. Snow pellets are typically a few to several millimeters in size and have small air pockets embedded within their structure and have visual remnants of ice crystals unlike sleet.

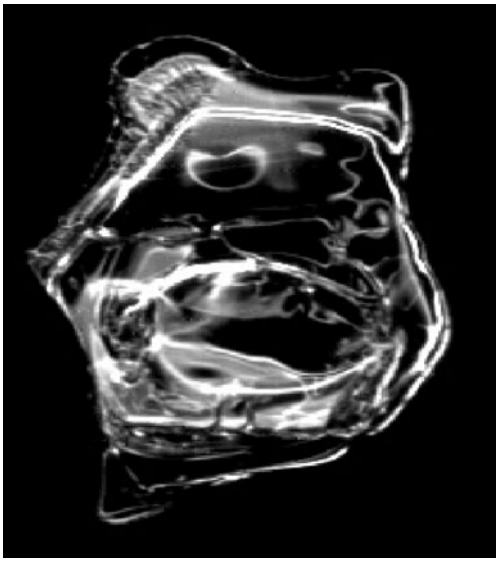

Snow Pellet, Figure 1 An image of partially broken and melt/refreeze snow grain.

SNOW PILLOW

A. K. Singh
DIAT (Deemed University), Girinagar, Pune, Maharashtra, India

The snow pillow provides a point value of the average water equivalent of snow which has accumulated on it. It is based on the detection of the hydrostatic pressure caused by snow. It is a large air mattress filled with an antifreeze fluid (mixture of methyl alcohol and water or a methanol–glycol–water solution, in the ratio of 1:1, having a specific gravity of 1). The fluid pressure responds to changes in the weight of snow on it, and is measured with a manometer or pressure transducer or load cell, as shown in Figure 1. Telemetry data acquisition systems (DAS) can be installed to provide continuous

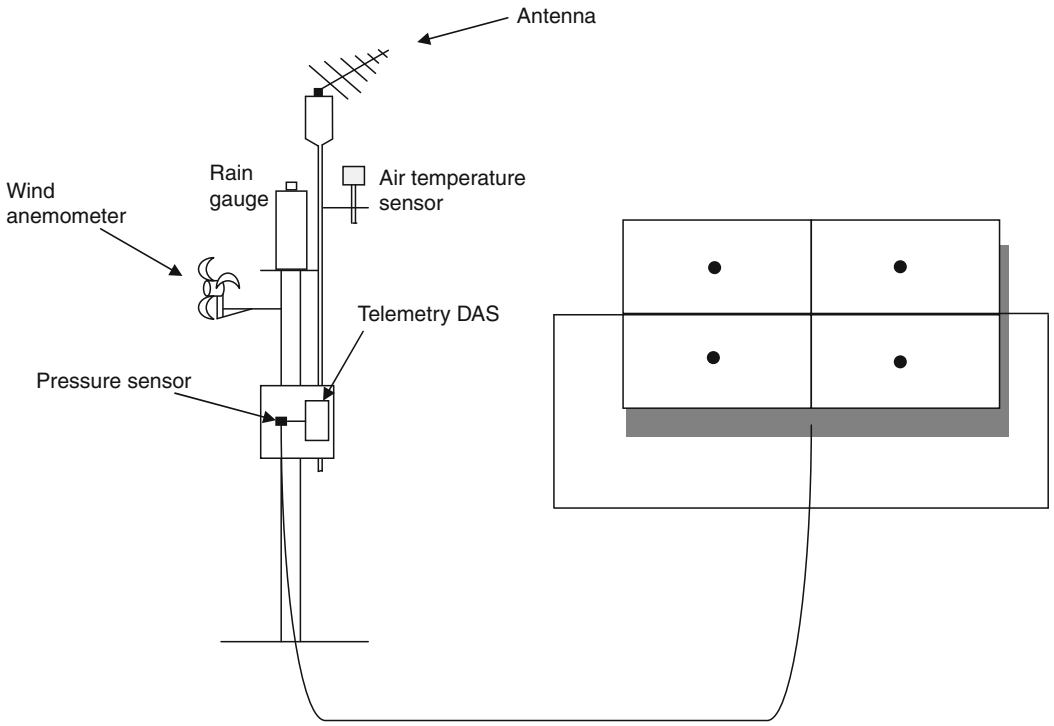

Snow Pillow, Figure 1 Schematic of snow pillow with telemetry data acquisition system.

measurements of water equivalent. Complete system consists of a DAS, a shaft encoder that tracks the movement of the float in the standpipe from the pillow, 12-volt battery for powering and mounted solar panel for recharging the batteries. A float connected to a shaft encoder records the distance the antifreeze is pushed up the standpipe. The DAS contains a transmitter to send the recorded data to the central station. Snow pillows are made up of different materials and come in various shapes and sizes. The stainless steel snow pillows have the problem of repair.

A small pillow used in a deep snow gives a pressure reading indicating a higher snow water equivalent than the actual. As the response of smaller pillows to the added weight of a heavy snowfall on a deep pack is longer than the larger pillows, it can produce an erroneous depth-time distribution for a storm. Intermittent freeze-thaw periods or rain on snow events may lead to the formation of ice layers within the pack, causing bridging, leading to lower values of the recorded water equivalent. In shallow snowpack the diurnal temperature changes may give spurious indications of snowfall or snowmelt due to expansion or contraction of the fluid in the pillow. Pillow sites should be near existing meteorological stations, or snow pillow should be equipped with certain meteorological instruments like precipitation gauge, thermograph, and anemometer.

Snow pillows are powerful tools for the study of precipitation measurements, particularly in mountain areas. It has been reported that pillows provide rough estimates of daily snowmelt losses from the snowpack. Pillow records can also be used to study meltwater formation as a function of climatic parameters. For the purpose of flood forecasting or inflow to reservoirs, it is of utmost importance to choose representative sites after surveying. Combined with measurements of snowmelt runoff, pillow records may also be useful for evaporation from snow cover.

SNOW PIT

A. K. Singh
DIAT (Deemed University), Girinagar, Pune, Maharashtra, India

The snow pit provides information about the stability of snow. It is a trench exposing a flat, vertical snow face from the snow surface to the ground, usually referred to as snow stratigraphy, as shown in Figure 1. Digging a snow pit reveals more about the snowpack structure than is visible from the surface and requires a little more practice and experience. Smoothen the uphill wall until it is vertical

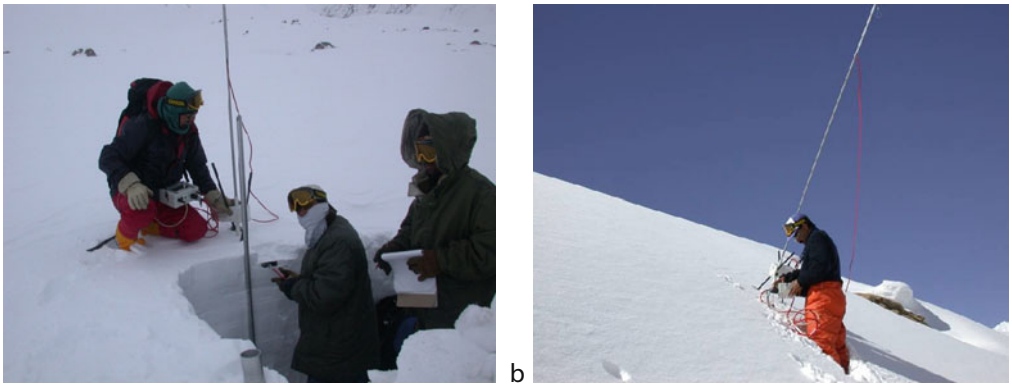

Snow Pit, Figure 1 Image (**a**) snow pit observation in progress, image (**b**) usage of Snow Micro Pen (SMP).

and the different layers of snow can be seen by pressing the snow layer so weak layers can be identified. After preparing the snow pit, temperatures on the data sheet are recorded and markings of each snow layer are done. For each layer, record the crystal size and type, hardness and density. Typical stratigraphy results are shown in Figure 2. The detection of snow layers and their mechanical behavior is most important in the assessment of snow pack stability. It allows study of the characteristics of the different layers of the snowpack that have developed as the snow has changed due to compaction and weather changes. Snow pits are used in mountainous areas to determine if one layer might slip on another causing an avalanche. The most effective snow pits should be dug near potential avalanche starting zones. As snow accumulates and changes over time, it develops layers marked by physical differences that are used to determine the history of the snowpack and are broadly classified as new snow, firn, or depth hoar. The new snow layer consists of new sharp crystals lying loosely on the top of the snow bank that are slowly being compacted by additional falling snow. The firn layer lies just below the new snow layer and consists of crystals that have lost their sharp edges due to evaporation, freezing, and compaction. They are rounded into more sphere-like shapes, during the process of becoming particles of ice. This snow is dense and the grains are more closely bonded together, which increases the mechanical strength of the firn layer. At the bottom of the snowpack lies the depth hoar layer consisting of snow crystals that have transformed (metamorphosed) into lumps of ice through evaporation, condensation, and compaction. This layer is weakly bonded than the firn or new snow layers. The depth hoar layer is loose and grainy and it is often nicknamed as sugar snow.

Many snow pits are not possible over a day by classical methods due to their time-consuming procedure. Recently an automated method has been developed, called SnowMicroPen (SMP) to identify the snow layers and their strength over a large area in a short interval of time. SMP motor and sensor is shown in Figure 3.

Bibliography

http://www.nasa.gov/pdf/186123main_SnowPitProcedures.pdf.

Satyawali, P. K., Pielmeier, C., Stucki, T., and Singh, A. K., 2009. Preliminary characterization of Alpine snow using SnowMicroPen. *Cold Regions Science and Technology*, **55**(3), 311–320.

SNOW RIPENING

A. K. Singh
DIAT (Deemed University), Girinagar, Pune, Maharashtra, India

Snow repining is the transition from a dry, subfreezing snow cover to isothermal snow, which can freely conduct water, that is, snow coming to full development, becoming mature for melt. It is a process during which the snow pack attains a state where it yields meltwater, including warming of the snowpack to 0°C. If the snow is ripe and air temperature is above freezing point, snowmelt occurs, otherwise positive energy first brings down snow to 0°C, that is, satisfying cold content of a few centimeters of top snow.

SNOW SKATING

Ashok Kumar Verma
Department of Geography and Environmental Studies, Cold Regions Research Center, Wilfrid Laurier University, Waterloo, ON, Canada

Synonyms

Ice skating; Roller skating; Skating; Snow boarding

Definition

Skating is defined as the sport where a person glides on the surface of ice or any other surface using the suitable

Station: 0108 Aspect: Zero Date: 21-Mar-06 Weather: 0000

Time Of Start:0645 Hrs Wind Direction & Speed:0000 Temp at Start:–7 Temp at End:–7

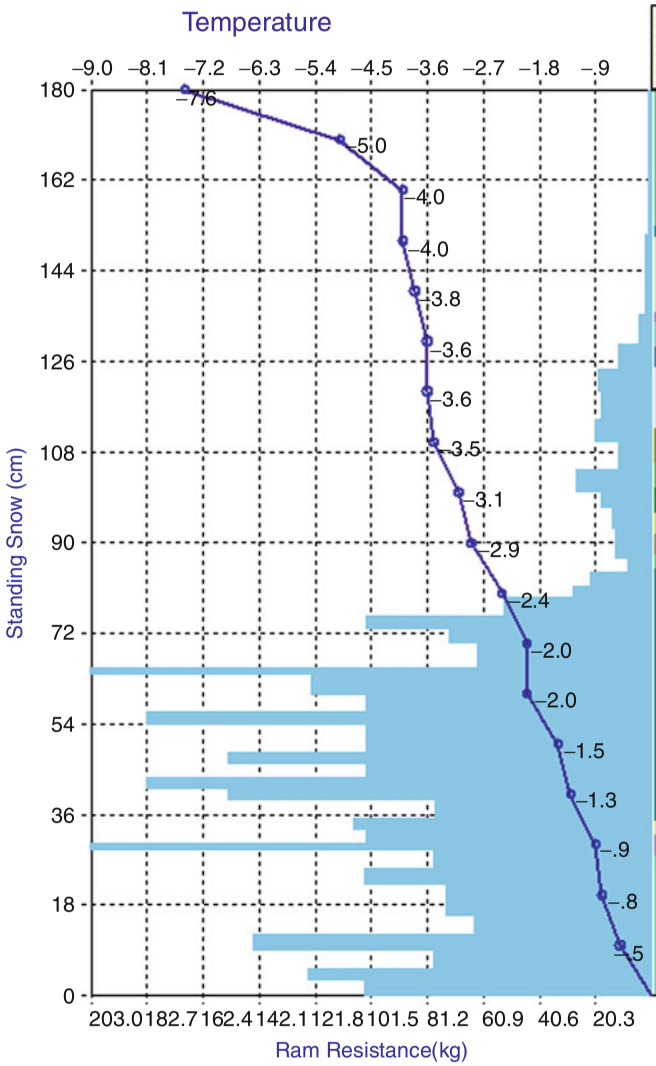

Layer From----- To-----	Layer No	Layer Thickness	Wetness	Grain Type	Grain Size	Hardness	Density (gm/ cubic cm)	Shear Strength(Kg/ 100 cm sqr)
153-180	17	27	Dry	(F S)	<1 mm	V Soft	0.12	2.5
151-153	16	02	Dry	(M G)	<1-2 mm	M Hard	0.4	0.7
136-151	15	15	Dry	(F L)	1 mm	M Soft	0.18	0.5
134-136	14	02	Dry	(M G)	2 mm	M Hard	0.35	xxx
129-134	13	05	Dry	(R G)	<1 mm	M Soft	0.28	5
125-129	12	04	Dry	(M G)	3-4 mm	V Hard		xxx
113-125	11	12	Dry	(R G)	<1 mm	M Hard	0.36	7
106-113	10	07	Dry	(M G)	1-2 mm	Hard		xxx
101-106	9	05	Dry	(M G)	1-2 mm	Hard	0.38	1.5
96-101	8	05	Dry	(M G)	1 mm	M Soft	0.37	6
92-96	7	04	Dry	(M G)	2-3 mm	V Hard	0.4	xxx
88-92	6	04	Dry	(R G)	1 mm	M Soft	0.33	0.5
85-88	5	03	Dry	(Ice)	X	V Hard		xxx
35-85	4	50	Moist	(R G)	1 mm	Hard	0.46	10
32-35	3	03	Moist	(R G)	<1 mm	Hard	0.4	10
28-32	2	04	Moist	(R G)	1-2 mm	Hard	0.49	10
0-28	1	28	Moist	(M G)	1 mm	Hard	0.48	10

Snow Pit, Figure 2 Record of stratigraphy profile with temperature profile, RAM profile, standing snow, temperature, snow type, grain type, etc. (Courtesy snow and Avalanche Study Establishment, SASE.)

Snow Pit, Figure 3 SnowMicroPen (SMP) motor, sensor assembly. (Courtesy Schneebeli, M, SLF, Davos, Switzerland.)

equipment such as bladelike runner or set of wheels attached to the shoe. Skating can be used for leisure activity, traveling, and in different forms of the sports activity as mentioned above in synonyms.

Origin: skating is regarded as the oldest winter sports back in times as long as 4,000 years in southern Finland as studied by Formenti and Minetti (2008). Skating as winter sports was quite famous in the Netherlands and other European countries in present. It is believed that skating in North America is brought by the British personnel during the eighteenth century (Flower, 1976). Earlier, the skates were made up of sharpened, flattened bone strapped to the bottom of the foot. With the advancement of the technology, the skates took form of steel blades, which invented by the Dutch in thirteenth century (Ice skating, 2009). The working principal of ice using skates is quite interesting. The metal blade at the bottom of the skates can glide with little friction over the surface of the ice. But variable leaning and digging of one of its edges into the ice will give skater a better ability to increase the friction and control of the movement.

The present-day skating had taken many forms such as roller skating, skateboard skating, and street skating. These forms use the wheels (often known as "spins") with skateboard instead the typical metal blade shoe. These forms of skating enhanced the outdoor sports activities, which were limited to the presence of snow and ice. Although, skating is a famous sport (winter or street), some hazard associated with this should be avoided as they may lead to serious injuries to head and legs. The practice and training of skate should be performed under suitable guidance and professional supervision.

Bibliography

Flower, R., 1976. *The history of skiing and other winter sports*. Toronto: Methuen.

Formenti, F., and Minetti, L. E., 2008. The first humans travelling on ice: an energy-saving strategy? *Biological Journal of the Linnean Society*, **93**(1), 1–7.

Ice skating, 2009. In *Wikipedia, The Free Encyclopedia*. http://en.wikipedia.org/w/index.php?title = Ice_skating&oldid = 283327568

SNOW SKIING

Ashok Kumar Verma
Department of Geography and Environmental Studies, Cold Regions Research Center, Wilfrid Laurier University, Waterloo, ON, Canada

The word Ski is derived from the Old Norse word "skio," which means split piece of wood or flat log (Flower and Killy, 1977; The History of Skiing, 2009; Skiing and Creation of Norwegian Identity, 1996).

The historical evidence of the ski is found in the Norway and Scandinavian literature that describe the ancient use of skiing for the livelihood (hunting), for military purpose, and as an efficient means of transportation. The oldest and accurate evidence documented in the region of Sweden and Norway dated back to 2,500–4,500 BC by archaeologists. The earliest reference of the skiing as winter sports is found in Procopius (560–559 AD), which mentions the race of Skridfinner – sliding finnes (Flower and Killy, 1977).

Present-day skiing is famous winter sports in all the cold climate countries such as North America, Europe, and some Asian countries and, recognized by the international Olympic organization and International Ski Federation. The worldwide popularity of ski as winter sports can be explained by the fact that the establishment of winter Olympic games for such sports. Over the time, skiing has evolved and divided into several categories and taken different forms of winter sports with respect to location and need namely, Alpine skiing, Backcountry skiing, Randonnee and Telemark skiing. In spite of its popularity as winter sports, the learning of ski by amateurs should be performed under proper guidance and supervision (Skiing, 2009). The ignorance of suitable learning environment and personnel can lead to fatal accidents causing major injuries and in some cases could even lead to death.

Bibliography

Flower, R., and Killy, J. C., 1977. *The History of Skiing and Other Winter Sports*. Toronto: Methuen.

Skiing, 2009. In *Wikipedia*, http://en.wikipedia.org/w/index.php?title=Skiing&oldid=283367370

Skiing, and Creation of Norwegian Identity, 1996. http://www.norway.org/News/archive/1996/199601skiing1.htm

The History of Skiing, 2009. The International Ski History Organisation (ISHA Resources). http://skiinghistory.org/

SNOW STORM

A. K. Singh
DIAT (Deemed University), Girinagar, Pune, Maharashtra, India

Steady snows of significant intensity accompanied by a certain amount of wind are often referred to as snowstorms. A massive snowstorm with strong winds (about 35 mph or more) is known as a blizzard. Snowstorms are usually considered to be less dangerous than ice storms. Mountain snowstorms can produce cornices and avalanches. Standing dead trees can be brought down by the weight of the snow, especially if it is wet or very dense. Even a few inches of dry snow can form drifts, many feet high under windy conditions. An additional danger, following a snowy winter, is spring flooding if the snow melts suddenly due to a dramatic rise in air temperature. Deaths can occur from hypothermia, infections brought on by frostbite, car accidents due to slippery roads, fires or carbon monoxide poisoning due to alternative heating methods after a storm causes a power outage, or heart attacks caused by overexertion while shovelling heavy wet snow.

SNOW AND VEGETATION INTERACTION

Christopher A. Hiemstra[1], Glen E. Liston[2]
[1]Cold Regions Research and Engineering Laboratory (CRREL), U.S. Army Corps of Engineers, ERDC, Fort Wainwright, AK, USA
[2]Cooperative Institute for Research in the Atmosphere, Colorado State University, Fort Collins, CO, USA

Definition

Snow and vegetation interaction describes how the assemblage of plants in an area influences snow accumulation and ablation and the subsequent effects of the snow on plants.

Introduction

Snow and vegetation interact in two principal ways. First, snow accumulation and ablation processes and patterns are influenced by vegetation's physical structure and spatial arrangement. Second, snow deposition and melt patterns affect vegetation's distribution and growth. These interactions take place at fine scales (1 mm to 100 m) and are common to all environments where snow and vegetation coexist. The most striking examples of snow and vegetation interaction are found where high winds, abundant snow, and isolated groups of trees interplay to create snow distributions that vary from 0.5 m to 5 m deep within horizontal distances of 100 m or less.

Vegetation effects on snow

Vegetation influences snow accumulation through canopy interception and by altering wind patterns within and around vegetation. All plants intercept snow to varying degrees as long as leaves, branches, or stems are exposed and there is a surface upon which snow can be deposited (see *Interception of Snow*). The exposed canopy's structure is important in determining the amount of interception and retention that occurs. For example, evergreen trees and shrubs retain leaves in winter; these leaves are densely arranged on their stems and provide abundant horizontal surface area. As a result, these leaves and branches are efficient at intercepting and retaining snow, even in windy locations. In contrast, deciduous trees and shrubs with vertically oriented stems present little surface area for snow interception. Moreover, that branch's surface can be smooth (e.g., aspen and birch) and light winds easily scour snow from the branches.

The rigidity of the plant also plays a role in interception. Branches with a snow burden may droop and jettison snow, or the stems may drop to the snow surface and become buried in the snowpack. Further, a plant's ability to intercept snow may change over time. In grasslands, leaves that were upright and readily intercepted snow in the fall become prostrate by mid-winter due to leaf and stem comminution through high winds, decomposition, and previous snow accumulation.

In areas where snow transport by wind is common, vegetation plays crucial roles in snow transport and resultant snow accumulation patterns. In windy environments, vegetation has a "snow holding depth," defined to be the maximum snow depth captured within and to the lee of the vegetation structure that is not available for wind redistribution (Liston and Elder, 2006). This depth varies as a function of vegetation height, canopy structure, and the spatial arrangement of individual plants. As one would expect, taller vegetation has a higher snow holding depth; in similar conditions, forested areas can retain more snow compared with grassland or alpine and arctic tundra. Structurally, plants with a dense canopy possess a larger snow holding depth compared with spreading plants of identical height. Areas dominated by many plants hold more snow than sparsely vegetated areas. As a general rule, vegetation can capture snow depths within ~60–90% of the plant's height, but this can vary substantially depending on vegetation height, structure, and spatial arrangement. If snow is shallower than the

vegetation's snow holding depth, the snow is generally not available for wind transport and snow redistribution in the environment will be limited. If snow depth exceeds this height and wind is sufficient, snow above the holding depth is available for transport and snow erosion will occur. In the case of taller forests, snow holding depth is almost always higher than actual snow depth.

In snowy and windy landscapes, snow depths frequently vary with dominant vegetation types as snow holding depths change through space. Agricultural areas in winter often feature recently tilled soils holding little-to-no snow while adjacent fields containing stubble from the previous growing season have a snowpack approximating the stubble height. Likewise, natural systems have varying snow holding depths corresponding with shifting vegetation types that exacerbate and emphasize snow–vegetation interactions. Vegetation's ability to produce deep snows is especially evident in upper treeline areas. On Libby Flats at 3,200 m elevation in the North American Rocky Mountains of southeast Wyoming, abundant winter snow precipitation (~71 cm SWE) and high winds (mean = 10 m/s) transport snow to the lee sides of tree patches and lines of trees (ribbon forests; Billings, 1969) that are 4–12 m tall and are maintained by snow deposition patterns (see below). At the end of each winter, 2–7 m of snow accumulate on the lee side of tree islands and ribbon forests and these drifts last well into summer (Figure 1). Trees are embedded in a matrix of subalpine meadow that has a smaller holding depth and acts as a source area for the lee sides of trees (Hiemstra et al., 2006). Drifts produced on the lee of trees in this area have a large effect on vegetation patterns, ecosystem processes, and growing season length (see below).

Vegetation can be used for snow management. On the high plains (shortgrass steppe with <20 cm holding depth) of North America, living snow fences consisting of several rows of trees and shrubs are planted upwind of roads susceptible to drifting snow. These windbreaks can be effective as long as the transplanted trees and shrubs remain vigorous. Additionally, crop stubble will often be left standing in the fields to retain winter snows needed to recharge soil moisture for the next crop.

While vegetation shapes snow accumulation patterns and overall distribution, it also affects snowpack metamorphism and ablation. A canopy influences soil temperatures before the snow arrives and alters subsequent thermal fluxes at the snow-soil interface and snowpack temperature gradients between the soil and upper snow surface. This gradient influences snow metamorphism occurring within the snowpack throughout the winter. Plant leaves, stems, and boles embedded in the snow conduct energy away from or into the snowpack depending on existing temperature gradients between the atmosphere and the ground. In environments where vegetation protrudes above the snowpack, shortwave radiation warms the exposed vegetation and longwave radiation emitted from the vegetation melts snow surrounding the vegetation (see *Snow Cover and Snowmelt in Forest Regions*). Snowpack properties and melting rates change with distance from exposed vegetation as heat islands associated with the vegetation are advected downwind over the remaining snow cover (Liston, 1995). In the Arctic, the snow-free season has arrived 1–9 days decade^{-1} earlier than in the recent past (Chapin et al., 2005) and increased shrub dominance (Sturm et al., 2005) will lengthen the snow-free season and alter energy budgets. In simulations

Snow and Vegetation Interaction, Figure 1 Large snowdrifts formed on the lee side of tree islands remain well into summer on Libby Flats (photo taken July 3, 1998). The prevailing winter wind direction is from left to right. Vegetation not covered by snow is growing, while vegetation covered by the snow awaits its growing season.

of a vegetation shift from shorter arctic tundra to taller arctic shrubland, snow melts 11 days earlier due to enhanced shrub cover and corresponding changes in the surface energy budget (Strack et al., 2007).

Vegetation is not always associated with accelerated snowmelt. A thicker canopy, such as that associated with forested environments, intercepts shortwave radiation above the snowpack and delays snowmelt. Vegetation can enhance the amount of snow in an area by capturing blowing snow and reducing sublimation.

Inasmuch as vegetation affects soil temperatures, snow accumulation patterns, ablation, and sublimation, vegetation can play an important role in resource management and water yield. Since vegetation plays such key roles in governing snow processes and distributions, it is critical to design observations and water resource forecast schemes around predominant vegetation types within watersheds. Further, vegetation can change slowly through succession or land cover change that gradually alters snow–vegetation interactions. Vegetation can also be disturbed (e.g., fire and widespread beetle outbreaks), consequently altering the snow cycle and energy and water budgets.

Snow effects on vegetation

Snow distribution has important implications for vegetation. Prevailing wind direction, snowfall, and resultant snow distribution patterns are often similar year after year (Walker et al., 2001), so that relatively steady-state environmental conditions are produced. These repeating conditions create characteristic spatial variation in ecosystem properties such as growing season length, soil and permafrost temperatures (Zhang, 2005), decomposition (Gilmanov et al., 2004), susceptibility to fungal predation (Cunningham et al., 2006), species composition (Billings, 2000), and primary production (Bowman and Fisk, 2001). Observations show strong correlations among snow season length and timing, temperatures, and vegetation growth (Jonas et al., 2008). Experiments with winter snow-free periods (Bokhorst et al., 2008) and earlier snowmelt dates (Wipf et al., 2009) show the importance of snow in terms of timing and insulation for vegetation. Vegetation exposed to harsh winter temperatures due to mid-winter snowmelt is susceptible to damage, and with advanced snow-free dates and accelerated growth, some plants may be damaged by extreme early-season temperatures before they are hardy.

Alpine vegetation distributions are often depicted in terms of a mesotopographic gradient (Johnson and Billings, 1962), where interplay among snow cover, wind exposure, and topographic position explain vegetation distribution patterns. For example, fellfields dominated by cushion plants are located on windy, snow-free ridge tops, while snowbed vegetation is predominant under long-lived lee-side snowbanks where growing season length is brief. Forest patterns, such as ribbon forests (Billings, 1969), have been explained by an abundance of leeward snow limiting tree survival to create alternating lines of forests and open glades. In areas where snow distributions repeat year after year, those patterns can be mirrored by vegetation distribution patterns and inferences can be made about snow depths based on existing vegetation and ecosystem patterns, and vice versa.

Snow can also physically affect trees by scouring and avalanches. While many plants are buried and protected by snow, taller shrubs and trees protrude above the snowpack and are exposed to saltating and suspended snow moving at and above the snow surface. Blowing snow crystals are abrasive and can damage leaf cuticles. This damage eventually leads to water loss and desiccation that kills plant leaves and meristems (Hadley and Smith, 1986). It is blowing snow that causes winter mortality of tree leaves and creates flagged trees commonly observed at treeline, where the only live branches above the snowpack are on the lee side of the tree's stem. Heavy snowfall events and avalanches can damage branches, produce scars, and uproot trees and the damage can be examined to study avalanche frequencies and distributions.

Summary

Vegetation plays a large role in snow distribution patterns; it interacts with snow through interception, by retaining blowing snow, and by reducing sublimation losses due to blowing snow. Vegetation can accelerate or delay snowmelt depending on canopy characteristics and the amount of incoming energy. In turn, snow affects ecosystem structure and function, including the distribution of vegetation in landscapes. The effect of snow on ecosystems is especially important in areas where most precipitation arrives as snow and growing seasons are relatively short.

Bibliography

Billings, W. D., 1969. Vegetational pattern near alpine timberline as affected by fire-snowdrift interactions. *Vegetatio*, **19**, 192–207.

Billings, W. D., 2000. Alpine vegetation. In Barbour, M. G., and Billings, W. D. (eds.), *North American Terrestrial Vegetation*. Cambridge: Cambridge University Press, pp. 537–572.

Bokhorst, S., Bjerke, J. W., Bowles, F. W., Melillo, J., Callaghan, T. V., and Phoenix, G. K., 2008. Impacts of extreme winter warming in the sub-Arctic: growing season responses of dwarf shrub heathland. *Global Change Biology*, **14**, 2603–2612.

Bowman, W. D., and Fisk, M. C., 2001. Primary production. In Bowman, W. D., and Seastedt, T. R. (eds.), *Structure and Function of An Alpine Ecosystem: Niwot Ridge, Colorado*. Oxford: Oxford University Press, pp. 177–197.

Chapin, F. S., Sturm, M., Serreze, M. C., McFadden, J. P., Key, J. R., Lloyd, A. H., McGuire, A. D., Rupp, T. S., Lynch, A. H., Schimel, J. P., Beringer, J., Chapman, W. L., Epstein, H. E., Euskirchen, E. S., Hinzman, L. D., Jia, G., Ping, C. L., Tape, K. D., Thompson, C. D. C., Walker, D. A., and Welker, J. M., 2005. Role of land-surface changes in Arctic summer warming. *Science*, **310**, 657–660.

Cunningham, C., Zimmermann, N. E., Stoeckli, V., and Bugmann, H., 2006. Growth response of Norway spruce saplings in two forest gaps in the Swiss Alps to artificial browsing, infection with black snow mold, and competition by ground vegetation. *Canadian Journal of Forest Research*, **36**, 2782–2793.

Gilmanov, T. G., Johnson, D. A., Saliendra, N. Z., Svejcar, T. J., Angell, R. F., and Clawson, K. L., 2004. Winter CO_2 fluxes

above sagebrush-steppe ecosystems in Idaho and Oregon. *Agricultural and Forest Meteorology*, **126**, 73–88.
Hadley, J. L., and Smith, W. K., 1986. Wind effects on needles of timberline conifers: seasonal influence on mortality. *Ecology*, **67**, 12–19.
Hiemstra, C. A., Liston, G. E., and Reiners, W. A., 2006. Observing, modelling, and validating snow redistribution by wind in a Wyoming upper treeline landscape. *Ecological Modelling*, **197**, 35–51.
Johnson, P. L., and Billings, W. D., 1962. The alpine vegetation of the Beartooth Plateau in relation to cryopedogenic processes and patterns. *Ecological Monographs*, **32**, 105–133.
Jonas, T., Rixen, C., Sturm, M., Stoeckli, V., 2008. How alpine plant growth is linked to snow cover and climate variability. *Journal of Geophysical Research-Biogeosciences*, **113**, G03013, doi:10.1029/2007JG000680.
Liston, G. E., 1995. Local advection of momentum, heat, and moisture during the melt of patchy snow covers. *Journal of Applied Meteorology*, **34**, 1705–1715.
Liston, G. E., and Elder, K., 2006. A distributed snow-evolution modeling system (SnowModel). *Journal of Hydrometeorology*, **7**, 1259–1276.
Strack, J. E., Pielke Sr., R. A., Liston, G. E., 2007. Arctic tundra shrub invasion and soot deposition: consequences for spring snowmelt and near-surface air temperatures. *Journal of Geophysical Research*, **112**, G04S44, doi:10.1029/2006JG000297.
Sturm, M., Schimel, J., Michaelson, G., Welker, J. M., Oberbauer, S. F., Liston, G. E., Fahnestock, J., and Romanovsky, V. E., 2005. Winter biological processes could help convert arctic tundra to shrubland. *Bioscience*, **55**, 17–26.
Walker, D. A., Billings, W. D., and de Molenaar, J. G., 2001. Snow-vegetation interactions in tundra environments. In Jones, H. G., Pomeroy, J. W., Walker, D. A., and Hoham, R. W. (eds.), *Snow Ecology: An Interdisciplinary Examination of Snow-Covered Ecosystems*. Cambridge: Cambridge University Press, pp. 266–324.
Wipf, S., Stoeckli, V., and Bebi, P., 2009. Winter climate change in alpine tundra: plant responses to changes in snow depth and snowmelt timing. *Climatic Change*, **94**, 105–121.
Zhang, T. J., 2005. Influence of the seasonal snow cover on the ground thermal regime: an overview. *Reviews of Geophysics*, **43**, RG4002, doi:10.1029/2004RG000157.

Cross-references

Global Outlook of Snowcover, Sea Ice, and Glaciers
Hydrologic Cycle and Snow
Melting Processes
Snow Cover and Snowmelt in Forest Regions
Snow Drift

SNOW WATER EQUIVALENT

Michael Durand
Byrd Polar Research Center, Ohio State University, Columbus, OH, USA

Definition

Snow water equivalent (SWE) is the equivalent depth of liquid water that would result from complete melting of a snowpack.

Introduction

In many parts of the world, snowmelt runoff is a critical water resource. It has been estimated that one-sixth of the global population lives in areas where streamflow is dominated by snowmelt runoff (Barrett et al., 2005). For water resource studies, and for applications such as long-term water supply forecasting, the liquid water equivalent stored in a snowpack is the most important quantity of interest, since SWE represents the amount of water that will be available during spring melt.

Snowpack accumulation on land results from atmospheric precipitation as snow. Snowpack is generally composed of air and frozen snow grains, as well as liquid water. At a point in space, snow density varies vertically with depth; the bulk density of the snowpack is defined such that the product of the snow depth and bulk density is equal to the SWE. Due to the presence of air within the matrix of snow grains, bulk density is generally less than that of pure ice, which is 917 kg m^{-3}; thus, SWE is generally less than the snow depth.

Measuring SWE

Manual in situ methods of measuring SWE are of two general types, both of which rely upon measurements of the snow mass, which can be converted to SWE. The first in situ type of SWE measurement is obtained by inserting a hollow pole vertically through the snowpack and into the underlying soil. The mass of the pole and the snow are then measured; as the mass of the pole is known, SWE can then be determined (Dingman, 2002). This method is generally practiced as part of a snow survey. The second type of in situ SWE measurement consists of vertical measurements of snow density at predefined intervals (e.g., 10 cm) through the snowpack. In order to obtain these measurements, a snow pit must be excavated. A snow pit also offers the opportunity to measure snowpack stratigraphy and the snowpack temperature profile in addition to the SWE; excavating a snow pit is generally far more labor intensive than snow surveys.

In contrast to the manual methods of measuring SWE, snow pillows are installed at a remote location, and consist of a pressure sensor that measures the mass of a snowpack that accumulates in a given location. Snow pillows can be configured to transmit snow mass observations to a central location where they can be archived. This approach allows for measurement of SWE in near-real time while obviating the need for potentially dangerous navigation of often complex terrain (e.g., in mountainous areas) by snow surveyors. As an example, the SNOw TELemetry (SNOTEL) network of snow pillows in the Western United States records SWE in several hundred locations (Serreze et al., 1999); data are made publicly available via World Wide Web archival and distribution.

Methods to measure SWE from airborne and spaceborne platforms have been developed over recent decades. For example, terrestrial radiation emitted at microwave frequencies is routinely measured from space by such

platforms as the Advanced Microwave Scanning Radiometer – EOS (AMSR-E) aboard the Terra and Aqua platforms. By observing the attenuation of the radiometric brightness at different microwave frequencies, global estimates of SWE can be inferred, albeit at coarse spatial scales (e.g., Chang et al., 1987). From airborne platforms, measurements of gamma radiation emitted by the earth surface can be used to infer SWE. The SWE retrieval exploits the fact that gamma radiation responds to isotopes in the upper 20 cm of soil; when the soil is covered by snow, the gamma emissions are modulated (Liston et al., 2008). For instance, the National Operational Hydrologic Remote Sensing Center (NOHRSC) in the USA performs regular airborne surveys using gamma radiation measurements (Fritzsche, 1982). Remote sensing of SWE is thus a field that is becoming more mature. Building on this remote sensing heritage, radar measurements at microwave frequencies can be used to infer SWE; the European Space Agency is currently planning the CoreH2O satellite mission to make high spatial resolution global measurements of SWE via microwave radar remote sensing (Rott et al., 2008).

Summary

SWE is an integrated measure of the potential water resources stored in a snowpack. For purposes of water resources planning, it is typically characterized by in situ measurements of snow mass; large-scale estimates are achieved by in situ measurement networks. Remote sensing estimates of SWE are becoming more mature. The upcoming CoreH2O mission has the goal of making high-resolution global measurements of SWE, enabling a significant advance in global cryospheric characterization.

Bibliography

Barrett, T. P., Adam, J. C., and Lettenmaier, D. P., 2005. Potential impacts of a warming climate on water availability in snow-dominated regions. *Nature*, **438**, 303.

Chang, A. T. C., Foster, J., and Hall, D., 1987. Nimbus-7 SMMR derived global snow cover parameters. *Annals of Glaciology*, **9**, 39.

Dingman, S. L., 2002. *Physical Hydrology*. New Jersey: Prentice Hall.

Fritzsche, A. E., 1982. The National Weather Service gamma snow system physics and calibration. Publication No. NWS-8201, EG&G, Inc., Las Vegas, NV, 37 pp.

Liston, G. E., Hiemstra, C. A., Elder, K., and Cline, D. W., 2008. Mesocell study area snow distributions for the Cold Land Processes Experiment (CLPX). *Journal of Hydrometeorology*, **9**, 957.

Rott, H., Cline, D., Duguay, C., Essery, R., Haas, C., Macelloni, G., Malnes, E., Pulliainen, J., Rebhan, H., and Yueh, S., 2008. CoReH2O – A Ku- and X-Band SAR Mission for Snow and Ice Monitoring, Alfred Wegener Institute for Polar and Marine Research: ePIC repository, Germany, 4 pp.

Serreze, M. C., Clark, M. P., Armstrong, R. L., McGinnis, D. A., and Pulwarty, R. S., 1999. Characteristics of the western United States snowpack from snowpack telemetry (SNOTEL) data. *Water Resources Research*, **35**, 2145.

Cross-references

Precipitation
Snow Density
Snow Depth
Snow Grains
Snow Pit
Stratigraphy of Snowpacks
Temperature Profile of Snowpack

SNOWBOARD

Amit Kumar
Department of Geology, Centre of Advanced Study in Geology, Punjab University, Chandigarh, India

The measurement of snow depth is made on the snowboard whose surface is kept free of snow before the snowfall. The snowboard is at least a 40 cm × 40 cm piece of plywood or lightweight metal and is placed on the surface of snow. The board is painted white or covered with while flannel, which provides a reference level for measurements.

Snowboard is also termed as a single thin, constructed with a laminated wood core with a steel edge, attached to the feet to ridden in snowboarding to descend a snow-covered slope area, and used to glide on snow. Snowboards generally have a length between 140 cm and 165 cm and a width between 24 cm and 27 cm. A different variety of snowboards exists according to riding preferences. Throughout the world, skiing sports develop great business in winter season. At high altitude areas, it offers exciting opportunities to develop snowboarding in mountain ranges. To enjoy snowboarding, which is the best sport that has gained immense popularity all over the world, the snowboard has been used worldwide.

SOLIFLUCTION

Stephen J. Walsh, Daniel J. Weiss
Department of Geography, University of North Carolina, Chapel Hill, NC, USA

Definition

Solifluction, the "slow gravitational downslope movement of water saturated, seasonally thawed materials" (Thomas and Goudie, 2000), is most commonly associated with alpine and/or arctic environments where seasonal and diurnal freeze-thaw cycles are prominent drivers of geomorphic activity (French, 1996). It is often coincident with cryoturbation (e.g., frost heaving and needle ice activity), the processes by which surficial materials, including soils and their residual parent materials, are mechanically mixed, moved, and sorted by repeated freezing and thawing. In contrast, solifluction and cryoturbation produce distinct features

including hummocks, stripes, sheets, lobes, and terraces (Matsuoka, 2001). Typically, these features are linear or quasi-linear, may be regularly spaced, and tend to occur parallel to the slope contour. Kessler and Werner (2003) identify the underlying mechanisms responsible for producing striped periglacial patterned ground on hillslopes, as feedback processes related to ice lens and stone transport within freezing soils.

Features and processes

Among identified solifluction features, lobes and terraces are most commonly observed and are frequently associated with alpine periglacial environments (French, 1996). Solifluction lobes and terraces are reported in areas including the Colorado Front Range, USA (Benedict, 1970), New Zealand (Billings and Mark, 1961), the Yukon Territory, Canada (Hugenholtz and Lewkowicz, 2002), Iceland (Douglas and Harrison 1996), the Olympic Mountains of Washington, USA (Hansen-Bristow and Price, 1985), Norway (Matthews et al., 1998), and the Northern Rocky Mountains of Montana, USA (Butler and Malanson, 1989). Solifluction terraces typically consist of flat areas (i.e., treads) covered by coarse materials that are adjacent to sloped areas (i.e., risers) covered by fine materials (Washburn, 1980). In contrast, solifluction lobes have a characteristic curved, lobate form (Benedict, 1970). Both lobes and terraces occur parallel to slope contours and often cover entire hillslopes. When occurring in areas covered by tundra, the alternating areas of surficial materials may produce turf-banked terraces and/or turf-banked lobes as vegetation establishes on the exposed fine materials. Vegetation does not, however, typically establish on the stone-covered treads, probably in response to mechanical disturbance from needle ice activity and frost heaving (Butler et al., 2004; Douglas and Harrison, 1996). Turf-banked terraces and lobes may also form in areas of relic solifluction features that are no longer experiencing downslope movement.

A key factor distinguishing solifluction from other processes influencing the production of periglacial patterned ground is slope angle, as solifluction requires slopes sufficiently gradual to retain water and yet sufficiently steep to allow downslope gravitational movement of materials. Further contributing to this process is permafrost that limits infiltration of water, thereby facilitating saturated conditions. The relationship between slope angle and patterned ground is explored, for example, by Butler and Malanson (1989), who categorize pattern ground types in alpine areas of Glacier National Park, Montana, USA as polygons, turf-banked terraces, and larger terraces dominated by frost shattering. Of these types, solifluction is considered most important for turf-banked terraces that are observed in areas with slope angles ranging from 5 to 22 degrees. This finding concurs with observations from Iceland by Douglas and Harrison (1996), who identify solifluction as the source of downslope movement for turf-banked terraces found on slopes ranging from approximately 5–19°. Likewise, Hansen-Bristow and Price (1985) report on turf-banked terraces in Olympic National Park, Washington, USA, that are coincident with slopes ranging from 5° to 20°. Several other environmental factors are proposed as contributing to the maintenance and formation of solifluction forms. These include a continental climate regime (Hansen-Bristow and Price, 1985), a threshold depth of snow (Hugenholtz and Lewkowicz, 2002), terrace and lobe orientation in relation to prevailing wind and the spatially variable pattern of snow scouring and drifting (Billings and Mark, 1961; Selkirk, 1998; Hugenholtz and Lewkowicz, 2002), mean annual air temperature depth of ice lens formation, slope inclination (Matsuoka, 2001), and presence of permafrost (Butler and Malanson, 1989).

Examples from Glacier National Park, Montana, USA

Solifluction features are often found in association with vegetated surfaces, and these surfaces may play a role in the formation of soliflucted landforms. Vegetation has been found to increase the soil moisture content, prevent rapid downslope movement, insulate the ground surface against extreme temperature, thereby depressing the freezing point of the soil, retarding surface runoff (Hansen-Bristow and Price, 1985), and altering the effective soil depth and stoniness of the soil (Malanson et al., 2002). The relationship between solifluction features and vegetation is not unidirectional, as these features may produce advantageous conditions for distinct vegetation types. For example, Butler et al. (2004) describe exfoliation of turf-banked terrace risers as a source of micro alluvial fans, occurring on stone-covered treads, that serve as seedling establishment sites above the existing alpine treeline. Solifluction features may also encourage tree line advance by providing topographic shelter for seedling establishment (Resler et al., 2005).

Turf-banked terraces found in Glacier National Park, Montana, USA are well described in the literature and provide an illustrative example of solifluction feature characteristics. Figure 1 shows a broad area of solifluction treads and risers on Lee Ridge, Glacier National Park, Montana, USA; Figure 2 is a more localized view of the tread/riser complex in the same geographic area. Turf-banked terraces found in the Park have treads and risers that typically range from less than 1 m to several meters in width. These sites are usually found on slight elevation gradients, with the individual stripes oriented parallel to the contours of the slope. Rock treads are covered with a thin veneer of coarse clasts (i.e., pebbles and cobbles), ranging from 3 to 8 cm in depth, that are typically coated with small populations of lichens, indicating a relict condition (Butler and Malanson, 1989). In contrast, vegetated risers are dominated by sand, silt, and clay (Butler and Malanson, 1989), and are populated by a dense ground cover of alpine tundra flora that is principally comprised of *Dryas octopetala* in association with *Salix reticulata, Carex ruspetris, Korbresia myosuroides, Oxytropis sericea,* and

Solifluction, Figure 1 A regional view of solifluction steps and risers on Lee Ridge, Glacier National Park, Montana, USA.

Solifluction, Figure 2 A local view of solifluction steps and risers on Lee Ridge, Glacier National Park, Montana, USA.

Selaginella densa (Bamberg and Major, 1968). Bamberg and Major (1968) use a soil movement plot to conclude that *Dryas* terraces are stable even though some amount of movement is recorded. This finding is confirmed by Butler and Malanson (1989), who hypothesize that no movement has taken place in the turf-banked terraces since the harsher climate of the neoglacial period. More recently, spatial patterns of turf-banked terraces, and their association with terrain settings, are explored using spatial digital technologies and geostatistical analysis (Walsh et al., 2003a, b).

Summary

Solifluction is a common feature of alpine environments throughout the world. Characterized by turf-banked, terraces and lobes, freeze-thaw conditions, in concert with moderate slope angles, can produce broad landscapes of patterned ground composed of alternating sequences of steps and risers. Vegetation, soil moisture, soil stoniness and depth, cryoturbation, terrain configuration, and climate conditions are among the factors that contribute to the formation of solifluction and dictate its geographic distribution.

Bibliography

Bamberg, S. A., and Major, J., 1968. Ecology of the vegetation and soils associated with calcareous parent materials in three alpine regions of Montana. *Ecological Monographs*, **38**, 127–167.

Benedict, J. B., 1970. Downslope soil movement in a colorado alpine region: rates, processes, and climatic significance. *Arctic and Alpine Research*, **2**, 165–226.

Billings, W. D., and Mark, A. F., 1961. Interactions between alpine tundra vegetation and patterned ground in the mountains of southern New Zealand. *Ecology*, **42**, 18–31.

Butler, D. R., and Malanson, G. P., 1989. Periglagial patterned ground, Waterton-glacier international peace park. *Canada and U.S.A. Zeitschrift fur Geomorphologie*, **33**, 43–57.

Butler, D. R., Malanson, G. P., and Resler, L. M., 2004. Turf-banked terrace tread and risers, turf exfoliation, and possible relationships with advancing treeline. *Catena*, **58**, 259–274.

Douglas, T. D., and Harrison, S., 1996. Turf-banked terraces in öraefi, southeast iceland: morphometry, rates of movement, and environmental controls. *Arctic and Alpine Research*, **28**, 228–236.

French, H. M., 1996. *The Periglacial Environment*. Essex: Longman.

Hansen-Bristow, K. J., and Price, L. W., 1985. Turf-banked terraces in the olympic mountains, Washington, USA. *Arctic and Alpine Research*, **17**, 261–270.

Hugenholtz, C. H., and Lewkowicz, A. G., 2002. Morphometry and Environmental Characteristics of Turf-Banked Solifluction Lobes, Kluane Range, Yukon Territory, Canada. *Permaforst and Periglacial Processes*, **13**, 301–313.

Kessler, M. A., and Werner, B. T., 2003. Self-organization of sorted patterned ground. *Science*, **299**, 380–383.

Malanson, G. P., Butler, D. R., Cairns, D. M., Welsh, T. E., and Resler, L. M., 2002. Variability in an edaphic indicator in alpine tundra. *Catena*, **49**(3), 203–215.

Matsuoka, N., 2001. Solifluction rates, processes and landforms: a global review. *Earth Science Reviews*, **55**, 366–374.

Matthews, J. A., Shakesby, R. A., Berrisford, M. S., and McEwen, L. J., 1998. Periglacial patterned ground on the styggedalsbreen glacier foreland, Jotunheimen, Southern Norway: micro-topographic, paraglacial and geoecological controls. *Permafrost and Periglacial Processes*, **9**, 147–166.

Resler, L. M., Butler, D. R., and Malanson, G. P., 2005. Topographic shelter and conifer establishment and mortality in an alpine environment, Glacier National Park, Montana. *Physical Geography*, **26**, 112–125.

Selkirk, J. M., 1998. Active vegetation-banked terraces on Macquarie Island. *Zeitschrift für Geomorphologie*, **42**, 483–496.

Thomas, D. S. G., and Goudie, A., 2000. *The Dictionary of Physical Geography*. Oxford: Blackwell.

Walsh, S. J., Bian, L., McKnight, S. A., Brown, D. G., and Hammer, E. S., 2003a. Solifluction steps and risers, lee ridge, Glacier National Park, Montana, USA: a scale and pattern analysis. *Geomorphology*, **55**(5 and 6), 381–398.

Walsh, S. J., Butler, D. R., Malanson, G. P., Crews-Meyer, K. A., Messina, J. P., and Xiao, N., 2003b. Mapping, modeling, and visualization of the influences of geomorphic processes on the alpine treeline ecotone, Glacier National Park, Montana, USA. *Geomorphology*, **53**(1–2), 129–145.

Washburn, A. L., 1980. *Geocryology: a survey of periglacial processes environments*. New York: Wiley.

Cross-references

Cryoturbation
Freezing and Thawing Index
Mountain Geomorphology
Periglacial
Permafrost

SOLUTE IN GLACIAL MELTWATERS

Martyn Tranter
Bristol Glaciology Centre, School of Geographical Sciences, University of Bristol, Bristol, UK

Introduction

Solutes in glacial meltwaters are generated by reactions that are comparable with other temperate and tropical latitudes, yet the factors controlling the production of solute are different. Factors controlling chemical weathering in other environments, such as the continual presence of water, soil, and vegetation (Drever, 2003), are not applicable to glacial environments, which are largely frozen for significant periods each year. The residence times of liquid water in glaciated catchments are often low (Knight, 1999), there are thin, skeletal soils at best, and vegetation is either absent or limited (French, 1996). However, glaciated catchments usually have high specific runoff, there are high concentrations of freshly comminuted rock flour, and adsorbed organic matter or surface precipitates that may hinder water-rock interactions are largely absent (Tranter, 2003). In short, the rapid flow of water over fine-grained, recently crushed, reactive mineral surfaces maximizes both the potential rates of chemical weathering and chemical erosion.

Composition of solutes

The chemical composition of glacial runoff from ice sheets, ice caps, and glaciers around the world is shown in Table 1 (after Brown, 2002; Tranter, 2003), which also includes the composition of global mean river water for comparative purposes. Sea salt, largely derived from marine aerosol, is a variable component of glacial runoff, and the dominant non-sea salt ions are Ca^{2+}–HCO_3^-–SO_4^{2-} – Mg^{2+}. The concentration of glacial runoff is usually inverse to discharge – hence low discharge waters are concentrated, whereas high discharge waters are dilute. The concentration of low discharge waters approaches ~1 meq/l (of positive charge) from smaller temperate, lower latitude glaciers, and ~3 meq/l for larger glaciers at higher latitudes. Glacial runoff is usually more dilute than global mean river water, and usually contains more K^+ and less Si for a given specific runoff (Anderson et al., 1997). The Ca^{2+}:Si and HCO_3^-:SO_4^{2-} ratio of glacial meltwaters are high and low, respectively, when compared with the principal world river waters, making glacial runoff an end member of global riverine water (Tranter, 2003). This is because glaciers preferentially weather carbonates and sulfides from the bedrock.

Glacial chemical weathering

The principal reactions that comminuted bedrock undergoes in glaciated terrain are summarized below, assuming that the bedrock is primarily composed of silicates and aluminosilicates.

Solute in Glacial Meltwaters, Table 1 The concentration of major ions in glacial runoff from different regions of the world (after Brown, 2002). Concentrations are reported in μeq/l

Region	Σ^+	Ca^{2+}	Mg^{2+}	Na^+	K^+	HCO_3^-	SO_4^{2-}	Cl^-	Source
Canadian High Arctic	280–3,500	260–2,600	21–640	1–190	0.1–39	210–690	59–3,900	–	1
Antarctica	550–3,100	72–1,300	120–336	360–1,400	0.8–110	91–1,600	34–1,200	0.6–1,000	2
Svalbard	330–1,900	120–1,000	99–540	110–270	5.1–41	110–940	96–760	5–310	3–5
Canadian Rockies	1,300–1,500	960–1,100	290–310	3.7–36	5.8–9.2	890–920	380–520	1.7–25	6
Iceland	170–960	110–350	30–120	30–480	2.8–12	190–570	26–130	30–87	7,8
Himalayas	130–940	75–590	6.6–230	25–65	22–51	200–730	160–410	1–22	9
Norway	20–930	8.8–623	1.6–66	8.3–210	1.0–29	1.4–680	7–140	0.9–190	10
European Alps	37–910	20–640	6–140	4.9–92	5.9–33	11–400	10–240	0.9–92	10, 11, 12
Alaska	670	550	36	25	61	430	260	2	13
Greenland	280–387	130–170	68–98	78–110	5–9	220–340	90–200	16–30	14
Cascades	56–150	35–80	8.3–20	2.5–17	9.7–37	83–100	7.9–29	–	15
Global mean runoff	1,200	670	280	220	33	850	170	160	16

Data sources. 1: Skidmore and Sharp (1999); 2: De Mora et al. (1994); 3: Hodgkins et al. (1997); 4: Hodson et al. (2000); 5: Wadham et al. (1997); 6: Sharp et al. (2002); 7: Raiswell and Thomas (1984); 8: Steinporsson and Oskarsson (1983); 9: Hasnain et al. (1989); 10: Brown (2002); 11: Collins (1979); 12: Thomas and Raiswell (1984); 13: Anderson et al. (2000); 14: Rasch et al., 2000; 15: Axtmann and Stallard, 1995; 16: Livingstone (1963)

Glacial comminution crushes bedrock and exposes the trace reactive components within crystalline aggregates more rapidly than would be the case in temperate and tropical soils, where new minerals are ultimately accessed via solubilization of the crystalline silicate lattices. Hence, glaciers are effective at solubilization of trace reactive components in the bedrock, which include carbonates, sulfides, and fluid inclusions. Laboratory experiments and direct sampling of waters from the glacier bed (Tranter et al., 1997, 2002) show that the initial reactions to occur when dilute snow and ice melt first access glacial flour are carbonate and silicate hydrolysis (Equations 1 and 2). These reactions raise the pH to high values (>9), lower the PCO_2 (to $\sim 10^{-6}$ atms), and maximize the water's potential to adsorb CO_2. Carbonate hydrolysis produces a solution with a Ca^{2+} concentration of ~200 μeq/l, with HCO_3^- the dominant anion.

$$\underset{\text{calcite}}{Ca_{1-x}(Mg_x)CO_3(s)} + H_2O(l) \leftrightarrow (1-x)Ca^{2+}(aq) + x\ Mg^{2+}(aq) + HCO_3^-(aq) + OH^-(aq) \quad (1)$$

$$\underset{\text{K-feldspar}}{KAlSi_3O_8(s)} + H_2O(l) \leftrightarrow \underset{\text{weathered feldspar surface}}{HAlSi_3O_8} + K^+(aq) + OH^-(aq) \quad (2)$$

The relatively dilute meltwater in contact with fine-grained glacial flour promotes the exchange of divalent ions from solution for monovalent ions on surface exchange sites. Hence, some of the Ca^{2+} and Mg^{2+} released from carbonate and silicate hydrolysis is exchanged for Na^+ and K^+.

$$\text{glacial flour} - Na_{(2-z)}, K_z(s) + (1-x)Ca^{2+}(aq) + x\ Mg^{2+}(aq) \leftrightarrow \text{glacial flour} - Ca_{(1-x)}, Mg_x(s) + (2-z)Na^+(aq) + zK^+(aq) \quad (3)$$

The high pH derived from hydrolysis enhances the dissolution of aluminosilicate lattices, since Al and Si become more soluble at pH > 9. Hydrolysis of carbonates results in a solution that is near saturation with calcite and aragonite. It is only in these types of waters that aluminosilicate dissolution is greater than carbonate dissolution. The influx of gases (including CO_2 and O_2), either from the atmosphere or from basal ice, and CO_2 produced by microbial respiration (see below) both lower the pH and the saturation with respect to carbonates. In addition, sulfide oxidation produces acidity (see below). Hence, almost all subglacial meltwaters are undersaturated with respect to calcium carbonate. The rapid dissolution kinetics of carbonates with respect to silicates means that carbonate dissolution continues to have a large impact on meltwater chemistry, despite carbonates being present often in only trace concentrations in the bedrock. For example, Haut Glacier d'Arolla has a bedrock, which is composed of metamorphic silicate rocks. Carbonates and sulfides are present in trace quantities in bedrock samples (0.00–0.58% and <0.005–0.71%, respectively). There are also occasional carbonate veins present in the schistose granite. Despite the bedrock being dominated by silicates, sulfide oxidation in subglacial environments dissolves carbonate to silicate in a ratio of ~5:1 (Tranter et al., 2002), compared to the global average of ~1.3:1 (Holland, 1978).

The acid hydrolysis of silicates and carbonates (Equations 4 and 5) that arises from the dissociation of CO_2 in solution is known as carbonation. Carbonation occurs in a restricted number of subglacial environments because ingress of atmospheric gases to these water-filled environments is restricted. It largely occurs in the major arterial channels at low flow, particularly near the terminus, and at the bottom of crevasses and moulins that reach the bed. Fine-grained sediment is flushed rapidly from these environments, and there is little time for the formation of secondary weathering products, such as clays, to form.

Hence, silicates dissolve incongruently, as crudely represented by Equation 4.

$$\underset{\text{anorthite}}{CaAl_2Si_2O_8(s)} + 2CO_2(aq) + 2H_2O(l) \leftrightarrow Ca^{2+}(aq) + 2HCO_3^-(aq) + \underset{\text{weathered feldspar surfaces}}{H_2Al_2Si_2O_8(s)} \quad (4)$$

$$\underset{\text{calcite}}{Ca_{1-x}(Mg_x)CO_3(s)} + CO_2(aq) + H_2O(l) \leftrightarrow (1-x)Ca^{2+}(aq) + xMg^{2+}(aq) + 2HCO_3(aq) \quad (5)$$

There is a limited body of evidence, which suggests that microbial oxidation of bedrock kerogen occurs (Wadham et al., 2004), and if this is the case, carbonation as a consequence of microbial respiration may occur in debris-rich environments, such as in the distributed drainage system and the channel marginal zone.

$$C_{org}(s) + O_2(aq) + H_2O(l) || CO_2(aq) + H_2O(l) \leftrightarrow H^+(aq) + HCO_3^-(aq) \quad (6)$$

The dominant reaction in subglacial environments is sulfide oxidation, since, following hydrolysis, this is the major reaction that provides protons to solution, so lowering the pH, decreasing the saturation index of carbonates, so allowing more carbonate dissolution (Equation 7). Sulfide oxidation occurs predominantly in debris-rich environments where comminuted bedrock is first in contact with water. It is microbially mediated, occurring several orders of magnitude faster than in sterile systems (Sharp et al., 1999). It consumes oxygen, driving down the pO_2 of the water.

$$\underset{\text{pyrite}}{4FeS_2(s)} + 16Ca_{1-x}(Mg_x)CO_3(s) + 15O_2(aq) + 14H_2O(l) \leftrightarrow 16(1-x)Ca^{2+}(aq) + 16xMg^{2+}(aq) + 16HCO_3^-(aq) + 8SO_4^{2-}(aq) + \underset{\text{ferric oxyhydroxides}}{4Fe(OH)_3(s)} \quad (7)$$

Earlier studies suggested that the limit on sulfide oxidation was the oxygen content of supraglacial melt, since subglacial supplies of oxygen are limited to that released from bubbles in the ice during regelation, the process of basal ice melting and refreezing as it flows around bedrock obstacles. However, studies of water samples from boreholes drilled to the glacier bed show that the SO_4^{2-} concentrations may be two or three times that allowed by the oxygen content of supraglacial meltwaters (Tranter et al., 2002). This suggests that oxidizing agents other than oxygen are present at the glacier bed. It seems very likely that microbially mediated sulfide oxidation drives certain sectors of the bed towards anoxia, and that in these anoxic conditions, Fe(III), rather than O_2, is used as an oxidizing agent (Equation 8). Sources of Fe(III) include the products of the oxidation of pyrite and other Fe(II) silicates in a previous oxic environment, as well as that found in magnetite and hematite.

$$FeS_2(s) + 14Fe^{3+}(aq) + 8H_2O(l) \leftrightarrow 15Fe^{2+}(aq) + 2SO_4^{2-}(aq) + 16H^+(aq) \quad (8)$$

Support for anoxia within subglacial environments comes from the $\delta^{18}O$–SO_4, which is enriched in ^{16}O when sulfide is oxidized in the absence of oxygen (Bottrell and Tranter, 2002).

The realization that there is microbial mediation of certain chemical weathering reactions in subglacial environments (Sharp et al., 1999; Skidmore et al., 2000; Bottrell and Tranter, 2002) has resulted in a paradigm shift, since the types of reactions that may occur in anoxic sectors of the bed include the common redox reactions that occur, for instance, in lake or marine sediments (Drever, 1988). A key difference in glacial systems is that the supply of new or recent organic matter is limited to that inwashed from the glacier surface, such as algae, insects and animal faces, or overridden soils during glacier advance. By contrast, the supply of old organic matter from comminuted rocks is plentiful. Given the thermodynamic instability of organic matter in the presence of O_2 or SO_4^{2-}, it seems likely that microbes will have evolved to colonize subglacial environments and utilize kerogen as an energy source. The first data to support this assertion is stable isotope analysis from Finsterwalderbreen, a small polythermal-based glacier on Svalbard, which has shale as a significant component of its bedrock (Wadham et al., 2004). The $\delta^{18}O$–SO_4 of waters upwelling from subglacial sediments are very enriched in $\delta^{18}O$, and the $\delta^{34}S$ is enriched in ^{34}S, which suggests that cyclical sulfate reduction and oxidation has been occurring. The $\delta^{13}C$ of DIC (dissolved inorganic carbon) is negative, consistent with the assertion that organic matter has been oxidized. Mass balance calculations suggest that a possible source of organic matter is kerogen, but the necromass of dead bacteria cannot be discounted. Whatever is the source of organic matter, sectors of the bed at Finsterwalderbreen are so anoxic that sulfate reduction is occurring (Equation 9).

$$\underset{\text{organic carbon}}{2CH_2O(s)} + SO_4^{2-}(aq) \leftrightarrow 2HCO_3^-(aq) + H_2S(aq) \quad (9)$$

It is possible that methanogenesis occurs under certain ice masses, since methanogens have been isolated from subglacial debris (Skidmore et al., 2000). The low $\delta^{13}C$–CH_4 and high concentration of methane found in gas bubbles within the basal ice of the Greenland Ice Sheet are consistent with there being methanogenesis within the basal organic-rich paleosols.

To date, there are few studies of glacial chemical weathering on bedrock with a significant evaporitic content. Work at John Evans Glacier in the Canadian High Arctic has shown that gypsum is dissolved in some areas of the bed, and that mixing of relatively concentrated Ca^{2+}–SO_4^{2-} waters with more dilute Ca^{2+}–HCO_3^-–SO_4^{2-} waters results in $CaCO_3$ precipitation due to the common ion effect (Skidmore (U. Montana) personal communication, 2010).

A key feature of the above chemical weathering scenarios is that relatively little atmospheric or biogenic CO_2 is involved. Hence, whereas ~23% and ~77% of solutes, excluding recycled sea salt, found in global mean river water is derived from the atmosphere and rock, respectively (Holland, 1978), atmospheric sources account for a maximum of 3–11% of solute in glacial runoff (after Hodson et al., 2000).

Bibliography

Anderson, S. P., Drever, J. I., and Humphrey, N. F., 1997. Chemical weathering in glacial environments. *Geology*, **25**, 399–402.

Anderson, S. P., Drever, J. I., Frost, C. D., and Holden, P., 2000. Chemical weathering in the foreland of a retreating glacier. *Geochimica et Cosmochimica Acta*, **64**, 1173–1189.

Axtmann, E. V., and Stallard, R. F., 1995. Chemical weathering in the South Cascade Glacier Basin, comparison of subglacial and extra-glacial weathering. *IAHS*, **228**, 431–439.

Bottrell, S. H., and Tranter, M., 2002. Sulphide oxidation under partially anoxic conditions at the bed of Haut Glacier d'Arolla, Switzerland. *Hydrological Processes*, **16**, 2363–2368.

Brown, G. H., 2002. Glacier meltwater hydrochemistry. *Applied Geochemistry*, **17**, 855–883.

Collins, D. N., 1979. Hydrochemistry of meltwaters draining from an alpine glacier. *Arctic and Alpine Research*, **11**, 307–324.

De Mora, S. J., Whitehead, R. F., and Gregory, M., 1994. The chemical composition of glacial melt water ponds and streams on the McMurdo Ice Shelf, Antarctica. *Antarctic Science*, **6**, 17–27.

Dokken, T. E., and Jansen, E., 1999. Rapid changes in the mechanism of ocean convection during the last glacial period. *Nature*, **401**, 458–461.

Drever, J. I., 1988. *The Geochemistry of Natural Waters*, 2nd edn. Englewood Cliffs, NJ: Prentice-Hall, 437 pp.

Drever, J. I., 2003. Surface and Ground Water, Weathering, Erosion and Soils. In Holland, H. D., and Turekian, K. K. (eds.), *Treatise on Geochemistry*, Vol. 5, Oxford and San Diego: Elsevier Pergamon.

French, H. M., 1996. *The Periglacial Environment*. 2nd edn. Reading, MA: Addison Wesley Longman, 341 pp.

Hasnain, S. I., Subramanian, V., and Dhanpal, K., 1989. Chemical characteristics and suspended sediment load of meltwaters from a Himalayan glacier in India. *Journal of Hydrology*, **106**, 99–108.

Hodgkins, R., Tranter, M., and Dowdeswell, J. A., 1997. Solute provenance, transport and denudation in a high Arctic glacierised catchment. *Hydrological Processes*, **11**, 1813–1832.

Hodson, A. J., Tranter, M., and Vatne, G., 2000. Contemporary rates of chemical weathering and atmospheric CO_2 sequestration in glaciated catchments: an Arctic perspective. *Earth Surface Processes and Landforms*, **25**, 1447–1471.

Holland, H. D., 1978. *The Chemistry of the Atmosphere and Oceans*. New York: Wiley. 351 pp.

Knight, P. G., 1999. *Glaciers*. Stanley Thornes: Cheltenham, 261 pp.

Livingstone, D. A., 1963. Chemical compositions of rivers and lakes, *U.S. Geological Survey Professional Paper 440-G*, 64 pp.

Raiswell, R., and Thomas, A. G., 1984. Solute acquisition in glacial meltwaters I. Fjällsjökull (south-east Iceland): bulk meltwaters with closed system characteristics. *Journal of Glaciology*, **30**, 35–43.

Rasch, M., Elbering, B., Jakobsen, B. H., and Hasholt, B., 2000. High-resolution measurements of water discharge, sediment, and solute transport in the River Zackenbergelven, Northeast Greenland. *Arctic, Antarctic and Alpine Research*, **32**, 336–345.

Sharp, M., Parkes, J., Cragg, B., Fairchild, I. J., Lamb, H., and Tranter, M., 1999. Bacterial populations at glacier beds and their relationship to rock weathering and carbon cycling. *Geology*, **27**, 107–110.

Sharp, M., Creaser, R. A., and Skidmore, M., 2002. Strontium isotope composition of runoff from a glaciated carbonate terrain. *Geochimica et Cosmochimica Acta*, **66**, 595–614.

Skidmore, M. L., and Sharp, M. J., 1999. Drainage system behaviour of a High-Arctic polythermal glacier. *Annals of Glaciology*, **28**, 209–215.

Skidmore, M. L., Foght, J. M., and Sharp, M. J., 2000. Microbial life beneath a High Arctic Glacier. *Applied Environmental Microbiology*, **66**, 3214–3220.

Steinporsson, S., and Oskarsson, N., 1983. Chemical monitoring of Jokulhaup water in Skeidara and the geothermal system in Grimsvotn, Iceland. *Jökull*, **33**, 73–86.

Thomas, A. G., and Raiswell, R., 1984. Solute acquisition in glacial meltwaters II. Argentiere (French Alps): bulk meltwaters with open system characteristics. *Journal of Glaciology*, **30**, 44–48.

Tranter, M., 2003. Chemical weathering in glacial and proglacial environments. In Holland, H. D., and Turekian, K. K. (eds.), *Treatise on Geochemistry*, Vol. 5, Surface and Ground Water, Weathering, Erosion and Soils (ed. J.I. Drever), pp. 189–205.

Tranter, M., Sharp, M. J., Brown, G. H., Willis, I. C., Hubbard, B. P., Nielsen, M. K., Smart, C. C., Gordon, S., Tulley, M., and Lamb, H. R., 1997. Variability in the chemical composition of in situ subglacial meltwaters. *Hydrological Processes*, **11**, 59–77.

Tranter, M., Sharp, M. J., Lamb, H. R., Brown, G. H., Hubbard, B. P., and Willis, I. C., 2002. Geochemical weathering at the bed of Haut Glacier d'Arolla, Switzerland – a new model. *Hydrological Processes*, **16**, 959–993.

Wadham, J. L., Hodson, A. J., Tranter, M., and Dowdeswell, J. A., 1997. The rate of chemical weathering beneath a quiescent, surge-type, polythermal based glacier, southern Spitsbergen. *Annals of Glaciology*, **24**, 27–31.

Wadham, J. L., Bottrell, S., Tranter, M., and Raiswell, R., 2004. Stable isotope evidence for microbial sulphate reduction at the bed of a polythermal high Arctic glacier. *Earth and Planetary Science Letters*, **219**, 341–355.

SOLUTES IN GLACIER ICE

Renoj Thayyen
Western Himalayan Regional Centre, National Institute of Hydrology, Jammu (J&K), India

Source

Dissolved ions (solute) in the glacier ice are mainly derived from the atmosphere by means of deposition of atmospheric particles on the glacier through precipitation. The deposition of atmospheric particle on the glacier is roughly proportional to their concentration in the atmosphere. Direct deposition of dust particles on the glacier, especially in the accumulation zone is also a major source

of solute in the glacier. At the subglacial zone of the glacier, solute entrainment happens in association with the relegation processes.

Processes

After the deposition in the accumulation zone of the glacier chemical constituents in the snowpack undergo various changes during the freeze thaw cycles. Preferential releases of ionic species from the snowpack occur during the densification processes. Impurities reach the ice grain boundary during recrystallization and reject most of the impurities to meltwater and the new ice formed will be purer. Solute concentration and its characteristics in the glacier ice with respect to the original solute characteristics of the snowpack are determined by the densification environment of the glacier. Glacier ice formation in subzero temperature ensures preservation of snowpack chemical characteristics to a great extent whereas in warmer climate, solute concentration in glacier ice undergoes major changes due to preferential elution processes.

Use

Atmospheric particle or aerosols originate from a variety of natural and manmade sources and chemical compositions of ice core provide good information on atmospheric particulate loading at the time of deposition and act as a good source of information for climate change studies. Radioactive isotopes derived from nuclear or volcanic activity is a very good time marker in the glacier ice.

Bibliography

Souchez, R. A., and Lemmens, M. M., 1987. Solutes. In Gurnell, A. M., and Clark, M. J. (eds.), *Glacio-fluvial Sediment Transfer: An Alpine Perspective*. Wiley: New York, pp. 285–303.

SPECIFIC MELT RATE

Pratap Singh
Tahal Consulting Engineers Ltd, New Delhi, India

The specific melt rate represents the melt rate over unit area and is represented in the unit of mm/day. Prevailing weather condition in a particular area has a control on the specific melt rate. Specific melt rate of snow/ice can be determined by allowing a small block of snow/ice to melt under natural weather conditions and observing the melt runoff and weather condition. Specific melt rate can be computed using energy balance approach or using temperature index approach. In general, empirical relationships are established between specific melt rate and mean daily temperature. The specific melt rate of glaciers ice is higher than that of snow due to lower albedo of ice. While computing the runoff from a snowfed or glacier fed basin, first specific melt rate is estimated and then runoff is derived by multiplying it with the representative area.

STABLE ISOTOPES

Bhishm Kumar
Hydrological Investigation Division, National Institute of Hydrology, Roorkee, Uttarakhand, India

The atoms of an element that do not decay with time or take infinite time to decay are called stable isotopes of that element (See *Oxygen Isotopes* and *Hydrogen Isotopes*).

Stable Isotopes, Table 1 Stable isotopes with their isotope ratio, abundance and commonly measured phases

Isotope	Ratio	% Natural Abundance	Reference (abundance ratio)	Commonly measured phases
^{2}H	$^{2}H/^{1}H$	0.015	VSMOW (1.5575×10^{-4})	H_2O, CH_2O, CH_4, H_2, OH^- minerals
^{3}He	$^{3}He/^{4}He$	0.000138	Atmospheric He (1.3×10^{-6})	He in water or gas, crustal fluids, basalt
^{6}Li	$^{6}Li/^{7}Li$	7.5	L-SVEC (8.32×10^{-2})	Saline waters, rocks
^{11}B	$^{11}B/^{10}B$	80.1	NBS 951 (4.04362)	Saline waters, clays, borate, rocks
^{13}C	$^{13}C/^{12}C$	1.11	VPDB (1.1237×10^{-2})	CO_2, carbonate, DIC, CH_4, organics
^{15}N	$^{15}N/^{14}N$	0.366	AIR N_2 (3.677×10^{-3})	N^2, NH_4^+, NO_3^-, N-organics
^{18}O	$^{18}O/^{16}O$	0.204	VSMOW (2.0052×10^{-3}) VPDB (2.0672×10^{-3})	H_2O,CH_2O,CO_2, sulfates NO_3^-, carbonates, silicates OH^- minerals
^{34}S	$^{34}S/^{32}S$	4.21	CDT (4.5005×10^{-3})	Sulfates, sulfides, H_2S, S-organics
^{37}Cl	$^{37}Cl/^{35}Cl$	24.23	SMOC (0.324)	Saline waters, rocks, evaporates, solvents
^{81}Br	$^{81}Br/^{79}Br$	49.31	SMOB	Developmental for saline waters
^{87}Sr	$^{87}Sr/^{86}Sr$	$^{87}Sr = 7.0$ $^{86}Sr = 9.86$	Absolute ratio measured	Water, carbonates, sulfates, feldspar

Over 2000 isotopes of 92 naturally occurring elements have been identified out of which several hundred are stable isotopes. But for hydrological investigations, we talk much about hydrogen and oxygen stable isotopes. As we know water molecule is made up of two hydrogen atoms and one oxygen atom therefore, many combinations (18) are possible out of which $^{1}H^{1}H^{16}O$, $^{1}HD^{16}O$, $HD^{18}O$, $^{1}H^{1}H^{17}O$, and $^{1}HD^{17}O$ are important. The stable isotopes with their isotope ratio, abundance, and commonly measured phases are listed in Table 1 (Clark and Fritz, 1997).

Bibliography

Clark, I., and Fritz, P., 1997. *Environmental Isotopes in Hydrogeology.* Boca Raton/New York: Lewis.

STAGE-DISCHARGE RELATIONSHIP

Amit Kumar
Centre of Advanced Study in Geology, Department of Geology, Punjab University, Chandigarh, India

Synonyms

Rating curve

Definition

The relationship between the amount of water flowing in a river or stream and stage at any particular point is usually known as stage–discharge relationship. Stage–discharge relationships for flow in rivers and channels are established by concurrent measurements of stage (y) and discharge (Q) (through velocity measurements, dilution methods, or other techniques) and the results are fitted graphically or statistically to yield the development of rating curves. The dynamic relationship between stage and discharge, which is unique to a particular selected station along the river, can be determined via mathematical relationships.

Introduction

Hydrologists, watershed managers are often interested in estimating stream discharge. Discharge is the flow rate of water passing a point on a stream at an instant in time; therefore, continuous flow measurement of river discharge is a hard and expensive task in hydrology. To overcome this problem, the stage reading at hydrometric gauges are permanently taken and the discharge of any time at which the actual discharge is unavailable will be estimated through a developed relationship between discharge and stage. To study the stage–discharge relation and the capability of long-term data in establishing a permanent stage–discharge relationship, and also to determine the best time to measure the discharge of rivers. More accurate values for discharge can be obtained when a permanent gauging station has been established on a stretch of a river where there is a stable relationship between stage and discharge, and this has been measured and recorded. Once this relationship is established, readings need only be taken of stage, because the discharge may then be read from a stage–discharge curve.

Stage–discharge relationship

Hydrological studies relied on stage–discharge relationships to monitor discharge in shallow streams of all depths. Hydrologists would typically get on a time-intensive program to rate a stream using a current meter to measure instantaneous discharge against several different stage events and a rating curve was developed. The stage–discharge relationship is based upon the relationship between stream water depth (stage) and discharge at a cross section. The relationship will be different for every cross section, and will change at a cross section as the cross section changes through time (aggrades or degrades).

The first step is to identify a permanent cross section. The cross section should be in a stable portion of the stream where the intensity of erosion and deposition is less. The second step is to install a stage staff or depth meter in the channel/well at the cross section. The stage staff must be fixed and permanent. Its stability and the cross section are crucial for developing a meaningful stage–discharge relationship. In the next step, the area of cross section of the river at a gauging site and the velocity of flow through the cross-sectional area are to be measured. The applied method at the cross section to estimate discharge over a wide range of value of discharge (low flow to peak flow) is known as area–velocity method. After enough observations, a stage–discharge relationship (equation) can be developed to correlate stage and discharge. Once the stage–discharge relationship is developed, discharge can be computed directly by only monitoring of the water level at the cross section over time. The extrapolation of computed values must be under the range of discharge used to develop such relationships.

If such relationship for a gauging station is and does not change with time constant, the control is said to be permanent. If it changes with time, it is called shifting control.

When measured value of stage and discharge are plotted on arithmetic paper, the result is an approximate parabolic curve, as shown in Figure 1. The curve can be expressed as

$$Q = a(h - h_0)^b \tag{1}$$

In which h_0 is a constant, representing the gauge reading for zero discharge, and a and b are rating curve constant. This relationship can also be expressed graphically by plotting the observed stage against corresponding discharge values in logarithmic paper, the plot is straight line, as shown in Figure 2. The equation becomes

$$\log Q = \log a + b \log(h - h_0) \tag{2}$$

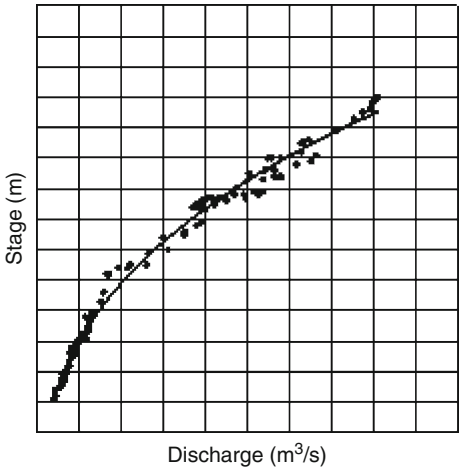

Stage-Discharge Relationship, Figure 1 Stage–discharge relationship curve (*arithmetic plot*).

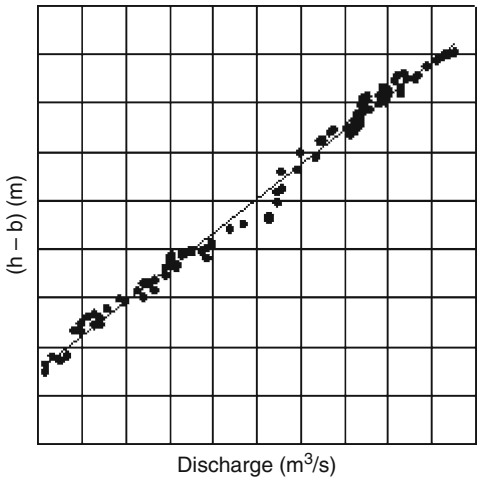

Stage-Discharge Relationship, Figure 2 Stage–discharge relationship curves (*logarithmic plot*).

The best value of constants a and b can be obtained using the least square method; however, constant h_0 must be found beforehand, and this can be estimated in several ways. A trial-and -error method can be used to yield h_0, which then gives the best-fit curve. Another way is to extrapolate the rating curve corresponding to $Q = 0$ and then plot log Q versus log $(h–h_0)$. If the plot is the straight line, then the value of h_0 obtained by extrapolation is acceptable. Otherwise, another value in the neighborhood of the previous value of h_0 is selected and the procedure is repeated.

A graphical method to determine h_0 has been reported by running (Wisler and Brater, 1959). According to this method, Q and h are plotted on arithmetic scale and a

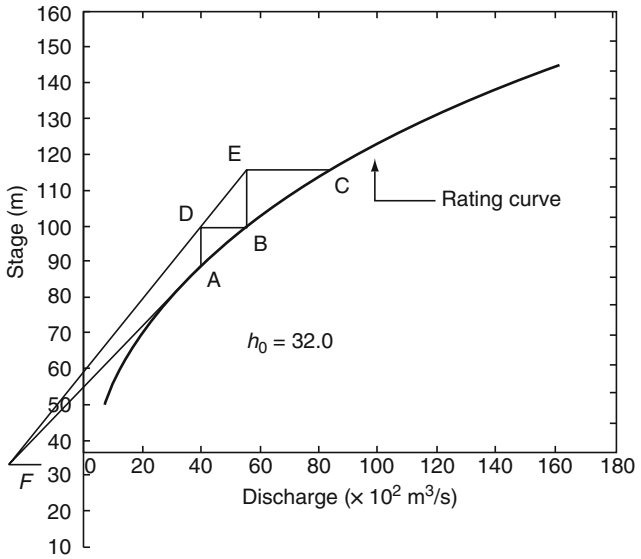

Stage-Discharge Relationship, Figure 3 Running's method for estimation of constant h_0.

smooth curve is drawn through plotted points. In Figure 3, three points, A, B, and C, are selected in such a way that their geometric progression is as follows.

$$\frac{Q_A}{Q} = \frac{Q_B}{Q} \tag{3}$$

The vertical lines are drawn at A and B, and horizontal lines drawn at B and C. Thus, D and E are obtained as intersection points with verticals. Two straight lines are drawn through E and D, and stage–discharge curve is assumed to be a parabola in this method.

Another method of computing h_0 is analytical. From a smooth curve of Q versus h, three values of discharge, Q_1, Q_2, and Q_3, are selected such that $Q_1/Q_2 = Q_2/Q_1$. The corresponding values of stage are h_1, h_2, and h_3. Then, using equation

$$\frac{(h_1 - h_0)^b}{(h_2 - h_0)^b} = \frac{(h_2 - h_0)^b}{(h_3 - h_0)^b} \tag{4}$$

$$\frac{(h_1 - h_0)}{(h_2 - h_0)} = \frac{(h_2 - h_0)}{(h_3 - h_0)} \tag{5}$$

$$h_0 = \frac{h_1 h_3 - {h_2}^2}{h_1 + h_3 - 2h_2} \tag{6}$$

Alternatively, all three parameters, a, b, and h_0, can be obtained by optimization.

The simple rating curve is generally satisfactory for a majority of streams where rapid fluctuation of stage is not experienced at gauging section. The adequacy of the curve is measured by the scatter of data around fitted

curve. When there is a permanent control, the rating curve is essentially permanent. If the rating curve is made using a range of stages from low to high, it can be used to interpolate the discharge for any stage of flow between the measured stages without measuring that flow. It is important to check the stability of the curve by parabolic discharge measurement, and to extend it with each new observed high stage. Changes in channel shape, due to scouring or sedimentation, can change the effect of control and thereby change the rating curve.

For some gauging stations, there may be two or more control each for a particular range of stage. The rating curve for such a station is discontinuous; the point of discontinuity corresponds to the stage reflecting the change in control. An example is the start of submergence of a weir control when the tail water level below the control rises above the lowest point of the control. Even under such conditions, the simple rating curve may be satisfactory if the control is permanent, free of backwater, and the stream slope is steep.

Summary

There have been a number of developments in recent years that have resulted in new and better estimation of stage and discharge relationships. Many types of equipments for both instantaneous measurements of flow and full-time monitoring of ungauged river were to be used for discharge measurements. Discharge is important for the hydrologic studies, considerable efforts to be made to collect this data as WMO recommended norms, by developing number of hygrometry stations in various geographical locations.

Bibliography

Herschy, R. W., 1978. *Hydrometry Principles and Practices*. Chichester, West Sussex: Wiley.
Herschy, R. W., 1985. *Streamflow Measurements*. Lonon and New York: Elsevier Applied Science.
Singh, P., and Singh, V. P., 2001. *Snow and Glacier Hydrology*. Dordrecht: Kluwer Academic.
Wisler, C. O., and Brater, E. F., 1959. *Hydrology*. New York: Wiley.

STATIONARY GLACIER

Renoj Thayyen
Western Himalayan Regional Centre, National Institute of Hydrology, Jammu (J&K), India

Synonyms

Standstill glacier

When horizontal velocity component of a glacier equals the horizontal component of ablation, glacier terminus remains stationery (Boulton, 1986). Glacier margins advance, retreat, or remain stationery in response to the variations in glacier mass balance. Frontal margins of the glacier will remain at same position when $U_{hx} = a_b/\tan \alpha$, where U_{hx} is the horizontal velocity component, a_b is the ablation rate, and α is the glacier surface slope. ($a_b/\tan \alpha$) constitute the horizontal component of ablation. While the position of the glacier termini is stationery, glacier ice itself is in motion but removed from the terminus region at a rate equal to the velocity.

Bibliography

Boulton, G. S., 1986. Push moraines and glacier contact fans in marine and terrestrial environments. *Sedimentology*, **33**, 677–698.

STRATIGRAPHY OF SNOWPACKS

Peter W. Nienow[1], Fay Campbell[2]
[1]School of Geosciences, University of Edinburgh, Edinburgh, UK
[2]Department of Geographical and Earth Sciences, University of Glasgow, Glasgow, UK

Definition

Snowpack stratigraphy. Snowpacks are often characterized by a number of distinctive "stratigraphic" layers in which the properties of the snow vary vertically in terms of density, crystal shape, grain size, and hardness. These individual layers when combined make up the stratigraphy of a snowpack.

Introduction

Any snowpack, whether of a seasonal or multi-year duration, will develop a layered structure (Figure 1) during its formation which will evolve through time. Each layer is formed by the deposition of falling snow, the redistribution of windblown snow, or a combination of these two processes. The initial snowpack is subsequently modified by compaction and thermal metamorphic processes resulting in the gradual densification of the snowpack. Surface melting, percolation, and under certain conditions, refreezing of meltwaters further modifies the snowpack and enhances the rate of densification. Snowpacks are typically heterogeneous with each layer varying in terms of density, crystal shape and grain size with subsequent implications for both porosity and permeability. An understanding of snowpack stratigraphy is important because the complex structure of an individual snowpack affects: (1) its stability, and therefore propensity to fail catastrophically in an avalanche; and (2) the snowpack hydrology (qv *Temperature Profile of Snowpack*) and therefore the rate at which meltwater is released from a given snowpack with implications for the runoff characteristics from snow-covered catchments. Snowpack

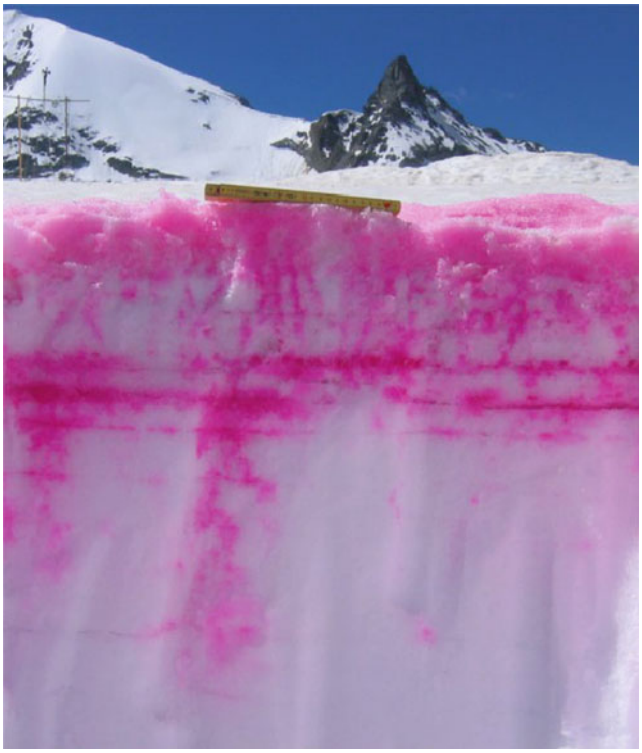

Stratigraphy of Snowpacks, Figure 1 Layered snowpack stratigraphy as revealed in a snow-pit, excavated 1½ h after a dye injection on the snowpack surface at Haut Glacier d'Arolla, Switzerland on 27 June 2004. The ruler at the surface is 20 cm long. (Photo: F. Campbell).

stratigraphy has traditionally been investigated in situ through the excavation of snow-pits and detailed vertical sampling of the snow characteristics of the walls therein (Fierz et al., 2009). More recently, numerical models have been developed to simulate the evolution of snowpack stratigraphy and stability (e.g., Brun et al., 1992; Jordan, 1991; Lehning et al., 2002).

Physical properties of the snowpack

The physical properties of the seasonal snowpack are controlled by processes operating on the snow during its formation in the atmosphere, deposition on the ground, and time on the ground. A thorough understanding of the processes of snowcover formation is therefore critical for understanding how the stratigraphy of a snowpack develops and evolves through time. More comprehensive discussions of snowpack development, characteristics, and processes from deposition to melt are provided by Male (1980), Marsh (2005), Lehning et al. (2002) and Pielmeier and Schneebeli (2003); a summary of those aspects most relevant to snowpack stratigraphy is given here.

Snowpack formation and evolution: dry snow processes

Snow Crystals (qv) forming in the atmosphere take on a range of sizes and a diverse variety of forms depending on the temperature and humidity of the atmosphere at the time of their formation and as they fall to the ground (Male, 1980). Crystal size and shape may be altered by wind action both as snowflakes fall to the ground and once deposited, with *Grains* (qv) broken and abraded into more equidimensional particles (Male, 1980).

As the seasonal snowpack is typically deposited by a series of winter storms, a characteristic layered (qv *Snow Layer*) structure develops, with varying layer properties depending initially on the conditions under which the snow was deposited. Between storms, the snowpack surface may be modified by freezing rain, packing by wind action, or surface melting and refreezing, resulting in the formation of thin, high-density layers which subsequently separate snow strata (Male, 1980). These "ice" layers, though rarely of solid ice, are relatively impermeable compared to the lower density and more permeable snow strata, and play an important role in controlling the physical properties of the snowpack, especially with respect to *Snow Hydrology* (qv) (Colbeck, 1975a; Campbell et al., 2006; Figure 1).

Once on the ground, snowflakes undergo a rapid *Snow Metamorphism* (qv) driven by water vapor gradients between convex and concave surfaces, allowing the snowpack to assume a lower energy state by reducing its total surface area relative to mass. In this process, known as equilibrium growth or equi-temperature metamorphism due to the small temperature gradients under which it takes place (Sommerfeld and LaChappelle, 1970), snowflakes and broken particles can be reduced to more spherical snow grains in a matter of days, and smaller grains melt and disappear as larger grains grow. In this way, grains may attain a diameter of up to 1 mm even while still below 0°C, and the rounding of grains can allow an increase in *Snow Density* (qv) to between 580 and 600 kg m^{-3} (Sommerfeld and LaChappelle, 1970), compared to only 50–70 kg m^{-3} for new snow deposited under calm conditions (Paterson, 1994).

If the snowpack is subject to a temperature gradient, the resulting movement of water vapor between grains that are at different temperatures drives kinetic growth metamorphism, producing characteristic faceted grains known as surface and depth hoar. More detailed information about the processes of equilibrium growth and kinetic growth metamorphism can be found in Sommerfeld and LaChappelle (1970) and Male (1980).

As metamorphism proceeds, the breaking up and rounding of dendritic particles is accompanied by the formation of bonds at points of contact between grains. This process, known as sintering, leads to an increase in snow density and strength. The snowpack, previously a matrix of single crystal or polycrystalline ice grains, becomes a complex three-dimensional network of connected particles (Male, 1980).

Snowpack formation and evolution: the metamorphism of wet snow

When liquid water is first introduced into the snowpack, it initiates a rapid metamorphism, whereby small ice grains are eliminated while larger grains grow rapidly until they reach diameters of 1–2 mm, with important implications for subsequent snowpack strength and hydrology (qv *Snow Hydrology*; *Stratigraphy of Snowpacks*). A thermodynamic analysis of the relationship between grain size and phase equilibrium temperature (Colbeck, 1975b) shows that this process can be understood as the result of differences in the melting temperature of small and large grains caused by the difference in their radii of curvature. Due to their smaller radius of curvature, melting temperature is higher for large grains than for small, and larger grains therefore exist at a higher temperature than smaller grains. This temperature difference drives heat flow by conduction toward the smaller grains. As a result, smaller grains decrease in size and eventually disappear, while larger grains increase in size, conserving the total mass.

The diverse grain forms found in both dry and wet snow at various stages of development are brought together by Fierz et al. (2009) in the International Classification for Seasonal Snow on the Ground. While primarily based on grain morphology, the scheme includes valuable information about the physical processes that lead to different grain types.

Snowpack structure

Metamorphism (qv *Snow Metamorphism*) of the snowpack through both dry and wet processes alters the initial snowpack stratigraphy and ensures that snowpack structure is continuously evolving following the initial deposition of falling or redistributed windblown snow. Investigations of snowpack stratigraphy, through snowpit studies (Fierz et al., 2009), typically reveal a horizontally layered structure in which crystal size, shape, and density vary with depth. These horizontal layers affect the permeability of the snowpack with implications for the transfer of surface meltwaters or liquid precipitation down through the snowpack (Figures 1 and 2). Where percolating meltwaters refreeze at depth, ice layers and ice lenses form. These layers may be spatially extensive where the boundary between two different stratigraphic units within the snowpack is consistent over long horizontal length scales (Pfeffer and Humphrey, 1998). If however the snowpack is characterized by a complex stratigraphy and snowpack permeability with numerous undulating stratigraphic boundaries, often due to the presence of sastrugi and windcrusts, the ice layers will rarely be spatially continuous even at short length scales of <1 m (Parry et al., 2007). The horizontal nature of the snowpack stratigraphy is disrupted by the downward percolation of water, which has been observed to percolate through both arctic and temperate snowpacks, via preferential flow-fingers or pipes (Figure 2) which occupy only a fraction of total snowpack volume but transmit a large proportion of flow (Marsh and Woo, 1984).

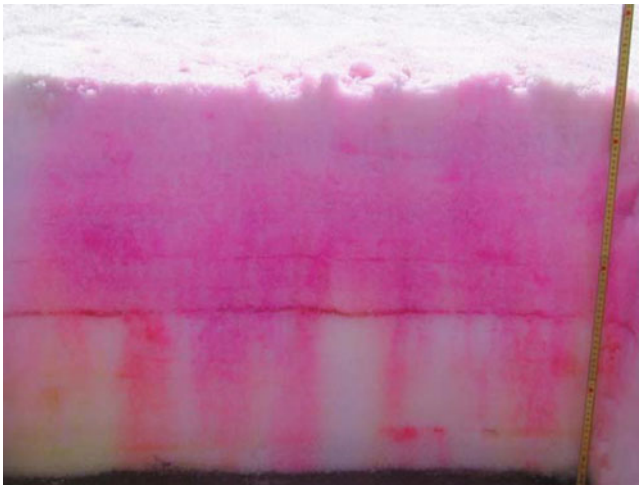

Stratigraphy of Snowpacks, Figure 2 The pattern of percolation as revealed by dye-stained surface meltwater in an excavated snow-pit 2½ h after a dye injection on the snowpack surface at Haut Glacier d'Arolla, Switzerland on 25 July 2004. An ice layer, 30 cm above the glacier surface, retains dye above it allowing continued downward flow through preferential flow-fingers. (Photo: F. Campbell).

The characteristic horizontal layering within a snowpack will affect the strength of the snowpack with implications for snowpack failure and avalanches. For example, the presence of a weakly bonded hoar layer within the snowpack provides a potential failure plane that will shear easily thus promoting the likelihood of an avalanche. As a result, avalanche forecasting is highly dependent on knowledge both of the in situ snowpack stratigraphy and our ability to predict, using models, how snowpack structure (and thus strength) will change through time (Lehning et al., 2002).

Modeling snowpack structure

The physical processes governing snow temperature evolution, grain metamorphism, densification, surface melt, and water transport have been brought together to produce comprehensive snow process models to simulate the energy and mass evolution of a snowpack through time given surface meteorological conditions. Well-established models include CROCUS, developed by the French national meteorological service (Brun et al., 1992), SNTHERM, from the US Army Corps of Engineers Cold Regions Research and Engineering Laboratory (CRREL) (Jordan, 1991), and the Swiss Federal Institute for Snow and Avalanche Research's SNOWPACK (Lehning et al., 2002). In the case of both CROCUS and SNOWPACK, the need for accurate snow stability information for avalanche warning purposes provided the impetus for detailed snowpack modeling, with SNOWPACK in particular including detailed information about snow microstructure

and resulting mechanical stability (Lehning et al., 2002). Advances in numerical modeling and the importance of effective prediction of snowpack stability ensure that investigations of snowpack stratigraphy will continue to be a well-researched area of snow science.

Summary

The processes that are responsible for the development of a snowpack ensure that it is characterized by internal "stratigraphic" layers in which the physical properties such as grain size, crystal type, density, and moisture content vary. Following the initiation of a snowpack as a result of snowfall or redistributed windblown snow, the stratigraphy of the snowpack continuously evolves due to physical compaction and the processes of both dry and wet-snow metamorphism. A detailed physical understanding of the processes that control snowpack stratigraphy is important because its complex structure affects: (1) the stability of the snowpack and its likelihood to fail as an avalanche; and (2) the permeability of the snowpack and the rate at which meltwaters are released from a given snowcover. There are numerous ways to characterize and investigate snowpacks as described in a detailed historical review on "Developments in the Stratigraphy of Snow" by Pielmeier and Schneebeli (2003). In recent decades, developments in both computational power and of the detailed understanding of snowpack processes has resulted in advances, through numerical modeling, in the simulation of the evolution of snowpack stratigraphy and stability (e.g., Brun et al., 1992; Jordan, 1991; Lehning et al., 2002).

Bibliography

Brun, E., David, P., Sudul, M., and Brunot, G., 1992. A numerical model to simulate snowcover stratigraphy for operational avalanche forecasting. *Journal of Glaciology*, **38**, 13–22.

Campbell, F., Nienow, P., and Purves, R., 2006. Role of the supraglacial snowpack in mediating meltwater delivery to the glacier system as inferred from dye tracer investigations. *Hydrological Processes*, **20**, 969–985.

Colbeck, S. C., 1975a. A theory for water flow through a layered snowpack. *Water Resources Research*, **11**(2), 261–266.

Colbeck, S. C., 1975b. Grain and bond growth in wet snow. In *Snow Mechanics: Proceedings of a symposium* held at Grindelwald, April 1974. IAHS Publication. Vol. 114, pp. 51–61.

Fierz, C., Armstrong, R. L., Durand, Y., Etchevers, P., Greene, E., McClung, D. M., Nishimura, K., Satyawali, P. K., and Sokratov, S. A. 2009. The international classification for seasonal snow on the ground. IHP-VII Technical Documents in Hydrology N°83, IACS Contribution N°1, UNESCO-IHP, Paris.

Jordan, R., 1991. A one-dimensional temperature model for a snow cover (91-16). US Army Corps of Engineers Cold Regions Research and Engineering Laboratory, Hanover, New Hampshire

Lehning, M., Bartelt, P., Brown, B., Fierz, C., and Satyawali, P., 2002. A physical SNOWPACK model for the Swiss avalanche warning. Part II: snow microstructure. *Cold Regions Science and Technology*, **35**, 147–167.

Male, D. H., 1980. The seasonal snowcover. In Colbeck, S. C. (ed.), *Dynamics of Snow and Ice Masses*. New York: Academic, pp. 305–395.

Marsh, P., 2005. HSA167 – water flow through snow and firn. In Anderson, M. (ed.), *The Encyclopedia of Hydrological Sciences*. London: Wiley.

Marsh, P., and Woo, M.-K., 1984. Wetting front advance and freezing of meltwater within a snow cover 1. Observations in the Canadian Arctic. *Water Resources Research*, **20**(12), 1853–1864.

Parry, V., Nienow, P., Mair, D., Scott, J., Hubbard, B., Steffen, K., and Wingham, D., 2007. Investigations of meltwater refreezing and density variations in the snowpack and firn within the percolation zone of the Greenland ice sheet. *Annals of Glaciology*, **46**, 61–68.

Paterson, W. S. B., 1994. *The Physics of Glaciers*, 3rd edn. Oxford: Butterworth Heinemann.

Pfeffer, W. T., and Humphrey, N. F., 1998. Formation of ice layers by infiltration and refreezing of meltwater. *Annals of Glaciology*, **26**, 83–91.

Pielmeier, C., and Schneebeli, M., 2003. Developments in the stratigraphy of snow. *Surveys in Geophysics*, **24**, 389–416.

Sommerfeld, R. A., and LaChappelle, E., 1970. The classification of snow metamorphism. *Journal of Glaciology*, **9**(55), 3–17.

Cross-references

Atmosphere-Snow/Ice Interactions
Layering of Snow
Snow Crystal Structure
Snow Density
Snow Grains
Snow Hydrology
Snow Metamorphism
Snow Pit

STREAMFLOW TRENDS IN MOUNTAINOUS REGIONS

Peter Molnar, Paolo Burlando, Francesca Pellicciotti
Institute of Environmental Engineering, ETH Zurich, Zurich, Switzerland

Definition

Streamflow is a hydrological variable measured at a defined river cross-section; it spatially integrates the runoff generating processes in the contributing watershed, including precipitation and air temperature. *Trends in streamflow* are progressive changes in the time series of streamflow that can be detected with *statistical methods* and their statistical significance can be assessed. Mountainous regions are particularly vulnerable to streamflow change because of their high specific runoff and the sensitivity to the distribution of precipitation and air temperature, and the processes of snow accumulation and melt.

Introduction

In the context of *climate change*, precipitation and temperature changes potentially have severe impacts on runoff in mountainous regions where the snowpack, glaciers, and small ice caps play a crucial role in runoff formation.

IPCC (2007) projects that widespread mass losses from glaciers and reductions in snow cover over recent decades will accelerate into the twenty-first century, reducing water availability, hydropower potential, and changing seasonality of flows in regions supplied by meltwater from major mountain ranges. It is therefore important to use statistical methods to detect gradual changes (trends) in streamflow from instrumental records and to attribute these changes to their possible causes.

In most cases, the *attribution* of discovered trends in streamflow to their causes is difficult. Because streamflow measurements integrate the runoff generating processes in the upstream watershed, they reflect not only the seasonal variability in precipitation and temperature, but also the variability in land surface properties (vegetation, soil, topographic characteristics such as slope and aspect, rock cover, glaciers, etc.). The existence of statistically significant trends in streamflow together with other hydroclimatic variables like precipitation and air temperature are an indication but not proof of causality. Only detailed knowledge about the physical processes of runoff formation in the tested basin can provide conclusive evidence.

In mountainous regions, there are additional issues related to *snow and ice*. Precipitation in winter builds the snowpack and contributes to streamflow in the following spring and summer seasons during snowmelt. The effect of temperature changes on the snowpack is therefore crucial for understanding streamflow trends (e.g., Stewart, 2009). Glacier change itself may result in both increasing or decreasing trends in streamflow during a warming trend, depending on the glacier mass balance (e.g., Huss et al., 2008). In the short-term, warming can lead to increased glacier runoff (e.g., Pellicciotti et al., 2010), while in the long-term, glacier recession can decrease the glacier mass to the point where a reduction in glacier runoff can result (e.g., Stahl and Moore, 2006).

An important element in any hydroclimatic trend detection is the choice of the *time period* over which data are tested. Hydroclimatic data generally exhibit variabilities at both short and long timescales. The time period is related to the purpose of the testing and should be chosen carefully so that discovered trends are not attributed erroneously to external factors when in fact they could be part of the natural long-term periodicity (e.g., Cohn and Lins, 2005; Laternser and Schneebeli, 2003). Furthermore, if trends in several variables are to be compared, it is fundamental that the time period is the same for all tested variables.

Methods

Several statistical tests for detecting changes in statistical properties of time series exist. Here, we focus only on the most common ones used in studies of gradual change (i.e., trends not jumps) in hydroclimatic data from the recent literature, with a special focus on streamflow. The details of the tests can be found in any statistical textbook, Helsel and Hirsch (1992) is recommended. Streamflow trend testing consists of four basic steps (Table 1).

Exploratory data analysis

In data preparation, attention should be paid to the type and resolution of data used. It is important to test streamflow for trends at several temporal resolutions. Daily data can indicate shifts in the distribution of streamflow, for example, the frequency of low and high flows (e.g., Birsan et al., 2005), while monthly and seasonal data can indicate the presence of seasonal shifts in the runoff regime, for example, the timing of spring snowmelt (e.g., Zhang et al., 2001). If daily data are available, it is advisable to study trends in quantiles Q_p, that is, daily flows exceeded with a frequency 1-p, for a range of p including minima and maxima on a seasonal basis. This gives an indication of shifts in the distributions of streamflow. Several time periods T should be tested, analyses could also be conducted on moving windows to identify more precisely in time when maximum change occurs (see Pellicciotti et al., 2010, for an effect of different time windows on trend detection). It is important to choose basins that are undisturbed, so that anthropogenic effects such as flow regulation, which are common in some mountain basins used for hydropower production, are ruled out.

Trend computation methods

The objective of testing is to compute a test statistic that quantifies the trend present in the data. In streamflow trend testing, there is a preference for nonparametric methods because the underlying distributions of the data are not known and are often non-normal. The four most common tests are listed in Table 1. Linear regression (LR) and Sen's robust slope estimator (SEN) estimate the magnitude of the trend slope b, which is useful when the magnitude of change itself is of importance. LR should be used only if the trend is linear. The Mann-Kendall (MK) test computes the test static Z and the Spearman rank correlation (RC) the test statistic t. These two tests have similar power and both are nonparametric methods not sensitive to outliers. The MK test is the most widely used test in the literature and is recommended for hydroclimatic data. It is distribution-free and captures linear and nonlinear monotonic trends. However, it is advisable to use more than one test in any trend detection study.

Testing statistical significance

At each site, the computed test statistic (b, Z, t) needs to be tested for its significance. The null hypothesis H_0 of no trend ($b = 0$, $Z = 0$, $t = 0$) is rejected at a chosen significance level α based on the computed test statistic and its distribution. For LR and SEN, the t-ratio is computed and tested with the Student's t distribution, for MK the test statistic Z is tested with the standard normal distribution, for RC the Student's t distribution may be used. In general if the test statistic, e.g., $|Z| > Z_{crit}(1 - \alpha/2)$ for a two-tailed

Streamflow Trends in Mountainous Regions, Table 1 Summary of the streamflow trend detection procedure

Steps and methods	Data/results	Selected references
1. Exploratory data analysis		
• Verifying data quality, aggregating data at different resolutions, computing daily quantiles, visual inspection of time series plots	Q (daily, monthly seasonal, annual) Daily quantiles Q_p	Kundzewicz and Robson (2004) Birsan et al. (2005) Lins and Slack (1999)
• Choice of trend testing time period/s T	Constant T Moving window T	
2. Trend computation methods		
• Trend slope – least squares linear regression, parametric method (LR)	Slope b, st.err. of b	Helsel and Hirsch (1992) Khaliq et al. (2009)
• Trend slope – Sen, nonparametric method (SEN)	Slope b, st.err. of b	
• Mann-Kendall test, nonparametric method (MK)	Test statistic Z	
• Spearman rank correlation test, nonparametric method (RC)	Test statistic t	
3. Testing statistical significance		
• Site significance: testing H_0 for b, Z, t	reject H_0 if $\|Z\| > Z_{crit}\ (1 - \alpha/2)$ $\|t\| > t_{crit}\ (1 - \alpha/2, DF)$	Khaliq et al. (2009) Kundzewicz and Robson (2004) Yue et al. (2002)
• Effect of serial correlation, methods – prewhitening, trend-free prewhitening, variance correction, resampling: permutation, bootstrap	Accounting for ρ	Burn and Elnur (2002) Livezey and Chen (1983) Zhang et al. (2001)
• Field significance: testing for the spatial congruence of site-significant trends in space (block bootstrap, Monte Carlo)	α_f -field significance level	
4. Assessing causality		
• Trend testing of other hydroclimatic data, for the same T (precipitation, temperature, snow, etc.) and examination of relations between variables and test statistics	Multivariate regression	Birsan et al. (2005) Kundzewicz and Robson (2004) Dery and Wood (2005) Lettenmaier et al. (1994)
• Examining dependence on long-term climate (climatic teleconnections)	ENSO, NAO, PDO indexes, etc.	Stahl and Moore (2006) Scherrer and Appenzeller (2004)
• Examining dependence on static basin properties	Assess vulnerability	Laternser and Schneebeli (2003)

test, then H_0 is rejected and it is concluded that the detected trend is statistically significant, that is, it is not likely to be due to random fluctuations, with the probability α of being wrong (Type I error). Sometimes a p-value is reported, that is, the probability that the computed test statistic would occur provided H_0 is true, values of $p < \alpha$ are statistically significant. Commonly used significance levels are $\alpha = 0.05, 0.1$. The power of a test is the test's ability to detect a trend when it really exists. The power is high when the detection error (Type II error) is low. The critical significance levels of the test statistics are affected by serial (auto) correlation in the data. Several methods have been developed to account for this (Table 1), details can be found in the review by Khaliq et al. (2009). The most commonly used method is the Trend-free prewhitening approach (Yue et al., 2002). Serial correlation is not likely to be high in inter-annual hydrological data, however it is advisable to compute the serial correlation coefficient for raw and detrended data to check if it is significantly $\rho > 0$. If serial correlation is an issue, variance correction and resampling methods have been found to perform well. In spatial studies, the field (spatial) significance of trends is tested by resampling (bootstrap) methods in order to identify if the spatial coherence of site-significant trends is nonrandom. For example, this could be the case for streamflow changes driven by large-scale regional climate shifts, the presence of glaciers, etc.

Assessing causality

The attribution of discovered trends in streamflow to their causes may be data-driven (indirect), for example, multivariate regression between streamflow and other hydroclimatic variables, or model-driven (direct), for example, by physically based rainfall-runoff modeling. The most common explanatory variables are precipitation (wet day frequency and intensity) and air temperature (minimum, maximum, mean), but if available, other variables like evaporation, snow cover duration and depth, glacier mass and length, etc. may be used. Long-term climate teleconnections may be examined by correlations with climate indexes such as ENSO, PDO, NAO, etc., which capture large-scale climate variability. Basin vulnerability to streamflow trends may also be examined by multivariate regression of trend statistics with static basin properties, such as basin area, average slope, soil type, rock and glacier coverage, vegetation cover, etc. (e.g., Birsan et al., 2005).

Example

An example of a streamflow trend testing procedure following the steps above is presented for the mountainous Oberried Basin, Simme River, central Switzerland. A 30-year record of daily streamflow (1971–2000) is studied for this 35.7 km^2 basin, which is 34.6% glaciated (Plaine Morte glacier) and has an average altitude of 2,370 m. Daily precipitation data are from the station Boltigen lower in the valley and daily minimum and maximum temperatures are measured at Adelboden in the neighboring valley for the same period.

In step (1) data were quality checked and aggregated to seasonal and annual totals, and seasonal quantiles Q_{min}, $Q_{0.1}$, ..., $Q_{0.9}$, Q_{max} were computed. Mean streamflow appears to be consistently increasing over the study period, especially in the summer (Figure 1a). There is pronounced seasonality typical of glacio-nival regimes, with highest flows in the snow and ice melt period in May-June-July. In step (2) the whole 30-year period was used for trend testing. The LR and MK trend tests were applied to the data and the trend slopes b and test statistic Z were computed. In step (3) statistically significant trends (α = 0.05) were found in Q in all seasons by both LR and MK tests. Quantile analyses showed that summer and spring increases were strongest for low and moderate flows (Figure 1b). But changes were statistically significant in most quantiles. Serial correlation was not present in the detrended data so prewhitening was not conducted. Field significance cannot be tested with one station. Assessing causality in step (4) focused on minimum temperatures T_{min} and precipitation P. Precipitation frequency and mean intensity did not show any meaningful trends in the study period, except for a small increasing trend in winter intensity. Statistically significant trends were however found for minimum temperature increases in spring and summer (Figure 1c). Spring in particular is a sensitive season because minimum temperatures fluctuate around 0°C, so even small increases may increase the likelihood of liquid precipitation and snowmelt. We also focused closer on the 10-year period 1984–1994 (Figure 1) where consistent increases in summer T_{min} were observed jointly with increases in runoff and glacier retreat and no major changes in P. The glacier retreated by almost 400 m between 1971 and 2000.

In summary, the seasonal MK Z for mean P, T_{min}, and Q in Figure 2a shows that temperature increases are likely the dominant reason for increases in streamflow, especially in the spring and summer months when they are

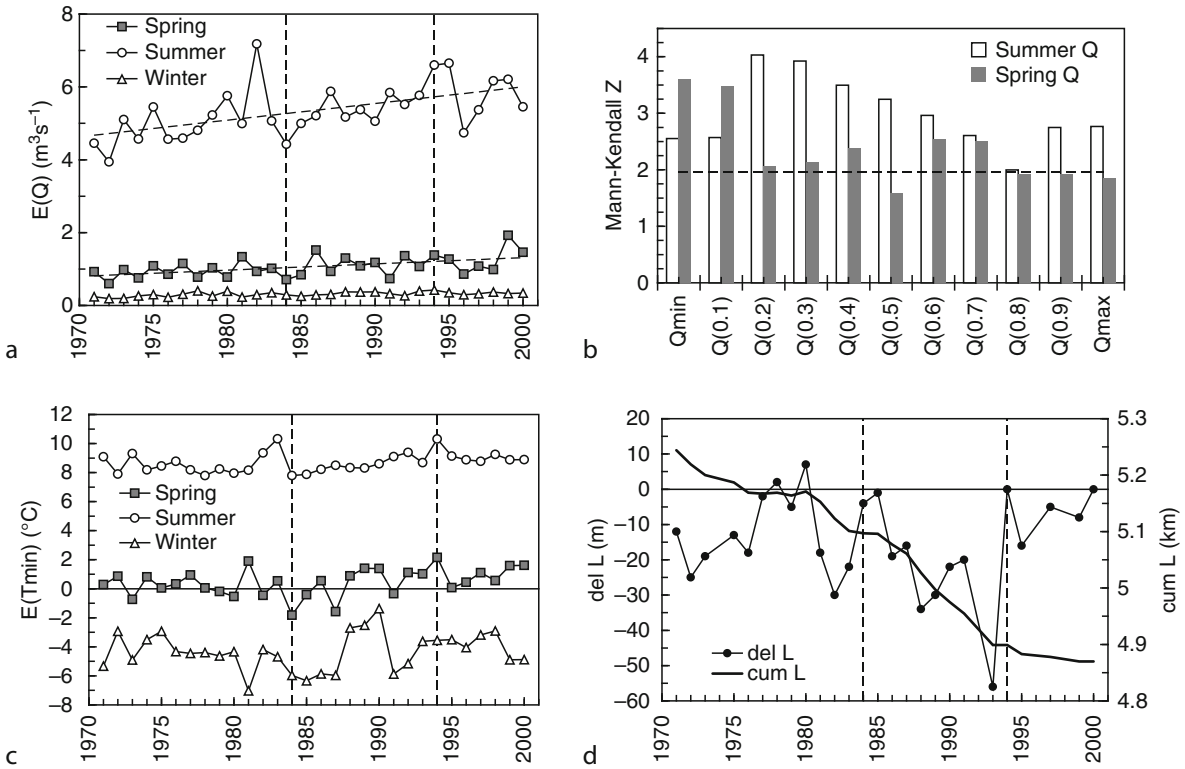

Streamflow Trends in Mountainous Regions, Figure 1 (**a**) Mean daily streamflow for the spring, summer, and winter seasons in Oberried (1971–2000) with linear trend line shown. (**b**) Mann-Kendall test statistics Z for quantiles Q_p of daily flows for the summer and spring seasons (Z_{crit} at $\alpha = 0.05$ is shown with dashed line). (**c**) Mean minimum daily temperature for the spring, summer, and winter seasons. (**d**) Plaine Morte annual glacier retreat (ΔL) and total glacier length (ΣL) for the studied period (data from Glaciological reports, 1881–2008). Vertical lines show the rapid glacier mass loss period 1984–1994.

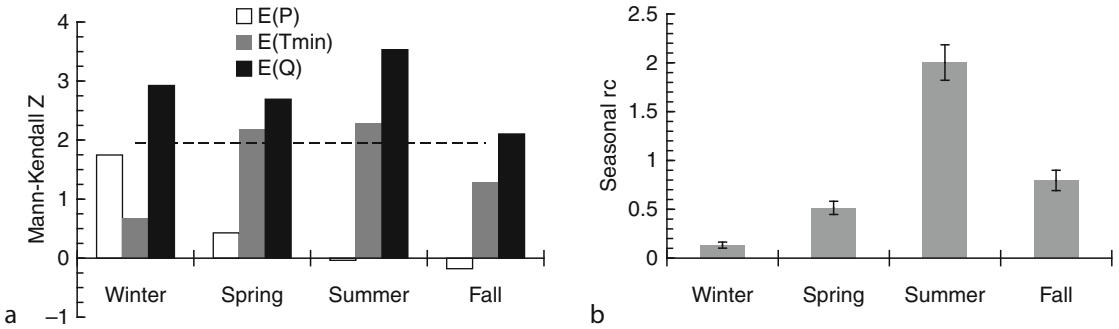

Streamflow Trends in Mountainous Regions, Figure 2 (**a**) Seasonal Mann-Kendall *Z* for mean precipitation, minimum temperature, and streamflow (Z_{crit} at $\alpha = 0.05$ is shown with dashed line). (**b**) Seasonal runoff coefficient (*rc*) computed as the ratio *rc* = E(*Q*)/E(*P*) with error bands due to altitude and wind corrections to convert point gauge precipitation to basin-wide estimates.

statistically significant ($\alpha = 0.05$). Small increases in winter precipitation may also contribute to the snowpack in winter and subsequent snowmelt. In Oberried, like in most mountain basins, the runoff coefficient *rc* (ratio between streamflow and precipitation) is strongly seasonal (Figure 2b). In fact in winter there is very little runoff $rc \approx 0$, while in summer $rc \approx 2$, which means that roughly half of the runoff volume comes from snow accumulated in the previous winter and from glacier melt.

Selected streamflow trend studies

Regional effects

There are large regional differences in streamflow trends in mountainous and/or cold environments, which are confounded by the fact that studies use different time periods. Main commonalities are that streamflow trends are often correlated with large-scale climate patterns (indexes such as NAO, PDO, etc.), with general warming, and less clearly with precipitation changes. For example, increasing trends in *Q* have been observed in the Eurasian Arctic rivers (1936–1999) (Peterson et al., 2002). In Canada, decreases in annual *Q* have been observed in the Pacific Climatic region (1960–1997) (Burn and Elnur, 2002) and in northern Canada (1964–2003) (Dery and Wood, 2005), as well as southern Canada (1967–1996) (Zhang et al., 2001). Predominantly increasing trends in *Q* were found in the continental USA (1944–1993) in particular for moderate and low quantiles, but there was regional variability (Lins and Slack, 1999) and often trends in streamflow were not entirely consistent with changes in precipitation and temperature (1948–1988) (Lettenmaier et al., 1994). Therefore, single site studies of streamflow trends should be examined in their regional context before any extrapolation of the results is made.

Glaciers and snow

In glacierized basins, summer streamflow has been found to increase due to glacier melt (e.g., Birsan et al., 2005; Pellicciotti et al., 2010) but also to decrease in areas where the glacier mass is past the critical point (e.g., Stahl and Moore, 2006). A review of other observations of glacier runoff changes can be found in Casassa et al. (2009). Single site case studies, like our Oberried example above or the study of Ye et al. (2005) of a glacier in Tianshan, show that summer runoff increases are primarily correlated with summer temperature rises and secondarily with precipitation increases. Pellicciotti et al. (2010) demonstrated that spring and summer streamflow increased for selected glacierised basins in the Swiss Alps, in relation to an increase in temperature and decrease in the seasonal snowpack. They also showed a shift in the timing of runoff due to earlier melt onset. However, they found that the magnitude and sign of trends vary with different time periods, in particular for those periods that include phases of positive glacier mass balance. Birsan et al. (2005) found a strong relation between upward streamflow trends and glacier coverage especially for summer moderate and low flow quantiles, which represent the snow and ice-melt contribution to flow. Similarly, Hodgkins (2009) found that higher summer flows were present in glaciated basins compared to non-glaciated ones during a shift from a cold to a warm phase of the PDO. In terms of melt, warming may also result in a shift in the seasonality and timing of flow (Pellicciotti et al., 2010). In several Canadian rivers, ice conditions have been found to begin and end earlier in more recent years (Zhang et al., 2001; Burn and Elnur, 2002). These observations suggest that temperature effects on streamflow trends should be a focus point of any trend detection study in mountainous regions, especially those with glaciers.

Summary

Streamflow trend detection is presented in four steps: (1) exploratory data analysis, (2) trend test methods and statistics, (3) testing for statistical significance, and (4) assessing the causality of streamflow trends. Trend detection is always connected with the choice of a time period, which should reflect the purpose of the analysis and be mindful of long-term climate oscillations that could be present. Streamflow trend attribution in mountainous regions to its causes is nontrivial, because it is difficult to separate the combination of precipitation and

temperature effects on runoff generation in high altitude catchments, the seasonal processes of snow accumulation and delayed snow melt, and the effect of the retreat and thinning of glaciers. A survey of studies highlights that streamflow trends are regionally dependent and should be investigated on a seasonal basis together with changes in precipitation and air temperature in order to capture the essence of streamflow change and its possible causes, in particular in glacierized basins.

Bibliography

Birsan, M. V., Molnar, P., Burlando, P., and Pfaundler, M., 2005. Streamflow trends in Switzerland. *Journal of Hydrology*, **314**, 312–329.

Burn, D. H., and Elnur, M. A. H., 2002. Detection of hydrologic trends and variability. *Journal of Hydrology*, **255**, 107–122.

Casassa, G., Lopez, P., Pouyaud, B., and Escobar, F., 2009. Detection of changes in glacial runoff in alpine basins: examples from North America, the Alps, central Asia and the Andes. *Hydrological Processes*, **23**, 31–41.

Cohn, T. A., and Lins, H. F., 2005. Nature's style: naturally trendy. *Geophysical Research Letters*, **32**, L23402, doi:10.1029/2005GL024476.

Dery, S. J., and Wood, E. F., 2005. Decreasing river discharge in northern Canada. *Geophysical Research Letters*, **32**, L10401, doi:10.1029/2005GL022845.

Glaciological reports (1881–2008). The Swiss Glaciers: Yearbooks of the Cryospheric Commission of the Swiss Academy of Sciences (SCNAT) published since 1964 by VAW, ETH Zurich, No. 1–124, (http://glaciology.ethz.ch/swiss-glaciers/).

Helsel, D. R., and Hirsch, R. M., 1992. Statistical methods in water resources. Studies in Environmental Science 49, Elsevier, Amsterdam, the Netherlands.

Hodgkins, G. A., 2009. Streamflow changes in Alaska between the cool phase (1947–1976) and the warm phase (1977–2006) of the Pacific Decadal Oscillation: the influence of glaciers. *Water Resources Research*, **45**, W06502, doi:10.1029/2008WR007575.

Huss, M., Farinotti, D., Bauder, A., and Funk, M., 2008. Modelling runoff from highly glacierized alpine drainage basins in a changing climate. *Hydrological Processes*, doi:10.1002/hyp.7055.

IPCC, 2007. Climate Change 2007. Fourth Assessment report of the Intergovernmental Panel on Climate Change, Synthesis Report, Geneva, Switzerland, 104 p.

Khaliq, M. N., Ouarda, T. B. M. J., Gachon, P., Sushama, L., and St-Hilaire, A., 2009. Identification of hydrological trends in the presence of serial and cross correlations: A review of selected methods and their application to annual flow regimes of Canadian rivers. *Journal of Hydrology*, **368**, 117–130.

Kundzewicz, Z. W., and Robson, A. J., 2004. Change detection in hydrological records – a review of the methodology. *Hydrological Sciences Journal*, **49**(1), 7–19.

Laternser, M., and Schneebeli, M., 2003. Long-term snow climate trends of the Swiss Alps (1931–99). *International Journal of Climatology*, **23**, 733–750.

Lettenmaier, D. P., Wood, E. F., and Wallis, J. R., 1994. Hydro-climatological trends in the continental US, 1948.88. *Journal of Climate*, **7**(4), 586–607.

Lins, H. F., and Slack, J. R., 1999. Streamflow trends in the United States. *Geophysical Research Letters*, **26**(2), 227–230.

Livezey, R. E., and Chen, W. Y., 1983. Statistical field significance and its determination by Monte Carlo techniques. *Monthly Weather Review*, **111**, 46–59.

Pellicciotti, F., Bauder, A., and Parola, M., 2010. Effect of glaciers on streamflow trends in the Swiss Alps. *Water Resources Research*, doi:10.1029/2009WR009039, in print.

Peterson, B. J., Holmes, R. M., McClelland, J. W., Vörösmarty, C. J., Lammers, R. B., Shiklomanov, A. I., Shiklomanov, I. A., and Rahmstorf, S., 2002. Increasing discharge to the Arctic Ocean. *Science*, **298**, 2171–2173.

Scherrer, S. C., and Appenzeller, C., 2004. Trends in Swiss Alpine snow days: The role of local- and large-scale climate variability. *Geophysical Research Letters*, **31**, L13215, doi:10.1029/2004GL020255.

Stahl, K., and Moore, R. D., 2006. Influence of watershed glacier coverage on summer streamflow in British Columbia. *Canada. Water Resource Research*, **42**, W06201, doi:10.1029/2006WR005022.

Stewart, I. T., 2009. Changes in snowpack and snowmelt runoff for key mountain regions. *Hydrological Processes*, **23**, 78–94.

Ye, B., Yang, D., Jiao, K., Han, T., Jin, Z., Yang, H., and Li, Z., 2005. The Urumqi river source Glacier No. 1, Tiashan, China: changes over the past 45 years. *Geophysical Research Letters*, **32**, L21504, doi:10.1029/2005GL024178.

Yue, S., Pilon, P., Phinney, B., and Cavadias, G., 2002. The influence of autocorrelation on the ability to detect trend in hydrological series. *Hydrological Processes*, **16**, 1807–1829.

Zhang, X., Harvey, K. D., Hogg, W. D., and Yuzyk, T. R., 2001. Trends in Canadian streamflow. *Water Resources Research*, **37**(4), 987–998.

Cross-references

Characteristics of Snow and Glacier Fed Rivers in Mountainous Regions with Special Reference to Himalayan Basins
Climate Change and Glaciers
Glacier Hydrology
Deglaciation
Hydrologic Cycle and Snow
Hydrological Response in Glacierized Basins
Runoff Generation
Runoff Observations
Snow Hydrology
Water Balance in the Glacierized Region

STRUCTURAL GLACIOLOGY

Michael J. Hambrey
Centre for Glaciology, Institute of Geography & Earth Sciences, Aberystwyth University, Aberystwyth, Ceredigion, UK

Synonyms

Glacier structure

Definition

Structural glaciology is the study of depositional and deformational structures in glaciers on all scales.

Structural glaciology

Glaciers demonstrate a wide range of structures that reflect their dynamic behavior. Such structures resemble those in rocks found in mountain belts, and as such, glaciers can serve as large-scale models of rock deformation

(Hambrey and Lawson, 2000). Interest in structural glaciology dates back to the early days of glaciology as a science, when pioneers such as James Forbes and John Tyndall investigated glaciers in the European Alps. However, it took the leap in understanding of the mechanics of glacier flow, triggered by Glen and Nye in the 1950s, and the subsequent introduction of structural geological principles to provide the basis for modern understanding of structures in glaciers.

Today, our knowledge of the structures of valley glaciers is well-founded, but up-scaling these ideas to ice sheets is still in its infancy. Structural glaciology is important not only for understanding glacier dynamics, but also in explaining water-routing through glaciers and glacial depositional landforms.

Glacier structures reflect both ductile and brittle deformation, and sometimes a combination of the two. Interpretation of structures requires consideration of two main concepts. Just as in rocks, ice is subject to multiple phases of deformation, referred to as "polyphase deformation." The early structures form in the upper reaches of the glacier, with later structures forming below and commonly overprinting pre-existing structures, resulting in complex associations of intersecting features. The second concept is that of cumulative (or finite) strain, since structures, once formed, continue to evolve under changing stress regimes. Adding increments of strain gives the cumulative strain, and may reflect both simple shear and pure shear. Such strains are expressed graphically as strain ellipses. They may be determined from direct measurements of velocity or by means of numerical modeling, supported by detailed 3-D mapping in the field (Hambrey and Lawson, 2000).

Before being subject to deformation, glacier ice is generally stratified from the progressive accumulation of snow and its conversion to *firn*. Internal deformation of ice under the action of gravity modifies and overprints this "primary structure." The most important ductile structures are:

- *Foliation*, which is a discontinuously layered structure originating from the simple shear and pure shear of pre-existing inhomogeneities, including stratification (Figure 1).
- *Folds*, which occur on scales from centimeters to kilometers, and reflect progressive compression or shear.
- *Boudinage*, a structure difficult to spot, but having the appearance of a string of sausages (from the French "boudin"); it results from ductility contrasts between different types of ice.
- *Ogives*, which are light and dark bands of clean and dirty ice respectively that commonly form below icefalls.

Brittle structures are dominated by *crevasses* – open V-shaped fractures in the ice, formed where ice is under tensile stress. They can be several tens of meters deep and several meters wide and are the main hazard to travel over glaciers, especially when snow-covered. Related to crevasses are *crevasse traces* which are closed water- or snow-filled crevasses, or tensional veins where the bounding ice walls have not physically separated. In addition, there are a variety of faults illustrating visible displacements, with thrust-faults being of particular importance through their role in recycling debris from the bed. A well illustrated account of glacier structures may be found in Hambrey and Alean (2004) and in their website, www.swisseduc.ch/glaciers/earth_icy_planet/glaciers05-en.html.

Structural Glaciology, Figure 1 Foliation in Gornergletscher, Switzerland, looking down-glacier toward the Matterhorn.

With different parts of a glacier developing their own distinctive suites of structures, depending on whether they are subject to shear, compression, or extension, the resulting structural assemblages may be of considerable complexity. Extensional flow regimes are dominated by crevasses and crevasse traces, the latter especially providing an historical record of dynamic regimes that may no longer exist. Compressive flow regimes, particularly at the base of an icefall typically show longitudinal foliation at the margins and arcuate foliation (derived from crevasse traces) across the middle. Within these structures folds on various scales can be identified. Icefalls may severely modify or even obliterate earlier structures. In the compressive zone near the snout foliation may be folded, whilst low-angle thrusts may develop, all superimposed on the aforementioned assemblages. Surge-type glaciers are a special case, and although they demonstrate all of the above attributes, they are further characterized by looped moraines and pervasive thrusting.

Understanding structures on glaciers aids interpretation of depositional landforms, including moraines dominated by folding and thrusting of ice and sediment, and of longitudinal ridges related to foliation, or transverse ridges related to crevassing. Thus, glacial geomorphological mapping needs to embrace knowledge of structural processes in the glaciers themselves.

Summary

Structural glaciology involves the investigation through mapping and 3-D analysis of the structures observed within glaciers. Analysis follows a structural geological approach on the grounds that glacier ice deforms in a manner resembling processes occurring in metamorphic rocks close to the melting temperature. The original primary structure comprises stratification of snow, firn, and ice in the accumulation area. Secondary structures include both brittle and ductile forms. Of these, brittle structures include crevasses, crevasse traces, faults, and thrusts; whereas ductile structures include foliation, folding, and boudinage. Structural glaciology is of fundamental importance in evaluating debris entrainment and transfer, and the subsequent deposition of sediment as landforms.

Bibliography

For a comprehensive review of structural glaciology

Hambrey, M. J., and Lawson, W., 2000. Structural styles and deformation fields in glaciers: a review. In Maltman, A. J., Hubbard, B., and Hambrey, M. J. (eds.), *Deformation of Glacial Materials*. London: Geological Society Special Publication 176, pp. 59–83.

For a layperson's account of glacier structures

Hambrey, M. J., and Alean, J., 2004. *Glaciers*. Cambridge: Cambridge Univ. Press. Chapter 5.
Illustrating a wide range of glacier structures. Available from World Wide Web: http://www.swisseduc.ch/glaciers/earth_icy_planet/glaciers05-en.html.

Cross-references

Crevasses
Englacial Processes
Forbes Band
Formation and Deformation of Basal Ice
Ogives
Sediment Entrainment, Transport, and Deposition

SUBGLACIAL BOREHOLE INSTRUMENTATION

Philip R. Porter
Division of Geography and Environmental Sciences, School of Life Sciences, University of Hertfordshire, Hatfield, Hertfordshire, UK

Definition

Subglacial borehole instrumentation: Instruments inserted via boreholes into the glacier substrate, usually used to measure basal motion and physical and hydraulic properties of basal sediments.

Introduction

Where glaciers overlie a sedimentary substrate, both sliding (Glacier Sliding) and deformation of subglacial sediments may contribute to total forward motion (Dynamics of Glaciers and Glacier Motion/Ice Velocity), yet the processes that control the partitioning of basal motion between sliding and deformation are not fully understood. This problem has arisen partially due to a lack of in situ monitoring of mechanical and hydrological conditions (Glacier Hydrology) at the ice-bed interface. However, hot-water drilling allows direct access to the ice-bed interface and direct monitoring of the processes of glacier basal motion (Subglacial Processes) is then made possible via the use of instrumented boreholes.

Much of the pioneering work to develop subglacial borehole instrumentation was carried out at Trapridge Glacier, Yukon Territory, Canada. Instruments are installed into the glacier substrate using a borehole percussion hammer, the operation of which is described in detail by Blake et al. (1992). Briefly, this comprises a 2 m long tubular structure around which is mounted a striker or "hammer" that can be repeatedly raised and dropped onto an anvil at the base of the hammer by an operator at the glacier surface. Subglacial instruments are housed within a "sheath" or attached to a "finger" at the base of the hammer below the anvil and the resultant percussive force drives the subglacial instrument progressively deeper into the substrate (see Blake et al., 1992).

This technique has been successfully used to install instruments into the substrate of Trapridge Glacier (e.g., Blake et al., 1992; Blake et al., 1994; Fischer and Clarke, 1997a; Fischer and Clarke, 1997b; Fischer et al., 1999; Kavanaugh and Clarke, 2001), Storglaciaren, Sweden (e.g., Iverson et al., 1994; Hooke et al., 1997; Fischer et al., 1998), Unteraargletscher, Switzerland (Fischer et al., 2001), and Bakaninbreen, Svalbard (e.g., Porter et al., 1997; Porter and Murray, 2001; Murray and Porter, 2001). Inevitably however, there are limitations associated with installing instruments in situ remotely from the surface beneath thick ice, aside from the obvious logistical demands. Firstly, the hot-water drilling process itself is likely to evacuate sediment from the base of the borehole to a depth of several decimeters (Blake et al., 1992) and it will inevitably take some time for sediment to intrude into the resultant void and for hydraulic and sedimentary equilibrium conditions to be reestablished. Secondly, although insertion depth can be monitored at the surface with an estimated accuracy of 0.01 m, exact placement of the sensor with respect to the ice-bed interface will always be unknown and careful interpretation of results is therefore required. Notwithstanding these issues, subglacial borehole instruments have the capacity to yield much useful information concerning basal motion and the factors that control it.

Measuring sliding

In order to effectively assess the relative contributions to glacier motion of sliding and sediment deformation, some independent measure of both these components of flow is required. Drag-spools are simple devices that give a continuous, quantitative measure of basal sliding. These instruments were first deployed beneath Trapridge Glacier (Blake et al., 1994). The drag-spool consists of a miniature multi-turn potentiometer attached to a spool, around which is wound several meters of thin string. This string passes out through a sealed plastic housing and is attached to a brass insertion tip. This tip is anchored in the subglacial sediment using the percussion hammer, while the drag-spool itself remains frozen and fixed into the borehole. As the glacier moves over its bed, the anchor remains fixed within the sediment and string is paid out from the spool. As displacement between drag-spool and anchor increases, progressive rotation of the spool and potentiometer causes a resistance change within the device (Figure 1). This resistance change is logged at the glacier surface and is converted to a glacier sliding rate using calibration data gained prior to installation.

Initial results from Trapridge Glacier indicated that basal sliding accounted for 50–70% of total glacier flow with measured basal sliding rates ranging from 40 to 80 mm d^{-1} and that peak sliding rates corresponded with rises in basal water pressure (as opposed to peak water pressure, Subglacial Drainage System) as recorded by pressure transducers suspended in boreholes (Blake et al., 1994). This latter finding conflicts with observations made elsewhere that peak glacier velocity and peak basal water pressure (Meltwater Pressure) generally coincide (e.g., Iken and Bindschadler, 1986; Kamb et al., 1985; Kamb and Engelhardt, 1987; Hooke et al., 1989). Fischer and Clarke (1997a) suggested that the relationship between sliding rate and rising basal water pressure observed beneath Trapridge Glacier could be explained in terms of "stick-slip" sliding processes operating at the ice-bed interface. As basal water pressure begins to rise, local strain buildup in the ice is released as basal ice decouples from the bed and the resultant increase in basal sliding is registered by drag-spools. However, once this strain is released, further increases in basal water pressure do not result in subsequent increases in the rate of basal sliding.

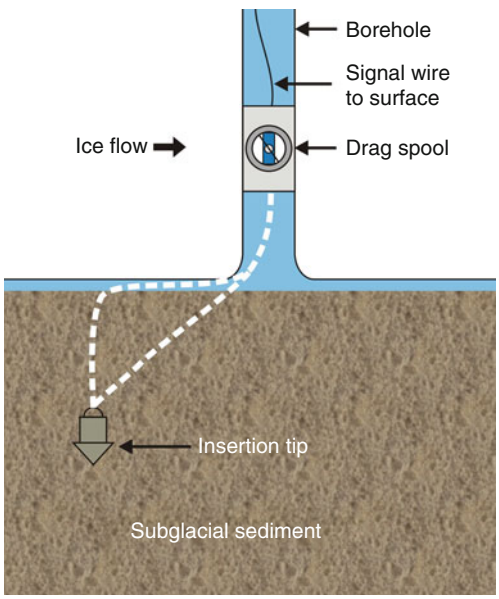

Subglacial Borehole Instrumentation, Figure 1 Conceptual diagram of a drag-spool installed within a borehole. Note the two possible locations for the drag-spool string (dashed white line) that will be dictated by sediment stiffness. Adapted from Blake et al. (1994) and Murray (1998).

Measuring deformation

Measuring the deformation rate of basal sediments is important both in order to assess the contribution of basal sediment deformation to flow and to obtain baseline stress and strain data to enhance understanding of the rheological properties of basal sediments. Qualitative measurements of total strain have been obtained from Trapridge Glacier using a resin filled tube (a "bed cast") inserted into basal sediments. A heating wire catalyzes the resin after several days of monitoring and the resultant deformation of the now-rigid tube once removed from basal sediments provides an indication of the extent of basal sediment deformation (Blake et al., 1992). A development of the bed cast is a rubber rod to which strain gauges are bonded (Blake et al., 1992). The advantage of the rubber rod over the bed cast technique is that a continuous, qualitative measure of strain rate can be obtained.

Quantitative assessment of the deformation rate of basal sediments can be made using strings of tilt cells inserted into basal sediments. A basic assumption is that, once installed, the tilt cell behaves as a clast within the basal sediment, becoming realigned as the sediment deforms. Thus, as the sediment deforms, the cell is tilted (Figure 2). Tilt cells are installed as "strings" of two or three cells allowing assessment of the vertical deformation profile and differentiation of the tilt data time series allows computation of instantaneous strain rates (Blake et al., 1992).

Tilt cells comprise two main designs. Firstly, leaf spring tilt cells comprise two pendulum weights attached to leaf springs orientated perpendicular to one another to which strain gauges are bonded. As the cell is tilted, the pendulum weights flex the leaf springs causing the resistance of the strain gauges to change. This resistance change can be related to angle of tilt once the cell has been calibrated. The operation and calibration of leaf spring tilt cells are described in detail by Blake et al. (1992).

Secondly, electrolytic tilt cells consist of a series of metal electrodes housed in a chamber containing a suitable electrolytic fluid that contacts the electrodes. Electrodes are arranged around a central common

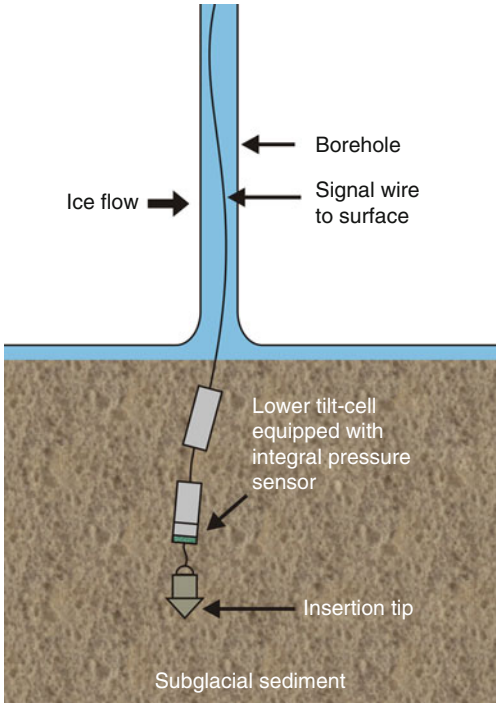

Subglacial Borehole Instrumentation, Figure 2 Conceptual diagram of a string of tilt cells installed within deforming subglacial sediments. Adapted from Murray (1998).

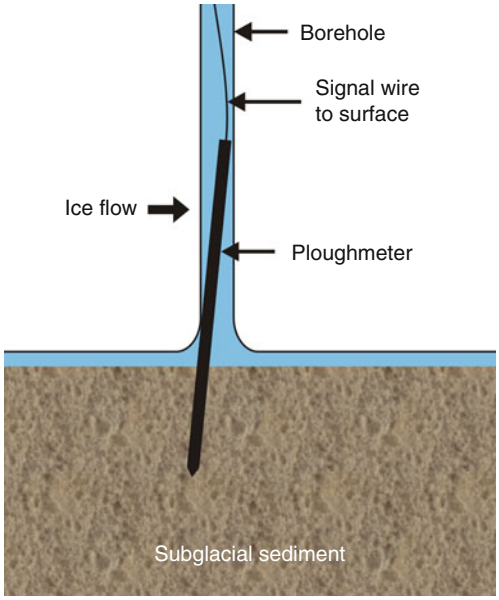

Subglacial Borehole Instrumentation, Figure 3 Conceptual diagram of a ploughmeter installed within a borehole. As the glacier flows over the sedimentary substrate, the ploughmeter is dragged through subglacial sediments. Adapted from Fischer and Clarke (1994) and Murray (1998).

electrode. In a dual-axis cell, four electrodes are mounted around the central electrode at 90° intervals in a "cross" configuration. As the cell is tilted, the outer electrodes either become immersed in, or emerge from the electrolyte depending on their position with respect to the central electrode, while the level of electrolyte in contact with the central electrode remains constant at all times. This has the effect of changing the impedance between electrodes that can be measured as a voltage change and related to angle and direction of tilt once the cell has been calibrated. Full details of the operation and calibration of electrolytic tilt cells are described by Blake et al. (1992) and Porter and Murray (2001). Strings of tilt cells are inserted vertically into basal sediments using a percussion hammer.

Data obtained from tilt cells installed beneath Trapridge Glacier show that subglacial strain rates vary in amplitude and polarity over short timescales. Observed negative strain rates may be a function of extrusion flow (Blake et al., 1992). A development of the basic electrolytic tilt cell was deployed at Bakaninbreen, Svalbard by Porter and Murray (2001). Here, the lowermost cell in each string was equipped with a pore-pressure transducer to allow relationships between sediment strain rates and water pressure fluctuations within deforming sediments to be assessed. At the time of installation, Bakaninbreen was in the late-active phase of a prolonged surge (Glacier Surging). Tilt cells were installed up- and down-glacier of a surge front. In common with observations at Trapridge Glacier, strain rates at Bakaninbreen fluctuated over short timescales, with periods of both positive and negative strain evident in the time series. Strain rates up-glacier of the surge front were an order of magnitude higher than those measured down-glacier of the surge front. Interpretation of tilt cell records indicated that deformation of basal sediments comprised the dominant mode of basal motion. However, in contrast to observations made elsewhere (e.g., Boulton and Hindmarsh, 1987), no consistent relationship between water pressure within basal sediments and strain rate was observed.

Assessing sediment properties

The ploughmeter is a device that enables assessment of properties of subglacial sediments such as viscosity and yield strength, and may also be used to infer sediment texture and assess glacier sliding rates (Fischer and Clarke, 1994; Fischer and Clarke, 1997b). The device consists of a steel rod onto which strain gauges are bonded near one end. It is hammered into the bed, such that all strain gauges are fully immersed into the subglacial sediment. The upper section of the device then becomes trapped in the ice, while the lower portion is dragged through the underlying sediment, effectively acting as an ice-entrained clast (Figure 3). This "plowing" action sets up stresses within the ploughmeter that cause changes in the resistance of the strain gauges that are monitored at the glacier surface and translated into an applied force by application of

calibration data. A full description of the device and its calibration is provided by Fischer and Clarke (1994).

Ploughmeter data makes it possible to obtain estimates of the rheological properties of basal sediments. If sediment is assumed to behave as a Newtonian viscous fluid, then an estimate of viscosity can be obtained. If sediment is assumed to behave as an ideal plastic solid (Plastic Flow and Plastic Deformation), then an estimate of yield strength (Bed Strength) can be obtained. Viscosity estimates gained from Trapridge Glacier range from 3.0×10^{-9} to 3.1×10^{10} Pa s (Fischer and Clarke, 1994), while estimates from ploughmeters installed beneath Bakaninbreen range from 1.1×10^{10} to $4.3\ 10^{10}$ Pa s (Porter, 1997). Applying an idea plastic solid model, yield strength estimates at Trapridge Glacier range from 48 to 57 kPa (Blake et al., 1992) and at Bakaninbreen they range from 6.6 to 411.6 kPa with high recorded values thought to be caused by ploughmeters moving into areas of frozen bed and by implication, areas of high-yield strength sediment (Murray and Porter, 2001). Comparison of calculated basal shear stress and yield strength data gained from ploughmeters at Bakaninbreen, allowed areas where stress exceeds yield strength to be identified (Porter et al., 1997). By implication, these areas are likely to be experiencing basal sediment deformation, an assertion that is supported by subsequent studies (Porter and Murray, 2001). Ploughmeter data has also been used to estimate glacier sliding rate based on clast collision frequency and associated force variations recorded by the device (Fischer and Clarke, 1997b).

The rheological properties of basal sediments have also been measured using a subglacial borehole instrument that has some conceptual similarities with the ploughmeter, dubbed a "dragometer" (Iverson et al., 1994). The device comprises a conical "fish" attached to a wire that runs up to a load cell installed in a metal tube that is trapped in the base of a borehole. The signal recorded by the load cell varies according to the forces applied to the "fish" which in turn relate to the residual strength of the subglacial sediments through which the "fish" is being dragged. A full description of the dragometer is provided by Iverson et al. (1994).

Data obtained from a dragometer installed in the bed of Storglaciären indicate an average residual strength for subglacial sediments of ~55 kPa (Iverson et al., 1994).

Hydraulic properties

Where ploughmeter data is collected alongside basal water pressure data from borehole pressure transducers, conclusions can be drawn regarding both the functioning of the basal hydrological system (e.g., Fischer et al., 1999; Kavanaugh and Clarke, 2001) and the hydraulic properties of basal sediments (e.g., Fischer et al., 1998; Fischer et al., 2001). Ploughmeter records and associated borehole water pressure records from Trapridge Glacier show good correspondence, with diurnal force fluctuations correlating well with large and rapid fluctuations in basal water pressure (Fischer et al., 1999). However, this correlation was observed to be in phase with one ploughmeter and out of phase with another in an adjacent borehole and was thought to arise from the existence of time-varying "sticky spots" beneath the glacier, whereby one ploughmeter is moving through an area where ice-bed coupling is enhanced (a "sticky spot") in response to a reduction of basal water pressure (Fischer et al., 1999).

Subsequent observations at Trapridge Glacier demonstrated that a series of "spring events" resulted in the failure of borehole pressure transducers and yielded significant force responses on ploughmeters, interpreted to result from strong basal motion associated with the establishment of a connected drainage system (Subglacial Drainage System) beneath the glacier (Kavanaugh and Clarke, 2001).

Ploughmeters installed beneath Unteraargletscher, Switzerland also displayed an inverse correlation with basal water pressure recorded by borehole pressure transducers and a significant time lag between the two signals (Fischer et al., 2001). This lag was thought to reflect the time taken for a pressure pulse in the subglacial drainage system to propagate through basal sediments to the insertion depth of the ploughmeter, thereby reducing sediment strength and associated force exerted on the ploughmeter. Assuming this assertion is correct, the hydraulic diffusivity of basal sediments can be estimated and values from Unteraargletscher range from 1.3×10^{-6} to 2.3×10^{-6} $m^2\ s^{-1}$. A similar ploughmeter force–water pressure relationship was measured at Storglaciären (Fischer et al., 1998) and again, using the propagation velocity of water pressure waves through basal sediments, calculated hydraulic diffusivity was found to range from 1.9×10^{-6} to 3.6×10^{-6} $m^2\ s^{-1}$.

Data concerning the hydraulic properties of basal sediments have also been obtained from pressure transducers installed within tilt cells inserted into basal sediments at Bakaninbreen (Porter and Murray, 2001). Here it was found that pore-water pressure fluctuations, as recorded by pore-pressure sensors installed within tilt cells, lagged borehole water pressure fluctuations by 37–49 h. Because the depth of insertion of tilt cells and integral pore-pressure sensor can be measured during installation, it is again possible to estimate hydraulic diffusivity using the propagation velocity of water pressure waves. Diffusivity values at Bakaninbreen range between 1.2×10^{-6} and 5.0×10^{-6} $m^2\ s^{-1}$ and if a value for specific storage of till is assumed then hydraulic conductivity of basal sediments can also be estimated. At Bakaninbreen, diffusivity ranges from 3.2×10^{-7} to 7.7×10^{-8} m s^{-1} which is in good agreement with values derived elsewhere (e.g., Boulton and Dent, 1974; Fountain, 1994; Iverson et al., 1994; Hubbard et al., 1995; Murray and Clarke, 1995). It is interesting to note, however, that at Bakaninbreen there is no clear relationship between basal water pressure fluctuations and strain rate as measured by tilt sensors (Porter and Murray, 2001). Furthermore, ploughmeters also showed only occasional strong relationships with basal water pressure and in contrast to observations made

elsewhere these correlations were mostly positive (Murray and Porter, 2001). At Bakaninbreen, it appears that there is weak coupling between sediment strength and water pressure fluctuations and that force fluctuations recorded by ploughmeters may arise from variations in granulometry (Granulometry) or ice-bed coupling (Murray and Porter, 2001).

Summary

The installation of subglacial borehole instruments has the capacity to yield much useful information concerning basal motion and the properties of basal sediments. Installation of borehole instrumentation is, however, logistically demanding and given inevitable uncertainties over instrument placement with respect to the ice-bed interface when installing remotely beneath thick ice, careful interpretation of results is required.

Bibliography

Blake, E. W., Clarke, G. K. C., and Gérin, M. C., 1992. Tools for examining subglacial bed deformation. *Journal of Glaciology*, **38**(130), 388–396.

Blake, E. W., Fischer, U. H., and Clarke, G. K. C., 1994. Direct measurement of sliding at the glacier bed. *Journal of Glaciology*, **40**(136), 595–599.

Boulton, G. S., and Dent, D. L., 1974. The nature and rates of post-depositional changes in recently deposited till from south-east Iceland. *Geografiska Annaler*, **56A**(3–4), 121–134.

Boulton, G. S., and Hindmarsh, R. C. A., 1987. Sediment deformation beneath glaciers: rheology and geological consequences. *Journal of Geophysical Research*, **92**(B9), 9059–9082.

Fischer, U. H., and Clarke, G. K. C., 1994. Ploughing of subglacial sediment. *Journal of Glaciology*, **40**(134), 97–106.

Fischer, U. H., and Clarke, G. K. C., 1997a. Stick-slip sliding behaviour at the base of a glacier. *Annals of Glaciology*, **24**, 390–396.

Fischer, U. H., and Clarke, G. K. C., 1997b. Clast collision frequency as an indicator of glacier sliding rate. *Journal of Glaciology*, **43**(145), 460–466.

Fischer, U. H., Iverson, N. R., Hanson, B., Hooke, R. Le B, and Jansson, P., 1998. Estimation of hydraulic properties of subglacial till from ploughmeter measurements. *Journal of Glaciology*, **44**(148), 517–522.

Fischer, U. H., Clarke, G. K. C., and Blatter, H., 1999. Evidence for temporally varying 'sticky spots' at the base of Trapridge Glacier, Yukon Territory, Canada. *Journal of Glaciology*, **45**(150), 352–360.

Fischer, U. H., Porter, P. R., Schuler, T., Evans, A. J., and Gudmundsson, G. H., 2001. Hydraulic and mechanical properties of glacial sediments beneath Unteraargletscher, Switzerland: Implications for glacier basal motion. *Hydrological Processes*, **15**(18), 3525–3540.

Fountain, A. G., 1994. Borehole water-level variations and implications for the subglacial hydraulics of South Cascade Glacier, Washington State, USA. *Journal of Glaciology*, **40**(135), 293–304.

Hooke, R. L., Calla, P., Holmlund, P., Nilsson, M., and Stroeven, A., 1989. A 3 year record of seasonal variations in surface velocity, Storglaciaren, Sweden. *Journal of Glaciology*, **35**(120), 235–247.

Hooke, R. Le B, Hanson, B., Iverson, N. R., Jansson, P., and Fischer, U. H., 1997. Rheology of till beneath Storglaciären, Sweden. *Journal of Glaciology*, **43**(143), 172–179.

Hubbard, B. P., Sharp, M. J., Willis, I. C., Nielsen, M. K., and Smart, C. C., 1995. Borehole water-level variation and the structure of the subglacial hydrological system of Haut Glacier d'Arolla, Valais, Switzerland. *Journal of Glaciology*, **41**(139), 572–583.

Iken, A., and Bindschadler, R. A., 1986. Combined measurements of sunglacial water pressure and surface velocity of Findelengletscher, Switzerland: conclusions about drainage system and sliding mechanism. *Journal of Glaciology*, **32**(110), 101–119.

Iverson, N. R., Jansson, P., and Hooke, R. Le B, 1994. In-situ measurement of the strength of deforming subglacial till. *Journal of Glaciology*, **40**(136), 497–503.

Kamb, B., and Engelhardt, H., 1987. Waves of accelerated motion in a glacier approaching surge: the minisurges of Variegated Glacier, Alaska, USA. *Journal of Glaciology*, **33**(113), 27–46.

Kamb, B., Raymond, C. F., Harrison, W. D., Engelhardt, H., Echelmeyer, K. A., Humphrey, N., Brugman, M. M., and Pfeffer, T., 1985. Glacier surge mechanism: 1982–1983 surge of variegated glacier, Alaska. *Science*, **227**(4686), 469–479.

Kavanaugh, J. L., and Clarke, G. K. C., 2001. Abrupt glacier motion and reorganization of basal shear stress following the establishment of a connected drainage system. *Journal of Glaciology*, **47**(158), 472–480.

Murray, T., 1998. Assessing the paradigm shift: deformable glacier beds. *Quaternary Science Reviews*, **16**, 995–1016.

Murray, T., and Clarke, G. K. C., 1995. Black-box modelling of the subglacial water system. *Journal of Glaciology, Journal of Geophysical Research*, **100**(B6), 10,231–10,245.

Murray, T., and Porter, P. R., 2001. Basal conditions beneath a soft-bedded polythermal surge-type glacier: Bakaninbreen, Svalbard. *Quaternary International*, **86**(1), 103–116.

Porter, P. R., 1997. Glacier surging: subglacial sediment deformation and ice-bed coupling. *Unpublished PhD thesis*, University of Leeds.

Porter, P. R., and Murray, T., 2001. Hydrological and mechanical properties of till beneath Bakaninbreen, Svalbard. *Journal of Glaciology*, **47**(157), 167–175.

Porter, P. R., Murray, T., and Dowdeswell, J. A., 1997. Sediment deformation and basal dynamics beneath a glacier surge front: Bakaninbreen, Svalbard. *Annals of Glaciology*, **24**, 21–26.

Cross-references

Bed Strength
Dynamics of Glaciers
Glacier Hydrology
Glacier Motion/Ice Velocity
Glacier Sliding
Glacier Surging
Plastic Flow
Subglacial Drainage System
Subglacial Processes

SUBGLACIAL DRAINAGE SYSTEM

Bryn Hubbard
Centre for Glaciology, Institute of Geography and Earth Sciences, Aberystwyth University, Aberystwyth, Ceredigion, Wales, UK

Synonyms

Basal drainage system; Subglacial hydrological system; Subglacial hydrology

Definition

Subglacial drainage systems are formed from the hydraulic pathways that contain and transfer water located close to the contact between an ice mass and its substrate. These pathways are commonly considered to be spatially discrete, e.g., flowing through dendritic networks of channels, or spatially dispersed, e.g., flowing through diffuse films. The subglacial drainage system can exchange water with the overlying englacial drainage system and the underlying groundwater drainage system. Extensive reviews of subglacial drainage have been provided by, among others, Flowers (2008), Hooke (1989), Hodgkins (1997) and Hubbard and Nienow (1997).

Introduction and significance

The investigation of subglacial hydrology forms an important branch of glaciology. However, it is important to note that well-developed subglacial drainage systems only exist at the bases of those temperate or polythermal ice masses that are at least partly warm based (i.e., are characterized by a basal interface that is melting).

Reconstructing the nature of, and changes in, subglacial drainage is important for several reasons. First, water located at the basal interface of any ice mass exerts a strong control over the way in which that ice mass moves. In general, the presence of subglacial water acts as a lubricating layer, speeding basal motion up by partially decoupling the ice mass from its (otherwise harder and/or rougher) substrate (e.g., Iken and Bindschadler, 1986). It is not only the presence of water that is important here but probably also the quantity of water stored at the glacier bed and its pressure (e.g., Bartholomaus et al., 2008), both of which change at a variety of timescales both across a single ice mass and between different ice masses. Recent so-called dynamic thinning, caused by a postulated increase in the delivery of surface-derived meltwater to the base of Greenland outlet glaciers (Zwally et al., 2002), is considered to be responsible for their speed up and retreat. Similarly, increases in lubricating basal meltwater may be responsible for at least facilitating, if not triggering, rapid speedups during the surge phase of *surge-type* glaciers (e.g., Kamb et al., 1985). Systematic representations of the links between subglacial drainage and ice mass motion are also important to computer modelers to allow them to improve the realism of their models of ice mass response to climate change.

Second, most of the water delivered from ice masses exits via the subglacial drainage system. In different settings and at different times, this water can represent a resource or a hazard. In terms of resource, subglacial water may be tapped directly from the glacier bed or shortly after it leaves the glacier for hydroelectric power generation and/or potable uses. Downstream extraction for domestic use and agricultural irrigation represents crucial supply issues in many populous but otherwise arid areas of the world. Understanding controls over changes in water delivery from glaciers at a variety of timescales is important for scientists to predict future supplies and to inform planners and policymakers. For example, ~2 billion people are dependent on water supplied by rivers that are fed by Himalayan glaciers – many of which are currently receding and are anticipated to continue to do so over the next several decades to centuries. Subglacial drainage can also be more immediately hazardous. *Jökulhlaups*, for example, probably represent the most visible hazard associated with subglacial water delivery. Taking the name from type events in Iceland, jökulhlaups (literally "glacier leaps") are large floods associated with the catastrophic release of water from subglacial lakes located in areas of high geothermal heating (e.g., Bjornsson, 2002). For example, the Grimsvötn jökulhlaup of 1996 discharged ~3 km^3 of meltwater in just over 2 days across its *sandur* (at a peak discharge of ~45,000 $m^3 s^{-1}$), causing an estimated ~US$15 million of infrastructural damage. Understanding the relationships between subglacial drainage and water delivery is therefore important to modelers, engineers, planners, and policymakers.

Third, water may be stored for long periods in isolated subglacial lakes, allowing distinctive microbiological forms to evolve. There are currently believed to be approaching 300 such lakes beneath the Antarctic Ice Sheet alone (Siegert et al., 2005; Smith et al., 2009), the largest known of which is Lake Vostok with surface dimensions of ~200 km and ~50 km, and an approximate volume of 5,400 km^3. In addition to the biological interest provided by these water bodies, research updates revealing ever-larger numbers of such lakes (e.g., Popov and Masolov, 2007) and the existence of hydraulic linkages between them (Fricker et al., 2007; Wingham et al., 2006) will probably transform our understanding of ice sheet drainage and motion over the next few decades.

Methods of empirical investigation

Revealing the dynamic nature of subglacial drainage represents a fundamental challenge for glaciologists. However, gaining direct access to undisturbed meltwater drainage pathways is at best challenging and at worst impossible. Consequently, researchers of subglacial drainage are continually developing and applying new methods and techniques (summarized in Hubbard and Glasser, 2005). Approaches to studying subglacial drainage fall into five broad categories.

1. *Investigations of the quantity and character of meltwater discharged from ice masses*. Analysis of the meltwater flowing from ice masses can provide important information about the subglacial flow pathways that it has followed beneath that ice mass. Simple discharge records, for example, when compared with the timing of water input to the ice mass, can inform on water transit times and water storage within the englacial and subglacial systems. Similarly, analysis of variations in

the fine sediment particles suspended in the water and of the chemical (ionic) composition of the water itself can also provide information relating to how long that water has spent at the glacier bed and under what broad conditions. For example, water that is routed efficiently through large subglacial channels will have little time to interact with reactive subglacial sediments and will be characterized by a rapid and peaked hydrograph. It will also be solute-poor relative to subglacial water that has been routed via diffuse flow pathways. Changes in the ratio of suspended sediment concentration to discharge of subglacially routed waters can be related to changes in subglacial sediment supply, with increases for example indicating the headward growth of channels or the tapping of new areas of the glacier bed (Fenn et al., 1985).

2. *Tracer investigations*. Tracers such as salt or, more commonly fluorescent dye (which can be detected at far lower concentrations and therefore requires lower dosages), can be added to the glacier drainage system at known locations and recorded as it exits the ice mass. The resulting breakthrough curve of dye concentration plotted against time can provide valuable information relating to the flow pathways followed by the water between the input location and the measuring station. For example, a rapidly-reached, narrow and flashy breakthrough curve will represent flow through a hydraulically more efficient, probably channelized, drainage system than a strongly attenuated breakthrough curve. In addition to such qualitative judgments, breakthrough curve analysis can yield quantitative data such as minimum flow speeds (given by dividing the straight-line distance between the input location and the measuring station by the time separating the tracer injection from the measurement) and dispersion (given by an analysis of the spread of the breakthrough curve relative to its velocity) (e.g., Burkimsher, 1983; Nienow et al., 1998).
3. *Proglacial bedrock investigations.* The methods outlined above provide useful information relating to real-time subglacial hydrological processes, but they are spatially integrated over large, and possibly unknown, flow lengths. In contrast, investigations of drainage-related geomorphic features etched into glaciated surfaces provide excellent spatial discrimination but poor temporal discrimination. Such studies can yield important information relating, in particular, to the structure and morphometry of the former subglacial drainage system and its individual flow pathways (e.g., Walder and Hallet, 1979). This information can be used to approximate former subglacial water discharges and pressures, and this information can in turn be used to inform reconstructions of former ice mass movement (e.g., Sharp et al., 1989).
4. *Borehole-based investigations*. Borehole-based investigations of subglacial drainage systems suffer from neither excessive spatial integration nor excessive temporal integration. However, the approach is logistically demanding, typically requiring multiple boreholes to be drilled to the bed of the ice mass concerned and then instrumented. Such boreholes can be created mechanically, which has the advantage of providing ice cores as well as access to the base of the ice mass (but which is logistically demanding and slow, typically yielding meters to tens of meters of borehole length per day), or thermally by pressurized hot water, which provides no ice core but which typically yields hundreds of meters of borehole length per day. Each such borehole provides direct access to a specific location on the ice mass bed, which can be investigated via several techniques. For example, our understanding of the relationship between subglacial drainage and ice mass motion has been revolutionized by synchronous borehole-based measurements of subglacial water pressure and surface measurements of ice velocity (Bartholomaus et al., 2008; Iken and Bindschadler, 1986). Where arrays of such boreholes can be drilled, spatial variability in multiple hydrological properties can be measured at high temporal resolution, providing the most detailed records available to date relating to subglacial drainage (e.g., Hubbard et al., 1995).
5. *Remotely sensed (geophysical and satellite-based) investigations.* The most widespread spatial coverage of information relating to subglacial drainage is supplied by remotely sensed data. However, while this information does provide good spatial coverage, it commonly yields first-order data that need to be interpreted in terms of specific subglacial properties. Such interpretations are rarely unequivocal, although inversion techniques can be used to infer hydrologically modulated variations in basal motion from satellite-based interferometric synthetic aperture radar (InSAR) (e.g., Magnusson et al., 2007). Ice surface radar also has the capacity to identify the presence of water at the ice-bed contact, and repeated radar measurements at a given site have the capacity to reveal changes in the nature of the interface and the distribution of that water (e.g., Smith et al., 2007). Recently, for example, repeat satellite-derived altimetry has revealed spatial variations in the surface elevation of ice masses pointing to coordinated, episodic water transfer between sub-ice lakes (e.g., Carter et al., 2009).

Configuration and change

Subglacial drainage networks are generally considered to fall into one of two broad categories. *Discrete* drainage systems are formed from a network of channels that may be cut upward into the overlying ice (named Röthlisberger channels or R-channels) (Röthlisberger, 1972) or cut downward into the underlying bedrock (named Nye channels or N-channels) (Nye, 1973). These networks are of broadly dendritic form, composed of small feeder streams

linking to create branch streams that in turn join to create a small number of trunk channels, each progressively flowing at low pressure and therefore drawing water from their smaller feeders. In contrast, *distributed* drainage systems form diffuse or anastomosing networks that do not evolve into progressively larger, lower-pressure channels. Such distributed systems can be formed of films, linked cavities, permeating flow through sub-ice sediments, or so-called canals, cut both upward into ice and downward into underlying sediments. These systems generally transfer water more slowly and at higher pressure for a given discharge than do discrete networks. Switching between the two can therefore raise or lower the pressure of subglacial meltwater, and correspondingly, ice motion (e.g., Fowler, 1987).

Controls over the structure of subglacial drainage systems, and of the individual flow pathways that comprise them, can change at a variety of timescales. Many subglacial drainage systems are correspondingly subject to spatial and temporal changes. For example, a change in the configuration of subglacial drainage pathways – from discrete (operating at relatively low pressure) to distributed (operating at relatively high pressure) – has been closely associated with the initiation of glacier surges (e.g., Fowler, 1987; Kamb et al., 1985 above). However, the most commonly recognized changes in subglacial drainage result from meteorological seasonality. Accordingly, the subglacial drainage system beneath mid-latitude valley glaciers can change from a diffuse network through the winter, when minimal and spatially diffuse water inputs derive from basal melting alone, to the summer, when large fluxes of surface meltwater are delivered to the glacier bed via point sources such as crevasses and moulins. However, this drainage system replacement is not instantaneous but time transgressive, with repeated dye tracer studies revealing that the distributed system is gradually replaced in an upglacier direction (dictated by the retreat of the surface snow line) by the channelized system (Nienow et al., 1998). While such wholesale seasonal changes are improbable at larger ice masses, subglacial drainage change is likely where summer surface melting occurs near the margins of large ice sheets, and over decades to centuries at larger ice masses that are subject to changing climatic conditions.

Conclusions

Subglacial drainage systems are important, diverse, and subject to change at various temporal and spatial scales. They are important because they (a) exert a strong influence on the basal motion of ice masses, (b) represent potential hazards and resource, and (c) can form large subglacial lakes. Subglacial drainage systems are diverse because they are composed of flow pathways that can have different specific configurations, which can in turn exist adjacent to each other and change over time. However, investigating the structure and dynamics of subglacial drainage systems is difficult, requiring major logistical effort and continual development of new methods and technologies. Despite these developments, the most pressing challenges that face researchers in the future are similar to those that have confronted researchers in the past. The most fundamental of these is probably still to obtain high (spatial- and temporal-) resolution records of changes in subglacial drainage systems at the ice mass scale, and to determine the physical controls responsible for those changes. This information would then be applied in a structured manner to allow future drainage system changes and meltwater discharges to be predicted. Additionally, perhaps the most interesting developments in the field of our exploration of subglacial drainage systems will come from obtaining the first direct access to major subglacial lakes, as well as their continued geophysical investigation.

Bibliography

Bartholomaus, T. C., et al., 2008. Response of glacier basal motion to transient water storage. *Nature Geoscience*, **1**, 33–37.

Bjornsson, H., 2002. Subglacial lakes and jokulhlaups in Iceland. *Global and Planetary Change*, **35**, 255–271.

Burkimsher, M., 1983. Investigations of glacier hydrological systems using dye tracer techniques: observations at Pasterzengletscher, Austria. *Journal of Glaciology*, **29**, 403–416.

Carter, S. P., et al., 2009. Dynamic distributed drainage implied by the flow evolution of the 1996–1998 Adventure Trench subglacial lake discharge. *Earth and Planetary Science Letters*, **283**, 24–37.

Fenn, C. R., et al., 1985. An evaluation of the use of suspended sediment rating curves for the prediction of suspended sediment concentration in a proglacial stream. *Geografiska Annaler: Series A, Physical Geography*, **67**, 71–82.

Flowers, G. E., 2008. Subglacial modulation of the hydrograph from glacierized basins. *Hydrological Processes*, **22**, 3903–3918.

Fowler, A. C., 1987. A theory of glacier surges. *Journal of Geophysical Research – Solid Earth and Planets*, **92**, 9111–9120.

Fricker, H. A., et al., 2007. An active subglacial water system in West Antarctica mapped from space. *Science*, **315**, 1544–1548.

Hodgkins, R., 1997. Glacier hydrology in Svalbard, Norwegian High Arctic. *Quaternary Science Reviews*, **16**, 957–973.

Hooke, R. L., 1989. Englacial and subglacial hydrology: a qualitative review. *Arctic and Alpine Research*, **21**, 221–233.

Hubbard, B., Glasser, N. F., 2005. *Field Techniques in Glaciology and Glacial Geomorphology*. West Sussex, England: Wiley.

Hubbard, B., and Nienow, P., 1997. Alpine subglacial hydrology. *Quaternary Science Reviews*, **16**, 939–955.

Hubbard, B. P., et al., 1995. Borehole water-level variations and the structure of the subglacial hydrological system of Haut Glacier d'Arolla, Valais, Switzerland. *Journal of Glaciology*, **41**, 572–583.

Iken, A., and Bindschadler, R. A., 1986. Combined measurements of subglacial water pressure and surface velocity of Findelengletscher, Switzerland: conclusions about drainage system and sliding mechanism. *Journal of Glaciology*, **32**, 101–119.

Kamb, B., et al., 1985. Glacier surge mechanism – 1982–1983 surge of variegated glacier, Alaska. *Science*, **227**, 469–479.

Magnusson, E., et al., 2007. The impact of jokulhlaups on basal sliding observed by SAR interferometry on Vatnajokull, Iceland. *Journal of Glaciology*, **53**, 232–240.

Nienow, P., et al., 1998. Seasonal changes in the morphology of the subglacial drainage system, Haut Glacier d'Arolla, Switzerland. *Earth Surface Processes and Landforms*, **23**, 825–843.
Nye, J., 1973. Water at the bed of the glacier. *International Association of Hydrological Sciences Publication*, **95**, 189–194.
Popov, S. V., and Masolov, V. N., 2007. Forty-seven new subglacial lakes in the 0–110 degrees E sector of East Antarctica. *Journal of Glaciology*, **53**, 289–297.
Röthlisberger, H., 1972. Water pressure in intra- and subglacial channels. *Journal of Glaciology*, **11**, 177–204.
Sharp, M., et al., 1989. Structure and Stability of the Former Subglacial Drainage System of the Glacier De Tsanfleuron, Switzerland. *Earth Surface Processes and Landforms*, **14**, 119–134.
Siegert, M. J., et al., 2005. A revised inventory of Antarctic subglacial lakes. *Antarctic Science*, **17**, 453–460.
Smith, A. M., et al., 2007. Rapid erosion, drumlin formation, and changing hydrology beneath an Antarctic ice stream. *Geology*, **35**, 127–130.
Smith, B. E., et al., 2009. An inventory of active subglacial lakes in Antarctica detected by ICESat (2003–2008). *Journal of Glaciology*, **55**, 573–595.
Walder, J. S., and Hallet, B., 1979. Geometry of former subglacial water channels and cavities. *Journal of Glaciology*, **23**, 335–346.
Wingham, D. J., et al., 2006. Rapid discharge connects Antarctic subglacial lakes. *Nature*, **440**, 1033–1036.
Zwally, H. J., et al., 2002. Surface melt-induced acceleration of Greenland ice-sheet flow. *Science*, **297**, 218–222.

Cross-references

Glacier Surging
Subglacial Lakes, Antarctic

SUBGLACIAL LAKES, ANTARCTIC

John C. Priscu
Department of Land Resources and Environmental Sciences, Montana State University, Bozeman, MT, USA

Definition

Subglacial lakes: Water-filled cavities located beneath glaciers and ice sheets

Introduction

Visual observations of what appeared to be floating ice by the crews of Russian aircraft flying missions over the Antarctic continent provide the earliest evidence of subglacial lakes. These observations were later verified by airborne radio-echo sounding, seismic data, and satellite imagery. We now know that more than 150 lakes exist beneath the Antarctic continent, and are connected by networks of subglacial streams and rivers, which may initiate and maintain rapid ice flow and should be considered in ice-sheet mass balance assessments (Siegert, 2000; Siegert et al., 2005). Morphometric data indicate that the volume of Antarctic subglacial lakes alone exceeds 10,000 km^3, with Lake Vostok (~5,400 km^3) and Lake 90° E (1,800 km^3) being the largest (Studinger et al., 2003, 2004). Antarctica lakes may hold over 8% of all lacustrine freshwater on Earth, enough to cover the whole continent with a uniform water layer ~1 m thick. Simple balance calculations reveal that the average water residence time in the subglacial zone of Antarctica is equal to ~1,000 years, which is likely a reflection of low liquid water generation rates coupled with slow rates of drainage of liquid water through subglacial environments (Priscu et al., 2008).

Over 60% of the lakes lie within 50 km of a local ice divide and 88% lie within 100 km of a local divide (Priscu et al., 2008) (Figure 1). The association of subglacial lakes with local ice divides and regions of high hydraulic fluid potential leads to a fundamental question concerning the evolution of subglacial lake environments: Does the evolving ice sheet control the location of subglacial lakes or does the fixed lithospheric character necessary for lake formation (e.g., basal morphology, geothermal flux, or the nature of sub-ice aquifers) constrain the evolution of ice sheet catchments? With the exception of central West Antarctica (where lakes are few), we know little about either the lithospheric character along these catchment boundaries or the history of their migration as discerned from layering within the ice sheet.

Origins of subglacial lakes

Deep subglacial lakes have probably been stable through many glacial cycles and may have developed novel ecosystems, in contrast to the shallower lakes (Dowdeswell and Siegert, 1999, 2002). Although arguments have been made for the tectonic origins of deep subglacial lakes, there continues to be debate about whether subglacial lakes in Antarctica reside in active tectonic basins or along old inactive zones of structural weakness that once provided guidance for subglacial erosion (Bell et al., 2006). Much of East Antarctica, where the majority of subglacial lakes have been found so far, is thought to have assembled 500–800 million years ago. However, our knowledge of the interior of the continent, the distribution of major tectonic boundaries, and old zones of structural weakness is limited due to a paucity of data.

The biology of subglacial systems

Much attention is currently focused on the exciting possibility that the subglacial environments of Antarctica may harbor microbial ecosystems under thousands of meters of ice, which have been isolated from the atmosphere for as long as the continent has been glaciated (20–25 million years). Profiles of prokaryotic cell abundance through the entire Vostok core reveal a two to sevenfold higher cell density in accretion ice than the overlying glacial ice, implying that Lake Vostok is a source of bacterial carbon beneath the ice sheet (Priscu et al., 1999; Christner et al., 2006). Data from the overlying accretion ice have been used to show that bacterial densities within Lake Vostok surface waters should be between 150 and 460 cells mL^{-1}.

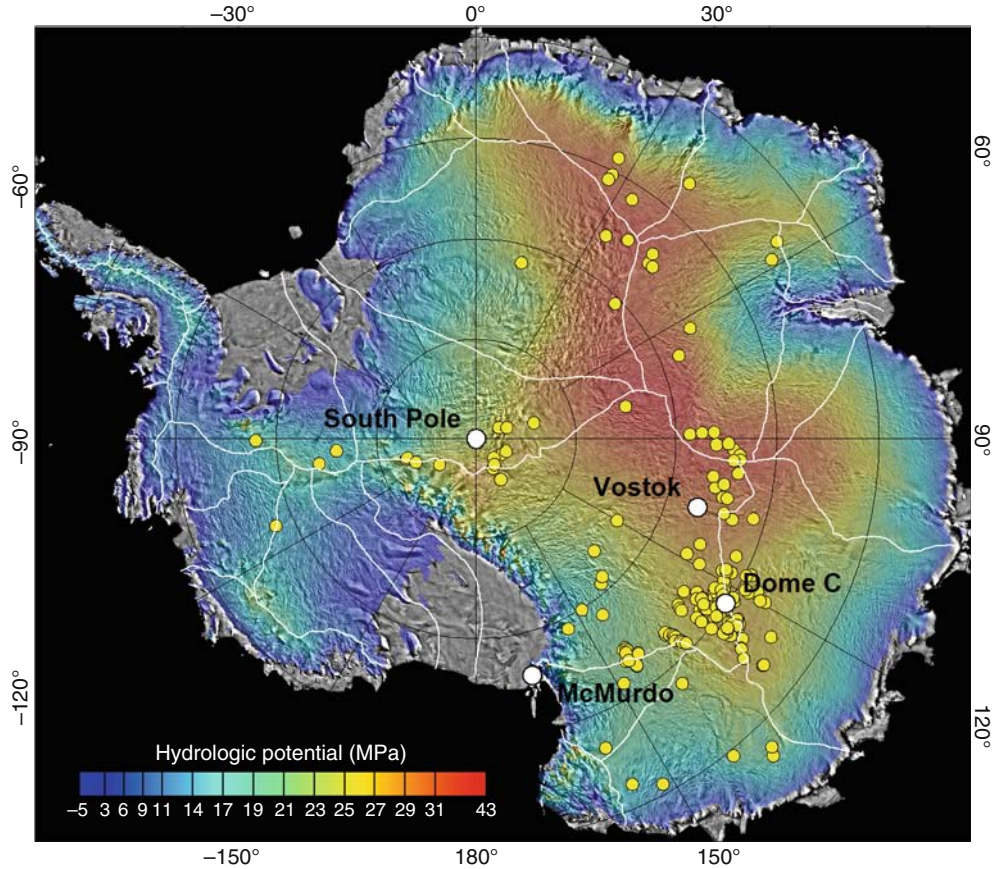

Subglacial Lakes, Antarctic, Figure 1 Map of Antarctica showing location of known subglacial lakes (*yellow circles*) in relation to ice divides (*white lines*) and hydrologic potential (*colored contours*). Modified from Priscu et al., 2008).

These values indicate that Lake Vostok is a highly oligotrophic system supporting relatively low levels of biomass. Sequence data obtained from DNA encoding for small subunit ribosomal RNA revealed that the microorganisms within Lake Vostok do not represent an evolutionarily distinct subglacial biota (Priscu and Christner, 2004). The time scale of isolation within Lake Vostok (>15 $\times 10^6$ year) is not long in terms of bacterial evolution compared to their 3.7 $\times$ 10^9 year history on Earth, and studies of species divergence of other bacteria have shown that species level divergence may take ~100 million years. Evidence for the presence of hydrothermal input is supported by the recent interpretation of He^3:He^4 data from accretion ice, which implies that there may be extensive faulting beneath Lake Vostok, which could introduce geochemical energy sources to the southern part of the lake (Petit et al., 2005). If this emerging picture is correct, Lake Vostok could harbor a unique assemblage of organisms fueled by chemical energy. While it seems inevitable that viable microorganisms from the overlying glacial ice, and in sediment scoured from bedrock adjacent to the lake, are regularly seeded into the lake, the question remains whether these or preexisting microorganisms have established an ecosystem in Lake Vostok. If a microbial ecosystem were found to exist within the water or sediment of these subsurface environments, they would represent one of the most extreme and unusual ecosystems on Earth.

Summary

The past 10 years have seen the study of subglacial lakes go from a curiosity to a focus of scientific research. We now know that more than 150 lakes exist beneath the Antarctic ice sheets, some of which rival the largest surface lakes on our planet in terms of size. These lakes appear to play a role in ice sheet dynamics (Llubes et al., 2006; Bell et al., 2007) and may harbor novel microorganisms, the mediate important microbial transformations. Several national programs plan to penetrate the subglacial environment over the next 5 years (Priscu et al., 2005). Data from these expeditions will yield the first samples from these environments and will change our view of polar regions.

Bibliography

Bell, R. E., Studinger, M., Fahnestock, M. A., and Shuman, A., 2006. Tectonically controlled subglacial lakes on the flanks of the Gamburtsev Subglacial Mountains. *East Antarctica Geophysical Research Letters*, **33**, L02504, doi:10.1029/2005GL025207.

Bell, R. E., Studinger, M., Shuman, A., Fahnestock, M. A., and Joughin, I., 2007. Large subglacial lakes in East Antarctica at the onset of fast-flowing ice streams. *Nature*, **445**, 904–907.

Christner, B. C., Royston-Bishop, G., Foreman, C. M., Arnold, B. R., Tranter, M., Welch, K. A., Lyons, W. B., Tsapin, A. I., Studinger, M., and Priscu, J. C., 2006. Limnological conditions in subglacial Lake Vostok, Antarctica. *Limnology and Oceanography*, **51**, 2485–2501.

Dowdeswell, J. A., and Siegert, M. J., 2002. The physiography of modern Antarctic subglacial lakes. *Global and Planetary Change*, **35**, 221–236.

Dowdeswell, J. A., and Siegert, M. J., 1999. The dimensions and topographic setting of Antarctic subglacial lakes and implications for large-scale water storage beneath continental ice sheets. *Geological Society of America Bulletin*, **111**, 254–263.

Llubes, M., Lanseau, C., and Rémy, F., 2006. Relations between basal condition, subglacial hydrological networks and geothermal flux in Antarctica. *Earth and Planetary Science Letters*, **241**, 655–662.

Petit, J. R., Alekhina, I., and Bulat, S., 2005. Lake Vostok, Antarctica: Exploring a Subglacial Lake and Searching for Life in an Extreme Environment. In Gargaud, M., Barbier, B., Martin, H., and Reisse, J. (eds.), *Lectures in Astrobiology, Vol. I, Series: Advances in Astrobiology and Biogeophysics*. Berlin: Springer, pp. 227–288.

Priscu, J. C., and Christner, B. C., 2004. Earth's icy biosphere. In Bull, A. T. (ed.), *Microbial Biodiversity and Bioprospecting*. Washington, DC: American Society for Microbiology Press, pp. 130–145.

Priscu, J. C., Adams, E. E., Lyons, W. B., Voytek, M. A., Mogk, D. W., Brown, R. L., McKay, C. P., Takacs, C. D., Welch, K. A., Wolf, C. F., Kirstein, J. D., and Avci, R., 1999. Geomicrobiology of subglacial ice above Lake Vostok, Antarctica. *Science*, **286**, 2141–2144.

Priscu, J. C., Kennicutt, M. C., III, Bell, R. E., Bulat, S. A., Ellis-Evans, J. C., Lukin, V. V., Petit, J.-R., Powell, R. D., Siegert, M. J., and Tabacco, I., 2005. Exploring subglacial antarctic lake environments. *EOS, Transactions of the American Geophysical Union*, **86**, 193–197.

Priscu, J. C., Christner, B. C., Foreman, C. M., and Royston-Bishop, G., 2006. Biological Material in Ice Cores. In Elias, S. A. (ed.), *Encyclopedia of Quaternary Sciences, Vol. 2*. UK: Elsevier, pp. 1156–1166.

Priscu, J. C., Tulaczyk, S., Studinger, M., Kennicutt, M. C., II, Christner, B. C., and Foreman, C. M., 2008. Antarctic subglacial water: origin, evolution and ecology. In Vincent, W., and Laybourn-Parry, J. (eds.), *Polar Lakes and Rivers*. UK: Oxford University Press, pp. 119–135.

Siegert, M. J., Carter, S., Tabacco, I., Popov, S., and Blankenship, D. D., 2005. A revised inventory of Antarctic subglacial lakes. *Antarctic Science*, **17**, 453–460.

Siegert, M. J., 2000. Antarctic subglacial lakes. *Earth Science Reviews*, **50**, 29–50.

Studinger, M., Karner, G. D., Bell, R. E., Levin, V., Raymond, C. A., and Tikku, A. A., 2003. Geophysical models for the tectonic framework of the Lake Vostok region, East Antarctica. *Earth and Planetary Science Letters*, **216**, 663–677.

Studinger, M., Bell, R. E., and Tikku, A. A., 2004. Estimating the depth and shape of subglacial Lake Vostok's water cavity from aerogravity data. *Geophysical Research Letters*, **31**, L12401, doi:10.1029/2004GL019801.

SUBGLACIAL PROCESSES

Sean Fitzsimons[1], Reginald Lorrain[2]
[1]Department of Geography, University of Otago, Dunedin, New Zealand
[2]Département des sciences de la Terre et de l'Environnement, Université Libre de Bruxelles, Bruxelles, Belgium

Synonyms

Basal processes; Subglacial sediment deformation

Definition

Subglacial processes are the thermal and mechanical processes immediately above and below the boundary between the ice and glacier bed that control glacier motion and processes of erosion, transportation, and deposition.

Introduction

In glaciology the term subglacial processes encompasses the thermal, mechanical, hydrological, and chemical processes that occur a few meters beneath and above the contact between a glacier and its substrate. These processes are of considerable importance because they determine the behavior of glaciers and ice sheets and are responsible for a range of phenomena that are expressed as spatial and temporal variations in the dynamic behavior of glaciers over a range of scales. Consideration of subglacial processes generally excludes processes that occur beneath floating ice masses. A recent, thorough review of subglacial processes was published by Clarke (2005).

Glacier beds

The nature and complexity of subglacial processes are controlled by the thermal conditions at the bed and by the material properties of the bed. The key thermal boundary condition at a glacier bed is the pressure melting point, which is the melting point of ice adjusted for pressure exerted by the weight of overlying ice. If the temperature is below the pressure melting point the ice is classified as cold-based and there is no bulk meltwater at the bed. In contrast, if the basal temperature is at the pressure melting point the glacier is classified warm-based and meltwater is freely available. Bed materials range from hard beds, which are characterized by lithified materials, to unconsolidated sediments such as till, sands, and gravels (soft beds). An additional complexity is that particles eroded from the bed can become entrained within the base of glaciers to form basal ice, which has mechanical properties that are quite distinct from ice of a meteoric origin (Fitzsimons, 2006). The combination of thermal and mechanical conditions, which can be simplified to three schematic velocity structures, are summarized by Figure 1.

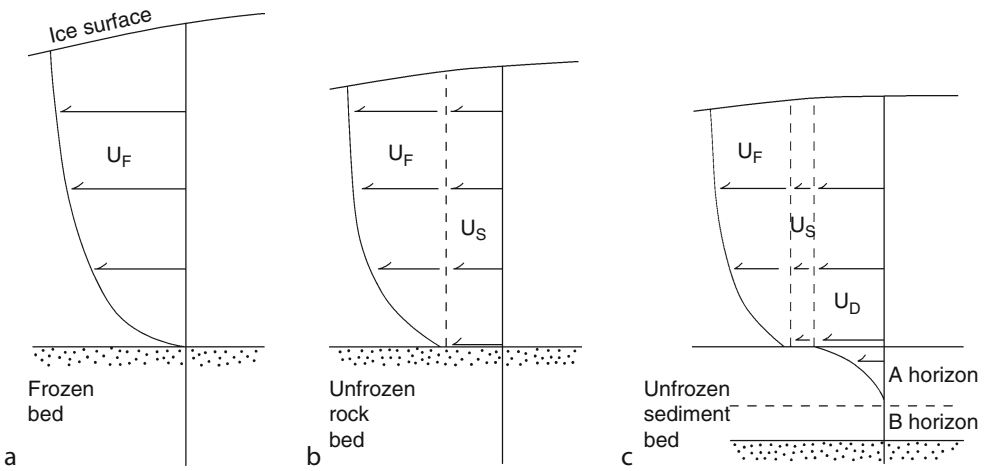

Subglacial Processes, Figure 1 Vertical velocity distributions associated with different thermal and mechanical conditions at glacier beds: (**a**) Shows the velocity distribution associated creep of ice above a frozen bed composed of rock or sediment. (**b**) Shows the velocity profile associated with creep and sliding above a warm rigid bed. (**c**) Shows the velocity profile associated with creep, sliding, and subglacial sediment deformation above a warm deformable bed. From Boulton (1996). Reprinted from the *Journal of Glaciology* with permission of the International Glaciological Society.

Thermal and mechanical processes

Most of our knowledge of subglacial processes comes from warm-based glaciers that have hard or soft beds. Warm, hard-bed glaciers are characterized by well-developed subglacial drainage systems, movement by basal sliding, and relatively high rates of erosion by processes of abrasion and plucking. Warm-based glaciers with soft beds are characterized by either rapid sliding that is facilitated by high subglacial water pressures that can uncouple the glacier from its bed, and/or result in deformation of subglacial sediment due to a decrease in shear strength of unconsolidated sediment caused by high pore water pressure.

An experiment conducted by Boulton (1979) beneath an Icelandic outlet glacier concluded that approximately 90% of glacier motion could be attributed to deformation of the uppermost 0.5 m of saturated till that formed the glacier bed. In such a situation, the "effective bed" of a glacier, that is, the surface below which there is no movement, is below the interface between the ice and the sediment. In the 1980s, seismic studies of active ice streams in Antarctica identified the presence of a layer of porous, saturated material beneath the ice, which was likely to be too weak to rigidly support the weight of the overlying ice, and therefore was probably undergoing deformation (Blankenship et al., 1986; Alley et al., 1986). The possibility that ice streams move principally by deformation of subglacial sediment forced a major rethinking of different chapters of glaciology and glacial geology that has been described as a paradigm shift (Boulton, 1986; Murray, 1997). This major shift in thinking has led to a large volume of published research on the nature of subglacial processes associated with warm-based glaciers underlain by soft beds.

A major focus of research into subglacial sediment deformation has involved investigations into processes beneath fast-flowing ice streams that drain the West Antarctic Ice Sheet. Although the ice streams only account for about 10% of the volume of the ice sheet they make up for up to 90% of the ice discharged to the ocean because they reach speeds of over 1,000 m/year, and are up to 60 km wide and 2,000 m thick. Despite numerous investigations into the basal processes associated with the fast flow of Antarctic ice streams it remains unclear whether the high velocities are sustained by subglacial sediment deformation, by fast sliding of ice over the substratum, or by a combination of both. In addition, studies of formerly glaciated landscapes show that ice streams also form on hard beds (Stokes and Clark, 2003), which suggests that the development of fast ice flow cannot be solely attributed to the presence of warm-based ice and a soft bed. A further complexity in our understanding of ice streams is that velocity can vary considerably over a range of timescales. For example, variations in the surface velocity of Whillans Ice Stream have been attributed to a single tidal cycle that is propagated through an ice shelf (Bindschadler et al., 2003), whereas the Kamb Ice Stream appears to have ceased flowing rapidly about 150 years ago. These studies, together with more recent research on the relationship between surface melting and acceleration of glacier flow (Zwally et al., 2002; Rignot and Kanagaratnam, 2006), demonstrate that the temporal variability of ice stream behavior forms an important component of understanding of the response of glaciers to climate change. The increase in velocity has been attributed to an increase in surface meltwater that rapidly migrates to the bed causing an increase in water pressure, which reduces effective normal stress causing accelerated sliding and/or subglacial sediment deformation.

Studying subglacial processes

Despite the difficulties of gaining direct access to glacier beds numerous successful field experiments have been conducted in such environments. The development of rapid hot-water drilling has facilitated the observation of subglacial conditions using cameras. Hot-water drilling has also enabled the deployment of a range of instruments designed to measure subglacial sediment deformation, sliding, bed strength, basal water pressures, and to sample subglacial sediment. Borehole-based instrumentation for observing and measuring subglacial processes has been reviewed by Fischer and Hubbard (2006).

Experiments have been conducted at Svartisen Subglacial Laboratory beneath Engabreen in Norway where Cohen et al. (2000) installed a concrete obstacle to measure bed shear stress. A later study in the laboratory was conducted by Iverson et al. (2003) who blasted a cavity in the bed and filled with it sediment to simulate subglacial till. After the ice closed over the cavity, the effective normal stress was experimentally controlled by changing the pore water pressure. The results showed that the sediment underwent shear at intermediate pore water pressures and that at higher pressures the ice moved over the till by plowing without deforming the sediment.

Uncertainties and questions raised by field experiments have stimulated laboratory experiments on the behavior of subglacial materials. This work has included direct shear tests on sediment collected from the bed of Antarctic ice streams (Kamb, 1991) and the construction of a ring shear device that permitted study of the mechanical behavior of materials under conditions of high shear strains (Iverson et al., 1997). These experiments concluded that the properties of deforming till exhibit the behavior of Coulomb (frictional) plastic material and that resistance to shear varies linearly with effective normal stress. The spatial and temporal variability of such processes has been highlighted by modeling studies, which suggested that local weakening of subglacial sediment could occur due to high pore water pressures in front of objects being dragged through a bed (Iverson, 1999). Similar measurements have been made with a "ploughmeter" to measure force and subglacial water pressure (Fischer et al., 2001). These data suggest that rapidly sliding glaciers might move by plowing through unconsolidated subglacial sediment rather than by penetrative deformation. Although the full complexity of the behavior of warm-based, soft-bed glaciers has yet to be fully understood, there is a clear consensus that the basal hydrological system controls the transient behavior of coupling between the glacier and its bed and whether movement is achieved by sliding or subglacial sediment deformation.

Our understanding of subglacial processes beneath cold-based glaciers with soft beds has also been advanced recently through a combination of field experiments conducted in tunnels excavated in glaciers, laboratory experiments, and modeling (Echelmeyer and Wang, 1987; Cuffey et al., 2000a, b; Fitzsimons et al., 1999, 2000). These studies have shown that cold-based glaciers can slide and ice-rich subglacial permafrost can be deformed and eroded (Figure 2).

Subglacial Processes, Figure 2 A 4.5 m thick excavation in deforming subglacial permafrost beneath Wright Lower Glacier in the McMurdo Dry Valleys, Antarctica. Measurements over 3 years demonstrate that deformation extends more than 3.5 m beneath the ice-permafrost boundary and that most deformation is accommodated by ice-rich layers between frozen sediment layers. The bolts and stakes have been used to measure strain and velocity over a period of 4 years.

Erosion, transportation, and deposition

In addition to acting as an important control of glacier dynamics, subglacial processes are also responsible for the processes of erosion, transportation and deposition that occur at the beds of glaciers. Exchanges of material between the bed and the glacier have two principal outcomes: the formation of a distinctive type of ice at the base of a glacier (basal ice) and the formation of distinctive erosional and depositional landforms. Basal ice is characterized by a relatively high debris content which frequently results in a stratified or banded appearance, high solute concentrations, and distinctive gas and isotopic composition, all of which distinguish the ice from overlying ice that has a meteoric origin. Studies of the chemistry of ice from the beds of glaciers have yielded new insights into the basal boundary conditions when the basal ice formed (Souchez et al., 1993; Souchez and Lorrain, 1991; Sleewaegen et al., 2003). For example, study of the stable isotope characteristics of basal ice exposed at the edge of the Greenland ice sheet suggested that there is considerable spatial variability in ice sheet erosion processes (Sugden et al., 1987). The presence of solid and dissolved contaminants together with associated changes in crystal structure and size result in markedly different mechanical behavior of basal ice from overlying meteoric ice. As a result, the lower few meters of glaciers are characterized by very high strain rates concentrated within the debris-bearing ice. For example, "amber ice" that occurs at the base of glaciers in the McMurdo dry valleys has been recognized as being soft compared to overlying white ice (Holdsworth and Bull, 1970). Later research on amber ice demonstrated that the small crystal size (<1 mm) is directly related to high strain rates (Cuffey et al., 2000b; Samyn et al., 2005).

The landforms left behind by formerly more extensive glaciers during the Pleistocene are testament to the processes that operate beneath glaciers. A wide variety of landforms have been used in a variety of ways to reconstruct the dimensions, behavior, and impact of glaciers on landscapes. However, there remains considerable uncertainty as to the origin of many distinctive landforms such as drumlins. Theories concerning their origin range from subglacial floods to instabilities in deforming beds to episodic erosion and depositional events. The most recent developments in understanding subglacial landforms have been driven by the acquisition of high definition remotely sensed imagery, both terrestrial and marine, that have permitted detailed mapping of glacial landforms such as lineations and moraines associated with ice streams (O'Cofaigh et al., 2002; Stokes and Clark, 2003).

Summary

The last few decades have seen enormous advances in understanding how glaciers interact with the substrates over which they flow. The central issue in our recently acquired understanding is the role of subglacial water as a means of uncoupling glaciers from their beds whether this is accomplished by rapid sliding, or subglacial sediment deformation. However, we have yet to develop an understanding of how spatial and temporal variability in subglacial processes is translated into the behavior of large glacial systems. Such an understanding is a prerequisite for the development of ice sheet models that parameterize subglacial processes.

Bibliography

Alley, R. B., Blankenship, D. D., Bentley, C. R., and Rooney, S. T., 1986. Deformation of till beneath ice stream B, West Antarctica. *Nature*, **322**, 57–59.

Bindschadler, R. A., King, M. A., Alley, R. B., Anandakrishnam, S., and Padman, L., 2003. Tidally controlled stick-slip discharge of a West Antarctic Ice Stream. *Science*, **301**, 1087–1091.

Blankenship, D. D., Bentley, C. R., Rooney, S. T., and Alley, R. B., 1986. Seismic measurements reveal a saturated porous layer beneath an active Antarctic ice stream. *Nature*, **322**, 54–57.

Boulton, G. S., 1979. Processes of glacier erosion on different substrata. *Journal of Glaciology*, **23**, 15–38.

Boulton, G. S., 1986. A paradigm shift in glaciology? *Nature*, **322**, 18.

Boulton, G. S., 1996. Theory of glacial erosion, transportation and deposition as a consequence of sediment deformation. *Journal of Glaciology*, **42**, 43–62.

Clarke, G. K. C., 2005. Subglacial Processes. *Annual Review of Earth and Planetary Sciences*, **33**, 247–276.

Cohen, D., Hooke, R., Le, B., Iverson, N. R., and Kohler, J., 2000. Sliding of ice past an obstacle at Engabreen, Norway. *Journal of Glaciology*, **46**, 599–610.

Cuffey, K. M., Conway, H., Gades, A., Hallet, B., Lorrain, R., Severinghaus, J. P., Steig, E. J., Vaughn, B., and White, J. W. C., 2000a. Entrainment at cold gacier beds. *Geology*, **28**, 351–354.

Cuffey, K. M., Conway, H., Gades, A., Hallet, B., Raymond, C. F., and Whitlow, S., 2000b. Deformation properties of subfreezing glacier ice: role of crystal size, chemical impurities, and rock particles inferred from in situ measurements. *Journal of Geophysical Research*, **105**(B12), 27,895–27,915.

Echelmeyer, K., and Wang, Z., 1987. Direct observations of basal sliding and deformation of glacial drift at subfreezing temperatures. *Journal of Glaciology*, **33**, 83–98.

Fischer, U. H., and Hubbard, B. P., 2006. Borehole-based subglacial instrumentation. In Knight, P. G. (ed.), *Glacier Science and Environmental Change*. Oxford: Blackwell, pp. 387–394.

Fischer, U. H., Porter, P. R., Schuler, T., Evans, A. J., and Gudmundsson, G. H., 2001. Hydraulic and mechanical properties of glacial sediments beneath Unteraargletscher, Switzerland: implications for glacier motion. *Hydrological Processes*, **15**, 3525–3540.

Fitzsimons, S. J., 2006. Mechanical behaviour and structure of the debris-rich basal ice layer. In Knight, P. G. (ed.), *Glacier Science and Environmental Change*. Oxford: Blackwell, pp. 329–335.

Fitzsimons, S. J., McManus, K. J., and Lorrain, R., 1999. Structure and strength of basal ice and substrate of a dry-based glacier: evidence for substrate deformation at sub-freezing temperatures. *Annals of Glaciology*, **28**, 236–240.

Fitzsimons, S. J., Lorrain, R., and Vandergoes, M., 2000. Behaviour of subglacial sediment and basal ice in a cold-based glacier. In Maltman, A. J., Hambrey, M. J., and Hubbard, B. (eds.), *Deformation of Glacial Materials*. Special Publication 176, Geological Society Publishing House, Bath, pp.181–190.

Holdsworth, G., and Bull, C., 1970. The flow law of cold ice; investigations on Meserve Glacier, Antarctica. *International Association of Hydrological Sciences Publication*, **86**, 204–216.

Iverson, N. R., 1999. Coupling between an glacier and a soft bed: II. Model results. *Journal of Glaciology*, **45**, 41–53.
Iverson, N. R., Baker, R. W., and Hooyer, T. S., 1997. A ring shear device for the study of till deformation: tests on a clayrich and a clay-poor till. *Quaternary Science Reviews*, **16**, 1057–1066.
Iverson, N. R., Cohen, C., and Hooyer, T. S., 2003. Effects of basal debris on glacier flow. *Science*, **301**, 81–84.
Kamb, B., 1991. Rheological nonlinearity and flow instability in the deforming bed mechanism of ice stream motion. *Journal of Geophysical Research*, **96**, 16585–16595.
Murray, T., 1997. Assessing the paradigm shift: deformable beds. *Quaternary Science Reviews*, **16**, 995–1016.
O'Cofaigh, C., Pudsey, C. J., Dowdeswell, J. A., and Morris, P., 2002. Evolution of subglacial bedforms along a paleo-ice stream, Antarctic Peninsula continental shelf. *Geophysical Research Letters*, **29**, 1199, doi:10.1029/2001GL01448.
Rignot, E., and Kanagaratnam, P., 2006. Changes in the velocity structure of the Greenland Ice Sheet. *Science*, **311**, 986–990.
Samyn, D., Svensson, A., Fitzsimons, S., and Lorrain, R., 2005. Ice crystal properties of amber ice and strain enhancement at the base of cold Antarctic glaciers. *Annals of Glaciology*, **40**, 185–190.
Sleewaegen, S., Samyn, D., Fitzsimons, S., and Lorrain, R., 2003. Equifinality of basal ice facies from an Antarctic cold-based glacier. *Annals of Glaciology*, **37**, 257–262.
Souchez, R., and Lorrain, R., 1991. *Ice Composition and Glacier Dynamics*. Berlin: Springer.
Souchez, R., Lemmens, M., Tison, J.-L., Lorrain, R., and Janssens, L., 1993. Reconstruction of basal boundary conditions at the Greenland Ice Sheet margin from gas composition in the ice. *Earth and Planetary Science Letters*, **118**(327–3), 33.
Stokes, C. R., and Clark, C. D., 2003. Laurentide ice streaming on the Canadian Shield: A conflict with the soft-bedded ice stream paradigm. *Geology*, **31**, 347–350.
Sugden, D. E., Knight, P. G., Livesey, N., Lorrain, R. D., Souchez, R. A., Tison, J.-L., and Jouzel, J., 1987. Evidence of two zones of debris entrainment beneath the Greenland ice sheet. *Nature*, **328**, 238–241.
Zwally, H. J., Adalati, W., Herring, T., Larson, K., Saba, J., and Steffen, K., 2002. Surface melt-induced acceleration of Greenland Ice-Sheet flow. *Science*, **297**, 218–222.

Cross-references

Bed Strength
Cold-Based Glaciers
Formation and Deformation of Basal Ice
Glacial Striations
Glacier Motion/Ice Velocity
Landforms of Glacial Erosion
Subglacial Drainage System

SUBGLACIAL VOLCANISM

Hugh Tuffen
Lancaster Environment Centre, Lancaster University, Lancaster, UK

Synonyms

Glaciovolcanism; Ice–volcano interaction

Definition

Strictly, volcanic activity beneath ice sheets or glaciers, but used generally to refer to volcanic eruptions where magma interacts with ice in any form, both on Earth and other planetary bodies (Glaciovolcanism). Subglacial volcanism may occur wherever volcanic vents are covered with bodies of ice, which may include small glaciers on the flanks of stratovolcanoes, substantial regional ice sheets, and even the Martian cryosphere (Smellie, 2000; Ice–Volcano Interactions).

Key localities of subglacial volcanism

Beneath past and present ice sheets: Iceland, Western Antarctic Ice Sheet, Antarctic Peninsula Ice Sheet, British Columbia.

At ice-covered stratovolcanoes: Andes, Cascades, Alaska, Aleutian Islands, Kamchatka

On other planets: Mars

Principal styles of subglacial volcanism

Tuya-building eruptions: Sustained, large-volume eruptions that melt through to the surface of ice sheets, forming distinctive "table mountains." Tuyas commonly consist of pillow lavas overlain by fragmental glassy volcanic deposits (hyaloclastites) that were emplaced within englacial lakes, and capped by subaerial lava flows formed when the ice surface was pierced (Smellie, 2000).

Tindar ridge-forming eruptions: eruptions from volcanic fissures beneath ice sheets that generate elongate ridges of pillow lavas and hyaloclastites. Example: Kalfstindar, Iceland (Smellie, 2000).

Magma–ice interaction at stratovolcanoes: interaction between lava or pyroclastic deposits and ice either on the flanks, or in the summit crater of a stratovolcano (Lescinsky and Fink, 2000).

The composition of magma erupted subglacially ranges from basalt to rhyolite (Smellie, 2000; McGarvie, 2009).

Hazards from subglacial volcanism

Melting of ice and snow can generate devastating meltwater floods (Guðmundsson et al., 1997; Glacier Lake Outburst Floods) and lahars (Major and Newhall, 1989). Explosive magma–meltwater interactions can lead to widespread ash fall.

Interesting features of subglacial volcanism

- The products of past subglacial eruptions can be used to reconstruct paleo-ice thicknesses in Iceland, Antarctica, and elsewhere (Smellie 2008; Ice–Volcano Interactions).
- Deglaciation is known to accelerate rates of volcanism in Iceland and other regions (Sigvaldason et al., 1992).
- Subglacial volcanoes may be an important environment for microbial life on Earth and even on Mars.

Bibliography

Guðmundsson, M. T., Sigmundsson, F., and Björnsson, H., 1997. Ice–volcano interaction of the 1996 Gjálp subglacial eruption, Vatnajökull, Iceland. *Nature*, **389**, 954–957.
Lescinsky, D. T., and Fink, J. H., 2000. Lava and ice interaction at stratovolcanoes: use of characteristic features to determine past glacial events and future volcanic hazards. *Journal of Geophysical Research*, **105**, 23711–23726.
Major, J. J., and Newhall, C. G., 1989. Snow and ice perturbation during historical volcanic eruptions and the formation of lahars and floods. *Bulletin of Volcanology*, **52**, 1–27.
McGarvie, D. W., 2009. Rhyolitic volcano–ice interactions in Iceland. *Journal of Volcanology and Geothermal Research*, **185**, 367–389.
Sigvaldason, G. E., Annertz, K., and Nilsson, M., 1992. Effect of glacier loading/deloading on volcanism: postglacial volcanic production rate of the Dyngjufjöll area, central Iceland. *Bulletin of Volcanology*, **54**, 385–392.
Smellie, J. L., 2000. Subglacial eruptions. In Sigurðsson, H., Houghton, B. F., McNutt, S. R., Rymer, H., and Stix, J. (eds.), *Encyclopaedia of Volcanoes*. London: Academic, pp. 403–418.
Smellie, J. L., 2008. Basaltic subglacial sheet-like sequences: Evidence for two types with different implications for the inferred thickness of associated ice. *Earth Science Reviews*, **88**, 60–88.

Cross-references

Andean Glaciers
Antarctica
Bottom Melting or Undermelt (Ice Shelf)
Glacier Lake Outburst Floods
Iceland Glaciers
Natural Hazards Associated with Glaciers and Permafrost
Subglacial Drainage System

SUBGLACIAL WEATHERING

Markus Konz
Institute of Environmental Engineering, Hydrology and Water Resources Management ETH Zürich, Zurich, Switzerland

Subglacial weathering is the study of mechanical and chemical changes in soil and rocks due to physical (e.g., grinding) and chemical (e.g., dissolution) processes in glacial environments. The subglacial hydrochemistry governs the rates of biogeochemical denudation and carbon cycling. These processes can have a significant impact on global biogeochemical cycles (Jones et al., 2002). Effluent glacier water transports dissolved and suspended matters that have been mobilized due to subglacial weathering and which can be used to determine nutrient and metal export and cycling (Mitchell et al., 2001, 2006; Mitchell and Brown, 2007).

Hydrologists use chemical analysis of glacier water to infer hydrological flow-paths in glacial drainage systems (Brown et al., 1996; Mitchell et al., 2006). The chemical signature of water samples can indicate the configuration and evolution of subglacial drainage systems.

Subglacial environments feature tough conditions for life due to a combination of low temperatures and lack of energy sources. However, recent investigations indicate an important abundance of bacterial populations in this habitat (see Hodson et al., 2008 for a review). The presence of bacteria is important for subglacial weathering reactions and these in turn supply energy to maintain bacterial populations.

Bibliography

Brown, G. H., Sharp, M., and Tranter, M., 1996. Experimental investigations of the weathering of suspended sediment by alpine glacial meltwater. *Hydrological Processes*, **10**, 579–597.
Hodson, A., Anesio, A. M., Tranter, M., Fountain, A., Osborn, M., Priscu, J., Laybourn-Parry, J., and Sattler, B., 2008. Glacial ecosystems. *Ecological Monographs*, **78**(1), 41–67.
Jones, I. W., Munhoven, G., Tranter, M., Huybrects, P., and Sharp, M., 2002. Modelled glacial and non-glacial HCO3 2, Si and Ge fluxes since the LGM: little potential for impact on atmospheric CO2 concentrations and marine Ge:Si ratio. *Global and Planetary Change*, **33**, 139–153.
Mitchell, A. C., and Brown, G. H., 2007. Diurnal hydrologicalphysicochemical controls and sampling methods for minor and trace elements in an alpine glacial hydrological system. *Journal of Hydrology*, **332**, 123–143.
Mitchell, A., Brown, G. H., and Fuge, R., 2001. Minor and trace element export from a glacierised Alpine headwater catchment (Haut Glacier d'Arolla, Switzerland). *Hydrological Processes*, **15**, 3499–3524.
Mitchell, A. C., Brown, G. H., and Fuge, R., 2006. Minor and trace elements as indicators of solute provenance and flow routing in a subglacial hydrological system. *Hydrological Processes*, **20**, 877–897.

SUBLIMATION FROM SNOW AND ICE

A. K. Singh
DIAT (Deemed University), Girinagar, Pune, Maharashtra, India

The process of ice changing directly into vapor without any intermediate liquid stage is often described by sublimation. The opposite of sublimation is "deposition," where water vapor changes directly into ice. The sublimation of ice or snow is driven by an imbalance between the saturation vapor pressure (or vapor density) at a given temperature, and the vapor pressure in the immediate vicinity of an ice surface. Sublimation process in snow controls the grain shape and size. Snow sublimation rate can be defined as the amount of mass lost per unit time and depends on particle surface area to mass ratio, vapor pressure gradients, and rate of air exchange around the snow crystal surface. Typically, these rates are higher when large vapor pressure gradients exist and rapid air exchange occurs.

It is not easy to actually see sublimation occurring, especially for ice. Sublimation occurs more readily when certain weather conditions are present, that is, on a dry and windy day with low relative humidity. Sublimation also occurs more at higher altitudes, where the air pressure is less than at lower altitudes. Sublimation is fairly slow since it takes quite a bit of energy for an ice molecule to escape the solid rigid structure to a gas. Sublimation will be enhanced under direct sunlight since photons of solar energy will add the energy necessary for solid ice molecules to escape. Sublimation will occur even at low sun angles but the amount of sublimation will be very weak. Since sun angle is a minimum at the start of winter and much higher in late winter, the sublimation power of the sun on surface snow will be much higher in late winter as compared to early winter on sunny days.

The sublimation rate of ice or snow has important implications on surface energy balance calculations, mass balance calculations, and studies of snow metamorphism.

Bibliography

Montesi, J., Elder, K., Schmidt, R. A., and Davis, R. E., 2004. Sublimation of Intercepted Snow within a Subalpine Forest Canopy at Two Elevations. *Journal of Hydrometeorology*, **5**(5), 763–773.

Neumann, T. A., Albert, M. R., Engel, C., Courville, Z., and Perron, F., 2009. Sublimation rate and the mass-transfer coefficient for snow sublimation. *International Journal of Heat and Mass Transfer*, **52**, 309–315.

SUMMER ACCUMULATION TYPE GLACIERS

Nozomu Naito
Department of Global Environment Studies, Hiroshima Institute of Technology, Hiroshima, Japan

Synonyms

Summer-accumulation type glacier

Definition

Accumulation. The process of adding of snow or ice to a glacier or its amount. Snowfall is generally the most popular process. In addition, frost, avalanche, refreezing of melt water, and catchment of blowing snow are other possible processes.

Ablation. The process of losing of glacier ice or snow or its amount. Melting is generally the most popular process. Then, evaporation, removal of snow by wind, and calving of icebergs are also possible.

Mass balance. The net mass change of glacier; accumulation subtracting ablation.

Introduction

Classical glaciology was initiated and has been developed through studies on glaciers in Europe and North America, where the main accumulation to the glaciers is snowfall in winter, and the main glacier ablation occurs in summer. The *Mass balance* of the glaciers is usually positive in winter, negative in summer, and then the annual *mass balance* is determined by the deduction of these two seasonal components. On the other hand, glaciers in Asia have been observed to have different characteristics since the 1970s (e.g., Ageta et al., 1980; Xie, 1980). These glaciers receive more accumulation in summer than in winter, and such glaciers have been called as *summer accumulation type glaciers* (Ageta, 1983; Ageta and Higuchi, 1984). In this definition, the periods of summer and winter are not explicitly defined, but they are generally regarded as warm and cold half years, respectively. Because climate in most parts of Asia is influenced by summer monsoon, most of the annual precipitation is concentrated in summer, while winter is cold but is a relatively dry season. Successive studies carried out on glaciers around the Himalayas and Tibetan Plateau have clarified that the *summer accumulation type glaciers* are very sensitive to changes in air temperature, as explained in what follows. Thus, *summer accumulation type glaciers* are considered to be much vulnerable to global warming.

Distribution

Summer accumulation type glaciers are extensively distributed in Asian highland regions influenced by Asian summer monsoon, i.e., the Himalayas, Tibetan Plateau, Qilian Mountains, Kunlun Mountains, Tien Shan, Pamir and so on. The Karakoram, however, is rather influenced by the westerlies, and receives much winter accumulation. In addition to the Asian glaciers, a part of the Andean glaciers are also revealed to be *summer accumulation type*, from an objectively analyzed meteorological datasets (Fujita, 2008).

Characteristics of mass balance

As most of the annual accumulation and ablation occur simultaneously in the same season on *summer accumulation type glaciers*, a change in climatic conditions in summer can induce a more drastic change in the glacier *mass balance* than that in winter. For example, an increase in summer air temperature will usually increase melting of glaciers. On the other hand, it will also decrease the snow fraction in precipitation, thereby decreasing accumulation. Moreover, it will lower the surface *albedo* of glaciers, thereby increasing absorption of solar radiation and melting. Thus, warming in summer has three negative effects on the *mass balance* of *summer accumulation type glaciers* (Ageta, 1983). In usual cases, warming in winter does not have such severe effects on the *mass balance* as warming in summer, because winter temperature is low enough below the melting point of ice.

As follows, the *albedo* effect on *mass balance* is probably the most important feature for *summer accumulation type glaciers*. Snowfall in summer keeps high *albedo* on the glacier surface and depresses melting. Due to this effect, the *equilibrium line altitude*, where the annual *mass*

balance is zero, is quite lowered, compared with a contrasting *winter accumulation type glacier*, which is assumed to have the same climate conditions except for only the seasonality of precipitation (Fujita and Ageta, 2000). In other words, *summer accumulation type glaciers* can exist as they are, owing to summer *accumulation*. In the case of winter accumulation, they should be smaller at higher altitudes or could not exist at all.

Sensitivity to climate changes

The above-mentioned significant characteristics in the *mass balance* of *summer accumulation type glaciers* deduce their high sensitivity to global warming, which have been investigated through numerical experiments. Not only *mass balance* but also dynamical response of *summer accumulation type glaciers* is more sensitive to temperature changes than that of *winter accumulation type glaciers* (Fujita and Ageta, 2000; Naito et al., 2001). On the other hand, the dynamical response to precipitation changes is more sensitive in the *winter accumulation type glaciers* (Naito et al., 2001). Moreover, precipitation seasonality and its concentration have a larger effect on the *mass balance* sensitivity to warming than latitude and the annual amount of precipitation (Fujita, 2008). These results indicate that forecasting the shrinkage of *summer accumulation type glaciers* to global warming requires an adequate consideration of their unique characteristics beyond simply applying any empirical relationship obtained for *winter accumulation type glaciers*.

Summary

Summer accumulation type glaciers receive more snowfall in summer than in winter. They are extensively distributed in Asian highland regions under summer monsoon climate, and parts of Andes. This type of glaciers are likely quite vulnerable to global warming, as decreasing summer snowfall reduces the surface *albedo*, and accelerates melting. In order to evaluate future shrinkages of this type of glaciers, the specific characteristics in their *mass balance* should be taken into account.

Bibliography

Ageta, Y., 1983. Characteristics of mass balance of the summer-accumulation type glacier in the Nepal Himalaya. *Seppyo*, **45**, 81–105 [in Japanese with an English abstract.].

Ageta, Y., and Higuchi, K., 1984. Estimation of mass balance components of a summer-accumulation type glacier in the Nepal Himalaya. *Geografiska Annaler*, **66 A**, 249–255.

Ageta, Y., Ohata, T., Tanaka, Y., Ikegami, K., and Higuchi, K., 1980. Mass balance of Glacier AX010 in Shrong Himal, east Nepal during the summer monsoon season. *Seppyo*, **41**(Special Issue), 34–41.

Fujita, K., 2008. Effect of precipitation seasonality on climatic sensitivity of glacier mass balance. *Earth and Planetary Science Letters*, **276**, 14–19.

Fujita, K., and Ageta, Y., 2000. Effect of summer accumulation on glacier mass balance on Tibetan Plateau revealed by mass-balance model. *Journal of Glaciology*, **46**, 244–252.

Naito, N., Ageta, Y., Nakawo, M., Waddington, E. D., Raymond, C. F., and Conway, H., 2001. Response sensitivity of a summer-accumulation type glacier to climate changes indicated with a glacier fluctuation model. *Bulletin of Glaciological Research*, **18**, 1–8.

Xie, Z., 1980. Mass balance of glaciers and its relationship with characteristics of glaciers. *Journal of Glaciology and Cryopedology*, **2**, 1–10 [in Chinese with an English abstract.].

Cross-references

Albedo
Andean Glaciers
Climate Change and Glaciers
Equilibrium-Line Altitude (ELA)
Glacier Mass Balance
Glaciers of the Karakoram Himalaya
Himalaya
Tibetan Plateau
Winter Accumulation Glacier

SUPER COOLING CLOUDS

P. Pradeep Kumar
Department of Atmospheric and Space Sciences, Pune University, Pune, India

As cloud forms and ascends it may be cooled to temperatures below 0°C. The water drops are expected to freeze, but in natural clouds this may not happen. Whether the water drops will freeze or not depends on the number of ice nuclei present in the cloud. Such drops are called as supercooled drops. For pure water droplets, the homogeneous freezing does not occur till −40°C. Supercooling of clouds till −15°C are not uncommon.

Bibliography

Rogers, R. R., 1979. *A Short Course on Cloud Physics*. New York: Pergamon, p. 234.

SUPERCOOLED WATER

Simon Cook
Centre for Glaciology, Institute of Geography & Earth Sciences, Aberystwyth University, Ceredigion, Wales, UK

Synonyms

Undercooling

Definition

Supercooled water. Water that remains in a liquid state when cooled below its melting (freezing) point.

Introduction

The freezing point of water (or the melting temperature of ice) varies depending upon the ambient pressure, the solute content of the water, whether the water is kept turbulent, and, where water and ice exist in soils or sediments, the interfacial forces between liquid water and ice. Typically, we think of water as a substance whose phase changes from liquid to solid as we cool it to 0°C, but there are several situations within cryospheric environments where water may exist in a liquid state at a temperature below the ambient freezing point. In this situation the water is referred to as being supercooled.

The transition of water to ice

As Block (2003) describes, the transition of water to ice via crystallization involves three stages: (1) supercooling, (2) formation of an ice nucleus, and (3) freezing to produce an ice crystal and growth of an ice front. Solutions supercool to varying degrees before spontaneously freezing. For example, perfectly pure and still water can remain liquid when cooled to approximately −40°C (Davis, 2001). In this supercooled state, liquid water is thermodynamically less stable than ice but it will remain in the liquid phase unless perturbed beyond a certain threshold. Such perturbations to the system could include further cooling, agitation of the water, or introduction of a freezing nucleus such as a sediment grain (seeding).

Pressure

The pressure dependence of the temperature at which ice melts and water freezes is of fundamental consequence to many aspects of cryospheric science. At atmospheric pressure, water will freeze at a temperature of 0°C, but with an increase in ambient pressure, the freezing point is depressed at a rate of 0.072°C per MPa (1 Pa = 1 N per square meter). So, for example, beneath glaciers and ice sheets, the freezing point of water is depressed by the pressure exerted by the ice thickness. The pressure beneath 2,000 m of ice is ∼17.6 MPa giving a melting point of −1.27°C (Benn and Evans, 1998). This pressure-determined melting/freezing temperature is referred to as the pressure melting point. Water at −1.27°C beneath 2,000 m of ice is not considered supercooled because its temperature is in equilibrium with the ambient pressure, but if that water were to flow from this area of high pressure to an area of lower pressure without freezing then it would be supercooled (e.g., Röthlisberger, 1968, 1972; Röthlisberger and Lang, 1987).

Glaciohydraulic Supercooling (qv) is a process that allows subglacial water to exist in a liquid state beneath ice masses in response to such pressure changes, and subsequently for this supercooled water to freeze to the glacier base to produce *basal ice* (qv *Formation and Deformation of Basal Ice*) and clog subglacial watercourses (e.g., Alley et al., 1998; Lawson et al., 1998; Cook et al., 2006). This mechanism of supercooling is implicitly associated with the flow of subglacial water through topographic basins or "overdeepenings." At the base of the overdeepening, the melting temperature is depressed beneath thick ice. As water is forced along a pressure gradient to ascend the reverse slope out of the overdeepening, the pressure melting temperature gradually rises toward 0°C as the overburden pressure decreases beneath thinner ice at the margin. For the water to remain in thermal equilibrium with the overlying temperate ice, the water must also warm as it moves along the gradient of decreasing pressure. Heat can be provided by a variety of potential sources, including: (a) viscous dissipation associated with water flow, (b) geothermal heat flux, (c) basal sliding, and (d) latent heat release if part of the water freezes. However, thermodynamic calculations suggest that if the adverse bed slope is sufficiently steep (more than 1.2–1.7 times the gradient of the ice-surface slope) then the heat generated and the rate of increase in water temperature will be insufficient to match the changing pressure melting point and it will become supercooled (Röthlisberger, 1972; Hooke, 1991; Alley et al., 1998). The minimum gradient of the adverse slope to allow supercooling varies dependent upon the air saturation state of the water. For the water to remain in thermal equilibrium with the overlying temperate ice, some of it must freeze to release latent heat, resulting in the production of *Frazil ice* (qv) (porous aggregates of lozenge-shaped crystals) and *Anchor Ice* (qv) (ice platelets anchored to the glacier or substrate). Sediment-laden water percolates through anchor and frazil ice until pore spaces freeze shut, and subsequent debris – ice segregation produces debris-laden basal ice (Alley et al., 1998; Lawson et al., 1998). The melting of this basal ice is suggested to have important implications for glacial geomorphology and landscape development (e.g., Larson et al., 2006), although there is still much uncertainty about the controls on the temporal and spatial pervasiveness of the process (e.g., Tweed et al., 2005; Cook et al., 2007).

Solutes

The presence of solutes within water may also depress its freezing point. In glaciers, the presence of solutes has an important impact on ice flow. The influence of solutes on the strain rate of glacier ice is variable as different solutes can either harden, soften, or have no effect on the ice (Nakamura and Jones, 1973). However, in situations where high solute concentrations act to depress the freezing point of water between ice crystals, the *Creep* (qv) of glacier ice may be enhanced (e.g., Wolff et al., 1988). Shreve (1984) demonstrated that glacier sliding could also be enhanced by elevated levels of solutes, in this case by sodium chloride (salt).

The depression of the freezing point by salt is of particular significance to sea ice scientists where supercooling and frazil ice formation occur as a result of differences in the salinities of waters. Martin (1981) explains that water becomes supercooled and produces frazil ice in Arctic river mouths or beneath pack ice where a layer of fresh meltwater at its freezing point (0°C) overlies a layer of

seawater at its freezing point (−1.6°C). Between 0.2 to 0.3 m of fresh water ice can grow beneath melting pack ice during the polar summer. Tsang and Hanley (1985) conducted experiments on ice formation for different supercoolings and initial salinities. Their results showed that the rate of frazil ice production was faster in fresh water than in saline water demonstrating that rates of sea ice formation depend to some extent on local salinity levels.

Block (2003) explains how, for terrestrial invertebrates which live in cold environments, solutes are important in maintaining body fluids in a liquid state. These "freeze avoiding" species may possess thermal hysteresis proteins (THPs) which depress the freezing point relative to the melting point of the body fluids, and which may be present together with compatible solutes that act as antifreezes (e.g., polyhydric alcohols and sugars).

Turbulence

The freezing point of water may be depressed by turbulence. This effect can pose a significant problem in rivers where frazil ice growth from turbulent supercooled water interrupts the operation of hydroelectric power stations (Martin, 1981). At low turbulence, frazil ice will float to the surface where it forms a pan, whereas when turbulence is high, frazil ice can be entrained into the flow and be carried to the bottom where it may attach to the channel bed and form anchor ice (Doering et al., 2001). Anchor ice can therefore alter the hydraulic characteristics of the flow. For example, the upper Niagara River experiences flow reductions of 20–30% as a result of anchor ice growth (Arden and Wigle, 1972).

Martin (1981) described how supercooling and frazil ice formation occur at the ocean surface due to the effect of turbulence. For leads (open water less than 100 m wide) and polynyas (width scale larger than 100 m) frazil ice will form where cold winds blow across regions of open water that is at the freezing point, agitating the water. In leads, frazil ice crystals form throughout the open water and are piled up to depths of 0.1–0.3 m at the edge of the lead due to wind and wave action. In polynyas, frazil ice tends to pile up in streaks aligned with wind direction to depths of around 1 m.

Interfacial effects

Soils and sediments encountered within cryospheric environments (i.e., permafrost and subglacial tills) can comprise a mixture of solid particles, air, ice, and liquid water. Supercooled water may exist in such situations as a consequence of solute content but of additional importance is the effect of premelting which itself can result from three related effects:

1. Ice–water interfacial tension – Interfacial tension results at an ice–water interface because of strong intermolecular forces between liquid water molecules at the interface. Hence a thin layer (on the order of nanometres) of supercooled liquid water will separate an ice lens growing in permafrost from a sediment particle (Rempel et al., 2004). Where the ice surface itself is curved, this will tend to promote the supercooling of pore-water that exists between sediment grains close to the ice front (Rempel et al., 2004).
2. Interfacial curvature – Higher interfacial tension is also promoted by enhanced curvature of sediment grains such that the finer grained a sediment is, the higher the curvature of the interface and the greater the depression of the freezing point (Christoffersen and Tulaczyk, 2003a; French, 2007).
3. Adsorption of liquid water onto a solid particle – The mineral properties of the soil particle also affect the thickness of the water layer that may be adsorbed to it (French, 2007). Adsorption refers to the forces that emanate from the particle surface which reduce the free energy of the water film.

Some important consequences of these effects include ice frost heaving in permafrost environments, and glacier motion. The deformation of the ground level in permafrost environments during winter cannot be fully explained by the volumetric expansion of water on freezing. Instead, it is due to the migration of premelted ice within the permafrost to a freezing front to produce segregation ice. The basic forcing mechanism is the repulsion between soil and water particles across the premelted water film which gives rise to low pressure within the water film (Rempel et al., 2004). Thus water in the surroundings is drawn toward the low pressure ice–water freezing interface where it may be frozen to produce segregation ice. Continued growth of the ice lens in this manner causes the ground to rupture – a process typically referred to as frost heaving (Dash et al., 1995).

Christoffersen and Tulaczyk (2003a, b) described a process of basal freeze-on beneath ice streams analogous to the process of frost heave in permafrost environments. In fine-grained subglacial till, water is unable to freeze due to interfacial effects and insufficient space for crystal growth. In polar ice streams, basal temperatures may be reduced by ice thinning, or by fast downward advection of cold surface ice. Reduced basal temperatures are accompanied by a decrease in water pressure at the ice–water interface producing a hydraulic gradient that drives the supercooled pore-water to the freezing front where it freezes to produce basal ice. Dewatering of the till in this manner causes it to consolidate and hence ice stream motion, which had once been accommodated by deformation of the saturated till layer, slows to the point of stagnation.

The existence of liquid water within glacier ice and subfreezing subglacial sediments is of fundamental importance for glacier motion of *Cold-Based Glaciers* (qv) and their geomorphic potential (Waller, 2001). Andersland and Alnouri (1970) demonstrated that at −12°C, frozen sand is much more resistant to loading than frozen clay because liquid water exists between clay particles due to interfacial effects, whereas water is completely frozen in

the sand sample. Echelmeyer and Zhongxiang (1987) suggested similarly that the existence of liquid water within subglacial sediments beneath Urumqi No. 1 Glacier reduced its creep strength by over 100 times relative to ice at a similar stress and temperature, enabling it to deform. This is contrary to previously held assumptions that cold-based glaciers were effectively frozen to their beds and were hence incapable of performing geomorphic work (e.g., Boulton, 1972).

Droplet size

When water is dispersed as tiny droplets in clouds, it can remain in a supercooled state in supercooled clouds. Clouds consist of water droplets at temperatures down to −12°C. *Rime Ice* (qv) may form from such masses of supercooled vapor or from water vapor carried by wind. On glaciers, rime ice development is most rapid in cool, humid conditions on surfaces that are exposed to wind (Benn and Evans, 1998). Rime ice formation can have a major impact on power supplies and telecommunication towers where it grows around cables and structures until they collapse under the additional weight (Makkonen, 2000). Rime ice accretion is also a major consideration in aeronautical engineering because aircraft must be resistant to rime ice formation since they routinely fly through supercooled vapor (Gent et al., 2000).

Summary

Whilst the transition from liquid water to ice is typically considered to occur at 0°C, there are a number of reasons why water can exist in a supercooled liquid state below this freezing point. Furthermore, the existence of supercooled water in the cryosphere has fundamental implications for important phenomena including frost heave of permafrost, glacier motion and dynamics, sea ice formation, the clogging of rivers and hydroelectric power inlets with frazil ice, and the design of power and telecommunications infrastructure and aircraft.

Bibliography

Alley, R. B., Lawson, D. E., Evenson, E. B., Strasser, J. C., and Larson, G. J., 1998. Glaciohydraulic supercooling: a freeze-on mechanism to create stratified, debris-rich basal ice: II theory. *Journal of Glaciology*, **44**, 563–569.

Andersland, O. B., and Alnouri, A., 1970. Time-dependent strength behaviour of frozen soils. *Journal of the Soil Mechanics and Foundations Division*, **SM4**, 1249–1265.

Arden, R. S., and Wigle, T. E., 1972. *Dynamics of Ice Formation in the Upper Niagara River. Proc.: The Role of Snow and Ice in Hydrology*. Banff: IAHS-UNESCO-WHO, pp. 1296–1313.

Benn, D. I., and Evans, D. J. A., 1998. *Glaciers and Glaciation*. London: Arnold.

Block, W., 2003. Water or ice? – the challenge for invertebrate cold survival. *Science Progress*, **86**, 77–101.

Boulton, G. S., 1972. The role of thermal regime in glacial sedimentation. In Price, R. J., and Sugden, D. E. (eds.), *Polar Geomorphology – Institute of British Geographers Special Publication Four*. Oxford: Alden, pp. 1–19.

Christoffersen, P., and Tulaczyk, S., 2003a. Response of subglacial sediments to basal freeze-on: I. Theory and comparison to observations from beneath the West Antarctic ice sheet. *Journal of Geophysical Research*, **108**(B4), 2222.

Christoffersen, P., and Tulaczyk, S., 2003b. Thermodynamics of basal freeze-on: predicting basal and subglacial signatures of stopped ice streams and interstream ridges. *Annals of Glaciology*, **36**, 233–243.

Cook, S. J., Waller, R. I., and Knight, P. G., 2006. Glaciohydraulic supercooling: the process and its significance. *Progress in Physical Geography*, **30**, 577–588.

Cook, S. J., Knight, P. G., Waller, R. I., Robinson, Z. P., and Adam, W. G., 2007. The geography of basal ice and its relationship to glaciohydraulic supercooling: Svínafellsjökull, southeast Iceland. *Quaternary Science Reviews*, **26**, 2309–2315.

Dash, J. G., Fu, H., and Wettlaufer, J. S., 1995. The premelting of ice and its environmental consequences. *Reports on Progress in Physics*, **58**, 115–167.

Davis, N., 2001. *Permafrost: A Guide to Frozen Ground in Transition*. Fairbanks: University of Alaska Press.

Doering, J. C., Bekeris, L. E., Morris, M. P., Dow, K. E., and Girling, W. C., 2001. Laboratory study of anchor ice growth. *Journal of Cold Regions Engineering*, **15**, 60–66.

Echelmeyer, K., and Zhongxiang, W., 1987. Direct observation of basal sliding and deformation of basal drift at sub-freezing temperatures. *Journal of Glaciology*, **33**, 83–98.

French, H. M., 2007. *The Periglacial Environment*. Chichester: Wiley.

Gent, R. W., Dart, N. P., and Cansdale, J. T., 2000. Aircraft icing. *Philosophical Transactions: Mathematical, Physical and Engineering Sciences*, **358**, 2873–2911.

Hooke, R. LeB., 1991. Positive feedbacks associated with erosion of glacial cirques and overdeepenings. *Geological Society of America Bulletin*, **103**, 1104–1108.

Larson, G. J., Lawson, D. E., Evenson, E. B., Alley, R. B., Knudsen, O., Lachniet, M. S., and Goetz, S. L., 2006. Glaciohydraulic supercooling in former ice sheets? *Geomorphology*, **75**, 20–32.

Lawson, D. E., Strasser, J. C., Evenson, E. B., Alley, R. B., Larson, G. J., and Arcone, S. A., 1998. Glaciohydraulic supercooling: a freeze-on mechanism to create stratified, debris-rich basal ice: I field evidence. *Journal of Glaciology*, **44**, 547–562.

Makkonen, L., 2000. Models for the growth of rime, glaze, icicles and wet snow on structures. *Philosophical Transactions: Mathematical, Physical and Engineering Sciences*, **358**, 2913–2939.

Martin, S., 1981. Frazil ice in rivers and oceans. *Annual Review of Fluid Mechanics*, **13**, 379–397.

Nakamura, T., and Jones, S. J., 1973. Mechanical properties of impure ice crystals. In Whalley, W. B., Jones, S. J., and Gold, L. W. (eds.), *Physics and Chemistry of Ice*. Ottawa: Royal Society of Canada, pp. 365–369.

Rempel, A. W., Wettlaufer, J. S., and Worster, M. G., 2004. Premelting dynamics in a continuum model of frost heave. *Journal of Fluid Mechanics*, **498**, 227–244.

Röthlisberger, H., 1968. Erosive processes which are likely to accentuate or reduce the bottom relief of valley glaciers. *International Association of Hydrological Sciences Publication*, **79**, 87–97.

Röthlisberger, H., 1972. Water pressure in intra- and subglacial channels. *Journal of Glaciology*, **11**, 177–202.

Röthlisberger, H., and Lang, H., 1987. Glacial hydrology. In Gurnell, A. M., and Clark, M. J. (eds.), *Glacio-Fluvial Sediment Transfer: An Alpine Perspective*. Chichester: Wiley.

Shreve, R. L., 1984. Glacier sliding at sub-freezing temperatures. *Journal of Glaciology*, **30**, 341–347.

Tsang, G., and Hanley, T. O'. D., 1985. Frazil formation in water of different salinities and supercoolings. *Journal of Glaciology*, **31**, 74–85.

Tweed, F. S., Roberts, M. J., and Russell, A. J., 2005. Hydrologic monitoring of supercooled discharge from Icelandic glaciers. *Quaternary Science Reviews*, **24**, 2308–2318.
Waller, R. I., 2001. The influence of basal processes on the dynamic behaviour of cold-based glaciers. *Quaternary International*, **86**, 117–128.
Wolff, E. W., Mulvaney, R., and Oates, K., 1988. The location of impurities in Antarctic ice. *Annals of Glaciology*, **11**, 194–197.

Cross-references

Anchor Ice
Cold-Based Glaciers
Creep
Formation and Deformation of Basal Ice
Frazil
Glaciohydraulic Supercooling
Rime Ice

SUPRA-GLACIAL DEBRIS ENTRAINMENTS

D. P. Dobhal
Wadia Institute of Himalayan Geology, Dehradun, India

Supra-glacial debris entrainments is defined as an unsorted and unstratified accumulation of sediments carried by the glacier along the bed and valley sides and deposited directly on glacier surface. They may occur by regelation or by the ice simply picking up the debris.

SURFACE ENERGY BALANCE

Michiel Van den Broeke[1], Xavier Fettweis[1,2], Thomas Mölg[3]
[1]Institute for Marine and Atmospheric Research, Utrecht University, Utrecht, Netherlands
[2]Department of Geography, University of Liège, Liège, Belgium
[3]Center for Climate & Cryosphere, University of Innsbruck, Innsbruck, Austria

Definition

The surface energy balance (SEB) describes the partitioning of energy fluxes toward and away from the surface. The local SEB determines the surface temperature of the Earth (T_s) and the associated exchange of energy between the surface and the atmosphere on one hand, and between the surface and the subsurface layers (whether it be soil, rock, water, snow, or ice, see Figure 1) on the other. When the surface consists of snow or ice, the SEB also determines the amount of energy that is available for sublimation and melting/freezing. These processes directly couple the SEB to the *surface mass balance* (SMB). In this entry, we describe the components of the SEB, and give six examples of the annual SEB cycle, all with a permanently snow-/ice-covered surface, but in widely varying geographical settings.

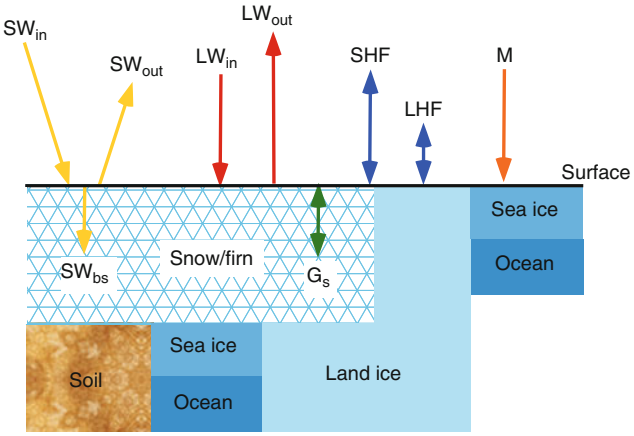

Surface Energy Balance, Figure 1 Components of the surface energy balance of snow, sea ice, and land ice. Length of arrows is only indicative.

Components of the surface energy balance

The SEB is defined as the sum of all fluxes of energy passing each second through a horizontal surface of unit area (Figure 1), with units J s^{-1} m^{-2} or W m^{-2}. *We define fluxes as positive when they are directed toward the surface,* i.e., *when they represent an energy gain for the surface.* For an infinitesimally thin surface layer without heat capacity (sometimes called a *skin layer*), these fluxes *balance,* i.e., their sum equals zero. If we neglect the heat added to the surface by falling snow, rain, or fog droplets, the SEB over a snow/ice surface can be written as:

$$M = SW_{in} + SW_{out} + SW_{bs} + LW_{in} + LW_{out} + SHF + LHF + G_s \left[Wm^{-2}\right] \quad (1)$$

In Equation 1, M is the melting flux when T_s equals 273.15 K, otherwise M = 0. Note that the melting temperature for sea ice surfaces can be lower than 273.15 K because the ice is saline in most cases. If $T_s < 273.15$ K and if there is liquid water available at the surface, M represents the freezing flux.

The abbreviations SW_{in} and SW_{out} represent the incoming and outgoing fluxes of shortwave (solar) radiation, SW_{bs} is the amount of shortwave radiation that is absorbed below the surface. LW_{in} and LW_{out} are the incoming and outgoing fluxes of longwave (terrestrial) radiation. Shortwave and longwave radiation are distinguished on the basis of their wavelength domain, determined from Planck's law by the temperature of the body that emits the radiation. If radiation originates from the surface of the Sun ($T_s \approx 5{,}800$ K), either directly or scattered in the Earth's atmosphere, nearly all energy is confined to wavelengths below 3 μm, hence the name *shortwave radiation*. If the radiation originates from the Earth-atmosphere system ($T_s \approx 200$–300 K), nearly all energy derives from wavelengths greater than 3 μm, hence the name *longwave*

radiation. SW and LW radiation fluxes are measured directly with broadband radiation sensors using selective filters.

At a sufficiently small distance above the surface, in the order of one to several mm, sensible heat exchange (SHF) and latent heat exchange (LHF) between the surface and air occurs predominantly by molecular conduction. Higher in the atmosphere, turbulence occurs as eddies (whirls) that vertically mix momentum, heat, and moisture. Turbulence is more effective in transporting scalars than molecular diffusion (Stull, 1988), and SHF and LHF are dominated by turbulent exchange. That is why they are usually referred to as *turbulent fluxes.*

Finally, G_s is the vertical heat flux below the surface, an expression of the molecular conduction of heat along temperature gradients in the snow/ice. The energy coming from the interior of the Earth, the geothermal heat flux, usually does not exceed 0.1 W m^{-2}, and is incorporated in G_s. The major components of the SEB are discussed separately below.

Shortwave radiation fluxes

When solar radiation impinges on the snow/ice surface, a part is absorbed at the surface, another part is reflected back to the atmosphere, and a third part penetrates to deeper layers and is absorbed below the surface. The net shortwave radiation flux (SW_{net}) is the total amount of shortwave radiation that is absorbed at or below the snow/ice surface. SW_{net} therefore equals the sum of downward (SW_{in}) and upward shortwave radiation (SW_{out}), and drives the daily and annual cycle in most SEB components.

SW_{in} is determined by (a) the amount of solar radiation impinging on the top of the atmosphere, (b) the amount of shortwave radiation that is scattered or absorbed in the atmosphere (depending notably on the cloudiness), and (c) the slope magnitude and orientation of the snow/ice surface. The instantaneous amount of solar radiation impinging on the top of the atmosphere (SW_{TOA}) depends on the solar constant, latitude, time of year, and time of day. Averaged over the year, the geographic poles receive about 40% of the insolation at the equator. But the temporal distribution of this energy is very different for different latitudes. As a rule of thumb, high-latitude (polar) regions experience a small daily cycle and a large annual cycle in SW_{TOA}, while tropical regions experience a large daily cycle and a small annual cycle in SW_{TOA} (Figure 2).

The amount of shortwave radiation that is scattered or absorbed in the atmosphere depends on the optical thickness of the atmosphere, which is mainly a function of vertically integrated water vapor mass and liquid water mass (clouds). The vertically integrated aerosol content also is important for shortwave radiation scattering. In the Polar Regions and for highly elevated tropical glaciers, the water vapor and aerosol content of the atmosphere is relatively low, so that the optical thickness is relatively small and the shortwave radiation intensity at the surface high. Explosive volcanic eruptions reduce the amount of solar energy reaching the surface; the El Chichón and Mount Pinatubo eruptions in 1983 and 1991 significantly impacted the SEB of Greenland (Fettweis, 2007). Glaciers or ice caps that are situated in temperate climates usually experience more cloudy conditions, limiting the amount of shortwave radiation that reaches the surface.

The orientation of glaciers with respect to the sun influences the amount of shortwave radiation impinging on the surface. If a glacier surface is steeply sloping and directed toward the sun, this can greatly enhance the amount of

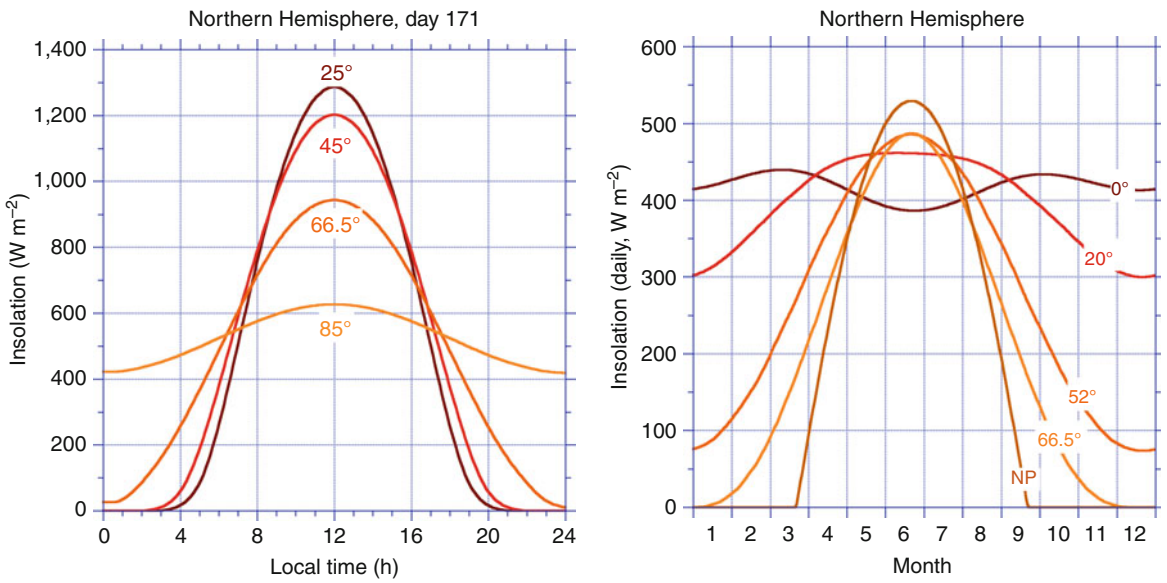

Surface Energy Balance, Figure 2 SW_{in} at the top of the atmosphere. Daily cycle in the northern hemisphere for June 20th (*left*) and annual cycle for the northern hemisphere based on daily means (*right*) of SW_{TOA} for various latitudes.

absorbed solar radiation and hence melting. On the other hand, if the sloping glacier is directed away from the sun, the solar rays hit the surface at an oblique angle, thereby decreasing the amount of shortwave radiation reaching the surface. Moreover, the surface can be shaded for parts of the day, eliminating the direct component of SW_{in}. For glacier melt modeling, the orientation of the glacier surface and the surrounding topography, therefore, needs to be explicitly taken into account (Klok and Oerlemans, 2002).

Part of the absorption (SW_{bs}) takes place below the surface (Grenfell and Maykut, 1977). Typical penetration depths are several cm in fine, dry-grained snow to several decimeters in ice (Brandt and Warren, 1993). This results in heating of the subsurface snow and ice layers (Kuipers Munneke and others, 2009) and may lead to subsurface melting (Van den Broeke and others, 2008b). When calculating the penetration of shortwave radiation in ice/snow, it is essential that the wavelength dependence of shortwave radiation absorption is taken into account, instead of using a bulk-extinction coefficient.

The fraction of shortwave radiation that is absorbed at or below the surface, is determined by the broadband surface albedo α, defined as:

$$\alpha = |SW_{out}|/SW_{in} \quad (2)$$

Snow albedo depends on the thickness, aerial coverage, and physical characteristics of the snow (grainsize, wetness, temperature), the thickness of the snow layer over dark soil and the spectrum and direction of the impinging solar radiation (wavelength distribution, solar zenith angle, ratio of diffuse to direct radiation, see Wiscombe and Warren, 1980, and entry on snow albedo). Clean, dry ice has an albedo of approximately 0.55, while clean, fresh snow has an albedo $\sim$0.85. The albedo of water ($<$0.1) is much lower than that of snow and ice, and meltwater that accumulates at the snow/ice surface can therefore have a significant impact on its albedo (Greuell, 2000).

Melting leads to rapid growth of snow grains and can lower the snow albedo to values near 0.75, i.e., increasing the amount of absorbed shortwave radiation by $\sim$70% compared to fresh snow. This represents the all-important albedo-melt feedback: melting lowers the albedo, which further enhances melt, etc. Typical low-ranging values of albedo (0.15–0.4) are found over ice and snow with a large dust load. The dust could have been melted out from the ice or blown onto it from the ice-free surroundings (Oerlemans and others, 2009). When seasonal snow or sea ice is replaced by the darker soil or sea surface, the amount of absorbed solar radiation may increase severalfold.

Figure 3 shows the global distribution of annual mean surface albedo, as derived from satellite measurements and radiative transfer modeling. The impact of snow and ice at high latitudes is clearly visible. The highest values ($>$0.8) are found over the interior dry snow zones of Greenland and Antarctica. The Arctic sea ice cover has a lower albedo, because it is melting for part of the year. The gradual transition toward lower values at mid-latitudes takes place over areas that are covered by seasonal snow or sea ice for part of the year. In the entry on snow albedo, the annual cycle of the albedo of Arctic sea ice is presented.

Longwave radiation fluxes

The net longwave radiation flux (LW_{net}) is the sum of incoming (LW_{in}) and outgoing (LW_{out}) longwave radiation fluxes. Over Greenland, LW_{in} appears the most sensitive SEB component for increased atmospheric concentrations of Greenhouse gases (Fettweis, 2007). Apart from exceptional cases, LW_{net} represents an energy loss for the surface, as the surface is generally warmer and has higher emissivity than the overlying atmosphere.

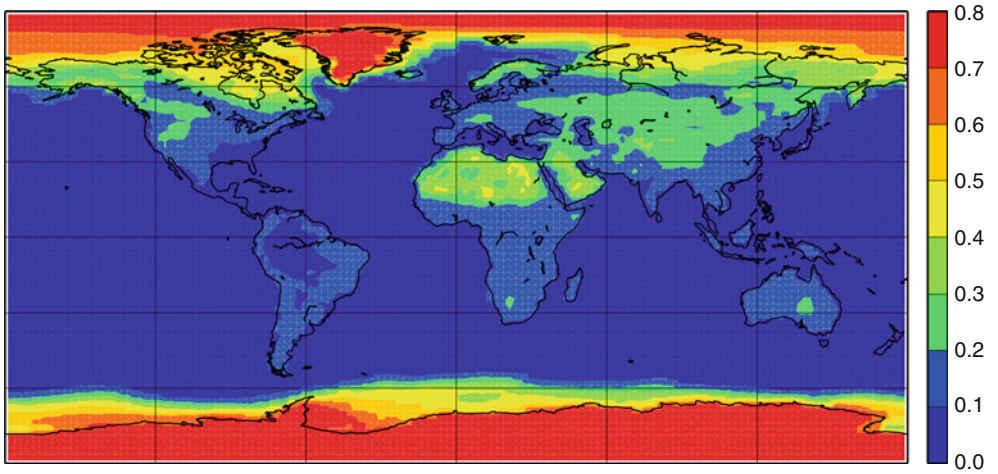

Surface Energy Balance, Figure 3 Satellite-derived surface broadband albedo, annual mean (based on data of Hatzianastassiou and others, 2004).

LW_{in} is determined by the effective emissivity (ε_{eff}) and effective radiation temperature (T_{eff}) of the atmosphere, while LW_{out} is determined by the emissivity (ε_s) and temperature (T_s) of the snow/ice surface. Using the Stephan–Boltzmann law, LW_{net} can be approximated by:

$$LW_{net} = \varepsilon_s \varepsilon_{eff} \sigma T_{eff}^4 - \varepsilon_s \sigma T_s^4 \quad (3)$$

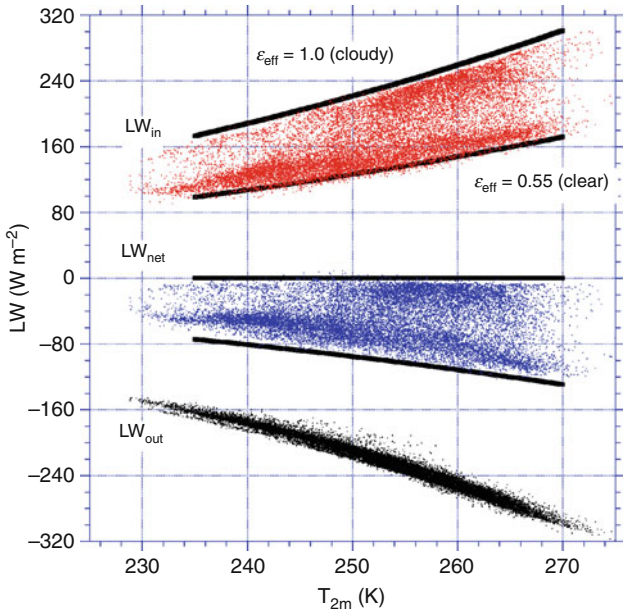

Surface Energy Balance, Figure 4 Observed hourly mean values of LW_{in} (*red dots*), LW_{out} (*black dots*), and LW_{net} (*blue dots*) as well as calculated from empirical formula (black lines, Equation 3) as a function of 2 m temperature for a non-melting location in Antarctica, at 1,100 m a.s.l. The upper and lower bounds of all three cases are for cloudy and clear sky conditions, respectively.

where the Stefan–Boltzmann constant $\sigma = 5.67 \times 10^{-8}$ W m^{-2} K^{-4}.

The surface emissivity of a dry snow surface is close to unity ($\varepsilon_s \approx 0.98$, Wiscombe and Warren, 1980) while the effective emissivity and radiation temperature of the atmosphere are complex functions of the vertical distribution of temperature, moisture, and other atmospheric compounds. In spite of this complexity, some general statements can be made. Under cloudy conditions, $\varepsilon_{eff} \approx 1$, and T_{eff} represents the cloud base temperature. When the cloud base is situated at low elevation, T_{eff} will not deviate much from T_s, so that LW_{net} will be zero or weakly negative. Under clear sky conditions, if 2 m air temperature is used as a measure for effective atmospheric radiative temperature, it is found that ε_{eff} can be approximated by a constant, to be determined empirically. Figure 4 shows an example for a location in Antarctica, where $\varepsilon_{eff} \approx 0.55$ (thick black lines in Figure 4). The resulting expression can be used to estimate LW_{in} and, if T_s is known (or assumed approximately equal to T_{2m}), to estimate LW_{out} and hence LW_{net}. The challenge lies in estimating LW_{in} for partly cloudy conditions, i.e., to interpolate between these two extremes (Kuipers Munneke and others, 2010).

Net radiation flux

Averaged over the year, $R_{net} = SW_{net} + LW_{net}$ is negative over much of the Polar Regions and in some highly elevated plateaus away from the Poles (e.g., the Tibetan Plateau, Figure 5). At these locations, cooling by LW_{net} exceeds warming by SW_{net}. This is remarkable, given that the Sun provides radiative energy for half of the time. The radiation deficit in the Polar Regions can be explained by factors that limit SW_{net}, such as the low Sun angle and the high albedo of the surface that usually consists of snow, glaciers, and sea ice. On the other hand, the snow effectively emits longwave radiation ($\varepsilon_s \approx 1$) while the polar

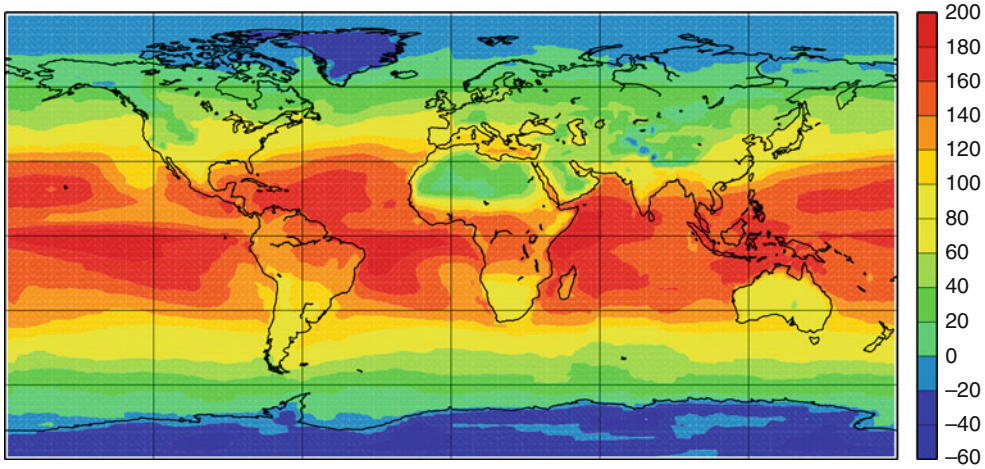

Surface Energy Balance, Figure 5 Annual average surface net radiation in W m^{-2} (*based on data of* Hatzianastassiou and others, 2004).

atmosphere is cold and dry, resulting in small ε_{eff}. This results in relatively strongly negative values of LW_{net}. Even at these sites, R_{net} will become positive around noon during sunny summer days, but when averaged over the year, the radiation balance is negative. Over a semi-infinite snow pack, this radiation deficit must be compensated by the sensible heat flux from the atmosphere, as the heat flux from the snowpack equals approximately zero when averaged over the year (see Section Subsurface heat flux). The latent heat flux is also likely to be small at polar sites (see Section latent heat flux), so that the most likely candidate is a flux of sensible heat from the atmosphere to the surface (next Section "Sensible heat flux"). Over sea ice, heat provided by the ocean through the subsurface heat flux compensates an important part of the radiative heat loss. Over open water in winter, much of the radiative heat loss is invested in cooling the upper ocean layers, resulting in the formation of sea ice.

Sensible heat flux

The turbulent flux of sensible heat, SHF (often referred to as the sensible heat flux), describes heat exchange between the surface and the air above it. In the surface layer, SHF can be directly measured using sonic anemometers that measure rapid (turbulent) fluctuations in temperature and vertical velocity. But these instruments are relatively vulnerable and expensive, which is why the sensible heat flux is often calculated, based on measured profiles of wind and temperature, in combination with surface-layer similarity theory (Stull, 1988). These calculations usually give satisfactory results over melting and non-melting snow and ice surfaces.

The sensible heat flux is directed away from the surface (negative) when the surface is warmer than the air, i.e., under statically unstable conditions in the atmospheric surface layer (SL). This upward heat transport is often referred to as convection. In the Polar Regions, convection is rare, and occurs, for instance, when cold polar air flows over open water, forming characteristic convective cloud straits. Weak convection also occurs during summer at highly elevated sites on the Polar Ice sheets, where temperatures are too low for sublimation to be significant (King and others, 2006).

In general, however, the negative net radiation cools the surface, which then becomes colder than the air above. Therefore, over snow and ice, SHF is commonly positive, i.e., directed toward the surface. The associated cooling of the atmospheric boundary layer often results in a surface-based temperature inversion, in which the temperature increases with height. In regions where the radiative heat loss is quasi-permanent during the Polar Night, i.e., the elevated interior plateaus of the Greenland and Antarctic ice sheets, the surface temperature inversion can become several tens of degrees (e.g., Vostok station in Figure 6). In the coastal areas and in the Arctic (Overland and others, 2000), the radiative cooling is weaker because of the more frequent occurrence of clouds, enhancing incoming

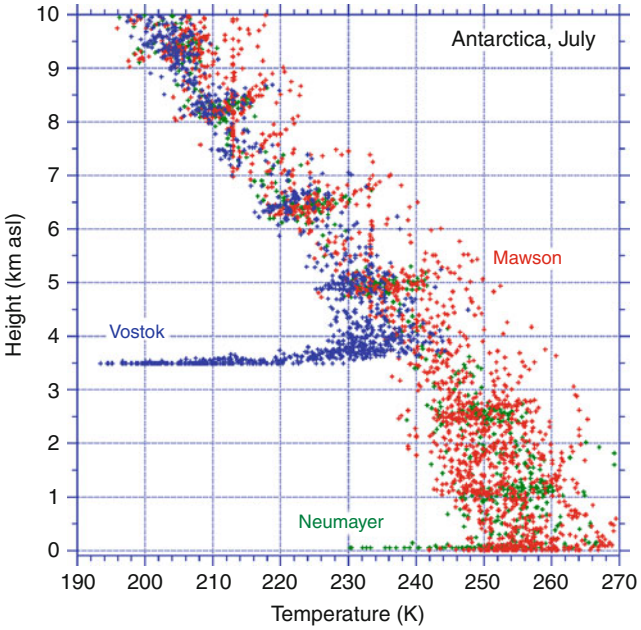

Surface Energy Balance, Figure 6 Wintertime (July) vertical temperature profiles from radiosondes measurements at three Antarctic stations. Atmospheric temperature profiles at South Pole are similar to Vostok.

longwave radiation, resulting in a weaker surface temperature inversion (e.g., Mawson and Neumayer in Figure 6).

Under these statically stable conditions, wind shear is a prerequisite for the generation of turbulent heat exchange. Wind shear is enhanced over rough surfaces, such as hummocky sea ice (Andreas and Claffey, 1995); over snow and ice surfaces that are relatively smooth, it requires relatively large wind speeds for the wind shear to become sufficiently large. Over ice sheets and glaciers, which have a sloping surface, this wind shear is often provided by *katabatic* forcing. The cold near-surface air is denser than the air in the free atmosphere at the same elevation, which sets up a horizontal pressure gradient over a sloping surface, forcing *katabatic* or downslope winds. Over the large ice sheets, katabatic winds can be very persistent. Because the katabatic forcing acts along the local slope, katabatic winds have a high *directional constancy.* Because of their direct coupling to the radiative cooling of the surface, katabatic winds efficiently generate the turbulence necessary to keep the sensible heat transport going in the stably stratified atmospheric surface layer.

Latent heat flux

Over a snow/ice surface at freezing temperatures, the latent heat flux (LHF) equals the amount of heat extracted from or added to the surface as a result of sublimation (the phase change from solid to water vapor) or deposition (phase transition from vapor to solid, i.e., rime formation). When the surface is melting and liquid water is available, LHF equals the amount of heat extracted from or added to

the surface as a result of evaporation (the phase change from liquid to gas) or condensation (phase transition from gas to liquid, i.e., dew formation). In mountainous areas and over sea ice, frost formation (from liquid to solid) may also be an important process. All these processes exchange not only heat but also mass with the surface, which couples the surface energy balance to the surface mass balance (the sum of all mass fluxes toward and away from the surface).

The LHF can be directly measured using instruments that measure the absorption of light by water vapor at a specific wavelength. Alternatively, LHF can be calculated using simultaneously measured vertical profiles of wind speed and specific humidity. The latter is often determined from relative humidity measurements, which are difficult to perform over snow and ice (Anderson, 1994).

Temperature plays a pivotal role in the magnitude of LHF through its influence on the moisture content of the air. The maximum moisture content of the air, and therewith its vertical gradients, is tightly coupled to temperature through the Clausius Clapeyron equation. Figure 7 (left) shows specific humidity as a function of 2 m temperature for a non-melting location in East Antarctica. Neglecting the temperature difference between the surface and 2 m for the moment and using the fact that the snow/ice surface is always saturated (i.e., the surface-specific humidity is represented by the upper boundary of the point cloud), the distance of individual points to the upper boundary represents the vertical moisture gradient, and therewith the sublimation potential. The undersaturation and therewith the vertical humidity gradient become small at low temperatures, resulting in low LHF values (Figure 7, right).

In summer, when the surface absorbs solar radiation and heats up, significant sublimation does occur at this site (significantly negative LHF). But even under very favorable conditions, the magnitude of LHF usually does not exceed several tens of W m^{-2}, which are small values compared to the mid-latitudes and tropics, where LHF can attain values of several hundreds of W m^{-2}. But this does not mean that LHF is unimportant for the hydrological cycle at high latitudes. An average LHF of only -1 W m^{-2} still represents a surface mass loss of 11 kg m^{-2}. For areas where snowfall and melt are small, such as the interior of the Greenland and Antarctic ice sheets, this potentially represents a considerable fraction of the annual snowfall.

When snowdrift takes place, sublimation from the surface ceases while the sublimation of drifting snow particles takes over. For snowdrift sublimation, which is thought to be an important term in the mass balance of the Greenland and Antarctic ice sheets and the seasonal snowpack at high northern latitudes (Box and others, 2006; Déry and Yau, 2001), no robust measurement techniques are yet available.

Subsurface heat flux

The subsurface heat flux (G) represents the conduction of heat into the subsurface strata; this flux is mainly driven by molecular conduction and therefore occurs along vertical temperature gradients in the snow/ice, following $G(z) = k\, dT(z)/dz$. The heat conductivity (k) of snow is mainly a function of snow density and grain structure, connecting the low heat conductivity of air ("zero" density snow) to that of ice (red curve in Figure 8). Since snow is

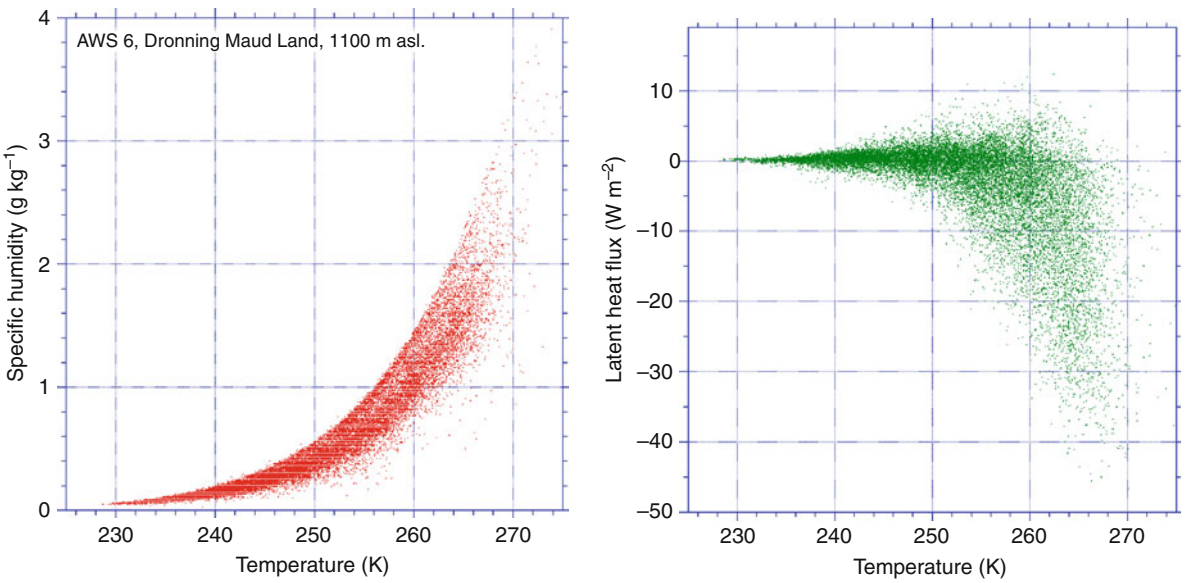

Surface Energy Balance, Figure 7 Observations of hourly 2 m specific humidity (*left*) and calculated latent heat flux LHF (*right*) as a function of 2 m temperature at an automatic weather station in East Antarctica.

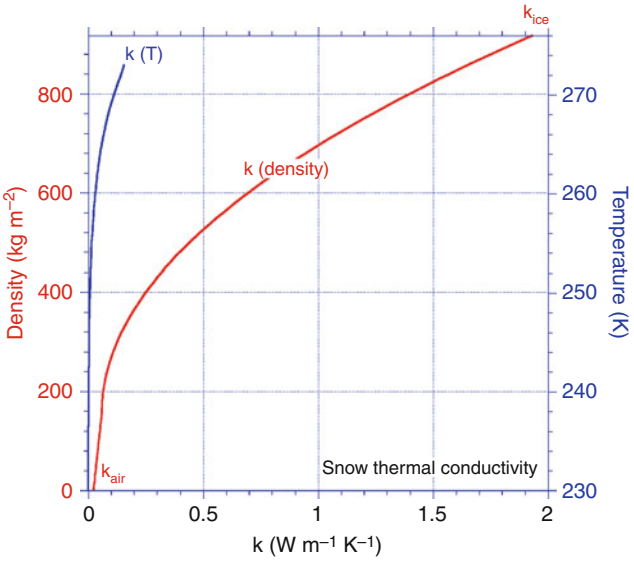

Surface Energy Balance, Figure 8 Value of heat conductivity k in snow is mainly a function of snow density and grain structure (*red curve*). A small part of the heat transport results from internal convection and from sublimation and subsequent deposition elsewhere in the snowpack, mainly a function of temperature (*blue curve*).

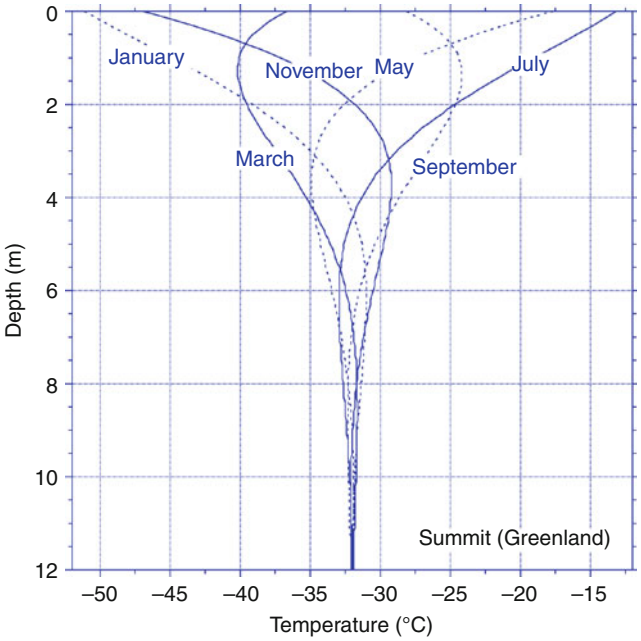

Surface Energy Balance, Figure 9 Theoretical temperature distribution in the snow at Summit, Greenland, forced by a sinusoidal temperature variation at the surface, and assuming a homogeneous snowpack with k = 0.5 W K^{-1} m^{-1}.

a porous medium, a small part of the heat transport results from internal convection and from sublimation and subsequent deposition elsewhere in the snowpack, both processes being a function of temperature (blue curve in Figure 8). This results in an effective heat conductivity that is the sum of conduction and internal convection/deposition.

In the surface energy balance, the surface value of G, G_s, is relevant. Over sea ice, G_s is an important SEB component (see further in this entry). Over a semi-infinite snowpack, G_s will be close to zero when averaged over the year; otherwise the snow layers below the surface would continuously cool or heat up. In the monthly average, G_s will be negative in summer, when the surface is warmer than the subsurface snow layers and heat is transported into the snowpack, and positive in winter, when the temperature gradient is reversed and heat is extracted from the deeper snow layers. But also monthly average values are usually small, typically several W m^{-2}. The real importance of G_s is in the daily cycle of the SEB. At times when turbulence is small, for instance under weak wind conditions, G_s is the only term that can compensate the radiative heat gains/losses; the chain of events is as follows: when the radiation balance becomes strongly positive/negative, and turbulence is weak, the surface temperature will quickly rise/fall. In response, the vertical temperature gradients between the subsurface and the surface will quickly grow, triggering a strongly negative/positive value of G_s, which compensates for the radiative heat exchange.

Because it transports heat, G(z) determines the ice/snow temperature distribution. Figure 9 shows the (theoretical) subsurface temperature distribution at Summit Station at the top of the Greenland ice sheet, as forced by a sinusoidal annual cycle in surface temperature, assuming a homogenous snowpack with constant density. In the absence of melting, the annual temperature variation vanishes below approximately 10 m depth. This means that at those depths, the temperature approximates the annual mean surface temperature. This technique is often used to estimate the annual mean surface temperature in the interior of the large ice sheets, where few observations are available. When melt occurs, the refreezing of the percolating meltwater releases heat into the snowpack and the underlying ice. Under these conditions, the technique of determining annual mean T_s is no longer applicable.

Melting and refreezing

If absorption of solar radiation has heated the snow/ice layers to the melting point, the excess energy produces melting ($M > 0$). The meltwater formed at the surface either runs off (when the surface is impermeable, i.e., ice), or penetrates the snowpack. Sea ice is an intermediate case where the water partly pools at the surface and partly percolates through or flows off the ice into the ocean. In the case of a snow pack, the meltwater may refreeze at some depth where the temperature is still below freezing. This refreezing of meltwater may constitute an important process for the mass balance of glaciers and sea ice

because the ice involved must be melted more than once before it is removed from the glacier. Moreover, upon refreezing, latent heat is released within the snowpack, which alters the subsurface temperature distribution. However, because the heat is released below the surface, as is the case with penetration of shortwave radiation, this heat source is not part of the surface energy balance. It merely influences the SEB through altering the subsurface heat flux by changing the subsurface temperature gradient. Gallée and Duynkerke (1997), for instance, showed that the daily cycle of surface melting and refreezing below the surface significantly impacts the SEB in Greenland. If it is not taken into account, the surface and subsurface temperatures are significantly underestimated.

Annual cycle of SEB over various permanent snow- and ice-covered surfaces

In this section, we discuss the idealized annual cycle, based on monthly means, of the SEB over various permanently snow- and ice-covered surfaces. The coordinates, elevation, surface type and basic climate conditions of these locations during different seasons are summarized in Table 1. For clarity, the annual cycles presented in the following figures have been smoothed using 3-month running means. For details of calculation and variability beyond the mean annual cycle, we refer to the original references.

North pole, arctic basin

While some SEB estimates are available from Russian drifting station and from various US drift stations such as SHEBA (Surface Heat Budget of the Arctic Ocean, Utta and others, 2002; Persson and others, 2002), here we present, for illustrative purposes, the idealized annual cycle of the SEB at the North Pole (90° North, NP), based on model/weather observations combined with an SEB model, assuming 2 m thick sea ice. The NP is situated over a frozen ocean surface that consists of snow-covered sea ice in winter and melting snow/ice in summer (Table 1). The wintertime SEB (Figure 10) is a first-order balance between (longwave) radiative cooling and heating by SHF and G_s. Especially G_s is significant; 30 W m^{-2} is the approximate amount of heat that flows from the warm ocean (−1.8°C) to the sea ice surface (−30°C), when the ice is 2 m thick. Because of the radiative cooling, the sea ice surface is colder than the overlying air, which, in combination with the moderate winds, generates a flux of sensible heat toward the surface. At the sea ice–ocean boundary, a semi-unlimited heat source is available from the deeper ocean. As a result, annual average G_s is significantly positive, driving freezing at the ice/ocean interface.

At these low temperatures, wintertime LHF is negligible. In spring, shortwave radiative heating increases surface temperature and specific humidity, resulting in weak sublimation. At sea level, the summer climate is relatively mild, even this far north, and frequent melting occurs. When melting starts in earnest in summer, the moisture and temperature gradients between the sea ice surface and the overlying air diminish, reducing the magnitude of the turbulent fluxes. Because the temperature gradient between ice surface and ice base also disappears, G_s goes to zero. All the absorbed shortwave radiation is invested in melting. The integrated amount of melt energy represents the removal of approximately 1.5 m of ice, less than the total ice thickness. In spite of bottom melting also taking place, sea ice at the North Pole usually survives the summer melt period, to form multiyear sea ice in the subsequent years.

Ablation zone of the west-greenland ice sheet

The Greenland ice sheet is the second largest ice mass in the world, and its southernmost part is situated in a subarctic climate. A site was selected in the lower ablation zone of the southwestern ice sheet (Table 1) for which reliable, multiyear meteorological observations are available (Van den Broeke et al., 2008a, b). In winter, surface radiative cooling is compensated in first order by SHF, with small contributions from LHF and G_s (Figure 11).

Surface Energy Balance, Table 1 Surface and climate characteristics of some SEB locations

Location name	Coordinates Elevation (m asl)	Surface type		Temperature (°C)		Wind speed (m s^{-1})	
		Summer	*Winter*	*Summer*	*Winter*	*Summer*	*Winter*
North Pole (Sea Ice)	90° N ~0 m	Melting snow/ice	Snow	−2	−30	6	5
West Greenland ablation zone	67° 06′N, 50° 07′ W 500 m	Melting ice	Snow	+3	−20	5	5
Morteratsch glacier	46° 24′ N, 9° 56′ E 2100 m	Melting ice	Snow	+9	−7	6	6
Neumayer (Antarctica)	70° 39′ S, 8° 15′ W 40 m	(Melting) snow	Snow	−5	−25	7	10
South Pole (Antarctica)	90° S 2830 m	Snow	Snow	−30	−60	5	7
		Dry season	*Wet season*	*Dry season*	*Wet season*	*Dry season*	*Wet season*
Kersten glacier (Kilimanjaro)	3° 05′ S, 37° 21′ E 5873 m	Ice	(Melting) snow	−7	−6	4	5

The subsurface heat flux G_s is heating the surface during winter, when the surface temperature is lower than the deeper snowpack temperature (Figure 9). In summer, the surface at this site is continuously at the melting point while the temperature deeper in the snowpack is several degrees lower than the melting point inducing a negative G_s.

Because in summer the air is usually warmer than 0°C, both SHF and LHF are directed toward the melting ice surface, contributing significantly to melt. Because of the sunny climate and relatively high temperatures in this part of Greenland, the total amount of summer ice melt at this site exceeds 4 m, among the largest values found in Greenland. Both SHF and LHF show a double maximum, one in winter and one in summer, which is caused by the double maximum in wind speed. In both seasons, atmospheric cooling through SHF maintains the katabatic winds. In winter, surface radiative cooling maintains the surface temperature deficit, while in summer the melting surface is responsible for a temperature deficit. Over melting ice surfaces, katabatic winds are sometimes called *glacier winds*.

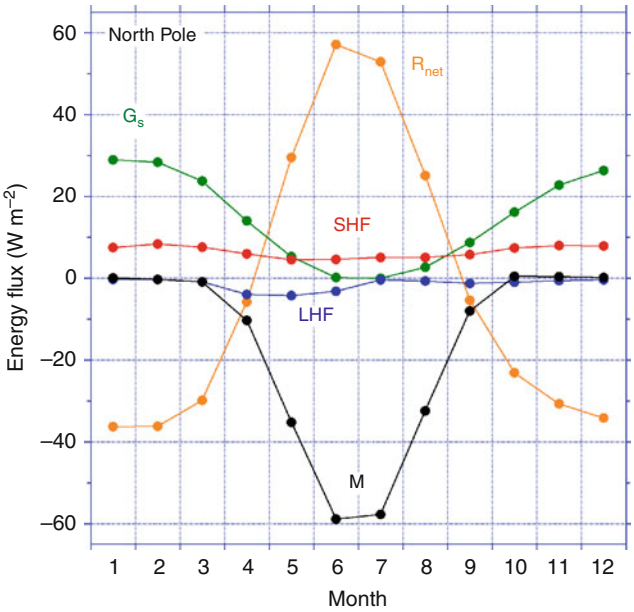

Surface Energy Balance, Figure 10 Annual cycle of SEB components at North Pole in the Arctic basin. Idealized results from model data and observations, assuming 2 m thick sea ice (see text).

Ablation zone of morteratsch glacier, swiss alps

Vadret da Morteratsch is a mid-latitude glacier in Switzerland (Table 1) and has one of the longest uninterrupted SEB records from the surface of a valley glacier (15 years, Oerlemans and others, 2009). The automatic weather station that produced the results shown in Figure 12 is situated in the ablation zone at the tongue of the glacier at 2,100 m asl. The winter SEB (Figure 12) is comparable to the Greenland ablation zone, with radiative heat losses being compensated mainly by SHF. In summer, the glacier tongue is surrounded by ice-free terrain, resulting in high summer air temperatures over the melting ice surface

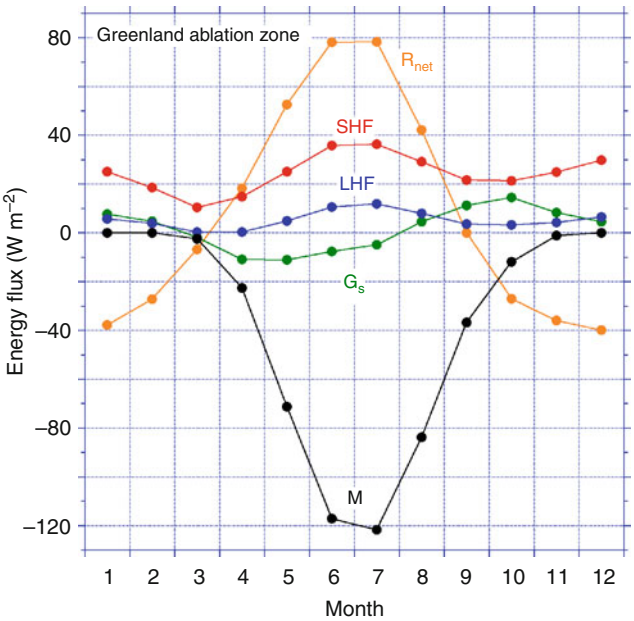

Surface Energy Balance, Figure 11 Annual cycle of SEB components in the lower ablation zone of the ice sheet in southwest Greenland. SEB calculated from 4 years of automatic weather station observations (see text).

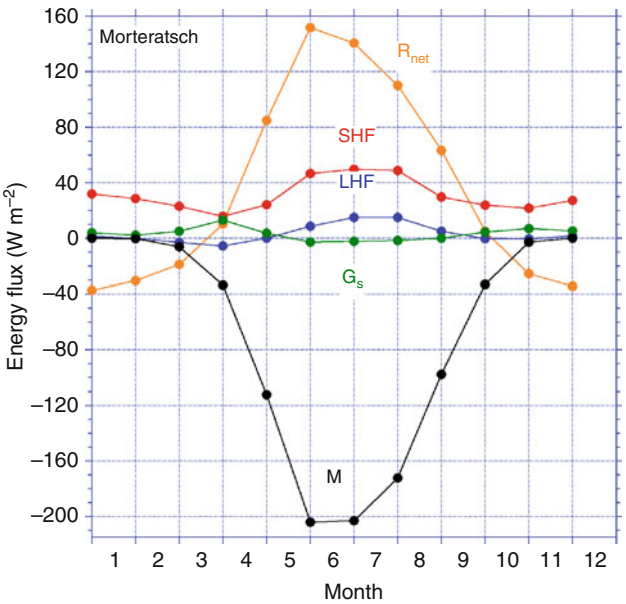

Surface Energy Balance, Figure 12 Annual cycle of SEB components in the ablation zone of the Morteratsch glacier, Switzerland. SEB calculated from 15 years of automatic weather station observations (see text).

(Table 1). This also results in dust accumulation, so that the surface albedo of the ice attains very low values (~0.15). This strongly enhances the absorption of shortwave radiation and therewith surface melting. As a result, R_{net} attains much higher values than in Greenland, while SHF and LHF are comparable, including the double annual maxima. The total melt for this location exceeds 7 m of ice, which has forced a strong retreat of the glacier in recent decades.

Kersten glacier, Kilimanjaro

This tropical glacier is situated between 5,100 and 5,900 m on the southern flank of Kilimanjaro, close to the equator (Table 1). Based on several years of AWS data and distributed energy balance modeling, the SEB, averaged over the entire glacier surface, could be determined (Mölg and others, 2009). The annual cycle (Figure 13) deviates strongly from other locations. As a result of its location close to the equator, the annual cycles in SW_{in} and ambient temperature are small, and thus there is no climatological summer or winter at this site; the seasonal variations are mostly forced by the wet and dry seasons. At these high elevations, the air contains little moisture and sublimation produces an important heat and mass loss year round. In the main wet season (April/May), sublimation strongly decreases. Net radiation is small, because SW_{net} is at a minimum, mainly due to high albedo. At the same time, as the air is moist and cloudy, cooling by LW_{net} is also small, resulting in small net radiation. In the core dry season (June–August) there is hardly any melt and ablation is controlled by sublimation. In these months, cooling by sublimation significantly exceeds warming by R_{net}, so that the surface remains significantly colder than the overlying air and SHF peaks. The most variable part of the year is the wet season around November/December. This season can start in October and last into January/February, but sometimes is totally absent. The occurrence of sublimation and the associated surface cooling is vital for limiting the melt amount throughout the year. Note that, even in the presence of moderate refreezing, melt (575 kg m^{-2} $year^{-1}$) still removes more mass than sublimation (450 kg m^{-2} $year^{-1}$) glacier-wide, because of the much smaller latent heat of fusion compared to evaporation/sublimation. However, at the glacier summit, sublimation dominates and accounts for 75% of the total annual mass loss.

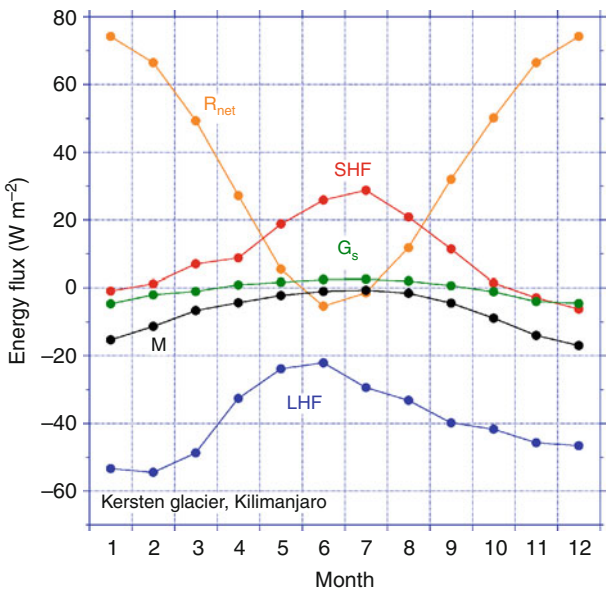

Surface Energy Balance, Figure 13 Annual cycle of SEB components on Kersten glacier, Kilimanjaro, Tanzania. SEB calculated from three years of automatic weather station observations in combination with a distributed energy balance model (see text).

Neumayer, antarctica

Neumayer station (Germany) is situated on Ekstrøm ice shelf in coastal East Antarctica, at approximately 70°S (Table 1). The station is situated relatively far to the north, at low elevation (40 m asl) and close to the Southern Ocean. The nearby ocean is ice-covered in winter, but ice free in summer. Being situated close to the circumpolar pressure trough, Neumayer experiences strong easterly winds year round with frequent occurrence of snowdrift (~40% of the time). The wind maximum in winter is caused by enhanced depression activity, not by katabatic forcing, because Neumayer is situated on a flat ice shelf, which does not allow for significant katabatic forcing. In spite of the proximity of the ocean, Neumayer has a cold climate with only occasional melting around noon during sunny summer days. The SEB (Figure 14) was calculated using 13 years of high-quality meteorological observations (König Langlo and Loose, 2007; Van den Broeke and others, 2009). In the absence of continuous melting, with slow snow metamorphosis, the surface albedo is high year round. Only after prolonged dry periods with daytime melt in summer does the albedo of the snow surface fall below 0.8; as a result, R_{net} is small and the radiation balance only becomes positive in summer. In combination with mild summer temperatures, this allows for significant sublimation (Figure 14). In winter, longwave radiative cooling dominates and is compensated by SHF and in second order by LHF and G_s.

South pole, east antarctica

The geographic South Pole is situated in the vast interior of the East Antarctic ice sheet at an altitude in excess of 2,800 m (Table 1). The South Pole experiences a wintertime surface inversion similar to Vostok Station in Figure 6. Because it is not situated on a dome, the wind climate shows an appreciable wintertime (katabatic) maximum which, because the surface slope is small, is much weaker than those measured over the steeper parts of the ice sheet closer to the coast. Snow metamorphism is slow at these low temperatures, resulting in a year-round high surface albedo. As a result, summertime net radiation is

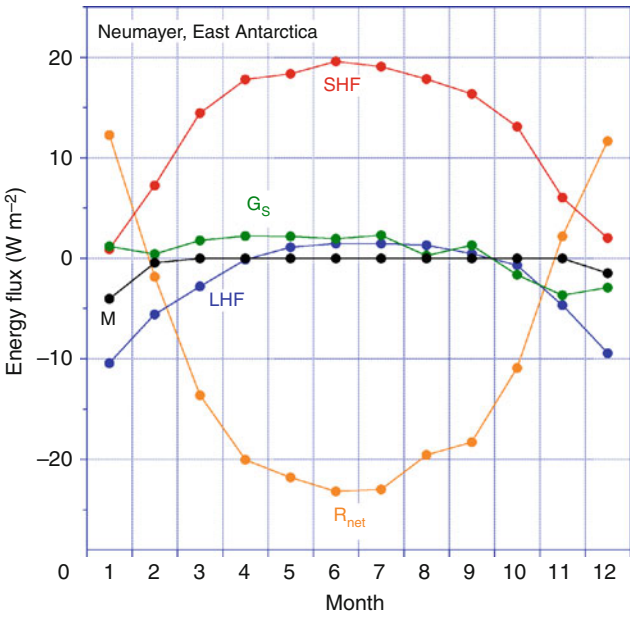

Surface Energy Balance, Figure 14 Annual cycle of SEB components at Neumayer, East Antarctica. SEB calculated based on 13 years of surface observations (see text).

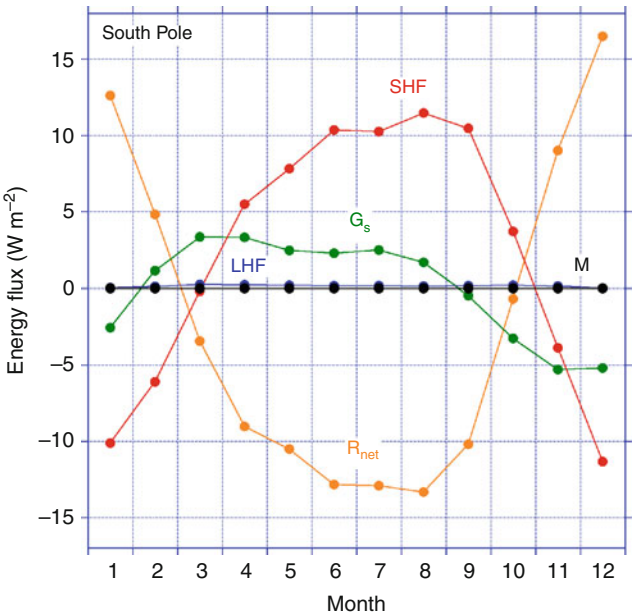

Surface Energy Balance, Figure 15 Annual cycle of SEB components at South Pole, East Antarctica. SEB calculated based on 3 years of surface observations (see text).

small, <15 W m^{-2}, and all fluxes are smaller in magnitude than at Neumayer (Figure 15). Summer temperatures are also too low to allow for significant sublimation to occur. In the absence of this heat sink, surface temperature can rise quickly above the air temperature during sunny summer days, allowing weak convection (negative SHF) and a shallow (~100 m) mixed boundary layer to develop (King and others, 2006; Van As and others, 2006). Because all other fluxes are small, monthly mean G_s becomes a significant component of the SEB at the South Pole, in spite of its small magnitude. The wintertime SEB is comparable to Neumayer, i.e., a first-order balance between radiative cooling and heating by SHF.

Summary

This entry describes the components of the surface energy balance (SEB) over snow and ice: shortwave and longwave radiation, the turbulent fluxes of sensible and latent heat, and the subsurface (conductive) heat flux. If the surface is melting, the sum of these fluxes determines the melt rate. We explicitly describe the idealized mean annual cycle of the surface energy balance components at six locations with permanently ice- or snow-covered surfaces, but with widely varying melt characteristics: sea ice at the North Pole, the ablation zone of the Greenland ice sheet, the ablation zone of the Morteratsch glacier in Switzerland, Kersten Glacier on the Kilimanjaro in Tanzania, Neumayer station in coastal East Antarctica, and South Pole station in interior East Antarctica.

Acknowledgments

We thank Gert König Langlo, Rianne Giesen, and Hans Oerlemans for providing data. Thomas Grenfell and an anonymous reviewer are thanked for improving the original manuscript.

Bibliography

Anderson, P. S., 1994. A method for rescaling humidity sensors at temperatures well below freezing. *Journal of Atmospheric and Oceanic Technology*, **11**, 1388–1391.

Andreas, E. L., and Claffey, K. J., 1995. Air-ice drag coefficients in the western Weddell Sea: 1. Values deduced from profile measurements. *Journal of Geophysical Research*, **100**, 4821–4831.

Box, J., Bromwich, D., Veenhuis, B., Bai, L.-S., Stroeve, J., Rogers, J., Steffen, K., Haran, T., and Wang, S.-H., 2006. Greenland ice sheet surface mass balance variability (1988–2004) from calibrated polar MM5 output. *Journal of Climate*, **19**, 2783–2800.

Brandt, R. E., and Warren, S. G., 1993. Solar heating rates and temperature profiles in Antarctic snow and ice. *Journal of Glaciology*, **39**, 99–110.

Déry, S. J., and Yau, M. K., 2001. Simulation of blowing snow in the Canadian Arctic using a double-moment model. *Boundary-Layer Meteorology*, **99**, 297–316.

Fettweis, X., 2007. Reconstruction of the 1979–2006 Greenland ice sheet surface mass balance using the regional climate model MAR. *The Cryosphere*, **1**, 21–40.

Gallée, H., and Duynkerke, P., 1997. Air-snow interactions and the surface energy and mass balance over the melting zone of west Greenland during GIMEX. *Journal of Geophysical Research*, **102**, 13813–13824.

Grenfell, T. C., and Maykut, G. A., 1977. The optical properties of ice and snow in the Arctic basin. *Journal of Glaciology*, **18**, 445–463.

Greuell, W., 2000. Melt-water accumulation on the surface of the Greenland ice sheet: effect on albedo and mass balance. *Geografiska Annaler*, **82A**, 489–498.
Hatzianastassiou, N., Matsoukas, C., Hatzidimitriou, D., Pavlakis, C., Drakakis, M., and Vardavas, I., 2004. Ten year radiation budget of the Earth: 1984–93. *International Journal of Climatology*, **24**, 1785–1802.
King, J. C., and Connolley, W. M., 1997. Validation of the surface energy balance over the Antarctic ice sheets in the UK meteorological office unified climate model. *J Climate*, **10**, 1273–1287.
King, J. C., Argentini, S. A., and Anderson, P. S., 2006. Contrasts between the summertime surface energy balance and boundary layer structure at Dome C and Halley stations, Antarctica. *Journal of Geophysical Research*, **111**, D02105, doi:10.1029/2005JD006130.
Klok, E. J., and Oerlemans, J., 2002. Model study of the spatial distribution of the energy and mass balance of Morteratschgletscher, Switzerland. *Journal of Glaciology*, **48**, 505–518.
König-Langlo, G. C., and Loose, B., 2007. The meteorological observatory at Neumayer stations (GvN and NM-II). *Antarctica, Polarforschung*, **76**, 25–38.
Kuipers Munneke, P., van den Broeke, M. R., Reijmer, C. H., Helsen, M. M., Boot, W., Schneebeli, M., and Steffen, K., 2009. The role of radiation penetration in the energy budget of the snowpack at Summit, Greenland. *The Cryosphere*, **3**, 155–165.
Kuipers Munneke, P., Reijmer, C. H., and van den Broeke, M. R., 2010. Assessing the retrieval of cloud properties from radiation measurements over snow and ice. *International Journal Climatology*, doi:10.1002/joc.2114.
Mölg, T., Cullen, N. J., Hardy, D. R., Winkler, M., and Kaser, G., 2009. Quantifying climate change in the tropical mid troposphere over East Africa from glacier shrinkage on Kilimanjaro. *Journal of Climate*, **22**, 4162–4181.
Oerlemans, J., Giessen, R. H., and van den Broeke, M. R., 2009. Retreating alpine glaciers: increased melt rates due to accumulation of dust (Vadret da Morteratsch, Switzerland). *Journal of Glaciology*, **55**, 729–736.
Overland, J. E., McNutt, S. L., Groves, J., Salo, S., Andreas, E. L., and Persson, P. O. G., 2000. Regional sensible and radiative heat flux estimates for the winter Arctic during the Surface Heat Budget of the Arctic ocean (SHEBA) experiment. *Journal of Geophysical Research*, **105**, 14093–14102.
Persson, P. O. G., Fairall, C. W., Andreas, E. L., Guest, P. S., and Perovich, D. K., 2002. Measurements near the atmospheric surface flux group tower at SHEBA: near-surface conditions and surface energy budget. *Journal of Geophysical Research*, **107** (C10), 8045, doi:10.1029/2000JC000705.
Stull, R. B., 1988. *An introduction to boundary layer meteorology*. Dordrecht/Boston/London: Kluwer Academic Publishers, p. 666.
Uttal, T., Curry, J. A., McPhee, M. G., Perovich, D. K., Moritz, R. E., Maslanik, J. A., Guest, P. S., Stern, H. L., Moore, J. A., Turenne, R., Heiberg, A., Serreze, M. C., Wylie, D. P., Persson, O. G., Paulson, C. A., Halle, C., Morison, J. H., Wheeler, P. A., Makshtas, A., Welch, H., Shupe, M. D., Intrieri, J. M., Stamnes, K., Lindsey, R. W., Pinkel, R., Pegau, W. S., Stanton, T. P., and Grenfell, T. C., 2002. The surface heat budget of the Arctic. *Bulletin of the American Meteorological Society*, **83**, 255–275.
Van As, D., van den Broeke, M. R., and Helsen, M. M., 2006. Structure and dynamics of the summertime atmospheric boundary layer over the Antarctic plateau, I: measurements and model validation. *Journal of Geophysical Research*, **111**, D007102, doi:10.1029/2005JD005948.
Van den Broeke, M. R., Smeets, C. J. P. P., Ettema, J., van der Veen, C., van de Wal, R. S. W., and Oerlemans, J., 2008a. Partitioning of melt energy and meltwater fluxes in the ablation zone of the west Greenland ice sheet. *The Cryosphere*, **2**, 179–189.
Van den Broeke, M., Smeets, P., Ettema, J., and Munneke, P. K., 2008b. Surface radiation balance in the ablation zone of the west Greenland ice sheet. *Journal of Geophysical Research*, **113**, D13105, doi:10.1029/2007JD009283.
Van den Broeke, M. R., König-Langlo, G., Picard, G., Kuipers Munneke, P., and Lenaerts, J., 2009. Surface energy balance, melt and sublimation at Neumayer station, East Antarctica. *Antarctic Science*, doi:10.1017/S0954102009990538.
Wiscombe, W., and Warren, S., 1980. A model for the spectral albedo of snow I. Pure snow. *Journal of Atmospheric Sciences*, **37**, 2712–2733.

Cross-references

Albedo
Arctic Hydroclimatology
Atmosphere-Snow/Ice Interactions
Climate Change and Glaciers
Degree-Days
Dry Snow
Firn
Glacier Mass Balance
Heat and Mass Transfer in Sea Ice
Ice Sheet
Ice Shelf
Katabatic Wind: In Relation with Snow and Glaciers
Kilimanjaro
Latent Heat of Condensation
Latent Heat of Fusion/Freezing
Latent Heat of Sublimation
Melting Processes
Physical Properties of Snow
Sea Ice
Snow
Snow Density
Snow Drift
Surface Temperature of Snow and Ice
Temperature Profile of Snowpack

SURFACE TEMPERATURE OF SNOW AND ICE

Dorothy K. Hall
Crysopheric Sciences Branch, Greenbelt, MD, USA

Definition

Land-Surface Temperature (LST) – surface temperature measurement from space over land areas, including land ice and snow.

Introduction and background

Thermal infrared (TIR) sensors facilitate surface temperature and melt-condition monitoring over extensive areas of snow and ice (Key and Haefliger, 1992; Stroeve and Steffen, 1998; Comiso, 2006; Hall et al., 2006, 2008a, b), especially when used with complementary satellite-derived passive- and active-microwave data.

The surface temperature (T) is not an intrinsic property of the surface; it varies with external factors such as meteorological conditions. Emissivity *is* an intrinsic property

of the surface and is independent of the temperature (Hook et al., 2007). Emissivity of snow and ice features is far less variable than the range encountered in a wide variety of land surfaces, leading to greater potential accuracies in retrieved land-surface temperature (LST) over snow and ice even when the emissivity is not known precisely. To obtain snow-surface temperatures to an accuracy of 0.01 K, the emissivity must be known to within 0.1% (Stroeve et al., 1996).

Analysis of the Advanced Very High Resolution Radiometer (AVHRR)-derived surface temperature of the Antarctic and Greenland ice sheets, ice caps, and smaller glaciers, available from the early 1980s, provides a method to evaluate melt and general climate trends as a surrogate for, and in addition to, air-temperature records that are obtained from relatively few and scattered in-situ observations (Stroeve and Steffen, 1998; Wang and Key, 2003, 2005a, b; Comiso, 2006). Satellite-derived "clear-sky" surface-temperature data are also useful for the validation of climate models and as input to data-assimilation models. However, AVHRR data, though highly valuable, have been acquired from a variety of instruments over a period >20 years, leading to satellite intercalibration issues. Newer data from the Earth Observation System (EOS) offer promise for validating the overlapping AVHRR record and extending the surface-temperature record over ice-covered areas into the future at a higher spatial resolution with improved instrument calibration.

One way to assess the accuracy of remotely sensed LSTs is to compare the values with in-situ surface temperatures under clear-sky conditions (Hall et al., 2008b). Various factors make that problematic, including the fact that the in-situ observations are point measurements while the satellite-derived observations represent LSTs from a much larger area. Also, in-situ observations from weather stations, and in particular the Greenland Climate Net-work (GC-Net) automatic weather station (AWSs) (Box, 2002) which are generally acquired at some height above the surface so that the measured air temperature must be extrapolated to calculate a surface temperature. That calculation is also affected by meteorological factors such as wind speed, but for higher wind-speed conditions, when the near-surface air is well mixed, near-surface air temperature is very close to the surface temperature. Also the AWS instruments record in-situ data at a "point" while the satellite instruments record data over an area varying in size from: 57 × 57 m Enhanced Thematic Mapper Plus (ETM+), 90 × 90 m Advanced Spaceborne Thermal Emission and Reflection Radiometer (ASTER), or to 1 × 1 km Earth Observing System Moderate Resolution Imaging Spectroradiometer (MODIS). Surface topography and other factors contribute to variability of surface temperature within a pixel, thus the AWS measurements may not be representative of the LST of the pixel as a whole. Without more information on the local spatial patterns, the AWS LST cannot be considered valid ground truth for the satellite measurements, with RMS uncertainty ~2°C or greater (Hall et al., 2008b; Koenig and Hall, in press).

Satellite-derived "clear-sky" LST products were studied from EOS instruments including the MODIS (Wan et al., 2002), the ASTER (Gillespie et al., 1998), and the ETM+ (Barsi et al., 2005) over snow and ice on Greenland. Satellite-derived LSTs were compared with in-situ air-temperature observations from the GC-Net. Results showed that MODIS, ASTER, and ETM+ provide reliable and consistent LSTs under clear-sky conditions and relatively flat terrain over snow and ice targets over a range of temperatures from −40°C to 0°C. The satellite-derived LSTs agree within a relative RMS uncertainty of ~0.5°C. The good agreement among the LSTs derived from the various satellite instruments is especially notable since different spectral channels and different retrieval algorithms are used to calculate LST from the raw satellite data. However accuracies are lower when LSTs are compared with AWS measurements.

Summary

The accuracy of measuring the surface temperature of snow and ice has been assessed. Difficulties are encountered when attempting to validate satellite data covering a large area (e.g., 1 × 1 km) with a point measurement (e.g., using air temperature data from meteorological stations or AWS), but relative validation between EOS IR sensors has provided accuracies of LST measurements over snow and ice of <1°C. To develop a long-term record of "clear-sky" surface temperature, satellite intercalibration remains an issue.

Bibliography

Barsi, J. A., Shott, J. R., Palluconi, F. D., and Hook, S. J., 2005. Validation of a Web-based atmospheric correction tool for single thermal band instruments. In *Proceedings of SPIE*, 5822, SPIE, Bellingham, doi:10.1117/12.619990.

Box, J. E., 2002. Survey of Greenland instrumental temperature records: 1873–2001. *International Journal of Climatology*, **22**, 1829–1847.

Comiso, J. C., 2006. Arctic warming signals from satellite observations. *Weather*, **61**(3), 70–76.

Gillespie, A. R., Rokugawa, S., Matsunaga, T., Cothern, J. S., Hook, S., and Kahle, A. B., 1998. A temperature and emissivity separation algorithm for Advanced Spaceborne Thermal Emission and Reflection Radiometer (ASTER) images. *IEEE Transactions on Geoscience and Remote Sensing*, **36**, 1113–1126.

Gillespie, A., Rokugawa, S., Hook, S. J., Matsunaga, T., and Kahle, A. B., 1999. *The ASTER temperature/emissivity separation algorithm theoretical basis document* (ATBD-AST-03) Version 2.4.

Hall, D. K., Williams, R. S., Jr., Casey, K. A., DiGirolamo, N. E., and Wan, Z., 2006. Satellite-derived, melt-season surface temperature of the Greenland ice sheet (2000–2005) and its relationship to mass balance. *Geophysical Research Letters*, **33**, L11501, doi:10.1029/2006GL026444.

Hall, D. K., Williams, R. S., Jr., Luthcke, S. B., and DiGirolamo, N. E., 2008a. Greenland ice sheet surface temperature, melt and mass loss: 2000–2006. *Journal of Glaciology*, **54**(184), 81–93.

Hall, D. K., Box, J. E., Casey, K. A., Hook, S. J., Shuman, C. A., and Steffen, K., 2008b. Comparison of satellite-derived ice and snow surface temperatures over Greenland from MODIS, ASTER,

ETM+ and in-situ observations. *Remote Sensing of Environment*, **112**(10), 3739–3749, doi:10.1016/j.rse.2008.05.007.
Hook, S. J., Vaughan, R. G., Tonooka, H., and Schladow, S. G., 2007. Absolute radiometric in-flight validation of mid infrared and thermal infrared data from ASTER and MODIS on the Terra spacecraft using the Lake Tahoe, CA/NV, USA, Automated Validation Site. *IEEE Transactions Geoscience and Remote Sensing*, **45**, 1798–1807.
Key, J., and Haefliger, M., 1992. Arctic ice surface temperature retrieval from AVHRR thermal channels. *Journal of Geophysical Research*, **97**(D5), 5885–5893.
Koenig, L. S., and Hall, D. K., in press. Comparison of satellite, thermochron and air temperatures at Summit, Greenland, 1 during the winter of 2008-09. *Journal of Glaciology*.
Stroeve, J., and Steffen, K., 1998. Variability of AVHRR-derived clear-sky surface temperature over the Greenland ice sheet. *Journal of Applied Meteorology*, **37**, 23–31.
Stroeve, J., Haefliger, M., and Steffen, K., 1996. Surface temperature from ERS-1 ATSR infrared thermal satellite data in polar regions. *Journal of Applied Meteorology*, **35**(8), 1231–1239.
Wan, Z., Zhang, Y., Zhang, Q., and Li, Z.-L., 2002. Validation of the land-surface temperature products retrieved from Terra Moderate Resolution Imaging Spectroradiometer data. *Remote Sensing of Environment*, **83**, 163–180.
Wang, X., and Key, J., 2003. Recent trends in Arctic surface, cloud, and radiation properties from space. *Science*, **299**(5613), 1725–1728.
Wang, X., and Key, J., 2005a. Arctic surface, cloud, and radiation properties based on the AVHRR Polar Pathfinder dataset, Part I: Spatial and temporal characteristics. *Journal of Climate*, **18**(14), 2558–2574.
Wang, X., and Key, J., 2005b. Arctic surface, cloud, and radiation properties based on the AVHRR Polar Pathfinder data set, Part II: Recent trends. *Journal of Climate*, **18**(14), 2575–2593.

Cross-references

Albedo
Arctic Hydroclimatology
Temperature Profile of Snowpack

SUSPENDED SEDIMENT CONCENTRATION

Veerle Vanacker
TECLIM, Earth and Life Institute, University of Louvain, Louvain-la-Neuve, BW, Belgium

Definition

Suspended sediment is generally transported within and at the same velocity as the surrounding fluid (water or wind). The stronger the flow and/or the finer the sediment, the greater the amount of sediment that can be suspended by turbulence.

Only the finer fraction (usually silt and clay fraction) of the suspended sediment can be continuously maintained in suspension by the flow turbulence. This fraction is often referred to as "wash load," and is typically not found in significant quantities at the bed surface. Its concentration is usually related to the sediment supply and is difficult to determine theoretically.

Most sediment particles are not continuously suspended, but are continuously settling through the surrounding fluid and may eventually return to the bed. This part of the total suspended sediment is referred to as "bed-material load," and its concentration can be estimated from the hydraulic parameters of the fluid and the composition of the bed material.

History and current techniques

The first measurements of suspended sediment go back at least to the samplings of the Rhone River (France) in the early 1800s (Garcia, 2008). The earliest suspended sediment samples were collected using instantaneous samplers. Later, more sophisticated samplers were developed that could be filled at a selected depth below the water surface.

The first sediment sampling and analytical methods used to differ strongly between the various monitoring programs (Glysson and Gray, 1997). The creation of the Federal Interagency Sedimentation Project (FISP) was important to standardize sediment samplers, sampling, and analytical techniques around the world. At present, a large number of both manually operated samplers and automatic samplers exist. Information on the use and calibration of these samplers can be obtained from the Federal Interagency Sedimentation Project (FISP, 2009).

In addition to these suspended sediment samplers, rapid progress is being made in developing new techniques for measuring the concentration of suspended sediment in fluids. These new methods are commonly based on optical backscatter, optical transmission, focused beam reflectance, laser diffraction, acoustic, nuclear, spectral reflectance, digital optical, and differential pressure principles to capture specific characteristics of the sediment–fluid mixture (Wren et al., 2000). At the moment, several of these advanced techniques still suffer from technical limitations that render their operation difficult in some environments. Continued technological improvements will undoubtedly lead to improved methods to collect data on suspended sediment concentration in the future.

Factors controlling variations in suspended sediment concentration

There is now a wealth of information from case studies worldwide that exemplify the large temporal and spatial variation that exists in suspended sediment concentration. It is becoming increasingly clear that variations in suspended sediment concentrations cannot be explained by natural biophysical factors only such as climate, geology, or topography.

Various studies have clearly shown that sediment fluxes from anthropogenically altered catchments are significant (Walling, 2006). Research at different spatial scales has indicated that humans have accelerated sediment production by agricultural activities, road construction, and intense logging, but have reduced the global sediment delivery to the oceans because of sediment retention in

reservoirs (Hooke, 2000; Syvitski et al., 2005; Vanacker et al., 2007).

In addition to global-scale analyses, simultaneous research on small catchments may contribute to yield complementary information on suspended sediment dynamics that would be difficult to obtain exclusively through large catchment studies.

Conclusions

In recent years, new techniques have been developed that will provide us a wealth of data on suspended sediment concentrations at spatial and temporal resolutions much higher than previously possible. In the future, this information will undoubtedly contribute to better understand the role of anthropogenic disturbances and climate change on terrestrial sediment fluxes.

Bibliography

Federal Interagency Sedimentation Project (FISP), 2009. Federal Interagency Sedimentation Project Home Page. (http://fisp.wes.army.mil, April 2009).

Garcia, M. H., 2008. *Sedimentation engineering: processes, management, modeling and practice.* ASCE Manual and Reports on Engineering Practice No. 110, American Society of Civil Engineers (ASCE).

Glysson, G. D., and Gray, J. R., 1997. Coordination and standardization of federal sedimentation activities. In *Proceedings of the U.S. Geological Survey Sediment Workshop*, Expanding sediment research capabilities in Today's USGS, Reston, Virginia, and Harpers Ferry, West Virginia, February 4–7, 1997. (http://water.usgs.giv/osw/techniques/workshop/glysson.html)

Hooke, R. Le. B., 2000. On the history of humans as geomorphic agents. *Geology*, **28**, 843–846.

Syvitski, J. P. M., Vorosmarty, C. J., Kettner, A. J., and Green, P., 2005. Impacts of humans on the flux of terrestrial sediment to the global coastal ocean. *Science*, **308**, 376–380.

Vanacker, V., Molina, A., Govers, G., Poesen, J., and Deckers, J., 2007. Spatial variation of suspended sediment concentrations in a tropical Andean river system: The Paute river, southern Ecuador. *Geomorphology*, **87**, 53–67.

Walling, D. E., 2006. Human impact on land-ocean sediment transfer by the world's rivers. *Geomorphology*, **79**, 192–216.

Wren, D. G., Barkdoll, B. D., Kuhnle, R. A., and Derrow, R. W., 2000. Field techniques for suspended-sediment measurement. *J Hydraul Eng*, **126**, 97–104.

Cross-references

Sediment Yield
Suspended Sediment Dynamics

SUSPENDED SEDIMENT DYNAMICS

Tim Stott
Physical Geography and Outdoor Education, Liverpool John Moores University, Liverpool, UK

Definition

Suspended sediment. The fine portion of a river or stream's sediment load which is normally carried in suspension. Suspended sediment is usually finer than 2 mm, although this boundary can vary significantly according to the stream's power and turbulence.

Dynamics. The branch of mechanics that deals with the motion and equilibrium of systems under the action of forces, usually from outside the system.

Introduction

Glaciers alternate between phases of accumulation and ablation. It is during ablation phases that most meltwater is discharged from glaciers. Even at low discharges, the meltwater is usually capable of entraining and transporting fine sediment in suspension. The dominant trend over the past few decades is that most glaciers worldwide are out of equilibrium with the current climate and they are slowly adjusting to seasonal changes in precipitation and higher temperatures by showing negative mass balance, significant volume loss, and retreat in most areas. In terms of landscape dynamics, this widespread and rapid retreat of mountain glaciers is revealing new expanses of fresh glacial debris, the stability, dynamics, and potential fluvial transport of which is beginning to gain the attention of research scientists. Meltwater streams and rivers draining glaciers and flowing across the fore field are called pro-glacial streams. Due to the large supply of sediment deposited beneath and in front of glaciers, pro-glacial streams can have high suspended sediment concentrations (SSC) during the peak (summer) melt season and during rainstorms. They are capable of transporting high suspended sediment loads.

Measurement methods

The most common approach to measuring suspended sediment dynamics in pro-glacial streams relies on retrieving discrete water samples at-a-point over time. This can be achieved by lowering a wide-mouthed bottle (usually 1 L capacity) into the flow and retrieving it when full. The highly turbulent nature of the flow usually means that suspended sediment is extremely well mixed and that values sampled at the stream margin will be representative of the whole cross section (see Gurnell et al., 1992). Water samples are then passed through pre-weighed filters (these are normally glass fiber such as Whatman GF/D 8 μm filters) on which the suspended sediment in the water sample is retained. Filters are then oven dried, and the filter plus dry sediment are weighed. The difference in the pre- and post-weight of the filter is due to the suspended sediment in the water sample. The weight of sediment divided by the volume of the water sample gives the SSC which is reported in mg/L. This method is known as the gravimetric method. However, in order to gain any meaningful understanding of suspended sediment dynamics, samples taken at a minimum of 3-hourly intervals are necessary, and most researchers reduce this time to 1 h or less if possible, which can be very labor intensive. Therefore, automatic pumping samplers (Figure 1) are used to

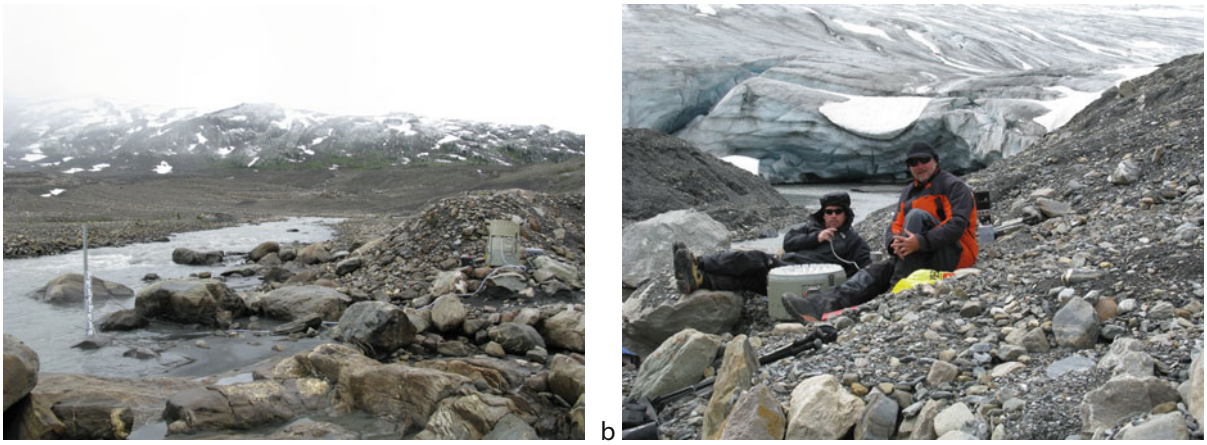

Suspended Sediment Dynamics, Figure 1 (**a**) Suspended sediment and discharge gauging site with stage board and ISCO automatic water sampler used to retrieve samples from Castle Creek draining the Roberts glacier, Cariboo Mountains, British Columbia with Roberts glacier in background (photo: Tim Stott). (**b**) Researchers filtering water samples retrieved by an ISCO automatic water sampler at Castle Creek which drains the Roberts glacier in background, Cariboo Mountains, British Columbia in summer 2008 (photo: Tim Stott).

Suspended Sediment Dynamics, Figure 2 Glass fiber 7 cm diameter filters which have been used to remove suspended sediment from a sequence on 1-hourly water samples collected in the Torrent du Glacier Noir, Ecrins National Park in SE France during July 2003. NB. The first sample (*top left*) was taken at 14:00 on day 1 and the last (*bottom right*) at 13:00 on day 2. The *top* row (14:00–17:00 on afternoon of day 1) and *bottom* rows (10:00–13:00 on day 2) show much higher SSCs as these will have coincided with times of highest discharge.

automatically pump water samples from the river via a 5–6 m tube (Figure 1a) into a series of 24 bottles (Figure 1b). The sampler is battery powered and the time interval at which samples are pumped can be determined by the operator. Figure 2 shows 24 filters which were collected from an Alpine pro-glacial torrent.

Since stream discharge has been shown to exert an important control over suspended sediment dynamics, this is normally measured at the same time that water samples are retrieved, or maybe even at greater frequency by means of electronic water level sensors such as a pressure transducer. The relationship between SSC and discharge (Q) shown in Figure 3 is known at a rating curve where $SSC = aQ^b$, where a and b are constants representing the intercept and slope of the rating plot, respectively.

Turbidity has successfully been used as a surrogate for SSC in pro-glacial streams (Clifford et al., 1995; Hodgkins, 1999; Irvine-Fynn et al., 2005; Stott and Mount, 2007a, b; Stott et al., 2008). Partech infrared (IR15C) 0–10,000 mg/L range turbidity sensors are a popular choice (Figure 4).

Turbidity sensors, such as the one shown in Figure 4, work by emitting a beam of light which is detected by a photoelectric cell on the opposite side of a gap. The instrument produces a voltage output which is proportional to the amount of light received by the light sensor. When the instrument is deployed in a stream, the proportion of the emitted light which is received by the light sensor is deemed to be proportional to the color or SSC of the stream water. The voltage output is logged by a data logger at any predetermined time interval (e.g., 10 s to 10 min) giving a far greater insight into the dynamics of the suspended sediment. However, in order to make useful meaning of the turbidity voltage data, gravimetrically determined samples are needed in order to calibrate the voltage output of the turbidity sensor (Figure 5).

The turbidity reading is sensitive to the particle size of the suspended sediment passing through the sensor gap which can scatter the light in different ways, hence the less-than-perfect relationship on Figure 4. So, the use of turbidity in pro-glacial streams can be a useful application to gain a more detailed picture of the suspended sediment

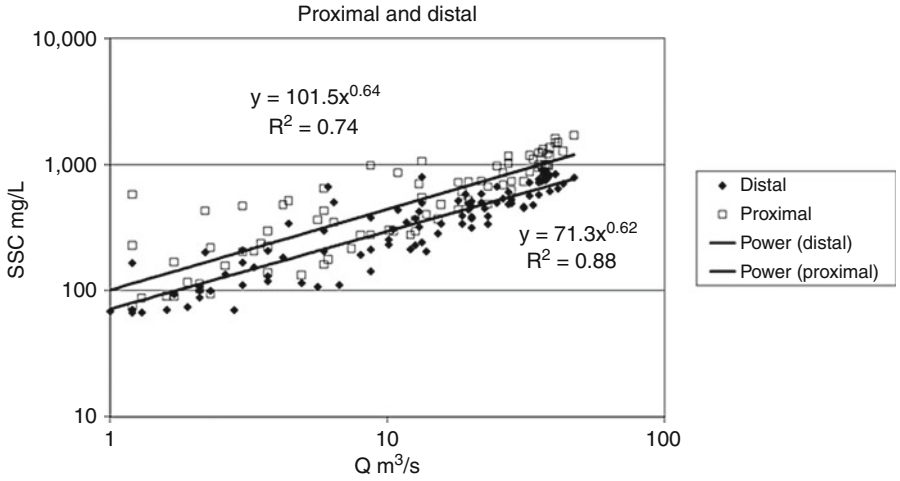

Suspended Sediment Dynamics, Figure 3 Suspended sediment concentration vs discharge rating relationship for proximal (50 m from glacier snout) and distal (600 m from glacier snout) sampling stations in the Ova da Morteratsch, Switzerland (From Stott et al., 2008).

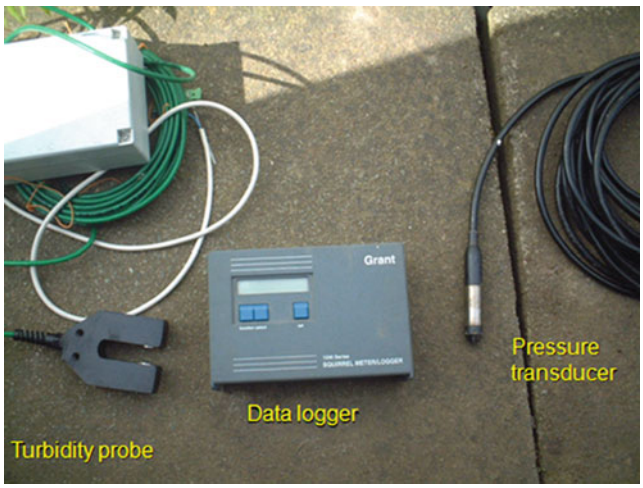

Suspended Sediment Dynamics, Figure 4 Partech turbidity sensor, data logger, and pressure transducer (photo: T. Stott).

dynamics, but it has limitations due to the difficulties of obtaining strong-enough calibration relationships.

Time series investigations

Figure 6 shows a typical time series plot for discharge and SSC predicted from turbidity sensors at two pro-glacial monitoring stations.

The predicted SSC record (Figure 6), while broadly responding to discharge fluctuations, shows SSC to be erratic, particularly at the proximal station. Some of the SSC peaks coincide with discharge peaks but others do not, suggesting that factors other than discharge are controlling SSC variations. One clear diurnal pattern is that discharge minimum consistently occurs at 09:10 each morning, after which it rises rapidly until it peaks sometime between 13:50 (e.g., 8 July) and 18:40 (e.g., 7 July), which seems to depend on the weather conditions (in particular air temperature). The SSC records behave differently, with proximal SSC behaving much more erratically, with greater variation, than the smoother less variable distal SSC. Nevertheless, diurnal variations are clear at both locations. Prior to 12 July, SSC at both stations rises and falls in response to discharge, until a cold weather spell on the night of 9–10 July occurred, when air temperature dropped to almost 0°C followed by cool days on 10 and 11 July causing discharge and SSC to fall. Some rain also fell on 9 and 10 July when daily totals of 24.8 and 1.8 mm were recorded. Warmer temperatures returned on 12 July after which peak discharge climbed steadily each day and a clear SSC exhaustion effect begins to appear. This can be seen clearly in Figure 5 where, following the minimum discharge at 09:10 in the morning, proximal SSC would fall and remain low for up to 6 h, not regaining its 09:10 am level until mid-afternoon, while distal SSC would start and continue to rise from 09:10 am with discharge. This suggests that the suspended sediment source during the morning and early afternoon was the pro-glacial area itself, whereas by mid-afternoon the proximal SSC would overtake the distal SSC suggesting that the suspended sediment source had now switched to the subglacial meltwater once the glacier had started to melt and the supra-, en-, and subglacial conduits had begun to flow. However, despite increasing air temperatures in the latter part of the record (13–19 July), SSC peaks in both proximal and distal records became progressively lower suggesting that the available sediment supply, apparent in the early part of the record, had become exhausted.

Figure 7 shows three examples of hydrographs and sedigraphs (generated using 5-min turbidity data) plotted using data gathered by Stott and Grove (2001) in the

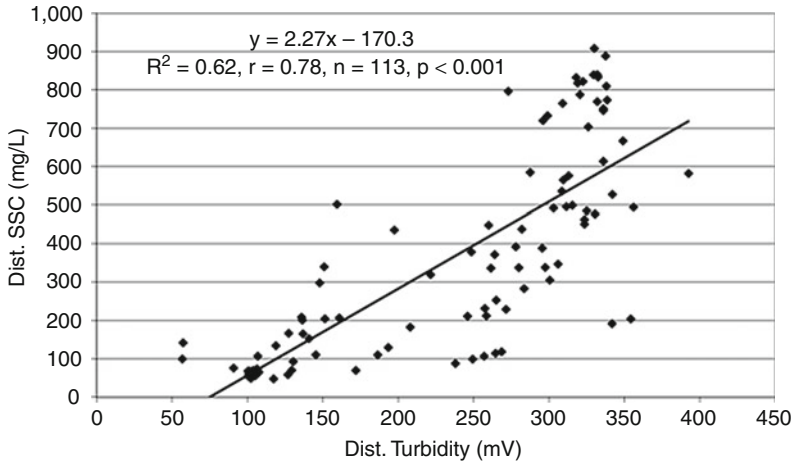

Suspended Sediment Dynamics, Figure 5 Suspended sediment concentration vs turbidity voltage calibration curve for Ova da Morteratsch, Bernina Alps, Switzerland after Stott et al. (2008). Note the large degree of scatter in the relationship.

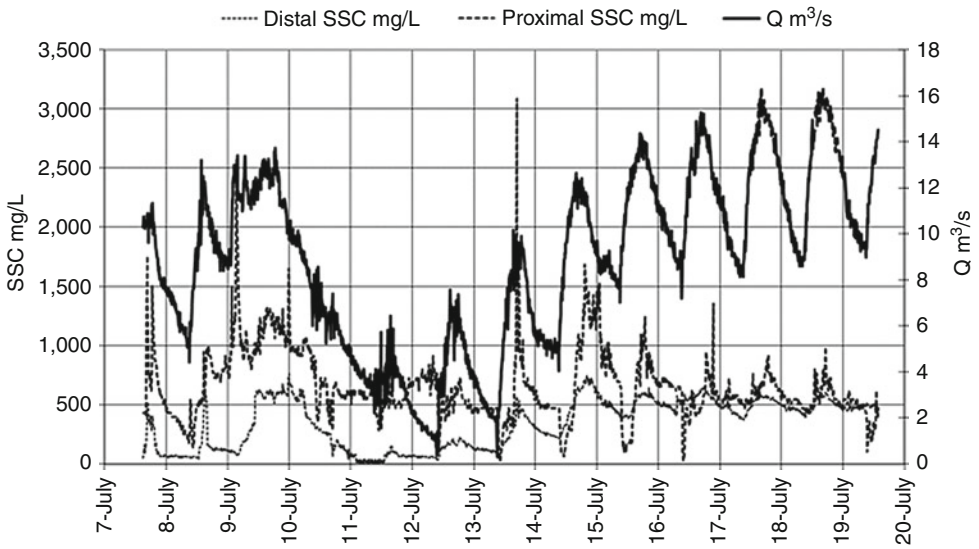

Suspended Sediment Dynamics, Figure 6 Time series plot for discharge and suspended sediment concentration predicted from turbidity sensors at two monitoring stations in the pro-glacial zone of the Morteratsch glacier, Switzerland in July 2007. The proximal station is 50 m from glacier snout, and the distal station is 600 m from the glacier snout (From Stott et al., 2008).

Skeldal River, NE Greenland in the 1998 melt season. At the same monitoring station during the study in August, SSC peaks before (Figure 7a), at the same time as (Figure 7b), and after the main hydrograph peak (Figure 7c).

This means that SSC can have very different values depending on which part of the hydrograph is being examined. For example, in Figure 7a, at a stage of 35 cm on the rising limb of the hydrograph SSC is 750 mg/L whereas when stage is 35 cm on the falling limb, around 10 h later, SSC is 550 mg/L. Where SSC can have different values at the same stage or discharge is known as the hysteresis effect.

Hysteresis

Figure 8 shows two examples of hysteresis loops in the SSC vs Q relationship in the Torrent du Glacier Noir, SE France (data from Stott and Mount, 2007a). Clearly, there is a large amount of scatter in the SSC vs Q relationship during both hydrographs.

However, when the sampling sequence is identified by numbers and the points are traced sequentially by arrows,

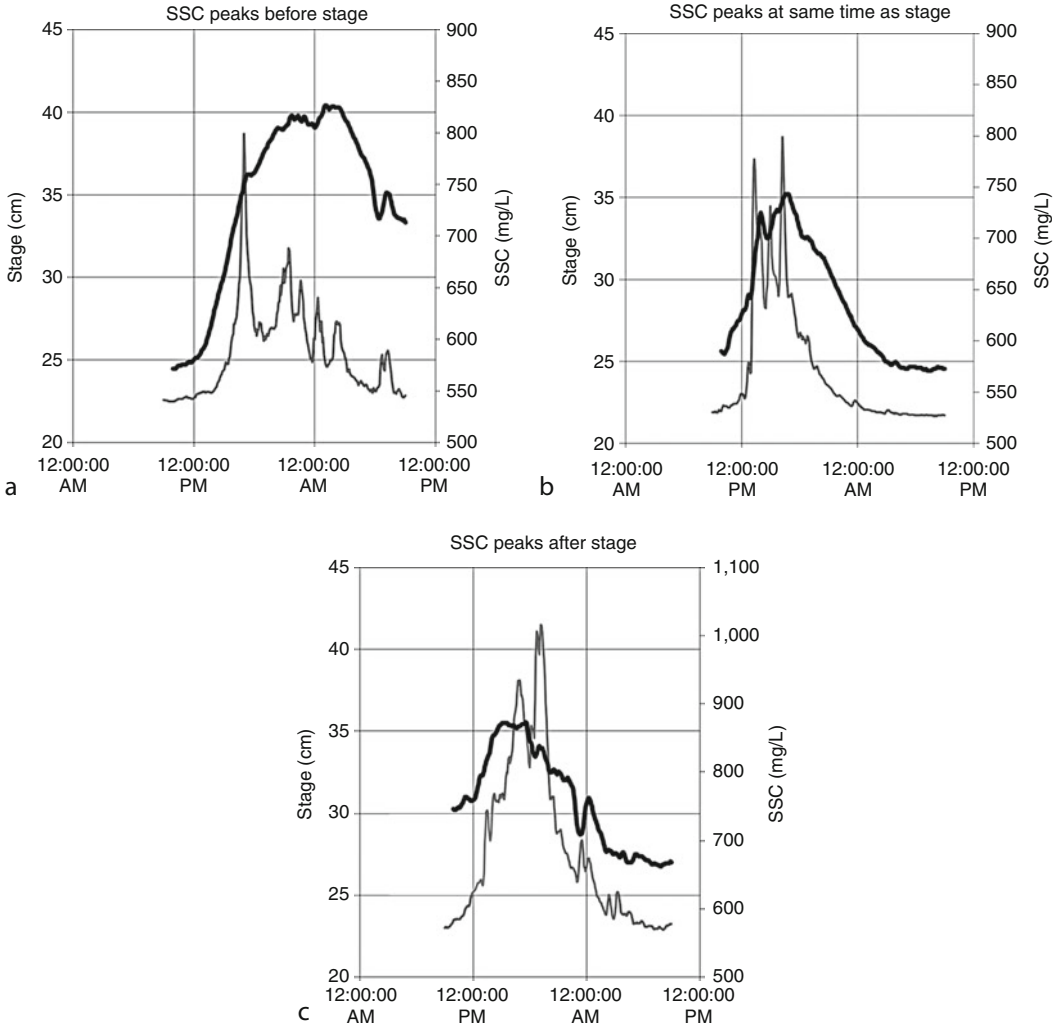

Suspended Sediment Dynamics, Figure 7 River stage (black line) and suspended sediment concentration (gray line) time series plots for the Skeldal River, NE Greenland (5-min data from a study by Stott and Grove, 2001), August 1998.

the loop nature of the hysteresis effect is visible in each of the flood events on 11 and 12 July 2003. While the loops are not perfect (they cross-over), the generally clockwise loop on 11 July (Figure 8a) suggests that SSC peaked before Q, whereas the anticlockwise loop in 12 July (Figure 8b) suggests that SSC peaked after Q.

Current investigations, controversies, and gaps in current knowledge

Future changes in pro-glacial suspended sediment dynamics are likely given the generally agreed forecasts for global warming this century (IPCC, 2007) and the likely continued retreat of glaciers. The consequences are likely to have greatest impact in the less economically developed parts of the world like the Himalaya (Singh et al., 2004) where changes in inputs of sediments to glacier-fed rivers have important implications for water abstraction and drinking water supply. Hydropower (HEP), large and small, is one of the most important of the renewables for electrical power production worldwide, providing 19% of the world's electricity (Paish, 2002) and set to increase. Small-scale hydro which draws water directly from streams and rivers with no dam or water storage, is one of the most cost-effective and environmentally benign energy technologies to be considered for rural electrification in less developed countries. Paish (2002) reports that the European Commission has a target to increase small hydro capacity by 4500 MW (50%) by the year 2010, and notes that turbines need to be protected from all the debris commonly found in rivers. Sediment entering intake pipes can be highly abrasive to turbines resulting in high maintenance and/or repair costs. A better understanding of sediment dynamics, and the likely future, will be important to HEP operators as it will allow planning of sediment flushing events and water intake at times when suspended sediment loads are likely to have least impact.

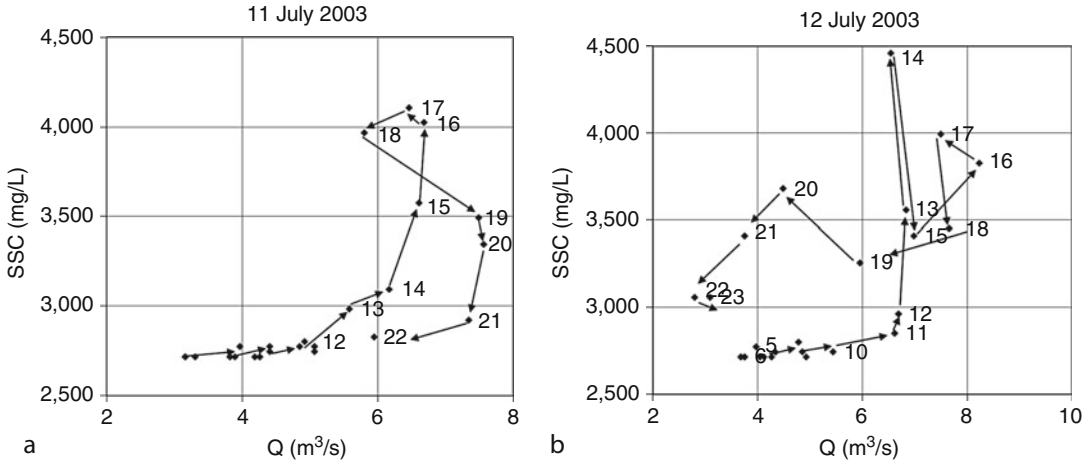

Suspended Sediment Dynamics, Figure 8 Examples of hysteresis loops in the SSC vs Q relationship for 1-hourly samples in the Torrent du Glacier Noir, SE France (data from Stott and Mount, 2007a), (**a**) clockwise on 11 July 2003, (**b**) anticlockwise on 12 July 2003.

High suspended sediment loads from mountain regions can result in sedimentation in lowland rivers which may affect stream ecology. Silt can clog river-bed gravels (Petticrew and Biickert, 1998), which in certain reaches contain salmon spawn so depriving the eggs of vital oxygen, thus jeopardizing successful salmon reproduction. River sedimentation can also impact channel dynamics in lowland river systems by causing decreases in channel capacity which can increase flood potential and lateral erosion, and may require expensive river dredging programs to avert such problems (Owens et al., 2005).

Summary

Suspended sediment dynamics is concerned with the motion and equilibrium of the fine portion of a river or stream's sediment load which is normally carried in suspension. Most meltwater is discharged from glaciers during ablation phases, and even at low discharges the meltwater is usually capable of entraining and transporting fine sediment in suspension, and at peak discharges pro-glacial streams are capable of transporting extremely high suspended sediment loads.

Changes in SSC are measured by collecting water samples in sequence at-a-point over time, then filtering the water through special glass fiber filters and measuring the weight change, known as the gravimetric method. Samples can be retrieved manually by dipping an empty bottle into the flow, or automatically using pumping samplers. Scatter plots of SSC vs Q are known as rating relationships. Turbidity can be used as a surrogate for SSC and has the advantage of being able to automatically scan at high frequency and log voltages to a data logger. However, SSC vs turbidity calibration relationships in pro-glacial streams, like SSC vs Q, tend to be less than perfect. Nevertheless, they can reveal patterns which might otherwise be missed by water sampling programs, and thereby aide interpretation of suspended sediment dynamics in pro-glacial streams. Examination of time series datasets from NE Greenland for SSC and Q show asynchronous SSC and Q patterns, with SSC peaking before, at the same time, and after the hydrograph peak in different flood events. A hysteresis effect in the SSC vs Q rating relationship is demonstrated for the Torrent du Glacier Noir in SE France.

Future changes in pro-glacial suspended sediment dynamics are likely given the generally agreed forecasts for global warming this century. The consequences are likely to be greatest in the less economically developed parts of the world like the Himalaya where glacier-fed rivers supply a high proportion of drinking water. Elsewhere, hydroelectricity generation often relies on abstracting water from glacier-fed rivers and changes in suspended sediment dynamics will have important implications for the timing and amount of abstraction since sediment-laden water causes problems concerned with increased abrasion and scour of pipes and turbines. Silt from pro-glacial zones can clog river-bed gravels downstream where certain reaches contain salmon spawn so depriving the eggs of vital oxygen, thus jeopardizing successful salmon reproduction. River sedimentation can also impact channel dynamics in lowland river systems by causing decreases in channel capacity which can increase flood potential and lateral erosion, and may require expensive river dredging programs to avert such problems.

Bibliography

Clifford, N. J., Richards, K. S., Brown, R. A., and Lane, S. N., 1995. Scales of variation of suspended sediment concentration and turbidity in a glacial meltwater stream. *Geografiska Annaler*, **77A**(1–2), 45–65.

Gurnell, A. M., Clark, M. J., Hill, C. T., and Greenhalgh, J., 1992. Reliability and representativeness of a suspended sediment concentration monitoring programme for a remote alpine proglacial river. In Bogen, J., Walling, D. E., and Day, T. (eds.), Erosion and Sediment Transport Monitoring in River Basins. *Proceedings of the Oslo Symposium* 24–28 August

1992, International Association of Hydrological Sciences Publication, 210, 191–200.
Hodgkins, R., 1999. Controls on suspended sediment transfer at a High-Arctic glacier determined from statistical modelling. *Earth Surface Processes and Landforms*, **24**(1), 1–21.
Hodgkins, R., Cooper, R., Wadham, J., and Tranter, M., 2003. Suspended sediment fluxes in a high-Arctic glacierised catchment: implications for fluvial sediment storage. *Sedimentary Geology*, **162**, 105–117.
IPCC. 2007. *Climate Change 2007: The Physical Science Basis, Contribution of Working Group I to the Fourth Assessment Report of the Intergovernmental Panel on Climate Change*. Fourth Assessment Report of the Intergovernmental Panel on Climate Change, Cambridge University Press. Available at http://www.ipcc.ch/ [accessed 21-10-07].
Irvine-Fynn, T. D. L., Moorman, B. J., Willis, I. C., Sjogren, D. B., Hodson, A. J., Mumford, P. N., Walter, F. S. A., and Williams, J. L. M., 2005. Geocryological processes linked to high Arctic proglacial stream suspended sediment dynamics: examples from Bylot Island, Nunavut, and Spitsbergen, Svalbard. *Hydrological Processes*, **19**(1), 115–135.
Owens, P. N., Batalla, R., Collins, A. J., Gomez, B., Hicks, D. M., Horowitz, A. J., Kondolf, G. M., Marden, M., Page, M. J., Peacock, D. H., Petticrew, E. L., Salomons, W., and Trustrum, N. A., 2005. Fine-grained sediment in river systems: environmental significance and management issues. *River Research and Applications*, **21**, 693–717.
Paish, O., 2002. Small hydro power: technology and current status. *Renewable & Sustainable Energy Reviews*, **6**(6), 537–556.
Petticrew, E. L., and Biickert, S. L. 1998. Characterization of sediment transport and storage in the upstream portion of the Fraser River (British Columbia, Canada). In Modeling Soil Erosion, Sediment Transport and Closely Related Hydrological Processes (*Proceedings of a Symposium held al Vienna*, July 1998). International Association of Hydrological Sciences Publication, **249**, 383–391.
Singh, P., Haritashya, U. K., Ramasastri, K. S., and Kumar, N., 2004. Diurnal variations in discharge and suspended sediment concentration, including runoff-delaying characteristics, of the Gangotri glacier in the Garhwal Himalayas. *Hydrological Processes*, **19**(7), 1445–1457.
Stott, T. A., and Grove, J. R., 2001. Short-term discharge and suspended sediment fluctuations in the proglacial Skeldal River, N. E. Greenland. *Hydrological Processes*, **15**, 407–423.
Stott, T. A., and Mount, N. J., 2007a. Alpine proglacial suspended sediment dynamics in warm and cool ablation seasons: implications for global warming? *Journal of Hydrology*, **332**(3–4), 259–270.
Stott T. A., and Mount, N. J., 2007b. The Impact of Rainstorms on Short-Term Spatial and Temporal Patterns of Suspended Sediment Transfer over A Proglacial Zone, Ecrins National Park, France, in Effects of River Sediments and Channel Processes on Social, Economic and Environmental Safety. In *Proceedings of the Tenth International Symposium on River Sedimentation*, Vol. V, River Sediment in the Environment: 259–266. Moscow. 1–4, August 2007.
Stott, T. A., Nuttall, A., Eden, N., Smith, K., and Maxwell, D., 2008. Suspended sediment dynamics in the Morteratsch proglacial zone, Bernina Alps, Switzerland. *Geografiska Annaler Series A Physical Geography*, **90**(4), 299–313.

Cross-references

Glacier Hydrology
Suspended Sediment Concentration
Suspended Sediment Load

SUSPENDED SEDIMENT LOAD

Amit Kumar
Department of Geology, Centre of Advanced Study in Geology, Punjab University, Chandigarh, India

Synonyms

Wash load

Definition

Almost all the world's streams carry sediment that originates from erosion processes in the basin that feed the streams. Sediment carried in a stream is classified as either suspended load or bed load. The suspended load is the fine-grained (clay and silt) sediment that remains in water during transportation. The bed load consists of the coarser fractions of the sediment (sands and gravels), moves by rolling, sliding, or saltation actions. Coarser sediments will be deposited first and suspended sediment load moves at approximately with the same velocity of the flowing water. From the general point of view, river is a main component of global water cycle and it plays an important role to transport sediment and other matter into the ocean (Garrels et al., 1975; Martin and Meybeck, 1979). In Himalayas, three major river systems: the Ganga, the Brahamputra, and Indus delivered a combined suspended sediment load of the order of 1.8×10^9 ton/year (Meybeck, 1976), which is about 9% of the total annual load carried from the continent to the oceans worldwide. Suspended sediment load can be satisfactory assessed directly from discharge and sediment concentration. Suspended sediment records are also used to estimating erosion rates in mountainous region, where the eroded material is transported as a sediment load.

Bibliography

Benn, D. I., and Evans, D. J. A., 1998. *Glaciers and Glaciation*. London: Arnold.
Garrels, R. M., Mackenzie, F. T., and Hunt, 1975. *Chemical Cycle and the Global Environment*. New York: William Kaufman. 260 pp.
Hambrey, M., and Alean, J., 2004. *Glaciers*, 2nd edn. New York: Cambridge University Press.
Lenzi, M. A., D' Agostino, V., and Billi, P., 1999. Bed-load transport in the instrumented catchment of the Rio Cordon: Part1. Analysis of bed-load records, condition and threshold of bad-load entrainment. *Catena*, **36**, 171–190.
Martin, J. M., and Meybeck, M., 1979. Elemental mass-balance of material carried by major world rivers. *Marine Chemistry*, **7**, 173–206.
Meybeck, M., 1976. Total mineral dissolved transport by world major rivers. *Hydrological Science Bulletin*, **21**, 265–284.
Milliman, J. D., and Meade, R. H., 1983. World-wide delivery of river sediment to the oceans. *Journal of Geology*, **91**, 1–21.

Cross-references

Sediment Entrainment, Transport, and Deposition
Suspended Sediment Load

SYNTHETIC APERTURE RADAR (SAR) INTERFEROMETRY FOR GLACIER MOVEMENT STUDIES

Y. S. Rao
Centre of Studies in Resources Engineering, Indian Institute of Technology, Powai, Mumbai, India

Synonyms

Mapping glacier movement

Definition

Glaciers move due to their own weight and the influence of gravity. Information about the movement of the glacier is very important for understanding the climate change, mass balance, and glacier dynamics. The movement can be measured using surveying techniques (stakes and theodolite), laser ranging, and global positioning systems. All these techniques are confined to a point measurement and consumes time and expensive to measure over large inaccessible and inhospitable areas. Remote sensing techniques are very useful and cost effective to map those areas for glacier movement. Synthetic Aperture Radar Interferometry (InSAR) is a powerful technique for measuring the glacier velocity and strain rate (velocity gradient) with centimeter accuracy. In this technique, the phase difference of two or more SAR images acquired from slightly different orbit positions or view angles and at different times is exploited to obtain topography and surface change due to earthquake, volcano, land subsidence, and glacier velocity mapping.

Introduction

InSAR is widely used to map the velocity of glaciers in Antarctica (Goldstein et al., 1993; Frolich and Doake, 1998) and Greenland (Joughin et al., 1995, 1996; Kwok and Fannestock, 1996; Rignot et al., 1995). However, its applicability to map the velocity of temperate glaciers is challenging due to steep topography, melting of snow, and atmospheric changes between two SAR acquisitions. In spite of these difficulties, InSAR was successfully applied to map the velocity of the temperate and alpine glaciers using ERS-1 and 2 SAR tandem data. The advantage with tandem data is that ERS-1 and 2 satellites with similar SAR system acquired data with a 1-day interval between August 1995 and June 1996. Within a 1-day interval, glacier velocity in many parts of the glacier except at terminus is less than the prescribed limit. The upper limit on differential displacement occurs when the phase change is equal to phase sampling rate in range (Vachon et al., 1996). It means that the change in displacement between adjacent resolution cells must be less than $\lambda/2$. This condition sets the upper limit for the detectable velocity gradient. For example, when ice blocks move more than $\lambda/2$ from one resolution cell to the next, phase cycles are no longer detectable on interferogram and phase unwrapping is impossible. However, if the scene coherence is retained, there is no upper limit on absolute displacement measurement. In order to retain the scene coherence, the upper limit on displacement would be roughly half the resolution cell. For ERS system, the value is 4.8 m/day as the slant range resolution is 9.6 m.

Repeat pass InSAR

Glacier velocity can be mapped using 2-pass and 3-pass differential SAR interferometric (DInSAR) techniques. In 2-pass technique, one image is acquired before an event (earthquake, volcano eruption, land subsidence, landslides, glacier movement, etc.) and another one after an event. A typical SAR interferometer is an extension of famous two slit Young's experiment and is shown in Figure 1a. The phase difference between the two images (i.e., interferogram phase) containing both topography and displacement phase can be written as (Rosen et al., 2000, Massonnet and Feigl, 1998; Madsen and Zebker, 1998)

$$\Delta\phi = -\frac{4\pi}{\lambda}\frac{B_n \delta h}{r \sin\theta} + \frac{4\pi}{\lambda}\delta r \tag{1}$$

where $\Delta\phi$ is the interferogram phase after correcting for flat earth surface phase, B_n is perpendicular baseline, δh is altitude difference between two point targets, λ is the wavelength of the SAR system used, θ is the SAR signal incidence angle, r is slant range distance, and δr is the displacement between the two scene acquisitions.

In order to obtain the displacement due to glacier motion, the first term in Equation 1 representing topography phase is to be removed. For this, one has to obtain the accurate topography information. In February 2000, shuttle radar topography mission (SRTM) flew around the globe for around 11 days and collected digital elevation models (DEMs) of the earth surface except the area around north and south poles. The DEMs derived from the SRTM data are freely available to the public. Using orbital parameters of the two SAR scenes and SRTM digital elevation models, synthetic phase corresponding topography can be obtained. The synthetic phase is subtracted from interferogram to get the differential interferogram, representing only phase due to displacement map. After removing the phase due to topography, the Equation 1 becomes

$$\Delta\phi_{\text{defo}} = \frac{4\pi}{\lambda}\delta r \tag{2}$$

From this equation, displacement corresponding to one phase cycle ($\Delta\phi_{\text{defo}} = 2\pi$, i.e., one fringe in differential interferogram) yields $\lambda/2$. This value for ERS-1&2 is 2.8 cm, SIR-C L-band is 12 cm, and TerraSAR-X is 1.5 cm. The entire procedure for obtaining displacement is shown in Figure 1b.

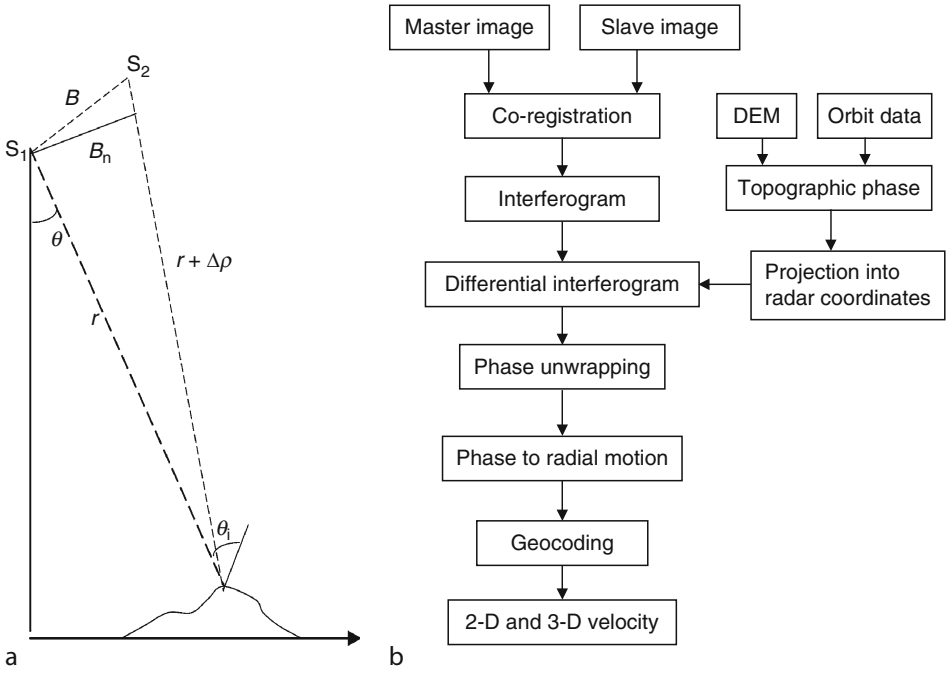

Synthetic Aperture Radar (SAR) Interferometry for Glacier Movement Studies, Figure 1 (**a**) Geometric configuration for InSAR and (**b**) flow diagram for 2-pass differential InSAR for glacier movement.

For typical ERS-1&2 SAR parameters λ = 5.6 cm, r = 850 km, θ = 23° baseline B_n=100 m, the first term (topographic) in Equation 1 becomes

$$\Delta\phi_{\text{topo}} = -0.06756\,\delta h \tag{3}$$

From this equation, the topographic height δh per one phase cycle ($\Delta\phi_{\text{topo}} = 2\pi$) becomes $\delta h = 93$ m. By comparing differential and topographic values, we can say that differential interferometry is 3,321 times greater sensitivity than topography. However, this sensitivity depends on the baseline value and decreases with increasing baseline. That is why DInSAR is better for lower baseline values. If DEM has some error of 30 m, then the error in displacement is about 1 cm (30 m/3,321 ≈ 1 cm).

Error in the baseline also creates an error in differential phase (Vachon et al., 1996). For ERS-1&2 tandem data, the error is about 0.4 cm/day. In addition to these topography and baseline-related errors, atmospheric changes will also affect the accuracy of displacement map (Zebker et al., 1997).

3-pass DInSAR is not useful for mapping the displacement map of temperate glaciers due to large interval (35 days) between two passes and melting of snow. However, this technique was applied by Kwok and Fannestock (1996) and Joughin et al. (1995) with several ERS SAR datasets over Greenland acquired with a 3-day interval to remove motion effects and obtain the topography. In this method, minimum three SAR images are required to form two interferograms. It is important to note that motion should be uniform throughout the acquisition period. By taking the difference of the two interferograms, motion is canceled and the resultant differential phase represents the topography. With this topography information, glacier motion can be obtained after removing the topography-related phase from the interferogram.

Phase coherence

For the analysis of glacier movement using InSAR, information about phase coherence is very important. In the interferometry processing, coherence is one of the products of InSAR technique. Interferometric complex correlation can be written as (Rosen et al., 2000)

$$\gamma = \frac{\langle g_1 g_2^* \rangle}{\sqrt{\langle |g_1|^2 \rangle \langle |g_2|^2 \rangle}}$$

where g_1 and g_2 represent the first and second SAR images, respectively, and angular brackets denote averaging over the ensemble of speckle realizations. The magnitude of the correlation $|\gamma|$ is usually known as coherence and varies from 0 to 1. The causes for the decorrelation between two images are due to temporal, spatial, and thermal noise. The total coherence of the image can be written as (Zebker and Villasenor, 1992)

$$\gamma_{\text{total}} = \gamma_{\text{temporal}}\gamma_{\text{spatial}}\gamma_{\text{thermal}}$$

The spatial decorrelation ($\gamma_{spatial}$) depends on sensor geometry and baseline separation between two acquisitions. The temporal decorrelation ($\gamma_{temporal}$) is due to changes in vegetation growth, snowdrift, snowmelt, glacier motion, permafrost freezing and thawing, soil moisture changes, agricultural practices, etc. that occur during repeat pass acquisition. The decorrelation due to thermal noise is related to signal to noise ratio of the sensor system.

Rignot et al. (1996) observed the coherence over San Rafael glacier, Chile using SIR-C L- and C-band and found that the coherence at L-band is better than C-band with a 1-day interval between two scenes as shown in Figure 2. Coherence is low ($\gamma < 0.4$) on the glacier at C-band, but higher on the plains surrounding Laguna San Rafael. Mountain peaks without vegetation also shows high coherence (γ = 0.7–0.8). The forest area shows low coherence (γ = 0.4–0.6) due to movement of leaves and volume scattering. At L-band, the coherence is high ($\gamma < 0.95$) at low elevations over the forest and also at slow moving part of the ice fields ($\gamma < 0.75$), intermediate over fast moving part of the glacier ($\gamma = 0.5$), moderate ($\gamma = 0.35$) in areas of high shear strain and low ($\gamma < 0.2$) over the open water and shadows. Snowmelting areas also show low coherence.

Using many ERS-1 and 2 tandem datasets, Vachon et al. (1996) and Mattar et al. (1998) observed change in coherence on different dates over Saskatchewan and Athabasca glaciers. It was found that on some dates, coherence is very low even for the tandem data and not useful for InSAR studies. They estimated the coherence using an averaging window size of 50 (azimuth) × 10 (range) samples.

Rao et al. (2008a) observed coherence change over three major Indian Himalayan glaciers, namely, Siachen, Gangotri, and Bara Shigri using ERS-1 and 2 tandem data and ENVISAT ASAR 35-day interval data. Among all these, Siachen glacier showed the highest coherence with ERS-1/2 tandem data acquired in descending pass as shown in Figure 3a. Low coherence was observed over Gangotri and Bara Shigri glaciers using the tandem data and shown in Figure 3b and c. ENVISAT ASAR 35-day interval data also gave good coherence outside glacier area. In glacier area, the coherence is completely lost due to large movement of the glacier within a 35-day interval and also changes in the debris on the glacier due to melting and precipitation. High-resolution TerraSAR-X images over Gangotri glacier with a 11-day interval also give poor coherence for the glacier part due to lower wavelength and fast movement of the glacier. However, good coherence and fringes are observed in the adjacent glacier area.

ALOS PALSAR L-band images over Qinghai-Tebetan plateau with interval 45–90 days also show low coherence over glacier area (Li et al., 2008). But the coherence obtained with a 45-day interval data as shown in Figure 4 is better than that obtained with a 90-day interval data. Due to longer wavelength of PALSAR and winter season, coherence was preserved between images acquired with a 45-day interval.

Intensity, coherence, and speckle-tracking methods

When the loss of coherence is high between interferometric SAR images, differential InSAR cannot be applied. An alternative to DInSAR for the estimation of glacier motion is offset tracking (Strozzi et al., 2002; Pattyn and Derauw, 2002). In the intensity tracking, image offsets in the slant range and azimuth directions are calculated using SAR intensity images, whereas in coherence-tracking method single look complex SAR images are used to calculate coherence and maximized the value by shifting the offset. This is done over entire image by tracking small patches of size 8 × 8 pixels which correspond to 160 m in the ground range and 30 in the azimuth direction for ERS SAR system. The offsets obtained through this procedure are due to orbit configurations and glacier movement. The offsets related to orbital geometry are estimated using precision orbit and ground control points and the offsets related to glacier displacement is separated. The accuracy of the offset-tracking methods is two times less than that we get using DInSAR studies (Strozzi et al., 2002). Advantage of offset-tracking method is that we get two-dimensional velocities in azimuth and range direction, whereas the DInSAR gives only in radar look direction (one direction). Rignot et al. (1996) also used intensity-tracking technique for the estimation of movement in crevasse areas.

Speckle tracking is similar to intensity and coherence tracking. Instead of correlating intensity or coherence between two images, it correlates speckle between two images for observing shifts between two images. The condition for this technique is that coherence between two images is necessary (Gray et al., 2001; Joughin, 2002; Short and Gray, 2004).

Three-dimensional flow estimation

Radar measures the displacement in the line of sight (LOS) direction. One single interferogram gives only one component of velocity. However, the true displacement may lie in any direction. Without additional information, it is not possible to separate horizontal and vertical displacement. Joughin et al. (1998), Mattar et al. (1998), Mohr et al. (1998), and Magnússon et al. (2007) combined the displacements obtained with ascending and descending pass data and surface slope to estimate three-dimensional ice velocity vector. They assumed that glacier flow is parallel to the topographic surface and also ice flows at a steady rate during acquisition of the ascending and descending passes. These assumptions may fail in some cases. The surface-parallel flow assumption fails in the regions of accumulation and ablation areas with bumpy terrain where vertical component motion is large and leads to errors. However, the horizontal component of motion is relatively unaffected by deviations in surface-parallel flow. The required inputs for the calculation of three component velocity vector are surface slope, angular separation of ascending and descending tracks α, and incidence angle (θ_i) which

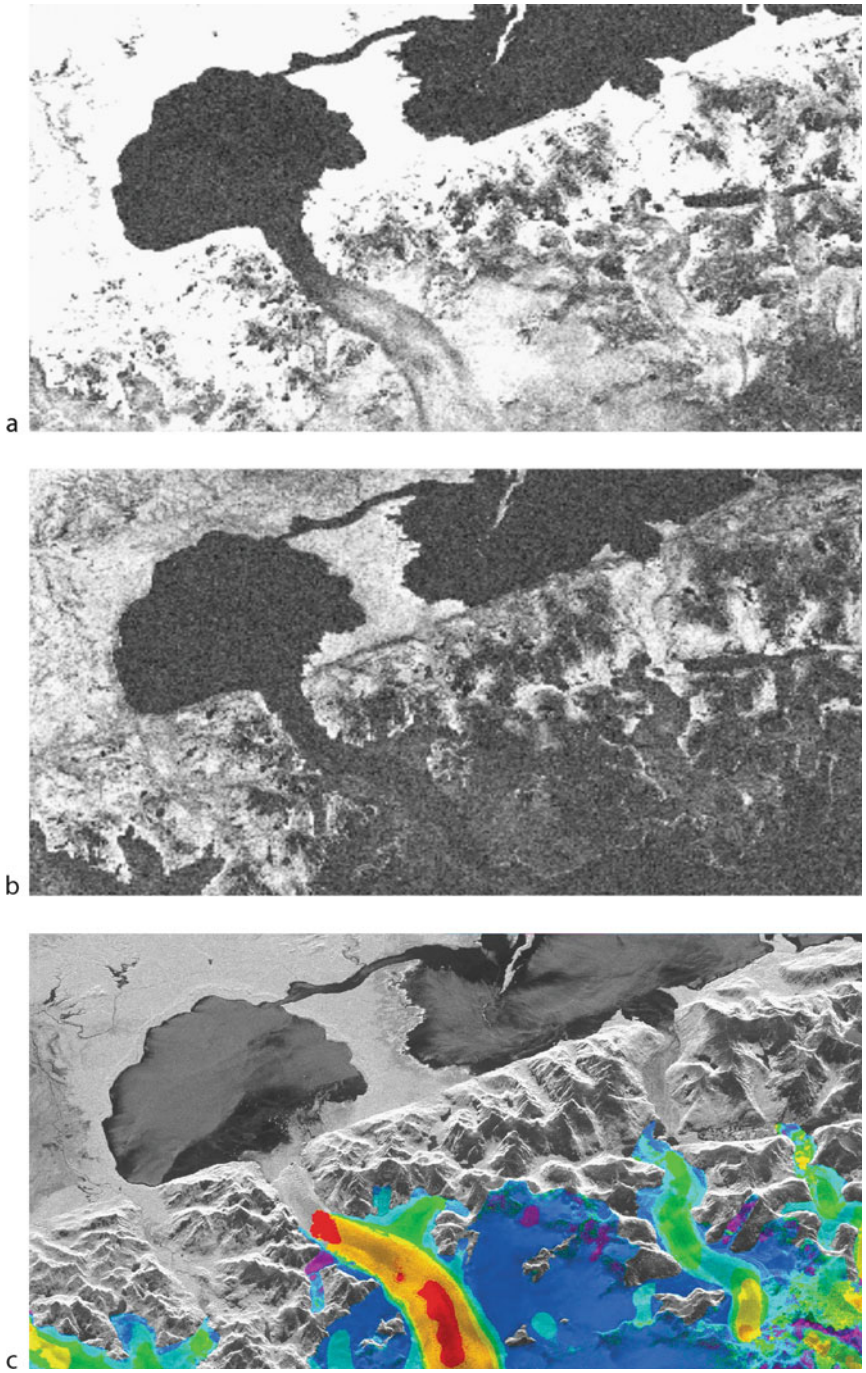

Synthetic Aperture Radar (SAR) Interferometry for Glacier Movement Studies, Figure 2 (**a**) Phase coherence between October 9 and 10, 1994 SIR-C L-band image pair, San Rafael Glacier, Chile. (**b**) phase coherence at C-band, and (**c**) ice motion derived using L-band data in the direction of radar illumination (Rignot et al., 1996). *Light purple* (<–3 cm/day), *purple* (–3 to –0.5 cm/day), *gray* (–0.5 to +0.5 cm/day), *blue* (0.5–3 cm/day), *light blue* (3–20 cm/day), *green* (20–45 cm/day), *yellow* (45–85 cm/day), *orange* (85–180 cm/day), and *red* (>180 cm/day). Negative sign is movement away from the radar and positive sign is movement toward the radar.

is defined with respect to local normal to the ellipsoid as shown in Figure 1, angle between ascending pass direction and reference x-axis and unwrapped phase corresponding to motion (Joughin et al., 1998).

Using single interferogram also, surface displacement can be estimated using range displacement (Vachon et al., 1996). For certain critical angles of surface slope and the direction of slope, the LOS displacement is

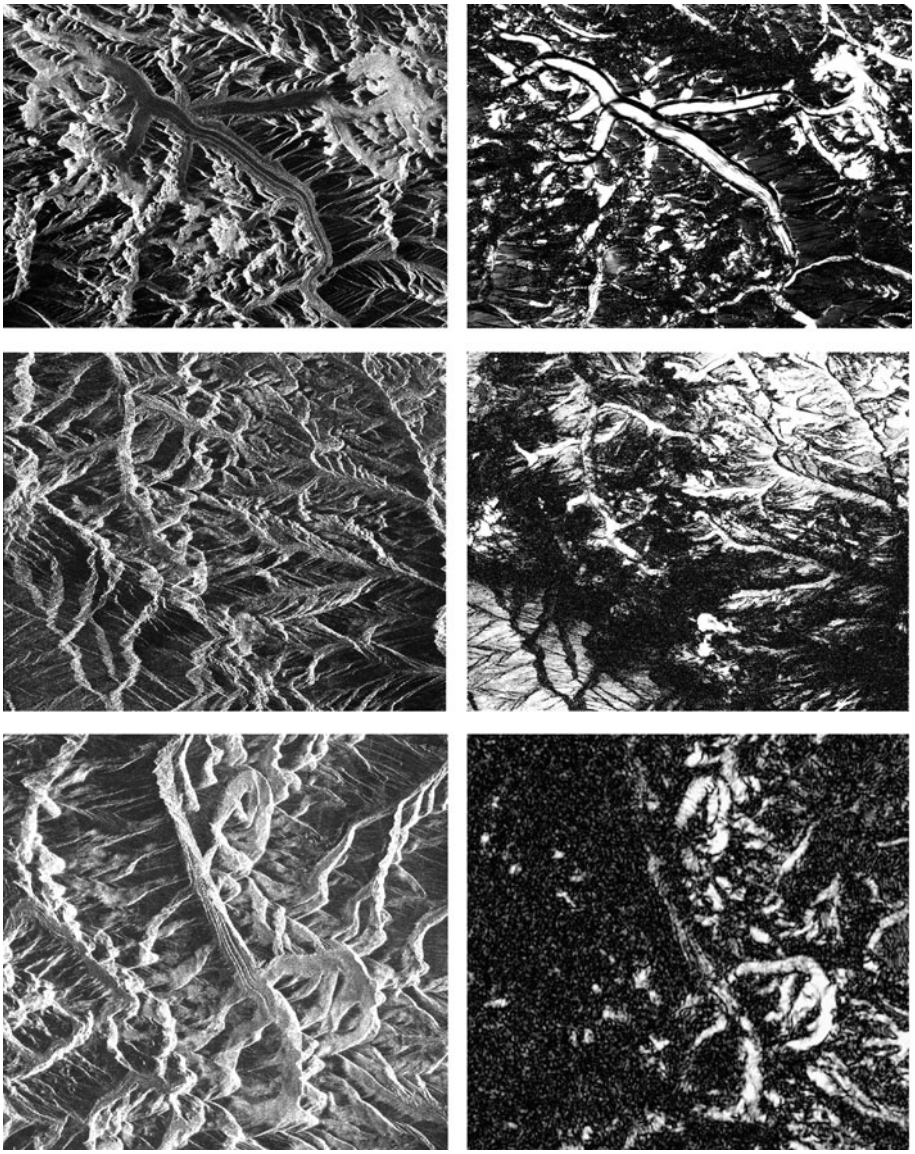

Synthetic Aperture Radar (SAR) Interferometry for Glacier Movement Studies, Figure 3 Interferometric coherence along with SAR intensity images are shown for Siachen (*top*), Gangotri (*middle*), and Bara Shigri (*bottom*) glaciers in Himalaya using ERS-1/2 tandem data.

perpendicular to the glacier displacement and surface displacement tends to infinity. To estimate the displacement from single LOS measurement, the LOS direction relative to displacement is outside the critical range.

Studies on land glaciers

InSAR studies on midlatitude alpine glaciers are very few. Vachon et al. (1996) studied surface displacement of Athabasca and Saskatchewan glaciers using several ERS-1/2 tandem pairs acquired with a 24 h interval. Topography information in the interferogram was removed using the DEM derived using airborne SAR data. The RMS error in their DEM is about 5 m that cause an error of 0.4 cm/day in displacement map at the baseline of 300 m. They also mentioned that the error in the baseline also causes 0.4 cm/day error in displacement map. Mattar et al. (1998) extended the same work and estimated three-dimensional surface flow field using surface-parallel flow assumption by combining ascending and descending passes. The LOS displacement of maximum 18 cm/day was observed for Saskatchewan glacier with ascending pass data, whereas 10 cm/day with descending pass data. The corresponding surface displacement along the center line of the Saskachewan glacier is 35 cm/day.

Rignot et al. (1996) studied San Rafael, Chile glacier using SIR-C L- and C-band October 1994 interferometric

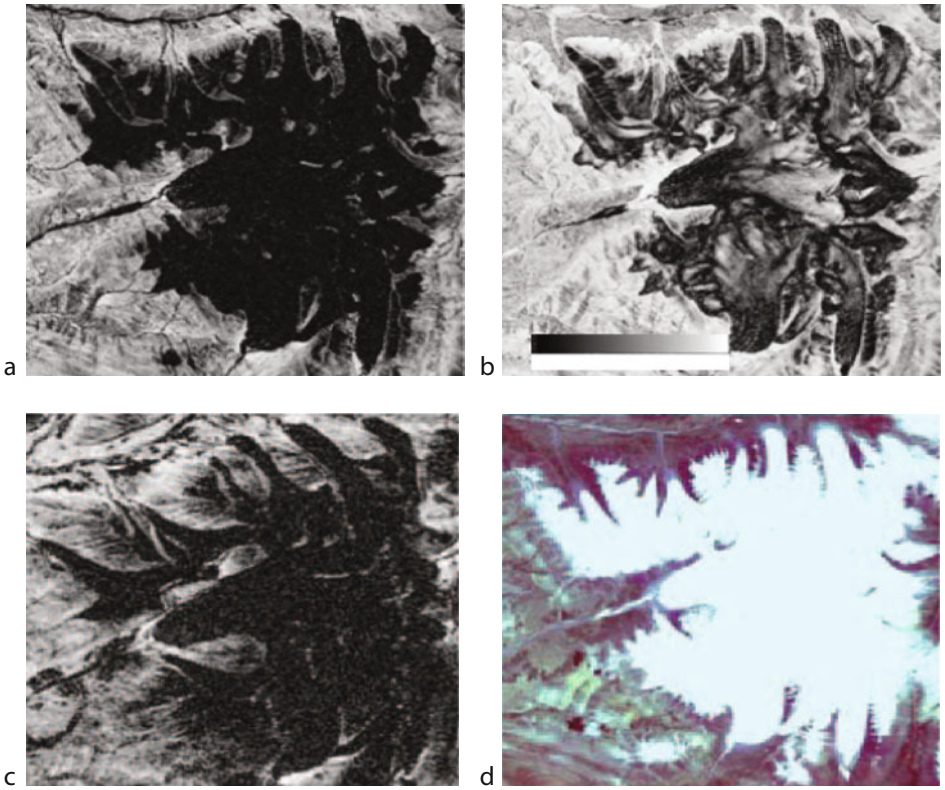

Synthetic Aperture Radar (SAR) Interferometry for Glacier Movement Studies, Figure 4 Phase coherence images over the glacier Dongkemadi in Qinghai-Tibetan plateau. (**a**) ALOS PALSAR pair June 11, 2006 and September 11, 2006 (**b**) ALOS PALSAR pair December 10, 2007 and January 25, 2008, (**c**) ENVISAT ASAR pair July 10, 2007 and August 14, 2007, and (**d**) TM image for the same area (Li et al., 2008).

data acquired with interval of 24 h. Due to shorter wavelength, C-band data did not give good coherence image for this area. However, L-band data preserved the coherence in many parts of the glacier and were used to map the surface topography over the glacier with accuracy of 10 m and measured the ice velocity with a precision of 4 mm/day. The LOS interferometric velocities were converted to surface displacement by assuming a flow direction and complemented by feature-tracking result near the calving front. Ice velocity map in radar LOS direction is shown in Figure 2c. InSAR observed ice velocity at the equilibrium line (1,200 m altitude) is 2.6 m/day (0.85 km/year) and increases rapidly before the glacier enters the narrower terminal valley. Just before 100 m from the calving front, ice velocity reaches 17.5 m/day (6.4 km/year). InSAR could estimate velocities upto 9 m/day. Feature-tracking method was used near the crevasse areas to estimate velocity upto 17.5 m/day. Effective starin-rate map was also generated using velocity map. Forster et al. (1999) studied Europa and Penguin glaciers in Chile using SIR-C L-band data and estimated ice velocity with a precision of 2 cm/day.

Michel and Rignot (1999) used SIR-C L-band October 1994 data to map Moreno glacier in Argentina. Both interferometry and feature tracking based on coherence have been used to map the glacier velocity and found that InSAR can measure ice velocity with a precision of 1.8 cm/day, while feature-tracking method can estimate with an accuracy of 14 cm/day.

Swiss Alpine glacier movement was studied by Strozzi et al. (2003). The glaciers covered in their study were the largest glacier Groβer Aletschgletscher and other glaciers Unteraargletscher, Fieschergletscher, and Grüebu Gletscher. As the ground truth data over Unteraargletscher glacier are available through various methods, interferometric derived LOS displacement map was obtained using ERS-1/2 tandem data for this glacier. The maximum velocity observed at the upper part of the glacier at steeper slopes is 4 cm/day and decreases gradually along the glacier. It was observed that radar is not sensitive to displacement measurement if the glacier flow is perpendicular to the radar look direction. It was suggested that the LOS surface displacement map of the glacier is useful to estimate mass balance distribution using the kinematic boundary condition without the use of ground measurements.

Himalayan glaciers movement

Rao et al. (2004, 2008a, b) mapped the movement of the major Himalayan glaciers, namely, Siachen, Gangotri, and Bara Shigri using ERS-1/2 tandem data. Siachen

glacier is the largest glacier located at higher elevation. It has a length of about 72 km and with varying width. It is the second largest glacier in the world outside the polar region. It feeds the Nubra river (also known as Shaksgam river) that flows parallel to the Karakoram range before entering into Tibet. The trunk glacier and its tributaries are in the form of a vast ice field. Continuous snowfall can be seen during winter periods. The average winter snowfall is about 10.5 m. The temperature varies from −10°C and −50°C. The elevation varies from the snout (3,620 m) to source of the glacier (i.e., Indira col) (5,753 m).

Gangotri glacier is a major source of water for many states of the North India. It is about 25 km long with varying width of 2.5–0.5 km and having many tributary glaciers. Some of these tributary glaciers are in turn having their own tributaries. The elevation over the main glacier varies from terminus (4,000 m) to the source of the glacier (6,000 m). The temperature at the glacier (terminus) varies from 10°C to –20°C. According to many reports, the glacier is retreating at alarming rates (20 m/year).

Bara Shigri glacier lies (N32°10'33", E77°40′09″) on Chandra-Bhaga river basin (Pir Panjal range) in Lahaul-Spiti district of Himachal Pradesh. The glacier is the largest in Himachal Pradesh with a length of 28 km (131 km^2) with elevation changing from terminus (4,000 m) to the source of the glacier (5,500 m). There are several glaciers around this glacier (Chhota Shigri, Hamta, etc.). All these glaciers are covered in one scene of the ERS-1/2 SAR data.

ERS-1/2 tandem data acquired on April 1 and 2, 1996 in descending pass with perpendicular baseline of 110 m and May 2 and 3, 1996 in ascending pass with baseline of 114 m were used to map the surface displacement of Siachen glacier. ERS-1/2 tandem pair acquired on March 25 and 26, 1996 in ascending pass with baseline of 75 m was used for Gangotri glacier studies. ERS-1/2 tandem pair acquired on May 2 and 3, 1996 in ascending pass with perpendicular baseline of 110 m was used to study the Bara Shigri glacier.

To get differential interferometric fringes, one has to follow several the steps given in Figure 1. Topography information from the interferogram was removed using SRTM 3 arc second DEM. Figure 5 shows ERS-1 SAR intensity, interferoram, differential interferogram and ice velocity in the LOS direction for Siachen glacier. Figure 5d shows velocity of the glacier in color. Negative (−) velocities represent movement away from the radar direction and positive (+) represents movement toward the radar direction.

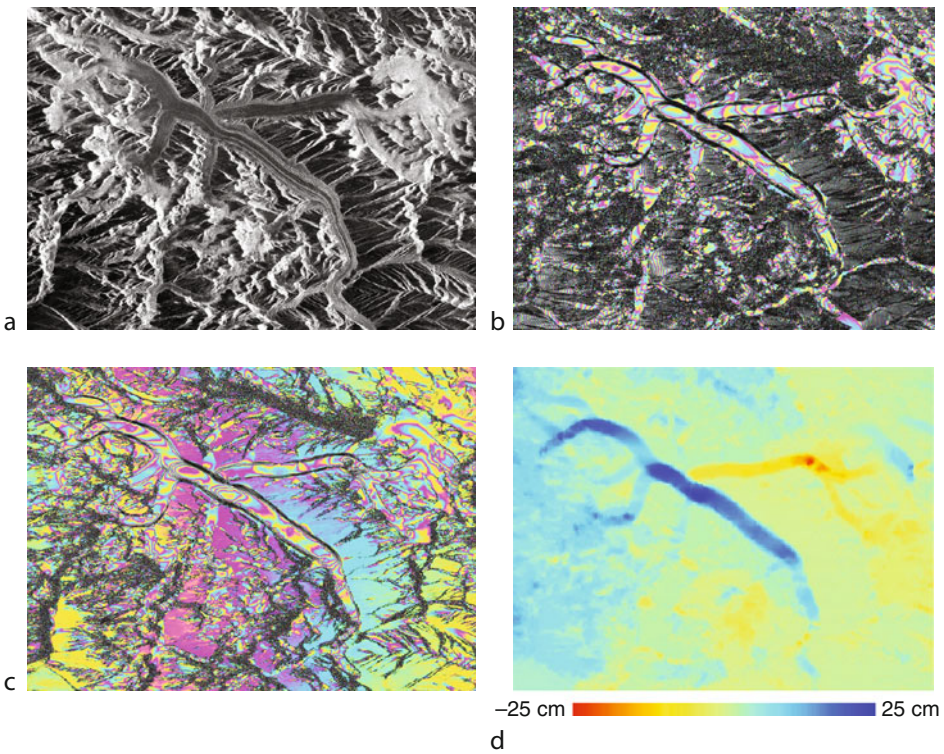

Synthetic Aperture Radar (SAR) Interferometry for Glacier Movement Studies, Figure 5 Synthetic Aperture Radar (SAR) images of April 1 and 2, 1996 acquired by ERS-1 and 2 satellites were processed using interferometric technique for estimating Siachen glacier movement. (**a**) SAR intensity image, (**b**) Interferogram with each fringe representing topographic height of 85 m, (**c**) Differential interferogram with each fringe representing 2.8 cm motion toward the radar direction, and (**d**) Surface displacement map in cm (*dark blue* represents (25 cm/day) movement toward the radar and red represents (–25 cm) away from the radar).

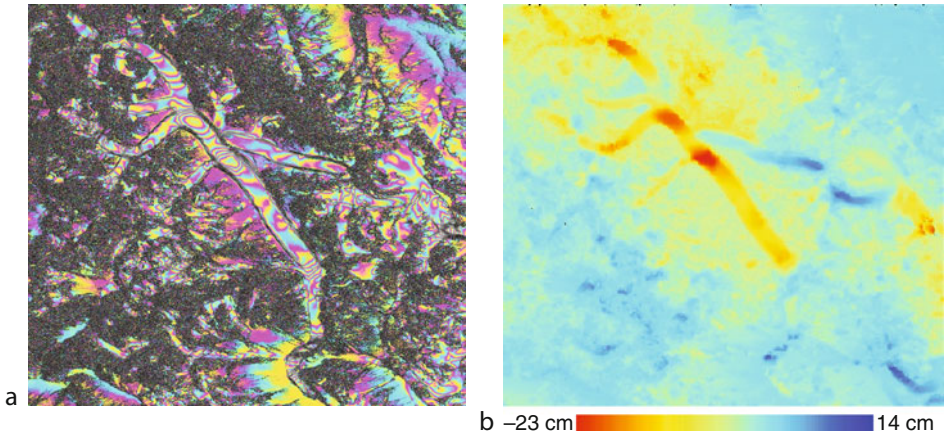

Synthetic Aperture Radar (SAR) Interferometry for Glacier Movement Studies, Figure 6 (**a**) Differential interferogram and (**b**) ice velocity in the radar direction for Siachen glacier obtained using ascending pass of ERS-1/2 SAR tandem data.

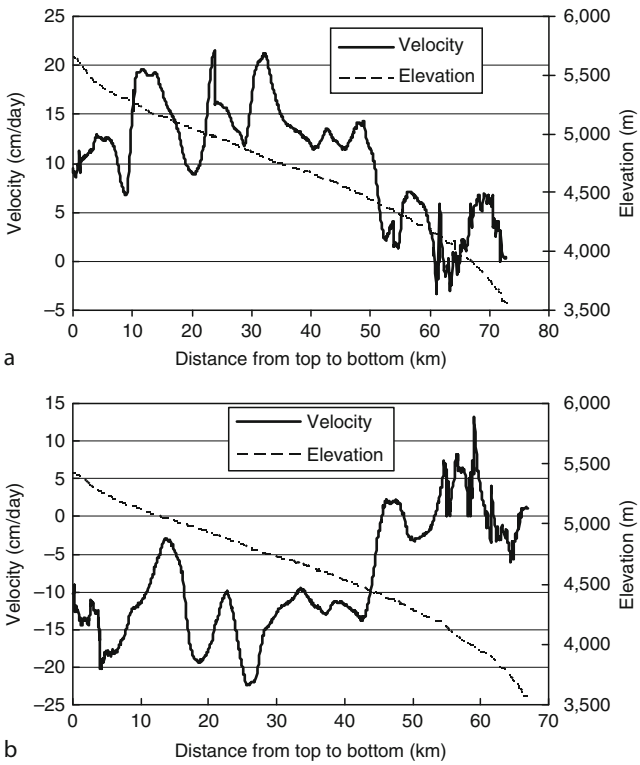

Synthetic Aperture Radar (SAR) Interferometry for Glacier Movement Studies, Figure 7 Ice velocity in the radar direction and surface elevation of Siachen glacier versus the distance from the top to terminus: (**a**) ascending and (**b**) descending pass.

Differential fringes over Siachen are more, particularly at higher elevation and also lower part of the glacier, that is, ablation area. Fringes are not seen at the middle part of the glacier. Above the Siachen glacier, there are small glaciers where fringes are observed. Fringes are also seen at some places where there are no glaciers. It may be due to differences between SRTM DEM and actual elevation present at the ground. At the joining place of tributaries with trunk of the glacier, round-shaped fringes (often called bull eye shape) are observed. It is due to the movement of ice over elevation and through a bump. Maximum number of fringes at the location is about 8 which is equal to 22.4 cm displacement toward the radar direction.

Similarly, differential fringes for ascending pass over Siachen are produced and shown in Figure 6. More differential fringes are seen for this pass particularly at the ablation area indicating that the glacier is moving faster in May than in April. We have also used ENVISAT ASAR datasets with interval of 35 days to 1 year for DInSAR studies. For the 35-day data, complete loss of coherence was observed on the glacier area. To estimate motion using the large interval data, intensity-tracking method can only be used.

Along the middle of the glacier, we took the velocity profile from highest elevation to lowest and shown in Figure 7 for both descending and ascending passes respectively. The X-axis is the distance in pixels down the glacier. Each pixel is about 20 m. In case of Gangotri, we observed positive velocity that indicates the movement of glacier away from the radar direction. For Siachen glacier, the trend of movement along the glacier varies depending on the descending and ascending passes. At the bump of the glacier (525 and 1,000 pixel number), there was steep change in displacement at the glacier. At the bottom of the glacier also, there is variation in the movement. The variation is highest at the ablation zone.

About two to three differential fringes (8.4 cm) were observed for Gangotri area particularly in higher elevation of the glacier. There was also displacement at some other areas due to DEM and baseline errors. Considering the

error in SRTM DEM which is about 30 m, the error in displacement map for Gangotri is less than 1 cm. Although we observed differential fringes for Bara Shigri glacier, we could not obtain displacement map due to phase unwrapping problems. We observed heavy coherence loss at this area. The differential fringes show that the maximum glacier movement is 5 cm/day.

Alaska surge glaciers

Bering glacier is the largest glacier in North American continent with 190 km length. Fatland and Lingle (1998, 2002) analyzed the glacier surge 1993–1995 using intereometric SAR data. Rabus and Fatland (2000) analyzed Black Rapids glacier in Alaska using ERS-1 SAR 3-day interval data. There is not much literature on catastrophic glacier using InSAR.

Summary

InSAR is a power tool for mapping glacier movement with centimeter accuracy at high spatial resolution. All satellite datasets may not be useful for InSAR applications due to large glacier movement, melting of snow, baseline requirements, and atmospheric changes. ERS-1/2 tandem data acquired with a 1-day interval was the best suitable data for mapping glacier movement. Limited data acquired by SIR-C were also used for glacier velocity mapping. For removing the topographic effects in the interferograms, SRTM digital elevation models have been used. Glacier velocity map generated with SAR data is in the line of radar direction. To obtain the three-dimensional velocity map, ascending and descending pass data are combined with an assumption that glacier movement is parallel to topographic surface. As most of the operating satellites give the data at the interval of 11–45 days, applications of InSAR for glacier movement is not feasible. To overcome the difficulty, intensity-, coherence-, and speckle-tracking methods have been used. As the resolution of the present satellites is better than the older satellites, glacier movement of even smaller glaciers can be mapped with greater accuracy.

Bibliography

Fatland, D. R., and Lingle, C. S., 2002. In SAR observations of the 1993–1995 Bering Glacier (Alaska, USA) surge and a surge hypothesis. *Journal of Glaciology*, **48**, 439–451.

Fatland, D. R., and Lingle, C. S., 1998. Analysis of the 1993–1995 Bering glacier (Alaska) surge using differential SAR interferometry. *Journal of Glaciology*, **44**(148), 532–546.

Forster, R. R., Rignot, E., Isacks, B. L., and Jezker, K. C., 1999. Interferometric radar observations of Glaciares Europa and Penguin, Hielo Patagonico Sur, Chile. *Journal of Glaciology*, **45**, 325–337.

Frolich, R. M., and Doake, G. S. M., 1998. Synthetic Aperture radar interferometry over Rutford ice stream and Carlsm inlet, Antarctica. *Journal of Glaciology*, **44**, 77–92.

Goldstein, R. M., Engelhardi, H., Kamb, B., and Frolich, R. M., 1993. Satellite radar interferometry for monitoring ice sheet motion: application to an Antarctic ice stream. *Science*, **262**, 525–1530.

Gray, A. L., Short, N., Mattar, K. E., and Jezek, K. C., 2001. Velocities and flux of the Filchner Ice Shelf and its tributaries determined from speckle tracking interferometry. *Canadian Journal of Remote Sensing*, **27**, 193–206.

Joughin, I., 2002. Ice-sheet velocity mapping: a combined interferometric and speckle tracking approach. *Annals of Glaciology*, **34**, 195–201.

Joughin, I. R., Winebrenner, D. P., and Fahnestock, M. A., 1995. Observations of ice-sheet motion in Greenland using satellite radar interferometry. *Geophysical Research Letters*, **22**, 571–574.

Joughin, I., Kwok, R., and Fahnestock, M., 1996. Estimation of ice sheet motion using satellite radar interferometry: Method and error analysis with application to the Humboldt Glacier, Greenland. *Journal of Glaciology*, **42**, 564–575.

Joughin, I. R., Kwok, R., and Fahnestock, M. A., 1998. Interferometric estimation of three-dimensional ice-flow using ascending and descending passes. *IEEE Transaction on Geosciences and Remote Sensing*, **36**, 25–37.

Kwok, R., and Fannestock, M. S., 1996. Ice sheet motion and topography from radar Interferometry. *IEEE Transaction on Geosciences and Remote Sensing*, **34**, 189–200.

Li, Z., Zhou, J., Tian, B., and Xie, Z., 2008. *The glacier identification using SAR interfermetric and polarimetric information in Qinghai-Tibetan plateau*. IV: Proceedings of IGARSS, pp. 1054–1056.

Madsen, S. N., and Zebker, H., 1998. Imaging radar interferometry. In Hdenderson, F. M., and Lewis, A. J. (eds.), *Principles and Applications of Imaging Radar, Manual of Remote Sensing.* Chapter 6, 3rd edn., Vol. 2, pp. 359–380.

Magnússon, E., Rott, H., Björnsson, H., and Pálsson, F., 2007. The Impact of jökulhlaups on basal sliding observed by SAR interferometry on Vatnajökul, Iceland. *Journal of Glaciology*, **53**, 232–240.

Massonnet, D., and Feigl, K. L., 1998. Radar interferometry and its application to changes in the earth's surface. *Reviews of Geophysics*, **36**, 441–500.

Mattar, E. K., Vachon, P. W., Geudtner, D., and Gray, A. L., 1998. Validation of Alpine glacier velocity measurements using ERS tandem-mission SAR data. *IEEE Transaction on Geosciences and Remote Sensing*, **36**, 974–984.

Michel, R., and Rignot, E., 1999. Flow of Glaciar Moreno, Argentina, from repeat pass shuttle imaging radar images: comparison of the phase correlation method with radar interferometry. *Journal of Glaciology*, **45**, 93–100.

Mohr, J. J., Reeh, N., and Madsen, S. N., 1998. Three-dimensional glacial flow and surface elevation measured with radar interferometry. *Nature*, **391**, 273–276.

Pattyn, F., and Derauw, D., 2002. DInSAR and coherence tracking applied to glaciology: the example of Shirase Glacier. *Journal of Glaciology*, **48**, 559–565.

Rabus, B. T., and Fatland, D. R., 2000. Comparison of SAR-interferometric and surveyed velocities on a mountain glacier: black rapids glacier, Alaska, U.S.A. *Journal of Glaciology*, **46**(152), 119–128.

Rao, Y. S., Venkataraman, G., Rao, K. S., and Snehmani, A., 2004. SAR interferometry for DEM generation and movement studies over Indian Glaciers. *Proceedings of IGARSS*, **2**, 1128–1131.

Rao, Y. S., Singh, G., Venkataraman, G., and Snehmani, A., 2008b. Application of SAR interferometry for DEM generation and movement studies over Himalayna glaciers. In *Proceedings of Natioanl Snow Science Workshop 2008 (NSSW-08)*, held during 11–12 January 2008, pp. 210–217.

Rao, Y. S., Kumar, V., Singh, G., Venkataraman, G., and Snehmani, A., 2008a. The loss of coherence in the InSAR images of Himalayan Glaciers. In *Proceedings of International Workshop on Snow, Ice, Glacier and Avalanches*, held at IIT Bombay during January 7–9, 2008, pp. 232–239.

Rignot, E., Jezek, K. C., and Sohn, H. G., 1995. Ice flow dynamics of the Greenland ice sheet from SAR interferometry. *Geophysical Research Letters*, **22**, 575–578.

Rignot, E., Forster, R., and Isacks, B., 1996. Interferometric observations of Glacier San Rafael. Chile. *Journal of Glaciology*, **42**, 279–291.

Rosen, A. P., Hensley, S., Joughin, I. R., Li, F. K., Madsen, S. N., Rodriguez, E., and Goldstein, R. M., 2000. Synthetic aperture radar interferometry. *Proceeding of IEEE*, **88**, 333–382.

Short, N. H., and Gray, A. L., 2004. Potential for RADARSAT-2 interferometry: glacier monitoring using speckle tracking. *Canadian Journal of Remote Sensing*, **30**, 504–509.

Strozzi, T. A., Luckman, T. M., Wegmüller, U., and Werner, C. L., 2002. Glacier motion estimation using SAR offset-tracking Procedures. *IEEE Transaction on Geosciences and Remote Sensing*, **40**, 2384–2391.

Strozzi, T., Gudmundsson, G. H., and Wegmuller, U., 2003. Estimation of the surface displacement of Swiss Alpine Glaciers using satellite radar interferometry, ERSeL eProceedings 2 1/2003 Observing our Cryosphere from Space: Techniques and Methods for Monitoring Snow and Ice with Regard to Climate Change, CD-ROM, 2003.

Vachon, P. W., Geudtner, D., Mattar, K., Gray, A. L., Brugman, M., and Cumming, I., 1996. Differential SAR interferometry measurements of Athabasca and Saskatchewan glacier flow rate. *Canadian Journal of Remote Sensing*, **22**, 287–296.

Zebker, H. A., and Villasenor, J., 1992. Decorrelation of interferometric radar echoes. *IEEE Transaction on Geosciences and Remote Sensing*, **30**, 950–959.

Zebker, H. A., Rosen, P. A., and Hensley, S., 1997. Atmospheric effects in interferometric synthetic aperture radar surface deformation and topographic maps. *Journal of Geophysical Research*, **102**(B4), 7547–7563.

Cross-references

Glacier Motion/Ice Velocity
Glacier Surging
Optical Remote Sensing of Alpine Glaciers